

## Functionalisation of Platinum Based Drugs Through Click Chemistry Strategies

### AUTHOR(S)

Eolann Kitteringham

### CITATION

Kitteringham, Eolann (2018): Functionalisation of Platinum Based Drugs Through Click Chemistry Strategies. Royal College of Surgeons in Ireland. Thesis. <https://doi.org/10.25419/rcsi.10803071.v1>

### DOI

[10.25419/rcsi.10803071.v1](https://doi.org/10.25419/rcsi.10803071.v1)

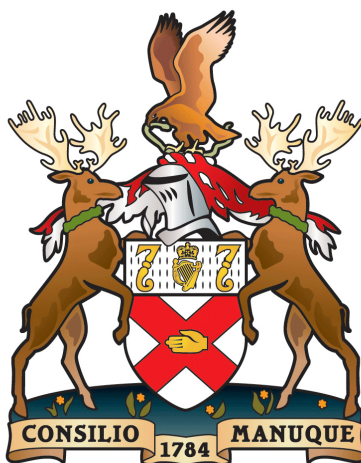
### LICENCE

CC BY-NC-SA 4.0

This work is made available under the above open licence by RCSI and has been printed from <https://repository.rcsi.com>. For more information please contact [repository@rcsi.com](mailto:repository@rcsi.com)

### URL

[https://repository.rcsi.com/articles/thesis/Functionalisation\\_of\\_Platinum\\_Based\\_Drugs\\_Through\\_Click\\_Chemistry\\_Strategies/10803071/1](https://repository.rcsi.com/articles/thesis/Functionalisation_of_Platinum_Based_Drugs_Through_Click_Chemistry_Strategies/10803071/1)



---

# RCSI

---

## Functionalisation of Platinum Based Drugs Through Click Chemistry Strategies

**Eolann Kitteringham B.Sc.**

Department of Chemistry, Royal College of Surgeons in Ireland

A thesis submitted to the School of Postgraduate Studies, Faculty of  
Medicine and Health Sciences, Royal College of Surgeons in  
Ireland, in fulfilment of the degree of Doctor of Philosophy

Under the supervision of Dr. Darren Griffith

**July 2018**

# Table of Contents

Declaration .....	i
Publications .....	ii
Acknowledgements .....	iii
Dedication .....	vi
Abstract .....	vii
Symbols and Abbreviations .....	ix
<b>Chapter 1</b> .....	1
<b>Cancer</b> .....	2
Ovarian Cancer .....	2
Treatments .....	3
<b>Metals in medicine</b> .....	4
Platinum (Pt) Chemistry .....	4
Gold (Au) Chemistry .....	6
Cisplatin – 1 <sup>st</sup> generation .....	6
Side effects and Pt resistance .....	9
<b>Next Generation Pt drugs</b> .....	11
Pt(IV) anticancer drugs .....	12
<b>Multifunctional Pt Drugs</b> .....	13
<b>Diagnostics</b> .....	15
Fluorophores .....	17
<b>Peptides in medicine</b> .....	22
Cell Penetrating Peptides .....	22
Heat Shock Proteins and HSP70 .....	25
<b>Steroids and hormones in medicine</b> .....	27
<b>Click Chemistry</b> .....	29
Triazole Chemistry .....	29
CuAAC .....	31
Bioorthogonal Chemistry .....	32
SPAAC .....	34
iEDDA .....	35
SPAAC vs iEDDA .....	38

<b>Conjugation of Bioactive molecules.....</b>	<b>38</b>
<b>Clicked Pt-fluorophore compounds .....</b>	<b>39</b>
<b>Targeted Pt Drug Delivery .....</b>	<b>41</b>
Pt-peptide conjugates .....	42
Pt-steroid conjugates .....	44
<b>Metal Chelating systems .....</b>	<b>46</b>
<b>Conclusion.....</b>	<b>49</b>
References .....	50
<b>Chapter 2 .....</b>	<b>66</b>
Instrumentation.....	67
Infrared spectroscopy .....	67
<sup>1</sup> H, <sup>13</sup> C, <sup>19</sup> F and <sup>195</sup> Pt Nuclear magnetic resonance spectroscopy .....	67
Mass spectrometry.....	67
Single Crystal X-ray diffraction methods .....	68
Elemental analysis .....	68
Ultraviolet-Visible Spectroscopy .....	68
Fluorescence Spectroscopy .....	68
HPLC .....	69
<b>Organic Syntheses .....</b>	<b>70</b>
General considerations and materials .....	70
Di- <i>tert</i> -butyl (2-hydroxypropane-1,3-diyl)dicarbamate <sup>4</sup> (1) .....	71
Di- <i>tert</i> -butyl ((propan-2-yl methanesulfonate)-1,3-diyl)dicarbamate <sup>4</sup> (2).....	72
Di- <i>tert</i> -butyl (2-azidopropane-1,3-diyl)dicarbamate <sup>4</sup> (3).....	73
2-azidopropane-1,3-diamine dihydrochloride <sup>5</sup> (DAP-N <sub>3</sub> .2HCl) (4) .....	74
Azidobenzene <sup>6</sup> (5) .....	75
2-(1-phenyl-1 <i>H</i> -1,2,3-triazol-4-yl)pyridine <sup>7</sup> (PTP) (6) .....	76
Di- <i>tert</i> -butyl (2-(4-(pyridin-2-yl)-1 <i>H</i> -1,2,3-triazol-1-yl)propane-1,3-diyl)dicarbamate (BOC <sub>2</sub> -PTPD) (7) .....	77
2-(4-(pyridin-2-yl)-1 <i>H</i> -1,2,3-triazol-1-yl)propane-1,3-diamine trihydrochloride (PTPD.3HCl) (8).....	78
Di- <i>tert</i> -butyl (2-(4-(phenyl)-1 <i>H</i> -1,2,3-triazol-1-yl)propane-1,3-diyl)dicarbamate – (BOC <sub>2</sub> -PhTPD) (9) .....	79
Di- <i>tert</i> -butyl (2-(4-(estradiol)-1 <i>H</i> -1,2,3-triazol-1-yl)propane-1,3-diyl)dicarbamate (10).....	80



(2-(4-(estradiol)-1 <i>H</i> -1,2,3-triazol-1-yl)propane-1,3-diyl) dihydrochloride (11)....	81
Di- <i>tert</i> -butyl (2-(4-(testosterone)-1 <i>H</i> -1,2,3-triazol-1-yl)propane-1,3-diyl)dicarbamate (12).....	82
(2-(4-(testosterone)-1 <i>H</i> -1,2,3-triazol-1-yl)propane-1,3-diyl) dihydrochloride (13).....	83
3,3'-((5-azido-1,3-phenylene)bis(ethyne-2,1-diyl))dipyridine (CageL-N <sub>3</sub> ) (14)....	84
3,3'-((5-(4-phenyl-1 <i>H</i> -1,2,3-triazol-4-yl)-1,3-phenylene)bis(ethyne-2,1-diyl))dipyridine (Cage-T-Ph) (15) .....	85
3,3'-((5-(4-(MAMP-NIR-AZA)-1 <i>H</i> -1,2,3-triazol-4-yl)-1,3-phenylene)bis(ethyne-2,1-diyl))dipyridine (Cage-T-MAMP) (16) .....	86
<b>Inorganic syntheses</b> .....	87
<i>cis</i> -[Pt(II)I <sub>2</sub> (DAP-N <sub>3</sub> )] <sup>5</sup> (17) .....	87
[Pt(II)(CBDCA)(DAP-N <sub>3</sub> )] <sup>5</sup> (18) .....	88
[Pt(II)Cl <sub>2</sub> (DAP-N <sub>3</sub> )] (19).....	89
[Pt(II)(CBDCA)(DAP-BCN-NIR-AZA)] fluorophore conjugate - Pt-Flu <sup>8</sup> (20)....	90
<i>cis</i> -[Pt(II)I <sub>2</sub> (NH <sub>3</sub> ) <sub>2</sub> ] – iodoplatin (21) .....	91
[Pt(II)(CBDCA)(NH <sub>3</sub> ) <sub>2</sub> ] – carboplatin <sup>9</sup> (22) .....	92
[Pt(II)I <sub>2</sub> (DACH)] <sup>10</sup> (23).....	93
[Pt(II)(DACH)(Ox)] – oxaliplatin <sup>11</sup> (24).....	94
[Pt(IV)(DACH)(OEt)(OH)(Ox)] (25) .....	95
[Pt(IV)(DACH)(OEt)(Ox)(succinato)] (26) .....	96
[Au(III)Cl <sub>3</sub> (PTP)] (27) .....	97
[Au(III)Cl <sub>3</sub> (BOC <sub>2</sub> -PTPD)] (28).....	98
Na <sub>0.5</sub> [Au(III)Cl <sub>2</sub> (PTPD)][Au(I)Cl <sub>2</sub> ][Au(III)Cl <sub>4</sub> ] <sub>0.5</sub> (29) .....	99
[Pt(II)Cl <sub>2</sub> (PTP)] (30) .....	100
[Pt(II)Cl <sub>2</sub> (PTPDH <sub>2</sub> )][PtCl <sub>4</sub> ] (31) .....	101
[Pt(II) <sub>3</sub> Cl <sub>4</sub> (PTPD) <sub>2</sub> ]Cl <sub>2</sub> (32).....	102
<i>cis</i> -[Pt(II)Cl <sub>2</sub> (DMSO) <sub>2</sub> ] <sup>15</sup> (33) .....	103
<i>cis</i> -[Pt(II)Cl <sub>2</sub> (DMSO)( <i>n</i> -propylamine)] (34).....	104
[Ag <sub>2</sub> (CBDCA)] <sup>17</sup> (35) .....	105
[Pt(II)(CBDCA)(DMSO) <sub>2</sub> ] <sup>16</sup> (36) .....	106
[Pt(II)(CBDCA)(DMSO)( <i>n</i> -propylamine)] <sup>16</sup> (37) .....	107
[Pt(II)(CBDCA)(2-(4-(estradiol)-1 <i>H</i> -1,2,3-triazol-1-yl)propane-1,3-diyl)] (38). 108	
[Pt(II)Cl <sub>2</sub> (2-(4-(estradiol)-1 <i>H</i> -1,2,3-triazol-1-yl)propane-1,3-diyl)] (39).....	109

Attempted synthesis of [Pt(II)(2-(4-(testosterone)-1 <i>H</i> -1,2,3-triazol-1-yl)propane-1,3-diyl)] (40) .....	110
Attempted synthesis of <i>cis</i> -[Pt(II)Cl <sub>2</sub> ( <i>n</i> -propylamine)(tetrazine-amine)] (41).....	111
Attempted synthesis of <i>cis</i> -[Pt(II)(CBDCA)( <i>n</i> -propylamine)(tetrazine-amine)] (42).....	112
<b>X-ray Crystallography</b> .....	113
[Pt(II)(CBDCA)(DAP-N <sub>3</sub> )] (18) .....	113
[Au(III)Cl <sub>3</sub> (PTP)] (27) .....	115
[Au(III)Cl <sub>2</sub> (PTPD)][Au(I)Cl <sub>2</sub> ][OH]{[NaAuCl <sub>4</sub> .2H <sub>2</sub> O]} <sub>n</sub> (29) .....	116
[Pt(II)Cl <sub>2</sub> (PTPDH <sub>2</sub> )] [PtCl <sub>4</sub> ] (31) .....	118
<i>cis</i> -[Pt(II)Cl <sub>2</sub> (DMSO)( <i>n</i> -propylamine)] (34).....	120
[Pt(II)(CBDCA)(DMSO)( <i>n</i> -propylamine)] (37) .....	121
<b>Peptide and peptide conjugate synthesis</b> .....	123
General considerations and materials .....	123
Solid phase synthesis .....	123
Peptide conjugation .....	123
Peptide cleavage .....	124
Peptide purification .....	124
<b><i>In vitro</i> cell culture</b> .....	126
Cell lines.....	126
Cell Culture .....	126
Cell passaging.....	127
Cell Counting .....	128
Cell Freezing .....	129
Cell thawing .....	129
<b>MTS Cell Proliferation Assay</b> .....	130
<i>In vitro</i> cytotoxicity evaluation .....	130
Statistical analysis .....	130
<b>Cellular Fluorescence Imaging</b> .....	131
Fixing of cells to microscope slide.....	131
Coverslip adherence .....	131
Widefield imaging.....	131
<b>DNA binding studies</b> .....	132
Preparation of DNA.....	132

DNA separation using agarose gel electrophoresis .....	132
References .....	133
<b>Chapter 3</b> .....	135
<b>Abstract</b> .....	136
<b>Introduction</b> .....	137
Rationale .....	140
<b>Chapter Aims</b> .....	141
<b>Synthesis of the Pt click template [Pt(CBDCA)(DAP-N<sub>3</sub>)] and corresponding Pt-Fluorophore click conjugate</b> .....	142
2-azidopropane-1,3-diamine dihydrochloride (DAP-N <sub>3</sub> .2HCl) .....	142
[Pt(II)(CBDCA)(DAP-N <sub>3</sub> )] .....	145
X-ray crystal analysis of [Pt(II)(CBDCA)(DAP-N <sub>3</sub> )] .....	145
[Pt(II)Cl <sub>2</sub> (DAP-N <sub>3</sub> )] .....	149
Pt-Flu Conjugation .....	149
<b>Biological analysis of Pt-Flu complex</b> .....	152
<i>In vitro</i> cytotoxicity evaluation .....	152
DNA Binding .....	156
<b>Fluorescent applications and analysis of Pt-Flu</b> .....	159
Fluorescent properties .....	159
Widefield cellular imaging .....	160
<b>Conclusion</b> .....	166
Future work .....	167
References .....	168
<b>Chapter 4</b> .....	171
<b>Abstract</b> .....	172
<b>Introduction</b> .....	173
Rationale .....	177
<b>Chapter Aims</b> .....	178
<b>Synthesis of Pt-peptide conjugates</b> .....	179
Solid phase peptide synthesis (SPPS) .....	179
Synthesis of [Pt(IV)(DACH)(OEt)(OH)(Ox)] .....	185
Pt(IV) peptide conjugation .....	186
Peptide cleavage and purification .....	187
<b><i>In vitro</i> analysis of Pt-peptide conjugates</b> .....	193

<i>In vitro</i> cytotoxicity .....	193
<b>Conclusion</b> .....	199
Future Work .....	200
References .....	201
<b>Chapter 5</b> .....	204
<b>Abstract</b> .....	205
<b>Introduction</b> .....	206
Rationale.....	208
<b>Chapter Aims</b> .....	209
<b>Synthesis of click ligand complexes</b> .....	210
PTP synthesis .....	210
PTPD synthesis.....	211
BOC <sub>2</sub> -PhTPD synthesis.....	212
<b>Synthesis of Metal PTP and PTPD complexes</b> .....	214
<b>Synthesis of Au complexes</b> .....	214
[AuCl <sub>3</sub> (PTP)] synthesis .....	214
X-ray crystal analysis of [Au(III)(PTP)Cl <sub>3</sub> ] (27) .....	215
[AuCl <sub>3</sub> (BOC <sub>2</sub> -PTPD)] synthesis .....	218
Na <sub>0.5</sub> [Au(III)Cl <sub>2</sub> (PTPD)][Au(I)Cl <sub>2</sub> ][Au(III)Cl <sub>4</sub> ] <sub>0.5</sub> synthesis.....	218
X-ray crystal analysis of [Au(III)Cl <sub>2</sub> (PTPD)][Au(I)Cl <sub>2</sub> ][OH]{[NaAuCl <sub>4</sub> .2H <sub>2</sub> O]} <sub>n</sub> .....	219
<b>Synthesis of Pt complexes</b> .....	223
[PtCl <sub>2</sub> (PTP)] synthesis.....	223
[PtCl <sub>2</sub> (PTPDH <sub>2</sub> )][PtCl <sub>4</sub> ] synthesis.....	223
X-ray crystal analysis of [Pt(II)Cl <sub>2</sub> (PTPD)][PtCl <sub>4</sub> ] .....	224
[Pt <sub>3</sub> Cl <sub>4</sub> (PTPD) <sub>2</sub> ]Cl <sub>2</sub> synthesis .....	226
<b>Crystallographic data</b> .....	228
<b>Conclusion</b> .....	230
Future Work .....	230
References .....	231
<b>Chapter 6</b> .....	235
<b>Abstract</b> .....	236
<b>Introduction</b> .....	236
Rationale.....	238

<b>Chapter Aims</b> .....	238
<b>Synthesis of azide cage ligands</b> .....	239
3,3'-((5-azido-1,3-phenylene)bis(ethyne-2,1-diyl))dipyridine (CageL-N <sub>3</sub> ) synthesis.....	239
Click reactions of CageL-N <sub>3</sub> .....	240
Fluorescent properties and analysis of Cage-T-MAMP .....	242
<b>Synthesis of Pt steroid complexes</b> .....	244
Pt-Steroid complexes.....	244
DAP-Estradiol synthesis.....	245
Platinum DAP-estradiol synthesis.....	247
DAP-Testosterone synthesis.....	248
Platinum DAP-testosterone attempted synthesis.....	250
<b>Synthesis of Pt DMSO <i>n</i>-propylamine complexes</b> .....	251
<i>cis</i> -[Pt(II)Cl <sub>2</sub> (DMSO) <sub>2</sub> ] synthesis.....	252
<i>cis</i> -[Pt(II)Cl <sub>2</sub> (DMSO)( <i>n</i> -pa)] synthesis .....	252
[Pt(II)(CBDCA)(DMSO) <sub>2</sub> ] synthesis .....	254
[Pt(II)(CBDCA)(DMSO)( <i>n</i> -pa)] synthesis.....	254
<b>Attempted synthesis of Pt-tetrazine</b> .....	258
<b>Conclusion and Future Work</b> .....	259
References .....	260
<b>Thesis Conclusion</b> .....	262
<b>Appendix</b> .....	265
Organic syntheses.....	266
Inorganic syntheses .....	294
Peptides .....	337
<i>In vitro</i> cytotoxicity data - Cell proliferation curves .....	344

## Declaration

I declare that this thesis, which I submit to RCSI for examination in consideration of the award of a higher degree Doctor of Philosophy is my own personal effort. Where any content present is the result of input or data from a related collaborative research programme this is duly acknowledged in the text such that it is possible to ascertain how much of the work is my own. I have not already obtained a degree in RCSI or elsewhere on the basis of this work. Furthermore, I took reasonable care to ensure that the work is original, and, to the best of my knowledge, does not breach copyright law, and has not been taken from other sources except where such work has been cited and acknowledged within the text.

This thesis represents a multidisciplinary project that comprises organic and inorganic synthesis, peptide chemistry, fluorescent imaging and cellular biology, all of which has been undertaken by the author except where otherwise stated.

Signed \_\_\_\_\_

Student Number \_\_\_\_\_

Date \_\_\_\_\_

## Publications

Kitteringham, E.; Wu, D.; Cheung, S.; Twamley, B.; O'Shea, D. F.; Griffith, D. M. Development of a novel carboplatin like cytoplasmic trackable near infrared fluorophore conjugate via strain-promoted azide alkyne cycloaddition. *Journal of Inorganic Biochemistry* **2018**, 182, 150-157.

Kitteringham, E.; Zhou, Z.; Twamley, B.; Griffith, D. M. Au(III) and Pt(II) complexes of a novel and versatile 1,4-disubstituted 1,2,3-triazole-based ligand possessing diverse secondary and tertiary coordinating groups. *Inorganic Chemistry*, **2018**, 57 (19), 12282-12290.

## Acknowledgements

Here it is, the eagerly awaited acknowledgments page. After 4 years of research in RCSI my full time student life is over at last, culminating in a PhD. It's fair and true to say that a PhD is very much a solitary undertaking, but it is not something you make it through alone. Anyone who knows me knows I don't normally like speaking out, but when I do I ramble and won't shut up! So, on these few pages I want to express my sincerest thanks, gratitude and love to everyone who helped me through it and have made it all possible.

Firstly I would like to thank my supervisor Dr. Darren Griffith. You have been a beacon of support and advice for me for the past 4 years. Without you constant encouragement, suggestions and the occasional bit of pressure this PhD would not have been possible. It's been a pleasure to work with you and a look forward to seeing the group grow and where its scientific ventures lead it with you steadfast at the reins.

To the Dazzlers' Bedazzlers: Aoife, Aisling and Donal, thank you all. You've all been a core support throughout these past 4 years, both within the lab and outside of it. Donal, we began at the same time allowing us to grow and motivate each other throughout our PhDs. The flat white "dates" helped too. Aoife, being the senior and leading lady of the group you kept me in line and passed on the vital chemistry tricks (and essential RCSI gossip) you can only gain by diving in first. And Aisling, as the newest group member you have kept me inspired and hopeful as I recall how I started out and provided the "next generation" PhD support for the Griffith Group. Sure we're great craic!

A big hand has to go to the Tea-Team: Emmet, Graeme, Suzanne, Aoife, Donal, Aisling Harrison, Siobhán, Alan, Hugh, Eanna, Tadhg, Will, Mike, Scott, Shona, Ruairí, James and Robbie. I will forever cherish my Tea-Cert. and the opportunity to mess and de-stress at teatime and lunch. I will miss the baked-goods on "Cake-Friday" and the post work drinks on "Pints-Friday" in The Swan. Your friendships have been invaluable.

Further thanks to Emmet for his leading role with the technical staff for keeping the lab in tip-top shape and providing support when anything broke down or needed replacing; along with thanks Graeme and Suzie for the additional lab technical support.

To the many other friends in the lab who I've met and learnt from over the past 4 years: Harrison, Dario, Daniele, Sandra, Caterina, Rosy, Roberta, Deborah, Ilaria, Elena, Vivi, Francesco, Grazia, Claudio, Martina, Federica, Claudia, Reece, Ziga, Tadhg, Haris, Ian and Shane. I'd especially like to thank Dan Wu for his collaborations and teaching me so



much right from day 1 when I was sharing space on a hot plate in your fumehood. I would also like to thank the rest of the Chemistry Department staff including: Yuan, Prof. Celine Marmion and Prof. Mauro Adamo. I would especially like to thank Dr. James Barlow and Prof. Pablo Sanz Miguel for agreeing to act as my internal and external examiners and the commitment needed to fulfil this duty.

In addition special thanks must go to my collaborators in RCSI: Prof. Donal O'Shea, Dr. Dan Wu, Prof. Marc Devocelle and Ms. Siobhán O'Flaherty and externally: Dr. Diego Montagner, and Prof. Angela Casini. Multi-disciplinary ventures are what science is all about and I've had a great experience working with you. I must also acknowledge RCSI for funding me through the Apjohn PhD Scholarship, making this all possible. I would also like to acknowledge Prof. Fiona Regan and especially Dr. James Chapman for giving me the opportunity to conduct research with you in MESTECH during my 2<sup>nd</sup> year summer in DCU. It gave me the taste for research and desire to pursue a PhD.

To the numerous students that have passed through my supervision in the lab I would like to especially thank Zehao "John" Zhou and I wish him the best in his own PhD in the USA. Conn, Jay and Nils, you have all shown me the pleasure that can come from teaching and passing on knowledge to an eager mind.

The thesis would not have been possible without the various analysts and support staff who assisted with my work. Dr. Brendan Twamley, Dr. John O'Brien and Dr. Gary Hessman from TCD, Dr. Jimmy Muldoon and Ms. Ann Connolly from UCD and Dr. Diego Montagner from MU without whom my spectral data would not have been! I would also like to thank Johnny, Mary, Shane and Seamus for their support and direction during my time with the MCT Department in addition to Dr. Brona Murphy of the Physiology Department for facilitating my cellular work and bio studies.

To the Shifts lads: Rob, Colm, Eoin and Dave. Our long standing school-boy friendship has been essential and the continuing sessions, travels and craic have kept me somewhat sane/insane throughout my PhD and I look forward to much more of it. To Colm and Rob especially, 22 years after meeting you on our first day of junior infants I couldn't think of 2 better people or friends to have frequently spent time with and am glad for the opportunity to have spent 2 years living and travelling with you guys. And next of course my main girlos: Katie and Cat. The chats in the Cullenswood sitting room were an endless source of entertainment, particularly as we slagged your significant others.

To my oldest friends Declan and Cian. It's important to know it is possible to have friends for life and even better to know it's true. Our long friendship which has grown from Downside Heights has been important throughout my PhD, where we have given each other the opportunity to not get tied down with work or show judgement. As part of the group Keith, for his shared humour and PhD experience, you have been a continual source of support, along with Gloria and Sarah. As a group you have all been valued friends and I look forward to many more games nights, PhD guilt free.

To my various kayaking crews in Skerries and DCU, particularly Kev and Roo, I am grateful for all the de-stressing whitewater, surf, freestyle and sea sessions we've had and am looking forward to having more time during the wet season this year.

To my family: my parents Emer and George and my sisters Aisling and Muireann. Thank you for the constant support and love throughout my pursuit of chemistry. Although none of you have a scientific background you had every confidence and supported me throughout, even if you didn't quite understand what it was I was actually doing! I may not always show it on my face but I do care. Thank you. My granny Eileen, from my earliest memories in Cork right up until now, you have always shown absolute faith in me, your grandson. I would like to thank you and Paddy for the lifetime of love you have shown me and giving me motivation to make you proud.

Last, but certainly not least, I must thank Sinéad. I met you at a certain annual RCSI social gathering at Christmas of my 2<sup>nd</sup> year and in true RCSI fashion things snowballed from there. You've shown me so much of what is out there in the world and together we've experienced a great deal more than I could have alone. During times of stress and uncertainty you have made me see that things happen for a reason and that it's ok to not get caught up in it. You were a critical source of support, confidence and love that I needed when I did not believe in myself. Words cannot fully reflect my feelings; it has meant everything to me.

Onwards and upwards! Eolann >

## Dedication

ES for a lifetime of love.

AMC for the invaluable support.

SC for having faith in me.

*ō F q p ø v " d g n k g x g " k p " { q w t u g n h 0*  
*Believe in me!*

*Believe in the me that believes in you ö*

## Abstract

Click Chemistry represents an exciting and important branch of synthetic chemistry with vast potential. Due to its versatility it is frequently used to modify and functionalise drugs, sensors and macromolecules for example, facilitating important advancements in many scientific fields. Furthermore, given its ability to generate unique compounds with relative simplicity, it is now at the forefront of modern chemical synthesis. This thesis explores how click chemistry conjugation strategies can be developed to functionalise Pt based drugs.

Cancer is one of the leading health issues worldwide, with 1 in 6 deaths being cancer related. Pt based drugs are used in 50% of all chemotherapy regimens. Despite the many successes of Pt drugs, the negative side effects associated with treatment often limit their effectiveness. In addition, many cancers become resistant to Pt based therapy over time. This thesis explores how click chemistry can play a role in enhancing the activity of Pt-based drugs and tracking Pt-based drugs through functionalisation.

Chapter 1 primarily provides an introduction to cancer, the medicinal chemistry of Pt-based drugs and click chemistry. A summary of research undertaken to date in relation to conjugation of Pt centres to secondary molecules is also provided.

Chapter 2 outlines the methods used to synthesise a number of novel organic compounds and ligands, as well as inorganic complexes. Peptide synthetic methods are also described, in addition to biological, *in vitro* and fluorescent imaging techniques and methods used.

Chapter 3 describes the development of a novel biocompatible Pt-fluorophore click complex and how the conjugation of a NIR fluorescent probe to a Pt drug may further our understanding of Pt cellular uptake and distribution. A Cu-free technique (SPAAC) was employed; the first of its kind, where the azide handle resides on the stable ammine carrier ligand. The *in vitro* cytotoxicity, DNA binding properties and widefield microscopy cellular imaging of the novel Pt-fluorophore complex were investigated.

The selective targeting of cancer cells over healthy cells is of prime interest in chemotherapeutic research, as the non-selective nature of Pt drugs is one of the biggest drawbacks associated with their use clinically. In addition, resistance to current Pt chemotherapy regimens is of major concern. Chapter 4 explores how peptides may be used to selectively target cancer and improve the potency of Pt drugs. The development of a novel Pt(IV)-peptide conjugate and its *in vitro* cytotoxicity is described.

Chapters 5 and 6 focus on synthesis of novel ligand scaffolds synthesised through click chemistry strategies with an emphasis on generating dual functional metal based drug complexes.

In chapter 5, the synthesis of a novel 1,4-disubstituted 1,2,3-triazole based multidentate ligand is described. Reaction of this ligand with Pt(II) and Au(III) precursors afforded novel complexes, the structures of three of which were characterised by X-ray crystallography, featuring interesting coordination modes. 1,4-disubstituted 1,2,3-triazole based multidentate ligands are demonstrated to be ideal platforms for the generation of multinuclear and mixed metal complexes.

Finally, chapter 6 features three independent subsections, which build on outputs from chapters 3 and 5 and describes the development of (i) click capable cage ligands, (ii) Pt-steroid complexes for enhanced cancer targeting and (iii) iEDDA capable Pt-tetrazine complexes.

## Symbols and Abbreviations

Å – Ångström	DAPI – 4',6-diamidino-2-phenylindole
aa – Amino acids	DCM – Dichloromethane
ABD – ATPase binding domain	DIBO – Dibenzocyclooctyne
ABIDO – Azadibenzocyclooctyne	DIC – <i>N,N</i> -Diisopropylcarbodiimide
ADP – Adenosine diphosphate	DPDP – Dipyridoxaldiphosphate
a.m.u – Atomic mass units	DPQ – Dipyrido[3,2- <i>f</i> :2',3'-
ATP – Adenosine triphosphate	<i>h</i> ]quinoxaline
Au – Gold	DPPN – Benzo[I]dipyrido[3,2- <i>α</i> :2',3'-
AR – Androgen receptors	<i>c</i> ]phenazine
Ar – Aryl/aromatic	DPPZ – Dipyrido[3,2- <i>α</i> :2',3'-
ATP – Adenosine triphosphate	<i>c</i> ]phenazine
BARAC – Biarylazacyclooctynone	DMF – <i>N,N</i> -dimethylformamide
b – Broad	DMSO – Dimethyl sulfoxide
BCN – bicyclo[6.1.0]nonyne	DNA – Deoxyribonucleic acid
bipy – 2,2'-bipyridine	DTPA –
BOC – <i>tert</i> -Butyloxycarbonyl	Diethylenetriaminepentaacetate
BOC <sub>2</sub> O – Di- <i>tert</i> -butyl dicarbonate	DR – Death receptors
BODIPY – Boron-fluorescent	<i>E. coli</i> – <i>Escherichia coli</i>
dipyrromethene	EA – Elemental analysis
btz – Di-(benzyl-triazole)	EDG – Electron donating groups
CBDCA – Cyclobutane dicarboxylato	EDTA – Ethylenediaminetetraacetic
CBDCAH <sub>2</sub> – Cyclobutane	acid
dicarboxylic acid	ER – Estrogen receptor
CDI – <i>N,N'</i> -carbonyldiimidazole	ESI – Electrospray ionization
CPP – Cell penetrating peptides	EtBr – Ethidium bromide
CRC – Colorectal cancer	FBS - Fetal bovine serum
CRT1 – Cu(I) transporter	Fmoc – Fluorenylmethyloxycarbonyl
CuAAC – Cu-promoted alkyne-azide	chloride
cycloaddition	FT – Fourier-transform
d - Doublet	g - grams
DACH – Diaminocyclohexane	GSH – Glutathione
DAP – 1,3-Diaminopropan-2-ol	GST – Glutathione <i>S</i> -transferase

h – Hour(s)	mM – Millimolar
HDAC – Histone deacetylase	mmol – Millimole
HIV – Human immunodeficiency virus	MS – Mass Spectrometry
HSAB – Hard soft Lewis acids and bases	MTS – 3-(4,5-dimethylthiazol-2-yl)-5-(3-carboxymethoxyphenyl)-2-(4-sulfophenyl)-2H-tetrazolium
HPLC – High performance liquid chromatography	MTT – 3-(4,5-dimethylthiazol-2-yl)-2,5-diphenyltetrazolium bromide
HSP – Heat shock protein	m/z – Mass to charge ratio
Hz – Hertz	<i>n</i> -pa – <i>n</i> -propylamine
I.D – Internal diameter	NaOX – Sodium oxalate
ICP – Inductively coupled plasma	NGR – Asparagine-glycine-arginine
iEDDA – Inverse electron demand Diels-Alder	NIR – Near infrared
IR – Infra-red	NIR-AZA – BF <sub>2</sub> -azadipyrromethenes
<i>J</i> – Coupling constants	NER – Nucleotide excision repair
K – Kelvin	NHS – <i>N</i> -Hydroxysuccinimide
kDa – Kilodaltons	nm – Nanometre
KLA – Acetyl-(KLAKLAK) <sub>2</sub> -NH <sub>2</sub>	NMP – <i>N</i> -methyl pyrrolidone
LMWP – Low molecular weight protamine	NMR – Nuclear magnetic resonance
M – Molar	OC – Open-circular
m – Multiplet	PA – Proton affinities
memHSP70 – Membrane bound HSP70	PBS – Phosphate-buffered saline
MRI – magnetic resonance imaging	pKa – Proton dissociation constant
MRSA – Methicillin-Resistant <i>Staphylococcus aureus</i>	ppm – parts per million
MAMP – mono-alkyne mono-phenol	Pt – Platinum
MBHA –Methylbenzhydramine	PI – Propidium iodide
mg – Milligram	POA – (2-propynyl)octanoic acid
min – Minute(s)	Py – Pyridyl
mL – Millilitre	q – Quartet
mm – Millimetres	RAFT – Regioselectively addressable functionalized template
	RGD – Arginine-glycine-aspartic acid
	ROS – Reactive oxygen species
	RNA – Ribonucleic acid

RP – Reverse phase	UV – Ultra-violet
rt – Room temperature	$\lambda_{\text{max}}$ abs – Max absorption wavelength
s – Singlet	$\lambda_{\text{max}}$ em – Max emission wavelength
SAHA – Suberoylanilide hydroxamic acid	3D – Three dimensional
SBD – Substrate binding domain	4D – Four dimensional
SC – Super coiled	°C – Degrees Celsius
ScP –Scrambled peptide	° – Degree
SDS – Sodium dodecyl sulphate	$\Phi$ – Quantum yield
SEM – Standard error mean	
SHRs – Steroid hormone receptors	
SPAAC – Strain-promoted alkyne-azide cycloaddition	
SPECT – Single-photon emission computed tomography	
SPPS – Solid phase peptide synthesis	
succ – Succinic Acid	
t – Triplet	
<i>t</i> Bu – <i>tert</i> -butyl	
TAE – Tris acetate-EDTA	
TAT – Trans-acting activator of transcription	
TBTA – <i>Tris</i> -(benzyltriazolylmethyl)amine	
TCO – <i>Trans</i> -cyclooctene	
TEA – Triethylamine	
terpy – 2,2':6',2''-terpyridine	
THF – Tetrahydrofuran	
TLC – Thin layer chromatography	
TPP – Tumour penetrating peptide	
tR – Retention time	
Trz - Triazole	
$\mu\text{m}$ – Micrometre	
$\mu\text{M}$ – Micro Molar	



# **Chapter 1**

## **Introduction**

## **Cancer**

Cancer is one of the most well-known and imposing diseases in today's society. As cancer is more prominent at an older age, its occurrence has increased substantially over the last century in developed nations, due to the general improvement in healthcare, which has resulted in an increased lifespan.<sup>1-4</sup> Furthermore, cancer is considered a "lifestyle disease" because choices in relation to diet, fitness, alcohol and tobacco use have all been shown to have a major influence on the development of the disease.<sup>2</sup> There are many forms of the disease, each named for the organ, tissue or cell type affected,<sup>5-6</sup> and although the survival rate has grown as a result of early detection and treatment through raised awareness,<sup>7</sup> it is the second most common cause of death in Ireland,<sup>8</sup> while globally it is the second biggest killer, with 1 in 6 of all deaths arising from some form of the disease.<sup>2</sup>

Within Ireland, the most prominent cancers are prostate, breast, colorectal, lung and skin melanomas. Although prostate and breast cancers make up 30% of all cancers in each gender, lung and colorectal are amongst the most problematic due to their higher occurrence and poor survival rates, with lung and colorectal cancers accounting for 21.1% and 11.8% of all invasive cancer related deaths, respectively.<sup>1</sup>

### **Colorectal Cancer**

Colorectal cancer (CRC) is the most reported form of the disease in Ireland, regardless of gender, and is the 2<sup>nd</sup> leading cause of cancer death.<sup>1, 5</sup> As with lung cancer, CRC is associated with a high mortality rate. The occurrence of CRC is higher in males than in females, with male mortality also being higher, probably due to the differences in lifestyle, dietary habits and the lower likelihood of men to seek medical consultation when faced with a health concern.<sup>1</sup> The 5 year survival rates have steadily improved<sup>1</sup> due to better early diagnosis and early treatment.<sup>9</sup> The development of platinum (Pt) drug resistance in CRC<sup>10</sup> and the negative side effects associated with current treatments have led to the research for alternative and more selective chemotherapies.<sup>11</sup>

### **Ovarian Cancer**

For females in Ireland, ovarian cancer is the 4<sup>th</sup> leading cause of cancer related mortality, accounting for 6.7% of all deaths. Although it only makes up 4% of all

invasive cancers, poor long term survival makes it one of the most deadly forms of cancer.<sup>1</sup> Furthermore, the survival rate over the past 20 years has not improved. Although it has a high (60-80%) response to treatment initially, recurrence and subsequent development of Pt drug resistance is common in 90% of metastatic cases. This leads to a 5 year net survival rate of 30%, making ovarian one of the most recurring forms of cancer.<sup>1, 12-14</sup>

## **Treatments**

There are a number of treatments available for cancers, which vary based on the type of cancer, the stage of cancer and how invasive the cancer in question may be. The three most common treatments may encompass one or all of the following: surgery to remove the tumorous growth, radiotherapy and drug therapy (chemotherapy).<sup>1, 7</sup>

Surgery is the most common treatment method but the extent of surgery may vary greatly based on the size and position of the tumour.<sup>1, 7, 15</sup> In many cases, this is very successful, particularly in instances where the cancer is localised within a single region. However, later stage cancers which are typically more aggressive, require more complicated and invasive surgical techniques and often potent chemotherapeutic regimens to eliminate aberrant cells at metastatic sites and to avert recurrence.<sup>7, 16-17</sup>

Radiotherapy is used to shrink tumour size by irradiating cells with X-rays, which induces DNA (deoxyribonucleic acid) damage, which in turn leads to programmed cell death and clearance of the tumour mass. Radiotherapy can be very effective, however its use can be limited by tumour location and proximity to healthy tissues and organs, in addition to the tumours size. In most instances, it is used in conjunction with another treatment or therapy.<sup>7, 18</sup> Surgery is often performed in conjunction with radiotherapy to remove larger dead tumour masses or to prevent recurrence through post-surgical radiation therapy.<sup>19-21</sup>

Hormone therapy is most commonly used in the treatment of prostate and breast cancers due to the specific demand and high level of receptors these organs have for hormonal steroids.<sup>5, 22-24</sup> In the case of prostate cancer, androgen receptors (AR) are upregulated and have an 80-90% dependency on them.<sup>25</sup> Androgen deprivation therapy is used to prevent the release of testosterone which is required for prostate cancer growth. The therapy results in tumour shrinkage.<sup>22</sup> For breast cancer, a test is

first carried out to determine whether the breast cancer is estrogen receptor (ER) positive or negative, ER(+) or ER(-).<sup>5</sup> Approximately 80% of breast cancers are estrogen sensitive<sup>26-27</sup> and may be treated with hormone therapy in a similar manner to prostate cancer.

Chemotherapy is broadly described as any treatment regime which uses a drug or chemical compound to elucidate an anticancer effect. There are a large number of drugs which perform this role, and a broad variety of combinations employed which are administered depending on type of cancer, stage of cancer and side effects.

For example, the triple therapy known as FOLFOX employs a three drug strategy made up of 5-Fluorouracil (which interferes with the DNA replication pathway), Leucovorin (which enhances the effects of 5-Fluorouracil) and oxaliplatin (by inducing ribosomal biogenesis stress<sup>28</sup>).<sup>29</sup> This chemotherapeutic cocktail is used to treat late stage CRC. The primary focus of this thesis will be on Pt-based anticancer chemotherapeutic drugs, as outlined below.

## Metals in medicine

Metals have a long history as key ingredients in many traditional natural remedies.<sup>30-31</sup> Today, metal based drugs are routinely used in the clinic as diagnostic agents and as therapeutics, with cisplatin, the platinum-based anticancer drug, well-known as the ‘poster boy’ of medicinal inorganic chemistry.<sup>11,32</sup>

### Platinum (Pt) Chemistry

Platinum (Pt) is a group 10 transition metal with an atomic number of 78, atomic mass of 195.08 a.m.u. (atomic mass units) and an electronic configuration of [Xe]4f<sup>14</sup>5d<sup>9</sup>6s<sup>1</sup>. It is most frequently found in the Pt(II) and Pt(IV) oxidation states, but may also form bimetallic complexes as Pt(I) and Pt(III), though this is uncommon. Pt is classified as a rare “soft” acid metal according to the HSAB (hard soft Lewis acids and bases) theory, and therefore binds strongly with soft ligand base donors such as nitrogen and sulphur.

Pt(II) forms square planar geometries with an 18 electron d<sup>8</sup> metal centre. The d<sub>xz</sub>, d<sub>yz</sub>, d<sub>z</sub><sup>2</sup> and d<sub>xy</sub> orbitals are occupied by electron pairs in a low spin state, leaving only

the highest energy  $d_{x^2-y^2}$  unoccupied (**Figure 1.1**). Pt(IV) forms more kinetically inert complexes which are thermally stable, with an octahedral geometry and with an 18 electron  $d^6$  metal centre. The complexes are low spin with the three  $t_{2g}$  orbitals ( $d_{xz}$ ,  $d_{yz}$ ,  $d_{xy}$ ) full, whilst leaving the two high energy  $e_g$  ( $d_{x^2-y^2}$ ,  $d_{z^2}$ ) orbitals unoccupied (**Figure 1.1**).

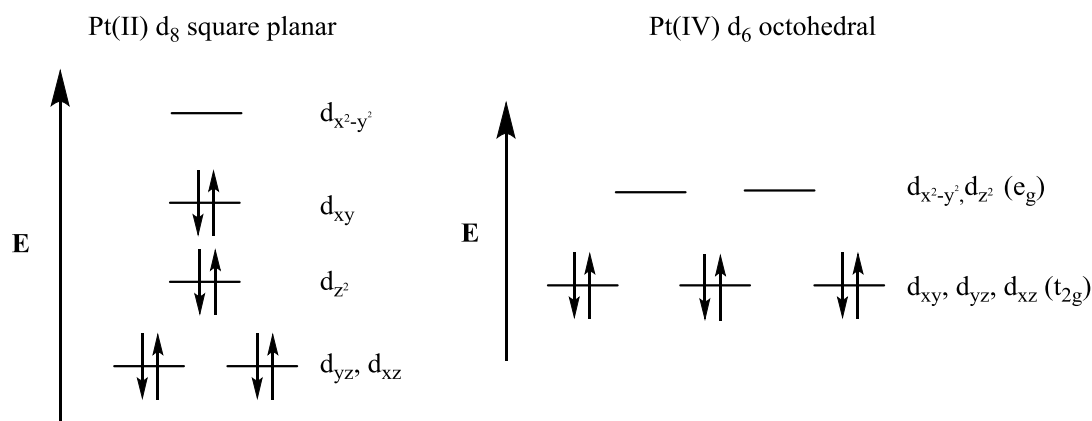
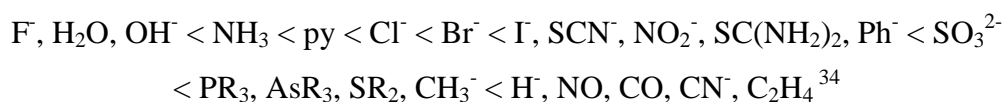


**Figure 1.1:** d-orbital level diagram for Pt(II) and Pt(IV) metal ions in a square planar and octahedral ligand field respectively.

Pt(II) and Pt(IV) follow the standard affinity for soft ligands as previously outlined by HSAB theory,<sup>33</sup> and Pt(II) reactions are influenced by the *trans* effect.<sup>34</sup>

The *trans* effect is the labilisation of ligands that are *trans* to other ligands and is used to primarily explain substitution patterns in Pt(II) chemistry. For example, it helps predict the likelihood of incoming ligands to coordinate in a *trans* conformation more rapidly than in a *cis* position with respect to ligand with a strong *trans* effect (such as many soft ligands).<sup>35</sup> The trend below shows the increasing intensity of the *trans* effect for a number of ligands:



Two main factors contribute to the magnitude of the *trans* effect; (i) the polarizability and (ii) the  $\pi$ -back-bonding ability of ligands, both of which weaken the Pt(II)-ligand bond. With respect to (i), the primary charge of Pt(II) induces a dipole with its ligands which can lengthen and weaken the bonds and (ii) where a strong  $\pi$ -back-bonding will weaken the *trans* ligand.<sup>34, 36</sup>

The *trans* effect is famously harnessed for the synthesis of cisplatin, which is synthesised by reacting  $[\text{PtCl}_4]^{2-}$  with ammonia.<sup>36</sup>

### Gold (Au) Chemistry

Gold (Au) is a group 11 transition metal with an atomic number of 78, atomic mass of 196.97 a.m.u. and an electronic configuration of  $[\text{Xe}]4f^{14}5d^{10}6s^1$ . It is most frequently found in the +1 and +3 oxidation states, but oxidation states ranging from -1 to +5 are also known.<sup>37</sup> Most Au drugs are associated with the +1 oxidation state such as Auranofin.<sup>37</sup>

Au, like Pt, is classified as a “soft” metal according to the HSAB theory and as such clinically used Au(I) complexes are bound by soft ligands, such as those containing thiols (sulphur) bonds and phosphines.<sup>37</sup>

Au(I) is an 18 electron  $d^{10}$  metal centre, with all d orbitals fully occupied (**Figure 1.2**) and forms linear complexes.

Au(III) complexes possess square planar geometries with an 18 electron  $d^8$  metal centre. The  $d_{xz}$ ,  $d_{yz}$ ,  $d_z^2$  and  $d_{xy}$  orbitals are occupied by paired electrons in a low spin state leaving the highest energy  $d_{x^2-y^2}$  unoccupied.

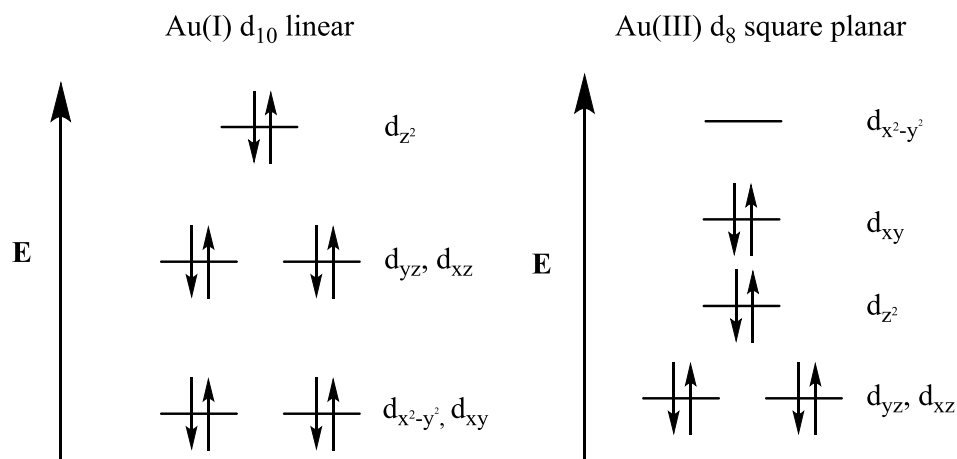


**Figure 1.2:** d-orbital level diagram for Au(I) and Au(III) metal ions in a linear and square planar ligand field respectively.

### Cisplatin –1<sup>st</sup> generation

*Cis*-diamminedichloroplatinum(II) (cisplatin) was the first Pt based anticancer drug brought to market, and the first used to target solid tumours. Although first synthesised in the early 1800s, in the 1960s Barnette Rosenberg serendipitously discovered that cisplatin had an anti-proliferative effect on *Escherichia coli* (*E.*

*coli*).<sup>38</sup> Cisplatin was approved by the FDA as an anticancer agent in 1978 and is now used clinically in a high proportion of chemotherapeutic regimens. Cisplatin's success certainly kick-started a surge of interest in metal based medicinal chemical research.

Structurally, cisplatin and other Pt(II) drug complexes follow the model outlined in **Figure 1.3**, where a Pt(II) metal centre is coordinated to *cis* am(m)ine and *cis* anionic ligands.

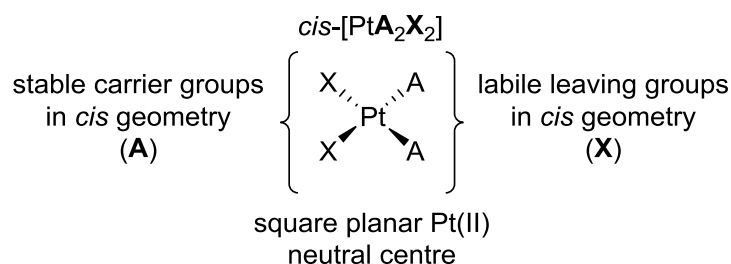
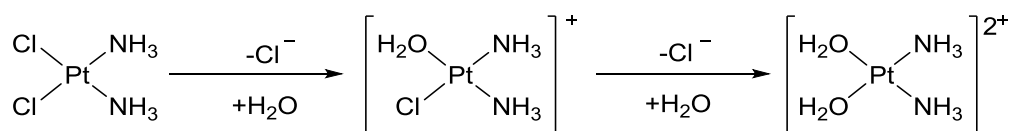


**Figure 1.3:** The “classical” *cis*-PtA<sub>2</sub>X<sub>2</sub> framework constitutes a Pt(II) metal centre coordinated to a stable carrier am(m)ine ligand (A) and a labile (di)anionic leaving group (X).

The am(m)ine groups are commonly referred to as carrier ligands as they remain bound to Pt following administration and intracellular transformation. The anionic labile ligands are known as leaving groups and become displaced following cellular uptake (**Figure 1.3**).

Cisplatin is injected intravenously and enters the cell by a combination of passive diffusion and active transport<sup>39</sup> (**Scheme 1.1**) *via* the Cu(I) transporter CRT1. Notably, genetic knockdown of CRT1 enhances Pt resistance both *in vitro* and *in vivo*.<sup>40-41</sup>

Following uptake, cisplatin must undergo a number of chemical interactions within the cell in order for DNA binding to occur. Upon entering the cell, cisplatin undergoes hydrolysis due to low chloride concentrations (4-10 mM) prompting the exchange of one or both chlorido ligands with H<sub>2</sub>O, forming an aquated Pt species (**Scheme 1.1**). This species is highly electrophilic and able to react with various cellular nucleophilic sites.



**Scheme 1.1:** Schematic representation of cisplatin hydrolysis in a cellular environment.

Cisplatin's primary mode of action against cancer cells is widely considered to be the formation of irreparable Pt-DNA adducts by binding to the N7 position of DNA bases, most notably with the purine base guanine and to a lesser extent adenine. The labile ligand(s) are substituted to form Pt-DNA crosslinks, which cause DNA damage and prevent DNA replication.<sup>42-45</sup>

The most prominent Pt-DNA adducts formed are intrastrand crosslinks, where Pt binds with two adjacent base pairs on the same DNA strand, namely as GpG 1,2-intrastrand and ApG 1,2-intrastrand crosslinks. GpXpG 1,3-intrastrand crosslinks occur less frequently, where Pt binds to two guanine bases separated by a single base (Figure 1.4). Interstrand crosslinking also occurs, with Pt binding to bases on opposite DNA strands.<sup>46</sup>

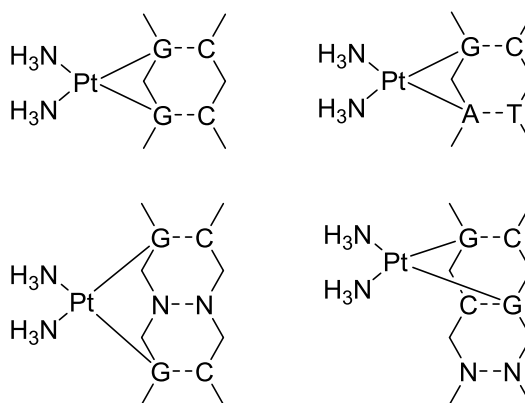


**Figure 1.4:** Structures of various DNA adducts formed with Pt; GpG 1,2-intrastrand, ApG 1,2-intrastrand, GpXpG 1,3-intrastrand, GpG 1,2-interstrand crosslinking.

GpG 1,2-intrastrand lesions are most associated with Pt cytotoxicity, as they severely disrupt the structure of DNA, by causing a bend towards the major groove, triggering a loss in helix stability.<sup>47</sup>

In addition, the presence of Pt further prevents DNA repair protein function, such as those associated with the nucleotide excision repair (NER) pathway. NER is a complex process involving more than twenty proteins. If DNA damage is beyond



repair DNA replication fails, the cell cannot replicate, thus committing the cell to apoptosis or programmed cell death.<sup>45, 48</sup>

Despite these widely observed and accepted claims, there is evidence that only low levels of administered Pt undergo nuclear DNA binding. In addition, given that there is still a high Pt drug cytotoxic response of certain cancer cells which have enhanced DNA repair mechanisms, it suggests that cytotoxicity may arise through other cellular means.<sup>49</sup> Cisplatin for example has also been linked with redox, endoplasmic reticulum stress and mitochondrial DNA damage.<sup>50</sup>

### Side effects and Pt resistance

With many types of cancer, there is no standard or single treatment method, even among cancers of the same tissue type.<sup>1, 51</sup> In order to treat cancer, a combination therapeutic regimen is often employed to give patients the highest chance of survival.<sup>1</sup> A major concern associated with clinically used drugs is their cytotoxicity to healthy cells, as many are non-selective to cancerous tissues, which greatly reduces quality of life.<sup>52</sup>

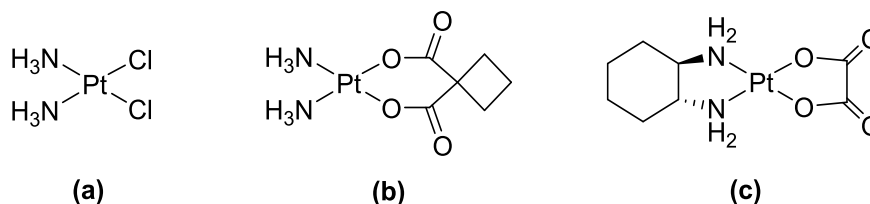


**Figure 1.5:** The chemical structures of the Pt drugs cisplatin, (b) carboplatin and (c) oxaliplatin.

Side effects associated with the clinically used Pt based anticancer drugs, cisplatin, carboplatin and oxaliplatin (**Figure 1.5**) has been severe enough that patients remove themselves from chemotherapy.<sup>53</sup> Some side effects include nausea and vomiting, organ damage, neurotoxicity and nephrotoxicity.<sup>52</sup>

As previously stated, many cancers are intrinsically resistant to available therapies or acquire resistance over time due to a variety of cellular defence mechanisms.<sup>1, 51</sup> Cancerous cells have been shown to undergo multiple gene mutations which can lead to a decrease in Pt complex intracellular uptake, an increase in cellular efflux of Pt drugs and increased repair of DNA damage for example.<sup>45, 52, 54</sup> Therefore many

treatments, though initially effective in reducing tumour size, fail over the longer term due to acquired resistance.<sup>55-56</sup>

There are four predominant categories which resistance may fall under which include: pre-target resistance, on-target resistance, post-target resistance and off-target resistance.<sup>56</sup>

The predominant mechanisms of pre-target resistance are decreased drug uptake and increased drug sequestration. As previously mentioned, the Cu(I) transport protein CRT1 is pivotal in cisplatin uptake, and genetic knockdown of CRT1 enhances Pt resistance.<sup>40-41</sup> Sequestering of Pt drugs naturally depletes the quantity of the active drug molecule. The cellular detoxification enzyme glutathione *S*-transferase (GST) and its substrate glutathione (GSH) contribute greatly to Pt resistance. The sulphur containing GSH acts as a scavenger and detoxifies Pt by forming an inert complex with Pt (Pt-GSH) which is unreactive.<sup>45, 57</sup> This reaction may occur with or without GST as a catalyst.<sup>45, 58</sup> GSH also aids in the detoxification process using transporter proteins which mediate Pt elimination through efflux of Pt-GSH type conjugates.<sup>45, 59</sup> Knockdown expression of GST in ovarian cancer has been shown to increase Pt sensitivity,<sup>60</sup> and using Pt complexes containing GSH inhibitors, such as ethacraplatin (**Figure 1.6**) can overcome Pt resistance.<sup>61-62</sup>

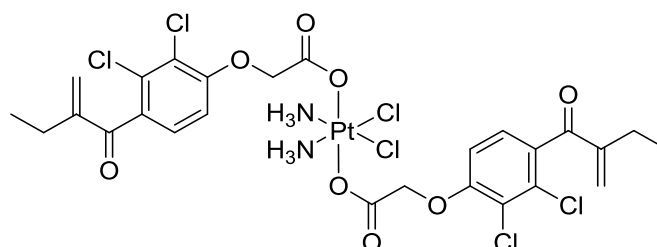


**Figure 1.6:** Ethacraplatin. A Pt(IV) drug which contains two molecules of the GSH inhibitor ethacrynic acid in the axial positions.

On-target resistance is associated with any mechanism which directly alters Pt-DNA binding and associated damage. The prominent mechanism of resistance to Pt drugs is through the enhanced expression and thus increased levels of the proteins of the NER<sup>48</sup> process, which improve the rate of DNA repair and increases Pt tolerance as a direct result.<sup>63-64</sup>

Post-target resistance relates to the alterations to processes which take place subsequent to Pt-DNA binding. When DNA adducts are beyond repair or cannot be effectively repaired, apoptosis is triggered through a lethal signalling cascade.

However, disruption to any of the associated proteins in this process can prevent cell death from occurring. A well-recognised example of post-target resistance involves the tumour suppressor protein p53. Cellular and protein mutations can lead to the loss of p53 function.<sup>65</sup> Irregular p53 function is common in cancer, with 50% of human cancers showing some form of mutation to the *TP53* gene.<sup>66-67</sup>

The final class of resistance is off-target resistance, where a process enhances cellular survival without being directly related to the cellular response to Pt drugs. For example, colorectal cancers are known to have increased levels of heat-shock proteins (HSP), which stabilise cellular proteins during a stress stimulus, such as Pt drug therapy.<sup>68</sup> The protective role HSPs fulfil in cancer cells prevents the initiation and activation of apoptosis, making it a biomolecule of interest if studying Pt drug resistance.

For the aforementioned reasons, overcoming resistance is a major objective in Pt drug research. The common approach currently employed in novel Pt drug development is the synthesis of dual or multifunctional Pt drugs. This will be the main focus of this thesis.

Multi target therapy is one of the tactics used in chemotherapy where a second active molecule is used in addition to Pt to enhance the cytotoxic effect.

## Next Generation Pt drugs

As previously discussed, Pt drugs play a critical role in anticancer chemotherapy and are used in 50% of cancer drug regimes. The 1<sup>st</sup> and 2<sup>nd</sup> generation of Pt drugs, cisplatin and carboplatin are known to kill cancer by forming irreparable Pt-DNA adducts.<sup>11</sup> Significantly, oxaliplatin was recently shown to induce its cytotoxic effect not through DNA binding but *via* induction of ribosomal biogenesis stress, disrupting ribosome synthesis, thus triggering cell death.<sup>28</sup>

A plethora of Pt complexes have been reported in the 40 years since the discovery and clinical use of cisplatin, but only carboplatin and oxaliplatin have also been approved for worldwide use. Although a number of other Pt complexes such as nedaplatin, lobaplatin and heptaplatin have been approved for use in specific countries, there have been limited successes in bringing new complexes beyond

clinical trials.<sup>32</sup> However, a frequent factor which has restricted the advancements of these new complexes are their lower cytotoxicities or similar limitations (resistance and side effects) as compared to the existing drugs. However, there has been a recent resurgence in this field and a number of interesting complexes have been developed with the aim of improving selectivity and sensitivity. To this end, new dual functional Pt(II/IV) complexes conjugated to targeting agents, diagnostic agents and/or additional bioactive moieties have been investigated.

### Pt(IV) anticancer drugs

To date, only Pt(II) complexes have been approved for clinical use, however a number of Pt(IV) complexes have recently shown potential in clinical trials, such as satraplatin (**Figure 1.7**).<sup>69-70</sup>

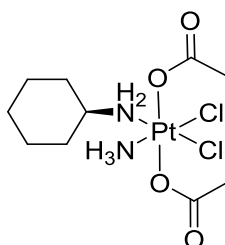
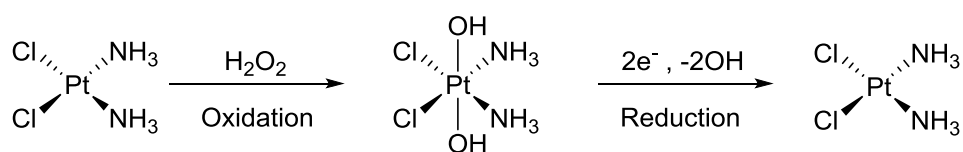


**Figure 1.7:** Pt(IV) anticancer complex satraplatin.

Pt(IV) complexes, in contrast to Pt(II), are not initially active and behave as prodrugs in a cellular environment. Pt(IV) must first undergo reduction in the reducing environment of the cell to form an active, traditional, Pt(II) drug (**Scheme 1.2**).<sup>71-73</sup>



**Scheme 1.2:** Pt(II) and Pt(IV) oxidation and reduction scheme.

An important advantage of developing Pt(IV) complexes is the ability to functionalise the axial hydroxo positions of Pt(IV) hydroxo complexes. The research community has primarily focussed on conjugating the following to one or both axial hydroxo groups; (i) an active drug molecule which is released upon reduction, (ii) a targeting moiety endowed with specificity for a particular tissue or cellular region or (iii), reporter molecules, which help track the drug.

## Multifunctional Pt Drugs

Pt drug resistance and non-specific targeting are of major concern in current chemotherapeutic medicine and there is an urgent need for the development of novel and better therapeutic agents for overcoming resistance and improving upon the negative side effects of current Pt drugs. This led to multi-functional therapies either through dual function drug design or co-administration.<sup>74-76</sup> Multifunctional Pt drugs can accomplish this through specific site targeting of cancer cells and/or targeting multiple mechanisms of resistance within tumour tissues.

The specific targeting of biomolecules is fundamental to chemical biology and medicinal chemistry, and is central to improving general population health. The emergence of new diseases and of drug resistant strains of many illnesses and infections, both bacterial and cancerous, means there is a constant need to develop new drugs in modern society. A number of traditional and novel approaches are currently employed in inorganic medicinal chemistry in order to create more potent and effective medicines.

Metal complexes provide an excellent platform for the rational design of drug candidates as therapeutic and diagnostic agents, due to the predictability and control of the pharmacodynamics and pharmacokinetics of such compounds. Metals can offer characteristic or accessible geometries, coordination numbers and redox states. Manipulation of such variables, by selection of appropriate ligands can lead to the fine tuning of electronic, chemical and photophysical properties of metal complexes. Ligand choice also contributes greatly to structural diversity, stability, ligand exchange kinetics and second coordination sphere interactions of metal complexes.<sup>32,</sup>

77

Surprisingly, given that numerous metallic elements play vital roles in biological systems, the majority of drug molecules are purely organic and do not attempt to exploit the potential advantages of metal-based complexes.

As previously mentioned, the administration of multiple drugs as a chemotherapeutic cocktail combination therapy, i.e. FOLFOX, can improve the treatment of cancer compared to the use of a single drug.<sup>78</sup> The success of strategies such as this proves

the effectiveness of multiple drug administration for targeting and inhibiting multiple pathways and elements associated with tumour cells.

McKay *et al.* and Johnstone *et al.* have both comprehensively reviewed many of the recent strategies employed to develop dual functionalised Pt drugs<sup>79-80</sup>

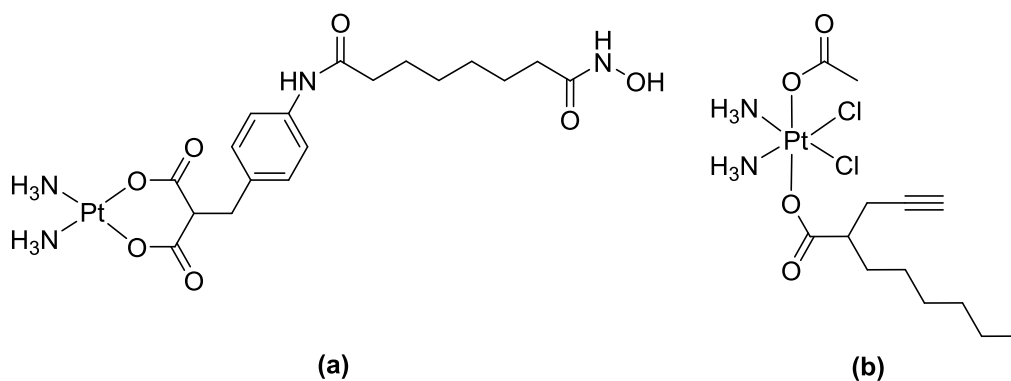


**Figure 1.8:** Structure of Pt HDAC inhibitor complexes (a)  $[\text{Pt(II)(mal-SAHA)(NH}_3)_2]^{81}$  and (b)  $[\text{Pt(IV)Cl}_2(\text{NH}_3)_2(\text{OAc})(\text{POA})]^{82}$ .

One interesting research strategy in dual therapeutic functional Pt drugs is through the use of histone deacetylase (HDAC) inhibitors. HDAC is involved in wrapping and unwrapping of DNA around histones during gene expression and DNA replication. Inhibition of this enzyme leaves DNA exposed in its uncoiled state, leaving it more liable to be platinated. Both suberoylanilide hydroxamic acid (SAHA) and (2-propynyl)octanoic acid (POA) have been identified as active HDAC inhibitors and utilised as ligands in both Pt(II)<sup>81</sup> and Pt(IV)<sup>82</sup> complexes (**Figure 1.8**). In both instances the HDAC inhibitor is “released” within the cell either by aquation of the labile Pt(II) ligand or reduction of Pt(IV) to Pt(II).

Song *et al.* investigated the use of a Pt(IV) complex with axial fluorescein ligands to track and determine the cellular reduction of Pt(IV). The fluorescein probe fluoresced only upon release following the reduction of Pt(IV) to the active Pt(II) complex, and therefore acted both as a therapeutic and a diagnostic agent.<sup>83</sup> Dual functional compounds which have both diagnostic and therapeutic properties are known as theranostic agents. They are of great interest in drug development and discovery due to their potential to actively track a drug complex and identify directly its localisation, processing and interactions.<sup>84</sup>

The use of another metal complex is sometimes employed in multifunctional therapies. For example, Au is most frequently used to make nanoparticles which have a wide range of uses including medical imaging and diagnosis,<sup>85-86</sup> anticancer treatment through photodynamic therapy<sup>87</sup> and therapeutic delivery and targeting,<sup>88</sup> as analytical probes<sup>89</sup> and in electronic technologies as conductors.<sup>90</sup> There has been a surge of interest in Au(III) square planar complexes as potential anticancer agents,<sup>91-94</sup> making Au a metal of interest in this thesis.

A prime example of rational multifunctional drug development was reported by Kumar *et al.* They utilised a Au nanoparticle that was functionalised with both a Pt(IV) drug and a targeting peptide moiety and reported enhanced tumour targeting and anticancer activity.<sup>95</sup>

This thesis will focus on the application of the diagnostic and targeting applications of new generation Pt drugs.

## Diagnostics

A rational design approach to the development of new anticancer treatments and methods for the early detection of disease are crucial to modern medicinal chemistry research. Diagnostic agents may be used in the developmental stage of rational drug design as they can be used to track and identify a drug or a drug candidate's cellular interactions and transport mechanisms.<sup>32, 84, 96-97</sup> Diagnostic agents may also be used to identify critical biomarkers such as proteins or antibodies associated with particular diseases or illnesses.<sup>98-100</sup>

Examples of diagnostics in medicine include magnetic resonance imaging (MRI) contrast agents,<sup>100</sup> single-photon emission computed tomography (SPECT) radioisotopic complexes,<sup>101-102</sup> and fluorescent dyes.<sup>97, 103-104</sup> In addition to clinically used diagnostics there is a plethora of simple pharmaceutical (over the counter) chemical diagnostic testing devices available to the general public, e.g. pregnancy tests, blood sugar strips and alcohol breathalysers.

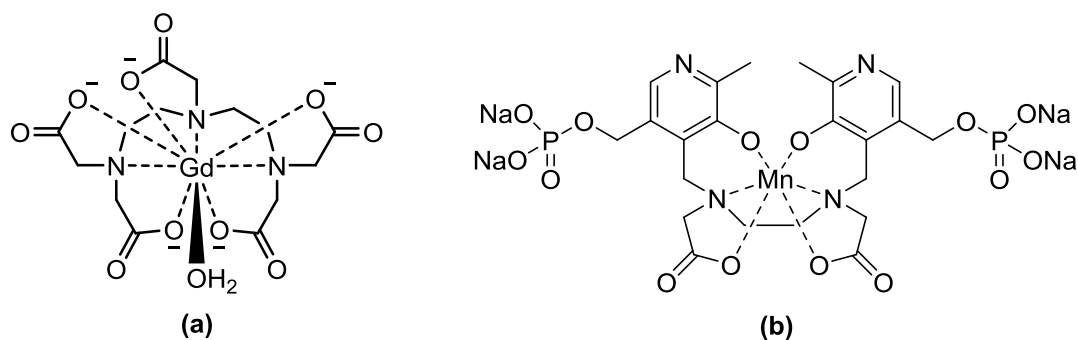


**Figure 1.9:** Clinically used MRI contrast agents (a) Magnevist<sup>105</sup>  $[\text{Gd}(\text{DTPA})(\text{H}_2\text{O})]^{2-}$ , (b) Teslascan<sup>106</sup>  $[\text{Mn}(\text{DPDP})]^{2-}$ , where DTPA = diethylenetriaminepentaacetate and DPDP = dipyridoxaldiphosphate.

MRI is used to generate an image of soft body tissues by generating a magnetic field which magnetically aligns the protons of water and small organic molecules. When the magnetic pulse ends there is a decay of the protons magnetic moment, known as relaxation time. This change can be detected and transformed into an image. Contrast agents may be added in order to improve (shorten) the relaxation time in imaging which can generate greater contrast between tissue types and improve the image resolution. The major classes used clinically utilise the strong paramagnetic properties of Gd, Mn and Fe to form complexes (**Figure 1.9**) which are capable of enhancing the image quality by reducing relaxation times. MRI may typically be used to scan the brain, liver and heart and can detect damaged tissues and tumours.<sup>105</sup>

The Tc isotope,  $^{99\text{m}}\text{Tc}$ , is used as a radioisotope as it is a  $\gamma$  ray emitter with a half-life *ca.* 6 hours, which can be detected and imaged using SPECT while minimising patient exposure to radiation.  $^{99\text{m}}\text{Tc}$  is used in a large number of SPECT imaging experiments in complexes with numerous multidentate ligands. Some complexes naturally locate in particular regions of the body, while others are attached to targeting agents.<sup>32</sup> Examples include Ceretec (**Figure 1.10a**), used to measure cerebral blood flow,<sup>107</sup> Cardiolite (**Figure 1.10b**) which specifically localises in cardiac tissues is used to assess cardio blood perfusion<sup>108</sup> and  $^{99\text{m}}\text{Tc}$  medronic acid (**Figure 1.10c**) which is used to identify bone breaks, regeneration and cancers due to its uptake by osteoblasts.<sup>109</sup>



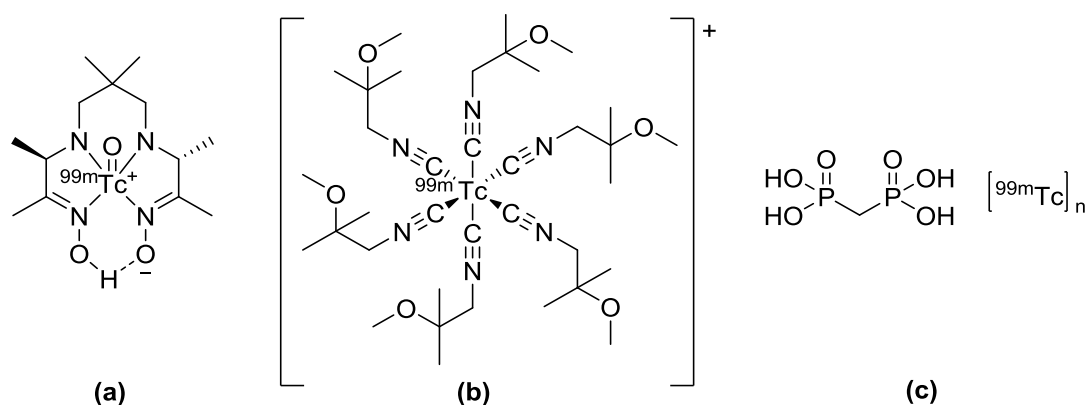


**Figure 1.10:** Clinically used  $^{99m}\text{Tc}$  imaging agents (a) Ceretec, (b) Cardiolite and (c)  $^{99m}\text{Tc}$  medronic acid.

Fluorophores are among the most frequently used diagnostic agents, due in part to the large variety available. Furthermore many can be readily modified to suit an application.

Fluorophores are the diagnostic agents employed in this thesis.

### Fluorophores

A fluorophore is a chemical which is capable of fluorescent emission upon excitation by light, where the emitted light is at a longer wavelength than the light absorbed. This is typically made possible by the presence of conjugated  $\pi$ -bond containing systems such as aromatic groups, cyclic or planar groups with several  $\pi$ -bonds. When a fluorescent molecule is excited by light, the molecule receives energy and is in an excited state. The molecule interacts with itself and surrounding molecules resulting in the emission of light of a different energy level and colour as it returns to its energy ground state.<sup>110</sup>

Fluorophores have a wide range of imaging applications in modern medicine, ranging from cellular and *in vivo* imaging to clinically approved fluorescent guided surgery.<sup>103, 111-113</sup>

A vast number of fluorescent probes are frequently used in clinical and research settings to detect and quantify key biomolecules associated with diseases such as cancer. Furthermore, fluorophores are routinely used to study the behaviour of drugs and drug candidates, i.e. to track the uptake, transport and processing of a drug within a cell.<sup>103, 111-113</sup> The variety of fluorophore families have allowed for a diverse

library of imaging agents to be developed and their properties tailored for a specific need or function.

Each fluorophore family is predominantly defined by their absorption, excitation and emission wavelengths. The common wavelength imaging range goes between 190 nm in the ultraviolet (UV) range up to 750 nm at the start of the infrared (IR) range.<sup>114</sup>

In an *in vitro* and *in vivo* system, excellent functionality and robustness of a probe is associated with high quantum yields, high extinction coefficients and photostability.<sup>115</sup> A great number of fluorophore species may be modified for specific qualitative and quantitative analysis of a particular biomarker, for example antibody tagging or specific organelle staining e.g. cell nucleus.<sup>104, 116</sup> Below is described a number of common *in vitro* applications for fluorescent materials.

The 4',6-diamidino-2-phenylindole (DAPI, **Figure 1.11a**) stain is perhaps the most commonly used dye in cellular microscopy. It has a high affinity for adenine-thymine rich regions of DNA and is thus used as a stain for the cell nucleus. It has low cellular permeability for live cells and is therefore frequently used in fixed cell imaging studies.<sup>117-118</sup>

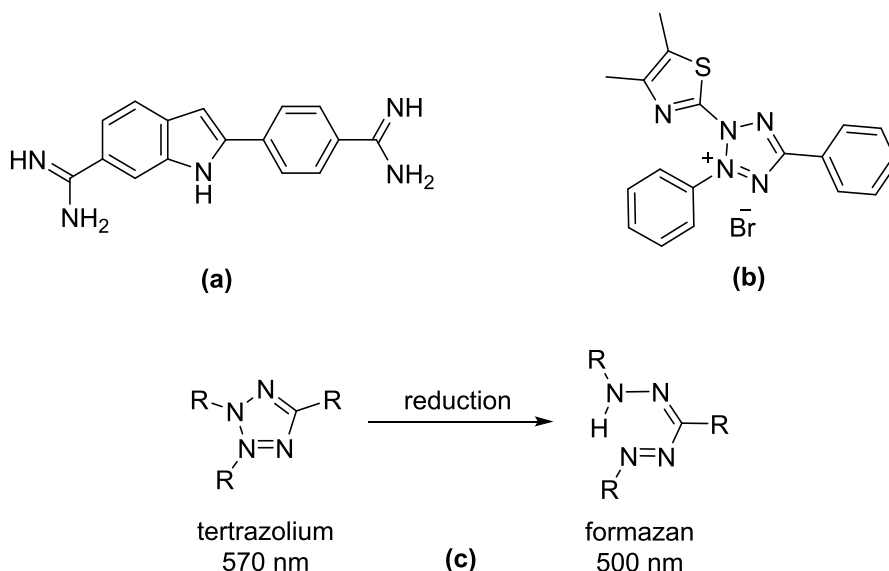


**Figure 1.11:** Fluorescent stains and dyes with *in vitro* applications: (a) DAPI ( $\lambda_{\text{max}}$  em 461 nm), (b) MTT ( $\lambda_{\text{max}}$  em 570 nm) and (c) reduction of tetrazolium rings to form a formazan group.

Switchable and on/off fluorescent materials are often used in colourimetric assaying techniques. Cytotoxicity and cell viability studies frequently use the MTT assay. (3-(4,5-dimethylthiazol-2-yl)-2,5-diphenyltetrazolium bromide (MTT) (**Figure 1.11b**) belongs to a family of agents known as tetrazolium dyes. In the presence of NAD(P)H-dependent cellular oxidoreductase enzymes in a living cell, MTT is reduced to form formazan (**Figure 1.11c**), which causes a shift in fluorescence from approximately 570 to 500 nm. It is used to determine cell viability based on the metabolic activity of a living cell.<sup>119-120</sup> Porphyrins, phthalocyanines and their derivatives are also used for their imaging properties in addition to multifunctional applications.<sup>121-122</sup> A number of these compounds show near-IR (NIR) emissions<sup>123</sup> however they are known to produce reactive oxygen species (ROS) within the cell and are therefore generally only used for imaging purposes.<sup>111</sup>

The limitations of many fluorescent compounds and their potential applications relate to their fluorescent properties e.g. photophysical properties, photostability (in solution) and emission wavelengths. Background labelling of the fluorescent probe through secondary and non-specific binding also reduces their function.<sup>124-125</sup>

Functional fluorophore design is of keen interest for *in vivo* imaging to generate bespoke imaging probes.<sup>126-127</sup> Of significant note from a medical and biofunctional stand point is the NIR range ( $\lambda=700-900$  nm). NIR fluorophores are desirable for use in a living system. NIR fluorophores such as boron-fluorescent dipyrromethenes (BODIPY) and in turn the BF<sub>2</sub>-azadipyrromethenes (NIR-AZA) and squaraine dyes for example, have been of prominent interest recently due to the favourable imaging properties they provide in an *in vivo* system, as NIR light penetrates through organic tissues. At lower wavelengths, interference from a biological system occurs due to the natural absorption of light by competing endogenous chromophore absorbance.<sup>128-131</sup>

A number of NIR dyes are also commercially available e.g. IRDye® 750 (from LI-COR Biosciences Inc.) (**Figure 1.12b**), which can label amino or thiol groups using the IRDye® 750 (*N*-Hydroxysuccinimide) NHS Ester and Maleimide derivatives respectively. Cy5.5® NHS Ester dye (from Lumiprobe, Lumiprobe GmbH) (**Figure 1.12a**) can label amino groups in peptides, proteins, and oligonucleotides. These dyes can readily be incorporated into the structure of antibodies and other biomarkers to

act as a fluorescent tag for identification and imaging purposes, as described in recent reports.<sup>132-134</sup>

Cy5.5 has been used to track the tumor uptake and distribution of a new targeted RNA (ribonucleic acid) therapy *in vivo*, with a view to further optimizing a delivery strategy.<sup>133</sup> Cy5.5 is one of the oldest and most widely used NIR dyes in *in vivo* cancer imaging,<sup>135-138</sup> however its lower emission wavelength of  $\lambda_{\text{max}}$  670 nm and low photostability is less favorable when compared to the BODIPY family of fluorophores,<sup>138</sup> and the IRDye® series.

Derivatives of the IRDye® 750 containing specific protein targeting moieties were used *in vivo* for the selective identification of tumor target proteins. In order to rationally develop this probe, a specific ligand pair of a target protein/biomolecule were determined and the NIR probe modified to contain two specific moieties to selectively bind with the desired target.<sup>134</sup>

There is an expanding research niche in the development and use of NIR fluorophores for practical surgical applications such as tumour imaging and fluorescence guided surgery.<sup>113</sup> The current strategies involve improving the emission strength of an NIR probe, specific targeting of a fluorophore and improving the time required for a viable image to be taken. The O'Shea research group has made substantial process in this field as described below.<sup>98, 128</sup>

The O'Shea research group have used NIR fluorophores for live imaging to study fundamental cellular process of lysosomes in cancer detection *in vivo*.<sup>128</sup> Grossi *et al.* developed a lysosome selective on/off NIR-AZA fluorophore (**Figure 1.12c**), which is pH responsive. Upon compartmentalisation in an acidic environment (~4.5 pH) within the lysosome, it turns “on” giving a fluorescence emission of  $\lambda_{\text{max}}$  707 nm, a process which is reversible through phenol/phenolate interconversion. This fluorophore used for 4D live cellular uptake and tracking studies and in *in vivo* mice models demonstrated high tumour localisation and targeting, validating its potential use in fluorescence guided surgery.<sup>128</sup>

In 2017, Daly *et al.* developed two NIR-AZA probes (**Figure 1.12d-e**) and tested the first preclinical *ex vivo* colonic lymph node mapping using common clinical and surgical imaging instruments and technology. This was achieved through the addition

of strong electron donating dimethylamino moieties to the NIR-AZA scaffold which helped produce a detectable bathochromic wavelength shift with emissions between 791-826 nm. A relatively low concentration of fluorophore solution was capable of rapidly staining specific colonic lymph nodes which did not spread from the injection site and “tattooed” a specific site of interest. Additional studies on recently resected tumorous colonic tissue (*ex vivo*) showed that fluorophore injected directly into the tumour migrated through the lymphatic vessels to distant nodes. This non-toxic method could be used as a means for lymph node mapping in surgery to identify the extended regions of diseased tissue mass over healthy tissue.<sup>98</sup>

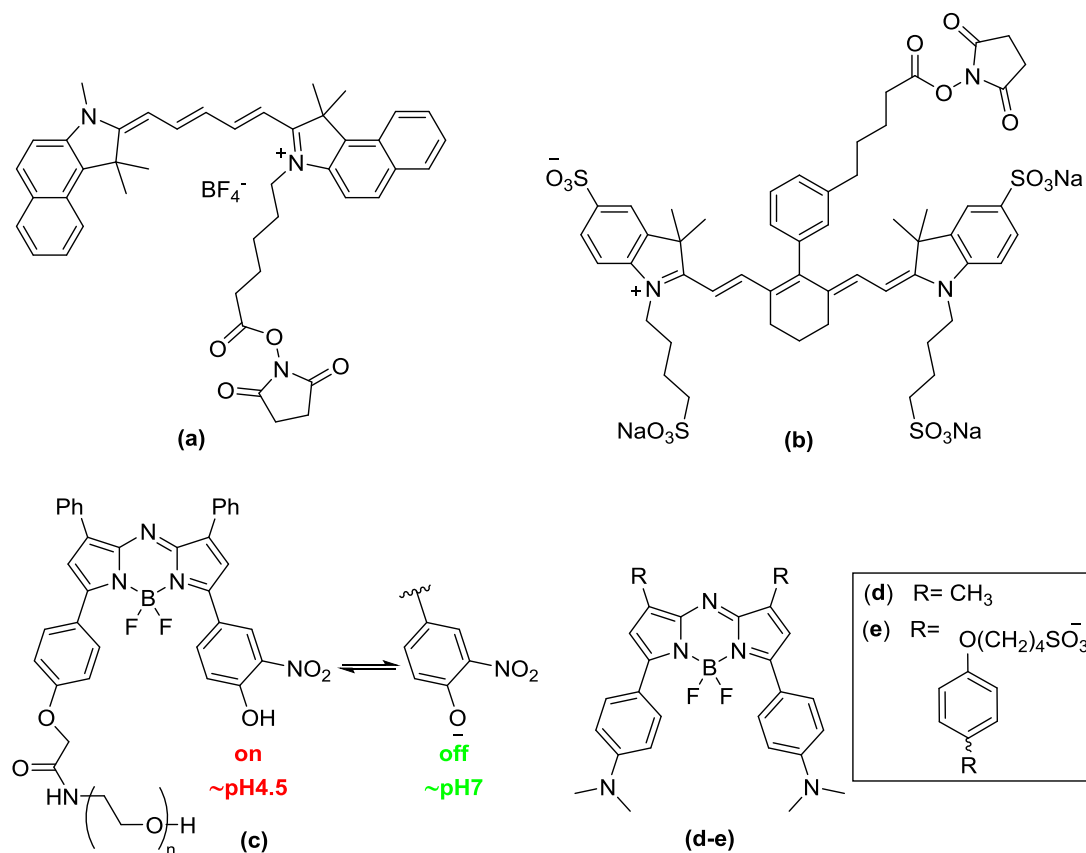


**Figure 1.12:** NIR Flu examples. (a) Cy5.5® NHS Ester reactive handle ( $\lambda_{\text{max}}$  em 710 nm), (b) IRDye® 750 NHS Ester reactive handle ( $\lambda_{\text{max}}$  em 776 nm in PBS), (c) Lysosomal responsive NIR-AZA fluorophore ( $\lambda_{\text{max}}$  em 707 nm),<sup>128</sup> (d) NIR-AZA ( $\lambda_{\text{max}}$  em 791 or 822 nm in THF or DMSO) and (e) ( $\lambda_{\text{max}}$  em 826 nm in DMSO).<sup>98</sup>

The significance of these final two real time fluorescent tools for the identification of key tissue structures and cellular markers shows the importance of diagnostic agents in modern medical research.

## Peptides in medicine

The identification and development of novel effective targeting agents are vitally important to the enhancement of modern medicine. Many existing clinical drugs suffer from dose limiting toxicity due to unspecific targeting within the body, for example cancer chemotherapeutics such as cisplatin.<sup>139-140</sup> Furthermore, some diseases respond poorly to existing drugs as these drugs lack the required selectivity to be truly effective.<sup>141-144</sup>

Peptide based pharmaceutical research is currently very strong given the improvements in the cost and ease of their synthesis. There are also now a growing number of established and well characterised biomolecules that can be effectively inhibited and/or targeted by synthetic peptides.<sup>74, 145</sup>

A peptide is a sequence of amino acids (aa) linked together through amide bond coupling reactions. The peptide chain may be linear or branched and considered to be anywhere between 2 and 50 aa in length, whereas proteins are considered to be greater than 50 aa in length.<sup>146</sup> Significantly, peptides are already clinically approved as therapies,<sup>74</sup> such as Leuporelin for prostate and breast cancer treatment,<sup>147</sup> the 100 unit peptide chain insulin glargine for long acting blood sugar control for diabetes<sup>148-149</sup> and atrial natriuretic peptides (ANP) used to treat cardiovascular disease and heart failure.<sup>150</sup> The use of peptides and specifically cell penetrating peptides (CPP) in targeting of cancers is currently very topical.<sup>75, 151-154</sup>

### Cell Penetrating Peptides

CPP are defined as short (fewer than 35 aa), non-toxic peptide sequences which are capable of translocation into cells both independently and when coupled to a cargo e.g. small organic molecule, protein, antibody or nanoparticle.<sup>145, 154</sup> The first example of a CPP was identified in 1988, transcription transactivating (Trans-acting activator of transcription) (TAT) peptide, derived from the human immunodeficiency virus1 (HIV-1).<sup>155</sup> Subsequently, additional CPPs and aptamers were identified in anticancer research, including penetratin, pVEC, RGD and Octaarginine.<sup>156-159</sup>

Since their discovery, the exact mechanism of entry of CPPs into cells has been widely investigated. There have been a number of conflicting reports and it is now widely accepted that there is no single fixed mode of cellular uptake/entry. In turn

different mechanisms of passive transport (energy independent) and active transport (energy dependent) have been proposed and established for a number of CPPs.<sup>160</sup>

Passive transport has been demonstrated through a number of mechanisms including the inverted micelle model, pore formation model, carpet like model and membrane thinning model (**Figure 1.13**).<sup>161-165</sup> These transport mechanisms are all thought to be induced by the ion charges of the amino acid sequences of the CPP interacting with the charged species present on the phospholipid bilayer of the cell membrane. In short, the proposed destabilization of the plasma membrane allows for the CPP to internalise within the cell.<sup>160</sup>

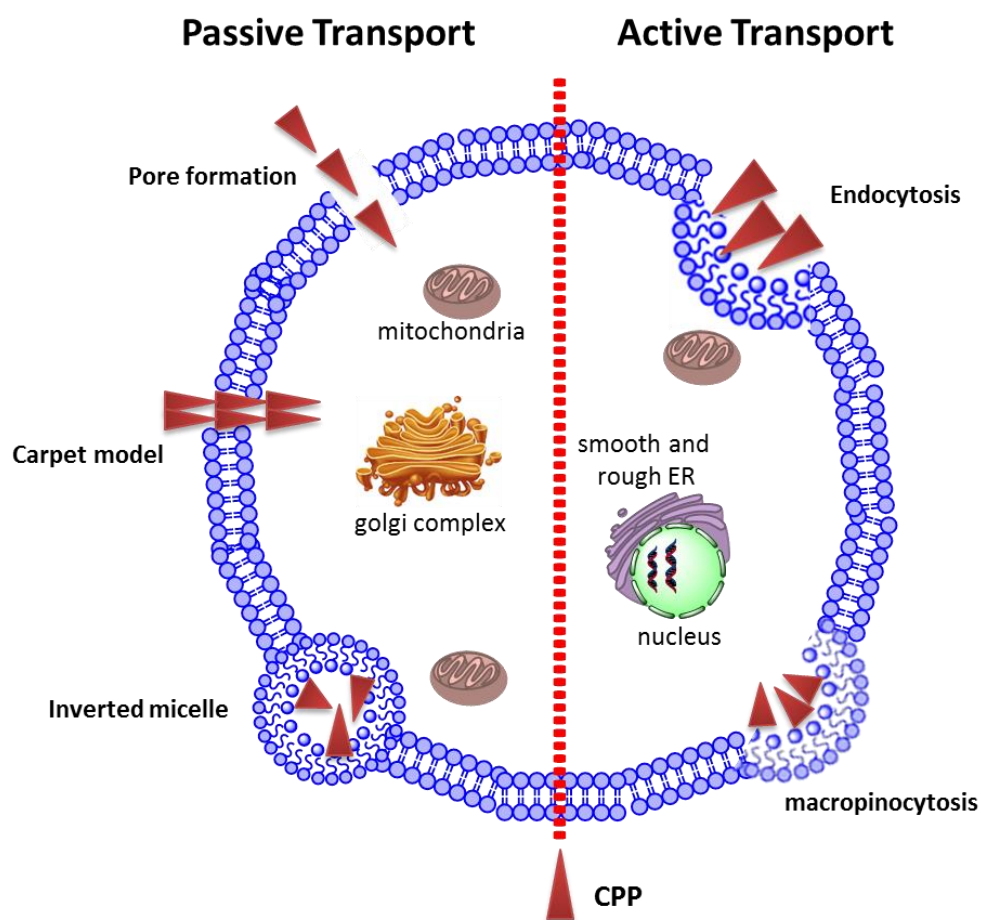


**Figure 1.13:** Mechanisms proposed for CPP cellular uptake. Adapted from *Int. J. Mol. Sci.* **2016**, *17* (11).<sup>166</sup>

The active transport of CPPs is most often associated with endocytosis, the mechanism responsible for uptake of particulates and macromolecules. This highly regulated and complex process occurs for all cells *via* the formation of new vesicles in the plasma membrane of the lipid bilayer engulfing the molecule in question and

transporting it within the cell. The three main mechanisms are phagocytosis, pinocytosis and receptor-mediated endocytosis<sup>167-168</sup> (**Figure 1.13**).

Given the effectiveness of CPPs, there has been a rapid growth in their conjugation to drug molecules. A number of studies have demonstrated that CPPs may be used to transport various cargos e.g. other proteins, active small molecules and siRNA (small interfering RNA), through the cell membrane, and essentially act as delivery moieties.<sup>169-171</sup> In turn, the use of CPPs has been investigated as a means to improve anticancer activity of drugs.

Octaarginine, for example, has been used to improve the delivery of paclitaxel (taxol) to ovarian cancer cells to improve the drug response in taxol-resistant tumour models.<sup>158</sup> pVEC has been used to deliver chlorambucil to breast cancer with increased cellular uptake in tumours leading to increased cytotoxicity while reducing uptake in non-tumorous tissues.<sup>156</sup>

Peptides with anticancer activity have been bound to CPPs demonstrating a positive anticancer effect. In one study, TATp and low molecular weight protamine (LMWP) were used with gelonin to target colorectal cancer where it induced complete inhibition of tumour growth.<sup>172</sup> Penetratin has been used in the delivery of pro-apoptotic peptide KLA (acetyl-(KLAKLAK)<sub>2</sub>-NH<sub>2</sub>) in a panel of 7 human cancer and 3 non-tumour cell lines and a selective increase in the cytotoxic activity *in vitro* against cancer cell lines over non-tumour was observed. This included improved activity against resistant cells.<sup>157</sup> The use of the tripeptide motif RGD (arginine-glycine-aspartic acid) is growing in popularity due to the simplicity of the structure. RGD targets  $\alpha\beta$  V and  $\alpha\beta$  V integrin receptors, which are found to be essential in tumour angiogenesis and metastasis, in addition to being upregulated in the tumour endothelium.<sup>159</sup>

Interestingly, the research group of Schatzschneider has reported a number of metal-peptide complexes which have displayed improved targeting *via* CPPs and activities as a result of conjugation to metal complexes.<sup>173-174</sup>

The few examples of CPP associated strategies described above have proved to be very effective in the studies described and clearly hold much promise clinically. In the majority of cases, the CPP targets a specific protein or enzyme that is either



upregulated or essential to the function of tumour cells and which make them distinct and effective targets.<sup>95, 151</sup> One such target, and the protein family of interest in this thesis, is heat-shock protein-70 (HSP70).

### Heat Shock Proteins and HSP70

HSPs were first identified by Rittosa in *Drosophila melanogaster* fruit fly through the identification of a gene that leads to the expression of proteins under heat stress.<sup>175</sup> As the HSP family of proteins was further investigated, it became clear that other cellular stresses result in HSP protein expression, such as elevated pH, hypoxia and ischemia.<sup>68</sup> Irrespective of the stress, HSPs aid in homeostasis by stabilising proteins and preventing denaturation that would normally occur during cellular stress. The major groups of the HSP family interact with one another, primarily functioning together to maintain cellular homeostasis.<sup>176</sup>

The six main classes are categorised with reference to their molecular mass in kilodaltons (kDa); HSP110, HSP90, HSP70, HSP60, HSP40 and small HSPs of 16-30 kDa.<sup>177</sup> These proteins interact and signal with one another in order to maintain, chaperone and correctly fold and unfold proteins during and following cellular stress. By behaving as a buffer system for proteins, they prevent damage and misfolding which often occurs during stress induced stimuli.<sup>178</sup> The HSP family function together and are highly dependent on many co-chaperone proteins, which are crucial to the heat shock response.<sup>176</sup>

There are thirteen members of the HSP70 family which are expressed on a basal level outside of cellular stress and perform cellular house-keeping roles. Not all HSP70 members are stress induced,<sup>179</sup> but their primary function is to maintain homeostasis in addition to a number of protein transportation roles through the cell and endoplasmic reticulum (ER).<sup>180-181</sup>

Of significance here are HSP70-1A and HSP70-1B, which have responsibility for major stress survival roles. These proteins are stress inducible and widely found in the cytosol, nucleus and lysosome.<sup>179</sup> The structures of HSP70-1A and B (generally referred to collectively as HSP70-1) only differ in sequence by two amino acids.<sup>182</sup> There are three major functional domains on the HSP70-1 structure; an N-terminal ATPase binding domain (ABD), a substrate binding domain (SBD) and a C-terminal domain which acts a “lid” for the SBD and mediates co-chaperone binding (**Figure**

**1.14).**<sup>183-184</sup> The SBD binds to neutral and hydrophobic aa residues on misfolded proteins.

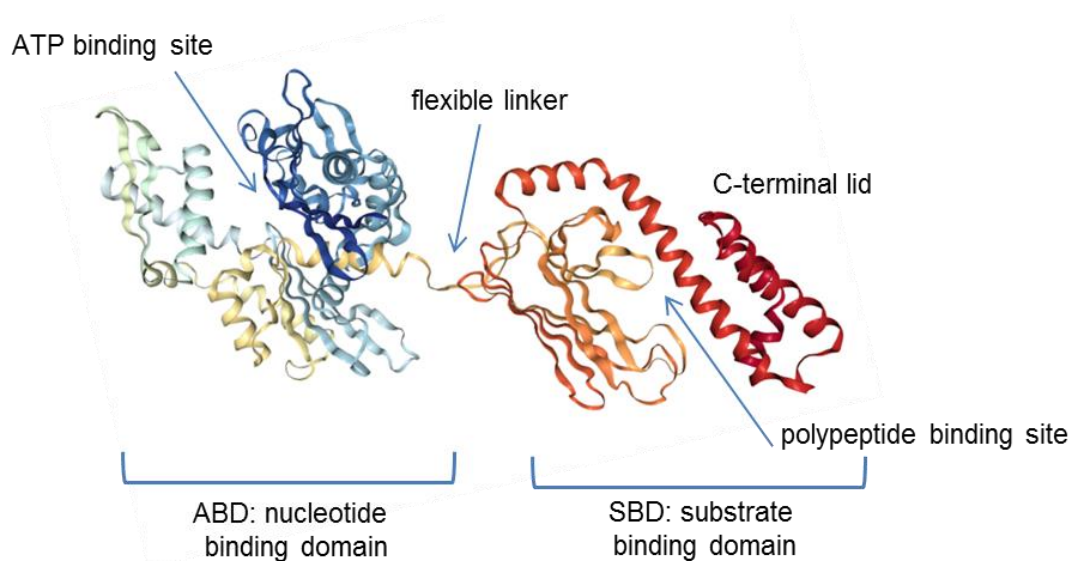


**Figure 1.14:** The solution structure of *E. coli* HSP70 homolog (DnaK) (PDB 2KHO), with the ABD, SBD and C-terminal helical domains indicated.<sup>68, 184</sup>

The expression of HSP70-1 is mediated by heat shock factors, a class of transcription factors, resulting in gene transcription of these proteins.<sup>185-186</sup> One of the major ways HSP70-1 accomplishes this is by preventing proteotoxicity, which is impaired cellular function as a result of incorrect protein folding. This irreversibly occurs when exposed hydrophobic stretches of misfolded proteins accumulate. As HSP70-1 shows high binding affinity for hydrophobic aa regions, they are capable of complexation to these misfolding proteins during cellular stress and retaining protein folding viability under conditions that would have otherwise been lethal.<sup>186-187</sup> Following the passing of the stress, HSP70-1 has a low binding affinity, due to ATP/ADP cellular levels, and the HSP70-1 protein dissociates from the complex.<sup>186</sup>

In 2013, Murphy reviewed the HSP70 family and how they play an essential role in cancer progress and prognosis.<sup>68</sup> Regulation of HSP70 within many cancer cells gives cancer a distinct survival advantage by interfering with apoptotic signalling pathways through various means.<sup>68</sup> A number of examples are described below.

HSP70 prevents intrinsic apoptosis by interfering with the translocation of the pro-apoptotic protein Bax, which is involved in the release and activation of caspases responsible for apoptosis.<sup>188</sup> HSP70 also prevents extrinsic apoptosis by binding and preventing recruitment of death receptors (DR), DR4 and DR5, which signal with

cell death inducing complexes.<sup>189</sup> In addition, HSP70 stabilises lysosomes, preventing cellular degradation.<sup>190</sup>

As mentioned, HSP70 is upregulated in numerous tumour cells which aid in their survival under cellular stress and is associated with cancer progression and poor prognosis,<sup>68</sup> however this upregulation also makes them molecules of interest as targets. A number of selective small molecule inhibitors of HSP70, such as Pifithrin- $\mu$ , VER-155008 and apoptozole<sup>191-193</sup> have been identified and show good inhibition of HSP70 and cytotoxicity towards cancer cells. Aoife McKeon, a former member of our research group, previously reported the essential role HSP70 plays in Pt drug resistant cell lines, and how inhibition of HSP70 with Pifithrin- $\mu$  improves the anticancer activity of Pt drugs.<sup>191</sup> Furthermore, she described in a separate study how conjugation of tumour penetrating peptide (TPP) to a Pt(IV) oxaliplatin type complex enhanced its cytotoxicity compared to oxaliplatin.<sup>195</sup> Of interest in this thesis is HSP70 as a target for delivery of an anticancer chemotherapeutic agent.

The 14-mer CPP known as TPP was derived from HSP70, and is capable of cellular penetration *via* membrane bound HSP70 (memHSP70).<sup>194-195</sup> Given the importance of HSP70 in cellular homeostasis during stress, its over-expression in cancer cells represents an ideal target protein in anticancer research.

## Steroids and hormones in medicine

As previously mentioned, hormone therapy is used in a number of human illnesses including treatment for cancer.<sup>5, 22-23</sup> Hormones are a class of signalling biomolecules which help in the regulation of many behavioural and physiological processes e.g. metabolism, mood, growth and sexual characteristics.<sup>196-198</sup> Steroids are one of the major classes of hormones.

The steroid structural core consists of 4 fused rings, three 6-membered (A, B and C rings) and one 5-membered (D ring), with the variant types distinguished by their side chain functional groups (**Figure 1.15**). Examples include estrogen, progesterone, testosterone and cholesterol.<sup>197</sup> Estradiol, progesterone and testosterone all belong to the class of sex hormones. Steroidal hormones are either endogenous (made within the body/cell) or exogenous (made outside of the body/cell).<sup>199-200</sup>

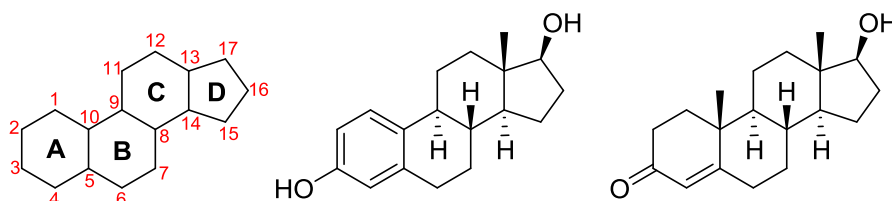


**Figure 1.15:** General ring labelling, structure and carbon number of steroid compounds (left) and the structures of the steroids estradiol (middle) and testosterone (right).

There have been a number of examples of transition metal steroid ligand complexes and dual functioning metal steroid complexes as potential chemotherapeutics.<sup>201-202</sup> Barrett *et al.* demonstrated the effectiveness of Cu-steroid (**Figure 1.16**) conjugates as antimicrobial complexes *in vitro* and *in vivo*. They complexed Cu with a novel steroid conjugated phenanthroline bidentate ligand and a second bidentate ligand such as dipyrdo[3,2-*f*:2',3'-*h*]quinoxaline (DPQ), dipyrdo[3,2-*a*:2',3'-*c*]phenazine (DPPZ) or benzo[*I*]dipyrdo[3,2-*a*:2',3'-*c*]phenazine (DPPN), which also possessed antimicrobial properties. Although the exact mode of action was not determined, the Cu complexes described demonstrate the potential benefits of employing steroid-based ligands to improve potency and targeted delivery of metal centres.<sup>201</sup>

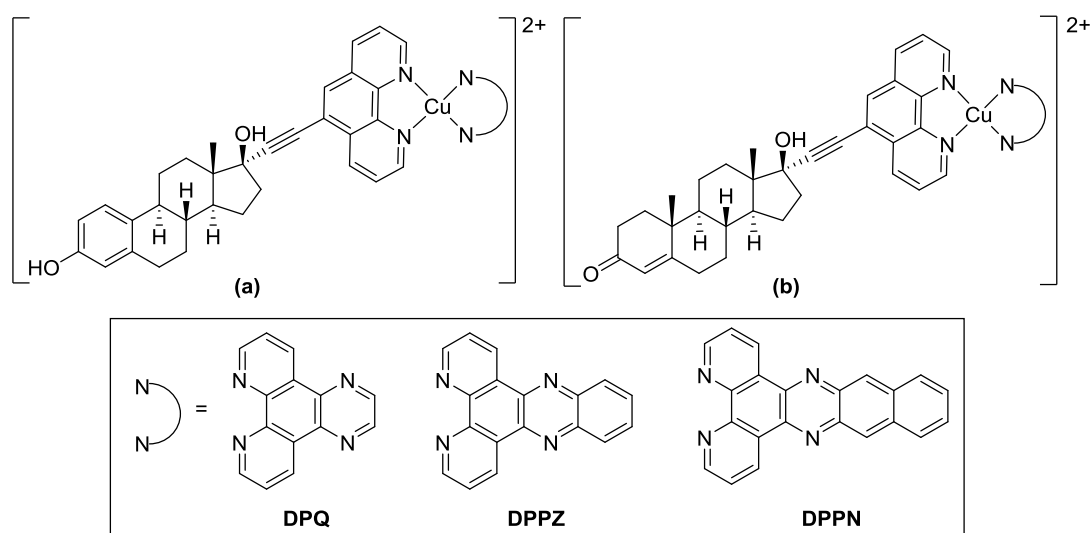


**Figure 1.16:** Structures of Cu-steroid antimicrobial complexes.<sup>201</sup>

Estradiol (of the estrogen class) and testosterone (of the androgen class) (**Figure 1.15**) are of particular interest to this thesis given their association with cancer. Estradiol and testosterone readily cross cell membranes due to their high

lipophilicity<sup>203-204</sup> but also their interactions with the steroid hormone receptors (SHRs), ER and AR respectively, which are upregulated in certain cancers.<sup>24-27, 205</sup> Therefore, steroid drug conjugates can potentially deliver a therapeutic payload *via* the natural steroid receptors present on the cell membrane.<sup>206-208</sup>

Drug conjugates of estradiol and testosterone are likely to possess improved cell permeability and targeting potential. Interestingly, the Lippard research group previously reported that tumour cells that are ER(+) become more sensitive to cisplatin and carboplatin therapy when treated with estrogens.<sup>209</sup> Recently, Johnstone *et al.* reviewed the topic of Pt-steroid complexes comprehensively used in anticancer research. Although the area was first investigated in the 1980s, there have been very few major advances on the methods, techniques and results described and only a limited number of Pt steroid complexes have better activity than the Pt drugs alone.<sup>80</sup>

## Click Chemistry

### Triazole Chemistry

A triazole is a five-membered heterocyclic ring of two carbons and three nitrogen atoms. It is typically formed following conjugation of two separate chemical moieties and is an extremely useful building block in the construction of ligands and coordination complexes,<sup>210-214</sup> which gives it a diverse range of applications including drug development, catalysis, metal ion sensing and imaging.<sup>210-211, 214</sup> There are two isomers of the triazole ring; 1,2,3-triazoles and 1,2,4-triazoles, each of which has two tautomers (**Figure 1.16a-d**). Substituted triazoles also exist giving rise to a number of regioisomers (**Figure 1.16e-f**) which further varies the chemical and physical properties of this unique moiety.

The 1*H*-1,2,3-triazole has a pK<sub>a</sub> of 9.3 making it weakly acidic. The N2 and N3 pyridine-type nitrogens are basic in property with proton affinities (PA) of 915 and 839 kJ mol<sup>-1</sup> respectively.<sup>211</sup> This trend is also observed for standard 1,4-disubstituted 1,2,3-triazoles.<sup>215</sup> N3 is more basic in nature by virtue of N2 having two adjacent nitrogen atoms, making N3 more prone to metal coordination.<sup>211</sup>

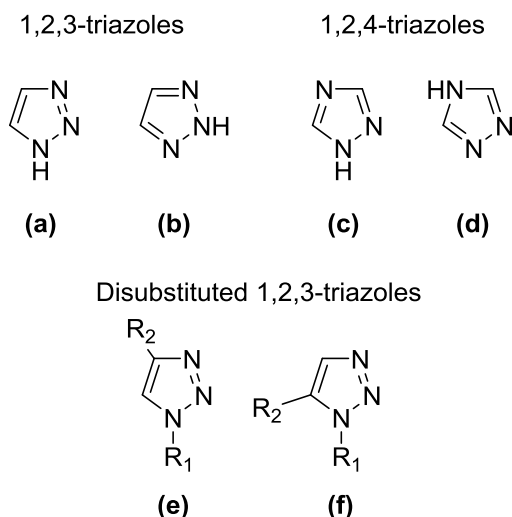
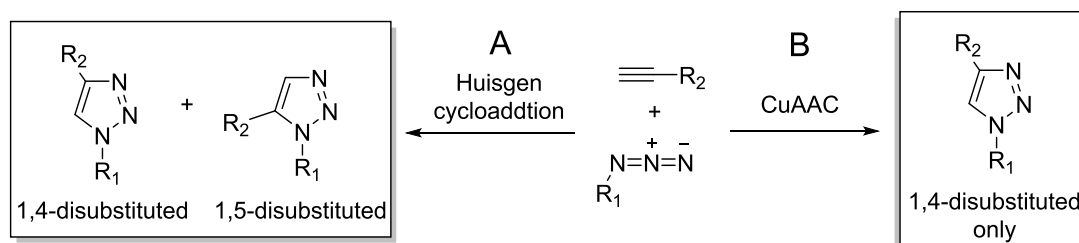


**Figure 1.16:** Structure of the four unsubstituted tautomers of the two possible triazole structures. (a) 1*H*- and (b) 2*H*- 1,2,3-triazole; and (c) 1*H*- and (d) 4*H*- 1,2,4-triazoles. Regioisomers of substituted 1,2,3-triazoles (e) 1,4 and (f) 1,5-disubstituted.

This work focuses specifically on 1,4-disubstituted 1,2,3-triazoles and their applications in medicinal and coordination chemistry.

There are two prominent synthetic methods used to generate substituted 1,2,3-triazoles, the earliest of which described is 1,3-dipolar cycloaddition, known as Huisgen cycloaddition (**Scheme 1.3A**). The reaction is a ring forming reaction between a terminal alkyne and an azide, and occurs spontaneously upon heating, forming a mixture of the 1,4- and 1,5-disubstituted regioisomers. As regioisomeric control is strongly desired in synthetic chemistry, the second and preferred synthetic method employed is the copper (Cu) promoted alkyne-azide cycloaddition (CuAAC), a prominent reaction in the field of “click” chemistry, which affords the 1,4 regioisomer only (**Scheme 1.3B**).

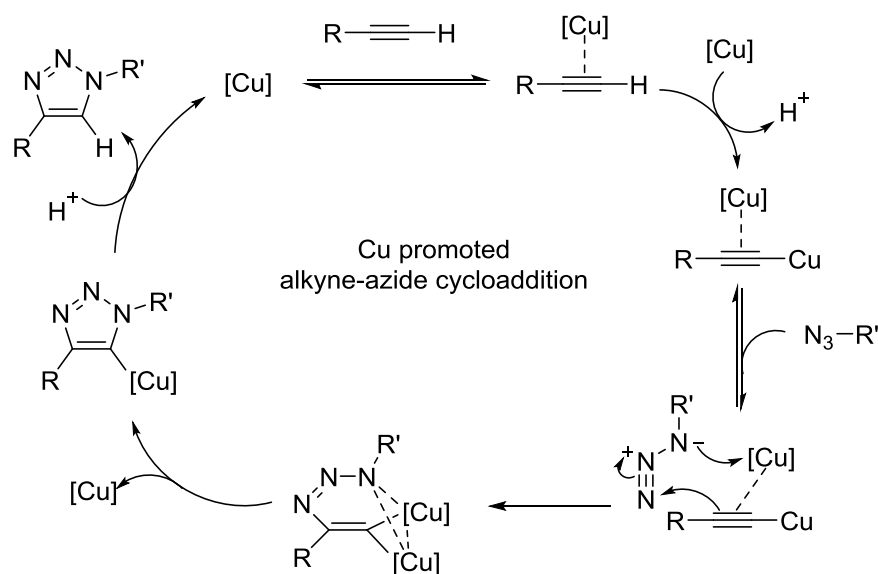


**Scheme 1.3:** Schematic model of the products of the 1,3-dipolar cycloadditions (A) Huisgen cycloaddition and (B) CuAAC.

## CuAAC

The term “click” chemistry was first introduced by Sharpless in 2001, describing a set of reactions which may be adapted from nature and which are rapid, high yielding and easy to isolate.<sup>216</sup> The most significant and common application of click chemistry reactions is the conjugation of two separate moieties into a single molecule, for example an active drug molecule and a targeting moiety forming a multifunctional agent.<sup>217</sup>

Copper catalysed alkyne-azide cycloaddition, or CuAAC,<sup>218</sup> is perhaps the most common of all the click reactions used in research today since its introduction, first published independently by Sharpless and Meldal in 2002.<sup>219-220</sup> It is a Huisgen cycloaddition reaction, which regioselectively generates 1,4-disubstituted 1,2,3-triazoles, with the respective R groups of the azide and alkyne moieties being retained in the N1 and C4 positions (**Scheme 1.4**).<sup>210, 219</sup>



**Scheme 1.4:** Mechanism of Cu promoted alkyne-azide cycloaddition.<sup>221</sup>

As a catalyst, the use of Cu(I) not only selectively generates 1,4-disubstituted triazoles, but also greatly increases the rate of the reaction at room temperature.<sup>220</sup> One of the earliest practical examples of CuAAC was in solid phase peptide conjugation, where Cu(I) coordinated to an acetylide peptide derivative of bombesin on a resin was conjugated to an azide containing functional group (e.g. azido-sugar and aryl azides), giving high conversion and pure click products.<sup>220</sup>

The robust nature of the reaction, and the ease of conjugation of two separate functional units, ensured that the popularity of CuAAC grew during the mid-2000s with a wide range of applications including polymer chemistry,<sup>222</sup> supramolecular chemistry,<sup>211, 218, 223</sup> metal sensing,<sup>224</sup> catalysis and, significantly, drug design.<sup>210, 225-226</sup>

CuAAC is extremely useful for the formation of many organic compounds and in many cases the desired product can be isolated and purified with relative ease. However, there are a number of drawbacks and limitations associated with CuAAC. Synthetically, the removal of Cu following a reaction may be difficult and Cu may also coordinate with a reactive group present on the alkyne or azide reactants during the reaction, both removing the catalyst and leading to undesirable inorganic by-products.<sup>227-228</sup>

From a biological stand point there is significant interest in performing click reactions on a cellular level, however the Cu catalysts employed are often toxic to cells,<sup>229</sup> causing oxidative stress as they catalyse the formation of ROS.<sup>230-231</sup> Interestingly, Hong *et al.* showed that it was possible to use CuAAC for cellular surface labelling while maintaining cell viability using tris(hydroxypropyltriazolyl)methylamine (THPTA) to stabilise Cu(I) during the reaction and prevent the formation of ROS.<sup>232</sup> Other approaches and Cu stabilising ligands have been used, and although Cu(I) toxicity is somewhat reduced the methods are tedious and not compatible with *in vivo* studies. Therefore there is a demand for better designed Cu catalysts for cellular CuAAC.<sup>232-235</sup>

To overcome these limitations, the Bertozzi group established two interlinked fields of click chemistry; (i) bioorthogonal chemistry<sup>236</sup> and (ii) Cu-free click.<sup>237</sup>

### Bioorthogonal Chemistry

Within the realm of click chemistry a subclass of reactions have emerged that are biocompatible and therefore may take place within a biological system without interfering with native biological processes.<sup>238-239</sup> This family of reactions have been classified as bioorthogonal chemistry. A few examples of bioorthogonal click reactions employed include strain-promoted alkyne-azide cycloaddition (SPAAC), inverse electron-demand Diels-Alder (iEDDA) and Staudinger ligation.<sup>239</sup>

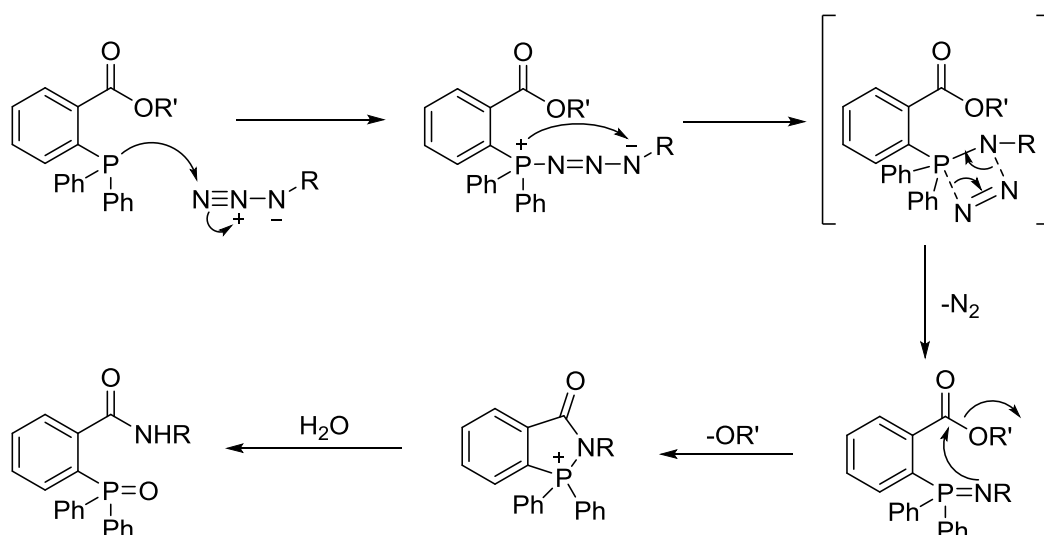


CuAAC has been at the forefront of bioorthogonal chemistry since the emergence of click chemistry but the necessity for a catalyst in a biological system is undesirable and impractical as previously discussed. This has given rise to what is known as Cu-free click chemistry; a group of truly bioorthogonal reactions which are biologically safe and require no catalyst or additional reagents to facilitate a click reaction.<sup>238</sup>

A number of criteria must be met for a compound or reaction to be considered bioorthogonal. Given that the reaction takes place in a cellular environment, the reaction must be stable to reduction in the cytosolic environment and inert to non-targeted cellular interference. The reagents cannot be water sensitive and should be stable to interactions with thiols, amines and other cellular nucleophiles. The compounds should also react readily, efficiently and rapidly at cellular temperatures.<sup>238-239</sup>

A major advantage of bioorthogonal chemistry in a living system is the fact that specific cellular sites, processes and biomolecules can be distinctly tracked and identified e.g. using a click capable probe.<sup>238-239</sup> A great number of compounds containing bioorthogonal handles (e.g. azides, cyclooctynes, cyclooctenes and tetrazines) have been synthesised and can now be modified to suit a practical need with relative ease, whether by attachment of a probe, tag or a protein.<sup>240</sup> Minor chemical modifications to the aforementioned handles facilitate control of reactivity and stability.<sup>125, 239, 241-244</sup>

Medicinally, azides were traditionally avoided for a long time as they were considered highly toxic<sup>216</sup> and are explosives when bound to heavy metals e.g. Pb (lead) and if not treated with care. However, they are now used prominently in the medicinal click chemistry field. The azide moiety is perhaps the most significant functional group in bioorthogonal chemistry due to the large number of click reactions in which it can take part in, and its relative biological inertness.<sup>237</sup>



**Scheme 1.5:** Mechanism of Staudinger ligation.<sup>245</sup>

The first example of bioorthogonal chemistry is the Staudinger ligation reaction (**Scheme 1.5**), a modified version of the Staudinger reaction<sup>246</sup> reported by the Bertozzi group. The reaction bioconjugates materials through amide bond linkage<sup>247</sup> and is the first example of bioorthogonal chemistry used in a living system.<sup>236</sup> However the reaction was limited by slow reaction rates and cellular oxidation of phosphines,<sup>229, 238</sup> leading to the development of alternative Cu-free approaches.

This section covers the Cu-free click reactions and products of prominent interest in this thesis.

### SPAAC

The most popular Cu-free click reaction is the SPAAC, whereby an azide undergoes 1,3-dipolar cycloaddition with a strained alkyne functional group, most commonly a cyclooctyne; the smallest stable cyclic alkyne.<sup>248</sup> This was first developed and reported by the Bertozzi group.<sup>237</sup> A wide range of cyclooctyne precursors were developed, such as bicyclo[6.1.0]nonyne (BCN), dibenzocyclooctyne (DIBO) and biarylazacyclooctynone (BARAC) (**Figure 1.17**). The 160° bond angle of the cyclooctyne<sup>238-239</sup> ring is key, given alkynes should typically have bond angles of 180°, as it increases the reactivity of the alkyne as a result of ring strain and therefore reacts readily with an azide without a catalyst (**Scheme 1.6**).<sup>248</sup>

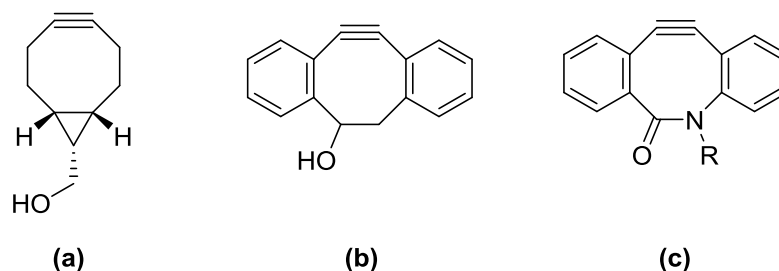
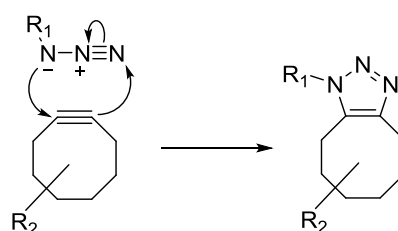


**Figure 1.17:** Structures of commonly employed strained cyclooctyne precursors (a) BCN, (b) DIBO and (c) BARAC.

There are a number of reasons why SPAAC is more desirable to CuAAC. A major driving factor outlined by McKay *et al.* is the toxicity of CuAAC, notably due to the Cu(I) ions ability to generate ROS.<sup>234</sup> SPAAC only requires two reagents for the reaction to occur, reducing the complexity of the reaction<sup>249</sup> and in turn high yields and single products tend to be produced.<sup>238</sup>



**Scheme 1.6:** SPAAC mechanism between a strained alkyne (as a cyclooctyne) and azide functional group as 1,3-dipolar cycloaddition.

There have been mixed results however, regarding improving the rate of SPAAC reactions<sup>243</sup> as compared to CuAAC reactions.<sup>79</sup> SPAAC, as with all alkyne-azide 1,3-dipolar reactions, follow 2<sup>nd</sup> order reaction rates.<sup>250</sup> The choice of strained alkyne used and modifications to respective R groups have been shown to modulate the rate of reaction.<sup>229, 251</sup> For example, BARAC (**Figure 1.17c**) derivatives are generally considered to be the fastest cyclooctynes to react with azides.<sup>252</sup>

### iEDDA

Another form of Cu-free click chemistry that is currently gaining popularity is iEDDA. Similar to SPAAC, the reaction occurs between a 3,6-disubstituted tetrazine-based heterocyclic ring and a dienophile such as a strained alkyne or a cyclic dienophile functional group (**Figure 1.18a-c**).<sup>125-126</sup> Like the previously mentioned cyclooctynes, a strained cyclic alkene moiety reacts rapidly with tetrazines due to the high level of ring strain, thus lowering the activation energy.<sup>243</sup>

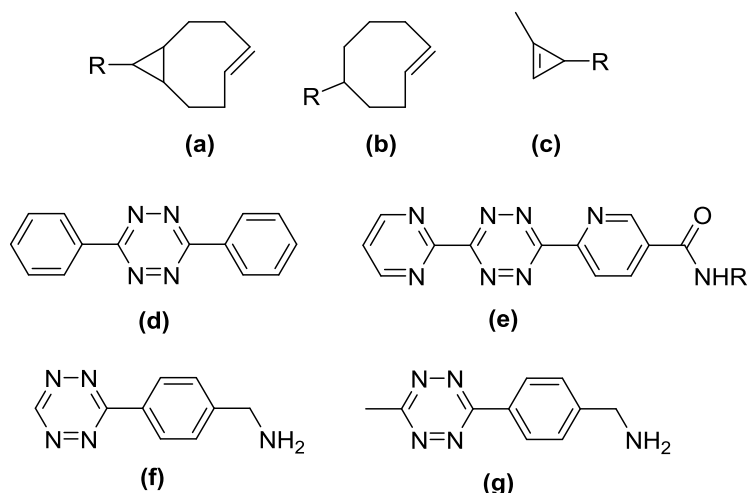
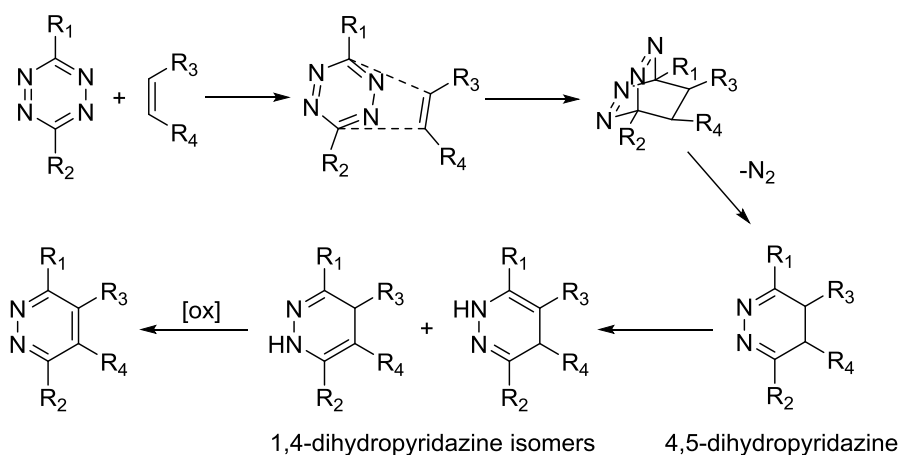


**Figure 1.18:** Examples of dienophile compounds used in iEDDA (a) *trans*-bicyclo[6.1.0]nonene, (b) *trans*-cyclooctene (TCO) and (c) 1-Methylcyclopropene (1-MCP). Commonly employed tetrazine compounds (d) diphenyltetrazine,<sup>242</sup> (e) 3,6-di(pyridin-2-yl)-1,2,4,5-tetrazine derivatives where R=functional moiety<sup>253</sup> and (f-g) 3-(benzylamino)-tetrazine derivatives.<sup>244</sup>

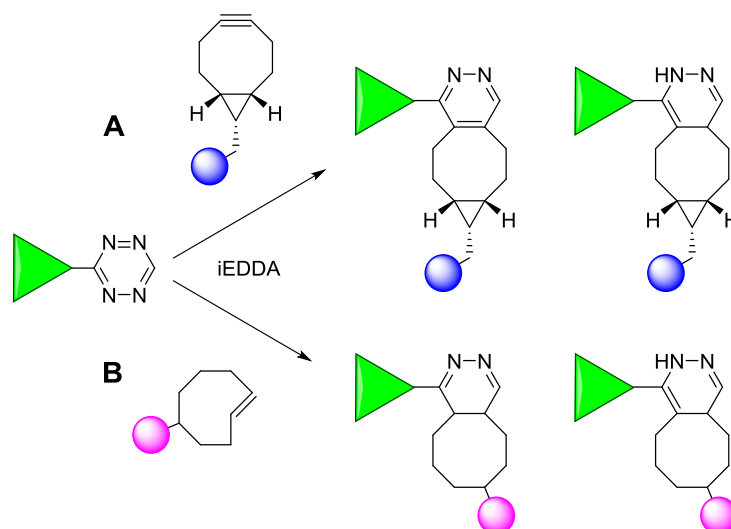
There are three predominant tetrazine ring isomers: 1,2,3,4-tetrazines, 1,2,3,5-tetrazines, and 1,2,4,5-tetrazines; also known as *v*-tetrazines, *as*-tetrazines and *s*-tetrazines respectively,<sup>254</sup> where only 1,2,4,5-tetrazines react under iEDDA conditions (**Figure 1.18d-g**). iEDDA follows a traditional inverse Diels-Alder type [4+2] cycloaddition ring forming reaction, where the tetrazine ring rearranges to form a new 6-membered ring with the loss of N<sub>2</sub> in a retro Diels-Alder reaction<sup>238</sup> (**Scheme 1.7**).<sup>243, 250</sup>



**Scheme 1.7:** Mechanism of iEDDA [4+2] inverse Diels-Alder cycloaddition between a tetrazine and dieneophile followed by retro Diels-Alder with the loss of N<sub>2</sub>.<sup>243, 250</sup>

As both alkyne (**Figure 1.17a-c**) and alkene (**Figure 1.18a-c**) groups behave as dienophiles and may be used for iEDDA, the diversity of potential products is greater than that of SPAAC. Although the iEDDA reaction with tetrazines was described as early as 1959 by Carboni and Lindsey,<sup>255</sup> it was not until the late 2000s, following the realisation of bioorthogonal click chemistry, that iEDDA was used primarily in the synthesis of pyridazine type compounds.<sup>255-256</sup> The significance of this reaction did not garner much interest until 2008, when its rapid rate of reaction in a biological system with a reactive dieneophile and its application when conjugated to a monoclonal antibody and clicked with a fluorescent probe containing a *trans*-cyclooctene was reported.<sup>257-258</sup>

The 2017 review by Oliveira and coworkers summarised the standard 2<sup>nd</sup> order reaction rates of the major click reactions in the field, showing a trend with reaction rate increasing such that: SPAAC < CuAAC < iEDDA.<sup>250</sup> It is noted that the iEDDA rate of reaction is fastest, but a number of modified SPAAC reactants did exhibit improved reaction rates relative to the CuAAC methods investigated.<sup>79, 125, 239, 243, 250, 259</sup> Similarly fine tuning of reaction rates are reported for alkyne-tetrazine reaction rates.<sup>242, 244</sup> Knall *et al.* also estimate that cyclooctene derivatives were more reactive than cyclooctyne derivatives for iEDDA.<sup>243, 250</sup>



**Scheme 1.8:** Scheme demonstrating iEDDA reaction between a tetrazine derivative and a strained cyclooctyne (A) or cyclooctene (B) derivative.

### SPAAC vs iEDDA

Much of the limiting factors for the SPAAC and iEDDA reactions are the stability and reactivity of the tetrazine and strained cyclooct-yne and -ene functional groups.

Karver *et al.* found the stability of tetrazine compounds in 37 °C FBS and PBS over 10 h varied from <5% to >60% decomposition and determined that tetrazines containing electron donating groups (EDG) are most stable.<sup>244</sup> Another report found 20% decomposition of di-2-pyridyltetrazine after 2 h in H<sub>2</sub>O.<sup>257</sup> Regardless, these cases reported excellent iEDDA reaction rates. McKay and coworkers reported on many of the limitations of the cyclooctyne class of compounds.<sup>79</sup> BARAC compounds were found to have a limiting  $t_{1/2}$  of 24 h in PBS where they undergo hydrolysis and are subject to molecular rearrangement,<sup>260</sup> while BCN showed poor stability in solution with only 6% of the starting compound remaining after 24 h.<sup>125</sup> Nucleophilic addition reactions in cells are observed, where for example nucleophiles such as glutathione and the sulphenic acid of cysteine residues react with the strained alkyne.<sup>261-263</sup>

One report demonstrated a practical limitation, showing that a high concentration of BCN and DBCO derivatised fluorophores were required for cellular labelling and the high background fluorescent labelling observed limited the use of SPAAC *in lieu* of iEDDA.<sup>125</sup> Murrey *et al.* also reported a drawback associated with iEDDA, due to potential products formed in the reaction due to specific organelle stability of TCO groups in addition to the poor shelf life of the TCO groups.

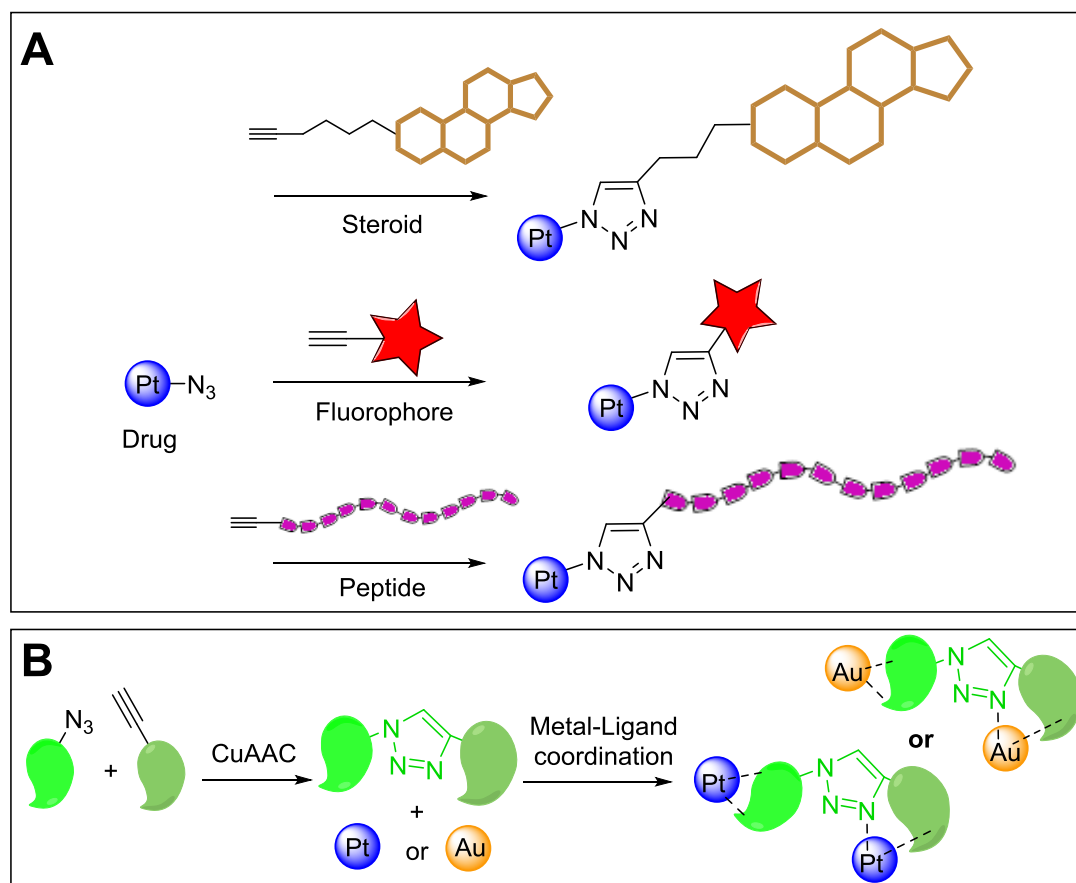
### Conjugation of Bioactive molecules

This thesis focuses on utilising click chemistry for A) bioconjugation of a click capable Pt drug to a moiety with a secondary functionality and B) development of novel ligand scaffolds to expand on the interesting coordination chemistry of triazole complexes.

Regarding A, the topics that will be further discussed and investigated throughout this work are the use of click chemistry to conjugate a Pt drug containing a reactive handle to (i) a fluorescent probe to track its movement and localisation and (ii), a

targeting peptide/steroid to enhance its selectivity for and uptake by cancer cells, (**Scheme 1.9A**).

Regarding B, novel 1,4-disubstituted 1,2,3 triazole based polydentate ligands will be designed and synthesised and their reactivity with Pt(II) and Au(III) centres investigated, (**Scheme 1.9B**).



**Scheme 1.9:** Click conjugation reactions between metals and ligands. **A:** Conjugation of functional molecules to Pt drugs. **B:** Polydentate ligand synthesis and coordination to Pt or Au.

### Clicked Pt-fluorophore compounds

Fluorescent probes are frequently used in research to identify key biomolecules associated with diseases such as cancer, and determine cellular transportation mechanisms to better understand how drugs interact with diseased cells. In addition, fluorophores are some of the most frequently used functional units in bioorthogonal click chemistry, due in part to the simplicity by which they can be modified as probes.<sup>96, 125</sup> The 2014 review of McKay *et al.* describes the vast use of CuAAC and

Cu-free methods which employ fluorophores to prepare bifunctional therapeutic and diagnostic agents. Within the current literature, there is a niche for fluorescent tagging of metals, with Pt being of major interest in this work.

The deRose research group have been one of the key players in this area, reviewing the click Pt fluorophore topic in 2015<sup>264</sup> and reporting a number of post-treatment CuAAC click reactions of Pt complexes with fluorophores.<sup>265-266</sup> These Pt-fluorophores (**Figure 1.19a-b**) have been used to detect the formation of Pt-DNA adducts as well as for imaging of HeLa cells post-treatment.

Zhang *et al.* reported a Pt(IV) complex prepared from a mono substituted azide handle in the axial ligand position capable of undergoing a CuAAC click reaction with a secondary component (**Figure 1.19c**); in this instance an alkyne-anthraquinone fluorophore,<sup>267</sup> but interestingly, no cellular study, fluorescent testing or imaging was undertaken, and the work remains a proof of concept.

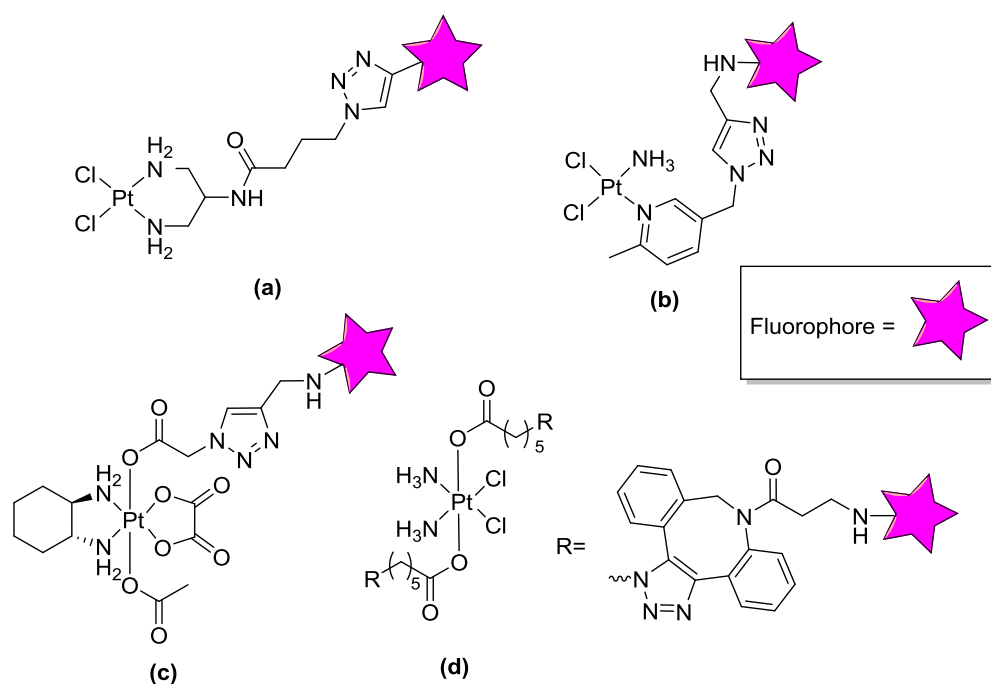


**Figure 1.19:** Examples of clicked Pt-fluorophore complexes generated from (a) *cis*-[Pt(2-azidobutyl)amido-1,3-propanediamine]Cl<sub>2</sub> with rhodamine or dansyl fluorophores,<sup>265</sup> (b) picazoplatin with dansyl fluorophore,<sup>266</sup> (c) [Pt(azidoacetic acid)(acetato)(DACH)(ox)] with anthraquinone fluorophore<sup>267</sup> and (d) [PtCl<sub>2</sub>(NH<sub>3</sub>)<sub>2</sub>(valeric-ABIDO-cy5.5)], Platin-cy5.5 reporter.<sup>217</sup>



Pathak and coworkers went a step further and synthesised the Pt(IV) complex Platin-Az, with a five carbon spacer (azido-valeric acid) axial ligand.<sup>217</sup> The addition of a spacer group is a common approach if the secondary handle is believed to interfere with or be interfered by the Pt drug. In this instance, given Pt can act as a fluorescent quencher, a spacer was added.<sup>83</sup> They utilised a cy5.5 functionalised ABIDO (azadibenzocyclooctyne) derivative to synthesise their fluorescent derivative *via* SPAAC and report a theranostic agent, Platin-cy5.5 (**Figure 1.19d**). The complex was visualised by live cell imaging in PC3 cells.<sup>217</sup> Although it was possible to track the live uptake and transport of the Platin-cy5.5, the IC<sub>50</sub> values of the ABIDO clicked Pt complex (without the fluorophore attached) was found to be lower compared to cisplatin and the unconjugated Platin-Az, and therefore the cytotoxicity of Platin-cy5.5 was not investigated.<sup>217</sup> Furthermore, the Platin-cy5.5 retained the strong NIR fluorescent properties of the free cy5.5 with an absorbance of 685 nm.

All of these particular examples are highly functional, but due to choice of fluorophores many fall outside of the desirable NIR range of interest for *in vivo* work.

## Targeted Pt Drug Delivery

The bifunctionalization of Pt drugs has been explored extensively since the turn of the millennium. As previously discussed, the limitations and side effects of the currently available Pt based anticancer therapies have driven the development of novel bifunctional drug candidates. A number of strategies have been developed in relation to this, many of which explore the conjugation of a bioactive moiety to Pt drugs to improve their anticancer properties. For improved targeting purposes examples include monoclonal antibodies,<sup>268-269</sup> sugars and carbohydrate units,<sup>80, 270</sup> hormones<sup>80, 271</sup> and peptide residues.<sup>195, 272-273</sup>

Cancer cells have a number of specific cellular distinctions to healthy ones, cancer type depending, which give cancer a distinct survival advantage. Upregulation or over-expression of metal ion receptors, homeostatic proteins and enzymes and hormone receptors to name a few may be exploited<sup>271</sup> and targeted to more effectively deliver a therapeutic payload.

For instance, colorectal cancers may have increased level of proteins such as HSP70.<sup>68</sup> It is also well known that hormones play a major role in cancer progression in prostate,<sup>274</sup> ovarian<sup>275</sup> and breast<sup>80, 276-277</sup> cancers, and in turn these cells have an increased level of steroid hormone receptors i.e. ER and AR.<sup>205</sup>

In this thesis, I investigated Pt-peptide and Pt-steroid derivatives with the aim of enhancing targeting and localisation of Pt drugs towards cancer cells.

### Pt-peptide conjugates

Pt-peptide conjugates have become a prominent topic in anticancer research with a number of new active complexes being reported for their ability to target cancer cells and improve anticancer activity.<sup>195, 272</sup> In many instances, the mechanism of conjugation is through cross-coupling *via* amide bond formation and also through click chemistry. It is also possible for Pt to form complexes directly with amino acid residues, predominantly through the amino groups but also through R group side chains which contain carboxylic acids or thiols for example.<sup>278-279</sup>

The first example of Pt-peptide conjugates developed for the purpose of tumour targeting was reported by the Lippard research group where tripeptide (RGD (**Figure 1.20a**) and NGR (asparagine-glycine-arginine) (**Figure 1.20b**)) targeting motifs were conjugated to a Pt(IV) cisplatin analogue through the axial ligands. The Pt(IV) peptide conjugates exhibited cytotoxicity against cancer cell lines, although to a lesser extent than cisplatin, the control.<sup>280</sup>

Subsequently, there have been a number of successful reports of targeting Pt(IV)-peptide conjugates. Gaviglio *et al.* synthesised two sets of mono- and di-conjugated Pt(IV)-peptide targeting complexes using two peptides; pseudo-neurotensin (pNT) (**Figure 1.20c**) as a targeting group for the NTR1 and NTR3 neurotensin receptors and the cyclic peptide octreotate, an analogue of somatostatin, the receptors (SSTRs) (**Figure 1.20d**) for which are upregulated in a number of cancers.<sup>281</sup> The cytotoxicity testing also demonstrated extremely positive improvements on cytotoxicity in most instances compared with the parent Pt(IV) complex in MCF-7, Panc1, HepG2 and PT45 cell lines. There was also inconsistency as to whether the mono- or di-conjugated Pt-peptide exhibited improved IC<sub>50</sub> values.<sup>281</sup>

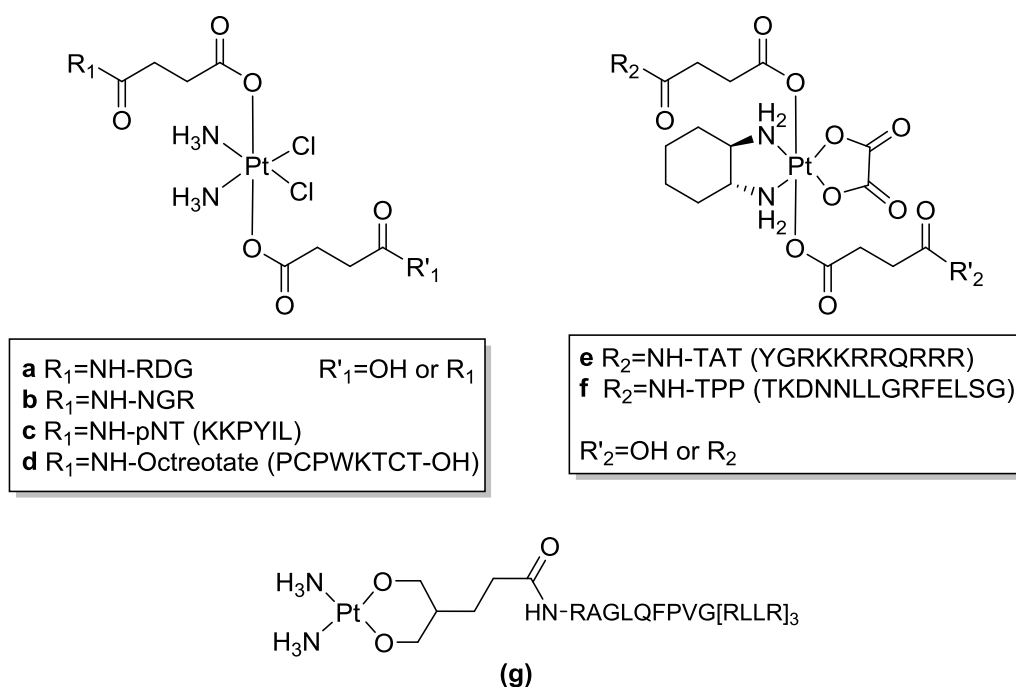


**Figure 1.20:** Recent Pt-peptide conjugates with dual functionality. Pt(IV) di-conjugates **(a-d)**  $[\text{PtCl}_2(\text{NH}_3)_2(\text{succ-R}_1)_2]$ ,<sup>280-281</sup> **(e-f)**  $[\text{Pt}(\text{DACH})(\text{Ox})(\text{succR}_2)_2]$ <sup>195, 272</sup> and **(g)** Pt(II) *cis*- $[\text{Pt}(\text{NH}_3)_2(\text{malBuf-2H})]$ .<sup>282</sup> In the instances of **a** to **f** a mono- and di-conjugated Pt-peptide may occur.

In addition the Keppler research group developed the first oxaliplatin tumour targeting Pt(IV)-peptide conjugate by conjugating the eleven amino acid TAT to an axial succinic acid ligand. This resulted in much improved cytotoxicity (up to 39 times more cytotoxic) of the Pt-peptide conjugate (**Figure 1.20e**) compared to the unconjugated precursor in the CH1, A549, SW480 and SK-OV-3 cell lines.<sup>272</sup>

Within our research group Aoife McKeon has already progressed the applications of the oxaliplatin based Pt(IV) conjugates<sup>195</sup> using the recently reported TPP (**Figure 1.20f**), which was developed to target the over expression of memHSP70 in colorectal cancer cells.<sup>194</sup> This demonstrated an enhanced anticancer effect and improved tumour selectivity of Pt-peptide conjugates in Pt resistant colorectal cancer cell lines, with respect to the clinical standard oxaliplatin.<sup>195</sup>

Pt(II)-peptides have also been synthesised, for example the Pt(II) conjugate of the cell penetrating and anti-proliferation peptide buforin IIb malonate derivative (malBuf) (**Figure 1.20g**) reported by Parker *et al.*<sup>282</sup>

In a separate instance Parker *et al.* had previously attempted a CuAAC click Pt-peptide conjugation reaction between a Pt(II) malonate-alkyne derivative and an azide functionalised peptide. The reaction was unsuccessful likely due to unfavourable interactions between the ligand, Pt source and Cu catalyst.<sup>228</sup> This shows the current limitations of Pt-peptide click strategies. However, other metal complexes have shown the ability to undergo click reactions to coordinate a peptide moiety directly, although yields varied and not all instances were successful.<sup>283</sup> It is also noteworthy that one of the earliest reports (2002) of click chemistry was to derivatise the cancer biomarker peptide, bombesin, *via* CuAAC with other functional units (as previously mentioned).<sup>220</sup> It is clear from the limited progression of clicked Pt-peptide conjugates in the 16 years since their first use in peptide chemistry that click chemistry may not represent an ideal strategy for conjugating Pt moieties to peptides directly.

Despite the limitations of these direct Pt click approaches, it is still possible to utilise click chemistry to generate a ligand or conjugation platform for a peptide of interest, in addition to peptide structural mimics.<sup>284</sup> For example a RAFT (regioselectively addressable functionalized template)-RGD targeting peptide ligand was successfully clicked to a Pt moiety using CuAAC by Massaguer *et al.* The RAFT was functionalised with four alkyne moieties and was clicked with an azide derivatised RGD peptide before conjugating to Pt, forming Pt(IV)-RAFT-[c(RGDfK)]<sub>4</sub>, which gave enhanced anticancer activity as compared to cisplatin and the single peptide derivative, Pt(IV)-[c(RGDfK)], in a number of instances.<sup>273</sup>

### **Pt-steroid conjugates**

The use of hormones and steroid drug conjugates is not a new strategy in anticancer treatments, with hormone therapy being prominent in the treatment of thyroid, breast and prostate cancer for instance.<sup>7</sup> As mentioned, many of the cancers in these organs have a high demand for endogenous steroids such as estradiol and testosterone and their exogenous derivatives.<sup>22</sup> As such these receptors are a strong target<sup>205</sup> for Pt based steroid conjugates. Different strategies of targeting and dual therapy that have been explored previously are described below.<sup>285</sup>

As early as the 1980s and 90s, Pt(II)-steroid complexes were being investigated for anticancer activity.<sup>286-287</sup> Many of the approaches undertaken investigate hormone receptor binding (e.g. AR and ER) and cellular cytotoxicity (**Figure 1.21**).

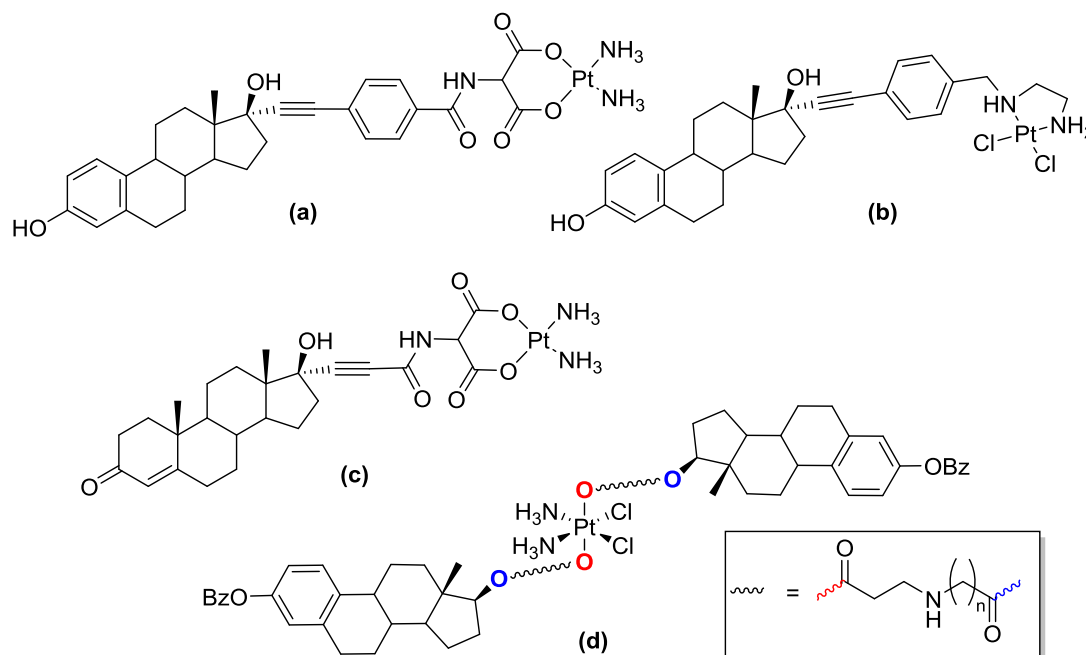


**Figure 1.21:** Examples of Pt-steroid complexes. (a-b) Pt(II) estrogen derivatives,<sup>288</sup> (c) Pt(II) malonate-testosterone derivative<sup>287</sup> and (d) Pt(IV) estrogen derivative.<sup>271</sup>

Previous studies demonstrate that co-administration and pre-treatment of cancer cells with estradiol improves Pt sensitivity,<sup>209</sup> but many of these Pt conjugates do not improve on overall activity when compared with cisplatin alone or co-administration treatments. In addition, at low Pt-steroid concentrations, cell growth increased in a number of instances, given the function of steroids in tumour growth.<sup>80, 285</sup>

**Figure 1.21d** shows a Pt(IV)-estrogen model which gave enhanced cytotoxic activity against breast cancer cell lines MCF-7 (ER(+)) as compared to HCC-1937(ER(-)). All derivatives tested gave  $\text{IC}_{50}\text{s} < 5.5 \mu\text{M}$  and also led to an upregulation of the high-mobility group (HMG) HMGB1, which is indicative of DNA damage and reduction of the Pt(IV) complex to Pt(II) within the cell.<sup>271</sup>

There has been extensive research carried out on estrogen derivatives for conjugation to Pt complexes, however there has been limited research and synthesis of non-estrogen derivatives e.g. testosterone, as evident in the reviews of Gust *et al.* and Johnstone *et al.*

Although a number of steroids with modified click handles have previously been investigated,<sup>289-290</sup> no click chemistry based approach has been explored, to the best of our knowledge, to generate a Pt-steroid complex.

## Metal Chelating systems

As previously mentioned, metal triazole complexes have a wide range of applications in this field such as catalysis, sensing, imaging and therapy.<sup>212, 291</sup> Triazoles can be modified easily to form multidentate ligands and in turn on reaction with selected metals the corresponding coordination complexes. The 1,2,3-triazole heterocyclic ring readily coordinates metal centres through a variety of modes; N2, N3 and C5 coordination for instance (**Figure 1.22**). Furthermore, selective alkylation (e.g. methylation) of 1,2,3-triazoles generates the corresponding 1,2,3-triazolylienes, which can be metalated to give the corresponding 1,2,3-triazolyliene coordination complexes (**Figure 1.22**).

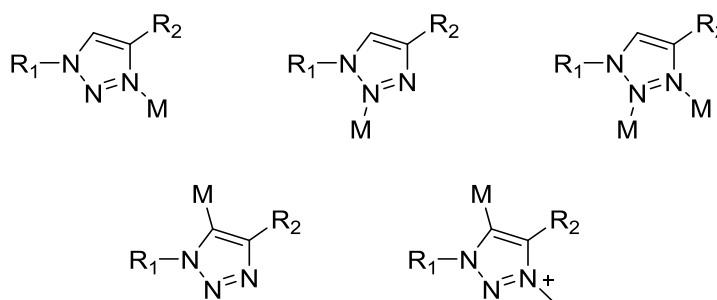


**Figure 1.22:** Metal coordination modes associated with 1,4-disubstituted 1,2,3-triazole ligands.

Schibli coined the phrase “click to chelate” and the Schibli group for example developed a technetium (<sup>99m</sup>Tc) triazole complex tethered to folic acid (**Figure 1.23a**). <sup>99m</sup>Tc is a metastable nuclear isomer of Technetium-99, which is used for SPECT, while folic acid is a targeting group. An azide derivative of folic acid was clicked with a terminal alkyne derivative of L-propargyl glycine to generate a 1,4-disubstituted 1,2,3-triazole as a tridentate ligand. This triazole essentially substituted a histidine group present in an established <sup>99m</sup>Tc tridentate ligand, **Figure 1.23a**. *In vivo* testing showed that the triazole-containing <sup>99m</sup>Tc complex gave equivalent imaging results to the histidine derivative, however the clicked triazole ligand was

synthesised in higher yield and fewer synthetic steps than the corresponding histidine ligand.<sup>99</sup>

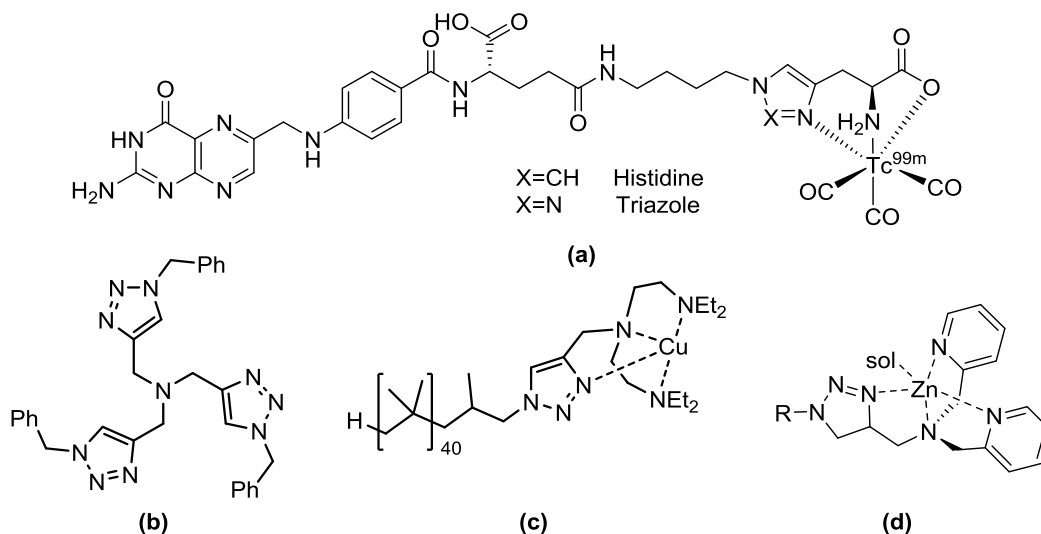


**Figure 1.23:** Metal functionalised triazole complexes (a) folic acid tagged  $^{99m}\text{Tc}$ ,<sup>99</sup> (b) triazole containing ligand, TBTA, which chelates catalytic Cu(I)<sup>292</sup> and (c) polymer supported triazole containing Cu(I) catalyst<sup>293</sup> and (d) Zn ion detecting polydentate ligand, where R=anthracene or *p*-anisoyl.<sup>224</sup>

Triazole based ligands were discovered serendipitously on attempting to improve the catalytic properties of Cu(I) in CuAAC reactions.<sup>292</sup> The tetradentate ligand *tris*-(benzyltriazolylmethyl)amine (TBTA) for example is believed to act by increasing the electron density of Cu(I) *via* the amine which further facilitates the formation of the Cu-acetylide complex, essential to the mechanism of CuAAC (**Figure 1.23b**).<sup>212</sup> Catalytic incorporation of Cu(I) into a triazole linked polymer resin has been employed in a similar manner (**Figure 1.23c**).<sup>293</sup> A number of potential transition metal catalysts of Pd, Ru, Rh and Ir have also been stabilised through triazole ligand complexation.<sup>294</sup>

Complexation of metals with a number of triazole containing ligands has been shown to display distinct fluorescent properties, leading to their use in metal ion detection.<sup>212</sup> Zhu *et al.* developed a number of polydentate triazole containing ligands used as Zn(II) sensors (**Figure 1.23d**). The ligands bind to a number of divalent metals e.g. Fe(II), Mg(II), but demonstrate selectivity for Zn(II) over other divalent ions in solution. Fluorescence increases significantly upon complexation with Zn(II) in addition to a shift in the emission maxima wavenumber.<sup>224</sup> A multitude of metal

ions including  $\text{Mg}^{2+}$ ,  $\text{Fe}^{2+}$ ,  $\text{Co}^{2+}$ ,  $\text{Cu}^{2+}$ ,  $\text{Ni}^{2+}$ ,  $\text{Ag}^+$ ,  $\text{Pb}^{2+}$  and  $\text{Hg}^{2+}$  may also be detected through triazole based metal responsive complex fluorescence. Interestingly, some of the metal ions are inversely detected by the reduction in fluorescence following coordination.<sup>295-298</sup> It is believed that the metal ions alter the fluorescence through these coordination interactions, leading to fluorescent quenching or enhancement.<sup>212</sup> 2-pyridyl-1,2,3-triazoles and 2,6-pyridyl-bis(1,2,3-triazole)s are of particular interest in coordination chemistry as they behave and bind with metals in a similar manner to the 2,2'-bipyridine (bipy) and 2,2':6',2''-terpyridine (terpy) ligands. Second and third row transition metal complexes of these substituted triazole ligands exhibit similar photophysical properties to their parent bipy or terpy complexes.<sup>214, 299</sup>

The Crowley and Elliot research groups have investigated a number of interesting triazole complexes for sensing and light-emitting purposes, as potential antibacterial and anticancer agents.

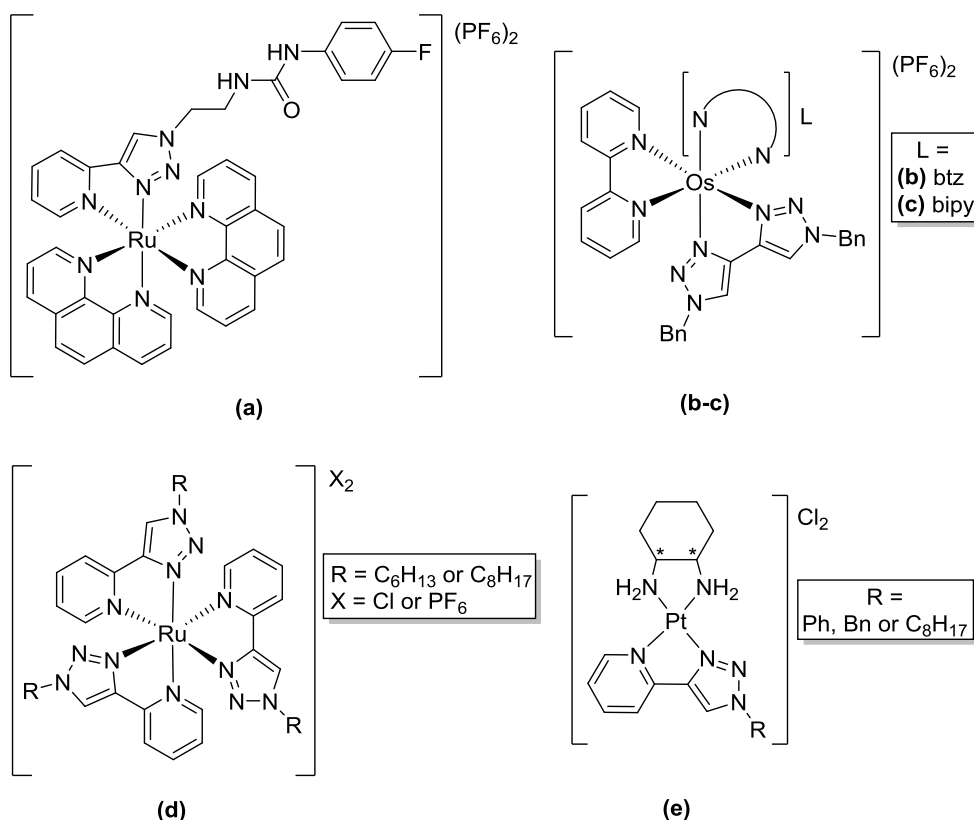


**Figure 1.24:** Metal triazole-based light-emitting and therapeutic complexes. (a)  $[\text{Ru}(\text{phen})_2(\text{pyridine-triazole-4-fluorophenyl urea})](\text{PF}_6)_2$ ,<sup>300</sup> (b)  $[\text{Os}(\text{bipy})(\text{btz})_2](\text{PF}_6)_2$ , (c)  $[\text{Os}(\text{bipy})_2(\text{btz})](\text{PF}_6)_2$ ,<sup>301</sup> (d)  $[\text{Ru}(\text{R-pyridine-triazole})_3]\text{X}_2$ ,<sup>302</sup> and (e)  $[\text{Pt}(\text{DACH})(2\text{-pyridyl-triazole-R})]\text{Cl}_2$ .<sup>303</sup>



Ghosh *et al.* developed a Ru(II) triazole-phenanthroline photochemical sensor (**Figure 1.24a**). The complex was also capable of ion extraction from solutions of oxyanions, including phosphates and carboxylates; however only the phosphate anion could be selectively sensed.<sup>300</sup>

In 2017, Elliot and coworkers<sup>299</sup> reviewed the various recent Rh, Ir, Os and Ru triazole complexes and their diverse selection of photophysical properties. They also developed two light-emitting electrochemical cells made from Os complexes containing bipy and di-(benzyl-triazole) (btz) ligands, which possessed NIR emission wavelengths of 713 and 724 nm, **Figures 1.24b** and **c** respectively. The two performed as extremely efficient fluorophores when compared to their Ru derivatives; however they suffered from poor stability, limiting their practical application.<sup>301</sup>

The complex  $[\text{Ru}(\text{R-pytri})_3]\text{X}_2$  (**Figure 1.24d**) was found to have antibacterial activity against a number of strains, including against Methicillin-Resistant *Staphylococcus aureus* (MRSA).<sup>302</sup>

Pages *et al.* have also synthesised a number of Pt(II) triazole based derivatives (**Figure 1.24e**) which displayed positive results against a series of different cancer cell lines and gave similar  $\text{IC}_{50}$  values to the three Pt drugs: cisplatin, carboplatin and oxaliplatin.<sup>303</sup>

## Conclusion

The formation of novel multifunctional metal complexes is of avid interest in many fields of chemistry. It is now easier than ever to combine separate functional units such as peptides, fluorophores and steroids, together into a single molecule. The reviewed work described shows the numerous attempts and strategies which have been explored to generate these complexes, with particular focus on Pt based anticancer agents. Click chemistry is an extremely versatile method which can be employed to generate these novel complexes, with relative ease.

## References

1. *National Cancer Registry Ireland* **2017**.
2. *World Health Organisation* **2018**.
3. Cancer Facts & Figures 2017. *American Cancer Society* **2017**.
4. White, M. C.; Holman, D. M.; Boehm, J. E.; Peipins, L. A.; Grossman, M.; Henley, S. J., Age and Cancer Risk: A Potentially Modifiable Relationship. *American journal of preventive medicine* **2014**, 46 (301), S7-15.
5. *Irish Cancer Society* **2014**.
6. What is Cancer? *National Cancer Institute* **2015**.
7. Miller Kimberly, D.; Siegel Rebecca, L.; Lin Chun, C.; Mariotto Angela, B.; Kramer Joan, L.; Rowland Julia, H.; Stein Kevin, D.; Alteri, R.; Jemal, A., Cancer treatment and survivorship statistics, 2016. *CA: A Cancer Journal for Clinicians* **2016**, 66 (4), 271-289.
8. Wilde, K. P. B. a. J., A report on All-Ireland mortality Data. Ireland, T. I. o. P. H. i., Ed. The Institute of Public Health in Ireland.: 2001.
9. Colorectal Cancer Facts & Figures 2017-2019. *American Cancer Society* **2017**.
10. Hammond, W. A.; Swaika, A.; Mody, K., Pharmacologic resistance in colorectal cancer: a review. *Therapeutic Advances in Medical Oncology* **2016**, 8 (1), 57-84.
11. Dasari, S.; Tchounwou, P. B., Cisplatin in cancer therapy: molecular mechanisms of action. *European journal of pharmacology* **2014**, 0, 364-378.
12. Kigawa, J., New Strategy for Overcoming Resistance to Chemotherapy of Ovarian Cancer. *Yonago Acta medica* **2013**, 56 (2), 43-50.
13. Galluzzi, L.; Vitale, I.; Michels, J.; Brenner, C.; Szabadkai, G.; Harel-Bellan, A.; Castedo, M.; Kroemer, G., Systems biology of cisplatin resistance: past, present and future. *Cell Death & Disease* **2014**, 5 (5), e1257.
14. Piccart, M. J.; Bertelsen, K.; James, K.; Cassidy, J.; Mangioni, C.; Simonsen, E.; Stuart, G.; Kaye, S.; Vergote, I.; Blom, R.; Grimshaw, R.; Atkinson, R. J.; Swenerton, K. D.; Trope, C.; Nardi, M.; Kaern, J.; Tumolo, S.; Timmers, P.; Roy, J. e.-A.; Lhoas, F. o.; Lindvall, B.; Bacon, M.; Birt, A.; Andersen, J. E.; Zee, B.; Paul, J.; Baron, B. T.; Pecorelli, S., Randomized Intergroup Trial of Cisplatin–Paclitaxel Versus Cisplatin–Cyclophosphamide in Women With Advanced Epithelial Ovarian Cancer: Three-Year Results. *JNCI: Journal of the National Cancer Institute* **2000**, 92 (9), 699-708.
15. Marley, A. R.; Nan, H., Epidemiology of colorectal cancer. *International Journal of Molecular Epidemiology and Genetics* **2016**, 7 (3), 105-114.
16. Coleman, R. L.; Monk, B. J.; Sood, A. K.; Herzog, T. J., Latest research and clinical treatment of advanced-stage epithelial ovarian cancer. *Nature reviews. Clinical oncology* **2013**, 10 (4), 211-224.
17. Vergote, I.; Tropé, C. G.; Amant, F.; Kristensen, G. B.; Ehlen, T.; Johnson, N.; Verheijen, R. H. M.; van der Burg, M. E. L.; Lacave, A. J.; Panici, P. B.; Kenter, G. G.; Casado, A.; Mendiola, C.; Coens, C.; Verleye, L.; Stuart, G. C. E.; Pecorelli, S.; Reed, N. S., Neoadjuvant Chemotherapy or Primary Surgery in Stage IIIC or IV Ovarian Cancer. *New England Journal of Medicine* **2010**, 363 (10), 943-953.
18. Formenti, S. C.; Demaria, S., Combining Radiotherapy and Cancer Immunotherapy: A Paradigm Shift. *JNCI: Journal of the National Cancer Institute* **2013**, 105 (4), 256-265.
19. Radiation Therapy to Treat Cancer. *National Cancer Institute* **2017**.
20. Paumier, A.; Le Péchoux, C., Post-operative radiation therapy. *Translational Lung Cancer Research* **2013**, 2 (5), 423-432.
21. Effects of radiotherapy and of differences in the extent of surgery for early breast cancer on local recurrence and 15-year survival: an overview of the randomised trials. *The Lancet* **2005**, 366 (9503), 2087-2106.
22. Hormone Therapy to Treat Cancer. *National Cancer Institute* **2015**.
23. Anzick, S. L.; Kononen, J.; Walker, R. L.; Azorsa, D. O.; Tanner, M. M.; Guan, X.-Y.; Sauter, G.; Kallioniemi, O.-P.; Trent, J. M.; Meltzer, P. S., AIB1, a Steroid Receptor Coactivator Amplified in Breast and Ovarian Cancer. *Science* **1997**, 277 (5328), 965.

24. Mantovani, A.; Allavena, P.; Sica, A.; Balkwill, F., Cancer-related inflammation. *Nature* **2008**, *454*, 436.
25. Heinlein, C. A.; Chang, C., Androgen Receptor in Prostate Cancer. *Endocrine Reviews* **2004**, *25* (2), 276-308.
26. Howlader, N.; Altekruse, S. F.; Li, C. I.; Chen, V. W.; Clarke, C. A.; Ries, L. A. G.; Cronin, K. A., US Incidence of Breast Cancer Subtypes Defined by Joint Hormone Receptor and HER2 Status. *JNCI Journal of the National Cancer Institute* **2014**, *106* (5), dju055.
27. How to Read Hormone Receptor Test Results. *Breastcancer.org* **2017**.
28. Bruno, P. M.; Liu, Y.; Park, G. Y.; Murai, J.; Koch, C. E.; Eisen, T. J.; Pritchard, J. R.; Pommier, Y.; Lippard, S. J.; Hemann, M. T., A subset of platinum-containing chemotherapeutic agents kills cells by inducing ribosome biogenesis stress. *Nat. Med.* **2017**, *23* (4), 461-471.
29. André, T.; Boni, C.; Mounedji-Boudiaf, L.; Navarro, M.; Tabernero, J.; Hickish, T.; Topham, C.; Zaninelli, M.; Clingan, P.; Bridgewater, J.; Tabah-Fisch, I.; de Gramont, A., Oxaliplatin, Fluorouracil, and Leucovorin as Adjuvant Treatment for Colon Cancer. *New England Journal of Medicine* **2004**, *350* (23), 2343-2351.
30. Orvig, C.; Abrams, M. J., Medicinal Inorganic Chemistry: Introduction. *Chemical Reviews* **1999**, *99* (9), 2201-2204.
31. Ernst, E., Toxic heavy metals and undeclared drugs in Asian herbal medicines. *Trends in Pharmacological Sciences* **2002**, *23* (3), 136-139.
32. Gaynor, D.; Griffith, D. M., The prevalence of metal-based drugs as therapeutic or diagnostic agents: beyond platinum. *Dalton Transactions* **2012**, *41* (43), 13239-13257.
33. Pearson, R. G., Hard and soft acids and bases and joe chatt. In *Modern Coordination Chemistry: The Legacy of Joseph Chatt*, Leigh, G. J.; Winterton, N., Eds. The Royal Society of Chemistry: 2002; pp 305-312.
34. Basolo, F., Mechanisms of platinum reactions. In *Modern Coordination Chemistry: The Legacy of Joseph Chatt*, Leigh, G. J.; Winterton, N., Eds. The Royal Society of Chemistry: 2002; pp 313-327.
35. Reedijk, J., New clues for platinum antitumor chemistry: Kinetically controlled metal binding to DNA. *Proceedings of the National Academy of Sciences* **2003**, *100* (7), 3611.
36. Roundhill, D. M., *Comprehensive Coordination Chemistry*. Pergamon: Oxford: **1987**; Vol. 5.
37. Shaw, C. F., Gold-Based Therapeutic Agents. *Chemical Reviews* **1999**, *99* (9), 2589-2600.
38. Rosenberg, B.; Vancamp, L.; Trosko, J. E.; Mansour, V. H., Platinum Compounds: a New Class of Potent Antitumour Agents. *Nature* **1969**, *222*, 385.
39. Gately, D. P.; Howell, S. B., Cellular accumulation of the anticancer agent cisplatin: A review. *British Journal Of Cancer* **1993**, *67*, 1171.
40. Ishida, S.; Lee, J.; Thiele, D. J.; Herskowitz, I., Uptake of the anticancer drug cisplatin mediated by the copper transporter Ctr1 in yeast and mammals. *Proceedings of the National Academy of Sciences of the United States of America* **2002**, *99* (22), 14298-14302.
41. Holzer, A. K.; Manorek, G. H.; Howell, S. B., Contribution of the Major Copper Influx Transporter CTR1 to the Cellular Accumulation of Cisplatin, Carboplatin, and Oxaliplatin. *Molecular Pharmacology* **2006**, *70* (4), 1390.
42. Bancroft, D. P.; Lepre, C. A.; Lippard, S. J., Platinum-195 NMR kinetic and mechanistic studies of cis- and trans-diamminedichloroplatinum(II) binding to DNA. *Journal of the American Chemical Society* **1990**, *112* (19), 6860-6871.
43. Eastman, A., The formation, isolation and characterization of DNA adducts produced by anticancer platinum complexes. *Pharmacology & Therapeutics* **1987**, *34* (2), 155-166.
44. Gavande, N. S.; VanderVere-Carozza, P. S.; Hinshaw, H. D.; Jalal, S. I.; Sears, C. R.; Pawelczak, K. S.; Turchi, J. J., DNA repair targeted therapy: The past or future of cancer treatment? *Pharmacology & Therapeutics* **2016**, *160*, 65-83.

45. Siddik, Z. H., Cisplatin: mode of cytotoxic action and molecular basis of resistance. *Oncogene* **2003**, 22 (47), 7265-7279.
46. Kelland, L. R., New platinum antitumor complexes. *Critical Reviews in Oncology/Hematology* **1993**, 15 (3), 191-219.
47. Pinto, A. L.; Lippard, S. J., Binding of the antitumor drug cis-diamminedichloroplatinum(II) (cisplatin) to DNA. *Biochimica et Biophysica Acta (BBA) - Reviews on Cancer* **1985**, 780 (3), 167-180.
48. Shuck, S. C.; Short, E. A.; Turchi, J. J., Eukaryotic nucleotide excision repair, from understanding mechanisms to influencing biology. *Cell research* **2008**, 18 (1), 64-72.
49. Basu, A.; Krishnamurthy, S., Cellular Responses to Cisplatin-Induced DNA Damage. *Journal of Nucleic Acids* **2010**, 2010, 201367.
50. Galluzzi, L.; Vitale, I.; Michels, J.; Brenner, C.; Szabadkai, G.; Harel-Bellan, A.; Castedo, M.; Kroemer, G., Systems biology of cisplatin resistance: past, present and future. *Cell Death & Disease* **2014**, 5 (5), e1257.
51. Johnstone, R. W.; Ruefli, A. A.; Lowe, S. W., Apoptosis: A Link between Cancer Genetics and Chemotherapy. *Cell* **2002**, 108 (2), 153-164.
52. Oun, R.; Moussa, Y. E.; Wheate, N. J., The side effects of platinum-based chemotherapy drugs: a review for chemists. *Dalton Transactions* **2018**, 47 (19), 6645-6653.
53. Windebank, A. J.; Grisold, W., Chemotherapy-induced neuropathy. *Journal of the Peripheral Nervous System* **2008**, 13 (1), 27-46.
54. Muggia, F., Platinum compounds 30 years after the introduction of cisplatin: Implications for the treatment of ovarian cancer. *Gynecologic Oncology* **2009**, 112 (1), 275-281.
55. Crystal, A. S.; Shaw, A. T.; Sequist, L. V.; Friboulet, L.; Niederst, M. J.; Lockerman, E. L.; Frias, R. L.; Gainor, J. F.; Amzallag, A.; Greninger, P.; Lee, D.; Kalsy, A.; Gomez-Caraballo, M.; Elamine, L.; Howe, E.; Hur, W.; Lifshits, E.; Robinson, H. E.; Katayama, R.; Faber, A. C.; Awad, M. M.; Ramaswamy, S.; Mino-Kenudson, M.; Iafrate, A. J.; Benes, C. H.; Engelman, J. A., Patient-derived models of acquired resistance can identify effective drug combinations for cancer. *Science* **2014**, 346 (6216), 1480.
56. Galluzzi, L.; Senovilla, L.; Vitale, I.; Michels, J.; Martins, I.; Kepp, O.; Castedo, M.; Kroemer, G., Molecular mechanisms of cisplatin resistance. *Oncogene* **2011**, 31, 1869.
57. Jansen, B. A. J.; Brouwer, J.; Reedijk, J., Glutathione induces cellular resistance against cationic dinuclear platinum anticancer drugs. *Journal of Inorganic Biochemistry* **2002**, 89 (3), 197-202.
58. Allocati, N.; Masulli, M.; Di Ilio, C.; Federici, L., Glutathione transferases: substrates, inhibitors and pro-drugs in cancer and neurodegenerative diseases. *Oncogenesis* **2018**, 7 (1), 8.
59. Chen, H. H. W.; Kuo, M. T., Role of Glutathione in the Regulation of Cisplatin Resistance in Cancer Chemotherapy. *Metal-Based Drugs* **2010**, 2010.
60. Sawers, L.; Ferguson, M. J.; Ihrig, B. R.; Young, H. C.; Chakravarty, P.; Wolf, C. R.; Smith, G., Glutathione S-transferase P1 (GSTP1) directly influences platinum drug chemosensitivity in ovarian tumour cell lines. *British Journal of Cancer* **2014**, 111 (6), 1150-1158.
61. Johansson, K.; Ito, M.; Schophuizen, C. M. S.; Mathew Thengumtharayil, S.; Heuser, V. D.; Zhang, J.; Shimoji, M.; Vahter, M.; Ang, W. H.; Dyson, P. J.; Shibata, A.; Shuto, S.; Ito, Y.; Abe, H.; Morgenstern, R., Characterization of New Potential Anticancer Drugs Designed To Overcome Glutathione Transferase Mediated Resistance. *Molecular Pharmaceutics* **2011**, 8 (5), 1698-1708.
62. Ang, W. H.; Khalaila, I.; Allardyce, C. S.; Juillerat-Jeanneret, L.; Dyson, P. J., Rational Design of Platinum(IV) Compounds to Overcome Glutathione-S-Transferase Mediated Drug Resistance. *Journal of the American Chemical Society* **2005**, 127 (5), 1382-1383.
63. Bellmunt, J.; Paz-Ares, L.; Cuello, M.; Cecere, F. L.; Albiol, S.; Guillem, V.; Gallardo, E.; Carles, J.; Mendez, P.; de la Cruz, J. J.; Taron, M.; Rosell, R.; Baselga, J.; On behalf of Spanish Oncology Genitourinary, G., Gene expression of ERCC1 as a novel

prognostic marker in advanced bladder cancer patients receiving cisplatin-based chemotherapy. *Annals of Oncology* **2007**, *18* (3), 522-528.

64. Kim, M. K.; Cho, K.-J.; Kwon, G. Y.; Park, S.-I.; Kim, Y. H.; Kim, J. H.; Song, H.-Y.; Shin, J. H.; Jung, H. Y.; Lee, G. H.; Choi, K. D.; Kim, S.-B., Patients with ERCC1-Negative Locally Advanced Esophageal Cancers May Benefit from Preoperative Chemoradiotherapy. *Clinical Cancer Research* **2008**, *14* (13), 4225.

65. Vousden, K. H.; Lane, D. P., p53 in health and disease. *Nature Reviews Molecular Cell Biology* **2007**, *8*, 275.

66. Muller, P. A. J.; Vousden, K. H., p53 mutations in cancer. *Nature Cell Biology* **2013**, *15*, 2.

67. Kirsch, D. G.; Kastan, M. B., Tumor-suppressor p53: implications for tumor development and prognosis. *Journal of Clinical Oncology* **1998**, *16* (9), 3158-3168.

68. Murphy, M. E., The HSP70 family and cancer. *Carcinogenesis* **2013**, *34* (6), 1181-1188.

69. Kelland, L. R.; Abel, G.; McKeage, M. J.; Jones, M.; Goddard, P. M.; Valenti, M.; Murrer, B. A.; Harrap, K. R., Preclinical Antitumor Evaluation of Bis-acetato-ammine-dichloro-cyclohexylamine Platinum(IV): an Orally Active Platinum Drug. *Cancer Research* **1993**, *53* (11), 2581.

70. Bhargava, A.; Vaishampayan, U. N., Satraplatin: leading the new generation of oral platinum agents. *Expert Opinion on Investigational Drugs* **2009**, *18* (11), 1787-1797.

71. Dhar, S.; Gu, F. X.; Langer, R.; Farokhzad, O. C.; Lippard, S. J., Targeted delivery of cisplatin to prostate cancer cells by aptamer functionalized Pt(IV) prodrug-PLGA-PEG nanoparticles. *Proceedings of the National Academy of Sciences* **2008**.

72. Wexselblatt, E.; Gibson, D., What do we know about the reduction of Pt(IV) prodrugs? *Journal of Inorganic Biochemistry* **2012**, *117*, 220-229.

73. Hall, M. D.; Hambley, T. W., Platinum(IV) antitumour compounds: their bioinorganic chemistry. *Coordination Chemistry Reviews* **2002**, *232* (1), 49-67.

74. Fosgerau, K.; Hoffmann, T., Peptide therapeutics: current status and future directions. *Drug Discovery Today* **2015**, *20* (1), 122-128.

75. Sugahara, K. N.; Teesalu, T.; Karmali, P. P.; Kotamraju, V. R.; Agemy, L.; Greenwald, D. R.; Ruoslahti, E., Co-administration of a Tumor-Penetrating Peptide Enhances the Efficacy of Cancer Drugs. *Science (New York, N.Y.)* **2010**, *328* (5981), 1031-1035.

76. Agemy, L.; Friedmann-Morvinski, D.; Kotamraju, V. R.; Roth, L.; Sugahara, K. N.; Girard, O. M.; Mattrey, R. F.; Verma, I. M.; Ruoslahti, E., Targeted nanoparticle enhanced proapoptotic peptide as potential therapy for glioblastoma. *Proceedings of the National Academy of Sciences* **2011**.

77. Barry, N. P. E.; Sadler, P. J., Exploration of the medical periodic table: towards new targets. *Chemical Communications* **2013**, *49* (45), 5106-5131.

78. Carrato, A., Adjuvant Treatment of Colorectal Cancer. *Gastrointestinal Cancer Research : GCR* **2008**, *2* (4 Suppl 2), S42-S46.

79. McKay, C. S.; Finn, M. G., Click Chemistry in Complex Mixtures: Bioorthogonal Bioconjugation. *Chemistry & biology* **2014**, *21* (9), 1075-1101.

80. Johnstone, T. C.; Suntharalingam, K.; Lippard, S. J., The Next Generation of Platinum Drugs: Targeted Pt(II) Agents, Nanoparticle Delivery, and Pt(IV) Prodrugs. *Chemical reviews* **2016**, *116* (5), 3436-3486.

81. Griffith, D.; Morgan, M. P.; Marmion, C. J., A novel anti-cancer bifunctional platinum drug candidate with dual DNA binding and histone deacetylase inhibitory activity. *Chemical Communications* **2009**, (44), 6735-6737.

82. Gabano, E.; Ravera, M.; Zanellato, I.; Tinello, S.; Gallina, A.; Rangone, B.; Gandin, V.; Marzano, C.; Bottone, M. G.; Osella, D., An unsymmetric cisplatin-based Pt(IV) derivative containing 2-(2-propynyl)octanoate: a very efficient multi-action antitumor prodrug candidate. *Dalton Transactions* **2017**, *46* (41), 14174-14185.

83. Song, Y.; Suntharalingam, K.; Yeung, J. S.; Royzen, M.; Lippard, S. J., Synthesis and Characterization of Pt(IV) Fluorescein Conjugates to Investigate Pt(IV) Intracellular Transformations. *Bioconjugate Chemistry* **2013**, *24* (10), 1733-1740.
84. Rizzo, L. Y.; Theek, B.; Storm, G.; Kiessling, F.; Lammers, T., Recent progress in nanomedicine: therapeutic, diagnostic and theranostic applications. *Current Opinion in Biotechnology* **2013**, *24* (6), 1159-1166.
85. Cai, W.; Gao, T.; Hong, H.; Sun, J., Applications of gold nanoparticles in cancer nanotechnology. *Nanotechnology, science and applications* **2008**, *2008* (1), 10.2147/NSA.S3788.
86. Saha, K.; Agasti, S. S.; Kim, C.; Li, X.; Rotello, V. M., Gold Nanoparticles in Chemical and Biological Sensing. *Chemical Reviews* **2012**, *112* (5), 2739-2779.
87. Cheng, Y.; Samia, A. C.; Meyers, J. D.; Panagopoulos, I.; Fei, B.; Burda, C., Highly Efficient Drug Delivery with Gold Nanoparticle Vectors for in Vivo Photodynamic Therapy of Cancer. *Journal of the American Chemical Society* **2008**, *130* (32), 10643-10647.
88. Brown, S. D.; Nativo, P.; Smith, J.-A.; Stirling, D.; Edwards, P. R.; Venugopal, B.; Flint, D. J.; Plumb, J. A.; Graham, D.; Wheate, N. J., Gold Nanoparticles for the Improved Anticancer Drug Delivery of the Active Component of Oxaliplatin. *Journal of the American Chemical Society* **2010**, *132* (13), 4678-4684.
89. Taton, T. A.; Mirkin, C. A.; Letsinger, R. L., Scanometric DNA Array Detection with Nanoparticle Probes. *Science* **2000**, *289* (5485), 1757.
90. Kim, Y.; Zhu, J.; Yeom, B.; Di Prima, M.; Su, X.; Kim, J.-G.; Yoo, S. J.; Uher, C.; Kotov, N. A., Stretchable nanoparticle conductors with self-organized conductive pathways. *Nature* **2013**, *500*, 59.
91. Boscutti, G.; Nardon, C.; Marchiò, L.; Crisma, M.; Biondi, B.; Dalzoppo, D.; Dalla Via, L.; Formaggio, F.; Casini, A.; Fregona, D., Anticancer Gold(III) Peptidomimetics: From Synthesis to in vitro and ex vivo Biological Evaluations. *ChemMedChem* **2018**, *13* (11), 1131-1145.
92. Ronconi, L.; Nardon, C.; Giulia, B.; Fregona, D., Perspective Gold(III)-Dithiocarbamate Anticancer Therapeutics: Learning from the Past, Moving to the Future. In *Advances in Anticancer Agents in Medicinal Chemistry*, Prudhomme, M., Ed. Bentham Books: **2013**; Vol. 2, pp 130-172.
93. Ronconi, L.; Fregona, D., The Midas touch in cancer chemotherapy: from platinum-to gold-dithiocarbamate complexes. *Dalton Transactions* **2009**, (48), 10670-10680.
94. Aikman, B.; de Almeida, A.; Meier-Menches, S. M.; Casini, A., Aquaporins in cancer development: opportunities for bioinorganic chemistry to contribute novel chemical probes and therapeutic agents. *Metallomics* **2018**, *10* (5), 696-712.
95. Kumar, A.; Huo, S.; Zhang, X.; Liu, J.; Tan, A.; Li, S.; Jin, S.; Xue, X.; Zhao, Y.; Ji, T.; Han, L.; Liu, H.; Zhang, X.; Zhang, J.; Zou, G.; Wang, T.; Tang, S.; Liang, X.-J., Neuropilin-1-Targeted Gold Nanoparticles Enhance Therapeutic Efficacy of Platinum(IV) Drug for Prostate Cancer Treatment. *ACS Nano* **2014**, *8* (5), 4205-4220.
96. Shieh, P.; Bertozzi, C. R., Design Strategies for Bioorthogonal Smart Probes. *Organic & biomolecular chemistry* **2014**, *12* (46), 9307-9320.
97. Willmann, J. K.; van Bruggen, N.; Dinkelborg, L. M.; Gambhir, S. S., Molecular imaging in drug development. *Nature Reviews Drug Discovery* **2008**, *7*, 591.
98. Daly, H. C.; Sampedro, G.; Bon, C.; Wu, D.; Ismail, G.; Cahill, R. A.; O'Shea, D. F., BF<sub>2</sub>-azadipyromethene NIR-emissive fluorophores with research and clinical potential. *European Journal of Medicinal Chemistry* **2017**, *135*, 392-400.
99. Mindt, T. L.; Müller, C.; Melis, M.; de Jong, M.; Schibli, R., "Click-to-Chelate": In Vitro and In Vivo Comparison of a <sup>99m</sup>Tc(CO)<sub>3</sub>-Labeled N(τ)-Histidine Folate Derivative with Its Isostructural, Clicked 1,2,3-Triazole Analogue. *Bioconjugate Chemistry* **2008**, *19* (8), 1689-1695.
100. Na Hyon, B.; Song In, C.; Hyeon, T., Inorganic Nanoparticles for MRI Contrast Agents. *Advanced Materials* **2009**, *21* (21), 2133-2148.

101. Tilkemeier, P. L.; Bourque, J.; Doukky, R.; Sanghani, R.; Weinberg, R. L., ASNC imaging guidelines for nuclear cardiology procedures. *Journal of Nuclear Cardiology* **2017**, *24* (6), 2064-2128.
102. Ho Shon, I. A.; Yan, W.; Roach, P. J.; Bernard, E. J.; Shields, M.; Sywak, M.; Sidhu, S.; Delbridge, L. W., Comparison of pinhole and SPECT 99mTc-MIBI imaging in primary hyperparathyroidism. *Nuclear Medicine Communications* **2008**, *29* (11), 949-955.
103. Zhang, R. R.; Schroeder, A. B.; Grudzinski, J. J.; Rosenthal, E. L.; Warram, J. M.; Pinchuk, A. N.; Eliceiri, K. W.; Kuo, J. S.; Weichert, J. P., Beyond the margins: real-time detection of cancer using targeted fluorophores. *Nature reviews. Clinical oncology* **2017**, *14* (6), 347-364.
104. Giepmans, B. N. G.; Adams, S. R.; Ellisman, M. H.; Tsien, R. Y., The Fluorescent Toolbox for Assessing Protein Location and Function. *Science* **2006**, *312* (5771), 217.
105. Caravan, P.; Ellison, J. J.; McMurry, T. J.; Laufer, R. B., Gadolinium(III) Chelates as MRI Contrast Agents: Structure, Dynamics, and Applications. *Chemical Reviews* **1999**, *99* (9), 2293-2352.
106. Karlsson, J. O. G.; Ignarro, L. J.; Lundström, I.; Jynge, P.; Almén, T., Calmangafodipir [Ca<sub>4</sub>Mn(DPDP)<sub>5</sub>], mangafodipir (MnDPDP) and MnPLED with special reference to their SOD mimetic and therapeutic properties. *Drug Discovery Today* **2015**, *20* (4), 411-421.
107. Moretti, J.-L.; Defer, G.; Cinotti, L.; Cesaro, P.; Degos, J.-D.; Vigneron, N.; Ducassou, D.; Holman, B. L., "Luxury perfusion" with 99mTc-HMPAO and 123I-IMP SPECT imaging during the subacute phase of stroke. *European Journal of Nuclear Medicine* **1990**, *16* (1), 17-22.
108. Sheikine, Y.; Berman Daniel, S.; Di Carli Marcelo, F., Technetium-99m-sestamibi Redistribution after Exercise Stress Test Identified by a Novel Cardiac Gamma Camera: Two Case Reports. *Clinical Cardiology* **2010**, *33* (4), E39-E45.
109. Uematsu, T.; Yuen, S.; Yukisawa, S.; Aramaki, T.; Morimoto, N.; Endo, M.; Furukawa, H.; Uchida, Y.; Watanabe, J., Comparison of FDG PET and SPECT for Detection of Bone Metastases in Breast Cancer. *American Journal of Roentgenology* **2005**, *184* (4), 1266-1273.
110. Stockert, J. C.; Blázquez-Castro, A., Chapter 3: Dyes and Fluorochromes. In *Fluorescence Microscopy in Life Sciences*, Bentham Science Publishers: **2017**; pp 61-95.
111. Pansare, V.; Hejazi, S.; Faenza, W.; Prud'homme, R. K., Review of Long-Wavelength Optical and NIR Imaging Materials: Contrast Agents, Fluorophores and Multifunctional Nano Carriers. *Chemistry of materials : a publication of the American Chemical Society* **2012**, *24* (5), 812-827.
112. Wolfbeis, O. S., An overview of nanoparticles commonly used in fluorescent bioimaging. *Chemical Society Reviews* **2015**, *44* (14), 4743-4768.
113. Haque, A.; Faizi, M. S. H.; Rather, J. A.; Khan, M. S., Next generation NIR fluorophores for tumor imaging and fluorescence-guided surgery: A review. *Bioorganic & Medicinal Chemistry* **2017**, *25* (7), 2017-2034.
114. Richards, A., *Alien Vision: Exploring the Electromagnetic Spectrum with Imaging Technology*. SPIE Press: **2001**.
115. Longmire, M. R.; Ogawa, M.; Hama, Y.; Kosaka, N.; Regino, C. A. S.; Choyke, P. L.; Kobayashi, H., Determination of Optimal Rhodamine Fluorophore for in Vivo Optical Imaging. *Bioconjugate Chemistry* **2008**, *19* (8), 1735-1742.
116. Cabantous, S.; Terwilliger, T. C.; Waldo, G. S., Protein tagging and detection with engineered self-assembling fragments of green fluorescent protein. *Nature Biotechnology* **2004**, *23*, 102.
117. Kapuscinski, J., DAPI: a DNA-Specific Fluorescent Probe. *Biotechnic & Histochemistry* **1995**, *70* (5), 220-233.
118. Zink, D.; Sadoni, N.; Stelzer, E., Visualizing chromatin and chromosomes in living cells. *Methods* **2003**, *29* (1), 42-50.

119. Riss, T. L.; Moravec, R. A.; Niles, A.; Duellman, S.; Benink, H. A.; Worzella, T. J.; Minor, L., Assay Guidance Manual [Internet]. *Eli Lilly & Company and the National Center for Advancing Translational Sciences* **2004**.
120. Mosmann, T., Rapid colorimetric assay for cellular growth and survival: Application to proliferation and cytotoxicity assays. *Journal of Immunological Methods* **1983**, *65* (1), 55-63.
121. Zhang, X.-a.; Lovejoy, K. S.; Jasanoff, A.; Lippard, S. J., Water-soluble porphyrins as a dual-function molecular imaging platform for MRI and fluorescence zinc sensing. *Proceedings of the National Academy of Sciences* **2007**, *104* (26), 10780.
122. Mauriello-Jimenez, C.; Croissant, J.; Maynadier, M.; Cattoën, X.; Wong Chi Man, M.; Vergnaud, J.; Chaleix, V.; Sol, V.; Garcia, M.; Gary-Bobo, M.; Raehm, L.; Durand, J.-O., Porphyrin-functionalized mesoporous organosilica nanoparticles for two-photon imaging of cancer cells and drug delivery. *Journal of Materials Chemistry B* **2015**, *3* (18), 3681-3684.
123. Tanaka, Y.; Shin, J.-Y.; Osuka, A., Facile Synthesis of Large meso-Pentafluorophenyl-Substituted Expanded Porphyrins. *European Journal of Organic Chemistry* **2008**, *2008* (8), 1341-1349.
124. Frangioni, J. V., In vivo near-infrared fluorescence imaging. *Current Opinion in Chemical Biology* **2003**, *7* (5), 626-634.
125. Murrey, H. E.; Judkins, J. C.; am Ende, C. W.; Ballard, T. E.; Fang, Y.; Riccardi, K.; Di, L.; Guilmette, E. R.; Schwartz, J. W.; Fox, J. M.; Johnson, D. S., Systematic Evaluation of Bioorthogonal Reactions in Live Cells with Clickable HaloTag Ligands: Implications for Intracellular Imaging. *Journal of the American Chemical Society* **2015**, *137* (35), 11461-11475.
126. de Moliner, F.; Kielland, N.; Lavilla, R.; Vendrell, M., Modern Synthetic Avenues for the Preparation of Functional Fluorophores. *Angewandte Chemie International Edition* **2016**, *56* (14), 3758-3769.
127. Li, Y.; Rey-Dios, R.; Roberts, D. W.; Valdés, P. A.; Cohen-Gadol, A. A., Intraoperative Fluorescence-Guided Resection of High-Grade Gliomas: A Comparison of the Present Techniques and Evolution of Future Strategies. *World Neurosurgery* **2014**, *82* (1), 175-185.
128. Grossi, M.; Morgunova, M.; Cheung, S.; Scholz, D.; Conroy, E.; Terrile, M.; Panarella, A.; Simpson, J. C.; Gallagher, W. M.; O'Shea, D. F., Lysosome triggered near-infrared fluorescence imaging of cellular trafficking processes in real time. *Nature Communications* **2016**, *7*, 10855.
129. Guo, Z.; Park, S.; Yoon, J.; Shin, I., Recent progress in the development of near-infrared fluorescent probes for bioimaging applications. *Chem. Soc. Rev.* **2014**, *43* (1), 16-29.
130. Yuan, L.; Lin, W.; Zheng, K.; He, L.; Huang, W., Far-red to near infrared analyte-responsive fluorescent probes based on organic fluorophore platforms for fluorescence imaging. *Chem. Soc. Rev.* **2013**, *42* (2), 622-661.
131. Ge, Y.; O'Shea, D. F., Azadipyrromethenes: from traditional dye chemistry to leading edge applications. *Chem. Soc. Rev.* **2016**, *45* (14), 3846-3864.
132. Sato, K.; Gorka, A. P.; Nagaya, T.; Michie, M. S.; Nani, R. R.; Nakamura, Y.; Coble, V. L.; Vasalatiy, O. V.; Swenson, R. E.; Choyke, P. L.; Schnermann, M. J.; Kobayashi, H., Role of Fluorophore Charge on the In Vivo Optical Imaging Properties of Near-Infrared Cyanine Dye/Monoclonal Antibody Conjugates. *Bioconjugate Chemistry* **2016**, *27* (2), 404-413.
133. Medarova, Z.; Pham, W.; Farrar, C.; Petkova, V.; Moore, A., In vivo imaging of siRNA delivery and silencing in tumors. *Nature Medicine* **2007**, *13*, 372.
134. Wichert, M.; Krall, N.; Decurtins, W.; Franzini, R. M.; Pretto, F.; Schneider, P.; Neri, D.; Scheuermann, J., Dual-display of small molecules enables the discovery of ligand pairs and facilitates affinity maturation. *Nature Chemistry* **2015**, *7*, 241.
135. Weissleder, R.; Tung, C.-H.; Mahmood, U.; Bogdanov Jr, A., In vivo imaging of tumors with protease-activated near-infrared fluorescent probes. *Nature Biotechnology* **1999**, *17*, 375.



136. Levi, J.; Cheng, Z.; Gheysens, O.; Patel, M.; Chan, C. T.; Wang, Y.; Namavari, M.; Gambhir, S. S., Fluorescent Fructose Derivatives for Imaging Breast Cancer Cells. *Bioconjugate Chemistry* **2007**, *18* (3), 628-634.
137. Garanger, E.; Boturyn, D.; Jin, Z.; Dumy, P.; Favrot, M.-C.; Coll, J.-L., New Multifunctional Molecular Conjugate Vector for Targeting, Imaging, and Therapy of Tumors. *Molecular Therapy* **2005**, *12* (6), 1168-1175.
138. Luo, S.; Zhang, E.; Su, Y.; Cheng, T.; Shi, C., A review of NIR dyes in cancer targeting and imaging. *Biomaterials* **2011**, *32* (29), 7127-7138.
139. Kelland, L., The resurgence of platinum-based cancer chemotherapy. *Nature Reviews Cancer* **2007**, *7*, 573.
140. Gordon, M. S.; Margolin, K.; Talpaz, M.; Sledge, G. W.; Holmgren, E.; Benjamin, R.; Stalter, S.; Shak, S.; Adelman, D. C., Phase I Safety and Pharmacokinetic Study of Recombinant Human Anti-Vascular Endothelial Growth Factor in Patients With Advanced Cancer. *Journal of Clinical Oncology* **2001**, *19* (3), 843-850.
141. Hardy, J.; Selkoe, D. J., The Amyloid Hypothesis of Alzheimer's Disease: Progress and Problems on the Road to Therapeutics. *Science* **2002**, *297* (5580), 353.
142. Xue, W.; Zender, L.; Miething, C.; Dickins, R. A.; Hernando, E.; Krizhanovsky, V.; Cordon-Cardo, C.; Lowe, S. W., Senescence and tumour clearance is triggered by p53 restoration in murine liver carcinomas. *Nature* **2007**, *445*, 656.
143. Aguirre-Ghiso, J. A., Models, mechanisms and clinical evidence for cancer dormancy. *Nature Reviews Cancer* **2007**, *7*, 834.
144. Yang, X.; Zhang, Y.; Hosaka, K.; Andersson, P.; Wang, J.; Tholander, F.; Cao, Z.; Morikawa, H.; Tegnér, J.; Yang, Y.; Iwamoto, H.; Lim, S.; Cao, Y., VEGF-B promotes cancer metastasis through a VEGF-A-independent mechanism and serves as a marker of poor prognosis for cancer patients. *Proceedings of the National Academy of Sciences* **2015**.
145. Shin, M. C.; Zhang, J.; Min, K. A.; Lee, K.; Byun, Y.; David, A. E.; He, H.; Yang, V. C., Cell-penetrating peptides: achievements and challenges in application for cancer treatment. *Journal of biomedical materials research. Part A* **2014**, *102* (2), 575-587.
146. M. Nic; J. Jirat; Kosata., B., IUPAC. Compendium of Chemical Terminology. In *The "Gold Book"*, Blackwell Scientific Publications: Oxford, 2006.
147. Plosker, G. L.; Brogden, R. N., Leuprorelin. *Drugs* **1994**, *48* (6), 930-967.
148. Waugh, N.; Cummins, E.; Royle, P.; Clar, C.; Marien, M., Newer agents for blood glucose control in type 2 diabetes: systematic review and economic evaluation. *Health Technol Assess* **2010**, *14* (36).
149. Hilgenfeld, R.; Seipke, G.; Berchtold, H.; Owens, D. R., The Evolution of Insulin Glargine and its Continuing Contribution to Diabetes Care. *Drugs* **2014**, *74* (8), 911-927.
150. Volpe, M.; Rubattu, S.; Burnett, J., Natriuretic peptides in cardiovascular diseases: current use and perspectives. *European Heart Journal* **2014**, *35* (7), 419-425.
151. Diener, C.; Garza Ramos Martínez, G.; Moreno Blas, D.; Castillo González, D. A.; Corzo, G.; Castro-Obregon, S.; Del Rio, G., Effective Design of Multifunctional Peptides by Combining Compatible Functions. *PLoS Computational Biology* **2016**, *12* (4), e1004786.
152. Ruoslahti, E., Tumor penetrating peptides for improved drug delivery. *Advanced Drug Delivery Reviews* **2017**, *110-111*, 3-12.
153. Raucher, D.; Ryu, J. S., Cell-penetrating peptides: strategies for anticancer treatment. *Trends in Molecular Medicine* **2015**, *21* (9), 560-570.
154. Regberg, J.; Srimanee, A.; Langel, Ü., Applications of Cell-Penetrating Peptides for Tumor Targeting and Future Cancer Therapies. *Pharmaceuticals* **2012**, *5* (9).
155. Frankel, A. D.; Pabo, C. O., Cellular uptake of the tat protein from human immunodeficiency virus. *Cell* **1988**, *55* (6), 1189-1193.
156. Myrberg, H.; Zhang, L.; Mäe, M.; Langel, Ü., Design of a Tumor-Homing Cell-Penetrating Peptide. *Bioconjugate Chemistry* **2008**, *19* (1), 70-75.
157. Alves, I. D.; Carré, M.; Montero, M.-P.; Castano, S.; Lecomte, S.; Marquant, R.; Lecorché, P.; Burlina, F.; Schatz, C.; Sagan, S.; Chassaing, G.; Braguer, D.; Lavielle, S., A proapoptotic peptide conjugated to penetratin selectively inhibits tumor cell growth. *Biochimica et Biophysica Acta (BBA) - Biomembranes* **2014**, *1838* (8), 2087-2098.

158. Dubikovskaya, E. A.; Thorne, S. H.; Pillow, T. H.; Contag, C. H.; Wender, P. A., Overcoming multidrug resistance of small-molecule therapeutics through conjugation with releasable octaarginine transporters. *Proceedings of the National Academy of Sciences* **2008**, *105* (34), 12128.
159. Desgrosellier, J. S.; Cheresch, D. A., Integrins in cancer: biological implications and therapeutic opportunities. *Nature reviews. Cancer* **2010**, *10* (1), 9-22.
160. Madani, F.; Lindberg, S.; Langel, Ü.; Futaki, S.; Gräslund, A., Mechanisms of Cellular Uptake of Cell-Penetrating Peptides. *Journal of Biophysics* **2011**, *2011*, 414729.
161. Prochiantz, A., Getting hydrophilic compounds into cells: lessons from homeopeptides. *Current Opinion in Neurobiology* **1996**, *6* (5), 629-634.
162. Prochiantz, A., Homeodomain-Derived Peptides: In and Out of the Cells. *Annals of the New York Academy of Sciences* **2006**, *886* (1), 172-179.
163. Matsuzaki, K.; Yoneyama, S.; Murase, O.; Miyajima, K., Transbilayer Transport of Ions and Lipids Coupled with Mastoparan X Translocation. *Biochemistry* **1996**, *35* (25), 8450-8456.
164. Shai, Y., Mode of action of membrane active antimicrobial peptides. *Peptide Science* **2004**, *66* (4), 236-248.
165. Ludtke, S.; He, K.; Huang, H., Membrane thinning caused by magainin 2. *Biochemistry* **1995**, *34* (51), 16764-16769.
166. Ye, J.; Liu, E.; Yu, Z.; Pei, X.; Chen, S.; Zhang, P.; Shin, M.-C.; Gong, J.; He, H.; Yang, C. V., CPP-Assisted Intracellular Drug Delivery, What Is Next? *International Journal of Molecular Sciences* **2016**, *17* (11).
167. Doherty, G. J.; McMahon, H. T., Mechanisms of Endocytosis. *Annual Review of Biochemistry* **2009**, *78* (1), 857-902.
168. Kumari, S.; Mg, S.; Mayor, S., Endocytosis unplugged: multiple ways to enter the cell. *Cell Research* **2010**, *20*, 256.
169. Fawell, S.; Seery, J.; Daikh, Y.; Moore, C.; Chen, L. L.; Pepinsky, B.; Barsoum, J., Tat-mediated delivery of heterologous proteins into cells. *Proceedings of the National Academy of Sciences* **1994**, *91* (2), 664.
170. Mäe, M.; Langel, Ü., Cell-penetrating peptides as vectors for peptide, protein and oligonucleotide delivery. *Current Opinion in Pharmacology* **2006**, *6* (5), 509-514.
171. Fang, B.; Jiang, L.; Zhang, M.; Ren, F. Z., A novel cell-penetrating peptide TAT-A1 delivers siRNA into tumor cells selectively. *Biochimie* **2013**, *95* (2), 251-257.
172. Park, Y. J.; Chang, L.-C.; Liang, J. F.; Moon, C.; Chung, C.-P.; Yang, V. C., Nontoxic membrane translocation peptide from protamine, low molecular weight protamine (LMWP), for enhanced intracellular protein delivery: in vitro and in vivo study. *The FASEB Journal* **2005**, *19* (11), 1555-1557.
173. Hu, W.; Splith, K.; Neundorff, I.; Merz, K.; Schatzschneider, U., Influence of the metal center and linker on the intracellular distribution and biological activity of organometal-peptide conjugates. *JBIC Journal of Biological Inorganic Chemistry* **2012**, *17* (2), 175-185.
174. Splith, K.; Hu, W.; Schatzschneider, U.; Gust, R.; Ott, I.; Onambele, L. A.; Prokop, A.; Neundorff, I., Protease-Activatable Organometal-Peptide Bioconjugates with Enhanced Cytotoxicity on Cancer Cells. *Bioconjugate Chemistry* **2010**, *21* (7), 1288-1296.
175. Ritossa, F., A new puffing pattern induced by temperature shock and DNP in drosophila. *Experientia* **1962**, *18* (12), 571-573.
176. Mayer, M. P.; Bukau, B., Hsp70 chaperones: Cellular functions and molecular mechanism. *Cellular and Molecular Life Sciences* **2005**, *62* (6), 670-684.
177. Lindquist, S.; Craig, E. A., The Heat-Shock Proteins. *Annual Review of Genetics* **1988**, *22* (1), 631-677.
178. Pirkkala, L.; Sistonen, L., Heat Shock Proteins (HSPs): Structure, Function and Genetics. *eLS* **2006**.
179. Daugaard, M.; Rohde, M.; Jäättelä, M., The heat shock protein 70 family: Highly homologous proteins with overlapping and distinct functions. *FEBS Letters* **2007**, *581* (19), 3702-3710.

180. Gething, M.-J.; Sambrook, J., Protein folding in the cell. *Nature* **1992**, 355, 33.
181. Lee, A. S., The ER chaperone and signaling regulator GRP78/BiP as a monitor of endoplasmic reticulum stress. *Methods* **2005**, 35 (4), 373-381.
182. Kampinga, H. H.; Hageman, J.; Vos, M. J.; Kubota, H.; Tanguay, R. M.; Bruford, E. A.; Cheetham, M. E.; Chen, B.; Hightower, L. E., Guidelines for the nomenclature of the human heat shock proteins. *Cell Stress & Chaperones* **2009**, 14 (1), 105-111.
183. Bork, P.; Sander, C.; Valencia, A., An ATPase domain common to prokaryotic cell cycle proteins, sugar kinases, actin, and hsp70 heat shock proteins. *Proceedings of the National Academy of Sciences* **1992**, 89 (16), 7290.
184. Bertelsen, E. B.; Chang, L.; Gestwicki, J. E.; Zuiderweg, E. R. P., Solution conformation of wild-type *E. coli* Hsp70 (DnaK) chaperone complexed with ADP and substrate. *Proceedings of the National Academy of Sciences* **2009**, 106 (21), 8471.
185. Qiu, Y.; Ye, X.; Hanson, P. J.; Zhang, H. M.; Zong, J.; Cho, B.; Yang, D., Hsp70-1: upregulation via selective phosphorylation of heat shock factor 1 during coxsackieviral infection and promotion of viral replication via the AU-rich element. *Cellular and Molecular Life Sciences* **2016**, 73 (5), 1067-1084.
186. Åkerfelt, M.; Morimoto, R. I.; Sistonen, L., Heat shock factors: integrators of cell stress, development and lifespan. *Nature Reviews Molecular Cell Biology* **2010**, 11, 545.
187. Jäättelä, M., Heat shock proteins as cellular lifeguards. *Annals of Medicine* **1999**, 31 (4), 261-271.
188. Stankiewicz, A. R.; Lachapelle, G.; Foo, C. P. Z.; Radicioni, S. M.; Mosser, D. D., Hsp70 Inhibits Heat-induced Apoptosis Upstream of Mitochondria by Preventing Bax Translocation. *Journal of Biological Chemistry* **2005**, 280 (46), 38729-38739.
189. Guo, F.; Sigua, C.; Bali, P.; George, P.; Fiskus, W.; Scuto, A.; Annavarapu, S.; Mouttaki, A.; Sondarva, G.; Wei, S.; Wu, J.; Djeu, J.; Bhalla, K., Mechanistic role of heat shock protein 70 in Bcr-Abl-mediated resistance to apoptosis in human acute leukemia cells. *Blood* **2005**, 105 (3), 1246.
190. Nylandsted, J.; Gyrð-Hansen, M.; Danielewicz, A.; Fehrenbacher, N.; Lademann, U.; Høyer-Hansen, M.; Weber, E.; Multhoff, G.; Rohde, M.; Jäättelä, M., Heat Shock Protein 70 Promotes Cell Survival by Inhibiting Lysosomal Membrane Permeabilization. *The Journal of Experimental Medicine* **2004**, 200 (4), 425-435.
191. McKeon, A. M.; Egan, A.; Chandanshive, J.; McMahon, H.; Griffith, M. D., Novel Improved Synthesis of HSP70 Inhibitor, Pifithrin- $\mu$ . In Vitro Synergy Quantification of Pifithrin- $\mu$  Combined with Pt Drugs in Prostate and Colorectal Cancer Cells. *Molecules* **2016**, 21 (7).
192. Schlecht, R.; Scholz, S. R.; Dahmen, H.; Wegener, A.; Sirrenberg, C.; Musil, D.; Bomke, J.; Eggenweiler, H.-M.; Mayer, M. P.; Bukau, B., Functional Analysis of Hsp70 Inhibitors. *PLOS ONE* **2013**, 8 (11), e78443.
193. Park, S.-H.; Kim, W.-J.; Li, H.; Seo, W.; Park, S.-H.; Kim, H.; Shin, S. C.; Zuiderweg, E. R. P.; Kim, E. E.; Sim, T.; Kim, N.-K.; Shin, I., Anti-leukemia activity of a Hsp70 inhibitor and its hybrid molecules. *Scientific Reports* **2017**, 7 (1), 3537.
194. Gehrmann, M.; Stangl, S.; Foulds, G. A.; Oellinger, R.; Breuninger, S.; Rad, R.; Pockley, A. G.; Multhoff, G., Tumor Imaging and Targeting Potential of an Hsp70-Derived 14-Mer Peptide. *PLOS ONE* **2014**, 9 (8), e105344.
195. McKeon, A. M.; Noonan, J.; Devocelle, M.; Murphy, B. M.; Griffith, D. M., Platinum(IV) oxaliplatin-peptide conjugates targeting memHsp70+ phenotype in colorectal cancer cells. *Chemical Communications* **2017**, 53 (82), 11318-11321.
196. Gibson, C. L., *Hormones and Behaviour: A Psychological Approach* (review). In *Perspectives in Biology and Medicine*, Johns Hopkins University Press: **2010**; pp 152-155.
197. Lednicer, D., *Steroid Chemistry at a Glance*. John Wiley & Sons: **2010**.
198. Zubeldia-Brenner, L.; Roselli, C. E.; Recabarren, S. E.; Gonzalez Deniselle, M. C.; Lara, H. E., Developmental and Functional Effects of Steroid Hormones on the Neuroendocrine Axis and Spinal Cord. *Journal of neuroendocrinology* **2016**, 28 (7), 10.1111/jne.12401.

199. Manber, R.; Armitage, R., Sex, Steroids, and Sleep: A Review. *Sleep* **1999**, 22 (5), 540-541.
200. Nwaru, B. I.; Nurmatov, U.; Sheikh, A., Endogenous and exogenous sex steroid hormones in asthma and allergy in females: protocol for a systematic review and meta-analysis. *Npj Primary Care Respiratory Medicine* **2016**, 26, 15078.
201. Barrett, S.; Delaney, S.; Kavanagh, K.; Montagner, D., Evaluation of in vitro and in vivo antibacterial activity of novel Cu(II)-steroid complexes. *Inorganica Chimica Acta* **2018**, 479, 261-265.
202. Le Bideau, F.; Dagonne, S., Synthesis of Transition-Metal Steroid Derivatives. *Chemical Reviews* **2013**, 113 (10), 7793-7850.
203. Heffner, L. J.; Schust, D. J., *The Reproductive System at a Glance*. 4th ed. ed.; Wiley-Blackwell: **2010**.
204. Albrecht, E. D.; Pepe, G. J., Steroid hormone regulation of angiogenesis in the primate endometrium. *Frontiers in Bioscience* **2003**, 8, 416-429.
205. Ahmad, N.; Kumar, R., Steroid hormone receptors in cancer development: A target for cancer therapeutics. *Cancer Letters* **2011**, 300 (1), 1-9.
206. Pérez Quiñones, J.; Szopko, R.; Schmidt, C.; Peniche Covas, C., Novel drug delivery systems: Chitosan conjugates covalently attached to steroids with potential anticancer and agrochemical activity. *Carbohydrate Polymers* **2011**, 84 (3), 858-864.
207. Jordan, V. C.; Brodie, A. M. H., Development and evolution of therapies targeted to the estrogen receptor for the treatment and prevention of breast cancer. *Steroids* **2007**, 72 (1), 7-25.
208. Sharman, W. M.; van Lier, J. E.; Allen, C. M., Targeted photodynamic therapy via receptor mediated delivery systems. *Advanced Drug Delivery Reviews* **2004**, 56 (1), 53-76.
209. He, Q.; Liang, C. H.; Lippard, S. J., Steroid hormones induce HMG1 overexpression and sensitize breast cancer cells to cisplatin and carboplatin. *Proceedings of the National Academy of Sciences* **2000**, 97 (11), 5768.
210. Crowley, J. D.; McMorran, D. A., Click-Triazole" Coordination Chemistry: Exploiting 1,4-Disubstituted-1,2,3-Triazoles as Ligands. In *Click Triazoles*, Košmrlj, J., Ed. Springer-Verlag Berlin Heidelberg: 2012; Vol. 28, pp 31-84.
211. Schulze, B.; Schubert, U. S., Beyond click chemistry - supramolecular interactions of 1,2,3-triazoles. *Chemical Society Reviews* **2014**, 43 (8), 2522-2571.
212. Struthers, H.; Mindt, T. L.; Schibli, R., Metal chelating systems synthesized using the copper(i) catalyzed azide-alkyne cycloaddition. *Dalton Transactions* **2010**, 39 (3), 675-696.
213. Suntrup, L.; Kleoff, M.; Sarkar, B., Serendipitous discoveries of new coordination modes of the 1,5-regioisomer of 1,2,3-triazoles enroute to the attempted synthesis of a carbon-anchored tri-mesoionic carbene. *Dalton Transactions* **2018**, 47 (24), 7992-8002.
214. van Hilst, Q. V. C.; Lagesse, N. R.; Preston, D.; Crowley, J. D., Functional metal complexes from CuAAC "click" bidentate and tridentate pyridyl-1,2,3-triazole ligands. *Dalton Transactions* **2018**, 47 (4), 997-1002.
215. Wang, K.; Chen, M.; Wang, Q.; Shi, X.; Lee, J. K., 1,2,3-Triazoles: Gas Phase Properties. *The Journal of Organic Chemistry* **2013**, 78 (14), 7249-7258.
216. Kolb Hartmuth, C.; Finn, M. G.; Sharpless, K. B., Click Chemistry: Diverse Chemical Function from a Few Good Reactions. *Angewandte Chemie International Edition* **2001**, 40 (11), 2004-2021.
217. Pathak, R. K.; McNitt, C. D.; Popik, V. V.; Dhar, S., A Versatile Bioorthogonal Copper-free Click Chemistry Platform to Functionalize Cisplatin Prodrugs. *Chemistry (Weinheim an der Bergstrasse, Germany)* **2014**, 20 (23), 6861-6865.
218. Liang, L.; Astruc, D., The copper(I)-catalyzed alkyne-azide cycloaddition (CuAAC) "click" reaction and its applications. An overview. *Coordination Chemistry Reviews* **2011**, 255 (23), 2933-2945.
219. Rostovtsev Vsevolod, V.; Green Luke, G.; Fokin Valery, V.; Sharpless, K. B., A Stepwise Huisgen Cycloaddition Process: Copper(I) Catalyzed Regioselective "Ligation" of

- Azides and Terminal Alkynes. *Angewandte Chemie International Edition* **2002**, *41* (14), 2596-2599.
220. Tornøe, C. W.; Christensen, C.; Meldal, M., Peptidotriazoles on Solid Phase: [1,2,3]-Triazoles by Regiospecific Copper(I)-Catalyzed 1,3-Dipolar Cycloadditions of Terminal Alkynes to Azides. *The Journal of Organic Chemistry* **2002**, *67* (9), 3057-3064.
221. Worrell, B. T.; Malik, J. A.; Fokin, V. V., Direct Evidence of a Dinuclear Copper Intermediate in Cu(I)-Catalyzed Azide-Alkyne Cycloadditions. *Science* **2013**, *340* (6131), 457.
222. Qin, A.; Lam, J. W. Y.; Tang, B. Z., Click Polymerization: Progresses, Challenges, and Opportunities. *Macromolecules* **2010**, *43* (21), 8693-8702.
223. Díaz, D. D.; Rajagopal, K.; Strable, E.; Schneider, J.; Finn, M. G., "Click" Chemistry in a Supramolecular Environment: Stabilization of Organogels by Copper(I)-Catalyzed Azide-Alkyne [3 + 2] Cycloaddition. *Journal of the American Chemical Society* **2006**, *128* (18), 6056-6057.
224. Huang, S.; Clark, R. J.; Zhu, L., Highly Sensitive Fluorescent Probes for Zinc Ion Based on Triazolyl-Containing Tetradentate Coordination Motifs. *Organic Letters* **2007**, *9* (24), 4999-5002.
225. van Hilst, Q. V. C.; Lagesse, N. R.; Preston, D.; Crowley, J. D., Functional metal complexes from CuAAC "click" bidentate and tridentate pyridyl-1,2,3-triazole ligands. *Dalton Trans.* **2018**, *47* (4), 997-1002.
226. Kolb, H. C.; Sharpless, K. B., The growing impact of click chemistry on drug discovery. *Drug Discovery Today* **2003**, *8* (24), 1128-1137.
227. Hein, C. D.; Liu, X.-M.; Wang, D., Click Chemistry, a Powerful Tool for Pharmaceutical Sciences. *Pharmaceutical research* **2008**, *25* (10), 2216-2230.
228. Parker, J. P.; Devocelle, M.; Marmion, C. J., Derivatisation of an Anti-Cancer Cationic Antimicrobial Peptide and its Complexation to Platinum(II). *Zeitschrift für anorganische und allgemeine Chemie* **2013**, *639* (8 9), 1628-1635.
229. Sletten, E. M.; Bertozzi, C. R., From Mechanism to Mouse: A Tale of Two Bioorthogonal Reactions. *Accounts of Chemical Research* **2011**, *44* (9), 666-676.
230. Hong, V.; Presolski Stanislav, I.; Ma, C.; Finn, M. G., Analysis and Optimization of Copper Catalyzed Azide-Alkyne Cycloaddition for Bioconjugation. *Angewandte Chemie International Edition* **2009**, *48* (52), 9879-9883.
231. Gaetke, L. M.; Chow, C. K., Copper toxicity, oxidative stress, and antioxidant nutrients. *Toxicology* **2003**, *189* (1), 147-163.
232. Hong, V.; Steinmetz, N. F.; Manchester, M.; Finn, M. G., Labeling Live Cells by Copper-Catalyzed Alkyne-Azide Click Chemistry. *Bioconjugate chemistry* **2010**, *21* (10), 1912-1916.
233. Uttamapinant, C.; Tangpeerachaikul, A.; Grecian, S.; Clarke, S.; Singh, U.; Slade, P.; Gee, K. R.; Ting, A. Y., Fast, Cell-compatible Click Chemistry with Copper-chelating Azides for Biomolecular Labeling. *Angewandte Chemie (International ed. in English)* **2012**, *51* (24), 5852-5856.
234. Besanceney-Webler, C.; Jiang, H.; Zheng, T.; Feng, L.; Soriano del Amo, D.; Wang, W.; Klivansky, L. M.; Marlow, F. L.; Liu, Y.; Wu, P., Raising the Efficacy of Bioorthogonal Click Reactions for Bioconjugation: A Comparative Study. *Angewandte Chemie (International ed. in English)* **2011**, *50* (35), 8051-8056.
235. Kennedy, D. C.; McKay, C. S.; Legault, M. C. B.; Danielson, D. C.; Blake, J. A.; Pegoraro, A. F.; Stollow, A.; Mester, Z.; Pezacki, J. P., Cellular Consequences of Copper Complexes Used To Catalyze Bioorthogonal Click Reactions. *Journal of the American Chemical Society* **2011**, *133* (44), 17993-18001.
236. Prescher, J. A.; Dube, D. H.; Bertozzi, C. R., Chemical remodelling of cell surfaces in living animals. *Nature* **2004**, *430*, 873.
237. Agard, N. J.; Baskin, J. M.; Prescher, J. A.; Lo, A.; Bertozzi, C. R., A Comparative Study of Bioorthogonal Reactions with Azides. *ACS Chemical Biology* **2006**, *1* (10), 644-648.

238. Jewett, J. C.; Bertozzi, C. R., Cu-free click cycloaddition reactions in chemical biology. *Chemical Society Reviews* **2010**, 39 (4), 1272-1279.
239. Patterson, D. M.; Nazarova, L. A.; Prescher, J. A., Finding the Right (Bioorthogonal) Chemistry. *ACS Chemical Biology* **2014**, 9 (3), 592-605.
240. Sletten Ellen, M.; Bertozzi Carolyn, R., Bioorthogonal Chemistry: Fishing for Selectivity in a Sea of Functionality. *Angewandte Chemie International Edition* **2009**, 48 (38), 6974-6998.
241. Ramil, C. P.; Lin, Q., Bioorthogonal chemistry: strategies and recent development. *Chemical communications (Cambridge, England)* **2013**, 49 (94), 11007-11022.
242. Chen, W.; Wang, D.; Dai, C.; Hamelberg, D.; Wang, B., Clicking 1,2,4,5-tetrazine and cyclooctynes with tunable reaction rates. *Chemical Communications* **2012**, 48 (12), 1736-1738.
243. Knall, A.-C.; Slugovc, C., Inverse electron demand Diels-Alder (iEDDA)-initiated conjugation: a (high) potential click chemistry scheme. *Chemical Society Reviews* **2013**, 42 (12), 5131-5142.
244. Karver, M. R.; Weissleder, R.; Hilderbrand, S. A., Synthesis and Evaluation of a Series of 1,2,4,5-Tetrazines for Bioorthogonal Conjugation. *Bioconjugate Chemistry* **2011**, 22 (11), 2263-2270.
245. Saxon, E.; Luchansky, S. J.; Hang, H. C.; Yu, C.; Lee, S. C.; Bertozzi, C. R., Investigating Cellular Metabolism of Synthetic Azidosugars with the Staudinger Ligation. *Journal of the American Chemical Society* **2002**, 124 (50), 14893-14902.
246. Staudinger, H.; Meyer, J., Über neue organische Phosphorverbindungen III. Phosphinmethylderivate und Phosphinimine. *Helvetica Chimica Acta* **1919**, 2 (1), 635-646.
247. Saxon, E.; Bertozzi, C. R., Cell Surface Engineering by a Modified Staudinger Reaction. *Science* **2000**, 287 (5460), 2007.
248. Schoenebeck, F.; Ess, D. H.; Jones, G. O.; Houk, K. N., Reactivity and Regioselectivity in 1,3-Dipolar Cycloadditions of Azides to Strained Alkynes and Alkenes: A Computational Study. *Journal of the American Chemical Society* **2009**, 131 (23), 8121-8133.
249. Zeng, D.; Zeglis, B. M.; Lewis, J. S.; Anderson, C. J., The Growing Impact of Bioorthogonal Click Chemistry on the Development of Radiopharmaceuticals. *Journal of nuclear medicine : official publication, Society of Nuclear Medicine* **2013**, 54 (6), 829-832.
250. Oliveira, B. L.; Guo, Z.; Bernardes, G. J. L., Inverse electron demand Diels-Alder reactions in chemical biology. *Chemical Society Reviews* **2017**, 46 (16), 4895-4950.
251. Seitchik, J. L.; Peeler, J. C.; Taylor, M. T.; Blackman, M. L.; Rhoads, T. W.; Cooley, R. B.; Refakis, C.; Fox, J. M.; Mehl, R. A., Genetically Encoded Tetrazine Amino Acid Directs Rapid Site-Specific In Vivo Bioorthogonal Ligation with trans-Cyclooctenes. *Journal of the American Chemical Society* **2012**, 134 (6), 2898-2901.
252. Gordon, C. G.; Mackey, J. L.; Jewett, J. C.; Sletten, E. M.; Houk, K. N.; Bertozzi, C. R., Reactivity of Biarylazacyclooctynones in Copper-Free Click Chemistry. *Journal of the American Chemical Society* **2012**, 134 (22), 9199-9208.
253. Lang, K.; Davis, L.; Torres-Kolbus, J.; Chou, C.; Deiters, A.; Chin, J. W., Genetically encoded norbornene directs site-specific cellular protein labelling via a rapid bioorthogonal reaction. *Nature chemistry* **2012**, 4 (4), 298-304.
254. de la Oliva, C. G. L., P. G. ; de Ocariz, C. O., Six Membered Heterocycles: Triazines, Tetrazines and Other Polyaza Systems. In *Modern Heterocyclic Chemistry*, **2011**; pp 1778-1864.
255. Carboni, R. A.; Lindsey, R. V., Reactions of Tetrazines with Unsaturated Compounds. A New Synthesis of Pyridazines. *Journal of the American Chemical Society* **1959**, 81 (16), 4342-4346.
256. Foster, R. A. A.; Willis, M. C., Tandem inverse-electron-demand hetero-/retro-Diels-Alder reactions for aromatic nitrogen heterocycle synthesis. *Chemical Society Reviews* **2013**, 42 (1), 63-76.

257. Blackman, M. L.; Royzen, M.; Fox, J. M., Tetrazine Ligation: Fast Bioconjugation Based on Inverse-Electron-Demand Diels–Alder Reactivity. *Journal of the American Chemical Society* **2008**, *130* (41), 13518-13519.
258. Devaraj, N. K.; Weissleder, R.; Hilderbrand, S. A., Tetrazine-Based Cycloadditions: Application to Pretargeted Live Cell Imaging. *Bioconjugate Chemistry* **2008**, *19* (12), 2297-2299.
259. Sauer, J.; Heldmann Dieter, K.; Hetzenegger, J.; Krauthan, J.; Sichert, H.; Schuster, J., 1,2,4,5 Tetrazine: Synthesis and Reactivity in [4+2] Cycloadditions. *European Journal of Organic Chemistry* **1998**, *1998* (12), 2885-2896.
260. Chigrinova, M.; McKay, C. S.; Beaulieu, L.-P. B.; Udachin, K. A.; Beauchemin, A. M.; Pezacki, J. P., Rearrangements and addition reactions of biarylazacyclooctynones and the implications to copper-free click chemistry. *Organic & Biomolecular Chemistry* **2013**, *11* (21), 3436-3441.
261. Beatty, K. E.; Fisk, J. D.; Smart, B. P.; Lu, Y. Y.; Szychowski, J.; Hangauer, M. J.; Baskin, J. M.; Bertozzi, C. R.; Tirrell, D. A., Live Cell Imaging of Cellular Proteins by a Strain Promoted Azide–Alkyne Cycloaddition. *ChemBioChem* **2010**, *11* (15), 2092-2095.
262. Chang, P. V.; Prescher, J. A.; Sletten, E. M.; Baskin, J. M.; Miller, I. A.; Agard, N. J.; Lo, A.; Bertozzi, C. R., Copper-free click chemistry in living animals. *Proceedings of the National Academy of Sciences* **2010**, *107* (5), 1821.
263. Poole, T. H.; Reisz, J. A.; Zhao, W.; Poole, L. B.; Furdui, C. M.; King, S. B., Strained Cycloalkynes as New Protein Sulfenic Acid Traps. *Journal of the American Chemical Society* **2014**, *136* (17), 6167-6170.
264. White, J. D.; Haley, M. M.; DeRose, V. J., Multifunctional Pt(II) Reagents: Covalent Modifications of Pt Complexes Enable Diverse Structural Variation and In-Cell Detection. *Accounts of Chemical Research* **2016**, *49* (1), 56-66.
265. Wirth, R.; White, J. D.; Moghaddam, A. D.; Ginzburg, A. L.; Zakharov, L. N.; Haley, M. M.; DeRose, V. J., Azide vs Alkyne Functionalization in Pt(II) Complexes for Post-treatment Click Modification: Solid-State Structure, Fluorescent Labeling, and Cellular Fate. *Journal of the American Chemical Society* **2015**, *137* (48), 15169-15175.
266. White, J. D.; Osborn, M. F.; Moghaddam, A. D.; Guzman, L. E.; Haley, M. M.; DeRose, V. J., Picazoplatin, an Azide-Containing Platinum(II) Derivative for Target Analysis by Click Chemistry. *Journal of the American Chemical Society* **2013**, *135* (32), 11680-11683.
267. Zhang, J. Z.; Bonnitcha, P.; Wexselblatt, E.; Klein, A. V.; Najajreh, Y.; Gibson, D.; Hambley, T. W., Facile Preparation of Mono-, Di- and Mixed-Carboxylato Platinum(IV) Complexes for Versatile Anticancer Prodrug Design. *Chem. Eur. J.* **2013**, *19* (5), 1672-1676.
268. Gupta, N.; Kancharla, J.; Kaushik, S.; Ansari, A.; Hossain, S.; Goyal, R.; Pandey, M.; Sivaccumar, J.; Hussain, S.; Sarkar, A.; Sengupta, A.; Mandal, S. K.; Roy, M.; Sengupta, S., Development of a facile antibody–drug conjugate platform for increased stability and homogeneity †Electronic supplementary information (ESI) available: Synthetic schemes and characterization data, experimental procedures, Fig. S1 and S2. See DOI: 10.1039/c6sc05149a Click here for additional data file. *Chemical Science* **2017**, *8* (3), 2387-2395.
269. Ahn, J.; Miura, Y.; Yamada, N.; Chida, T.; Liu, X.; Kim, A.; Sato, R.; Tsumura, R.; Koga, Y.; Yasunaga, M.; Nishiyama, N.; Matsumura, Y.; Cabral, H.; Kataoka, K., Antibody fragment-conjugated polymeric micelles incorporating platinum drugs for targeted therapy of pancreatic cancer. *Biomaterials* **2015**, *39*, 23-30.
270. Tanaka, M.; Kataoka, H.; Yano, S.; Ohi, H.; Kawamoto, K.; Shibahara, T.; Mizoshita, T.; Mori, Y.; Tanida, S.; Kamiya, T.; Joh, T., Anti-cancer effects of newly developed chemotherapeutic agent, glycoconjugated palladium (II) complex, against cisplatin-resistant gastric cancer cells. *BMC Cancer* **2013**, *13*, 237-237.
271. Barnes, K. R.; Kutikov, A.; Lippard, S. J., Synthesis, Characterization, and Cytotoxicity of a Series of Estrogen-Tethered Platinum(IV) Complexes. *Chemistry & Biology* **2004**, *11* (4), 557-564.

272. Abramkin, S.; Valiahdi, S. M.; Jakupec, M. A.; Galanski, M.; Metzler-Nolte, N.; Keppler, B. K., Solid-phase synthesis of oxaliplatin-TAT peptide bioconjugates. *Dalton Transactions* **2012**, 41 (10), 3001-3005.
273. Massaguer, A.; Gonzalez-Canto, A.; Escribano, E.; Barrabes, S.; Artigas, G.; Moreno, V.; Marchan, V., Integrin-targeted delivery into cancer cells of a Pt(IV) pro-drug through conjugation to RGD-containing peptides. *Dalton Transactions* **2015**, 44 (1), 202-212.
274. Hu, R.; Dunn, T. A.; Wei, S.; Isharwal, S.; Veltri, R. W.; Humphreys, E.; Han, M.; Partin, A. W.; Vessella, R. L.; Isaacs, W. B.; Bova, G. S.; Luo, J., Ligand-Independent Androgen Receptor Variants Derived from Splicing of Cryptic Exons Signify Hormone-Refractory Prostate Cancer. *Cancer Research* **2009**, 69 (1), 16.
275. Albanito, L.; Madeo, A.; Lappano, R.; Vivacqua, A.; Rago, V.; Carpino, A.; Oprea, T. I.; Prossnitz, E. R.; Musti, A. M.; Andò, S.; Maggiolini, M., G Protein-Coupled Receptor 30 (GPR30) Mediates Gene Expression Changes and Growth Response to 17 $\beta$ -Estradiol and Selective GPR30 Ligand G-1 in Ovarian Cancer Cells. *Cancer Research* **2007**, 67 (4), 1859.
276. Early Breast Cancer Trialists' Collaborative, G., Relevance of breast cancer hormone receptors and other factors to the efficacy of adjuvant tamoxifen: patient-level meta-analysis of randomised trials. *The Lancet* **2011**, 378 (9793), 771-784.
277. Carlsson, J.; Nordgren, H.; Sjöström, J.; Wester, K.; Villman, K.; Bengtsson, N. O.; Ostenstad, B.; Lundqvist, H.; Blomqvist, C., HER2 expression in breast cancer primary tumours and corresponding metastases. Original data and literature review. *British Journal Of Cancer* **2004**, 90, 2344.
278. Kantoury, M.; Eslami Moghadam, M.; Tarlani Ali, A.; Divsalar, A., Structure Effect of Some New Anticancer Pt(II) Complexes of Amino Acid Derivatives with Small Branched or Linear Hydrocarbon Chains on Their DNA Interaction. *Chemical Biology & Drug Design* **2016**, 88 (1), 76-87.
279. Iakovidis, A.; Hadjiliadis, N., Complex compounds of platinum (II) and (IV) with amino acids, peptides and their derivatives. *Coordination Chemistry Reviews* **1994**, 135-136, 17-63.
280. Mukhopadhyay, S.; Barnés, C. M.; Haskel, A.; Short, S. M.; Barnes, K. R.; Lippard, S. J., Conjugated Platinum(IV)-Peptide Complexes for Targeting Angiogenic Tumor Vasculature. *Bioconjugate Chemistry* **2008**, 19 (1), 39-49.
281. Gaviglio, L.; Gross, A.; Metzler-Nolte, N.; Ravera, M., Synthesis and in vitro cytotoxicity of cis,cis,trans-diamminedichlorodisuccinatoplatinum(IV)-peptide bioconjugates. *Metallomics* **2012**, 4 (3), 260-266.
282. Parker, J. P.; Devocelle, M.; Morgan, M. P.; Marmion, C. J., Derivatisation of buforin IIb, a cationic henicosapeptide, to afford its complexation to platinum(II) resulting in a novel platinum(II)-buforin IIb conjugate with anti-cancer activity. *Dalton Transactions* **2016**, 45 (33), 13038-13041.
283. Pai, S.; Radacki, K.; Schatzschneider, U., Sonogashira, CuAAC, and Oxime Ligations for the Synthesis of MnI Tricarbonyl PhotoCORM Peptide Conjugates. *European Journal of Inorganic Chemistry* **2014**, 2014 (18), 2886-2895.
284. Li, H.; Aneja, R.; Chaiken, I., Click Chemistry in Peptide-Based Drug Design. *Molecules (Basel, Switzerland)* **2013**, 18 (8), 9797-9817.
285. Gust, R.; Beck, W.; Jaouen, G.; Schönenberger, H., *Optimization of cisplatin for the treatment of hormone dependent tumoral diseases Part 1: Use of steroidal ligands*. 2009; Vol. 253, p 2742-2759.
286. Ehrenstorfer-Schäfers, E.-M.; Steiner, N.; Altman, J.; Beck, W., Metal Complexes of Biologically Important Ligands, LV [1] Binding of Steroidal Hormones through  $\alpha$ -Amino Acid Ligands to Platinum(II) and Palladium(II). *Z. Naturforsch* **1990**, 45b, 817-827.
287. Gandolfi, O.; C. Apfelbaum, H.; Migron, Y.; Blum, J., *Syntheses of cis-dichlorodiammineplatinum analogs having steroidal hormones bound to the metal atom via malonato bridges*. 1989; Vol. 161, p 113-123.
288. Gabano, E.; Cassino, C.; Bonetti, S.; Prandi, C.; Colangelo, D.; Ghiglia, A.; Osella, D., Synthesis and characterisation of estrogenic carriers for cytotoxic Pt(II) fragments:



- biological activity of the resulting complexes. *Organic & Biomolecular Chemistry* **2005**, *3* (19), 3531-3539.
289. Hu, J.; Lu, J. R.; Ju, Y., Steroid/Triterpenoid Functional Molecules based on “Click Chemistry”. *Chemistry óAn Asian Journal* **2011**, *6* (10), 2636-2647.
290. Budelier, M. M.; Cheng, W. W. L.; Bergdoll, L.; Chen, Z.-W.; Abramson, J.; Krishnan, K.; Qian, M.; Covey, D. F.; Janetka, J. W.; Evers, A. S., Click chemistry reagent for identification of sites of covalent ligand incorporation in integral membrane proteins. *Analytical chemistry* **2017**, *89* (4), 2636-2644.
291. Mindt, T. L.; Struthers, H.; Brans, L.; Anguelov, T.; Schweinsberg, C.; Maes, V.; Tourwé, D.; Schibli, R., “Click to Chelate”: Synthesis and Installation of Metal Chelates into Biomolecules in a Single Step. *Journal of the American Chemical Society* **2006**, *128* (47), 15096-15097.
292. Chan, T. R.; Hilgraf, R.; Sharpless, K. B.; Fokin, V. V., Polytriazoles as Copper(I)-Stabilizing Ligands in Catalysis. *Organic Letters* **2004**, *6* (17), 2853-2855.
293. Bergbreiter, D. E.; Hamilton, P. N.; Koshti, N. M., Self-Separating Homogeneous Copper (I) Catalysts. *Journal of the American Chemical Society* **2007**, *129* (35), 10666-10667.
294. Mathew, P.; Neels, A.; Albrecht, M., 1,2,3-Triazolylienes as Versatile Abnormal Carbene Ligands for Late Transition Metals. *Journal of the American Chemical Society* **2008**, *130* (41), 13534-13535.
295. Lin-Na, Z. H. U.; Shao-Long, G.; Shu-Ling, G.; Chu-Luo, Y.; Jin-Gui, Q. I. N., Novel Pyrene-armed Calix[4]arenes through Triazole Connection: Ratiometric Fluorescent Chemosensor for Zn<sup>2+</sup> and Promising Structure for Integrated Logic Gates. *Chinese Journal of Chemistry* **2008**, *26* (8), 1424-1430.
296. Park, S. Y.; Yoon, J. H.; Hong, C. S.; Souane, R.; Kim, J. S.; Matthews, S. E.; Vicens, J., A Pyrenyl-Appended Triazole-Based Calix[4]arene as a Fluorescent Sensor for Cd<sup>2+</sup> and Zn<sup>2+</sup>. *The Journal of Organic Chemistry* **2008**, *73* (21), 8212-8218.
297. Maisonneuve, S.; Fang, Q.; Xie, J., Benzothiadiazoyl-triazoyl cyclodextrin: a selective fluoroionophore for Ni(II). *Tetrahedron* **2008**, *64* (37), 8716-8720.
298. David, O.; Maisonneuve, S.; Xie, J., Generation of new fluorophore by Click chemistry: synthesis and properties of  $\beta$ -cyclodextrin substituted by 2-pyridyl triazole. *Tetrahedron Letters* **2007**, *48* (37), 6527-6530.
299. Scattergood, P. A.; Elliott, P. I. P., An unexpected journey from highly tunable phosphorescence to novel photochemistry of 1,2,3-triazole-based complexes. *Dalton Transactions* **2017**, *46* (47), 16343-16356.
300. Ghosh, T. K.; Chakraborty, S.; Chowdhury, B.; Ghosh, P., Bis-Heteroleptic Ruthenium(II) Complex of Pendant Urea Functionalized Pyridyl Triazole and Phenathroline for Recognition, Sensing, and Extraction of Oxyanions. *Inorganic Chemistry* **2017**, *56* (9), 5371-5382.
301. Ross, D. A. W.; Scattergood, P. A.; Babaei, A.; Pertegas, A.; Bolink, H. J.; Elliott, P. I. P., Luminescent osmium(ii) bi-1,2,3-triazol-4-yl complexes: photophysical characterisation and application in light-emitting electrochemical cells. *Dalton Transactions* **2016**, *45* (18), 7748-7757.
302. Kumar, S. V.; Scottwell, S. Ø.; Waugh, E.; McAdam, C. J.; Hanton, L. R.; Brooks, H. J. L.; Crowley, J. D., Antimicrobial Properties of Tris(heteroleptic) Ruthenium(II) 2-Pyridyl-1,2,3-triazole “Click” Complexes against Pathogenic Bacteria, Including Methicillin-Resistant Staphylococcus aureus (MRSA). *Inorganic Chemistry* **2016**, *55* (19), 9767-9777.
303. Pages, B. J.; Sakoff, J.; Gilbert, J.; Zhang, Y.; Li, F.; Preston, D.; Crowley, J. D.; Aldrich-Wright, J. R., Investigating the cytotoxicity of platinum(II) complexes incorporating bidentate pyridyl-1,2,3-triazole “click” ligands. *Journal of Inorganic Biochemistry* **2016**, *165*, 92-99.

## **Chapter 2**

### **Materials and Methods**

## Instrumentation

### Infrared spectroscopy

Infrared spectroscopy (IR) measurements were obtained using a Nicolet iS10 FT-IR (Fourier-transform-IR) (*Thermo Fisher Scientific, Waltham, Massachusetts, USA*). The infrared spectra were recorded from 400-4000 wavenumbers ( $\text{cm}^{-1}$ ) and analysed using OMNIC™ software (*ver. 9.6, Thermo Fisher Scientific*).

### $^1\text{H}$ , $^{13}\text{C}$ , $^{19}\text{F}$ and $^{195}\text{Pt}$ Nuclear magnetic resonance spectroscopy

$^1\text{H}$ ,  $^{13}\text{C}$  and  $^{19}\text{F}$  Nuclear magnetic resonance (NMR) experiments were performed using a Bruker DX-400 spectrometer (*Bruker, Billerica, Massachusetts, USA*) at room temperature.  $^{195}\text{Pt}$  NMR was performed by Dr. Diego Montagner in the School of Chemistry, Maynooth University, or by Dr. John O'Brien in the School of Chemistry, Trinity College Dublin. The spectra were analysed using MestReNova software (*ver. 6.0.2-5475, Mestrelab, Santiago de Compostela, Spain*). Chemical shifts ( $\delta$ ) are given in parts per million (ppm) using the residual proton signals in the indicated solvents as internal standards, and coupling constants ( $J$ ) are quoted in hertz (Hz). Proton multiplicities are assigned using the following abbreviations; broad (b), singlet (s), doublet (d), triplet (t), quartet (q) and multiplet (m).<sup>1</sup>  $J$  values were calculated using multiplet analysis reporting with MestReNova.

### Mass spectrometry

Electron spray ionisation (ESI) mass spectrometry (MS) experiments were performed using an Advion Expression CMS instrument (*Advion, Ithaca, New York, USA*) at the Department of Chemistry, The Royal College of Surgeons in Ireland or on a Quattro *O k e t liquid* chromatography instrument (*Micromass, Waters Corp., Milford, Massachusetts, USA*) at the School of Chemistry and Chemical Biology, University College Dublin. High resolution (accurate) mass spectrometry (HRMS) experiments were performed by Dr. Jimmy Muldoon on a liquid chromatography time-of-flight (LCT) Classic instrument with ESI (*Micromass, Waters Corp., Milford, Massachusetts, USA*) at the School of Chemistry and Chemical Biology, University College Dublin or by Dr. Gary Hessman on a Bruker Compact™ HRMS with ESI at the School of Chemistry, Trinity College Dublin.

### **Single Crystal X-ray diffraction methods**

All X-ray crystallographic measurements were performed by Dr. Brendan Twamley at the School of Chemistry, Trinity College Dublin. X-ray structural analyses for all samples were performed on a Bruker D8 Quest ECO at 100(2) K with an Oxford Cryostream cryostat (*Oxford Cryosystems Ltd, Oxford, UK*), with samples mounted on a MiTeGen microloop (*MiTeGen, Itasca, New York, USA*) using Mo K $\alpha$  radiation ( $\lambda = 0.71073$ ). Bruker APEX software was used to collect and reduce data and determine the space group. Absorption corrections were applied using SADABS. Structures were solved with the XT structure solution program using Intrinsic Phasing and refined with the XL refinement package using Least Squares minimisation in Olex2. All non-hydrogen atoms were refined anisotropically. Hydrogen atoms were assigned to calculated positions using a riding model with appropriately fixed isotropic thermal parameters.

### **Elemental analysis**

Elemental analysis (C, H, N, S, Cl) was performed by Ms. Ann Connolly using an Exeter Analytical CE 440 elemental analyser (*Exeter Analytical Ltd, University of Warwick Science Park, The Venture Centre, Coventry, UK*) in the Micro-analytical laboratory at the School of Chemistry and Chemical Biology, University College Dublin.

### **Ultraviolet-Visible Spectroscopy**

UV-vis experiments were recorded using a Varian Cary 50 Scan UV-visible spectrophotometer (*Agilent Technologies, Santa Clara, California, USA*) using 1 cm path length quartz cuvettes. The UV-Vis spectra were analysed using Cary WinUV software (*ver. 3.0, Agilent Technologies, Santa Clara, California, USA*).

### **Fluorescence Spectroscopy**

Fluorescence emission measurements were conducted with a Varian Cary Eclipse Fluorescence spectrophotometer (*Agilent Technologies, Santa Clara, California, USA*) using an excited and emissive slit of 5 nm. The emission spectra were analysed using Cary Eclipse software (*ver. 3.0, Agilent Technologies, Santa Clara, California, USA*).

## HPLC

Chromatographic analysis and purification was performed on a Shimadzu Prominence LC system equipped with a Shimadzu SPD-20AV prominence UV/vis Detector (*Shimadzu Corp. Kyoto, Kyoto Prefecture, Japan*). YMC 5  $\mu\text{m}$  columns used for analytical HPLC were triart phenyl (150 Å, 4.6 mm, 4.6 x 250 mm I.D.) and triart C18 (110 Å, 4.6 mm, 4.6 x 250 mm I.D.) and for preparative HPLC were triart phenyl (150 Å, 10 mm, 4.6 x 250 mm I.D.) and triart C18 (110 Å, 4.6 mm, 10 x 250 mm I.D) (*YMC America Inc., Allentown, Pennsylvania, USA*). Flow rates of 0.7-1 mL/min (analytical) or 3-4 mL/min (semi-preparative) were used. Wavelength detections at 210, 280, 600 nm and 650 nm were used. Retention times (tR) for analytical RP-HPLC are reported in minutes.

## Organic Syntheses

### General considerations and materials

All commercially available reagents and solvents were purchased from Sigma Aldrich (*Sigma Aldrich Ireland Ltd., Arklow, Co Wicklow*). Sodium azide was sourced from TCI chemicals (*Tokyo Chemical Industry UK Ltd., Oxford, UK*) and  $K_2PtCl_4$  was sourced from Alfa Chemicals (*Alfa Chemicals Ltd, Binfield, Bracknell, UK*). All reagents were used as supplied without further purification unless otherwise stated. All reactions which are described as ‘anhydrous’ were conducted in oven-dried glassware ( $>120\text{ }^{\circ}\text{C}$ ) using syringe cap-septum technique, in anhydrous solvents under an inert  $N_2$  or argon atmosphere.

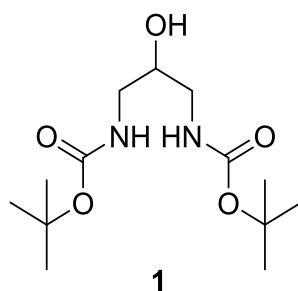
NIR fluorophores mono-alkyne mono-phenol (MAMP) NIR  $BF_2$ -azadipyrromethene (NIR-AZA) and bicyclo[6.1.0]non-4-yne (BCN) NIR-AZA were synthesised in house by Dr. Dan Wu.<sup>2-3</sup>

Cage ligand precursor 3,5-bis(pyridin-3-ylethynyl)aniline was synthesised and provided by the research group of Prof. Angela Casini, School of Chemistry, Cardiff University.

Estradiol and testosterone ligand starting materials ethinylestradiol and ethisterone were provided by Dr. Diego Montagner, School of Chemistry, Maynooth University.

Analytical thin layer chromatography (TLC) was carried out using pre-coated silica (*Merck DC silica gel 60 F254*) plates which were visualised under ultraviolet light (254 nm). Flash column chromatography was carried out using silica gel 60 (40 – 63  $\mu\text{m}$ ).

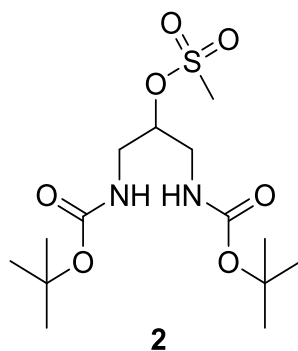
**Di-*tert*-butyl (2-hydroxypropane-1,3-diyl)dicarbamate<sup>4</sup> (1)**



1,3-Diaminopropan-2-ol (DAP) (5.915 g, 65.6 mmol) was dissolved in a 1:1 mixture of THF (tetrahydrofuran) and deionised water (70 mL) and stirred at 0 °C. Di-*tert*-butyl dicarbonate (BOC<sub>2</sub>O) (25 g, 114.56 mmol) dissolved in THF (10 mL) was added dropwise and the solution stirred at room temperature (rt) overnight, giving an opaque yellow mixture. The THF was removed under reduced pressure and the residue was extracted with Et<sub>2</sub>O (3 x 60 mL) and washed with brine (2 x 50 mL). The organic layers were dried over Na<sub>2</sub>SO<sub>4</sub>, filtered and concentrated under reduced pressure to give a viscous oil which was air dried overnight to yield **1** as a white solid (18.945 g, 99.5 %).

<sup>1</sup>H NMR (400 MHz, CDCl<sub>3</sub>) δ: 5.11 (s, 2H, NH), 3.73 (m, *J* = 10.1, 5.1 Hz, 1H, CH), 3.64 (bs, 1H, OH), 3.32-3.05 (m, 4H, CH<sub>2</sub>), 1.44 (s, 18H, C(CH<sub>3</sub>)<sub>3</sub>) ppm.

**Di-*tert*-butyl ((propan-2-yl methanesulfonate)-1,3-diyl)dicarbamate<sup>4</sup> (2)**



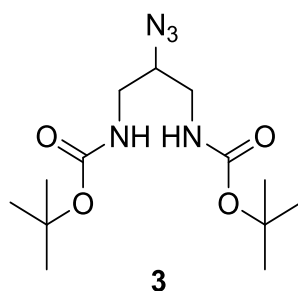
Triethylamine (TEA) (5 mL, 35.87 mmol) was added to a solution of **1** (5.309 g, 18.28 mmol) dissolved in dichloromethane (DCM) (100 mL) and purged with argon for 10 min. Methane sulfonyl chloride (MS-Cl) (3.39 mL, 43.87 mmol) was added drop-wise over 30 mins at 0 °C, giving a yellow solution and subsequently stirred at rt overnight. The unreacted MS-Cl was quenched with water (20 mL) and the solution was washed with brine (150 mL) and 10% aqueous NaHCO<sub>3</sub> (100 mL). The organic layer was dried over MgSO<sub>4</sub>, filtered and concentrated under reduced pressure to yield **2** as light yellow solid (6.597 g, 88 %).

<sup>1</sup>H NMR (400 MHz, CDCl<sub>3</sub>) δ: 5.18 (s, 2H, NH), 4.66 (d, *J* = 4.2 Hz, 1H, CH), 3.39 (tdd, *J* = 20.4, 9.6, 4.9 Hz, 4H, CH<sub>2</sub>), 3.09 (s, 3H, CH<sub>3</sub>), 1.43 (s, 18H, C(CH<sub>3</sub>)<sub>3</sub>) ppm.

<sup>13</sup>C NMR (101 MHz, CDCl<sub>3</sub>) δ: 156.34, 80.1, 79.1, 52.6, 40.8, 38.1, 28.3 ppm.



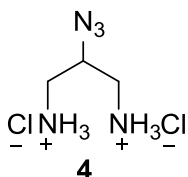
**Di-*tert*-butyl (2-azidopropane-1,3-diyl)dicarbamate<sup>4</sup> (3)**



$\text{NaN}_3$  (0.95 g, 14.613 mmol) and **2** (1.282 g, 3.4794 mmol) were dissolved in anhydrous *N,N*-dimethylformamide (DMF) (12 mL) and purged with  $\text{N}_2$  for 15 min and stirred at 80 °C overnight under  $\text{N}_2$ . The solution was cooled and washed with water (20 mL) and extracted into EtOAc (3 x 25 mL), followed by subsequent washes with water (2 x 25 mL) and brine (30 mL). The organic layer was dried over  $\text{MgSO}_4$ , filtered and concentrated under reduced pressure to give a dark yellow oil. This was recrystallized in hexane to yield **3** as a white solid (1.036 g, 94 %).

$^1\text{H}$  NMR (400 MHz,  $\text{CDCl}_3$ )  $\delta$ : 5.06 (s, 2H, NH), 3.64 (dd,  $J = 6.5, 3.9$  Hz, 1H, CH), 3.48 – 3.06 (m, 4H,  $\text{CH}_2$ ), 1.44 (s, 18H,  $\text{C}(\text{CH}_3)_3$ ) ppm.  $^{13}\text{C}$  NMR (101 MHz,  $\text{CDCl}_3$ )  $\delta$ : 155.2, 78.9, 59.9, 39.8, 27.3 ppm.

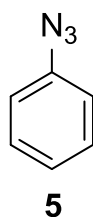
**2-azidopropane-1,3-diamine dihydrochloride<sup>5</sup> (DAP-N<sub>3</sub>.2HCl) (4)**



6M HCl (8 mL) was added to **3** (2.682 g, 8.504 mmol) dissolved in EtOAc (8 mL), stirred for at rt for 4 h and chilled at 4 °C overnight. The white crystals were vacuum filtered and washed with cold EtOAc (2 mL) to yield **4** (1.224 g, 77 %).

<sup>1</sup>H NMR (400 MHz, DMSO-*d*<sub>6</sub>) δ: 8.55 (s, 6H, NH<sub>3</sub>), 4.29 (tt, *J* = 8.5, 4.1 Hz, 1H, CH), 3.16 (dd, *J* = 13.4, 4.1 Hz, 2H, CH<sub>2</sub>), 2.91 (dd, *J* = 13.4, 8.7 Hz, 2H, CH<sub>2</sub>) ppm. <sup>13</sup>C NMR (101 MHz, DMSO-*d*<sub>6</sub>) δ: 57.0 (s, CH), 39.8 (s, CH<sub>2</sub>) ppm. <sup>1</sup>H NMR (400 MHz, D<sub>2</sub>O) δ: 4.24 (dd, *J* = 10.4, 7.0 Hz, 1H, CH), 3.34 (dd, *J* = 13.6, 3.7 Hz, 2H, CH<sub>2</sub>), 3.11 (dd, *J* = 13.6, 9.2 Hz, 2H, CH<sub>2</sub>) ppm. EA calc. % for C<sub>3</sub>H<sub>11</sub>Cl<sub>2</sub>N<sub>5</sub> requires C, 19.16; H, 5.90; N, 37.24; Cl, 37.70, found: C, 19.38, H, 5.96, N, 35.71, Cl 37.90%. FT-IR <sub>max</sub> (cm<sup>-1</sup>): 3061, 2954, 2848, 2538, 2135, 2078, 1979, 1591, 1573, 1510, 1471, 1406, 1361, 1324, 1279, 1203, 1144, 1081.

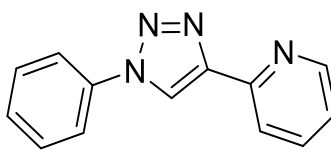
**Azidobenzene<sup>6</sup> (5)**



To a mixture of aniline (1.096 mL, 12 mmol) and 6M HCl (12 mL) was added  $\text{NaNO}_2$  (1.242 g, 18 mmol) dissolved in water (25 mL) slowly and stirred for 30 min at 0 °C.  $\text{NaN}_3$  (2.34 g 36 mmol) in water (50 mL) was added dropwise stirred for 2 h. The product was extracted into EtOAc (3 x 75 mL) and washed with water. The organic layers were dried with  $\text{Na}_2\text{SO}_4$ , filtered and concentrated under reduced pressure to yield **5** as a pale yellow oil in quantitative yield (1.415 g, 99 %)

$^1\text{H}$  NMR (400 MHz,  $\text{CDCl}_3$ )  $\delta$ : 7.42 – 7.34 (m, 2H, *ArH*), 7.20 – 7.14 (m, 1H, *ArH*), 7.06 (dt,  $J = 8.7, 1.7$  Hz, 2H, *ArH*) ppm.  $^{13}\text{C}$  NMR (101 MHz,  $\text{CDCl}_3$ )  $\delta$ : 140.1, 129.9, 125.0, 119.2 ppm.

**2-(1-phenyl-1*H*-1,2,3-triazol-4-yl)pyridine<sup>7</sup> (PTP) (**6**)**

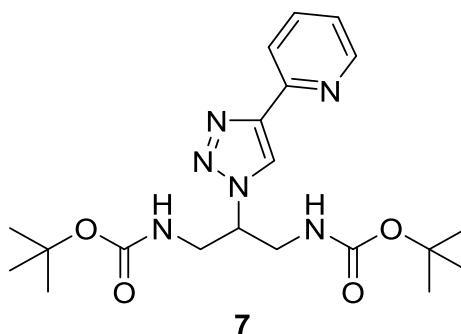


**6**

2-ethylene-pyridine (1.211 mL, 12 mmol) and **5** (1.499 mL 12 mmol) were dissolved in 3:2 MeOH:H<sub>2</sub>O (100 mL). CuSO<sub>4</sub>·5H<sub>2</sub>O (157 mg, 0.629 mmol) and sodium ascorbate (3.784 g, 19.1 mmol) in water was added and the reaction was stirred at rt for 1 h. The reaction was quenched with saturated ammonium chloride (50 mL) and extracted into DCM (2 x 75 mL). The organic layer was washed with brine (60 mL), dried over Na<sub>2</sub>SO<sub>4</sub>, filtered and concentrated under reduced pressure. The crude product was subject to column chromatography on silica using 10:1 DCM:EtOAc to yield **7** as a pale yellow crystalline solid (1.346 g, 50 %).

<sup>1</sup>H NMR (400 MHz, CDCl<sub>3</sub>) δ: 8.61 (m, *J* = 6.5 Hz, 2H, Trz*H* and Pyr*H*), 8.26 (d, *J* = 7.9 Hz, 1H, Py*H*), 7.85 – 7.78 (m, 3H, 1 Pyr*H* and 2 Ar*H*), 7.54 (dt, *J* = 10.3, 1.9 Hz, 2H, Ar*H*), 7.49 – 7.43 (m, 1H, Py*H*), 7.30 – 7.23 (m, 1H, Ar*H*) ppm. <sup>13</sup>C NMR (101 MHz, CDCl<sub>3</sub>) δ: 150.1, 149.6, 149.1, 137.2, 130.0, 129.0, 123.2, 120.6, 120.6, 120.1, 29.8 ppm. FT-IR <sub>max</sub> (cm<sup>-1</sup>): 3111, 3051, 2981, 2889, 1592, 1568, 1502, 1472, 1463, 1435, 1405, 1355, 1275, 1254, 1148, 1091, 1074, 843, 793, 757, 723, 708, 688.

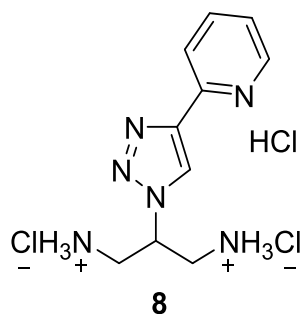
**Di-*tert*-butyl (2-(4-(pyridin-2-yl)-1*H*-1,2,3-triazol-1-yl)propane-1,3-diyl)dicarbamate (BOC<sub>2</sub>-PTPD) (**7**)**



2-ethynylpyridine (392  $\mu$ L, 3.879 mmol) and **3** (1.223 g, 3.879 mmol) were dissolved in 3:2 MeOH:H<sub>2</sub>O (100 mL). CuSO<sub>4</sub>·5H<sub>2</sub>O (48 mg, 0.192 mmol) and sodium ascorbate (1.1 g, 5.552 mmol) in water (10 mL) was added, and the reaction was stirred at rt for 2 h. The reaction was quenched with saturated ammonium chloride (50 mL) and extracted into DCM (2 x 75 mL). The organic layer was washed with brine (60 mL), dried over Na<sub>2</sub>SO<sub>4</sub>, filtered and concentrated under reduced pressure. The crude product was subjected to column chromatography on silica using 10:1 DCM:EtOAc, to yield **7** as a green yellow crystalline solid (1.597 g, 98 %).

<sup>1</sup>H NMR (400 MHz, CDCl<sub>3</sub>)  $\delta$ : 8.60 (s, 1H, TrzH), 8.24 – 8.11 (m, 2H, PyrH), 7.78 (t,  $J$  = 7.6 Hz, 1H, PyrH), 7.25 – 7.22 (m, 1H, PyrH), 5.29 (d,  $J$  = 6.7 Hz, 2H, NH), 4.78 – 4.71 (m, 1H, CH), 3.86 – 3.54 (m, 4H, CH<sub>2</sub>), 1.43 (d,  $J$  = 6.4 Hz, 18H, C(CH<sub>3</sub>)<sub>3</sub>) ppm. <sup>13</sup>C NMR (101 MHz, CDCl<sub>3</sub>)  $\delta$ : 156.5, 147.8, 130.4, 129.1, 128.5, 125.8, 120.3, 80.3, 60.5, 41.4, 28.5 ppm. ESI-MS:  $m/z$  ([M+H]<sup>+</sup>) 419.3. FT-IR<sub>max</sub> (cm<sup>-1</sup>): 3265, 2979, 2920, 1698, 1609, 1534, 1477, 1424, 1395, 1366, 1338, 1282, 1253, 1175, 1145, 1086, 1020, 782.

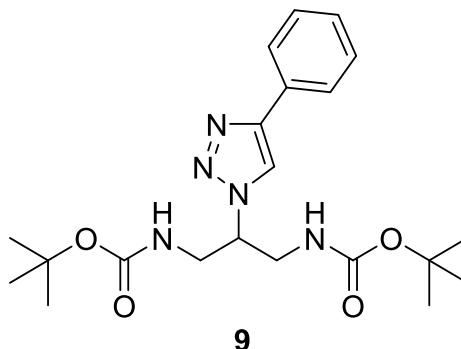
**2-(4-(pyridin-2-yl)-1*H*-1,2,3-triazol-1-yl)propane-1,3-diamine trihydrochloride (PTPD.3HCl) (**8**)**



6M HCl (8 mL) was added to **7** (550 mg, 1.314 mmol) dissolved in EtOAc (8 mL) of giving a dark green/black solution which was stirred at rt for 3 h. The white solid formed was filtered under vacuum to yield **8** (402 mg, 93 %).

$^1\text{H}$  NMR (400 MHz,  $\text{D}_2\text{O}$ )  $\delta$ : 9.12 (s, 1H, Pyr*H*), 8.78 (d,  $J = 5.7$  Hz, 1H, Trz*H*), 8.64 (t,  $J = 7.9$  Hz, 1H, Pyr*H*), 8.42 (d,  $J = 8.1$  Hz, 1H, Pyr*H*), 8.01 (t,  $J = 6.7$  Hz, 1H, Pyr*H*), 5.55 (td,  $J = 9.6, 4.7$  Hz, 1H, CH), 3.81 (ddd,  $J = 17.8, 14.1, 6.8$  Hz, 4H,  $\text{CH}_2$ ) ppm.  $^{13}\text{C}$  NMR (101 MHz,  $\text{D}_2\text{O}$ )  $\delta$ : 147.3, 142.0, 141.7, 140.6, 127.3, 126.3, 124.7, 57.5, 40.8 ppm. ESI-MS:  $m/z$  ( $[\text{M}-3\text{HCl}]^+$ ) 219.1. EA calc. % for  $\text{C}_{10}\text{H}_{17}\text{Cl}_3\text{N}_6$  requires C, 36.66; H, 5.23; N, 25.65% found C, 36.68; H, 5.20; N, 25.62 %. FT-IR  $_{\text{max}}$  ( $\text{cm}^{-1}$ ): 3066, 2854, 2009, 1610, 1496, 1219, 1093, 957, 921, 865, 790.

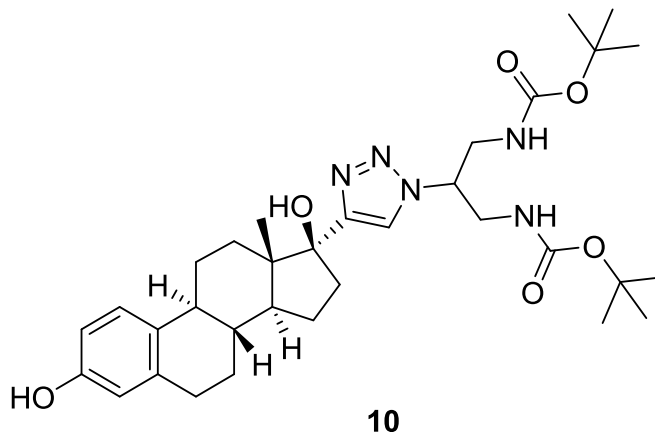
**Di-*tert*-butyl (2-(4-(phenyl)-1*H*-1,2,3-triazol-1-yl)propane-1,3-diyl)dicarbamate  
–(BOC<sub>2</sub>-PhTPD) (9)**



Phenylacetylene (348  $\mu$ L, 3.171 mmol) and **3** (1 g, 3.171 mmol) were dissolved in 3:2 MeOH:H<sub>2</sub>O (80 mL). CuSO<sub>4</sub>·5H<sub>2</sub>O (46 mg, 0.184 mmol) and sodium ascorbate (1.274 g, 6.34 mmol) in water (10 mL) was added and the reaction was stirred at rt for 2 h. The reaction was quenched with saturated ammonium chloride (50 mL) and extracted into DCM (2 x 75 mL). The organic layer was washed with brine (60 mL), dried over Na<sub>2</sub>SO<sub>4</sub>, filtered and concentrated under reduced pressure. The crude product was subject to column chromatography on silica using 9:1 DCM:MeOH to yield **9** as a white crystalline solid (744 mg, 56 %).

<sup>1</sup>H NMR (400 MHz, CDCl<sub>3</sub>)  $\delta$ : 7.87 (s, 1H, TrzH), 7.81 (d,  $J$  = 7.3 Hz, 2H, ArH), 7.43 (t,  $J$  = 7.6 Hz, 2H, ArH), 7.34 (t,  $J$  = 7.4 Hz, 1H, ArH), 5.46 – 4.91 (m, 2H, NH), 4.70 (p,  $J$  = 5.7 Hz, 1H, CH), 3.87 – 3.51 (dm, 4H CH<sub>2</sub>), 1.43 (s, 18H, C(CH<sub>3</sub>)<sub>3</sub>) ppm. <sup>13</sup>C NMR (101 MHz, CDCl<sub>3</sub>)  $\delta$ : 156.5, 147.8, 130.4, 129.1, 128.5, 125.8, 120.3, 80.3, 60.5, 41.4, 28.5 ppm. FT-IR<sub>max</sub> (cm<sup>-1</sup>): 3372, 3237, 3111, 3057, 2981, 2937, 1698, 1532, 1484, 1458, 1437, 1391, 1366, 1335, 1270, 1253, 1158, 1110, 1090, 1050, 1003, 851, 768, 721, 696.

**Di-*tert*-butyl (2-(4-(estradiol)-1*H*-1,2,3-triazol-1-yl)propane-1,3-diyl)dicarbamate (10)**

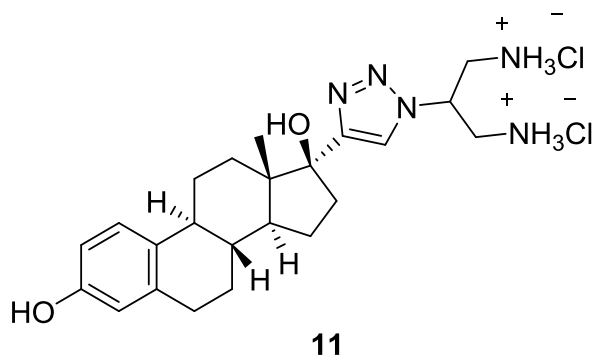


Ethinylestradiol (400 mg, 1.349 mmol) and **3** (425 mg, 1.349 mmol) were dissolved in 1:4 MeOH:H<sub>2</sub>O (50 mL). CuSO<sub>4</sub>·5H<sub>2</sub>O (34 mg, 0.135 mmol) and sodium ascorbate (534 mg, 2.698 mmol) in water (10 mL) was added and the reaction was stirred for 2 days at 40 °C. The reaction was quenched with saturated ammonium chloride (40 mL) and extracted into EtOAc (3 x 70 mL). The organic layer was washed with brine (70 mL), dried over Na<sub>2</sub>SO<sub>4</sub>, filtered and concentrated under reduced pressure. The crude product was subject to column chromatography on silica using 9:1 DCM:MeOH to yield **10** as a yellow crystalline solid (800 mg, 97 %).

<sup>1</sup>H NMR (400 MHz, CDCl<sub>3</sub>) δ: 7.65 (bs, 1H), 6.98 (bs, 1H), 6.56 (m, 2H), 5.58 (m, 2H), 4.65 (m, 1H), 3.78 (m, 2H), 3.54 (m, 2H), 3.17 (m, 1H), 2.74 (m, 2H), 2.35 (m, *J* = 18.3 Hz, 1H), 2.09 (m, 1H), 1.88 (m, *J* = 12.6 Hz, 3H), 1.55 (m, *J* = 28.2 Hz, 3H), 1.42 (bs, *J* = 4.2 Hz, 23H), 1.02 (s, 3H), 0.60 (m, 1H) ppm. <sup>13</sup>C NMR (101 MHz, CDCl<sub>3</sub>) δ: 207.5, 171.44, 156.7, 153.9, 138.2, 132.1, 126.4, 115.5, 113.0, 80.3, 60.6, 53.6, 48.6, 43.3, 41.3, 41.1, 39.5, 33.1, 31.1, 29.8, 28.4, 27.4, 26.3, 23.6, 21.2, 14.3 ppm. ESI-MS: *m/z* ([M+H]<sup>+</sup>) 612.5, ([M+Na]<sup>+</sup>) 634.5.



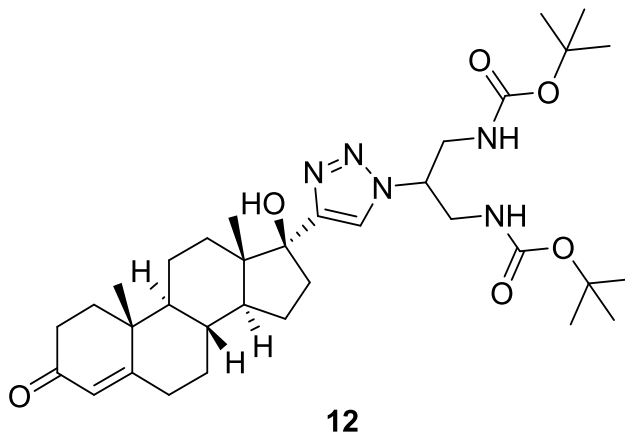
**(2-(4-(estradiol)-1*H*-1,2,3-triazol-1-yl)propane-1,3-diyl) dihydrochloride (11)**



**10** (800 mg, 1.308 mmol) was dissolved in EtOAc (5 mL) and 6M HCl (5 mL) was added. The solution was stirred at rt for 2 h and stored at -18 °C for 4 h. The resultant white precipitate was vacuum filtered, washing with EtOAc to yield **11** as an off-white solid (604 mg, 95 %).

<sup>1</sup>H NMR (400 MHz, D<sub>2</sub>O)  $\delta$ : 8.06 (s, 1H), 7.12 (d,  $J$  = 8.2 Hz, 1H), 6.61 (d,  $J$  = 8.2 Hz, 2H), 5.29 (td,  $J$  = 9.1, 4.4 Hz, 1H), 3.72 (ddd,  $J$  = 13.2, 9.3, 3.6 Hz, 2H), 3.63 (dd,  $J$  = 13.5, 3.7 Hz, 2H), 2.74 (d,  $J$  = 5.6 Hz, 2H), 2.43 – 2.32 (m, 1H), 2.17 – 2.05 (m, 2H), 1.95 – 1.81 (m, 3H), 1.66 – 1.48 (m, 3H), 1.47 – 1.32 (m, 2H), 1.32 – 1.11 (m, 2H), 0.97 (s, 3H), 0.78 (t,  $J$  = 12.7, 9.0 Hz, 1H) ppm. <sup>13</sup>C NMR (101 MHz, D<sub>2</sub>O)  $\delta$ : 154.4, 153.2, 138.9, 132.6, 126.7, 124.0, 115.3, 112.9, 82.7, 56.6, 47.9, 46.9, 42.7, 40.7, 40.6, 38.9, 36.7, 32.2, 28.9, 26.8, 25.6, 22.9, 13.7 ppm. ESI-MS:  $m/z$  ([M-2Cl]<sup>2+</sup>) 412.4, ([M-Cl]<sup>+</sup>) 446.5. FT-IR  $\nu_{\text{max}}$  (cm<sup>-1</sup>): 2930, 1608, 1581, 1498, 1453, 1354, 1284, 1247, 1138, 1018, 915, 872, 818, 785.

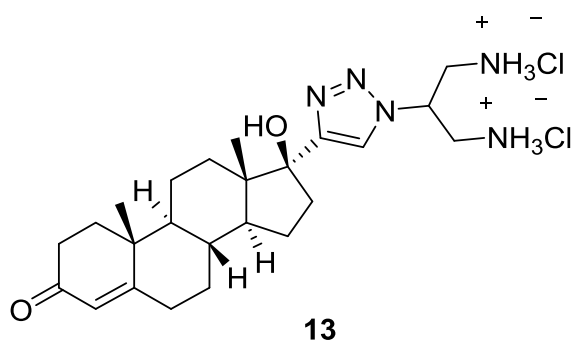
**Di-*tert*-butyl (2-(4-(testosterone)-1*H*-1,2,3-triazol-1-yl)propane-1,3-diyl)dicarbamate (12)**



Ethisterone (400 mg, 1.280 mmol) and **3** (404 mg, 1.280 mmol) were dissolved in 1:4 MeOH:H<sub>2</sub>O (50 mL). CuSO<sub>4</sub>·5H<sub>2</sub>O (32 mg, 0.128 mmol) and sodium ascorbate (507 mg, 2.560 mmol) in water (10 mL) were added and the reaction was stirred for 2 days at 40 °C. The reaction was quenched with saturated ammonium chloride (30 mL) and extracted into EtOAc (3 x 70 mL). The organic layer was washed with brine (70 mL), dried over Na<sub>2</sub>SO<sub>4</sub>, filtered and concentrated under reduced pressure. The crude product was subject to column chromatography on silica using 9:1 DCM:MeOH to yield **12** as a yellow crystalline solid (757 mg, 94 %).

<sup>1</sup>H NMR (400 MHz, CDCl<sub>3</sub>) δ: 7.58 (s, 1H), 5.67 (s, 1H), 5.52 (d, *J* = 4.9 Hz, 2H), 4.59 (s, 1H), 3.85 – 3.66 (m, 2H), 3.48 (m, *J* = 11.9 Hz, 2H), 3.22 (bs, 1H), 2.33 (dt, *J* = 35.7, 9.1 Hz, 5H), 2.08 (t, *J* = 11.7 Hz, 1H), 1.96 – 1.79 (m, 3H), 1.67 – 1.54 (m, 2H), 1.42 (d, *J* = 18.7 Hz, 20H), 1.16 (d, *J* = 9.2 Hz, 3H), 1.07 – 0.98 (m, 4H), 0.73 (td, *J* = 11.4, 3.7 Hz, 1H), 0.42 (t, *J* = 10.5 Hz, 1H) ppm. <sup>13</sup>C NMR (101 MHz, CDCl<sub>3</sub>) δ: 199.6, 171.4, 156.5, 153.6, 123.9, 122.1, 82.3, 80.1, 60.0, 53.1, 48.9, 46.9, 41.2, 38.6, 37.9, 36.3, 35.6, 34.0, 32.9, 32.7, 31.5, 28.4, 23.8, 20.6, 17.5, 14.4 ppm. ESI-MS: *m/z* ([M+H]<sup>+</sup>) 628.5, ([M+Na]<sup>+</sup>) 650.5.

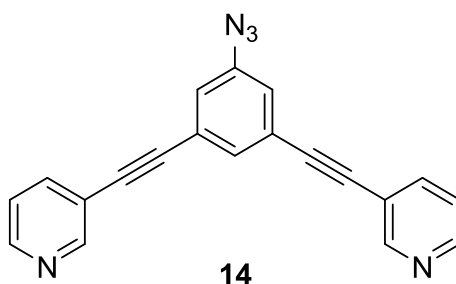
**(2-(4-(testosterone)-1H-1,2,3-triazol-1-yl)propane-1,3-diyl) dihydrochloride (13)**



**12** (220 mg, 0.3504 mmol) was dissolved in EtOAc (1.5 mL) and 6M HCl (1.2 mL) was added. The solution was stirred at rt for 4 h and stored at -18 °C overnight. The resultant white precipitate was vacuum filtered, washing with EtOAc to yield **13** as an off-white solid (38 mg, 22 %).

$^1\text{H}$  NMR (400 MHz,  $\text{MeOD-}d_4$ )  $\delta$ : 5.72 (s, 1H), 3.35 (s, 1H), 2.89 (s, 1H), 2.56 – 2.44 (m, 2H), 2.35 – 2.26 (m, 2H), 2.25 – 2.18 (m, 1H), 2.11 (d,  $J = 12.8$  Hz, 1H), 2.03 – 1.86 (m, 2H), 1.81 – 1.60 (m, 6H), 1.59 – 1.34 (m, 4H), 1.29 (s, 1H), 1.25 (s, 3H), 1.01 (m,  $J = 26.4, 18.6, 8.5$  Hz, 3H), 0.89 (s, 3H) ppm.  $^{13}\text{C}$  NMR (101 MHz,  $\text{MeOD-}d_4$ )  $\delta$ : 202.4, 175.1, 124.2, 80.3, 74.9, 55.3, 51.2, 47.8, 40.0, 39.8, 37.5, 36.8, 34.7, 33.9, 33.7, 32.9, 23.9, 21.9, 17.7, 13.2 ppm. ESI-MS:  $m/z$  ( $[\text{M}-2\text{Cl}]^{2+}$ ) 428.5.

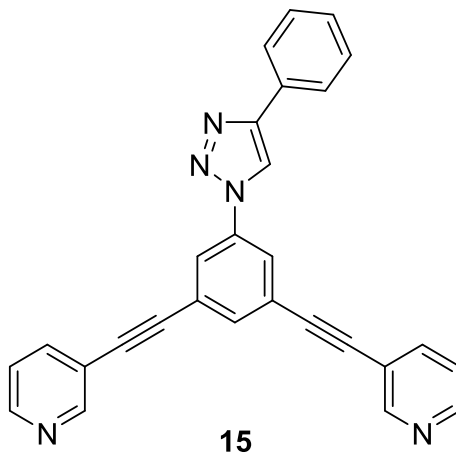
**3,3'-((5-azido-1,3-phenylene)bis(ethyne-2,1-diyl))dipyridine (CageL-N<sub>3</sub>) (**14**)**



To a solution of 3,5-bis(pyridin-3-ylethynyl)aniline (125 mg, 0.423 mmol) in 6M HCl (3 mL) was added NaNO<sub>2</sub> (35 mg, 0.508 mmol) dissolved in water (3 mL) slowly and stirred for 30 min at 0 °C. NaN<sub>3</sub> (55 mg 0.847 mmol) in water (3 mL) was added dropwise and stirred at rt for 2 h. The solution was brought to pH 8.5 with a 2 M solution of NaOH to give a pale brown precipitate which was vacuum filtered and washed with H<sub>2</sub>O and Et<sub>2</sub>O to yield **14** as a pale brown solid (134 mg, 98 %).

<sup>1</sup>H NMR (400 MHz, CDCl<sub>3</sub>) δ: 8.77 (d, *J* = 1.2 Hz, 2H), 8.59 (dd, *J* = 4.8, 1.3 Hz, 2H), 7.82 (dt, *J* = 7.9, 1.7 Hz, 2H), 7.51 (s, 1H), 7.32 (dd, *J* = 7.7, 4.9 Hz, 2H), 7.19 (d, *J* = 1.1 Hz, 2H) ppm. <sup>13</sup>C NMR (101 MHz, CDCl<sub>3</sub>) δ: 152.5, 149.2, 141.0, 138.7, 131.3, 124.7, 123.3, 122.3, 119.9, 90.7, 87.7 ppm. ESI-MS: *m/z* ([M+H]<sup>+</sup>) 322.4, ([M-N<sub>2</sub>]<sup>+</sup>) 294.3, ([M-N<sub>3</sub>]<sup>+</sup>) 279.2. FT-IR <sub>max</sub> (cm<sup>-1</sup>): 3415, 3072, 2981, 2362, 2219, 2107, 1665, 1578, 1560, 1475, 1442, 1407, 1360, 1275, 1248, 1187, 1171, 1119.

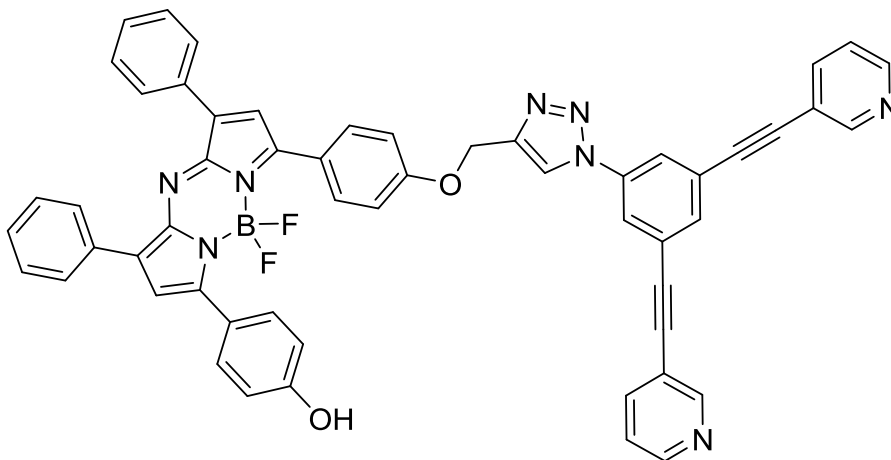
**3,3'-((5-(4-phenyl-1*H*-1,2,3-triazol-4-yl)-1,3-phenylene)bis(ethyne-2,1-diyl))dipyridine (Cage-T-Ph) (**15**)**



To a solution of **14** (20 mg, 0.0622 mmol) dissolved in DCM (0.5 mL) and diluted with 3:1 MeOH:H<sub>2</sub>O (6 mL) was added phenylacetylene (6.83  $\mu$ L, 0.0622 mmol). CuSO<sub>4</sub>·5H<sub>2</sub>O (2 mg, 0.006 mmol) and sodium ascorbate (16.4 mg, 0.083 mmol) in water (2 mL) was added and the reaction was stirred at rt for 5 h. The reaction was quenched with saturated ammonium chloride (20 mL) and extracted into DCM (3 x 20 mL). The organic layer was washed with brine (30 mL), dried over Na<sub>2</sub>SO<sub>4</sub>, filtered and concentrated under reduced pressure. The crude product was subject to column chromatography on silica using 9:1 DCM:MeOH to yield **15** as a white solid (25.2 mg, 96 %).

<sup>1</sup>H NMR (400 MHz, CDCl<sub>3</sub>)  $\delta$ : 8.80 (s, 2H), 8.60 (s, 2H), 8.27 (s, 1H), 7.98 (d,  $J$  = 1.3 Hz, 2H), 7.91 (d,  $J$  = 7.2 Hz, 2H), 7.84 (dt,  $J$  = 7.9, 1.7 Hz, 2H), 7.78 (s, 1H), 7.47 (t,  $J$  = 7.5 Hz, 2H), 7.38 (t,  $J$  = 7.4 Hz, 1H), 7.33 (dd,  $J$  = 7.7, 5.0 Hz, 2H) ppm. <sup>13</sup>C NMR (101 MHz, CDCl<sub>3</sub>)  $\delta$ : 152.5, 149.4, 148.9, 138.8, 137.4, 134.5, 130.0, 129.1, 128.8, 126.0, 125.0, 123.3, 123.3, 119.7, 117.4, 90.3, 88.5 ppm. ESI-MS:  $m/z$  ([M+H]<sup>+</sup>) 424.2. FT-IR  $\nu_{\text{max}}$  (cm<sup>-1</sup>): 3125, 3095, 3032, 2920, 1590, 1583, 1560, 1472, 1438, 1411, 1228, 1187, 1072, 1053, 1016, 861, 805, 701, 678.

**3,3'-((5-(4-(MAMP-NIR-AZA)-1*H*-1,2,3-triazol-4-yl)-1,3-phenylene)bis(ethyne-2,1-diyl))dipyridine (Cage-T-MAMP) (**16**)**



**16**

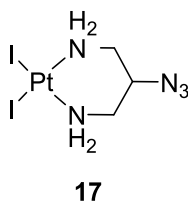
**16** was synthesised following preparation adapted from Murtagh *et al.*<sup>3</sup> Fluorescent analysis was performed in conjunction with Dr. Dan Wu, RCSI.

To a solution of fluorophore MAMP-NIR-AZA (18.2 mg, 0.032 mmol) dissolved in THF (4 mL) was added **14** (9.9 mg, 0.031 mmol) in H<sub>2</sub>O (2 mL) and THF (2 mL). CuSO<sub>4</sub>·5H<sub>2</sub>O (2 mg, 40% mole eq.) and sodium ascorbate (1.6 mg, 40% mol eq.) in water (1 mL) was added and the reaction was stirred at rt for 1 h. The THF was removed under reduced pressure and the residue diluted with H<sub>2</sub>O (10 mL) extracted into EtOAc (2 x 25 mL). The organic layer was washed with brine (20 mL), H<sub>2</sub>O (20 mL), dried over Na<sub>2</sub>SO<sub>4</sub>, filtered and concentrated under reduced pressure. The crude product was subject to column chromatography on silica using 85:15 DCM:EtOAc gradually increasing to 1:1 to yield **16** as a brown-green solid (11.9 mg, 43 %).

<sup>1</sup>H NMR (400 MHz, DMSO-*d*<sub>6</sub>)  $\delta$ : 10.61 (s, 1H), 10.39 (s, 1H), 9.21 (s, 1H), 8.86 (s, 2H), 8.66 (s, 2H), 8.29 (m, 1H), 8.17 (m, 5H), 8.08 (m, 2H), 7.95 (s, 1H), 7.66 (s, 1H), 7.52 (m, 8H), 7.31 (m, 2H), 7.17 (m, 3H), 6.95 (m, 2H), 5.43 (s, 1H), 3.92 (d, *J* = 5.7 Hz, 2H) ppm. <sup>19</sup>F NMR (376 MHz, DMSO-*d*<sub>6</sub>)  $\delta$ : -130.40 (q, *J* = 33.5 Hz, 2F) ppm. ESI-MS: *m/z* ([*M*-H]<sup>-</sup>) 887.4.  $\lambda_{\text{max}}$  abs (CHCl<sub>3</sub>): 680 nm,  $\lambda_{\text{max}}$  em (CHCl<sub>3</sub>): 716 nm.

## Inorganic syntheses

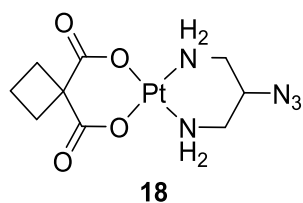
### *cis*-[Pt(II)I<sub>2</sub>(DAP-N<sub>3</sub>)]<sup>5</sup> (**17**)



KI (2.7 g, 16.262 mmol) dissolved in water (4 mL) was added drop-wise to a solution of K<sub>2</sub>[PtCl<sub>4</sub>] (1.5 g, 3.614 mmol) in water (11 mL) forming [PtI<sub>4</sub>]<sup>2-</sup>. A solution of **4** (680 mg, 3.614 mmol) and NaOH (292 mg, 7.3 mmol) in water (5 mL) was added drop-wise to the Pt solution and stirred at 60 °C for 5 min and chilled overnight at 4 °C yielding a brown solid which was vacuum filtered and washed with cold MeOH and Et<sub>2</sub>O. This yielded **17** as a light brown solid (1.957 g, 94 %).

<sup>1</sup>H NMR (400 MHz, DMSO-*d*<sub>6</sub>) δ: 5.85 – 5.32 (m, 4H, NH<sub>2</sub>), 4.26 – 4.15 (m, 1H, CH), 2.92 (qd, *J* = 13.3, 5.8 Hz, 2H, CH<sub>2</sub>), 2.71 – 2.54 (m, 2H, CH<sub>2</sub>) ppm. FT-IR<sub>max</sub> (cm<sup>-1</sup>): 3192, 2933, 2108, 1593, 1494, 1445, 1352, 1199, 1053.

**[Pt(II)(CBDCA)(DAP-N<sub>3</sub>)]<sup>5</sup> (**18**)**



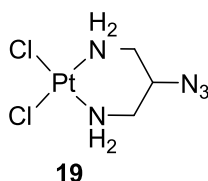
A solution of AgNO<sub>3</sub> (241 mg, 1.418 mmol) dissolved in water (3 mL) was added to a solution of **17** (410 mg, 0.727 mmol) in water (10 mL) and stirred overnight in darkness at rt. The reaction was filtered over celite to remove the resultant insoluble AgI. Cyclobutane 1,1-dicarboxylic acid (CBDCAH<sub>2</sub>) (105 mg, 0.727 mmol) and NaOH (58 mg, 1.454 mmol) dissolved in water (3 mL) were added to the filtrate and stirred in darkness at rt for 24 h. The reaction was concentrated under reduced pressure and the resulting precipitate was collected by vacuum filtration, washed with cold water, EtOH and Et<sub>2</sub>O, and dried over P<sub>2</sub>O<sub>5</sub> to yield **18** as a white solid (140 mg, 43 %).

<sup>1</sup>H NMR (400 MHz, DMSO-*d*<sub>6</sub>) δ: 5.54 – 5.28 (dm, 4H, NH<sub>2</sub>), 3.92 (t, *J* = 6.3 Hz, 1H, CH), 2.65 (dt, *J* = 11.8, 7.9 Hz, 4H, CH<sub>2</sub>), 2.55 – 2.45 (m, 4H, CH<sub>2</sub>) (overlap DMSO-*d*<sub>6</sub>), 1.70 – 1.58 (m, 2H, CH<sub>2</sub>) ppm. <sup>1</sup>H NMR (400 MHz, MeOD-*d*<sub>4</sub>) δ 4.10 (dt, *J* = 7.1, 3.4 Hz, 1H), 2.89 – 2.80 (m, 4H), 2.78 (d, *J* = 3.7 Hz, 4H), 1.91 – 1.77 (m, 2H) ppm. <sup>13</sup>C NMR (101 MHz, DMSO-*d*<sub>6</sub>) δ: 177.5, 58.6, 55.6, 45.3, 30.5, 34.9 ppm. <sup>195</sup>Pt NMR (108 MHz, DMSO-*d*<sub>6</sub>) δ: -1938.33 ppm. ESI-MS: *m/z* ([M-H]<sup>-</sup>) 452.4, ([M+H]<sup>+</sup>) 453.3, ([M+Na]<sup>+</sup>) 474.8. EA calc. % for C<sub>9</sub>H<sub>15</sub>N<sub>5</sub>O<sub>4</sub>Pt·0.5H<sub>2</sub>O requires C, 23.43; H, 3.50; N, 15.18 %, found C, 23.69; H, 3.21; N, 14.77 %. FT-IR<sub>max</sub> (cm<sup>-1</sup>): 3534, 3287, 3172, 3094, 2951, 2100, 1597, 1542, 1438.

Single crystals suitable for X-ray diffraction analysis were obtained on standing the filtrate at 4 °C for two weeks.<sup>8</sup>



**[Pt(II)Cl<sub>2</sub>(DAP-N<sub>3</sub>)] (**19**)**

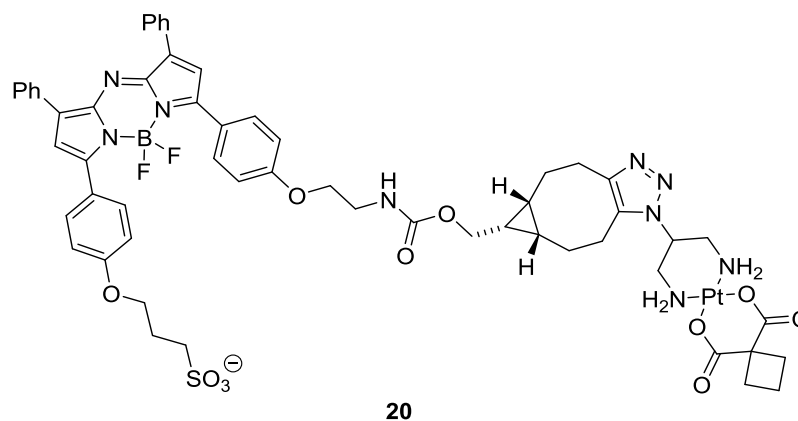


**19** was synthesised by the following preparation modified from Urankar *et al.*

A solution of AgNO<sub>3</sub> (250 mg, 1.472 mmol) dissolved in water (3 mL) was added to a solution of **17** (425 mg, 0.754 mmol) in water (7 mL) with 1 mL of DMF and stirred overnight in darkness at rt. The reaction was filtered over celite to remove the resultant insoluble AgI. KCl (141 mg, 1.885 mmol) in water (3 mL) was added to the filtrate and stirred in darkness at rt for 24 h. The reaction was left to stand at 4 °C for 3 days and the resultant yellow solid formed was collected by vacuum filtration, concentrated and washed with cold water, EtOH and Et<sub>2</sub>O, and dried over P<sub>2</sub>O<sub>5</sub> to yield **19** as a yellow solid (123 mg, 43 %).

<sup>1</sup>H NMR (400 MHz, DMSO-*d*<sub>6</sub>) δ 5.88 – 5.40 (bm, 4H, NH<sub>2</sub>), 4.17 (s, 1H, CH), 2.88 – 2.57 (m, 4H, CH<sub>2</sub>) ppm. <sup>13</sup>C NMR (101 MHz, DMSO-*d*<sub>6</sub>) δ: 58.0, 44.2, 42.7 ppm. EA calc. % for C<sub>3</sub>H<sub>9</sub>N<sub>5</sub>Cl<sub>2</sub>Pt.H<sub>2</sub>O requires C, 9.03; H, 2.78; N, 17.55; Cl, 17.76 %, found C, 9.25; H, 2.80; N, 17.34; Cl, 18.12 %. FT-IR <sub>max</sub> (cm<sup>-1</sup>): 3222, 3179, 3116, 2935, 2110, 1587, 1258.

**[Pt(II)(CBDCA)(DAP-BCN-NIR-AZA)] fluorophore conjugate - Pt-Flu<sup>8</sup> (20)**

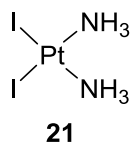


**18** (6.24 mg, 0.0138 mmol) was dissolved in 1:1 water:MeOH (5 mL) and added to fluorophore BCN-NIR-AZA (10 mg, 0.0115 mmol) in 1:1 MeOH:H<sub>2</sub>O (3 mL) and the solution was stirred for 200 min at rt. Reaction progress was monitored by analytical RP-HPLC in 70:30 MeCN:H<sub>2</sub>O and ESI-MS. The reaction mixture was purified by sephadex size exclusion chromatography and preparative RP-HPLC with 70:30 MeCN:H<sub>2</sub>O as eluent. The pure fractions were combined and concentrated under reduced pressure, frozen in liquid nitrogen and lyophilized to give conjugate **20** as a fine green solid (6.2 mg, 41 %).

<sup>1</sup>H NMR (400 MHz, 60% CD<sub>3</sub>CN + 40% D<sub>2</sub>O)  $\delta$ : 8.00 (bs, 6H), 7.84 (d,  $J$  = 24.4 Hz, 2H), 7.41-7.28 (m, 6H), 7.19 (bs, 2H), 7.00 (bs, 4H), 4.28-4.08 (m, 5H), 3.44 (bs, 1H), 2.91 (bs, 7H), 2.73 (bs, 7H), 2.21-2.01 (m, 5H), 1.77 (bs, 3H), 1.50 (bs, 1H), 1.22-1.10 (m, 3H), 0.92 (bs, 2H) ppm (NH<sub>2</sub> are not classified as overlaid with water peak). <sup>19</sup>F NMR (376 MHz, 60% CD<sub>3</sub>CN + 40% D<sub>2</sub>O)  $\delta$ : -130.96 (q,  $J$  = 32.0 Hz, 2F) ppm. <sup>195</sup>Pt NMR (500 MHz, MeOD-*d*<sub>4</sub>)  $\delta$ : -1957.96 ppm.

$\lambda_{\text{max}}$  abs (H<sub>2</sub>O/1% SDS): 699 nm,  $\lambda_{\text{max}}$  em (H<sub>2</sub>O/1% SDS): 721 nm. HR-MS (ESI):  $m/z$  ([M-H]<sup>-</sup>): C<sub>57</sub>H<sub>59</sub>BF<sub>2</sub>N<sub>9</sub>O<sub>11</sub>PtS, requires: 1321.3769, found: 1320.3612. RP-HPLC: Triart Phenyl 5 mm HPLC column (150 x 4.6 mm I.D), isocratic 60:40 MeCN:H<sub>2</sub>O as an eluent, t<sub>R</sub>: 1.19 min. Purity > 98%.

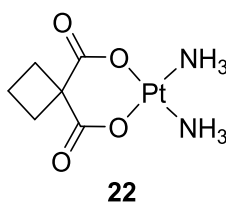
***cis*-[Pt(II)I<sub>2</sub>(NH<sub>3</sub>)<sub>2</sub>] –iodoplatin (**21**)**



KI (3 g, 18.07 mmol) in water (7 mL) was added drop-wise to a solution of K<sub>2</sub>[PtCl<sub>4</sub>] (1 g, 2.109 mmol) in water (10 mL) and was heated to 50 °C for 30 min forming a brown/black solution K<sub>2</sub>[PtI<sub>4</sub>]. Concentrated ammonium hydroxide was added dropwise with stirring until the brown colour was replaced by a yellow solution with a yellow precipitate which was vacuum filtered at once, washing with warm water, cold EtOH and Et<sub>2</sub>O. This yielded **21** as a yellow crystalline solid (967 mg, 83%).

FT-IR<sub>max</sub> (cm<sup>-1</sup>): 3255, 2009, 2981, 1520, 1380.

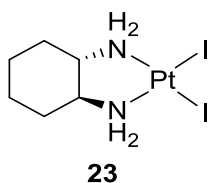
**[Pt(II)(CBDCA)(NH<sub>3</sub>)<sub>2</sub>] –carboplatin<sup>9</sup> (**22**)**



A solution of AgNO<sub>3</sub> (549 mg, 3.231 mmol) dissolved in water (10 mL) was added to a suspension of **21** (800 mg, 1.657 mmol) in water (30 mL) and stirred overnight in darkness at rt. The reaction was filtered over celite to remove the resultant insoluble AgI. CBDCAH<sub>2</sub> (227 mg, 1.574 mmol) and NaOH (126 mg, 3.148 mmol) dissolved in water (5 mL) were added to the filtrate and stirred in darkness at rt for 24 h. The reaction was concentrated under reduced pressure and the resulting precipitate was collected by vacuum filtration, washed with cold water, EtOH and Et<sub>2</sub>O, and dried over P<sub>2</sub>O<sub>5</sub> to yield **22** as a white solid (345 mg, 59 %).

<sup>1</sup>H NMR (400 MHz, D<sub>2</sub>O) δ: 2.84 (t, *J* = 7.9 Hz, 4H, CH<sub>2</sub>), 1.86 (t, *J* = 7.9 Hz, 2H, CH<sub>2</sub>) ppm. <sup>13</sup>C NMR (101 MHz, D<sub>2</sub>O) δ: 181.9, 56.2, 31.0, 15.3 ppm. ESI-MS: *m/z* ([M+H]<sup>+</sup>) 372, ([2M+Na]<sup>+</sup>) 764.7. EA calc. % for C<sub>6</sub>H<sub>10</sub>N<sub>2</sub>O<sub>4</sub>Pt requires C, 19.41; H, 3.26; N, 7.55, found C, 19.35; H, 3.11; N, 7.17 %. FT-IR <sub>max</sub> (cm<sup>-1</sup>): 3659, 3255, 2981, 2971, 2889, 1599, 1473, 1376, 1344.

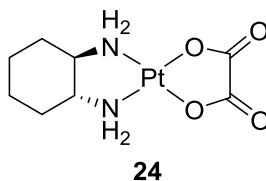
**[Pt(II)I<sub>2</sub>(DACH)]<sup>10</sup> (**23**)**



K<sub>2</sub>[PtCl<sub>4</sub>] (2.07 g, 4.97 mmol) was dissolved in water (50 mL) and KI (3.2g, 18.9 mmol) in water (10 mL) was added and the solution stirred for 30 min. (1*R*,2*R*)-(-)-1,2-Diaminocyclohexane (DACH) (0.591 g, 4.97 mmol) in water (10 mL) was added dropwise and stirred at rt for 18 h in darkness. The pale yellow/brown solid was vacuum filtered to yield **23** as a brown solid (2.629 g, 94 %).

<sup>1</sup>H NMR (400 MHz, DMSO-*d*<sub>6</sub>) δ: 6.26 – 5.65 (m, 4H, NH<sub>2</sub>), 2.33 (s, 2H, CH<sub>2</sub>), 1.96 (dd, *J* = 40.5, 11.3 Hz, 2H, CH<sub>2</sub>), 1.51 (s, 2H, CH<sub>2</sub>), 1.30 (d, *J* = 8.7 Hz, 2H, CH<sub>2</sub>), 1.10 – 0.98 (m, 2H, CH) ppm. <sup>13</sup>C NMR (101 MHz, DMSO-*d*<sub>6</sub>) δ: 63.7, 60.4, 30.8, 23.8 ppm. FT-IR <sub>max</sub> (cm<sup>-1</sup>): 3655, 3252, 3180, 3108, 2981, 2971, 2938, 2865, 1557, 1394.

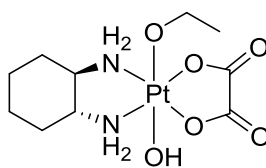
**[Pt(II)(DACH)(Ox)] –oxaliplatin<sup>11</sup> (**24**)**



A solution of AgNO<sub>3</sub> (632mg, 3.72 mmol) dissolved in water (10 mL) was added to a solution of **23** (1.100 g, 1.908 mmol) in water (40 mL) and stirred overnight in darkness at rt. The reaction was filtered over celite to remove the resultant insoluble AgI. Sodium oxalate (NaOx) (243 mg, 1.81 mmol) in water (3 mL) was added to the filtrate which was filtered immediately to remove any Ag<sub>2</sub>(Ox) precipitate and then stirred in darkness at rt for 24 h.. The filtrate was concentrated under reduced pressure and the resulting precipitate was collected by vacuum filtration, washed with cold water, EtOH and Et<sub>2</sub>O, and dried over P<sub>2</sub>O<sub>5</sub> to yield **24** as a white solid (590 mg, 82 %).

<sup>1</sup>H NMR (400 MHz, DMSO-*d*<sub>6</sub>) δ: 6.10 (d, *J* = 8.5 Hz, 2H, NH<sub>2</sub>), 5.37 (t, *J* = 9.4 Hz, 2H, NH<sub>2</sub>), 2.01 (s, 2H, CH<sub>2</sub>), 1.82 (d, *J* = 12.3 Hz, 2H, CH<sub>2</sub>), 1.45 (d, *J* = 8.3 Hz, 2H, CH<sub>2</sub>), 1.20 (d, *J* = 9.9 Hz, 2H, CH<sub>2</sub>), 1.01 (t, *J* = 9.8 Hz, 2H, CH<sub>2</sub>) ppm. <sup>13</sup>C NMR (101 MHz, DMSO-*d*<sub>6</sub>) δ: 166.4, 62.3, 32.0, 24.5 ppm. ESI-MS: *m/z* ([M+H]<sup>+</sup>) 398, ([M+Na]<sup>+</sup>) 420.2. EA calc. % for C<sub>8</sub>H<sub>14</sub>N<sub>2</sub>O<sub>4</sub>Pt.0.5H<sub>2</sub>O requires C, 23.65; H, 3.72; N, 6.89, found C, 23.75; H, 3.43; N, 6.69 %. FT-IR <sub>max</sub> (cm<sup>-1</sup>): 3657, 3367, 3181, 2981, 2971, 2889, 1630, 1380, 1318.

**[Pt(IV)(DACH)(OEt)(OH)(Ox)] (25)**



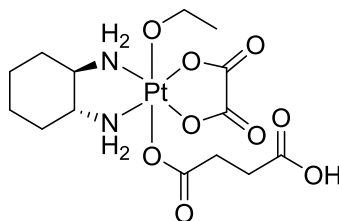
**25**

**25** was synthesised by the following preparation modified from Feazell *et al.*<sup>12</sup>

A solution of **24** (382 mg, 0.962 mmol) suspended in EtOH (400 mL) and 1 mL of 50 % wt/v H<sub>2</sub>O<sub>2</sub> in water was heated to 70 °C with stirring for 5 h, giving rise to a pale white solution. The solvent was removed under reduced pressure giving rise to a yellow oily residue. The addition of Et<sub>2</sub>O (20 mL) gave a precipitate which was collected by vacuum filtration, washing with cold EtOH and Et<sub>2</sub>O to yield **25** as a yellow solid (405 mg, 92 %).

<sup>1</sup>H NMR (400 MHz, DMSO-*d*<sub>6</sub>) δ: 10.23 (s, 1H, OH), 7.89 (s, 1H, NH), 7.37 (s, 1H, NH), 7.03 (s, 1H, NH), 6.42 (s, 1H, NH), 3.20 (dt, *J* = 6.7, 5.6 Hz, 2H, CH<sub>2</sub>), 2.14 – 1.86 (m, 3H, CH<sub>3</sub>), 1.57 – 1.33 (m, 5H, DACH), 1.14 – 0.99 (m, 5H, DACH) ppm. <sup>13</sup>C NMR (101 MHz, DMSO-*d*<sub>6</sub>) δ: 164.9, 164.9, 62.8, 61.1, 60.9, 60.4, 56.5, 30.9, 24.2, 18.9 ppm. <sup>195</sup>Pt NMR (86 MHz, DMSO-*d*<sub>6</sub>) δ: 1296.79 ppm. ESI-MS: *m/z* ([M+H]<sup>+</sup>) no signal. EA calc. % for C<sub>10</sub>H<sub>19</sub>N<sub>2</sub>O<sub>6</sub>Pt requires C, 19.41; H, 3.26; N, 7.55, found C, 19.35; H, 3.11; N, 7.17 %. FT-IR <sub>max</sub> (cm<sup>-1</sup>): 3436, 3177, 2981, 2971, 1705, 1663, 1585, 1359.

**[Pt(IV)(DACH)(OEt)(Ox)(succinato)] (26)**



**26**

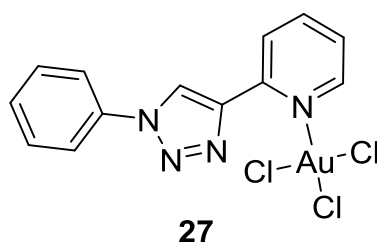
**26** was synthesised by the following preparation modified from Feazell *et al.*<sup>12</sup>

A solution of **25** (245 mg, 0.533 mmol) dissolved in DMF (3 mL) was heated to 75 °C. To this was added succinic anhydride (80 mg, 0.80 mmol) in DMF (1 mL) and stirred for 18 h, giving a dark brown solution. This was reduced under vacuum giving an oil. The addition of acetone precipitated a white solid, which was vacuum filtered and washed with acetone and Et<sub>2</sub>O to yield **26** as a brown solid (210 mg, 70 %).

<sup>1</sup>H NMR (400 MHz, DMF-*d*<sub>7</sub>) δ: 12.42 (s, 1H), 8.93 (s, 1H), 8.75 – 8.18 (m, 1H), 7.84 (s, 1H), 7.04 (s, 1H), 3.10 (q, *J* = 6.8 Hz, 1H), 2.92 (m, *J* = 3.7, 1.8 Hz, 2H), 2.84 (s, 1H), 2.75 (m, *J* = 3.8, 1.9 Hz, 2H), 2.49 (dd, *J* = 23.8, 18.3 Hz, 5H), 2.26 (dd, *J* = 21.6, 11.2 Hz, 1.5H), 1.57 (s, 3.5H), 1.26 (d, *J* = 10.7 Hz, 2H), 1.08 (dt, *J* = 22.1, 6.9 Hz, 2H) ppm. <sup>13</sup>C NMR (101 MHz, DMF-*d*<sub>7</sub>) δ: 174.19, 173.9, 65.5, 64.2, 62.3, 60.2, 24.2, 15.9, 15.1 ppm. <sup>1</sup>H NMR (400 MHz, DMSO-*d*<sub>6</sub>) δ: 12.09 (s, 1H), 8.62 – 6.88 (bm, 4H, NH<sub>2</sub>), 3.03 (q, *J* = 13.6, 6.7 Hz, 4H), 2.38 (m, 4H), 1.50 (m, 5H), 1.20 – 0.96 (m, 8H). <sup>195</sup>Pt NMR (86 MHz, DMSO-*d*<sub>6</sub>) δ: 1366.95 ppm. ESI-MS: *m/z* ([M+Na]<sup>+</sup>) 582.3 EA calc. % for C<sub>14</sub>H<sub>24</sub>N<sub>2</sub>O<sub>9</sub>Pt requires C, 30.06; H, 4.32; N, 5.01, found C, 30.15; H, 4.37; N, 4.81 %. FT-IR <sub>max</sub> (cm<sup>-1</sup>): 3656, 3178, 2981, 2971, 2889, 1714, 1652, 1462, 1380.



**[Au(III)Cl<sub>3</sub>(PTP)] (27)**



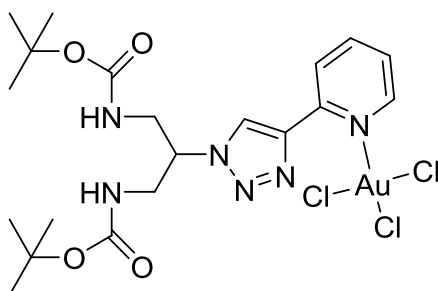
The following reaction was carried out under my supervision by Mr. Zehao Zhou, a visiting exchange student from Soochow University, China.

Na[AuCl<sub>4</sub>].2H<sub>2</sub>O (90 mg, 0.23 mmol) and **6** (50 mg, 0.23 mmol) were dissolved in MeOH (10 mL) and stirred at rt for 18 h. The solid precipitate was collected by vacuum filtration, washed with cold MeOH and dried to yield **27** as a yellow solid (100 mg, 83 %).

<sup>1</sup>H NMR (400 MHz, Acetone-*d*<sub>6</sub>) δ: 9.63 (s, 1H, TrzH), 9.31 (d, <sup>3</sup>*J* = 5.8 Hz, 1H, ArH), 8.49 (d, *J* = 3.8 Hz, 2H, ArH), 8.05 (dd, <sup>3</sup>*J* = 5.8 Hz, <sup>4</sup>*J* = 3.8 Hz, 2H, ArH), 7.96 (dd, <sup>3</sup>*J* = 9.4, <sup>4</sup>*J* = 5.8 Hz, 1H, ArH), 7.74 – 7.67 (m, 2H, ArH), 7.62 (dd, <sup>3</sup>*J* = 10.6, <sup>4</sup>*J* = 4.3 Hz, 1H, ArH) ppm. ESI-MS: *m/z* [(PTP+H)<sup>+</sup>] 223.1, [(AuCl<sub>3</sub>+H)<sup>+</sup>] 303.2. EA calc. % for C<sub>13</sub>H<sub>10</sub>AuCl<sub>3</sub>N<sub>4</sub>.0.5CH<sub>3</sub>OH requires C, 29.94; H, 2.23; N, 10.35; Cl, 19.69, found C, 29.84 H, 1.81 N, 10.35 Cl, 19.31 %. FT-IR<sub>max</sub> (cm<sup>-1</sup>): 3101, 1604, 1593, 1571, 1556, 1503, 1474, 1468, 1447, 1424, 1238, 1170, 1107, 1040, 774, 757.

Single crystals suitable for X-ray diffraction analysis were obtained by slow evaporation of a solution of **27** in acetone at rt.

**[Au(III)Cl<sub>3</sub>(BOC<sub>2</sub>-PTPD)] (28)**

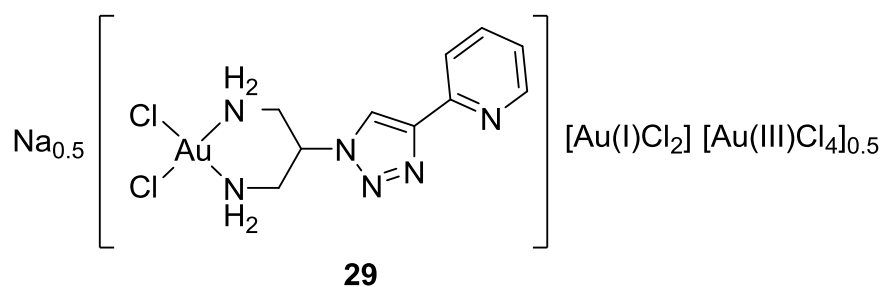


**28**

The following reaction was carried out under my supervision by Mr. Zehao Zhou, a visiting exchange student from Soochow University, China.

Na[AuCl<sub>4</sub>].2H<sub>2</sub>O (95 mg, 0.24 mmol) and **7** (100 mg, 0.24 mmol) were dissolved in MeOH (10 mL) and stirred at rt for 18 h. The addition of water (10 mL) induced precipitation of a yellow solid, which was collected by vacuum filtration, washed with cold water and dried to yield **28** (158 mg, 91%).

<sup>1</sup>H NMR (400 MHz, Acetone-*d*<sub>6</sub>) δ: 8.98 (s, 1H, TrzH), 8.94 (d, <sup>3</sup>*J* = 5.3 Hz, 1H, ArH), 8.58 (t, *J* = 7.7 Hz, 1H, ArH), 8.47 (d, *J* = 8.0 Hz, 1H, ArH), 7.93 (t, *J* = 6.3 Hz, 1H, ArH), 5.10 – 5.00 (m, 1H, CH), 3.77 – 3.63 (m, 4H, CH<sub>2</sub>), 1.34 (s, 18H, C(CH<sub>3</sub>)<sub>3</sub>) ppm. ESI-MS: *m/z* [(M-Cl)<sup>+</sup>] 685.1. EA calc. % for C<sub>20</sub>H<sub>30</sub>AuCl<sub>3</sub>N<sub>6</sub>O<sub>4</sub>·1.25CH<sub>3</sub>OH requires C, 33.50; H, 4.63; N, 11.03; Cl, 13.96, found C, 33.34 H, 4.02 N, 10.91 Cl, 13.64 %. FT-IR<sub>max</sub> (cm<sup>-1</sup>): 3333, 3133, 1667, 1606, 1568, 1515, 1428, 1366, 1315, 1250, 1161, 1113, 981, 781.

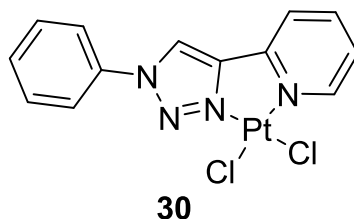


Na[AuCl<sub>4</sub>].2H<sub>2</sub>O (200 mg, 0.502 mmol) dissolved in water (8 mL) was added to a solution of **8** (82 mg, 0.251 mmol) and NaOH (30 mg, 0.75 mmol) in water (3 mL) and stirred at rt for 24 h. The solid, which precipitated instantly, was collected by vacuum filtration, washed with water and Et<sub>2</sub>O to yield **29** as a pale yellow-brown solid (108 mg, 46%).

ESI-MS: *m/z* [AuCl<sub>2</sub>(PTPD)<sup>+</sup>] 485.1. EA calc. % for C<sub>10</sub>H<sub>14</sub>Au<sub>2.5</sub>Cl<sub>6</sub>N<sub>6</sub>Na<sub>0.5</sub> requires C, 12.85; H, 1.51; N, 8.99; Cl, 22.75, found C, 13.25; H, 1.44; N, 8.99; Cl, 22.64 %. FT-IR <sub>max</sub> (cm<sup>-1</sup>): 3095, 2948, 2354, 1605, 1569, 1471, 1446, 1346, 1231, 1031, 910, 777.

Single crystals suitable for X-ray diffraction analysis were obtained by slow evaporation from the filtrate at rt.

**[Pt(II)Cl<sub>2</sub>(PTP)] (30)**

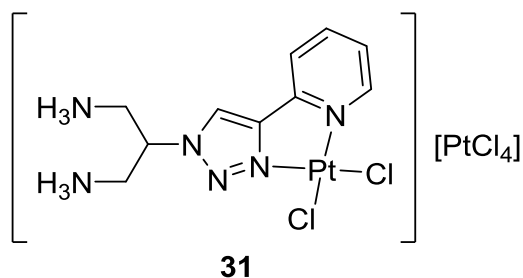


Novel synthetic procedure of the previously reported compound **30**.<sup>13-14</sup>

K<sub>2</sub>[PtCl<sub>4</sub>] (373 mg, 0.899 mmol) dissolved in water (10 mL) was added to a solution of **6** (200 mg, 0.899 mmol) MeOH (10 mL) and stirred at rt for 4 days. The solid precipitate was collected by vacuum filtration washing with cold MeOH and dried to yield **30** as a yellow solid (166 mg, 35 %).

<sup>1</sup>H NMR (400 MHz, DMF-*d*<sub>7</sub>) δ: 9.96 (s, 1H, TrzH), 9.53 (d, <sup>3</sup>*J* = 5.9 Hz, 1H, ArH), 8.48 (td, <sup>3</sup>*J* = 7.8 Hz and <sup>4</sup>*J* = 1.2 Hz, 1H, ArH), 8.35 (d, <sup>3</sup>*J* = 7.4 Hz, 1H, ArH), 8.06 (d, <sup>3</sup>*J* = 7.4 Hz, 2H, ArH), 7.89 – 7.83 (m, 3H, ArH), 7.81-7.68 (m, 3H, ArH) ppm. <sup>13</sup>C NMR (101 MHz, DMF-*d*<sub>7</sub>) δ: 149.6, 148.8, 141.0, 136.6, 130.7, 130.4, 126.3, 124.8, 122.5, 121.3 ppm. ESI-MS: *m/z* [(M+H)<sup>+</sup>] 489. EA calc. % for C<sub>13</sub>H<sub>10</sub>Cl<sub>2</sub>N<sub>4</sub>Pt·0.5CH<sub>3</sub>OH requires C, 32.16; H, 2.40; N, 11.11; Cl, 14.06, found C, 31.81; H, 1.95; N, 10.99; Cl, 13.68 %. FT-IR <sub>max</sub> (cm<sup>-1</sup>): 3146, 2981, 2889, 1628, 1594, 1500, 1463, 1285, 1150, 1106, 1074, 968, 766.

**[Pt(II)Cl<sub>2</sub>(PTPDH<sub>2</sub>)] [PtCl<sub>4</sub>] (**31**)**

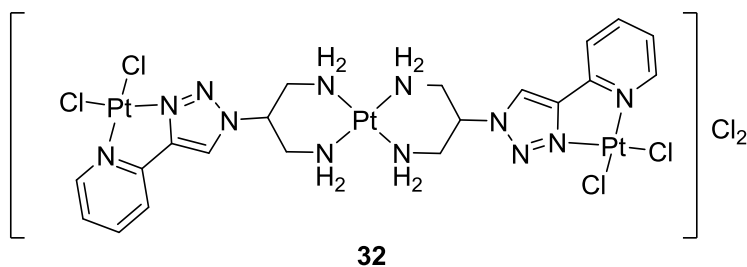


K<sub>2</sub>[PtCl<sub>4</sub>] (104 mg, 0.251 mmol) and **8** (82 mg, 0.251 mmol) were dissolved in acetic acid (6.5 mL) and refluxed at 115 °C for 4 days. The solution was cooled to rt and the solid precipitate was vacuum filtered, washing with water, MeOH, EtOH and Et<sub>2</sub>O to yield **31** as a pale brown solid (50 mg, 24 %).

<sup>1</sup>H NMR (400 MHz, D<sub>2</sub>O) δ: 8.88 (s, 1H), 8.66 (s, 1H), 8.40 (d, *J* = 47.6 Hz, 6H), 8.11 (d, *J* = 7.8 Hz, 1H), 7.99 (t, *J* = 7.5 Hz, 1H), 7.43 (s, 1H), 5.40 (s, 1H), 3.55 – 3.42 (m, 4H) ppm. ESI-MS: *m/z* [(PtCl<sub>2</sub>PTPD<sup>2+</sup>+H)<sup>+</sup>] 484.6, [(PtCl<sub>2</sub>PTPD+2Na)<sup>+</sup>] 532.4. EA calc. % C<sub>10</sub>H<sub>16</sub>Cl<sub>6</sub>N<sub>6</sub>Pt<sub>2</sub>·0.5CH<sub>3</sub>COOH requires C, 15.49; H, 2.13; N, 9.85; found C, 15.52; H, 1.87; N, 9.69 %. FT-IR <sub>max</sub> (cm<sup>-1</sup>): 3093, 2981, 2360, 1587, 1493, 1466, 1382, 1281, 1250, 1131, 1099, 953, 778.

Single crystals suitable for X-ray diffraction analysis were obtained by slow evaporation from the filtrate and washings at rt.

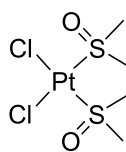
**[Pt(II)<sub>3</sub>Cl<sub>4</sub>(PTPD)<sub>2</sub>]Cl<sub>2</sub> (**32**)**



K<sub>2</sub>[PtCl<sub>4</sub>] (300 mg, 0.72 mmol) dissolved in water (5 mL) was added to a solution of **8** (118 mg, 0.36 mmol) and KOH (43 mg, 0.11 mmol) in water (5 mL). The solution was stirred at rt for 3 days and a pale yellow solid was collected by vacuum filtration, washed with water, EtOH and Et<sub>2</sub>O and dried to yield **32** (193 mg, 65 %).

HR-MS (ESI): *m/z* ([M-Cl]<sup>+</sup>): C<sub>20</sub>H<sub>28</sub>Cl<sub>5</sub>N<sub>12</sub>Pt<sub>3</sub>, requires: 1198.9897, found: 1198.9928; ([Pt(PTPD)Cl<sub>2</sub>+H]<sup>+</sup>): C<sub>10</sub>H<sub>15</sub>Cl<sub>2</sub>N<sub>6</sub>Pt, requires: 485.2560, found: 485.0369. (2[Pt(PTPD)Cl<sub>2</sub>+H]<sup>+</sup>): 2[C<sub>10</sub>H<sub>15</sub>Cl<sub>2</sub>N<sub>6</sub>Pt], requires: 969.5040, found: 969.0676. EA calc. % C<sub>20</sub>H<sub>28</sub>Cl<sub>6</sub>N<sub>12</sub>Pt<sub>3</sub> requires C, 19.46; H, 2.29; N, 13.62; Cl, 17.23, found C, 19.37; H, 2.30; N, 13.36; Cl, 16.98 %. FT-IR<sub>max</sub> (cm<sup>-1</sup>): 3516, 3194, 3105, 2980, 2889, 2360, 1614, 1602, 1578, 1470, 1410, 1382, 1225, 1141, 1031, 966, 789, 742.

*cis*-[Pt(II)Cl<sub>2</sub>(DMSO)<sub>2</sub>]<sup>15</sup> (**33**)

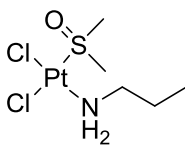


**33**

DMSO (0.77 mL, 10.8 mmol) was added to a solution of K<sub>2</sub>[PtCl<sub>4</sub>] (1.5 g, 3.6 mmol) in water (15 mL) and the mixture stirred at rt in the dark for 18 h. The resulting precipitate was collected by vacuum filtration, washed with cold water, EtOH and Et<sub>2</sub>O, and dried over P<sub>2</sub>O<sub>5</sub> to yield **33** as a light yellow solid (1.398 g, 92 %).

EA calc. % for C<sub>4</sub>H<sub>12</sub>Cl<sub>2</sub>O<sub>2</sub>S<sub>2</sub>Pt requires C, 11.38; H, 2.86; Cl, 16.79; S, 15.19, found C, 11.30; H, 2.79; Cl, 16.96; S, 14.79 %. FT-IR <sub>max</sub> (cm<sup>-1</sup>): 3037, 2981, 2916, 1473, 1462, 1383, 1299, 1251, 1152, 1131, 1016.

***cis*-[Pt(II)Cl<sub>2</sub>(DMSO)(*n*-propylamine)] (**34**)**



**34**

**34** was synthesised by the following preparation modified from Bitha *et al.*<sup>16</sup>

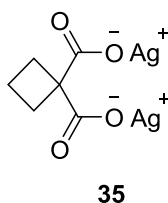
A suspension of **33** (100 mg, 0.237 mmol) in water (4 mL) was heated to 40°C and *n*-propylamine (23 µL, 0.237mmol) and stirred for 2 h resulting in a pale yellow solution. The solution was concentrated to approx. 1 mL and cooled at 4 °C overnight. The resultant pale yellow solid was vacuum filtered, washing with cold MeOH and Et<sub>2</sub>O to yield **34** (63 mg, 66 %).

<sup>1</sup>H NMR (400 MHz, D<sub>2</sub>O) δ: 3.54 – 3.40 (bd, 6H), 2.83 – 2.70 (m, 2H), 1.67 (dt, *J* = 14.8, 7.4 Hz, 2H), 0.91 (td, *J* = 7.4, 1.2 Hz, 3H) ppm. ESI-MS: *m/z* ([M+Na]<sup>+</sup>) 426.3. EA calc. % for C<sub>5</sub>H<sub>15</sub>Cl<sub>2</sub>NOSPt requires C, 14.89; H, 3.75; Cl, 17.58; S, 7.95, found C, 14.86; H, 3.58; Cl, 17.80; S, 8.23 %. FT-IR <sub>max</sub> (cm<sup>-1</sup>): 3248, 3202, 3120, 3009, 2970, 2929, 1572, 1470, 1453, 1446, 1409, 1381, 1120, 1098.

Single crystals suitable for X-ray diffraction analysis were obtained by slow evaporation of the filtrate.



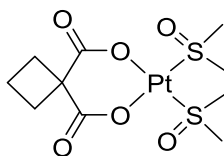
**[Ag<sub>2</sub>(CBDCA)]<sup>17</sup> (**35**)**



CBDCAH<sub>2</sub> (500 mg, 3.469 mmol) was dissolved in water (10 mL) with NaOH (277 mg, 6.938 mmol). To this was added AgNO<sub>3</sub> (1.178 g, 6.938 mmol) in water (6 mL) and the reaction was stirred in darkness at rt for 2 h. A white precipitate was collected by vacuum filtration and washed with water and Et<sub>2</sub>O to yield **35** as a white solid (1.162 g, 94 %).

FT-IR <sub>max</sub> (cm<sup>-1</sup>): 2980, 2941, 1542, 1495, 1453, 1435, 1396, 1344, 1253, 1228, 1155, 1124.

**[Pt(II)(CBDCA)(DMSO)<sub>2</sub>]<sup>16</sup> (**36**)**

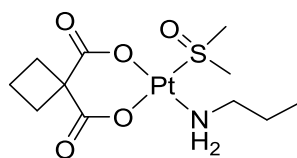


**36**

**35** (212 mg, 0.592 mmol) in water (10 mL) was added to a suspension of **33** (250 mg, 0.592 mmol) in water (15 mL) and stirred at rt in darkness for 18 h. The AgCl precipitate was removed by filtration over celite and the filtrate reduced under pressure to yield a colourless solid precipitate. The solution was let stand at 4 °C for 4 h and vacuum filtered, washing with acetone and Et<sub>2</sub>O to yield **36** as a white crystalline solid (145 mg, 50 %).

<sup>1</sup>H NMR (400 MHz, D<sub>2</sub>O) δ: 3.50 (s, 12H), 2.73 (t, *J* = 7.9 Hz, 4H), 1.92 – 1.81 (m, 2H) ppm. <sup>13</sup>C NMR (101 MHz, D<sub>2</sub>O) δ: 179.4, 55.6, 42.2, 30.6, 15.2 ppm. ESI-MS: *m/z* ([M+Na]<sup>+</sup>) 516.2, ([2M+Na]<sup>+</sup>) 1009.5. EA calc. % for C<sub>10</sub>H<sub>18</sub>O<sub>6</sub>S<sub>2</sub>Pt requires C, 24.34; H, 3.68; S, 12.99, found C, 24.19; H, 3.45; S, 12.56 %. FT-IR <sub>max</sub> (cm<sup>-1</sup>): 3650, 3509, 2981, 2971, 1660, 1602, 1544, 1352, 1320, 1160, 1117.

**[Pt(II)(CBDCA)(DMSO)(*n*-propylamine)]<sup>16</sup> (**37**)**



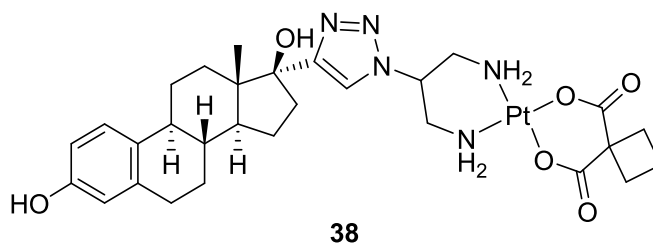
**37**

A suspension of **36** (82 mg, 0.166 mmol) in water (5 mL) was heated to 40°C and *n*-propylamine (13.67 µL, 0.166 mmol) and stirred for 2 h resulting in a pale yellow solution. The solution was concentrated to approx. 1 mL and cooled at 4 °C overnight. The resultant white crystalline solid was vacuum filtered and washed with cold MeOH and Et<sub>2</sub>O to yield **37** (48 mg, 61 %).

<sup>1</sup>H NMR (400 MHz, D<sub>2</sub>O) δ: 3.44 (s, 6H), 2.82 – 2.68 (m, 4H), 2.66 – 2.58 (m, 2H), 1.90 – 1.80 (m, 2H), 1.72 – 1.60 (m, 2H), 0.89 (t, *J* = 7.4 Hz, 3H) ppm. <sup>13</sup>C NMR (101 MHz, D<sub>2</sub>O) δ: 180.4, 55.9, 48.0, 42.7, 30.8, 23.3, 15.2, 10.1 ppm. ESI-MS: *m/z* ([M+H]<sup>+</sup>) 475.2, ([M+Na]<sup>+</sup>) 497.1, ([2M+H]<sup>+</sup>) 949.3, ([2M+Na]<sup>+</sup>) 971.4. EA calc. % for C<sub>11</sub>H<sub>21</sub>NO<sub>5</sub>SPt.Na requires C, 26.56; H, 4.26; N, 2.82, found C, 26.86; H, 4.13; N, 2.69 %. FT-IR <sub>max</sub> (cm<sup>-1</sup>): 3252, 3203, 3095, 2990, 2967, 2909, 1655, 1615, 1360, 1136, 1109, 1086, 1030.

Single crystals suitable for X-ray diffraction analysis were obtained by cooling of the concentrated mother liquor at 4 °C.

**[Pt(II)(CBDCA)(2-(4-(estradiol)-1*H*-1,2,3-triazol-1-yl)propane-1,3-diyl)] (38)**



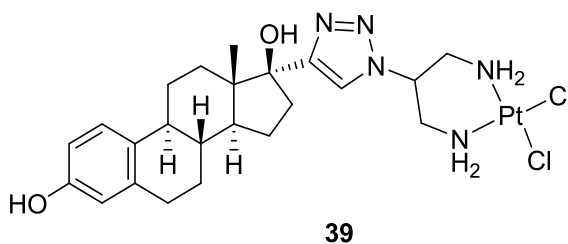
**36** (114 mg, 0.240 mmol) was dissolved in water (10 mL) at 100 °C. A solution of **11** (116 mg, 0.240 mmol) and NaOH (19.2 mg, 0.480 mmol) in water (5 mL) and DMF (0.5 mL) was heated, and added drop-wise to the solution of **36** and stirred at 100 °C for 6 h, producing an off-white solid which was vacuum filtered and washed with water, EtOH and Et<sub>2</sub>O. This yielded **38** as an off white solid (133.3 mg, 74%).

<sup>1</sup>H NMR (400 MHz, DMF-*d*<sub>7</sub>) δ 9.34 (s, 1H), 8.29 (s, 1H), 7.21 (d, *J* = 8.6 Hz, 1H), 6.76 (d, *J* = 8.4 Hz, 1H), 6.72 (s, 1H), 5.84 – 5.11 (m, 4H), 3.50 (m, *J* = 19.9, 10.1 Hz, 2H), 3.32 – 3.21 (m, 1H), 2.66 – 2.52 (m, 2H), 2.27 (m, *J* = 28.0, 15.5, 8.2 Hz, 3H), 2.13 – 1.87 (m, 4H), 1.79 – 1.39 (m, 7H), 1.21 (s, 2H), 1.14 – 1.04 (m, 1H), 0.87 (m, *J* = 14.9, 8.4 Hz, 1H) ppm.

<sup>1</sup>H NMR (400 MHz, DMSO-*d*<sub>6</sub>) δ: 9.00 (s, 1H), 7.96 (d, *J* = 7.2 Hz, 1H), 6.95 (d, *J* = 8.6 Hz, 1H), 6.50 – 6.39 (m, 2H), 5.56 – 5.09 (bm, 4H), 4.61 (m, 1H), 2.94 (m, *J* = 9.7 Hz, 1H), 2.68 (m, *J* = 5.6 Hz, 2H), 2.59 (m, *J* = 11.9 Hz, 1H), 2.27 (m, *J* = 23.0, 13.6 Hz, 2H), 2.12 – 2.03 (m, 1H), 1.99 – 1.57 (m, 6H), 1.50 – 1.13 (m, 6H), 0.91 (s, 3H), 0.56 – 0.45 (m, 1H) ppm. <sup>195</sup>Pt NMR (86 MHz, DMSO-*d*<sub>6</sub>) δ: -3245.61 ppm.

EA calc. % for C<sub>29</sub>H<sub>39</sub>O<sub>6</sub>N<sub>5</sub>Pt.1.5H<sub>2</sub>O requires C, 44.90; H, 5.46; N, 9.03, found C, 44.75; H, 5.46; N, 9.12 %. FT-IR <sub>max</sub> (cm<sup>-1</sup>): 3384, 3195, 3116, 2932, 2870, 1648, 1609, 1585, 1500, 1448, 1378, 1356, 1289, 1235, 1153, 1053, 1022, 913, 870, 847, 787.

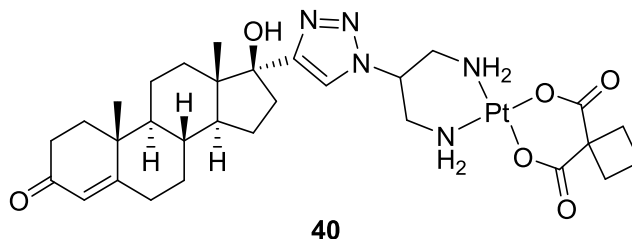
**[Pt(II)Cl<sub>2</sub>(2-(4-(estradiol)-1*H*-1,2,3-triazol-1-yl)propane-1,3-diyl)] (39)**



**33** (100 mg, 0.237 mmol) was dissolved in DMF (1 mL) at rt. To a solution of **11** (114 mg, 0.237 mmol) in DMF (1 mL) was added DBU (70.9  $\mu$ L, 0.474 mmol) giving a solution which was added drop-wise to the solution of **33** and stirred at rt for 2 days. Water (3 mL) was added to the flask giving an off white precipitate. which was cooled to 4 °C for 4 h. The off-white solid was vacuum filtered and washed with water and Et<sub>2</sub>O and dried over P<sub>2</sub>O<sub>5</sub>. This yielded **39** as a brown-orange crystalline solid (92.9 mg, 58%).

<sup>1</sup>H NMR (400 MHz, DMF-*d*<sub>7</sub>)  $\delta$ : 9.12 (s, 1H), 8.08 (s, 1H), 6.99 (d, *J* = 8.4 Hz, 1H), 6.55 (d, *J* = 8.4 Hz, 1H), 6.51 (s, 1H), 5.51 (d, *J* = 33.7 Hz, 3H), 5.12 (s, 1H), 5.05 (t, *J* = 10.1 Hz, 1H), 3.47 (s, 4H), 3.30 (d, *J* = 12.2 Hz, 2H), 3.10 – 3.02 (m, 1H), 2.46 – 2.34 (m, 1H), 2.14 – 1.99 (m, 2H), 1.93 – 1.64 (m, 5H), 1.56 – 1.44 (m, 2H), 1.41 – 1.17 (m, 3H), 1.00 (s, 3H), 0.65 (td, *J* = 12.6, 3.5 Hz, 1H) ppm. <sup>195</sup>Pt NMR (86 MHz, DMSO-*d*<sub>6</sub>)  $\delta$ : -2277.74 ppm. EA calc. % for C<sub>23</sub>H<sub>33</sub>Cl<sub>2</sub>N<sub>5</sub>O<sub>2</sub>Pt.0.25H<sub>2</sub>O requires C, 40.50; H, 4.95; N, 10.27, found C, 40.71; H, 5.32; N, 10.41 %. FT-IR <sub>max</sub> (cm<sup>-1</sup>): 3189, 3120, 2925, 2871, 1652, 1609, 1498, 1436, 1386, 1288, 1251, 1224, 1131, 1098, 1060, 1024, 913, 871, 819, 787, 661.

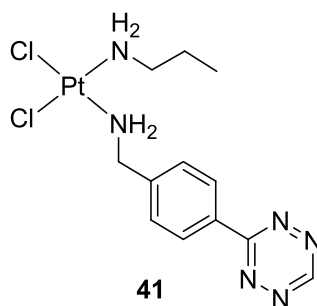
**Attempted synthesis of [Pt(II)(2-(4-(testosterone)-1H-1,2,3-triazol-1-yl)propane-1,3-diyl)] (40)**



**36** (32.2 mg, 0.0679 mmol) was dissolved in water (3 mL) at 100 °C. A solution of **13** (34 mg, 0.0679 mmol) and NaOH (5.5 mg, 0.136 mmol) in water (2 mL) and DMF (0.5 mL) was heated to form a solution which was added drop-wise to the solution of **36** and stirred at 100 °C for 6 h giving an off-white solid which was vacuum filtered and washed with water, EtOH and Et<sub>2</sub>O. This yielded an off white solid of 33 mg, which did not correlate with the theoretical values of **40**.

Attempted product analysis: <sup>1</sup>H NMR (400 MHz, DMF-*d*<sub>7</sub>) δ: 5.66 (s, 1H), 5.38 (s, 1H), 3.50 (m, 3H), 3.36 (s, 1H), 2.53 – 2.41 (m, 2H), 2.33 – 2.13 (m, 3H), 2.06 (m, 1H), 2.02 – 1.93 (m, 1H), 1.90 – 1.82 (m, 1H), 1.77 – 1.59 (m, 6H), 1.45 (m, 3H), 1.24 (s, 3H), 1.05 – 0.91 (m, 2H), 0.89 (s, 3H) ppm. ESI-MS: *m/z* (unassigned) 570.3. EA calc. % C<sub>30</sub>H<sub>43</sub>N<sub>5</sub>O<sub>6</sub>Pt requires C, 47.12; H, 5.67; N, 9.16, found C, 71.29; H, 5.95; N, 2.10 %. FT-IR <sub>max</sub> (cm<sup>-1</sup>): 3400, 3259, 2934, 2920, 1656, 1645, 1612, 1429, 1381, 1329, 1232, 1191, 1152, 1125, 1069, 1060, 992, 949, 922, 689, 784, 724, 698, 680.

**Attempted synthesis of *cis*-[Pt(II)Cl<sub>2</sub>(*n*-propylamine)(tetrazine-amine) (**41**)**

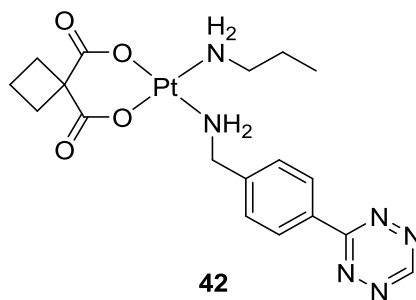


The synthesis of **41** was attempted following a preparation modified from Bitha *et al.*<sup>16</sup>

**34** (18 mg, 0.045 mmol) was dissolved in water (2.5 mL) at 100 °C. A solution of tetrazine-amine.HCl (10 mg, 0.045 mmol) and NaOH (1.8 mg, 0.045 mmol) in water (2 mL) and DMF (0.5 mL) was added to the solution of **34** and heated for 4 h. The solution was concentrated under vacuum to approx. 1 mL and cooled at 4 °C overnight. The resultant brown solid was vacuum filtered, washing with cold MeOH and Et<sub>2</sub>O to yield 16 mg, which did not correlate with the theoretical values of **41**.

Analysis of the solid was not possible by NMR or MS and IR and elemental analysis could not conclusively identify the product formed.

**Attempted synthesis of *cis*-[Pt(II)(CBDCA)(*n*-propylamine)(tetrazine-amine)]  
(**42**)**



The synthesis of **42** was attempted following a preparation modified from Bitha *et al.*<sup>16</sup>

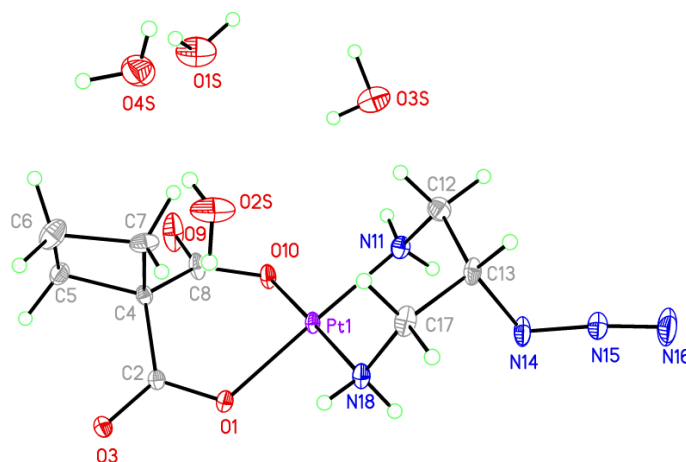
**37** (21.2 mg, 0.0447 mmol) was dissolved in water (2.5 mL) at 100 °C. A solution of tetrazine-amine.HCl (10 mg, 0.0447 mmol) and NaOH (1.8 mg, 0.0447 mmol) in water (2.2 mL) and DMF (0.3 mL) was added to the solution of **37** and heated for 4 h. The solution was concentrated under vacuum to approx. 1 mL and cooled at 4 °C overnight. The resultant orange-brown solid was vacuum filtered, washing with cold MeOH and Et<sub>2</sub>O to yield 18 mg, which did not correlate with the theoretical values of **42**.

Analysis of the solid was not possible by NMR or MS and IR and elemental analysis could not conclusively identify the product formed.



## X-ray Crystallography

### [Pt(II)(CBDCA)(DAP-N<sub>3</sub>)] (18)



A clear colourless needle fragment-like specimen of C<sub>9</sub>H<sub>23</sub>N<sub>5</sub>O<sub>8</sub>Pt, approximate dimensions 0.050 mm x 0.110 mm x 0.160 mm, was used for the X-ray crystallographic analysis. The X-ray intensity data were measured at 100(2)K using an Oxford Cryosystems low temperature device using a MiTeGen micromount. Bruker APEX software was used to correct for Lorentz and polarization effects.

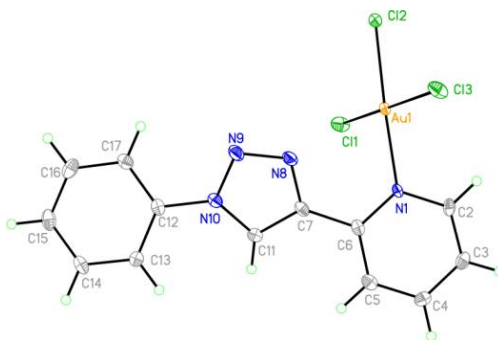
A total of 755 frames were collected. The total exposure time was 3.24 hours. The frames were integrated with the Bruker SAINT software package using a wide-frame algorithm. The integration of the data using a triclinic unit cell yielded a total of 35734 reflections to a maximum  $\theta$  angle of 35.14° (0.62 Å resolution), of which 7321 were independent (average redundancy 4.881, completeness = 99.6%,  $R_{\text{int}}$  = 9.75%,  $R_{\text{sig}}$  = 5.23%) and 6540 (89.33%) were greater than  $2\sigma(F^2)$ . The final cell constants of  $a$  = 8.1972(2) Å,  $b$  = 10.0512(3) Å,  $c$  = 11.2870(3) Å,  $\alpha$  = 64.3846(12)°,  $\beta$  = 80.5246(14)°,  $\gamma$  = 82.4160(14)°, volume = 825.18(4) Å<sup>3</sup>, are based upon the refinement of the XYZ-centroids of 9977 reflections above 20  $\sigma(I)$  with 6.229° <  $2\theta$  < 68.65°. Data were corrected for absorption effects using the Multi-Scan method (SADABS). The ratio of minimum to maximum apparent transmission was 0.686. The calculated minimum and maximum transmission coefficients (based on crystal size) are 0.1995 and 0.2910.

The structure was solved and refined using the Bruker SHELXTL Software Package, using the space group  $P\bar{1}$ , with  $Z = 2$  for the formula unit, C<sub>9</sub>H<sub>23</sub>N<sub>5</sub>O<sub>8</sub>Pt. The final anisotropic full-matrix least-squares refinement on  $F^2$  with 239 variables converged

at  $R1 = 3.25\%$ , for the observed data and  $wR2 = 8.19\%$  for all data. The goodness-of-fit was 1.071. The largest peak in the final difference electron density synthesis was  $3.699 \text{ e}^-/\text{\AA}^3$  and the largest hole was  $-3.814 \text{ e}^-/\text{\AA}^3$  with an RMS deviation of  $0.260 \text{ e}^-/\text{\AA}^3$ . On the basis of the final model, the calculated density was  $2.111 \text{ g/cm}^3$  and  $F(000)$ , 508  $\text{e}^-$ .

**Refinement Note:** Residual Densities (e.g.  $0.68 \text{\AA}$  from Pt1) of ca.  $-3.81 \text{ e}^-/\text{\AA}^3$  are absorption artefacts and could not be modelled or eliminated. Amino donor N-H and O3s hydrogen atoms were refined with restraints (DFIX).

**[Au(III)Cl<sub>3</sub>(PTP)] (27)**

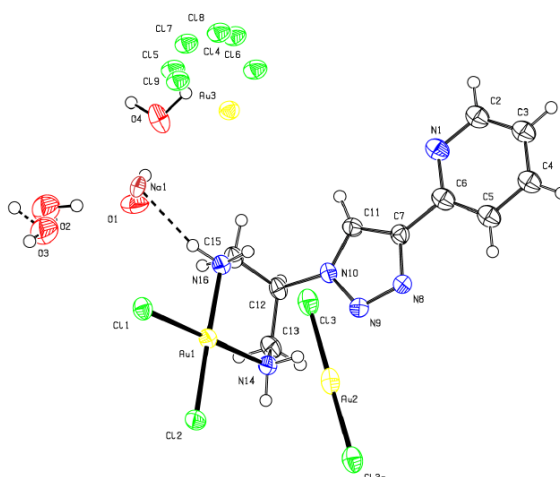


A specimen of C<sub>13</sub>H<sub>10</sub>AuCl<sub>3</sub>N<sub>4</sub>, approximate dimensions 0.160 mm x 0.240 mm x 0.280 mm, was used for the X-ray crystallographic analysis. The X-ray intensity data were measured at 100(2)K using an Oxford Cryosystems low temperature device using a MiTeGen micromount. Bruker APEX software was used to correct for Lorentz and polarization effects.

A total of 513 frames were collected. The total exposure time was 0.23 hours. The integration of the data using a triclinic unit cell yielded a total of 11304 reflections to a maximum  $\theta$  angle of 28.41° (0.75 Å resolution), of which 3795 were independent (average redundancy 2.979, completeness = 99.2%,  $R_{\text{int}}$  = 4.62%,  $R_{\text{sig}}$  = 4.95%) and 3415(89.99%) were greater than  $2\sigma(F^2)$ . The final cell constants of  $a$  = 6.960(3) Å,  $b$  = 9.060(4) Å,  $c$  = 12.468(6) Å,  $\alpha$  = 88.87(3)°,  $\beta$  = 76.044(16)°,  $\gamma$  = 86.372(11)°, volume = 761.5(6) Å<sup>3</sup>, are based upon the refinement of the XYZ-centroids of reflections above 20  $\sigma(I)$ . Data were corrected for absorption effects using the Multi-Scan method (SADABS). The ratio of minimum to maximum apparent transmission was 0.467. The calculated minimum and maximum transmission coefficients (based on crystal size) are 0.3481 and 0.7457.

The structure was solved using the Bruker APEX Software Package and refined with XL in Olex2, using the space group  $P\bar{1}$ , with  $Z$  = 2 for the formula unit, C<sub>13</sub>H<sub>10</sub>AuCl<sub>3</sub>N<sub>4</sub>. The final anisotropic full-matrix least-squares refinement on  $F^2$  with 190 variables converged at  $R1$  = 2.60%, for the observed data and  $wR2$  = 5.79% for all data. The goodness-of-fit was 1.067. The largest peak in the final difference electron density synthesis was 1.195 e<sup>-</sup>/Å<sup>3</sup> and the largest hole was -2.065 e<sup>-</sup>/Å<sup>3</sup> with an RMS deviation of 0.202 e<sup>-</sup>/Å<sup>3</sup>. On the basis of the final model, the calculated density was 2.292 g/cm<sup>3</sup> and  $F(000)$ , 492 e<sup>-</sup>.

**[Au(III)Cl<sub>2</sub>(PTPD)][Au(I)Cl<sub>2</sub>][OH]{[NaAuCl<sub>4</sub>·2H<sub>2</sub>O]}<sub>n</sub> (29)**



A specimen of C<sub>20</sub>H<sub>36.60</sub>Au<sub>3.80</sub>Cl<sub>19.21</sub>N<sub>12</sub>Na<sub>0.80</sub>O<sub>4.40</sub>, approximate dimensions 0.080 mm x 0.080 mm x 0.180 mm, was used for the X-ray crystallographic analysis. The X-ray intensity data were measured at 100(2)K using an Oxford Cryosystems low temperature device using a MiTeGen micromount. Bruker APEX software was used to correct for Lorentz and polarization effects.

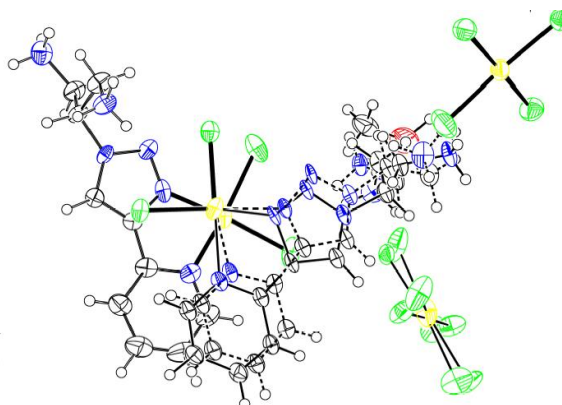
A total of 1504 frames were collected. The total exposure time was 4.66 hours. The frames were integrated with the Bruker SAINT software package using a wide-frame algorithm. The integration of the data using a monoclinic unit cell yielded a total of 40737 reflections to a maximum  $\theta$  angle of 26.47° (0.80 Å resolution), of which 4212 were independent (average redundancy 9.672, completeness = 99.9%,  $R_{\text{int}}$  = 2.93%,  $R_{\text{sig}}$  = 1.36%) and 3849 (91.38%) were greater than  $2\sigma(F^2)$ . The final cell constants of  $a = 15.2675(6)$  Å,  $b = 18.9896(7)$  Å,  $c = 7.1416(3)$  Å,  $\beta = 99.1035(11)^\circ$ , volume = 2044.44(14) Å<sup>3</sup>, are based upon the refinement of the XYZ-centroids of 9939 reflections above  $20\sigma(I)$  with  $5.815^\circ < 2\theta < 52.93^\circ$ . Data were corrected for absorption effects using the Multi-Scan method (SADABS). The ratio of minimum to maximum apparent transmission was 0.290. The calculated minimum and maximum transmission coefficients (based on crystal size) are 0.0080 and 0.0276.

The structure was solved using the Bruker APEX Software Package and refined with XL in Olex2, using the space group  $P2_1/c$ , with  $Z = 2$  for the formula unit, C<sub>20</sub>H<sub>30.80</sub>Au<sub>3.80</sub>Cl<sub>9.20</sub>N<sub>12</sub>Na<sub>1.60</sub>O<sub>3.20</sub>. The final anisotropic full-matrix least-squares refinement on  $F^2$  with 224 variables converged at  $R1 = 2.73\%$ , for the observed data and  $wR2 = 7.25\%$  for all data. The goodness-of-fit was 1.101. The largest peak in the

final difference electron density synthesis was  $1.221 \text{ e}^-/\text{\AA}^3$  and the largest hole was  $-0.872 \text{ e}^-/\text{\AA}^3$  with an RMS deviation of  $0.158 \text{ e}^-/\text{\AA}^3$ . On the basis of the final model, the calculated density was  $2.602 \text{ g/cm}^3$  and  $F(000)$ , 1469  $\text{e}^-$ .

**Refinement Note:** the asymmetric unit the counter ions  $\text{AuCl}_2$  and  $\text{OH}^-$  are only 50% occupied. The  $\text{OH}^-$  occupies the same space as the Na (40% occupied) in the charge neutral  $[\text{Na}(\text{H}_2\text{O})_2\text{AuCl}_4]_n$  which is only partially occupied. This moiety was modelled with restraints (DFIX, SADI, SIMU, ISOR) and constraints (EADP O2, O3 and Cl4;Cl5; Cl6;Cl7; Cl8; Cl9) with the Cl atoms in three separate locations (43, 32 and 5% occupancy, refined to a total of 80% using SUMP). The hydroxide is coordinated to a water molecule at 50% occupancy and the Na is also coordinated to two water molecules at 40% and 80% occupancy. Hydrogen atoms were added to the water molecules to align as best as possible to hydrogen bonding receptors.

**[Pt(II)Cl<sub>2</sub>(PTPDH<sub>2</sub>)][PtCl<sub>4</sub>] (31)**



A specimen of C<sub>10.25</sub>H<sub>17</sub>Cl<sub>6</sub>N<sub>6</sub>O<sub>0.25</sub>Pt<sub>2</sub>, approximate dimensions 0.030 mm x 0.030 mm x 0.130 mm, was used for the X-ray crystallographic analysis. The X-ray intensity data were measured at 100(2)K on a Bruker D8 Quest ECO with an Oxford Cryosystems low temperature device using a MiTeGen micromount. Bruker APEX software was used to correct for Lorentz and polarization effects.

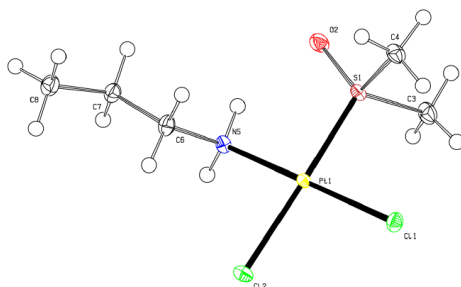
A total of 1030 frames were collected. The total exposure time was 12.31 hours. The frames were integrated with the Bruker SAINT software package using a narrow-frame algorithm. The integration of the data using a triclinic unit cell yielded a total of 36729 reflections to a maximum  $\theta$  angle of 26.56° (0.79 Å resolution), of which 9231 were independent (average redundancy 3.979, completeness = 97.5%,  $R_{\text{int}}$  = 8.91%,  $R_{\text{sig}}$  = 8.35%) and 6034 (65.37%) were greater than  $2\sigma(F^2)$ . The final cell constants of  $a = 12.4400(6)$  Å,  $b = 13.3881(6)$  Å,  $c = 15.1617(7)$  Å,  $\alpha = 76.6984(17)^\circ$ ,  $\beta = 68.0193(18)^\circ$ ,  $\gamma = 89.2239(19)^\circ$ , volume = 2271.40(19) Å<sup>3</sup>, are based upon the refinement of the XYZ-centroids of 9864 reflections above 20  $\sigma(I)$  with  $5.665^\circ < 2\theta < 53.00^\circ$ . Data were corrected for absorption effects using the Multi-Scan method (SADABS). The ratio of minimum to maximum apparent transmission was 0.604. The calculated minimum and maximum transmission coefficients (based on crystal size) are 0.4504 and 0.7454.

The structure was solved with the XT structure solution program using Intrinsic Phasing and refined with the XL refinement package using Least Squares minimisation with Olex2, using the space group  $P\bar{1}$ , with  $Z = 4$  for the formula unit, C<sub>10.25</sub>H<sub>17</sub>Cl<sub>6</sub>N<sub>6</sub>O<sub>0.25</sub>Pt<sub>2</sub>. The final anisotropic full-matrix least-squares refinement on

$F^2$  with 648 variables converged at  $R1 = 4.95\%$ , for the observed data and  $wR2 = 11.31\%$  for all data. The goodness-of-fit was 1.030. The largest peak in the final difference electron density synthesis was  $1.977 \text{ e}^-/\text{\AA}^3$  and the largest hole was  $-2.523 \text{ e}^-/\text{\AA}^3$  with an RMS deviation of  $0.262 \text{ e}^-/\text{\AA}^3$ . On the basis of the final model, the calculated density was  $2.431 \text{ g/cm}^3$  and  $F(000)$ , 1522  $\text{e}^-$ .

**Refinement Note:** One ligand was disordered in two locations ca. 50% and modelled with restraints (SADI, SIMU, ISOR). One  $\text{PtCl}_4$  moiety also modelled in two positions at 50% occupancy with one restraint (SMIU). Half occupied methanol molecule modelled with restraints (ISOR). The remaining solvent in the void ( $\text{H}_2\text{O}/\text{MeOH}$ ) was removed from the data using the subroutine SQUEEZE<sup>18</sup> (155 electrons in a 330 cubic Angstrom solvent accessible void, approx. 5MeOH, 6H<sub>2</sub>O per unit cell).

***cis*-[Pt(II)Cl<sub>2</sub>(DMSO)(*n*-propylamine)] (34)**



A specimen of C<sub>5</sub>H<sub>15</sub>Cl<sub>2</sub>NOPtS, approximate dimensions 0.080 mm x 0.220 mm x 0.260 mm, was used for the X-ray crystallographic analysis. The X-ray intensity data were measured at 100(2)K on a Bruker B8 Quest Eco with an Oxford Cryostream low temperature device using a MiTeGen micromount. Bruker APEX software was used to correct for Lorentz and polarization effects.

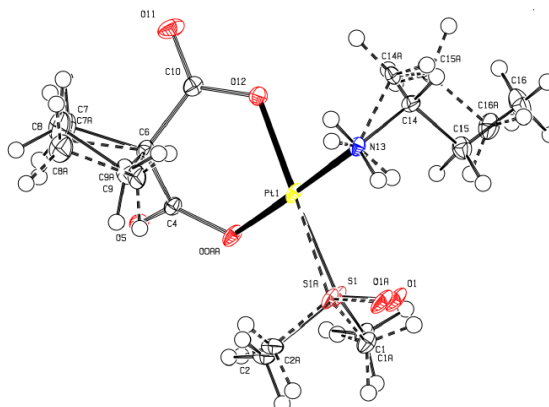
A total of 756 frames were collected. The total exposure time was 1.68 hours. The integration of the data using a monoclinic unit cell yielded a total of 19325 reflections to a maximum  $\theta$  angle of 30.64° (0.70 Å resolution), of which 3431 were independent (average redundancy 5.632, completeness = 99.7%,  $R_{\text{int}} = 2.76\%$ ,  $R_{\text{sig}} = 1.99\%$ ) and 3200 (93.27%) were greater than  $2\sigma(F^2)$ . The final cell constants of  $a = 20.9490(8)\text{Å}$ ,  $b = 7.3231(3)\text{Å}$ ,  $c = 16.9429(7)\text{Å}$ ,  $\beta = 121.1433(12)^\circ$ , volume = 2224.63(16) Å<sup>3</sup>, are based upon the refinement of the XYZ-centroids of reflections above 20  $\sigma(I)$ . The calculated minimum and maximum transmission coefficients (based on crystal size) are 0.4115 and 0.7461.

The structure was solved with the XT structure solution program using Intrinsic Phasing and refined with the XL refinement package using Least Squares minimisation with Olex2, using the space group C2/c, with  $Z = 8$  for the formula unit, C<sub>5</sub>H<sub>15</sub>Cl<sub>2</sub>NOPtS. The final anisotropic full-matrix least-squares refinement on  $F^2$  with 111 variables converged at  $R1 = 1.57\%$ , for the observed data and  $wR2 = 3.49\%$  for all data. The goodness-of-fit was 1.105. The largest peak in the final difference electron density synthesis was 0.763 e<sup>-</sup>/Å<sup>3</sup> and the largest hole was -1.594 e<sup>-</sup>/Å<sup>3</sup> with an RMS deviation of 0.152 e<sup>-</sup>/Å<sup>3</sup>. On the basis of the final model, the calculated density was 2.408 g/cm<sup>3</sup> and  $F(000)$ , 1504 e<sup>-</sup>.

**Refinement Note:** Donor N-H atoms located on the difference map and refined with restraints (DFIX).



**[Pt(II)(CBDCA)(DMSO)(*n*-propylamine)] (37)**



A specimen of  $C_{11}H_{21}NO_5PtS$ , approximate dimensions 0.040 mm x 0.140 mm x 0.290 mm, was used for the X-ray crystallographic analysis. The X-ray intensity data were measured at 100(2)K on a Bruker B8 Quest Eco with an Oxford Cryostream low temperature device using a MiTeGen micromount. Bruker APEX software was used to correct for Lorentz and polarization effects.

A total of 1272 frames were collected. The total exposure time was 4.71 hours. The integration of the data using a monoclinic unit cell yielded a total of 44917 reflections to a maximum  $\theta$  angle of  $33.34^\circ$  (0.65 Å resolution), of which 5646 were independent (average redundancy 7.956, completeness = 99.7%,  $R_{\text{int}} = 3.69\%$ ,  $R_{\text{sig}} = 2.08\%$ ) and 5240 (92.81%) were greater than  $2\sigma(F^2)$ . The final cell constants of  $a = 8.2289(3)$  Å,  $b = 9.9801(3)$  Å,  $c = 17.8668(6)$  Å,  $\beta = 94.9380(10)^\circ$ , volume =  $1461.87(8)$  Å<sup>3</sup>, are based upon the refinement of the XYZ-centroids of reflections above  $20\sigma(I)$ . The calculated minimum and maximum transmission coefficients (based on crystal size) are 0.1640 and 0.6960.

The structure was solved with the XT structure solution program using Intrinsic Phasing and refined with the XL refinement package using Least Squares minimisation with Olex2, using the space group  $P2_1/n$ , with  $Z = 4$  for the formula unit,  $C_{11}H_{21}NO_5PtS$ . The final anisotropic full-matrix least-squares refinement on  $F^2$  with 247 variables converged at  $R1 = 1.95\%$ , for the observed data and  $wR2 = 4.31\%$  for all data. The goodness-of-fit was 1.117. The largest peak in the final difference electron density synthesis was  $1.738\text{ e}^-/\text{\AA}^3$  and the largest hole was  $-1.961\text{ e}^-/\text{\AA}^3$  with

an RMS deviation of  $0.146 \text{ e}^-/\text{\AA}^3$ . On the basis of the final model, the calculated density was  $2.156 \text{ g/cm}^3$  and  $F(000)$ , 912  $\text{e}^-$ .

**Refinement Note:** DMSO, propylamine and cyclobutane groups all disordered in two locations with occupancies of 67:33; 57:43 and 57:43% respectively. Restraints (SADI, SIMU for propyl amine and cyclobutane and SADI for S-O distances) and constraints (EADP in DMSO) were used in the model for convergence.

## Peptide and peptide conjugate synthesis

### General considerations and materials

All chemicals and solvents were used as received from commercial suppliers. 9-Fluorenylmethyloxy carbonyl (Fmoc) protected amino acids; Fmoc-Lys(Boc)-OH, Fmoc-Asp(OiBu)-OH, Fmoc-Asn(Trt)-OH, Fmoc-Leu-OH, Fmoc-Gly-OH, Fmoc-Phe-OH, and Fmoc-Glu(OtBu)-OH were purchased from Merck (*Merck Millipore, Cork, Ireland*). Fmoc-Thr(*t*Bu)-OH, Fmoc-Arg(Pbf)-OH, Fmoc-Ser(*t*Bu)-OH, Rink amide 4-methylbenzhydrylamine (MBHA) resin, *N,N*-diisopropylcarbodiimide (DIC), oxyma pure, piperidine, *N*-methyl-2-pyrrolidone, *N,N'*-carbonyldiimidazole (CDI), piperidine, phenol, trifluoroacetic acid (TFA), succinic anhydride, anhydrous DMF and anhydrous DCM were purchased from Sigma Aldrich (*Sigma Aldrich Ireland Ltd., Wicklow, Ireland*). Syringe reactors were purchased from MultiSynTech GmbH (*MultiSynTech GmbH, Witten, Germany*).

### Solid phase synthesis

Peptide sequences were assembled by automated solid phase peptide synthesis on a CEM Liberty Blue™ Microwave Peptide Synthesizer (*CEM Microwave Technology, Ireland Ltd, Dublin*) using L-amino acids protected with Fmoc.<sup>19</sup> The synthesis was carried out in accordance to the Fmoc/*t*Bu strategy where the peptide chain is assembled sequentially from a rink MBHA resin (*Sigma Aldrich, Arklow, Wicklow*) using DIC and oxyma pure coupling chemistry. Single coupling cycles using a 10-fold excess of Fmoc-amino acids were employed. The Fmoc/*t*Bu strategy utilises a relatively mild de-protection scheme where removal of Fmoc was carried out using 20% (v/v) piperidine in *N*-methyl pyrrolidone (NMP).<sup>20</sup> The reaction was monitored by the UV absorbance of the dibenzofulvene side product at 301 nm.

### Peptide conjugation

Attachment of the [Pt(IV)(DACH)(OEt)(Ox)(Succ)] **26** to the Rink Amide MBHA resin-bound peptide was performed manually in a 5 mL syringe (0.05 mmol scale) fitted with a Teflon frit and stopcock. Following completion of the peptide sequence and final Fmoc deprotection on the N-terminal, the resin was agitated in DMF (2 mL) for 30 min to facilitate swelling, after which the DMF was drained. Quantities of the reagents were calculated relative to 0.05 mmol of the original peptide on resin.

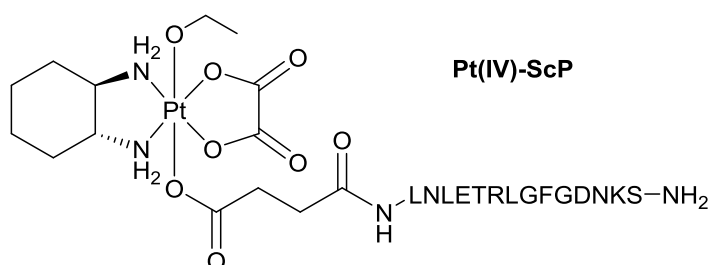
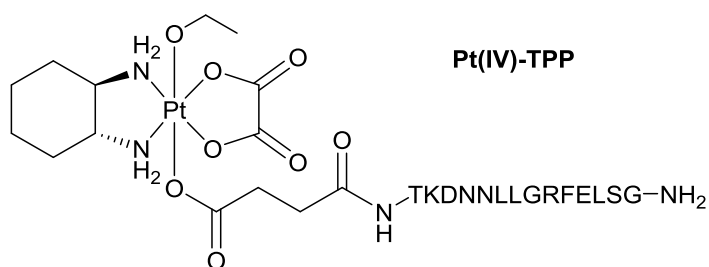
To [Pt(IV)(DACH)(OEt)(Ox)(Succ)], **26**, (112 mg, 0.2 mmol) in anhydrous DMF (1 mL) at 60 °C was added a solution of CDI (68 mg, 0.42 mmol) in anhydrous DMF (1 mL), and the mixture stirred at 60 °C for a further 10 min. The reaction was cooled to rt and transferred into a reactor containing the pre-swelled polymer-bound peptide, and stirred for 48 h. Following conjugation, the resin was washed with DMF in order to remove any excess unreacted activated Pt precursor before washing with DCM and drying under vacuum.<sup>21</sup>

### **Peptide cleavage**

Following Pt-peptide conjugation the resulting Pt-peptide conjugates were cleaved from the resin and side-chain protecting groups removed using a mixture of TFA 95%, phenol 2.5% and water 2.5% (total 3 mL). The peptide cleavage cocktail was prepared fresh each time, added to the resin and stirred at rt for 2 h. Upon reaction completion the resin was filtered and the crude Pt-peptide conjugate mixture was precipitated using a minimal amount of Et<sub>2</sub>O, and collected by centrifugation for 4 min at 2,500 rpm. The resulting supernatant was disposed of and the resulting precipitated peptide re-suspended in Et<sub>2</sub>O (10 mL). The suspension was centrifuged and this process was repeated three times. The final Pt-peptide conjugate pellet was left to air dry before being dissolved in distilled water, frozen in liquid nitrogen, and lyophilized to give a white powder.

### **Peptide purification**

Chromatographic analysis and peptide purification was performed using analytical and preparative RP-HPLC: Triart C18 5 mm columns. Crude products were dissolved in a H<sub>2</sub>O:MeOH (95:5) mixture. Mobile phase A: 0.1% TFA/H<sub>2</sub>O and mobile phase B: 0.1% TFA/MeOH were used with a gradient of 5–85–5% B over 65 min with a flow rate of 1 mL/min (analytical) or 4 mL/min (semi-preparative). Double wavelength detection at 214 and 254 nm was used.



**Pt-TPP**; (4 mg, 3.8%),  $^1\text{H}$  NMR (400 MHz,  $\text{D}_2\text{O}$ )  $\delta$ : 7.34 (dd,  $J = 13.6, 7.2$  Hz, 3H), 7.28 (d,  $J = 7.3$  Hz, 2H), 4.65 (dd,  $J = 15.7, 6.8$  Hz, 5H), 4.45 (s, 2H), 4.39 – 4.30 (m, 5H), 4.30 – 4.17 (m, 4H), 3.94 (d,  $J = 3.8$  Hz, 2H), 3.92 – 3.88 (m, 3H), 3.36 (s, 2H), 3.25 – 3.11 (m, 5H), 3.06 – 2.98 (m, 3H), 2.91 – 2.75 (m, 7H), 2.71 – 2.58 (m, 5H), 2.36 (s, 2H), 2.28 (d,  $J = 14.6$  Hz, 2H), 2.24 (s, 3H), 2.07 (s, 3H), 1.67 (dd,  $J = 22.5, 8.8$  Hz, 15H), 1.50 – 1.41 (m, 4H), 1.22 (d,  $J = 6.3$  Hz, 5H), 1.16 (t,  $J = 6.9$  Hz, 3H), 0.92 (ddd,  $J = 18.6, 12.6, 6.5$  Hz, 15H) ppm.  $^{195}\text{Pt}$  NMR (86 MHz,  $\text{D}_2\text{O}$ )  $\delta$ : 1379.14 ppm. HRMS (ESI+)  $m/z$ : 1054.4160 ( $\text{M}+2\text{H}^+$ ) $^{2+}$ ,  $t_R$ : 38.96 min, purity 100%.

**Pt-ScP**; (3.2 mg, 1.9%)  $^1\text{H}$  NMR (400 MHz,  $\text{D}_2\text{O}$ )  $\delta$ : 7.41 – 7.31 (m, 3H), 7.27 (d,  $J = 6.9$  Hz, 2H), 4.67 (dt,  $J = 27.7, 7.3$  Hz, 4H), 4.41 (t,  $J = 5.1$  Hz, 1H), 4.30 (dd,  $J = 34.2, 11.9$  Hz, 8H), 4.00 – 3.82 (m, 7H), 3.36 (s, 2H), 3.18 (d,  $J = 3.7$  Hz, 5H), 3.02 (dd,  $J = 19.6, 12.4$  Hz, 3H), 2.94 – 2.76 (m, 7H), 2.67 (s, 2H), 2.59 (s, 1H), 2.55 – 2.42 (m, 4H), 2.30 (s, 2H), 2.24 (s, 1H), 2.14 (s, 1H), 2.06 (s, 1H), 1.85 (d,  $J = 36.9$  Hz, 5H), 1.65 (s, 15H), 1.45 (s, 3H), 1.22 (d,  $J = 5.8$  Hz, 4H), 1.16 (t,  $J = 6.9$  Hz, 2H), 0.98 – 0.83 (m, 17H) ppm. HRMS (ESI+)  $m/z$ : 1054.3705 ( $\text{M}+2\text{H}^+$ ) $^{2+}$ ,  $t_R$ : 38.56 min, purity 100%.

The free peptides **TPP** and **ScP** were cleaved and purified using the above methods on a 0.1 mmol scale stirring at rt for 90 min. **TPP**; (30.8 mg, 20%), HRMS (ESI+)  $m/z$ : 1561.71 ( $\text{M}+\text{H}^+$ ) $^+$ ,  $t_R$ : 38.79 min, purity >95.73%. **ScP**; (59.3 mg, 38 %), HRMS (ESI+)  $m/z$ : 1561.55 ( $\text{M}+\text{H}^+$ ) $^+$ ,  $t_R$ : 35.90 min, purity >97.08%.

## *In vitro* cell culture

### Cell lines

A2780P and A2780cis human ovarian carcinoma cells were obtained from the European Collection of Authenticated Cell Cultures (ECACC, a part of Public Health England) through Sigma Aldrich (*Sigma Aldrich Ireland Ltd., Arklow, Co Wicklow*).

**Table 2.1:** Appropriate seeding densities for ovarian and colorectal cancer cell lines.

Name	Source	Morphology	Comment
<b>A2780P</b>	human ovarian carcinoma	epithelial, adherent	wild type
<b>A2780cis</b>	human ovarian carcinoma	epithelial, adherent	cisplatin resistant
<b>HCT116 wt</b>	human colon carcinoma	epithelial, adherent	wild type
<b>HT29</b>	human colon adenocarcinoma	epithelial, adherent	wild type

### Cell Culture

All commercially available materials were purchased from Sigma Aldrich unless otherwise stated, and were used as supplied within 6 months of the purchase date. All culture materials were stored below 5 °C and heated to 37 °C before use.

A2780P, A2780cis and HCT116 wt were cultured in RPMI 1640 with L-glutamine (2 mM) (*EuroClone, Wheterby, UK*) supplemented with 10% Fetal Bovine Serum (FBS) (*Biosera, East Sussex, UK*) and 100 U/mL penicillin and 100 µg/mL streptomycin (*EuroClone, Wheterby, UK*). HT29 cell lines were cultured in Dulbecco's Modified Eagle Medium (DMEM) supplemented with 10% FBS, 1% L-glutamine and 1% penicillin-streptomycin.

In this work, media refers to complete medium with all supplements. In order to retain resistance, solutions of 1 µM cisplatin in media was added to the A2780cis cells every third passage.

All cells were kept in an incubator set to 5% CO<sub>2</sub> at 37 °C. All cells were cultured in a sterile mycoplasma-free facility and were tested regularly for the presence of

mycoplasma contamination with MycoAlert™ Mycoplasma Detection Kit (Lonza, Basel, Switzerland).

#### Phosphate-buffered saline (PBS)

PBS is an isotonic solution with a pH of 7.4 used for washing cells in culture. PBS contains sodium chloride, potassium chloride and phosphate buffer dissolved in deionised water, with a concentration of 137 mM sodium chloride, 10 mM phosphate buffer and 2.7 mM potassium chloride per 200 mL of deionised water. PBS was dispensed in 20 mL aliquots and stored at 4 °C until required for washing.

#### FBS

FBS is the supernatant fraction remaining after the natural coagulation of fetal calf blood. FBS is commonly used as a serum supplement for *in vitro* cell culture as it provides cells with nutrients for differentiation and proliferation, as well as a number of hormones and growth factors. FBS was heat inactivated at 55 °C in a water bath for 30 min, before being dispensed in 50 mL aliquots and stored at -20 °C until required for addition to medium. It was then defrosted, heated to 37 °C in a water bath and added to medium in a 1:10 dilution.

#### Penicillin-Streptomycin solution

Penicillin-Streptomycin is an antibiotic solution stabilised with 10,000 units penicillin and 10 mg streptomycin/mL in 0.9% NaCl. Penicillin interferes with the cell wall synthesis of Gram-positive bacteria, while streptomycin disrupts protein synthesis, particularly in Gram-negative bacteria. This solution was dispensed as 10 mL aliquots and stored at -20 °C until required for addition to medium. It was then defrosted, heated to 37 °C in a water bath for 30 min and added in a 1:100 dilution.

#### Cell passaging

Once cells in culture had reached approximately 70% confluency, the old media was removed and the cells washed with PBS solution to remove any remaining residual media. This step is necessary as culture media contains  $Mg^{2+}$  and  $Ca^{2+}$  cations which inhibit the activity of trypsin. Trypsin-EDTA (0.25%) was then added and the cells left to detach in an incubator for approx. 5 min (**Table 2.2**). Trypsin acts by cleaving adhesion proteins involved in cell-cell and cell-matrix interactions. These adhesion proteins in turn rely on the presence of calcium and so trypsin is supplemented with EDTA as it is a divalent cation chelator and functions to reduce the number of

cations and adhesion proteins present that may inhibit trypsin. This combination of trypsin-EDTA breaks up the extra cellular matrix of cells and causes adherent cell detachment from the flask surface. Once detached, medium was added (at least three times the amount) to inactivate the trypsin-EDTA, and the cell suspension was transferred to a centrifuge tube. Cell pellets were formed by centrifugation at 1,000 rpm for 3 min. The resulting pellet was re-suspended in fresh media and cells were counted, and seeded in new culture flasks at appropriate seeding densities with reference to **Table 2.3**.

**Table 2.2:** Appropriate trypsin amounts relative to cell culture dish size.

Dish	Area mm <sup>2</sup>	Media mL
T-25	2500	1
T-75	7500	3

### Cell Counting

Cell pellets were re-suspended in appropriate culture media (5 mL) and the concentrated cell suspension (10 µL) was then mixed with 0.4% trypan blue stain (10 µL). 10 µL of this mixture was pipetted into a Countess™ Cell Counting Chamber Slide (*Invitrogen, Thermo Fisher Scientific, Waltham, Massachusetts, USA*). Each slide has 2 x 10 µL chambers which may each be inserted into the Countess™ Automated Cell Counter (*Invitrogen, Thermo Fisher Scientific, Waltham, Massachusetts, USA*). The cells in the chamber were visualised and analysed to determine the number of living, dead and total cells present, as well as the cell viability %. Using the calculator function the volume of the cell suspension could be determined to create a stock solution of known concentration e.g. the required concentration of A2780 cells was  $1 \times 10^5$  cells/mL to give a seeding density  $1 \times 10^4$  cells/100 µL in each well of a 96 well plate.

The required volume was then taken from the thoroughly mixed cell suspension and added to each well/plate. The number of cells seeded was based on several factors including the nature of the cell line, the dimensions of a single cell and the duration of an experiment. The seeding densities used are outlined in **Table 2.3**.



**Table 2.3:** Appropriate seeding densities for ovarian and colorectal cancer cell lines.

Cell Line	Dish	Area mm <sup>2</sup>	Seeding density	Media mL
<b>A2780P</b>	8-well	93	$1 \times 10^4$	0.2
	96-well	50	$1 \times 10^4$	0.1
	T-25	2500	$5 \times 10^5$	5
	T-75	7500	$1.5 \times 10^6$	15
<b>A2780cis</b>	8-well	93	$1 \times 10^4$	0.2
	96-well	50	$1 \times 10^4$	0.1
	T-25	2500	$5 \times 10^5$	5
	T-75	7500	$1.5 \times 10^6$	15
<b>HCT116 wt</b>	96-well	50	$6 \times 10^3$	0.1
	T-25	2500	$6 \times 10^5$	5
	T-75	7500	$2 \times 10^6$	15
<b>HT29</b>	96-well	50	$6 \times 10^3$	0.1
	T-25	2500	$5 \times 10^5$	5
	T-75	7500	$1.5 \times 10^6$	15

### Cell Freezing

For long-term storage cells require to be kept in temperatures below -80 °C. Cells were cultured as normal and once they had reached approximately 70% confluency cells were harvested and centrifuged. The resulting pellet was re-dissolved in freezing media (1 mL) which contains 85% of the appropriate culture medium with 15% DMSO. DMSO plays a cyroprotective role as it increases the solubility of the cell membrane, preventing the formation of large ice crystals in the cell cytoplasm which can occur as a result of rapid temperature drop. To avoid this process the cryotube vials were initially placed in a CoolCell™ LX Freezing Container which slows down the rate of freezing to -1 °C/1 min, preventing cell rupture. The cryotubes were then transferred to a -80 °C freezer, and for long term storage to a -178 °C liquid nitrogen tank until further use.

### Cell thawing

The cryotube vial was removed from liquid nitrogen and slowly defrosted in a water bath at 37 °C. The thawed cell solution was added to appropriate culture media (5

mL) and the cell suspension spun for 3 min at 1000 rpm, and the supernatant removed. The remaining pellet was re-suspended in media and the cell suspension re-spun to ensure no DMSO remained. The final cell pellet in fresh media (1 mL) was transferred to the appropriate cell culture flask, and total volume adjusted as necessary (**Table 2.3**).

## **MTS Cell Proliferation Assay**

### ***In vitro* cytotoxicity evaluation**

Cells were cultivated in 96-well culture plates and seeded at densities outlined in **Table 2.3** in appropriate culture media. The media was removed 24 h after seeding and cells were treated with a particular test compound solution (100  $\mu$ L) at various working concentrations. After 72 h of treatment [3-(4,5-dimethylthiazol-2-yl)-5-(3-carboxymethoxyphenyl)-2-(4-sulfo phenyl)-2*H*-tetrazolium, inner salt, (MTS) (*Promega, Southampton, UK*) (20  $\mu$ L) was added to each well, and the plates were incubated for 2 h at 37 °C. Following incubation, the absorbance was measured at 490 nm for 1 second using a Wallac 1420 Victor 3V plate reader (*Perkin-Elmer Life Sciences, Boston, USA*). The percentage of surviving cells relative to untreated controls was evaluated. The IC<sub>50</sub> value, defined as the drug concentration required to inhibit cell proliferation by 50%, was determined for each test compound graphically from dose-response plots using GraphPad Prism (*ver 5.1., GraphPad Software Inc. La Jolla, California, USA*).

### **Statistical analysis**

Statistical analysis for all experiments was carried out using GraphPad Prism. Difference between two values were analysed using an unpaired Student's t-test with the significance level set to  $p < 0.05$ .

## Cellular Fluorescence Imaging

### Fixing of cells to microscope slide

Cells were cultivated onto an ibidi 8-well removable chamber slide (*Martinsried, Munich, Germany*) and seeded at densities outlined in **Table 2.3** in appropriate media. The media was removed 14 h after seeding and the cells were treated with 5  $\mu$ M test compound solution (200  $\mu$ L) for a variety of time points. Following exposure, cells were washed with PBS (200  $\mu$ L) in triplicate to remove excess test compound and media and the cells were fixed to the slide with 4 % para-formaldehyde (PFA) in PBS by incubation at 37 °C for 10 min. The excess PFA was removed and the wells were washed with PBS (200  $\mu$ L) in triplicate and 100  $\mu$ L of PBS was added to each well to prevent fixed cell degradation.

### Coverslip adherence

The coverslip was attached to the 8-well chamber slide by first removing the PBS from the wells. The 8-well detachable divider was removed leaving behind the slide. Excess PBS was carefully dried from the slide and Vectashield® containing DAPI (*Vector Laboratories, Maravai Life Sciences, Burlingame, California, USA*) (9.5  $\mu$ L) to counterstain the nuclei was added and the coverslip was mounted, removing all air bubbles. The coverslip was secured in place using nail polish to prevent the slide drying out. The prepared slide was stored in darkness at 4 °C in darkness.

### Widefield imaging

Imaging was performed on an Olympus IX73 epi-fluorescent widefield microscope (*Olympus Corp., Shinjuku, Tokyo, Japan*) equipped with a Lumencor Spectra X (*Lumencor Inc., Bearverton, Oregon, USA*) solid state diode illumination source containing LEDs capable of excitation at 405 and 640 nm. Images were acquired with an Olympus 60X/ 14.5 oil DIC objective (*Olympus Corp., Shinjuku, Tokyo, Japan*). The camera was an iXon 88 EMCCD (*Andor Technology Ltd, Belfast, United Kingdom*) controlled by MetaMorph (*ver. 7.8, Sunnyvale, California, USA*). Camera settings for fluorescence were 100 ms exposure and 1000X EM gain. Camera settings for the Hoechst 33342 fluorescence were 20 ms exposure and 1000X EM gain. Images were processed using ImageJ software (*Wayne Rasband, Fiji, National Institute of Health, USA*).

## DNA binding studies

### Preparation of DNA

pUC19 DNA plasmid was sourced from Brennan & Co. (*Brennan & Company, Stillorgan, Dublin*), prepared from cultures of *E.coli*. The double-stranded circular plasmid DNA is 2686 base pairs in length. For each experiment DNA (200 ng) was prepared from a working solution of source pUC19 DNA (50 µg/mL) to give a final concentration of 60 µM diluted with 10 mM NaClO<sub>4</sub> buffer.

### DNA separation using agarose gel electrophoresis

DNA fragments were separated based on their size and length using agarose gel electrophoresis. A 1% w/v agarose gel was first prepared in Tris acetate-EDTA (TAE) buffer (40 mM Tris-acetate, 1 mM EDTA) (1.5 g in 150 mL), and a 20-well comb inserted as a space holder for sample loading. The percentage of agarose gel used was determined based on the size of DNA fragments with respect to kilobases (kb).

Test compound solutions (5 µL) at various working concentrations were aliquoted in eppendorfs and DNA (5 µL) was added. The samples were then incubated in the dark for 48 h at 37 °C. Following incubation, loading buffer (40% sucrose, 0.1M EDTA (pH 8), 0.5% SDS, 0.05% bromophenol blue) was added to each sample (2 µL). The DNA samples containing loading buffer (12 µL) were loaded onto each lane of the agarose gel where lane 1 contains a DNA molecular marker ladder (6 µL) in TAE buffer (4 µL) with loading gel (2 µL).

The gels were placed in TAE running buffer and an electric current was applied across the gel. As DNA constitutes a negatively charged sugar-phosphate backbone an electric current causes the negatively charged nucleic acids to migrate through the gel towards the positively charged electrode. Samples were initially run at 150 V, increasing to 200 V. On completion (~ 60 min) the current was stopped and the gel stained by placing it in an ethidium bromide (EtBr) solution (0.5 µM/mL) for 40 min. The gels were washed with deionised water to remove any remaining excess EtBr and visualized using an Amersham™ Imager 600 transilluminator (*GE Healthcare Life Sciences, Buckinghamshire, UK*). The gels were excited with midrange UV (312 nm) which is the fluorescence excitation maximum of EtBr.

## References

1. Gottlieb, H. E.; Kotlyar, V.; Nudelman, A., NMR chemical shifts of common laboratory solvents as trace impurities. *The Journal of organic chemistry* **1997**, 62 (21), 7512-7515.
2. Wu, D.; Cheung, S.; O'Sullivan, C. J.; Gao, Y.; Chen, Z.-L.; O'Shea, D. F., Strained alkyne substituted near infrared BF 2 azadipyromethene fluorochrome. *RSC Advances* **2016**, 6 (90), 87373-87379.
3. Murtagh, J.; Frimannsson, D. O.; O'Shea, D. F., Azide Conjugatable and pH Responsive Near-Infrared Fluorescent Imaging Probes. *Organic Letters* **2009**, 11 (23), 5386-5389.
4. Karim, K. J. A.; Binauld, S.; Scarano, W.; Stenzel, M. H., Macromolecular platinum-drugs based on statistical and block copolymer structures and their DNA binding ability. *Polymer Chemistry* **2013**, 4 (22), 5542-5554.
5. Urankar, D.; Košmrlj, J., Preparation of diazenecarboxamide–carboplatin conjugates by click chemistry. *Inorganica Chimica Acta* **2010**, 363 (14), 3817-3822.
6. Dai, Z.-C.; Chen, Y.-F.; Zhang, M.; Li, S.-K.; Yang, T.-T.; Shen, L.; Wang, J.-X.; Qian, S.-S.; Zhu, H.-L.; Ye, Y.-H., Synthesis and antifungal activity of 1, 2, 3-triazole phenylhydrazone derivatives. *Organic & biomolecular chemistry* **2015**, 13 (2), 477-486.
7. Bolje, A.; Urankar, D.; Košmrlj, J., Synthesis and NMR Analysis of 1,4-Disubstituted 1,2,3-Triazoles Tethered to Pyridine, Pyrimidine, and Pyrazine Rings. *European Journal of Organic Chemistry* **2014**, 2014 (36), 8167-8181.
8. Kitteringham, E.; Wu, D.; Cheung, S.; Twamley, B.; O'Shea, D. F.; Griffith, D. M., Development of a novel carboplatin like cytoplasmic trackable near infrared fluorophore conjugate via strain-promoted azide alkyne cycloaddition. *Journal of Inorganic Biochemistry* **2018**, 182, 150-157.
9. Varbanov, H. P.; Valiahdi, S. M.; Kowol, C. R.; Jakupec, M. A.; Galanski, M.; Keppler, B. K., Novel tetracarboxylatoplatinum (IV) complexes as carboplatin prodrugs. *Dalton Transactions* **2012**, 41 (47), 14404-14415.
10. Failes, T. W.; Hall, M. D.; Hambley, T. W., The first examples of platinum amine hydroxamate complexes: structures and biological activity. *Dalton Transactions* **2003**, (8), 1596-1600.
11. Williams, K. M.; Poynter, A. D.; Hendrie, J. D.; Jackson, D. C.; Martin, V. K., Comparison of N-acetylmethionine reactivity between oxaliplatin and an oxaliplatin derivative with chiral (S,S) amine nitrogen atoms. *Inorganica Chimica Acta* **2013**, 401, 64-69.
12. Feazell, R. P.; Nakayama-Ratchford, N.; Dai, H.; Lippard, S. J., Soluble Single-Walled Carbon Nanotubes as Longboat Delivery Systems for Platinum(IV) Anticancer Drug Design. *Journal of the American Chemical Society* **2007**, 129 (27), 8438-8439.
13. Schweinfurth, D.; Pattacini, R.; Strobel, S.; Sarkar, B., New 1,2,3-triazole ligands through click reactions and their palladium and platinum complexes. *Dalton Transactions* **2009**, (42), 9291-9297.
14. Lo, W. K. C.; Huff, G. S.; Cubanski, J. R.; Kennedy, A. D. W.; McAdam, C. J.; McMorran, D. A.; Gordon, K. C.; Crowley, J. D., Comparison of Inverse and Regular 2-Pyridyl-1,2,3-triazole “Click” Complexes: Structures, Stability, Electrochemical, and Photophysical Properties. *Inorganic Chemistry* **2015**, 54 (4), 1572-1587.
15. Shahabadi, N.; Heidari, L., Synthesis, characterization and multi-spectroscopic DNA interaction studies of a new platinum complex containing the drug metformin. *Spectrochimica Acta Part A: Molecular and Biomolecular Spectroscopy* **2014**, 128, 377-385.
16. Bitha, P.; Morton, G. O.; Dunne, T. S.; Delos Santos, E. F.; Lin, Y. I.; Boone, S. R.; Haltiwanger, R. C.; Pierpont, C. G., (Malonato)bis[sulfinylbis(methane)-S]platinum(II) compounds: versatile synthons for a new general synthesis of antitumor symmetrical and dissymmetrical (malonato)platinum(II) complexes. *Inorganic Chemistry* **1990**, 29 (4), 645-652.

17. Saha, P.; Descôteaux, C.; Brasseur, K.; Fortin, S.; Leblanc, V.; Parent, S.; Asselin, É.; Bérubé, G., Synthesis, antiproliferative activity and estrogen receptor  $\alpha$  affinity of novel estradiol-linked platinum(II) complex analogs to carboplatin and oxaliplatin. Potential vector complexes to target estrogen-dependent tissues. *European Journal of Medicinal Chemistry* **2012**, *48*, 385-390.
18. Spek, A. L., Structure validation in chemical crystallography. *Acta Cryst.* **2009**, *D65*, 148-155.
19. Merrifield, R. B., Solid Phase Peptide Synthesis. I. The Synthesis of a Tetrapeptide. *Journal of the American Chemical Society* **1963**, *85* (14), 2149-2154.
20. Carpino, L. A.; Han, G. Y., 9-Fluorenylmethoxycarbonyl amino-protecting group. *The Journal of Organic Chemistry* **1972**, *37* (22), 3404-3409.
21. Abramkin, S.; Valiahdi, S. M.; Jakupec, M. A.; Galanski, M.; Metzler-Nolte, N.; Keppler, B. K., Solid-phase synthesis of oxaliplatin-TAT peptide bioconjugates. *Dalton Transactions* **2012**, *41* (10), 3001-3005.

## **Chapter 3**

**Novel platinum(II)-fluorophore conjugation *via* SPAAC. Synthesis, characterisation, DNA binding, *in vitro* cytotoxicity and NIR cytoplasmic imaging of ovarian cancer cells**

## Abstract

The successful design and pre-clicked synthesis of a non-toxic and cytosol trackable carboplatin-like near infrared fluorophore conjugate *via* strain-promoted azide alkyne cycloaddition (SPAAC) is reported. Reaction of *cis*-[Pt(2-azidopropane-1,3-diamine)(CBDCA)] and a bicyclo[6.1.0]non-4-yne NIR-AZA fluorophore gave the corresponding clicked Pt-Fluorophore conjugate. The X-ray crystal structure of *cis*-[Pt(CBDCA)(DAP-N<sub>3</sub>)] was determined featuring the azide on the bidentate 1,3-diaminopropane ligand. The Pt-fluorophore conjugate is the first example of a Pt conjugate clicked *via* SPAAC where the reactive azide handle is on the ammine carrier ligand. The *in vitro* cytotoxicity and widefield fluorescence imaging of the Pt-Fluorophore conjugate in A2780P and A2780cis cells and the Pt DNA binding experiments by gel electrophoresis are described.

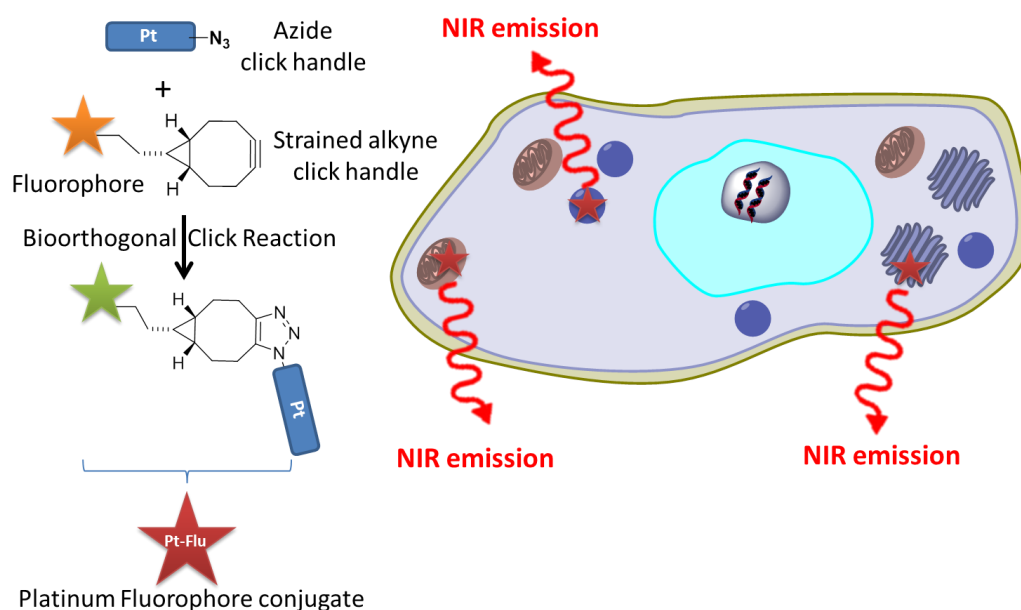


**Figure 3.1:** Graphical hypothesis of the aims of this work. Synthesis of a clicked Pt-Flu conjugate, followed by treatment *in cellulo*.



## Introduction

Metal-based drugs have a wide range of medicinal applications and are routinely used as therapeutics and diagnostics in a clinical setting.<sup>1-2</sup> In particular, platinum (Pt) drugs such as cisplatin, carboplatin and oxaliplatin (**Figure 3.2**) have played a very important and well documented role in treating cancer and are employed in nearly 50% of anticancer regimens.<sup>3</sup>

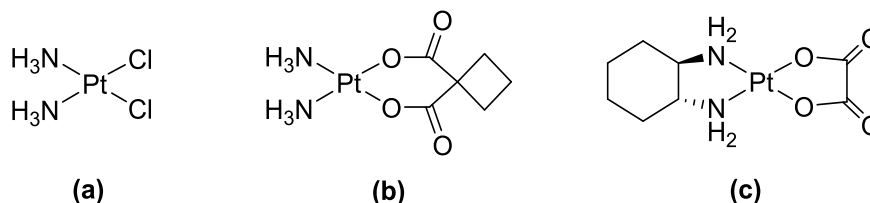


**Figure 3.2:** Structures of (a) cisplatin ( $cis-[PtCl_2(NH_3)_2]$ ), (b) carboplatin ( $[Pt(CBDCA)(NH_3)_2]$ , CBDCA = cyclobutane dicarboxylate) and (c) oxaliplatin ( $[Pt(DACH)(Ox)]$  DACH = 1*R*,2*R*-cyclohexane-1,2-diamine and Ox = oxalate).

The cytotoxicity of Pt drugs, which hydrolyse (loss of chlorido or carboxylate ligands) inside cells, has traditionally been primarily attributed to their ability to covalently bind DNA, forming DNA adducts, leading to DNA damage responses and ultimately programmed cell death, apoptosis.<sup>3-4</sup>

However, given that only 1% of intracellular cisplatin forms adducts with nuclear DNA and that Pt drugs exert noteworthy cytotoxic effects in enucleated cells it is apparent that the effects of Pt drugs are likely both nuclear and cytoplasmic.<sup>5</sup> Intracellularly activated electrophilic Pt centres for example can interact with cytoplasmic nucleophiles, including mitochondrial DNA (mtDNA), RNA as well as multiple mitochondrial and extramitochondrial proteins which may for instance induce oxidative and reticular stress.<sup>5-6</sup> Significantly, it is becoming increasingly clear that the exact biomolecular mechanisms of action of Pt drugs are not implicit.<sup>5</sup> Lippard *et al.* for example have recently demonstrated that oxaliplatin, in contrast to cisplatin and carboplatin, does not kill cells *via* the DNA-damage response but by inducing ribosome biogenesis stress.<sup>7</sup> Therefore it is clear that the exact biomolecular mechanisms of action of Pt drugs and in particular the extranuclear or cytoplasmic effects of Pt drugs are not fully understood.<sup>5</sup>

Trackable metal-based drugs which incorporate an organic fluorophore offer the prospect of real-time imaging of important biological processes *in vitro* and providing vital information concerning the biodistribution, cellular transport, subcellular localization, and mechanisms of action and resistance to metallothrapeutics.<sup>8-10</sup>

The near-infrared (NIR) spectral region (700–900 nm) provides ideal imaging spectral wavelengths, reduced light toxicity and does not interfere with competing endogenous chromophore absorbance.<sup>8-10</sup> Significantly, NIR probes have been successfully employed to image tumours *in vitro* and *in vivo* and as sensors for ROS, RNS, thiols, ions, pH and enzyme activities.<sup>6</sup>

The BF<sub>2</sub>-azadipyrromethene (NIR-AZA) fluorophore class, which have absorptions of c. 690 nm with emission at c. 725 nm in formulated aqueous solution,<sup>11-12</sup> offer excellent photophysical and stability properties and have attracted the attention of many research teams,<sup>10, 13</sup> including those interested in tracking metal-based drugs.<sup>14</sup>

The previously reported, BCN-NIR-AZA (**Figure 3.3**) possesses a strain-promoting bicyclo[6.1.0]non-4-yne (BCN) conjugation group, an aqueous solubilizing alkyl-sulfonate group and excellent NIR photophysical properties;  $\lambda_{\text{abs}} = 690 \text{ nm}$  ( $\epsilon = 72,000 \text{ M}^{-1} \text{ cm}^{-1}$ ) and  $\lambda_{\text{Flu}} = 722 \text{ nm}$  ( $\Phi_{\text{Flu}} = 0.18$ ) in aqueous buffer. It was recently for example successfully employed as conjugate to a tumour targeting cyclic RGD peptide for real-time cellular imaging and *in vivo* tumour visualization.<sup>15</sup>

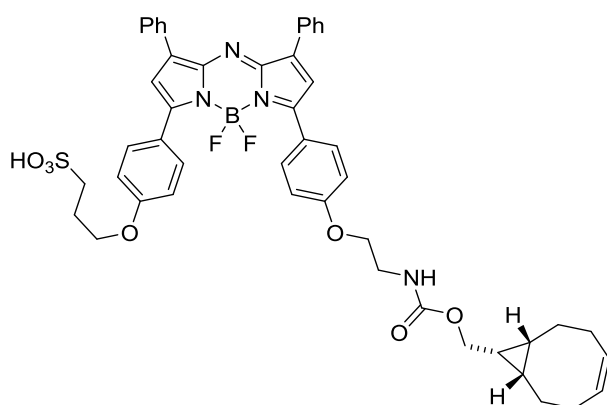


**Figure 3.3:** Structure of strained alkyne bearing BCN-NIR-AZA fluorophore.

Specifically, a number of Pt(II) anticancer type compounds have been reported where boron-fluorescent dipyrromethene (BODIPY) moieties have been tethered to

Pt centres *via* prior direct covalent modification of the ammine carrier ligands, **Figure 3.4a-c**. For instance, Miller *et al.* developed BODIPY tethered Pt complexes for high resolution imaging of cancer *in vivo*,<sup>16</sup> Hall and coworkers to monitor the fate of cisplatin analogues,<sup>17</sup> and Mitra *et al.* for mitochondria targeted phototoxicity, **Figure 3.4**.<sup>18</sup>

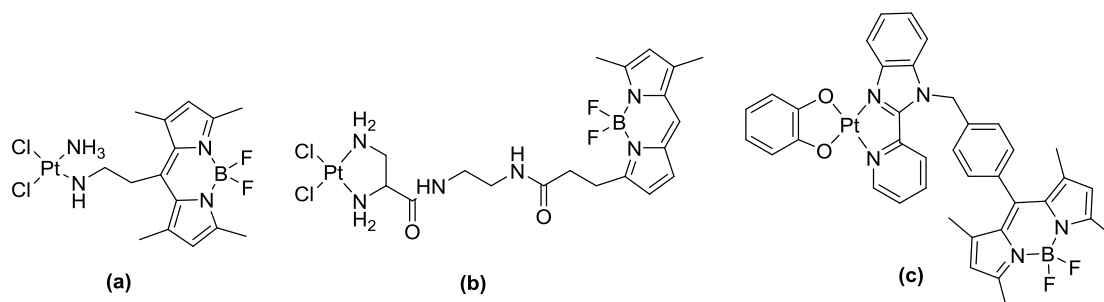


**Figure 3.4:** (a-c) Structures of previously reported Pt-BODIPY conjugates generated through direct covalent modification of the ammine carrier ligands.<sup>17-18</sup>

Furthermore, a number of Pt complexes which offer a general synthetic approach to the functionalization of Pt centres have been developed, including those that possess reactive azide handles that facilitate click reactions, **Figure 3.5a-c**.<sup>6, 19-20</sup> Dhar *et al.* for example developed the Pt(IV) precursor, Platin-Az, **Figure 3.5c** which enables installation of new functionalities *via* strain-promoted azide alkyne cycloadditions (SPAACs). The azides, which are found on a labile Pt(IV) axial ligand, and which are lost on reduction to Pt(II) *in cellulo*, were clicked with azadibenzocyclooctyne (ADIBO) derivatives including the near-infrared fluorescent reporter, Cy5.5, which was used to visualize the cellular uptake of Pt in prostate cancer cells.<sup>21</sup>

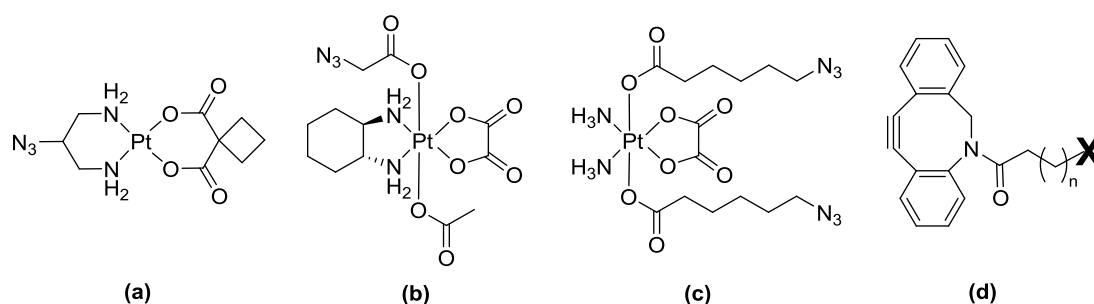


**Figure 3.5:** (a-c) Structures of previously reported Pt azide complexes and (d) structure of azadibenzocyclooctyne (ADIBO) derivative where **X** could be a targeting ligand, antibody, fluorescent reporter or therapeutic.

SPAAC reactions offer a number of synthetic advantages in a biological system. The alkyne and azide functional groups are biorthogonal and do not interfere with endogenous biomolecules within a biological system.<sup>22</sup> The use of a strained cyclooctyne moiety instead of a traditional terminal alkyne also removes the need for a Cu(I) catalyst, which is toxic in many cellular environments, limiting the scope for live cell imaging.<sup>23</sup> Furthermore, the absence of a catalyst and other coupling reagents also aids purification of clicked product. Finally, as the SPAAC is biorthogonal, it provides the ideal template for reactions both *in vitro* and *in vivo*.

*cis*-[Pt(2-azidopropane-1,3-diamine)(CBDCA)] possesses a reactive azide handle on the stable ammine carrier ligand, in contrast for example to Platin-Az, **Figure 3.5c**, offering better biocompatibility. Previously, [Pt(II)(CBDCA)(DAP-N<sub>3</sub>)] and its cisplatin derivative have been investigated for their Cu(I) promoted click reactions to conjugate them to organic scaffolds with potential biological relevance, with the cisplatin complex being further investigated *ex cellulo* for its DNA binding potential by White *et al.*<sup>6</sup>

### Rationale

The imaging and tracking of anticancer drugs such as carboplatin is of considerable interest to the scientific community. Given there are still question marks over the exact mechanisms of action of Pt drugs and on average only 1% of Pt drugs which enter cancer cells bind with DNA, we sought to develop a biorthogonal platform that would help (i) investigate the cellular uptake, efflux and/or the cytoplasmic distribution in cancer cells of Pt drugs (ii) identify novel extranuclear cellular targets associated with Pt drugs and (iii) provide valuable information on the biodistribution of Pt drugs *in vivo*.

Fluorescent probes are routinely conjugated to bioactive molecules to probe cellular and physiological processes. SPAAC was selected as the preferred conjugation strategy as it facilitates both the *ex cellulo* synthesis and the *in cellulo* synthesis of Pt fluorophore conjugates and removes the requirement for potentially toxic Cu(I).

[Pt(CBDCA)(DAP-N<sub>3</sub>)] was selected as it serves as a carboplatin mimic, which possesses the required reactive azide handle on the ammine carrier ligand.

BODIPY was selected as the fluorophore of choice given its well-recognised favourable photophysical properties but also because it is known to be relatively non-toxic and not to accumulate in the nucleus of cells, thereby facilitating investigations in the cytoplasm.

To this end, cytotoxicity and DNA binding studies of the Pt-Flu conjugate were carried out as well as cellular imaging studies in two ovarian cancer cell lines.

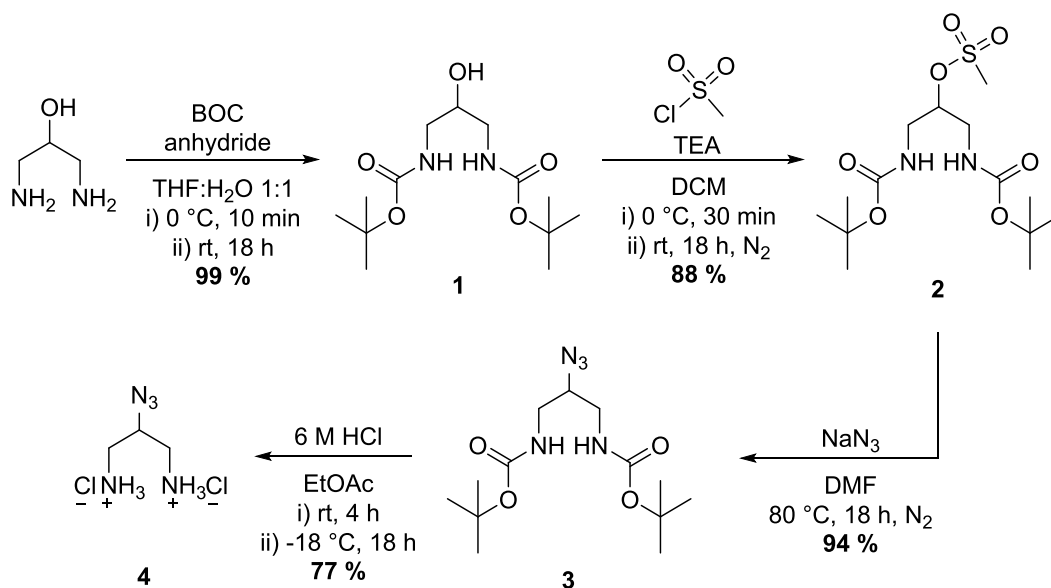
### Chapter Aims

- ◁ To synthesise and characterize a novel Pt-Flu conjugate *via* strain promoted alkyne-azide cycloaddition (SPAAC).
- ◁ To investigate the *in vitro* cytotoxicity of the Pt-Flu conjugate against cisplatin sensitive and cisplatin resistant ovarian cancer cell lines.
- ◁ To examine the DNA binding ability of the Pt-Flu conjugate.
- ◁ To investigate the fluorescent and imaging properties of the Pt-Flu conjugate *in vitro* in cisplatin sensitive and cisplatin resistant ovarian cancer cell lines

## Synthesis of the Pt click template [Pt(CBDCA)(DAP-N<sub>3</sub>)] and corresponding Pt-Fluorophore click conjugate

### 2-azidopropane-1,3-diamine dihydrochloride (DAP-N<sub>3</sub>.2HCl)

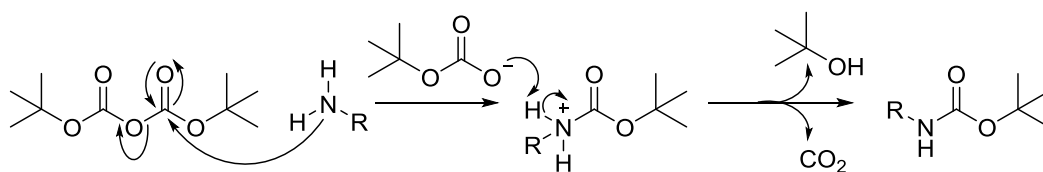
The synthesis of DAP-N<sub>3</sub>.2HCl **4** was carried out in 4 steps (**Scheme 3.1**) using the previously reported method of Karim *et al.* by the conversion of 1,3-diamine-propan-2-ol to **4**.



**Scheme 3.1:** Synthetic route to DAP-N<sub>3</sub> **4**.

The synthetic route involved BOC protection of the amines, generation of a mesylate (MeS) leaving group from the alcohol, azide substitution of the MeS group and final acid deprotection (6 M HCl) of the amines to give **4** as a hydrochloride salt in 77% yield.

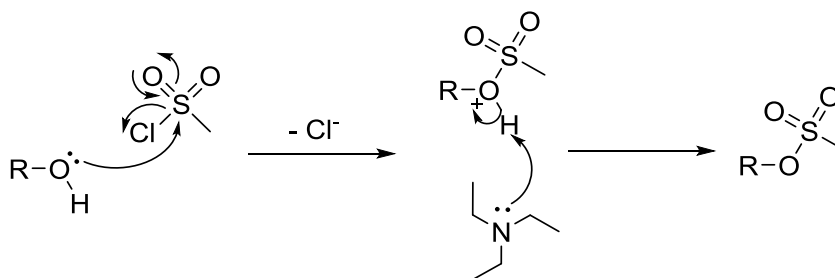
**1** was formed by the protection of two amine groups on DAP-OH (1, 3-diaminopropan-2-ol) with BOC<sub>2</sub>O by slow addition at 0 °C. This is an example of nucleophilic acyl substitution. The mechanism of this reaction occurs in two steps; i) the addition of the primary amine through the carbonyl group of BOC<sub>2</sub>O, followed by ii) elimination of the *tert*-butanoic anion. The *tert*-butanoic anion acts as a base which picks up the proton from the ammonium cation formed, resulting in the carbamate. The *tert*-butanoic acid formed may further decompose to *tert*-butanol and carbon dioxide (**Scheme 3.2**).



**Scheme 3.2:** Scheme demonstrating BOC protection of a primary amine.

The BOC protection reduces reactivity of the nucleophilic amine groups in downstream reactions. The viscous oil formed solidifies upon extended air exposure as a pale yellow sticky solid. The BOC protected product **1** was characterised by  $^1\text{H}$  NMR ( $\text{CDCl}_3$ ) spectroscopy where a single, large peak at 1.44 ppm correlates for the eighteen protons of the two symmetrical BOC groups attached, serving as the diagnostic signal.

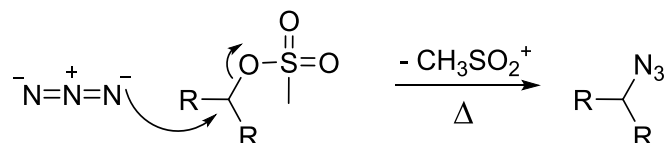
Alcohols become good leaving groups if they are converted to the corresponding mesylates, tosylates and triflates. For example, alkyl mesylates can perform all of the substitution reactions of the corresponding alkyl halides. Compound **2** was synthesised on reaction of **1** with methanesulfonyl chloride in the presence of the non-nucleophilic base TEA (**Scheme 3.3**), *via* nucleophilic substitution. The alcohol first becomes deprotonated and reacts with the sulfonyl group which acts as an electrophile. A chloride anion is lost as a result, later generating HCl with the proton in solution from the alcohol. The reaction afforded the mesylate and BOC protected derivative of DAP, **2**.



**Scheme 3.3:** Reaction scheme demonstrating nucleophilic substitution of methanesulfonyl chloride.

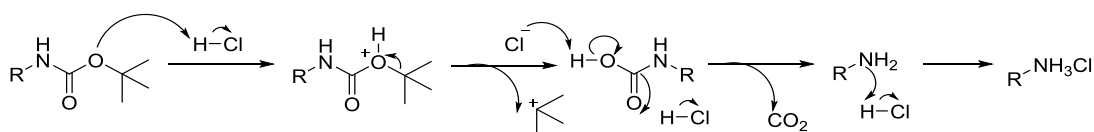
Compound **2** was characterised by  $^1\text{H}$  NMR ( $\text{CDCl}_3$ ) spectroscopy and a single diagnostic peak at 3.09 ppm correlating to the three methyl protons of the MeS group was evident in the spectrum. Likewise, in the  $^{13}\text{C}$  NMR spectrum, a resonance observed at 38.16 ppm is associated with the methyl of the MeS group carbon.

The third step of the reaction was the heating of **2** with sodium azide to yield BOC protected DAP-N<sub>3</sub>, **3**, by substitution of the MeS group with an N<sub>3</sub> via S<sub>N</sub>2 substitution (**Scheme 3.4**). The product **3** was characterised by <sup>1</sup>H NMR (CDCl<sub>3</sub>) spectroscopy with the loss of the single diagnostic peak which correlated to the methyl group of MeS, along with a shift in the single proton of carbon number 2 of the propane chain from 4.66 to 3.64 ppm. In the <sup>13</sup>C NMR spectrum, the loss of the methyl carbon associated with MeS was also observed.



**Scheme 3.4:** Reaction scheme demonstrating nucleophilic substitution of methanesulfonate with an azide.

The final step in the synthesis of DAP-N<sub>3</sub> was the acid deprotection of the amines and concomitant formation of the dihydrochloride salt (**Scheme 3.5**), giving compound **4**. The BOC deprotection was performed using 6 M HCl (excess) in a 1:1 mixture with EtOAc. There are a number of steps to this reaction. First, the *tert*-butyl carbamate is protonated by HCl and the loss of the *tert*-butyl cation results in carbamic acid formation. The chloride ion deprotonates the carbamic acid, resulting in decarboxylation of the carbamic acid and forms the free amine. The amine interacts with the excess HCl in solution to form a hydrochloride salt, DAP-N<sub>3</sub>.2HCl, which precipitates from solution upon cooling in EtOAc.



**Scheme 3.5:** Scheme demonstrating acid deprotection of BOC protected amines.

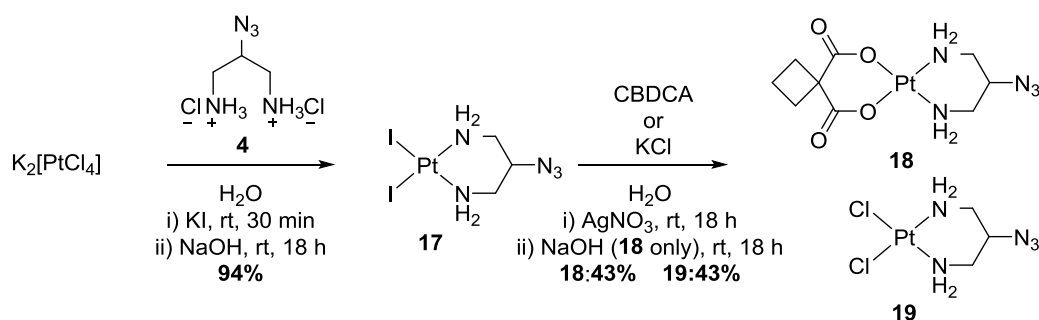
The product **4** was characterised by <sup>1</sup>H NMR (DMSO-*d*<sub>6</sub>) spectroscopy by a single, broad resonance peak at 8.55 ppm integrating for the six protons of the two NH<sub>3</sub> groups along with the loss of the large broad singlet of the 18 BOC *tert*-butyl protons. The protons of propane are observed and integrate for 1:2:2 as one methine and four methylene protons across two signals at 4.29, 3.16 and 2.91 ppm respectively; akin to compounds **1-3** and matching previously reported data.<sup>24</sup> The compound was additionally analysed using D<sub>2</sub>O as a solvent. Elemental analysis data is consistent with the proposed structure of compound **4**. FT-IR analysis of **4**



demonstrated the presence of the azide stretch within the characteristic region at  $2135\text{ cm}^{-1}$ .

### [Pt(II)(CBDCA)(DAP-N<sub>3</sub>)]

[Pt(II)(CBDCA)(DAP-N<sub>3</sub>)], **18** was synthesised in two steps following the previous published method of Urankur *et al.* using standard Pt synthetic methodology and procedures.<sup>24</sup> [PtI<sub>4</sub>]<sup>2-</sup> was first formed in solution by the stirring of K<sub>2</sub>[PtCl<sub>4</sub>] with excess KI in water. To this was added DAP-N<sub>3</sub>, which was generated by reacting two equivalents of NaOH with DAP-N<sub>3</sub>.2HCl, in water. DAP-N<sub>3</sub> readily coordinates to Pt forming the intermediate [Pt(II)I<sub>2</sub>(DAP-N<sub>3</sub>)], which was subsequently stirred with AgNO<sub>3</sub> overnight, in darkness. The AgI precipitate was removed by celite filtration. Na<sub>2</sub>CBDCA was added to the filtrate and stirred overnight. The solution was concentrated under vacuum and the resultant precipitate collected as **18**.



**Scheme 3.6:** Scheme demonstrating the two step synthesis of [Pt(II)(CBDCA)(DAP-N<sub>3</sub>)] and [Pt(II)Cl<sub>2</sub>(DAP-N<sub>3</sub>)].

The characterisation was informed by <sup>1</sup>H, <sup>13</sup>C and <sup>195</sup>Pt (MeOD-*d*<sub>4</sub> and DMSO-*d*<sub>6</sub>) NMR spectroscopy, ESI-mass spectroscopy (MS) and FT-IR, which correlated with the previously reported structure of Urankur *et al.* Elemental analysis also correlated with the theoretical values demonstrating the formation of the desired complex. In addition the previously unreported crystal structure of the complex was solved as seen in **Figure 3.6**.

### X-ray crystal analysis of [Pt(II)(CBDCA)(DAP-N<sub>3</sub>)]

The ORTEP structure is reported in **Figure 3.7**, while the data relating to the crystal and refinement patterns is reported in **Table 3.1**. Crystal data and structure refinement for [Pt(II)(CBDCA)(DAP-N<sub>3</sub>)] are shown in **Table 3.2**.

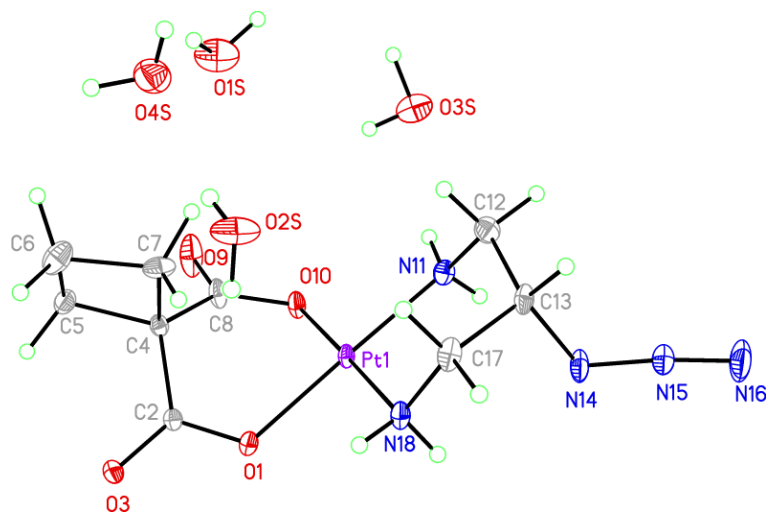


**Figure 3.6:** ORTEP diagram of [Pt(II)(CBDCA)(DAP-N<sub>3</sub>)], with 4 H<sub>2</sub>O included, and atomic displacement parameters shown at 50% probability.

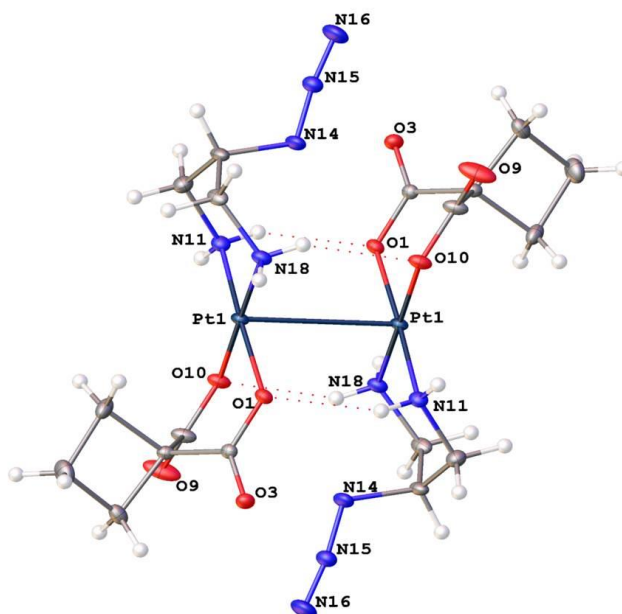


**Figure 3.7:** ORTEP diagram of the [Pt(II)(CBDCA)(DAP-N<sub>3</sub>)] dimer over inversion centre with atomic displacement parameters shown at 50% probability.

**Table 3.1:** Selected bond lengths [ $\text{\AA}$ ] and angles [ $^\circ$ ] determined for  $[\text{Pt(II)(CBDCA)(DAP-N}_3)]$ .

Bond	Length $\text{\AA}$	Bond	Angles $^\circ$
C(4)-C(5)	1.550(5)	C(5)-C(4)-C(7)	88.8(3)
C(4)-C(7)	1.582(5)	C(6)-C(5)-C(4)	90.2(3)
C(5)-C(6)	1.546(6)	C(7)-C(6)-C(5)	90.4(3)
C(6)-C(7)	1.542(6)	C(6)-C(7)-C(4)	89.2(3)
N(11)-Pt(1)	2.028(3)	O(10)-Pt(1)-N(11)	87.22(11)
N(14)-N(15)	1.241(4)	N(18)-Pt(1)-O(1)	88.35(11)
N(15)-N(16)	1.126(5)	O(1)-Pt(1)-N(11)	176.34(11)
N(18)-Pt(1)	2.025(3)	O(10)-Pt(1)-N(18)	179.00(10)
O(1)-Pt(1)	2.026(2)	N(18)-Pt(1)-N(11)	93.77(12)
O(10)-Pt(1)	2.011(3)	O(10)-Pt(1)-O(1)	90.65(10)
Pt(1)-Pt(1)#1	3.1201(2)	N(16)-N(15)-N(14)	172.3(4)
		N(11)-Pt(1)-Pt(1)#1	92.49(9)
		N(18)-Pt(1)-Pt(1)#1	90.77(9)
		O(1)-Pt(1)-Pt(1)#1	84.49(7)
		O(10)-Pt(1)-Pt(1)#1	89.11(8)

**Table 3.2:** Crystal data and structure refinement for  $[\text{Pt(II)(CBDCA)(DAP-N}_3)]$ 

Empirical formula	$\text{C}_9\text{H}_{23}\text{N}_5\text{O}_8\text{Pt}$
Formula weight	524.41
Temperature	99.99 K
Wavelength	0.71073 $\text{\AA}$
Crystal system	Triclinic

Space group	P $\bar{1}$
Unit cell dimensions	a = 8.1972(2) Å, U = 64.3846(12)°. b = 10.0512(3) Å, V = 80.5246(14)°. c = 11.2870(3) Å, $\beta$ = 82.4160(14)°.
Volume	825.18(4) Å <sup>3</sup>
Z	2
Density (calculated)	2.111 Mg/m <sup>3</sup>
Absorption coefficient	8.550 mm <sup>-1</sup>
F(000)	508
Crystal size	0.16 x 0.11 x 0.05 mm <sup>3</sup>
Theta range for data collection	3.036 to 35.139°.
Index ranges	-13 ≤ h ≤ 13, -16 ≤ k ≤ 16, -18 ≤ l ≤ 18
Reflections collected	35734
Independent reflections	7321 [R(int) = 0.0975]
Completeness to theta = 26.000°	99.8 %
Absorption correction	Semi-empirical from equivalents
Max. and min. transmission	0.2910 and 0.1995
Refinement method	Full-matrix least-squares on F <sup>2</sup>
Data / restraints / parameters	7321 / 4 / 239
Goodness-of-fit on F <sup>2</sup>	1.071
Final R indices [I > 2σ(I)]	R1 = 0.0325, wR2 = 0.0789
R indices (all data)	R1 = 0.0394, wR2 = 0.0819
Largest diff. peak and hole	3.699 and -3.814 e.Å <sup>-3</sup>

The molecular structure of *cis*-[Pt(II)(CBDCA)(DAP-N<sub>3</sub>)] in **Figure 3.7** clearly shows the typical Pt(II) square planar geometry. The bond angles of the central Pt substituents for example, O(1)-Pt(1)-N(11), O(10)-Pt(1)-N(18), N(18)-Pt(1)-N(11) and O(10)-Pt(1)-O(1) are 176.34(11), 179.00(10), 93.77(12), 90.65(10)° respectively.

With regard to the azido group, recorded bond lengths and angles have been compared to previously reported azide structures. The N(14)=N(15) and N(15)=N(16) bond lengths of 1.241(4) and 1.126(5) Å respectively corresponded to

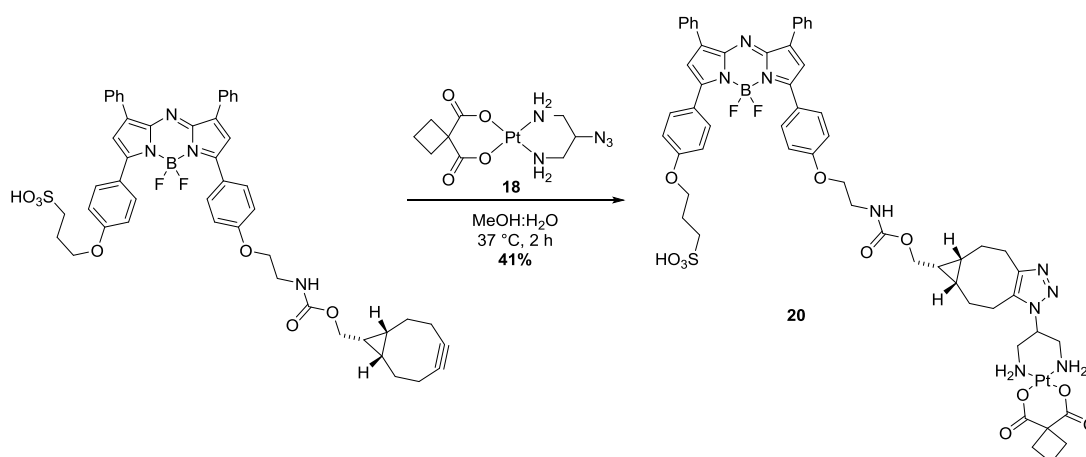
the reported N=N lengths of 1.25 and 1.13 Å, as did the distorted linear bond angle of N(16)-N(15)-N(14) being 172.3(4)° compared to 173.6°. <sup>25</sup>

Each ligand surrounding the Pt centre forms a 6 membered chelate ring. The DAP-N<sub>3</sub> group adopts a distorted chair conformation with an axial azido substituent. The cyclobutane dicarboxylate group displays a distorted boat conformation. The dimer complex forms hydrogen bonded dimers with 4 N-H...O interactions. The molecules lie parallel over an inversion centre with a Pt...Pt distance of 3.1201(2) Å. This type of close Pt-Pt interaction has been noted previously. <sup>26-28</sup>

### [Pt(II)Cl<sub>2</sub>(DAP-N<sub>3</sub>)]

[Pt(II)Cl<sub>2</sub>(DAP-N<sub>3</sub>)], **19** was synthesised as per the method above (**Figure 3.6**), previously reported by Urankur *et al.* The characterisation was informed by <sup>1</sup>H, <sup>13</sup>C (DMSO-*d*<sub>6</sub>) NMR spectroscopy, Elemental analysis and FT-IR, which correlated with the previously reported structure. <sup>24</sup>

### Pt-Flu Conjugation



**Scheme 3.7:** Synthetic route for synthesis of Pt-Flu *via* SPAAC

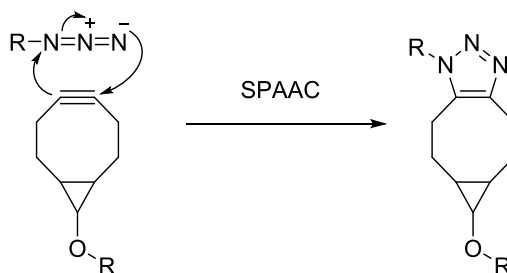
The conjugation of Pt complex **18** with the BCN-NIR-AZA fluorophore (**Flu**) was performed in a single step by stirring at rt for 2 h generating compound **20** (**Pt-Flu**) as proposed in **Scheme 3.7**. **Pt-Flu** was purified by RP-preparative HPLC using 7:3 MeCN:H<sub>2</sub>O as the eluent. The pure fractions were combined and dried by lyophilisation. It was characterised by <sup>1</sup>H, <sup>19</sup>F (60% CD<sub>3</sub>CN + 40% D<sub>2</sub>O) and <sup>195</sup>Pt

(MeOD- $d_4$ ) NMR spectroscopy, HR MS, analytical trace RP-HPLC and UV-vis absorption and emission spectroscopy.

The HR ESI-MS spectrum of **Pt-Flu** in the negative mode featured the required molecular ion for  $C_{57}H_{59}BF_2N_9O_{11}PtS$  (calc.: 1320.3769) at 1320.3612 a.m.u and the expected Pt isotopic pattern. The  $^{19}F$  spectrum of **Pt-Flu** exhibits a standard quartet signal at -130.96 ppm, which is typical of BODIPY compounds<sup>15</sup> and the  $^{195}Pt$  NMR spectrum gives a signal at -1957.96 ppm, a region which correlates with Pt(II) diamino dicarboxylato complexes.<sup>29</sup>

The  $^1H$  NMR spectrum is poorly resolved given the difficulty in recording  $^1H$  NMR spectra of BODIPY derivatives and particularly those that possess an alkyl sulfonate group. Regardless, signals associated with the 20 protons of the four benzene rings ( $8\times H$  and  $10\times H$ ) and the boron-dipyrromethene ( $2\times H$ ) moiety are found from 7 to 8 ppm, integrating for 20. The amines of the DAP group and the amide proton are not observed in  $CD_3CN/D_2O$ . The carbon 2 proton associated with the DAP ligand is found at 3.44 ppm and integrates for one proton. The remaining 33 protons are the methylene protons associated with the alkyl sulfonate chain ( $6\times H$ ), the phenoxyethyl carbamate group ( $4\times H$ ), the DAP ligand ( $4\times H$ ), cyclobutanedicarboxylato ligand ( $6\times H$ ) and the protons associated with the bicyclo[6.1.0]non-4-ene group ( $13\times H$ ).

The reaction is a form of click chemistry known as strain-promoted alkyne-azide cycloaddition (SPAAC). Unlike traditional alkyne-azide click chemistry this reaction does not require the generation of a Cu(I) catalyst. Instead, the reaction is driven by the reactivity of the strained alkyne, cyclooctyne, as shown in **Scheme 3.8**. Although there are a number of examples of Pt(II) and Pt(IV) complexes with incorporated azide handles utilizing both SPACC and BODIBY fluorophores, this is the first reported example of SPAAC of a Pt(II) complex with the bicyclo[6.1.0]non-4-ene group and where the reactive azide on a stable ammine carrier ligand is conjugated to a BODIPY fluorophore.<sup>6, 17-20</sup>



**Scheme 3.8:** Scheme demonstrating the reaction mechanism of the copper-free SPAAC click reaction.

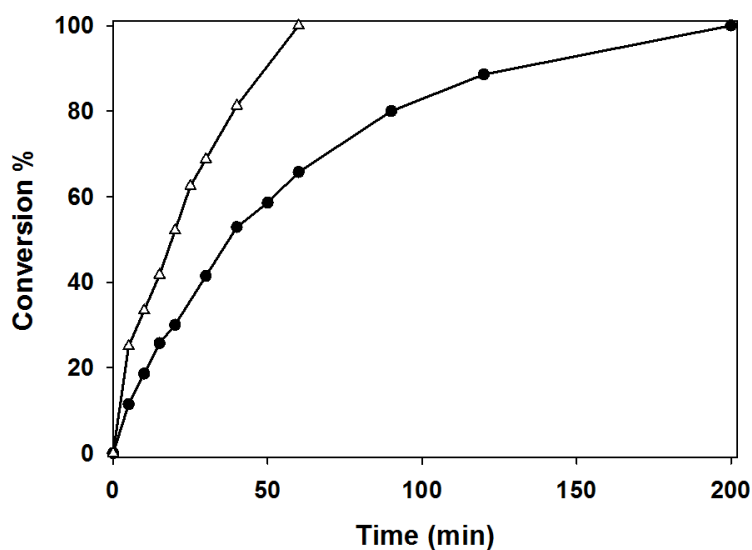


**Figure 3.8:** Plot of the conversion of **Flu** to **Pt-Flu** react 1:1 in MeOH:H<sub>2</sub>O with 1.2 eq. of [Pt(CBDCA)(DAP-N<sub>3</sub>)] **18**. Reactions performed at rt (●) and 37 °C (Δ).

Reaction progress was monitored using analytical trace HPLC in 70 % acetonitrile and 30 % 25 mM NH<sub>4</sub>HCO<sub>2</sub> buffer in water, where samples were taken directly from the reaction solution at the required time points. 100 % conversion was normalised and taken to be the time at which the free fluorophore peak no longer reduced. At 37 °C, the conversion rate reaches its max after 60 min. At rt, the conversion is noticeably slower than at the higher temperature, taking 200 min to reach its maximum (**Figure 3.8**).

Significantly, the conversion plots demonstrate that the formation of **Pt-Flu** is completed more rapidly at 37 °C than at rt. This demonstrates the potential applicability for this reaction within a cellular or *in vivo* model due to the increased reactivity at a biologically relevant temperature.

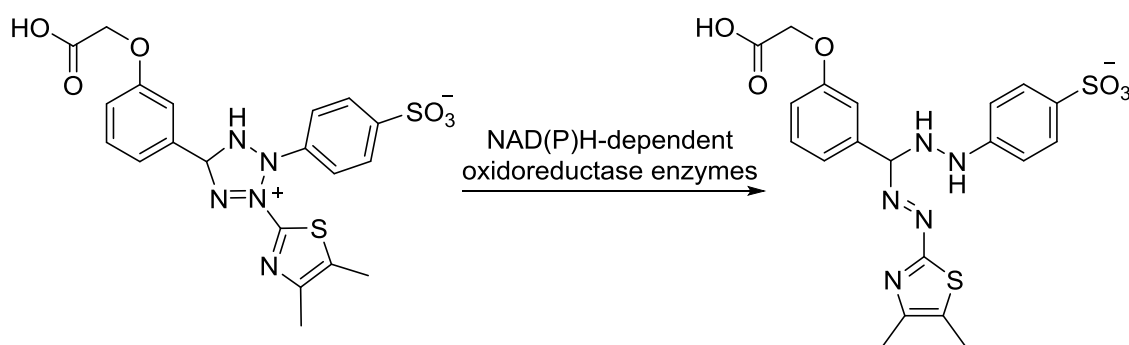
## Biological analysis of Pt-Flu complex

### *In vitro* cytotoxicity evaluation

*In vitro* cytotoxicity experiments were undertaken ( $n = 3$ ) to establish how the cisplatin sensitive and cisplatin resistant ovarian cancer cell lines, A2780P and A2780cis respectively, responded to treatment with cisplatin, carboplatin, [Pt(II)(CBDCA)(DAP-N<sub>3</sub>)] **18**, *cis*-[Pt(II)(Cl)<sub>2</sub>(DAP-N<sub>3</sub>)] **19**, strained alkyne bearing NIR-AZA fluorophore(**Flu**) and the **Pt-Flu** conjugate **20**. Stock solutions of these test compounds were prepared fresh in culture medium and diluted to various working concentrations as per **Table 3.3**.

**Table 3.3:** The range of drug concentration used per cell line.

	A2780P	A2780cis
<b>Carboplatin</b>	12.5 - 200 $\mu$ M	12.5 - 200 $\mu$ M
<b>[Pt(CBDCA)(DAP-N<sub>3</sub>)] 18</b>	12.5 - 200 $\mu$ M	12.5 - 200 $\mu$ M
<b>Flu</b>	50 - 200 $\mu$ M	50 - 200 $\mu$ M
<b>Pt-Flu 20</b>	50 - 200 $\mu$ M	50 - 200 $\mu$ M
<b>Cisplatin</b>	0.39 - 50 $\mu$ M	0.39 - 50 $\mu$ M
<b>[PtCl<sub>2</sub>(DAP-N<sub>3</sub>)] 19</b>	0.39 - 50 $\mu$ M	0.39 - 50 $\mu$ M



**Scheme 3.9:** Scheme demonstrating the conversion of MTS into aqueous, soluble formazan by dehydrogenase enzymes found in the metabolically active cells.

All test compounds were synthesised following literary procedures, and **Flu** kindly provided by Dr. Dan Wu.<sup>15</sup> Cell growth was determined by an MTS inner salt assay, a colourimetric test based on the ability of viable cells to reduce a yellow tetrazolium salt to blue formazan (**Scheme 3.9**).<sup>30</sup> Dose-response plots based on 72 h treatment ( $n$



= 3) were generated using GraphPad Prism and IC<sub>50</sub> values, defined as the drug concentration required to inhibit cell growth by 50 %, were determined (**Table 3.4**).

**Table 3.4.** IC<sub>50</sub> values calculated for ovarian cancer cell lines treated for 72 h. Error shown as  $\pm$  SEM.

Compound	A2780P ( $\mu$ M)	A2780cis ( $\mu$ M)	Resistance factor
<b>Carboplatin</b>	71.9 $\pm$ 2.02	149.8 $\pm$ 2.39	2.08
<b>[Pt(CBDCA)(DAP-N<sub>3</sub>)] 18</b>	61.4 $\pm$ 3.35	134.3 $\pm$ 3.38	2.19
<b>Flu</b>	>200	>200	-
<b>Pt-Flu 20</b>	>200	>200	-
<b>Cisplatin</b>	4.5 $\pm$ 0.425	15.8 $\pm$ 1.62	3.51
<b>[PtCl<sub>2</sub>(DAP-N<sub>3</sub>)] 19</b>	12.0 $\pm$ 0.57	36.2 $\pm$ 3.13	3.02

Cisplatin, which is the Pt drug of choice in a large variety of cancers and solid tumours,<sup>31</sup> exhibited superior cytotoxicity to all other compounds in both the Pt sensitive and resistant ovarian cancer cell lines, A2780P and A2780cis respectively. However, with reference to the *in vitro* cytotoxicity data, there is a noteworthy difference between the Pt drug concentration required to inhibit cell growth for the Pt dichlorido complexes (cisplatin and **19**) and Pt dicarboxylato complexes (carboplatin and **18**) tested. Therefore each complex will be discussed independently.

In the A2780P cell line, the cisplatin type complexes required a concentration of 4.5 - 12.0  $\mu$ M to inhibit cell growth, whereas the carboplatin type derivatives required a higher concentration with a range of 61.4 - 71.9  $\mu$ M to exhibit the same cytotoxic effect. With respect to the A2780cis cell line, the Pt drugs followed a similar pattern with a range of 15.8 - 36.2  $\mu$ M for cisplatin and 134.3 - 149.8  $\mu$ M for carboplatin. As expected and outlined, there is a noticeable reduction in the cytotoxicity of the Pt drugs in the Pt resistant A2780cis cell line with resistance factors of the carboplatin type derivatives being circa 2.1 and the cisplatin type being >3 when compared against A2780P cells. This observation was in agreement with previously published reports of cisplatin and carboplatin cytotoxicity.<sup>32-33</sup>

The carboplatin derivative **[Pt(CBDCA)DAP-N<sub>3</sub>]** was found to be marginally more cytotoxic than carboplatin with lower IC<sub>50</sub>s against both cell lines, with the resistance observed for carboplatin against A2780cis also retained. Although this compound

and its copper catalysed click reaction has been previously reported, this is the first instance of its *in vitro* cytotoxicity being determined.<sup>24</sup> Interestingly, Dhar and coworkers also observed that incorporation of the azide moiety in Platin-Az conferred slightly higher cytotoxicity than the non azide analogue, *cis,trans*-[Pt(NH<sub>3</sub>)<sub>2</sub>Cl<sub>2</sub>[OOC(CH<sub>2</sub>)<sub>2</sub>-CH<sub>3</sub>)]<sub>2</sub>, butyroplatin.<sup>20</sup> Significantly, the cytotoxicity of **18** was retained when compared to carboplatin meaning that it represents an ideal Pt-based click template which can participate in post treatment bioconjugation reactions given it possesses an azide on the stable ammine carrier ligand.

In contrast to **18** and carboplatin, **19**, the cisplatin like DAP-N<sub>3</sub> derivative, was found to possess IC<sub>50</sub> values three times higher than cisplatin (12.0 vs 4.5 μM against A2780P and 36.2 vs 15.8 μM against A2780cis respectively). Therefore, **19** was not brought forward for conjugation with **Flu** as it was not an ideal model when compared with **18**.

As predicted, **Flu** was found to be non-cytotoxic against both cell lines with no appreciable reduction in cell proliferation observed at the upper concentration of this study, 200 μM. This agrees with literature precedent where most examples of BODIBY fluorophores used *in vitro* exhibited little or no cytotoxicity.<sup>34-36</sup> In a 2015 review by Kowada *et al.*<sup>37</sup> on the topic of BODIPY fluorescence for cellular imaging, only one fluorophore reported nuclear accumulation, that of a fluorophore-trimethoprim (TMP) conjugate, where the antibiotic TMP acts as a protein tag which facilitates the nuclear uptake.<sup>34</sup>

**Pt-Flu** was also found to be non-cytotoxic with an IC<sub>50</sub> >200 μM and no noteworthy activity exhibited *in vitro*. This observation is likely due to decreased nuclear accumulation of **Pt-Flu** as compared to both carboplatin and [Pt(CBDCA)(DAP-N<sub>3</sub>)], and is likely due to the relatively bulky size and lipophilicity of the fluorophore. This observation is of significance as such properties may prevent permeation into the nucleus (the traditional target site of Pt drugs), a frequent observation for BODIBY compounds.<sup>34</sup> For example, Jagodinsky *et al.* found that their cisplatin BODIPY fluorophore conjugates were relatively non-cytotoxic against KB 3-1, KB-CP.5 and KB CP20 cell lines. The IC<sub>50</sub> values were considerably larger for the Pt-BOBIPY complexes when compared to their relevant cisplatin compounds alone.<sup>17</sup> They also reported that nuclear localisation occurred at concentrations of 50-

100  $\mu\text{M}$ . It is therefore reasonable to suggest that the conjugation of **Flu** eliminates the anti-proliferation activity in this instance.

In turn, BODIPY based fluorophores are ideal candidates to act as cytoplasmic reporters to investigate and examine the movements and targets of Pt complexes. The identification of new non-DNA targets is a growing area of interest<sup>38</sup> and the development of Pt-Flu conjugates as cytoplasmic trackable probes may have important roles to play in investigating the uptake and non-nuclear effect of Pt-based anticancer complexes.

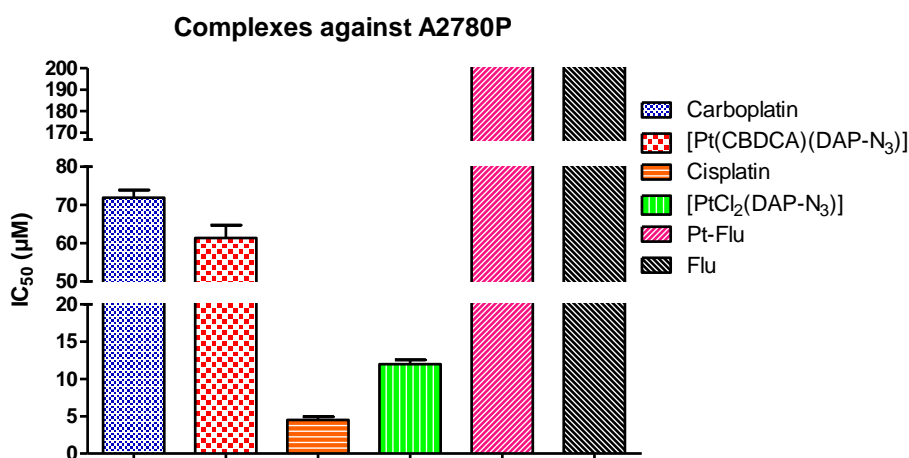


**Figure 3.9:** Cell proliferation ( $n = 3$ ) after 72 h treatment with compounds against A2780P cells with IC<sub>50</sub> values; for carboplatin 71.9  $\mu\text{M}$ , [Pt(CBDCA)(DAP-N<sub>3</sub>)] 4  $\mu\text{M}$ , **Flu** and **Pt-Flu** >200  $\mu\text{M}$ , cisplatin 4.5  $\mu\text{M}$  and [PtCl<sub>2</sub>(DAP-N<sub>3</sub>)] 12.0  $\mu\text{M}$ .



**Figure 3.10:** Cell proliferation ( $n = 3$ ) after 72 h treatment with compounds against A2780cis cells with IC<sub>50</sub> values; carboplatin 149.8  $\mu\text{M}$ , [Pt(CBDCA)(DAP-N<sub>3</sub>)] 134.3  $\mu\text{M}$ , **Flu** and **Pt-Flu** >200  $\mu\text{M}$ , cisplatin 15.8  $\mu\text{M}$  and [PtCl<sub>2</sub>(DAP-N<sub>3</sub>)] 36.2  $\mu\text{M}$ .

### DNA Binding

A well-established electrophoretic technique was used to investigate the effect of the Pt-Flu conjugate on pUC19 plasmid DNA supercoiling, where changes in DNA mobility are taken as evidence of a direct metal-DNA interaction leading to DNA unwinding.<sup>39-41</sup> The experiments were conducted on circular plasmid bacterial DNA, isolated from *E. coli*, which can exist in 3 forms: (I) supercoiled (SC), (II) open-circular (OC) and (III) linear/nicked. In normal circumstances, the DNA plasmid exists in the SC form, in which it is tightly wound so it can fit within bacterial cells. However, when SC DNA is exposed to a DNA binding agent, the supercoils unwind as a result of rotation around the phosphodiester backbone, generating the OC form.<sup>39, 41-42</sup> It is noteworthy that particular DNA damaging agents may also give rise to nicks in the plasmid, resulting in a long chain or multiple small fragments of DNA.<sup>43</sup>

Significantly, different forms of DNA travel at different rates through an agarose gel matrix and in turn separate. The matrix may be considered like a mesh or net. As such, the SC DNA runs through the gel faster as it is tightly packed and experiences less resistance as compared to the less tightly packed OC form. Linear DNA is slower again as it may spread out to the DNAs full length. Nicked fragments may vary in size and result in multiple bands appearing on the gel.

Gel electrophoresis was employed against test compounds Pt-Flu and Flu to investigate their DNA binding activities and compared against [Pt(CBDCA)(DAP-N<sub>3</sub>)], and carboplatin as a control and known DNA binder.<sup>44</sup> These tests determined that as expected all Pt containing complexes were capable of causing DNA band migration. In direct contrast, the free Flu did not cause band migration.

**Figure 3.11** shows an agarose gel in which increasing amounts of Pt-Flu have bound to negatively SC, closed circular pUC19 plasmid DNA. The rate of migration of the SC band decreases until it co-migrates with the OC relaxed band as seen between 200 and 275  $\mu$ M. This DNA mobility shift confirms Pt Flu conjugate can bind to nucleotides and cause unwinding of the DNA. Similar effects are shown for carboplatin and [Pt(CBDCA)(DAP-N<sub>3</sub>)]. In contrast, increasing the concentration of BCN-NIR-AZA fluorophore does not induce a migratory shift of supercoiled DNA

to its open circular form suggesting little or no direct interaction with DNA, **Figure 3.11**.

The cytotoxicity of Pt-based complexes is typically associated with DNA binding in the nucleus of cells. The **Pt-Flu** conjugate can bind DNA even though it was found to be non-cytotoxic; therefore it is highly likely that the Pt-Flu does not effectively enter the nucleus, bind to nuclear DNA and exact a DNA induced cytotoxic effect.

Interestingly, **18** required a lower concentration to induce a band shift from the SC to the OC form as compared to carboplatin (**Figure 3.11A-B**). **18** was found to be the most potent DNA binder investigated, with complete conversion to OC observed at 100  $\mu\text{M}$  compared to the 175 and 250  $\mu\text{M}$  observed for carboplatin and Pt-Flu respectively (**Figure 3.11**).<sup>44</sup>

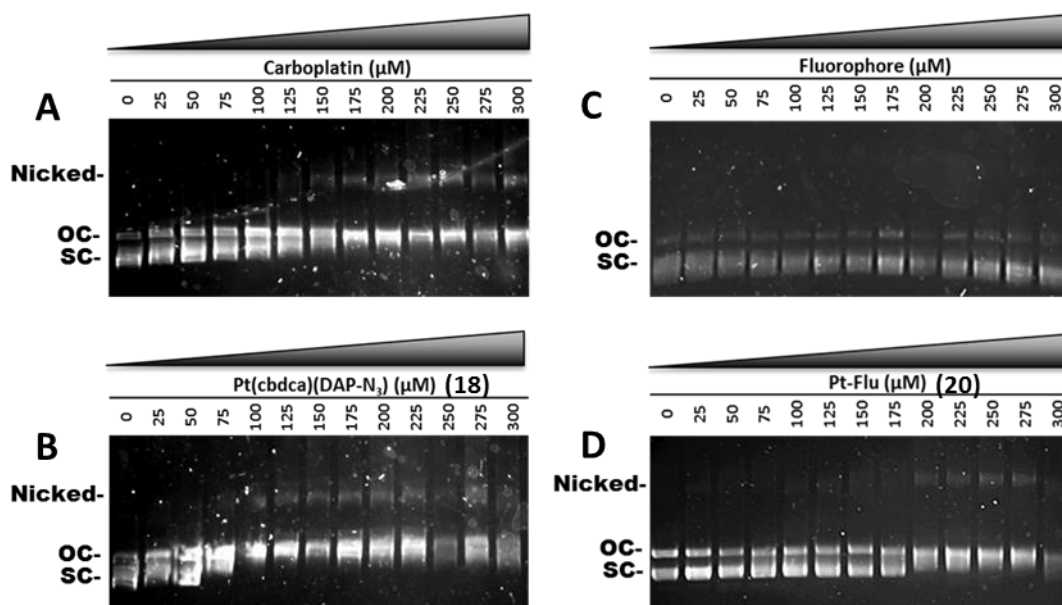


**Figure 3.11:** Gels of carboplatin,  $[\text{Pt}(\text{CBDCA})(\text{DAP-N}_3)]$  (**18**), Flu and Pt-Flu (**20**) demonstrating the interaction with circular pUC19 plasmid DNA after 48 h of incubation at 37 °C. 200 ng of DNA at a concentration of 60  $\mu\text{M}$  was used in each sample against a concentration range from 0 to 300  $\mu\text{M}$ .

In **Figure 3.11**, it is noteworthy that at the higher concentrations of the Pt complexes the appearance of the nicked/linear DNA band is observed. This band begins to form where the OC form dominates the SC band and is indicative of DNA damage.

The free fluorophore did not exhibit any DNA binding activity. The large aromatic BODIPY moiety in the fluorophore could potentially  $\pi$  stack with DNA bases and act

as a minor groove binder or DNA intercalator as has been previously reported for phenanthroline type derivatives, especially their metal complexes.<sup>45-47</sup> As predicted, this did not occur. The 2015 work by Jagodinsky *et al.* demonstrated and concluded that a cisplatin BODIPY conjugate could not induce DNA damage independent of the Pt containing portion of the complex<sup>48</sup>, corroborating the results observed in this study.

In summary, the three Pt containing complexes demonstrated the ability to bind to DNA and induce DNA band migration in a gel electrophoretic experiment. [Pt(CBDCA)(DAP-N<sub>3</sub>)] gave the best activity against pUC19 DNA at a concentration of 100  $\mu$ M, followed by clinically used standard carboplatin (175  $\mu$ M) and the Pt-Flu conjugate (250  $\mu$ M). Although the three Pt drugs were structurally similar, Pt-Flu gave the lowest level of activity which may be due to the bulky fluorophore group sterically hindering its binding to the DNA plasmid. The free Flu did not exhibit any DNA binding activity as predicted.

## Fluorescent applications and analysis of Pt-Flu

### Fluorescent properties

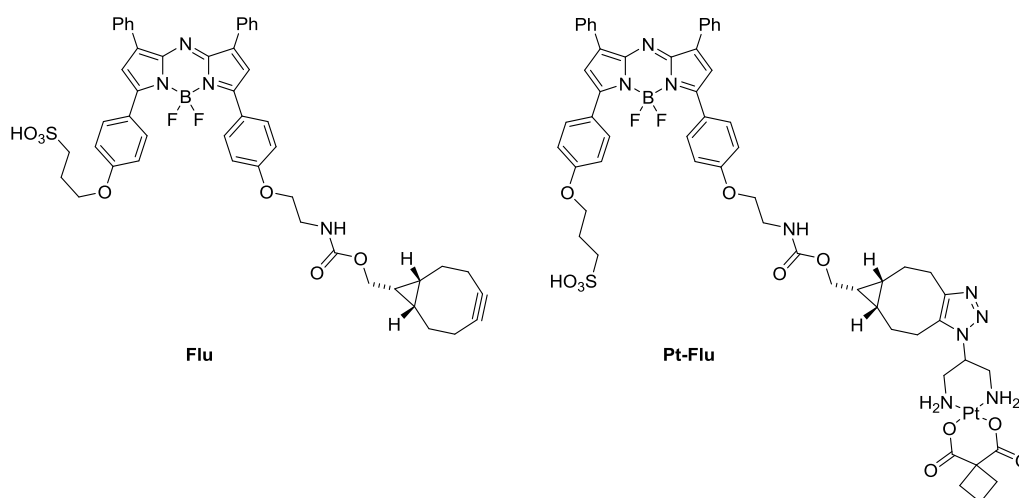
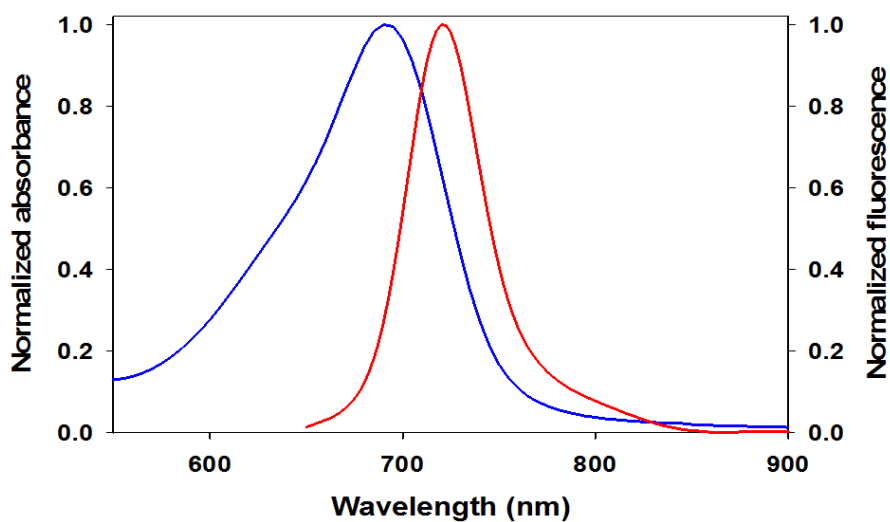


**Figure 3.12:** Structures of Flu and Pt-Flu.



Compound	max abs (nm)	Ext. coeff. ( $M^{-1}cm^{-1}$ )	max em (nm)	flu <sup>c</sup>
Flu	690	72,000	722	0.18
Pt-Flu	695	64,000	720	0.11

**Figure 3.13:** UV-vis and fluorescence properties of BCN-NIR-AZA and Pt BCN-NIR-AZA fluorophore conjugate. Graph displaying the absorbance (blue) and fluorescent emission (red) of the Pt-Flu conjugate.

The BF<sub>2</sub>-Azadipyrrromethene compounds are valued for their photostability as well as their excellent NIR spectral properties. However, as the photophysical properties of the molecule are sensitive to structural modification, the absorbance and fluorescence spectra were obtained before and after conjugation of Flu to Pt. The results for the Pt-Flu conjugate in H<sub>2</sub>O/1% SDS ( $\lambda_{\text{maxabs}} = 695 \text{ nm}$ ,  $\lambda_{\text{maxem}} = 720 \text{ nm}$ ) were found to maintain the excellent NIR spectral properties of the free fluorophore, with only minor differences in the  $\lambda_{\text{maxabs}}$  and  $\lambda_{\text{maxem}}$  in aqueous solution observed (**Figure 3.13.**). On conjugation to Pt, the extinction coefficient dropped from 72,000 to 64,000 and quantum yield from 0.18 to 0.11.<sup>15</sup>

### Widefield cellular imaging

To visualize the cellular uptake and distribution of the fluorophore and Pt-Flu conjugate, ovarian cancer cells A2780P and A2780cis were seeded on a chamber slide and incubated with 5  $\mu\text{M}$  of the test compounds for 15, 30, 60 or 120 minutes, with a control of 120 min with no compound, followed by fixation using 4% paraformaldehyde and nuclear co-staining with DAPI (4',6-diamidino-2-phenylindole), before being imaged using widefield microscopy.

The widefield images showed that an effective internalization of **Flu** and **Pt-Flu** conjugate had occurred with a cumulative localization throughout the cytosol over 120 minutes in both A2780P and A2780cis cell lines as can be seen in **Figure 3.14.** There was no discernible difference in the level of fluorescence that was detected in the A2780P and the A2780cis cell lines.

**Figures 3.15** and **3.16** demonstrate the accumulation of **Pt-Flu** and **Flu** in both cell lines from 30 to 120 min and show a steady uptake of the complexes over time. No noteworthy difference in the rate of uptake or distribution patterns of **Flu** as compared to **Pt-Flu** were observed in either cell line at the time points studied. The rapid uptake and distribution make the practical applications of this compound viable for *in vivo* use.



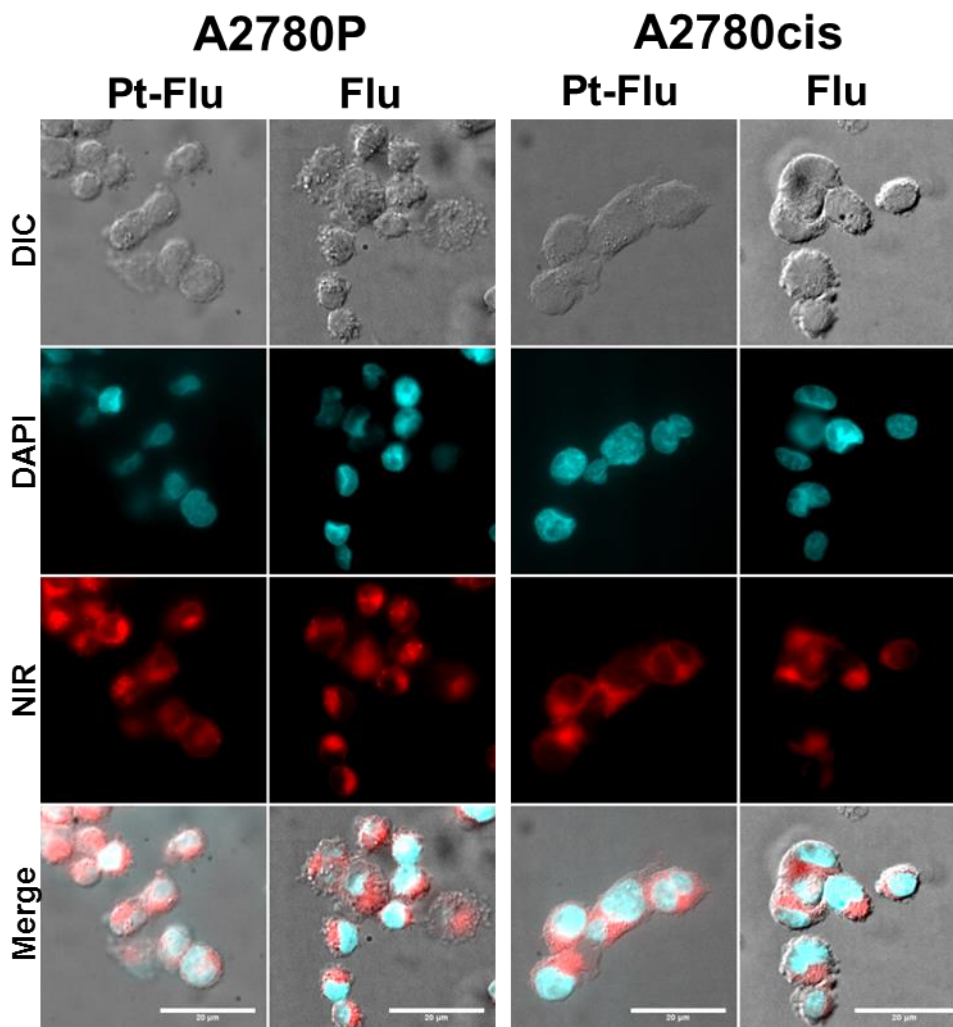


**Figure 3.14:** Widefield fluorescent images of fixed A2780P and A2780cis ovarian cancer cells following 120 min incubation at 37 °C with **Flu** and **Pt-Flu** at 5  $\mu$ M. DIC; white light, DAPI; nucleus stain, NIR; fluorescence of test compounds and composite merged image showing localisation of test compounds within the cytoplasm. Scale bars 20  $\mu$ m.

As already discussed, the compounds demonstrated good distribution throughout the cytosol, but significantly **Flu** and **Pt-Flu** do not visibly localize in the nucleus of either cell line, but predominate in the cytoplasm. This further supports the findings from the *in vitro* cytotoxicity and DNA binding studies, suggesting that the lack of cytotoxicity observed for the Pt-Flu is likely, in part, due to its inability to access and bind to nuclear DNA, despite DNA binding potential as evidenced through the gel electrophoresis experiments.

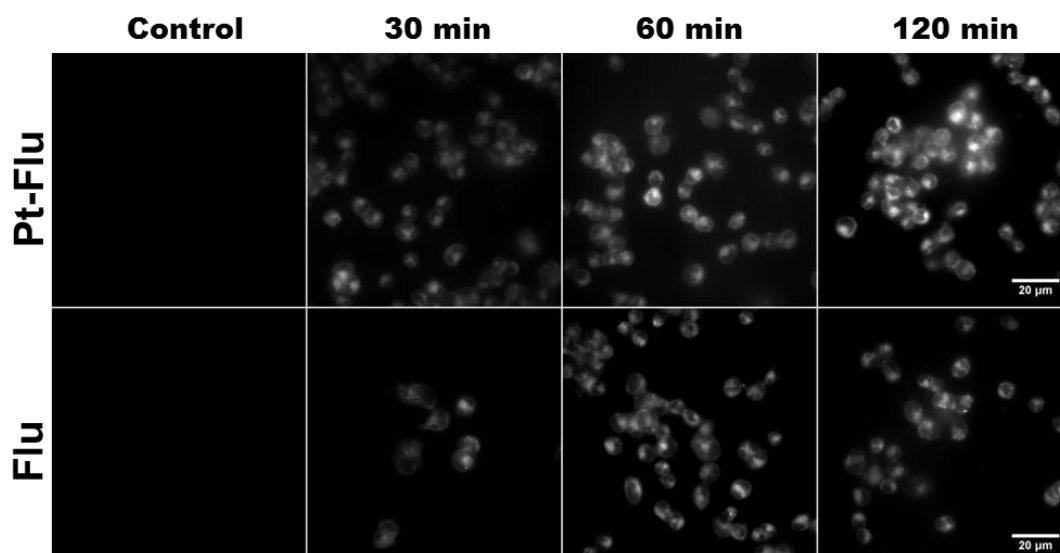


**Figure 3.15:** NIR widefield images of fixed A2780P cells following 30 min, 60 min and 120 min incubation at 37 °C with **Flu** and **Pt-Flu** at 5 μM, where control was 120 min with no complex. Increased time shows the rise in cellular uptake. Scale bars 20 μm.

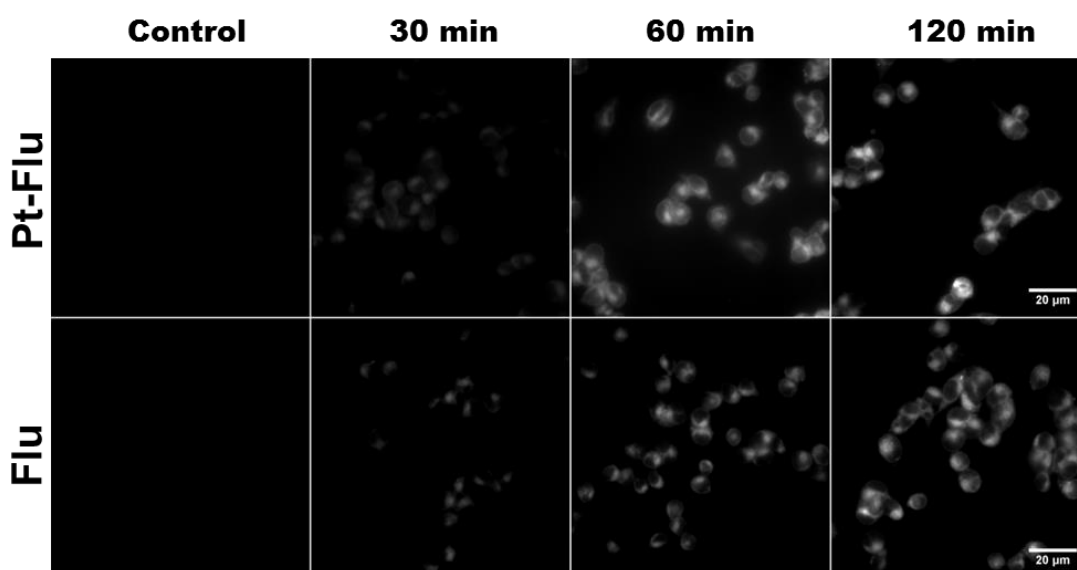


**Figure 3.16:** NIR widefield images of fixed A2780cis cells following 30 min, 60 min and 120 min incubation at 37 °C with **Flu** and **Pt-Flu** at 5 μM, where control was 120 min with no complex. Increased time shows the rise in cellular uptake. Scale bars 20 μm.

It is apparent that the properties associated with the Pt-fluorophore conjugate are strongly influenced by the physical properties of the bulky organic fluorophore and

as anticipated its distribution in cellular environments is exclusively in the cytoplasm.<sup>34-36</sup>

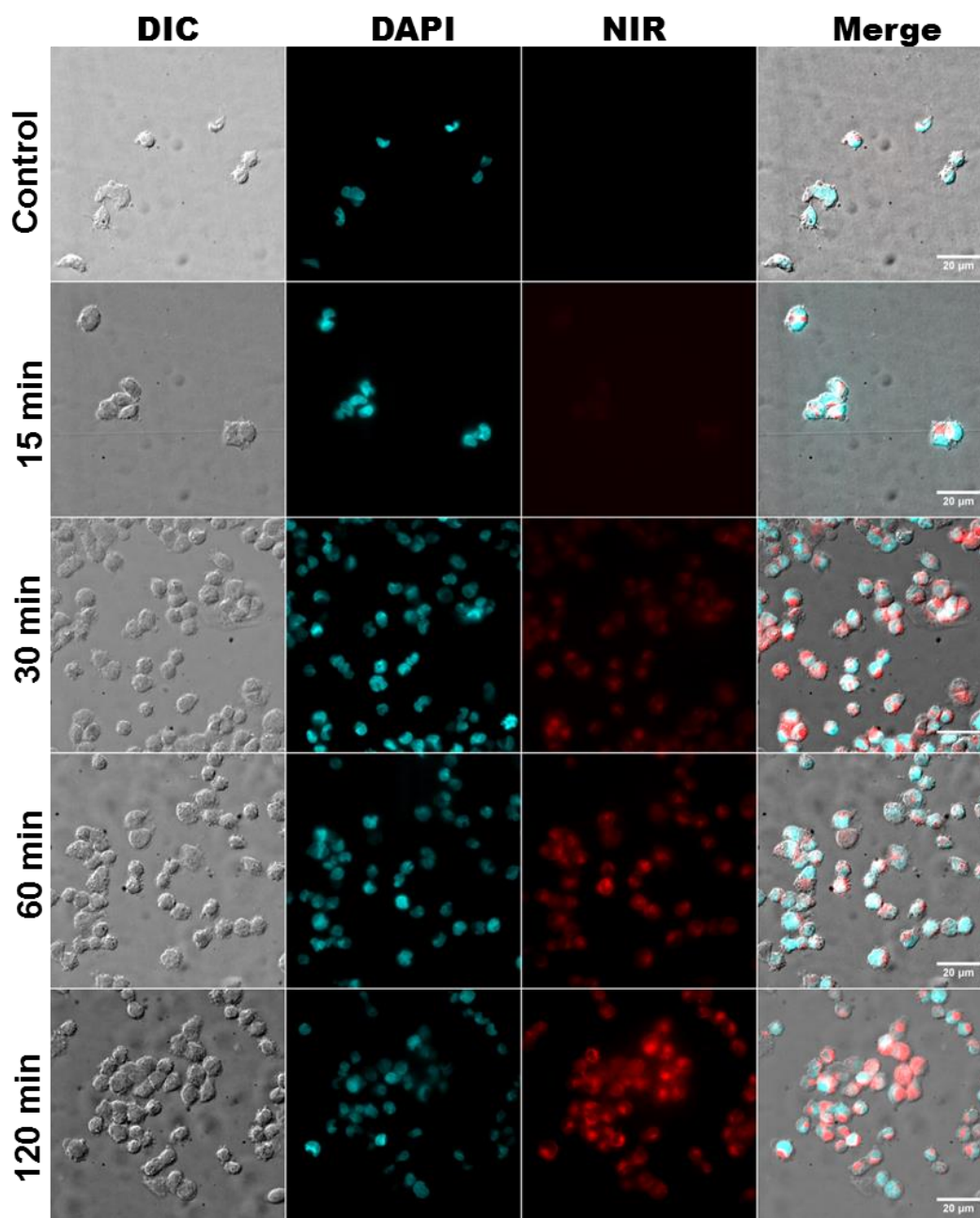


**Figure 3.17:** Widfield images of fixed A2780P cells following 15, 30, 60 and 120 min incubation at 37 °C with **Pt-Flu** at 5 μM, where control was 120 min with no complex. Increased time shows the rise in cellular uptake by the NIR images. Scale bars 20 μm.

However at 120 min **Pt-Flu** shows a high level of emission from specific regions which may be a result of Pt being incorporated into vesicles or localising within or at

other cellular target sites. These regions present themselves as small spherical regions which give a higher intensity of fluorescence (**Figure 3.18**).

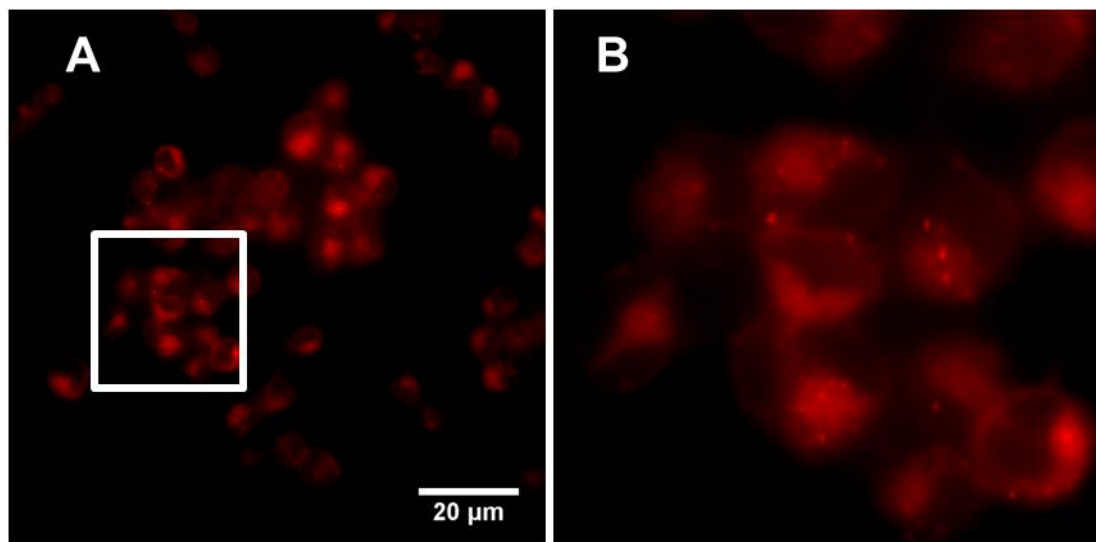


**Figure 3.18:** Widefield images of fixed A2780P cells following 120 min incubation at 37 °C with **Pt-Flu** at 5  $\mu$ M using 640 nm NIR light. (A) shows the full image and (B) shows the zoomed view (white box) which displays regions of higher **Pt-Flu** accumulation. Scale bars 20  $\mu$ m.

Recent work by Lippard and coworkers has highlighted that oxaliplatin exhibits its cytotoxic activity not by nuclear DNA binding but by inducing ribosome biogenesis stress.<sup>7</sup> Recently, the cisplatin derivative azidoplatin was found to induce endoplasmic reticulum stress as a part of its Pt drug activity and potential new targets were identified using post fluorescent labelling of a bacterial protein with Pt bound following incubation.<sup>38</sup> This study was limited though to highlighting that Pt-Flu was distributed throughout the cytoplasm and could not with certainty establish which organelles or specific region(s) within the cell were associated with higher distribution.

It was possible to visualise the cells exposed to Pt-Flu in 3D using z-stack imaging techniques. The 3D environment of the cell could be visualised and it was possible to detect specific regions of localisation. The composite z-stack images of the DAPI and NIR wavelength images therefore have the potential to provide valuable information absent from 2-D images (**Figure 3.19** and **Figure 3.20-22** animated gifs in digital appendix).

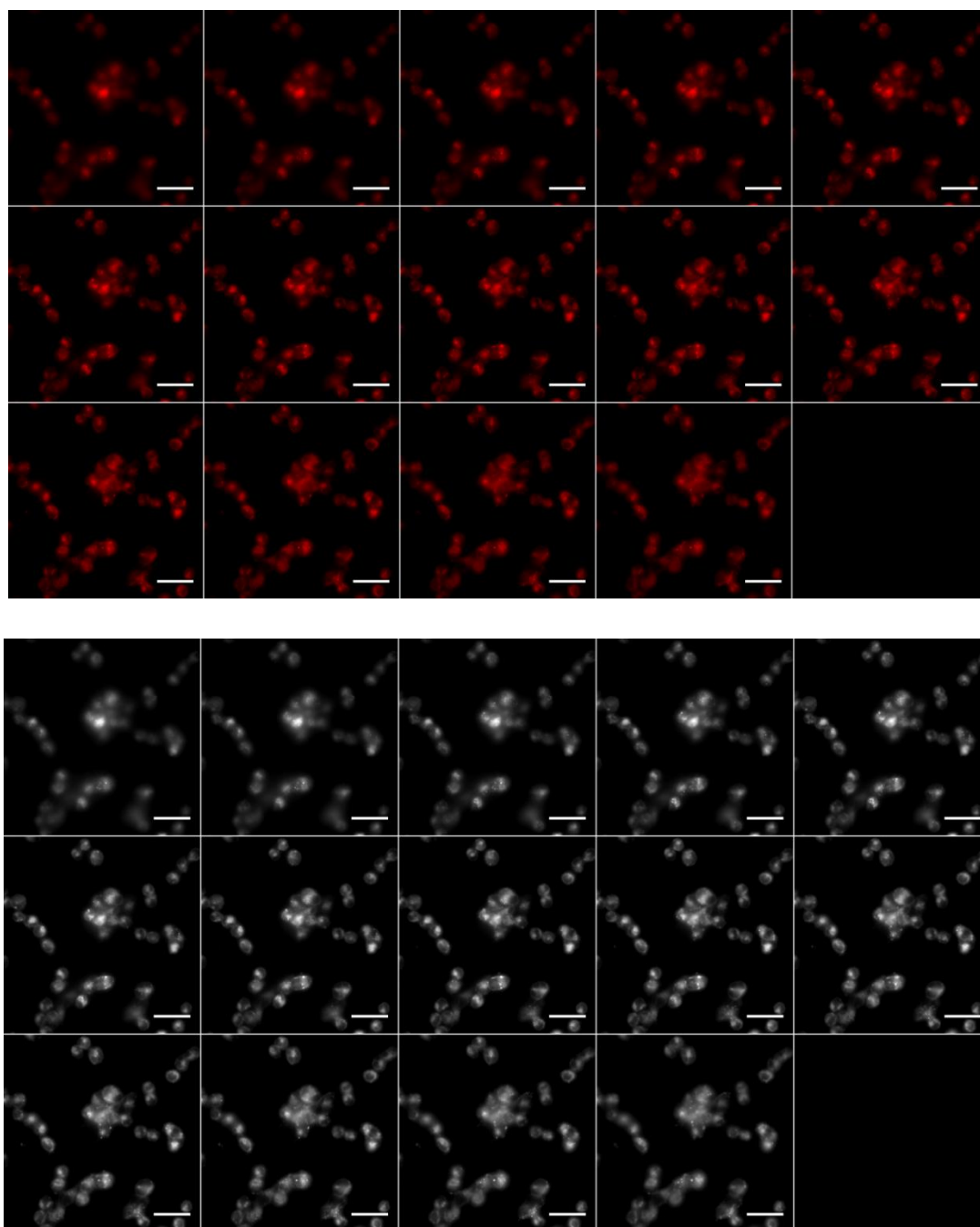


**Figure 3.19:** Widefield z-stack slice images of fixed A2780P cells following 120 min incubation at 37 °C with **Pt-Flu** at 5  $\mu$ M using 640 nm NIR light. Individual image slices show distribution throughout the cell including specific regions of localisation. Top image shows red filter applied and the bottom image displaying no filter. Scale bars 20  $\mu$ m.

## Conclusion

A novel non-toxic carboplatin-like Pt BODIPY fluorophore conjugate was successfully synthesised *via* SPAAC on reaction of [Pt(II)(CBDCA)(DAP-N<sub>3</sub>)] and a strained alkyne bearing the BCN-NIR-AZA fluorophore. This is the first example of a copper free click reaction where the azide was on the stable ammine carrier ligand of a Pt(II) complex with conjugation to a fluorophore of the BODIPY class. The X-ray crystal structure of the previously synthesised [Pt(II)(CBDCA)(DAP-N<sub>3</sub>)] was determined, along with the first IC<sub>50</sub> values for this complex to be reported. *In vitro* cytotoxicity, DNA binding and *in cellulo* fluorescent imaging properties of the non-toxic Pt-Flu conjugate were also reported. The **Pt-Flu** effectively binds to recombinant DNA, is readily taken up by ovarian cancer cells and disperses uniformly throughout the cytoplasm. Significantly, this conjugate was found to be non-toxic as expected and likely due to the predicted poor nuclear accumulation.

The first *in vitro* cytotoxicity data for [Pt(II)(CBDCA)(DAP-N<sub>3</sub>)] has been reported, highlighting that it retains the cytotoxicity associated with carboplatin and can serve as a good carboplatin click template.

Ultimately, the conjugation strategy described is the first example using SPACC where the azide handle resides on the Pt stable ammine carrier ligand, and in turn should serve as an important precedent for future studies.

**Future work**

The bioorthogonal click reaction described should be investigated in cells pre-treated with cytotoxic [Pt(II)(CBDCA)(DAP-N<sub>3</sub>)] with a view to investigating the cellular transport and cytoplasmic localization of [Pt(II)(CBDCA)(DAP-N<sub>3</sub>)] as a surrogate for carboplatin, over time. Such a study may have an important role to play in the ongoing investigation of the non-nuclear effects of Pt-based drugs.

In addition to identifying additional targets, the *in cellulo* SPAAC click reaction must be further studied in order to identify and qualify a means by which the successful conjugation reaction may be confirmed e.g. ICP-MS.

DeRose *et al.* for example in recent years have investigated DNA hairpin strand interactions with click capable Pt(II) derivatives and analysed after incubation by post click incorporation of a fluorescent agent using a copper catalysed click.<sup>49-50</sup>

The widefield imaging gave valuable insights into the potential applications of the Pt-Flu conjugate as a cytoplasmic trackable Pt drug. Further work is still needed in order to specifically determine non-DNA targets and binding sites. This may be investigated by screening against other cellular dyes in addition to DAPI and through live imaging for real time **Pt-Flu** uptake.

## References

1. Gaynor, D.; Griffith, D. M., The prevalence of metal-based drugs as therapeutic or diagnostic agents: beyond platinum. *Dalton Transactions* **2012**, 41 (43), 13239-13257.
2. Keogan, D.; Griffith, D., Current and Potential Applications of Bismuth-Based Drugs. *Molecules* **2014**, 19 (9), 15258-15297.
3. Wheate, N. J.; Walker, S.; Craig, G. E.; Oun, R., The status of platinum anticancer drugs in the clinic and in clinical trials *Dalton Trans.* **2010**, 39, 8113-8127.
4. Kelland, L., The resurgence of platinum-based cancer chemotherapy. *Nat. Rev.* **2007**, 7 (8), 573-584.
5. Galluzzi, L.; Vitale, I.; Michels, J.; Brenner, C.; Szabadkai, G.; Harel-Bellan, A.; Castedo, M.; Kroemer, G., Systems biology of cisplatin resistance: past, present and future. *Cell death & disease* **2014**, 5, e1257.
6. White, J. D.; Haley, M. M.; DeRose, V. J., Multifunctional Pt(II) Reagents: Covalent Modifications of Pt Complexes Enable Diverse Structural Variation and In-Cell Detection. *Acc. Chem. Res.* **2016**, 49 (1), 56-66.
7. Bruno, P. M.; Liu, Y.; Park, G. Y.; Murai, J.; Koch, C. E.; Eisen, T. J.; Pritchard, J. R.; Pommier, Y.; Lippard, S. J.; Hemann, M. T., A subset of platinum-containing chemotherapeutic agents kills cells by inducing ribosome biogenesis stress. *Nat. Med.* **2017**, 23 (4), 461-471.
8. Guo, Z.; Park, S.; Yoon, J.; Shin, I., Recent progress in the development of near-infrared fluorescent probes for bioimaging applications. *Chem. Soc. Rev.* **2014**, 43 (1), 16-29.
9. Yuan, L.; Lin, W.; Zheng, K.; He, L.; Huang, W., Far-red to near infrared analyte-responsive fluorescent probes based on organic fluorophore platforms for fluorescence imaging. *Chem. Soc. Rev.* **2013**, 42 (2), 622-661.
10. Ge, Y.; O'Shea, D. F., Azadipyrromethenes: from traditional dye chemistry to leading edge applications. *Chem. Soc. Rev.* **2016**, 45 (14), 3846-3864.
11. Wu, D.; Cheung, S.; Devocelle, M.; Zhang, L.-J.; Chen, Z.-L.; O'Shea, D. F., Synthesis and assessment of a maleimide functionalized BF<sub>2</sub> azadipyrromethene near-infrared fluorochrome. *Chem. Commun.* **2015**, 51 (93), 16667-16670.
12. Grossi, M.; Morgunova, M.; Cheung, S.; Scholz, D.; Conroy, E.; Terrile, M.; Panarella, A.; Simpson, J. C.; Gallagher, W. M.; O'Shea, D. F., Lysosome triggered near-infrared fluorescence imaging of cellular trafficking processes in real time. *Nat. Commun.* **2016**, 7, 10855.
13. Wu, D.; Sedgwick, A. C.; Gunnlaugsson, T.; Akkaya, E. U.; Yoon, J.; James, T. D., Fluorescent chemosensors: the past, present and future. *Chem. Soc. Rev.* **2017**.
14. Bertrand, B.; Doulain, P. E.; Goze, C.; Bodio, E., Development of trackable metal-based drugs: new generation of therapeutic agents. *Dalton Trans.* **2016**, 45 (33), 13005-11.
15. Wu, D.; Cheung, S.; O'Sullivan, C. J.; Gao, Y.; Chen, Z.-L.; O'Shea, D. F., Strained alkyne substituted near infrared BF<sub>2</sub> azadipyrromethene fluorochrome. *RSC Adv.* **2016**, 6 (90), 87373-87379.
16. Miller, M. A.; Askevold, B.; Yang, K. S.; Kohler, R. H.; Weissleder, R., Platinum Compounds for High-Resolution In Vivo Cancer Imaging. *ChemMedChem* **2014**, 9 (6), 1131-1135.
17. Jagodinsky, J. C.; Sulima, A.; Cao, Y.; Poprawski, J. E.; Blackman, B. N.; Lloyd, J. R.; Swenson, R. E.; Gottesman, M. M.; Hall, M. D., Evaluation of fluorophore-tethered platinum complexes to monitor the fate of cisplatin analogs. *Journal of biological inorganic chemistry : JBIC : a publication of the Society of Biological Inorganic Chemistry* **2015**, 20 (7), 1081-95.
18. Mitra, K.; Gautam, S.; Kondaiah, P.; Chakravarty, A. R., BODIPY-Appended 2-(2-Pyridyl)benzimidazole Platinum(II) Catecholates for Mitochondria-Targeted Photocytotoxicity. *ChemMedChem* **2016**, 11 (17), 1956-1967.



19. Reithofer, M. R.; Chan, K.-H.; Lakshmanan, A.; Lam, D. H.; Mishra, A.; Gopalan, B.; Joshi, M.; Wang, S.; Hauser, C. A. E., Ligation of anti-cancer drugs to self-assembling ultrashort peptides by click chemistry for localized therapy. *Chem. Sci.* **2014**, *5* (2), 625-630.
20. Pathak, R. K.; McNitt, C. D.; Popik, V. V.; Dhar, S., Copper-Free Click-Chemistry Platform to Functionalize Cisplatin Prodrugs. *Chem. Eur. J.* **2014**, *20* (23), 6861-6865.
21. Zhang, J. Z.; Bonnitcha, P.; Wexselblatt, E.; Klein, A. V.; Najajreh, Y.; Gibson, D.; Hambley, T. W., Facile Preparation of Mono-, Di- and Mixed-Carboxylato Platinum(IV) Complexes for Versatile Anticancer Prodrug Design. *Chem. Eur. J.* **2013**, *19* (5), 1672-1676.
22. Best, M. D., Click Chemistry and Bioorthogonal Reactions: Unprecedented Selectivity in the Labeling of Biological Molecules. *Biochemistry* **2009**, *48* (28), 6571-6584.
23. Jewett, J. C.; Bertozzi, C. R., Cu-free click cycloaddition reactions in chemical biology. *Chemical Society Reviews* **2010**, *39* (4), 1272-1279.
24. Urankar, D.; Košmrlj, J., Preparation of diazenecarboxamide-carboplatin conjugates by click chemistry. *Inorg. Chim. Acta* **2010**, *363* (14), 3817-3822.
25. Chen, F.-F.; Wang, F., Electronic Structure of the Azide Group in 3 $\epsilon$ -Azido-3 $\epsilon$ -deoxythymidine (AZT) Compared to Small Azide Compounds. *Molecules* **2009**, *14* (7), 2656.
26. Anderson, B. M.; Hurst, S. K., Platinum Stacking Interactions in Homoleptic Platinum Polymers. *Eur. J. Inorg. Chem.* **2009**, *2009* (21), 3041-3054.
27. Newman, C. P.; Cave, G. W. V.; Wong, M.; Errington, W.; Alcock, N. W.; Rourke, J. P., Di-metallated platinum carbonyl complexes: platinum-platinum interactions in the solid state. *Dalton Trans.* **2001**, (18), 2678-2682.
28. Constable, E. C.; Henney, R. P. G.; Leese, T. A.; Tocher, D. A., Cyclopalladated and cycloplatinated complexes of 6-phenyl-2,2[prime or minute]-bipyridine: platinum-platinum interactions in the solid state. *Chemical Commun.* **1990**, (6), 513-515.
29. Rochon, F. D.; Massarweh, G., Synthesis, multinuclear magnetic resonance and crystal structures of Pt(II) complexes containing amines and bidentate carboxylate ligands. *Inorganica Chimica Acta* **2006**, *359* (12), 4095-4104.
30. Stockert, J. C.; Blázquez-Castro, A.; Cañete, M.; Horobin, R. W.; Villanueva, Á., MTT assay for cell viability: Intracellular localization of the formazan product is in lipid droplets. *Acta Histochemica* **2012**, *114* (8), 785-796.
31. Dasari, S.; Tchounwou, P. B., Cisplatin in cancer therapy: molecular mechanisms of action. *European journal of pharmacology* **2014**, *0*, 364-378.
32. Bose, R. N.; Maurmann, L.; Mishur, R. J.; Yasui, L.; Gupta, S.; Grayburn, W. S.; Hofstetter, H.; Salley, T., Non-DNA-binding platinum anticancer agents: Cytotoxic activities of platinum-phosphato complexes towards human ovarian cancer cells. *Proc. Nat. Acad. Sci.* **2008**, *105* (47), 18314-18319.
33. Mohell, N.; Alfredsson, J.; Fransson, Å.; Uustalu, M.; Byström, S.; Gullbo, J.; Hallberg, A.; Bykov, V. J. N.; Björklund, U.; Wiman, K. G., APR-246 overcomes resistance to cisplatin and doxorubicin in ovarian cancer cells. *Cell Death & Disease* **2015**, *6*, e1794.
34. Miller, L. W.; Cai, Y.; Sheetz, M. P.; Cornish, V. W., In vivo protein labeling with trimethoprim conjugates: a flexible chemical tag. *Nature Methods* **2005**, *2*, 255.
35. Jiang, X.-D.; Gao, R.; Yue, Y.; Sun, G.-T.; Zhao, W., A NIR BODIPY dye bearing 3,4,4a-trihydroxanthene moieties. *Organic & Biomolecular Chemistry* **2012**, *10* (34), 6861-6865.
36. Zhang, H.-X.; Chen, J.-B.; Guo, X.-F.; Wang, H.; Zhang, H.-S., Highly Sensitive Low-Background Fluorescent Probes for Imaging of Nitric Oxide in Cells and Tissues. *Analytical Chemistry* **2014**, *86* (6), 3115-3123.
37. Kowada, T.; Maeda, H.; Kikuchi, K., BODIPY-based probes for the fluorescence imaging of biomolecules in living cells. *Chemical Society Reviews* **2015**, *44* (14), 4953-4972.
38. Cunningham, R. M.; DeRose, V. J., Platinum Binds Proteins in the Endoplasmic Reticulum of *S. cerevisiae* and Induces Endoplasmic Reticulum Stress. *ACS Chemical Biology* **2017**, *12* (11), 2737-2745.

39. Onoa, G. B.; Cervantes, G.; Moreno, V.; Prieto, M. J., Study of the interaction of DNA with cisplatin and other Pd(II) and Pt(II) complexes by atomic force microscopy. *Nucleic Acids Research* **1998**, 26 (6), 1473-1480.
40. Jamieson, E. R.; Lippard, S. J., Structure, Recognition, and Processing of Cisplatin–DNA Adducts. *Chemical Reviews* **1999**, 99 (9), 2467-2498.
41. Malina, J.; Hannon, M. J.; Brabec, V., DNA binding of dinuclear iron(II) metallosupramolecular cylinders. DNA unwinding and sequence preference. *Nucleic Acids Research* **2008**, 36 (11), 3630-3638.
42. Rezaee, M.; Alizadeh, E.; Hunting, D.; Sanche, L., DNA-Platinum Thin Films for Use in Chemoradiation Therapy Studies. *Bioinorganic Chemistry and Applications* **2012**, 2012, 923914.
43. Prisecaru, A.; Molphy, Z.; Kipping, R. G.; Peterson, E. J.; Qu, Y.; Kellett, A.; Farrell, N. P., The phosphate clamp: sequence selective nucleic acid binding profiles and conformational induction of endonuclease inhibition by cationic Triplatin complexes. *Nucleic Acids Research* **2014**, 42 (22), 13474-13487.
44. Sorokanich, R. S.; Di Pasqua, A. J.; Geier, M.; Dabrowiak, J. C., Influence of Carbonate on the Binding of Carboplatin to DNA. *Chemistry & Biodiversity* **2008**, 5 (8), 1540-1544.
45. Shahabadi, N.; Mohammadi, S.; Alizadeh, R., DNA Interaction Studies of a New Platinum(II) Complex Containing Different Aromatic Dinitrogen Ligands. *Bioinorganic Chemistry and Applications* **2011**, 2011.
46. Molphy, Z.; Prisecaru, A.; Slator, C.; Barron, N.; McCann, M.; Colleran, J.; Chandran, D.; Gathergood, N.; Kellett, A., Copper Phenanthrene Oxidative Chemical Nucleases. *Inorganic Chemistry* **2014**, 53 (10), 5392-5404.
47. McGivern, T. J. P.; Afsharpour, S.; Marmion, C. J., Copper complexes as artificial DNA metallonucleases: From Sigman's reagent to next generation anti-cancer agent? *Inorganica Chimica Acta* **2018**, 472, 12-39.
48. Jagodinsky, J. C.; Sulima, A.; Cao, Y.; Poprawski, J. E.; Blackman, B. N.; Lloyd, J. R.; Swenson, R. E.; Gottesman, M. M.; Hall, M. D., Evaluation of fluorophore-tethered platinum complexes to monitor the fate of cisplatin analogs. *Journal of biological inorganic chemistry : JBIC : a publication of the Society of Biological Inorganic Chemistry* **2015**, 20 (7), 1081-1095.
49. Wirth, R.; White, J. D.; Moghaddam, A. D.; Ginzburg, A. L.; Zakharov, L. N.; Haley, M. M.; DeRose, V. J., Azide vs Alkyne Functionalization in Pt(II) Complexes for Post-treatment Click Modification: Solid-State Structure, Fluorescent Labeling, and Cellular Fate. *Journal of the American Chemical Society* **2015**, 137 (48), 15169-15175.
50. White, J. D.; Osborn, M. F.; Moghaddam, A. D.; Guzman, L. E.; Haley, M. M.; DeRose, V. J., Picazoplatin, an Azide-Containing Platinum(II) Derivative for Target Analysis by Click Chemistry. *Journal of the American Chemical Society* **2013**, 135 (32), 11680-11683.

## **Chapter 4**

**Novel platinum(IV) oxaliplatin-peptide mono-conjugates for targeting of colorectal cancer cells**

## Abstract

A selectively mono-functionalized novel Pt(IV) tumour targeting peptide (TPP) conjugate [Pt(DACH)(OEt)(Ox)(succTPP)] (Pt-TPP) has been synthesised. TPP has the potential to target membrane bound heat shock protein 70 (memHSP70), which is upregulated in many cancers and in turn potentially bestows selective targeting on conjugation to Pt anticancer drugs. The synthesis and *in vitro* cytotoxicity of the Pt-TPP conjugate, the novel unsymmetrical Pt(IV) precursor [Pt(DACH)(OEt)(Ox)(succ)], oxaliplatin and control compounds are described. Pt-TPP exhibits similar cytotoxic effects as compared to oxaliplatin, and enhanced activity compared to the [Pt(DACH)(OEt)(Ox)(succ)] precursor, against colorectal cancer cells lines HCT116 and HT29.

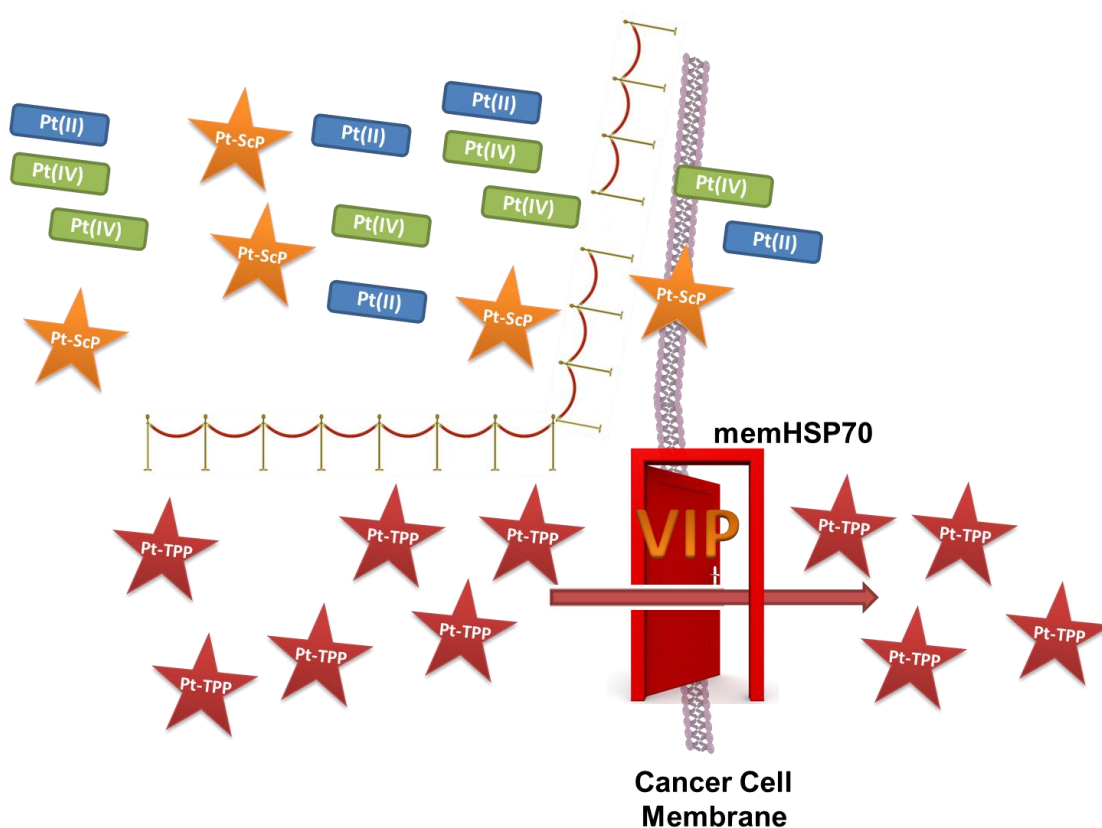


**Figure 4.1:** Graphical hypothesis of the aims of this work. Synthesis of a cancer cell targeting Pt-peptide conjugate followed by treatment *in vitro*.

## Introduction

The three platinum (Pt)-based drugs, cisplatin, carboplatin and oxaliplatin are marketed worldwide and are found in over 50% of all chemotherapeutic regimens.<sup>1</sup> There are multiple modes of actions associated with these drugs. Upon hydrolysis of their labile chlorido or dicarboxylato ligands inside cells, they are believed to induce oxidative and reticular stress, mitochondrial DNA damage but most importantly, nuclear DNA damage. Irreparable DNA damage through the formation of DNA adducts ultimately triggers cell death, apoptosis.<sup>1-3</sup>

Cisplatin and carboplatin have very similar cytotoxic profiles given they share the same ammine carrier ligands. Notably, oxaliplatin, which has a diamminocyclohexane carrier ligand, is administered as a critical component of late stage colorectal cancer (CRC) treatment regimens, partially due to the inherent resistance of CRC to cisplatin and carboplatin.<sup>4</sup> Recent important work by Lippard and co-workers has also shown that oxaliplatin does not primarily kill cancer cells *via* DNA-damage mediated processes, as is the case with cisplatin and carboplatin, but instead by inducing ribosome biogenesis stress, which triggers cell death.<sup>5</sup>

Although Pt drugs are used clinically to great effect, there are a number of drawbacks and limitations to their use, including poor bio-selectivity for cancerous cells over healthy tissues resulting in severe negative side effects including neurotoxicity, nephrotoxicity, nausea and vomiting amongst others.<sup>6</sup> Significantly, a number of cancers are also intrinsically resistant or over time develop resistance to Pt drugs.<sup>3, 6</sup>

For these reasons, enhancing tumour selectivity of Pt drugs is a major objective in the development of innovative Pt anticancer agents. One such approach is the synthesis of Pt drugs which facilitate conjugation to a selective targeting molecule. Pt(IV) prodrugs are often used in order to increase the pharmacological properties and diversity of Pt complexes through the functionalisation of their axial ligands.<sup>7</sup>

Pt(IV) complexes have an octahedral geometry and are generally considered to be activated following reduction in the hypoxic and reducing cellular environment of cancer cells to form the corresponding active Pt(II) complex on release of the two axial ligands.<sup>7</sup> Satraplatin (**Figure 4.2a**) is one such Pt(IV) complex and is currently being investigated in stage III clinical trials.<sup>8-9</sup>

In recent years, there have been increasing numbers of reports describing the conjugation of bioactive molecules which may endow secondary functionality to Pt(IV) complexes *via* their axial ligands. In these so-called bifunctional Pt(IV) prodrugs, a biomolecule is often coordinated to a Pt(IV) centre *via* a carboxylate functionality. The biomolecules generally (i) play a role in drug targeting and delivery or (ii) possess inherent anticancer properties or (iii) act as reporters. Bioactive molecules include peptides, antibodies, fluorescent probes and small molecule inhibitors (**Figure 4.2**).

For instance, Brabec and co-workers have synthesised an oxaliplatin Pt(IV) prodrug containing the histone deacetylase inhibitor valproic acid (VPA) (**Figure 4.2b**).<sup>10</sup> Similarly, Ang and co-workers have synthesised the Pt(IV) conjugate ethacraplatin (**Figure 4.2c**), based on cisplatin with two ethacrynic acid (EA) axial ligands, where EA is an active inhibitor of glutathione-S-transferase (GST).<sup>11-12</sup> McKeon *et al.* and Abramkin *et al.* have developed Pt-peptide conjugates capable of targeted cell penetration, **Figure 4.2d-e**.<sup>4, 13</sup>

Much research has been undertaken into peptides in recent years due to their inherent biocompatibility, increasing ease of synthesis and their ability to recognise and inhibit key cellular pathways. The role of cell penetrating peptides (CPP) has been of particular interest in rational drug design, due to the ability of CPPs to recognise particular cellular components and in turn potentially facilitate targeted drug delivery and selective uptake. By exploiting a protein specific to tumour cells, it may be possible to selectively target cancerous tissues through a “Trojan horse” approach.<sup>4,13</sup> As such, identification and structural characterisation of cellular components is being widely investigated to determine their significance in cancer progression and whether they may be exploited for active targeting.<sup>4, 14</sup>

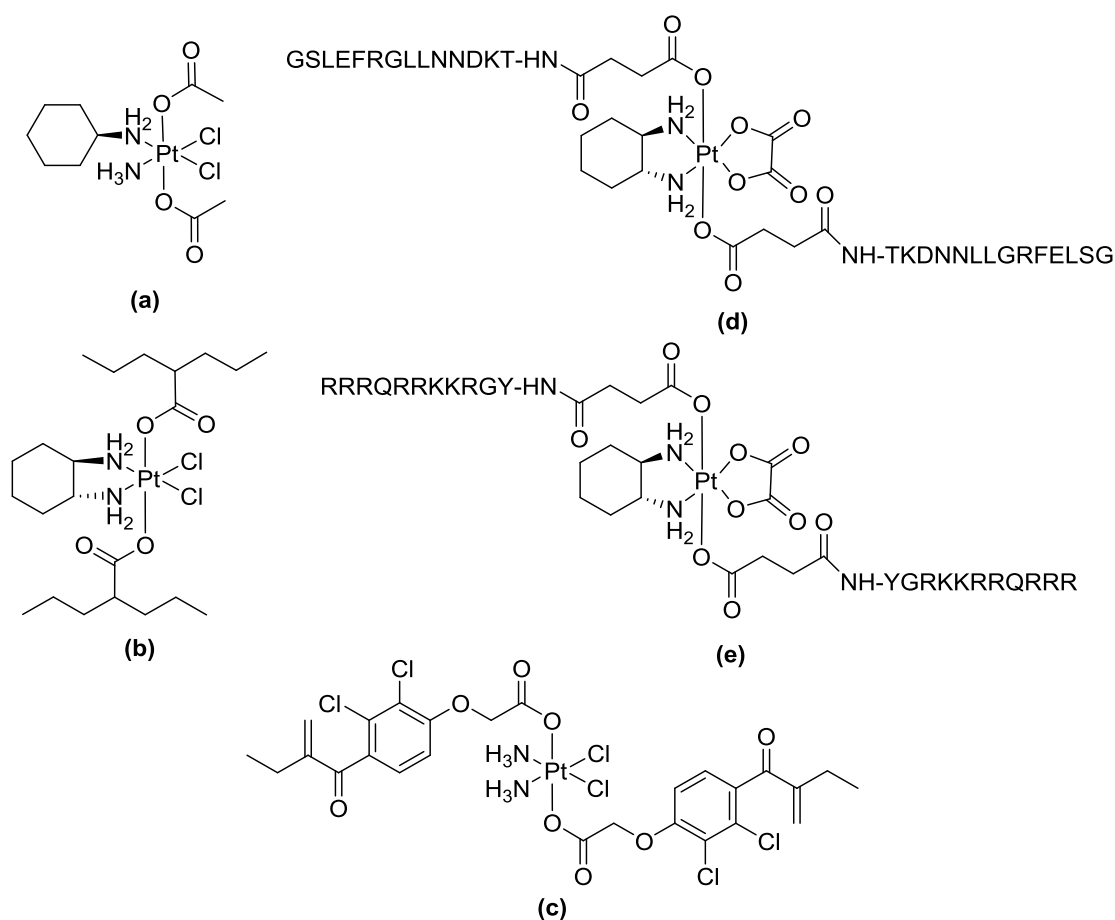


**Figure 4.2:** Structures of satraplatin (a),<sup>9</sup>  $[\text{PtCl}_2(\text{DACH})(\text{VPA})_2]$  (b),<sup>10</sup> ethacraplatin (c)<sup>11</sup> and the cell penetrating peptide conjugates  $[\text{Pt}(\text{DACH})(\text{Ox})(\text{succTPP})_2]$  (d)<sup>13</sup> and  $[\text{Pt}(\text{DACH})(\text{Ox})(\text{succTAT})_2]$  (e).<sup>4</sup>

Heat-shock protein 70 (HSP70) is a biomolecule of interest as a bio-target in anticancer treatment. There are thirteen HSP70 family members, whose primary function is to maintain homeostasis following a cellular stress response to stimuli, for example hypoxia, temperature fluctuations and exposure to heavy metals (e.g. Pt drugs). They function by forming an intermediate structure with neutral and hydrophobic amino acid (aa) residues found on client proteins. Stabilisation is enhanced through the action of other co-chaperones such as HSP40, which improves protein binding affinity, ensuring that the protein shape and viability is maintained until the stress has passed.<sup>15-17</sup> Significantly, in many cancers including CRC, the level of HSP70 is found to be upregulated, thus giving cancer cells a distinct survival advantage over healthy tissues and cells. HSP70 is therefore associated with cancer

progression and poor prognosis.<sup>16</sup> It is also significant that inhibition of HSP70 is associated with an anti-cancer effect.<sup>16, 18</sup>

Significantly, the selective expression of HSP70 on the plasma membrane (memHSP70) of cultured cancer cells including colorectal cancer cells has been reported. In addition, memHSP70 was found to be present on 50% of tumours in a 1,000 patient cohort but not expressed in healthy non-cancerous cells. memHSP70 therefore represents an excellent candidate for the selective targeting of cancer cells.<sup>14</sup> Gehrmann *et al.* previously described the tumour penetrating peptide (TPP, TKDNNLLGRFELSG), a 14-mer peptide derived from HSP70 which matches an epitope within the oligomerization domain of the HSP70 molecule (aa 450–463). The specific binding and rapid internalisation of TPP in membrane HSP70 positive (memHSP70+) tumour cells was reported.<sup>14</sup> Therefore, TPP offers significant potential as a targeting moiety for cancer cells which over express memHSP70.

Aoife McKeon, a PhD student in Dr. Darren Griffith's research group at RCSI, successfully synthesised and characterised novel platinum TPP conjugates upon activation of the two free succinato carboxylic acid groups on the previously reported *cis,cis,trans*-dichlorido(*trans*-(1*R*,2*R*)diaminocyclohexane)oxalatodisuccinato platinum(IV) complex (*cis,cis,trans*-[Pt(1*R*,2*R*-DACH)(Ox)(succ)<sub>2</sub>])<sup>19</sup> with CDI, and subsequent coupling with the deprotected N-terminal threonine of the resin bound **TPP** sequence.

McKeon *et al.* determined that Pt(IV) conjugates possessing mono and di-TPP peptide sequences [Pt(1*R*,2*R*-DACH)(Ox)(succ)(succTPP)] and [Pt(1*R*,2*R*-DACH)(Ox)(succTPP)<sub>2</sub>] could induce cell apoptosis to a greater extent than oxaliplatin alone in Pt resistant HT29 colorectal cancer cells with relatively high memHSP70+ expression. Substitution of TPP with scrambled peptide (ScP) essentially abolished the observed cytotoxicity in the Pt(IV) peptide conjugates. This report suggests that TPP does endow a Pt(IV) oxaliplatin type complex, with the potential for the targeting of cancer cells through the specific binding and internalization by memHSP70+ tumour cells *via* endosomal pathways.

Although the Pt(IV) TPP conjugates were successful in improving Pt drug activity against CRC, there were a number of synthetic drawbacks including low yields and challenges in relation to the separation and purification of the Pt(IV) mono and di-



peptide conjugates. Specifically, the production of a Pt(IV) mono peptide conjugate naturally reduces the yield of the preferred Pt(IV) di peptide conjugate product and in addition the Pt(IV) mono and di peptide conjugates have similar HPLC retention times, which further reduces the yield post purification.<sup>13</sup>

To overcome these drawbacks, the use of an unsymmetrical Pt(IV) complex, i.e. one which possesses two unique axial ligands, could reduce the number of side-products formed in the coupling reaction and in turn simplify purification. A number of unsymmetrical Pt(IV) complexes have been previously reported, such as the Pt(IV) cisplatin and oxaliplatin derivatives which possess a single succinato ligand (**Figure 4.3**).<sup>20-21</sup>

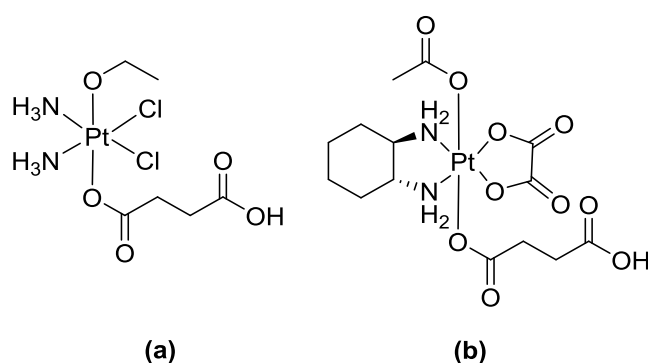


**Figure 4.3:** Structures of *cis,cis,trans*-[Pt(NH<sub>3</sub>)<sub>2</sub>Cl<sub>2</sub>(OEt)(succ)] (a),<sup>20</sup> (OC-6-44)-Acetato(3-carboxypropanoato)(1*R*,2*R*-cyclohexanediamine)oxalatoplatinum(IV) (b).<sup>21</sup>

Novel unsymmetrical Pt(IV) mono peptide conjugates have been synthesised and characterised. The *in vitro* cytotoxicity of the complexes against colorectal cancer cells was investigated.

### Rationale

Conjugation of TPP and ScP to an unsymmetrical Pt(IV) conjugate, [Pt(DACH)(OEt)(Ox)(succ)], which possesses only one reactive succinato group should generate the corresponding Pt(IV) mono peptide conjugates in increased yield and subsequently isolate the complexes with less complications relative to the strategy of McKeon *et al.*

## Chapter Aims

- ◁ To synthesise novel unsymmetrical Pt(IV) conjugates with two unique axial ligands attached.
- ◁ To synthesise the 14-mer TPP derived from HSP70, and the corresponding scrambled peptide sequence, ScP.
- ◁ To synthesise Pt(IV) mono TPP conjugate and Pt(IV) mono ScP conjugate *via* amide bond formation.
- ◁ To investigate the *in vitro* cytotoxicity of the Pt-peptide conjugates against a panel of colorectal cancer cell lines which contain differential levels of memHSP70 expression.

## Synthesis of Pt-peptide conjugates

### Solid phase peptide synthesis (SPPS)

Peptide sequences were prepared from L- $\alpha$ -amino acids that comprise the general structure in **Figure 4.4**. For clarity, for the remainder of this work peptides are consistently written from the N to the C terminus in standard peptide nomenclature using one letter codes for the individual amino acids (**Table 4.1**).

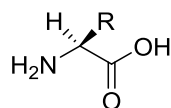


**Figure 4.4:** General chemical structure of L- $\alpha$ -amino acids.

**Table 4.1.** Amino acids with one letter codes and side chains indicated.<sup>[a]</sup>

Amino Acid	Letter Code	-R Group	-R-Properties <sup>[b]</sup>
glycine	G	-H	
lysine	K	-(CH <sub>2</sub> ) <sub>4</sub> NH <sub>2</sub>	positively charged
arginine	R	-(CH <sub>2</sub> )NHC(-NH)NH <sub>2</sub>	positively charged
aspartic acid	D	-CH <sub>2</sub> COOH	negatively charged
glutamic acid	E	-(CH <sub>2</sub> ) <sub>2</sub> COOH	negatively charged
threonine	T	-CH(CH <sub>3</sub> )OH	polar uncharged
serine	S	-CH <sub>2</sub> OH	polar uncharged
asparagine	N	-CH <sub>2</sub> CONH <sub>2</sub>	polar uncharged
leucine	L	-CH <sub>2</sub> (CH)(CH <sub>3</sub> ) <sub>2</sub>	hydrophobic
phenylalanine	F	-CH <sub>2</sub> Ph	hydrophobic

[a] amino acids listed refer to those that were used in SPPS, not all amino acid [b] side chains are charged at physiological pH 7.4.

Peptide sequences TPP (TKDNNLLGRFELSG) and ScP (LLETRLGFGDNKS) were assembled using microwave assisted SPPS from a rink amide MBHA resin.<sup>22</sup> Rink amide MBHA resin consists of a crosslinked polystyrene support which provides moderately high loading and produces the completed peptide as a peptide-amide, as opposed to a peptide-acid. The peptide syntheses were carried out in accordance with the well-established Fmoc/*t*Bu protection strategy, a process which involves incrementally synthesising the peptide in a defined direction from the C- to the N- terminus.<sup>23</sup> All of the amino acids employed in the syntheses possess an Fmoc

protected N $\alpha$ -amino group and a free C-terminal carboxylic acid. Fmoc is employed as a temporary protecting group and is base sensitive.<sup>23</sup> In contrast, any side-chain functional groups present on the amino acids are semi-permanently protected with an acid labile protecting group (**Figure 4.5, Table 4.2**). This model is known as orthogonal protection and facilitates the separate removal of multiple protecting groups using a dedicated set of reaction conditions.

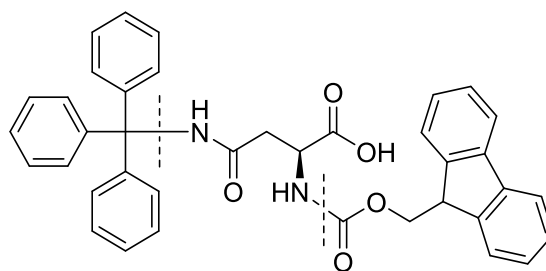


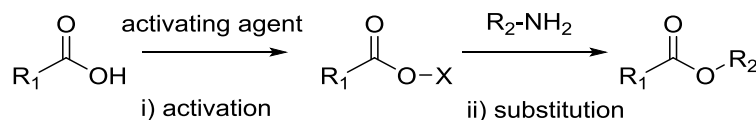
**Figure 4.5.** Fmoc-Asn(trt)-OH. The amine is protected by a base sensitive Fmoc group, while the side chain is protected by an acid labile trt group. The C-terminal carboxylic acid is left free.

**Table 4.2.** Amino acids with one letter codes and side chains indicated.<sup>[a]</sup>

Amino Acid	-Amino	-R Side Chain
glycine	Fmoc	
lysine	Fmoc	Boc
arginine	Fmoc	Pdf
aspartic acid	Fmoc	OtBu
glutamic acid	Fmoc	OtBu
threonine	Fmoc	tBu
serine	Fmoc	tBu
asparagine	Fmoc	trt
leucine	Fmoc	
phenylalanine	Fmoc	

The coupling of amino acids linked *via* amide bonds is the most crucial step in peptide synthesis. Amide bond formation in general is a condensation reaction, however equilibrium favours an acid-base reaction on mixing an acid with an amine, which results in the formation of a stable salt product.<sup>24</sup> In order to promote the amide condensation reaction a good leaving group is first attached to the carbonyl

carbon of the acid in the form of an activating agent. As such, amino acid coupling is typically described in two consecutive steps; i) activation of an acyl moiety followed by ii) nucleophilic acyl substitution with an amino group (**Scheme 4.1**).<sup>24</sup>



**Scheme 4.1:** Reaction scheme demonstrating amide bond formation produced by the activation of a carboxylic acid group on amino acid  $\text{R}_1$  by incorporating a leaving group X, in order to facilitate attack by the amino group of a second amino acid  $\text{R}_2$ .

In order to facilitate rapid amino acid coupling in high yield, a number of activating agents are available, each with associated advantages and disadvantages. As no one coupling reagent is suited for all amino acid substrates, it is therefore necessary to consider the reaction itself when selecting the reagent. Phosphonium and aminium type reagents such as 1-[bis(dimethylamino)methylene]-1*H*-1,2,3-triazolo[4,5-*b*]pyridinium3-oxidhexafluoro phosphate (HATU) and *N,N*-diisopropylethyl amine (DIEA) for example together with a base are frequently used and these compounds have been shown to demonstrate high coupling rates (**Figure 4.6**).<sup>25</sup> However, due to potential racemization of amino acids in the presence of a base, the use of carbodiimide compounds is often favoured. Base is not necessary in this scenario and the reaction occurs *via* addition of a carboxy group to the carbodiimide functionality to generate an *O*-acyl isourea species, which are excellent acylating agents.<sup>26</sup>

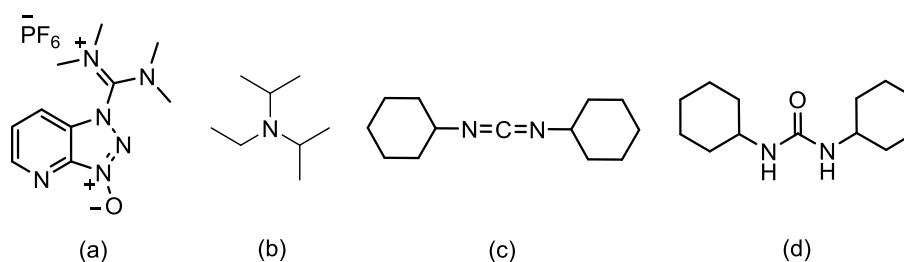
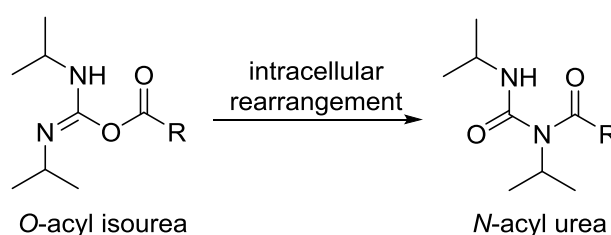


**Figure 4.6:** Chemical structures of activating agent HATU (a), DIEA (b) DCC (c) and DCU (d).

Dicyclohexylcarbodiimide (DCC) has been employed as one of the most popular carbodiimide coupling reagents, but is restricted by the generation of the unwanted side product dicyclohexylurea (DCU), which displays limited solubility in most organic solvents (**Figure 4.6**). Issues with the removal of this reaction by-product has

led to the use of other reagents such as *N,N*-diisopropylcarbodiimide (DIC). DIC acts in a similar manner to DCC, however its corresponding urea is soluble in solvents typically employed in SPPS, and thus may be easily eliminated as a result.

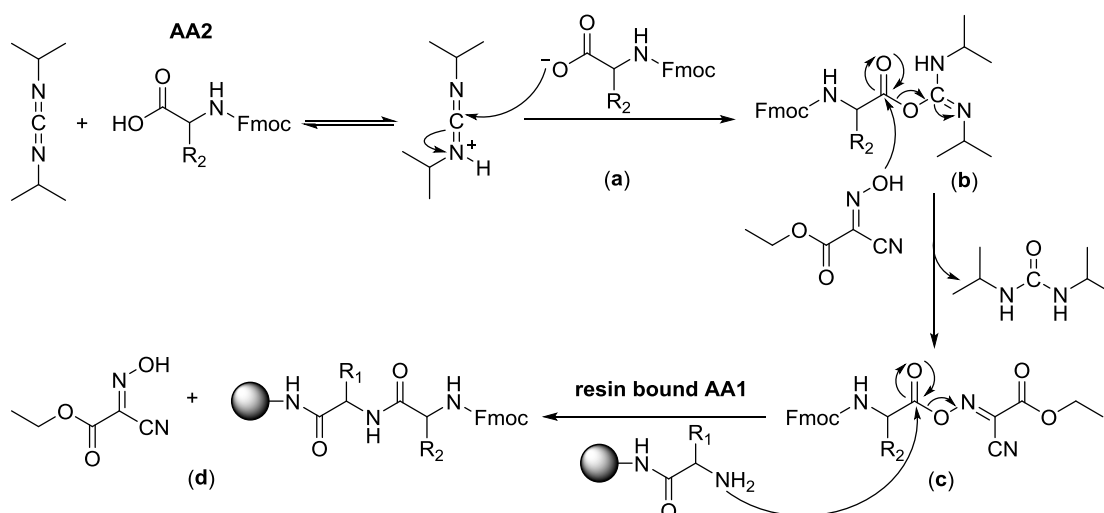
As carbodiimide compounds are associated with the formation of a highly reactive *O*-acyl isourea, their use is not always preferred. This species has the ability to undergo intracellular acyl transfer resulting in the corresponding *N*-acyl urea which consequently reduces yield and presents a difficulty during purification (**Scheme 4.2**). Additionally, the *O*-acyl isourea has the potential to undergo extensive racemization with any susceptible carboxy species.<sup>26</sup>



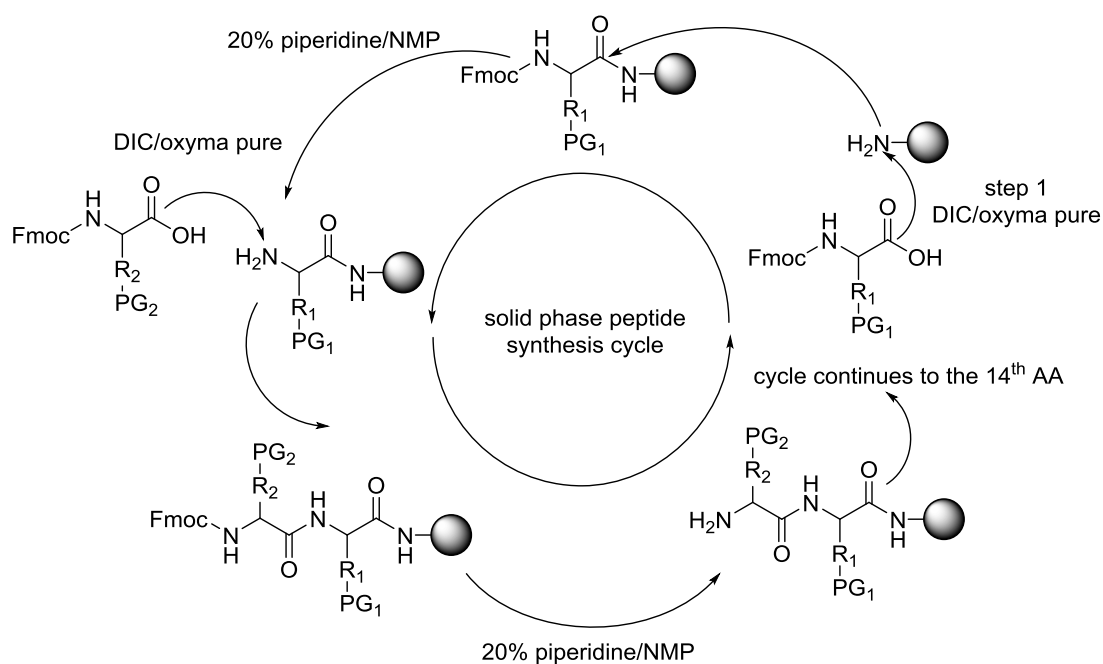
**Scheme 4.2:** Reaction scheme demonstrating the *O*-acyl isourea product formed in DIC coupling and the subsequent rearrangement to an *N*-acyl urea.

To overcome this drawback, DIC in conjunction with a suitable  $\alpha$ -nucleophile is commonly employed. The selection of an appropriate nucleophile that will readily react with the *O*-acyl isourea prevents any side reactions, subsequently forming a less potent acylation agent. This product is still capable of amide bond formation, but racemization is less favoured. Oxyma pure (ethyl cyano(hydroxyimino)acetate) is the preferred reagent in this reaction, as it is a non-explosive alternative to 1-hydroxybenzotriazole (HOBt), which is highly explosive under anhydrous conditions.<sup>27</sup>

The DIC/oxyma pure coupling mechanism shown in **Scheme 4.3** depicts one amino acid bound to the resin (AA1), with a second amino acid to be added (AA2). The carboxylate anion of AA2 reacts with DIC (**Scheme 4.3a**) and the reaction generates an *O*-acyl species (**Scheme 4.3b**). This reaction product reacts readily with nucleophilic oxyma pure to form an active ester, while diisopropyl urea is eliminated (**Scheme 4.3c**). Acylation of the newly formed active ester occurs by the addition of the nucleophilic amine of AA1. Following amide bond formation, oxyma pure is eliminated resulting in a dipeptide coupled to the resin (**Scheme 4.3d**).



**Scheme 4.3:** Reaction scheme demonstrating the addition of AA2 to resin bound AA1 using DIC/oxyma pure coupling chemistry.



**Scheme 4.4:** Reaction scheme demonstrating the incremental steps of amino acid DIC/oxyma pure coupling onto an insoluble rink amide MBHA resin, followed by Fmoc deprotection with piperidine in NMP where R = amino acid side chain and n = the number of amino acids.

Single coupling cycles using a 10-fold excess of Fmoc-amino acids and DIC/oxyma pure coupling chemistry were employed. An excess of the reagents relative to the immobilised peptide at each stage of the synthesis is vital to ensure high levels of

conversion. Subsequent to each amino acid coupling, intermittent steps of Fmoc deprotection were performed (**Scheme 4.4**). As shown above, Fmoc is base sensitive and was removed by the application of 20% (v/v) piperidine in NMP.

Completion of the 14 amino acid sequences and final Fmoc deprotection on the N-terminal afforded the desired TPP and ScP peptides as indicated in **Figures 4.7** and **4.8** respectively.

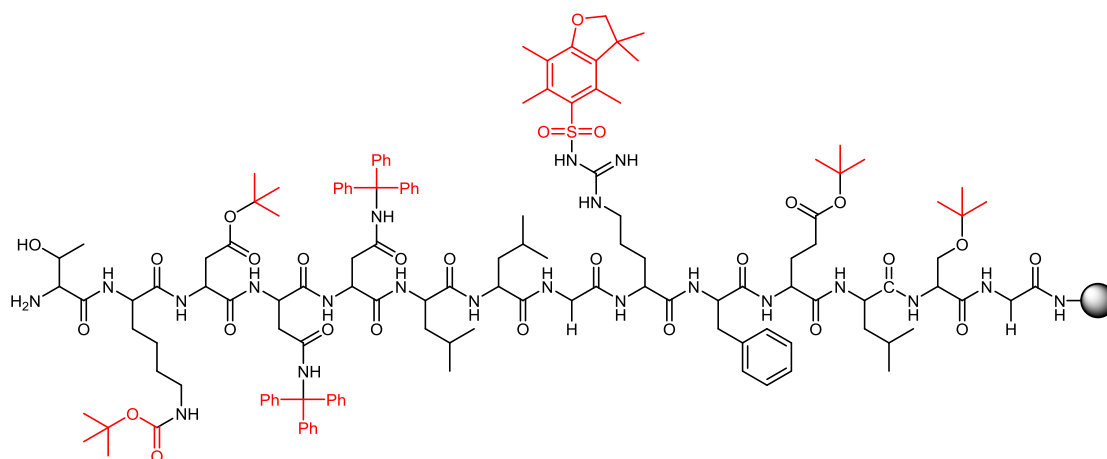


**Figure 4.7:** Chemical structure of 14-mer TPP (TKDNNLLGRFELSG) bound to a resin amide MBHA resin following SPPS and final Fmoc deprotection with semi-permanent side chain protecting groups (highlighted in red) still intact.

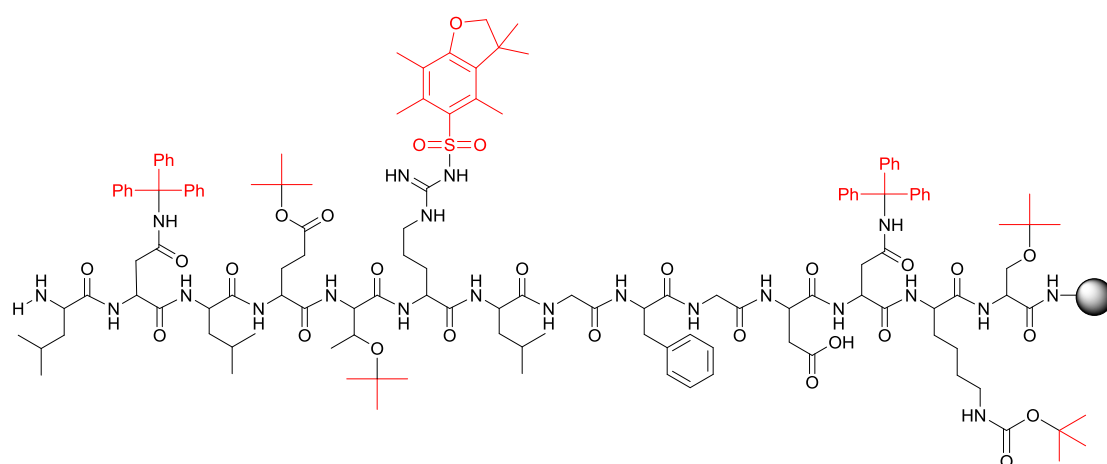


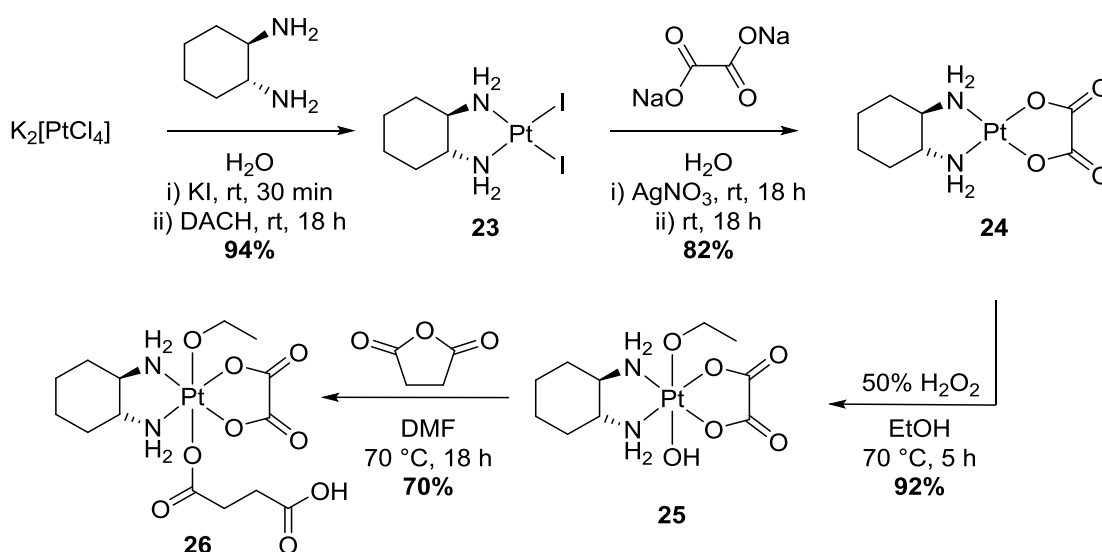
**Figure 4.8:** Chemical structure of 14-mer ScP (LNLETRLGRGDNKS) bound to a resin amide MBHA resin following SPPS and final Fmoc deprotection with semi-permanent side chain protecting groups (highlighted in red) still intact.



**Synthesis of [Pt(IV)(DACH)(OEt)(OH)(Ox)]**

[Pt(IV)(DACH)(OEt)(Ox)(succ)] was synthesised in two steps starting from oxaliplatin as per **Scheme 4.5**. The synthesis was developed through modification of the methods reported by Feazell *et al.*

Oxaliplatin (**24**) was first oxidised by heating at 70 °C with 50% wt/vol H<sub>2</sub>O<sub>2</sub> in EtOH to form [Pt(IV)(DACH)(OEt)(OH)(Ox)] complex **25**. Subsequently, the complex was dissolved at 70 °C in anhydrous DMF, followed by the addition of succinic anhydride in anhydrous DMF to form [Pt(IV)(DACH)(OEt)(Ox)(succ)] complex **26** as a light brown solid with a 70% yield.



**Scheme 4.5:** Synthetic route to [Pt(IV)(DACH)(OEt)(Ox)(succ)].

[Pt(IV)(DACH)(OEt)(OH)(Ox)], **25** was characterised by elemental analysis, and NMR and IR spectroscopy. Elemental analysis for **25** is consistent with the expected values for [Pt(IV)(DACH)(OEt)(OH)(Ox)]. The IR spectrum shows a broad peak at 3436 cm<sup>-1</sup> which is indicative of the OH ligand. In the <sup>1</sup>H NMR spectrum (DMSO-*d*<sub>6</sub>) diagnostic resonances associated with the ethoxide protons were evident as a quartet integrating for two protons at 3.20 ppm and a multiplet integrating for three protons at 1.86 ppm. In the <sup>13</sup>C NMR spectrum two peaks at 18.94 and 56.49 ppm appear in the predicted region for ethoxide CH<sub>2</sub> and CH<sub>3</sub> carbons. The <sup>195</sup>Pt NMR spectrum displayed a peak at 1296.79 ppm, which is consistent with Pt(IV) complexes.<sup>28</sup>

[Pt(IV)(Ox)(DACH)(OEt)(Ox)(succ)], **26** was characterised by elemental analysis NMR and IR spectroscopy and mass spectrometry. Elemental analysis for **26**

correlated with the required values for one oxalate, one DACH, one ethoxide and one succinate group per Pt centre. In the IR spectrum, the broad peak of the OH ligand at  $3436\text{ cm}^{-1}$  was no longer present, indicating that the hydroxo ligand had been substituted and two (C=O) peaks were evident at  $1714$  and  $1652\text{ cm}^{-1}$ . In the  $^1\text{H}$  NMR spectrum ( $\text{DMF-}d_7$ ), two multiplets observed at  $2.75$  and  $2.92\text{ ppm}$ , both integrating for two protons, are characteristic of the two  $\text{CH}_2$  moieties on the succinato ligand along with the diagnostic resonance corresponding to the carboxylic acid proton, evident as a broad singlet at  $12.42\text{ ppm}$ . The  $^{13}\text{C}$  NMR spectrum revealed two diagnostics peaks at  $174.19$  and  $173.89\text{ ppm}$ , which confirm the presence of the coordinated and terminal succinic acid functional group carbons generated on reaction of the Pt(IV) precursor with succinic anhydride. The  $^{195}\text{Pt}$  NMR ( $\text{DMSO-}d_6$ ) spectrum of **26** displayed a single peak at  $1366.95\text{ ppm}$ , demonstrating a distinct shift in position in comparison to complex **25**. ESI-MS in positive mode aided the identification of the  $\text{M}+\text{Na}$  with a mass peak of  $582.3\text{ a.m.u.}$

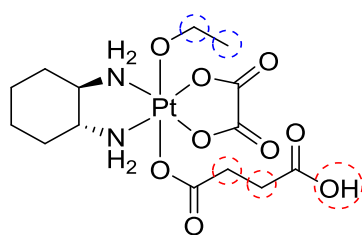
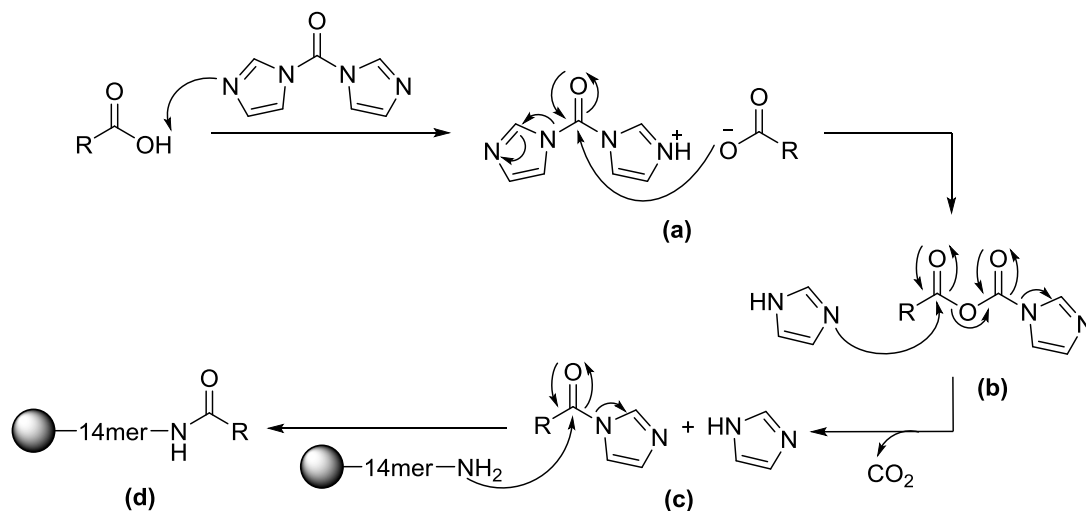


**Figure 4.9:** Chemical structure of Pt(IV) complex **26** and the protons which serve as diagnostic peaks in  $^1\text{H}$  NMR spectrum, indicated in red for succinato and blue for ethoxide.

#### Pt(IV) peptide conjugation

Pt(IV) peptide conjugation was performed manually using the resin-bound peptide with side chain protecting groups *in situ* in order to avoid any undesired reactions between the carboxylic acid of the platinum complex and free amino groups on the lysine, arginine and asparagine. The structure of **26** comprises a bidentate *trans*-(1*R*,2*R*) DACH ligand and an oxalato ligand in the equatorial positions. In addition to the axial ethoxide ligand, a second axial ligand, the succinato group which possesses a free carboxylic acid group, was activated on reaction with CDI (**Scheme 4.6a**) to form an acyl carboxy imidazole (**Scheme 4.6b**) which readily rearranges with loss of  $\text{CO}_2$  to yield an acyl imidazole species (**Scheme 4.6c**). The activated Pt

complex was subsequently treated with TPP or ScP in a 4:1 ratio to afford the corresponding Pt-TPP or Pt-ScP conjugates through amide bond formation (**Scheme 4.6d**).



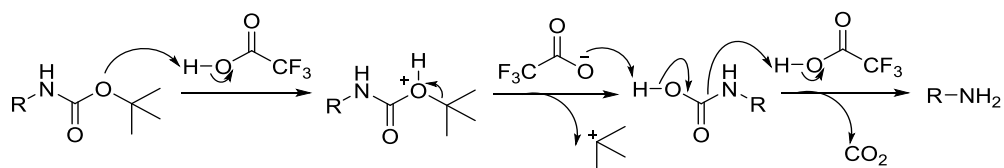
**Scheme 4.6:** Reaction scheme demonstrating Pt-peptide coupling using CDI where  $R = [Pt(IV)(DACH)(oxalato)(ethoxido)(succinato)]$  and 14-mer = resin bound TPP or ScP.

### Peptide cleavage and purification

Following Pt-peptide conjugation, the resin was thoroughly washed with DMF to remove any excess unreacted active precursor **26**, and the corresponding conjugates were subsequently cleaved from the resin and the side-chain protecting groups removed. This was achieved under acidic conditions as the semi-permanent side chain protecting groups are acid labile. A cleavage cocktail consisting 95% TFA sufficiently removed the various protecting groups employed by different amino acids; *Ot*Bu, *t*Bu, Trt, Pbf and Boc. In addition, electrophilic species are formed during the acidolytic deprotection, and for this reason the cleavage cocktail comprised 2.5% water and 2.5% phenol. These reagents possess nucleophilic scavenger activity and consequently prevent reactive side products from recombining with liberated nucleophilic amino acid side chain functional groups.

The reaction mechanism of TFA deprotection is demonstrated in **Scheme 4.7**, where an amino acid is protected with BOC. The *tert*-butyl carbamate becomes protonated in the presence of TFA (**Scheme 4.7**), and the loss of the *tert*-butyl cation results in carbamic acid formation (**Scheme 4.7**). The *tert*-butyl cation is quenched by a

suitable scavenger agent in order to prevent nucleophilic substrates from being alkylated. Decarboxylation of the carbamic acid generates the free amine (**Scheme 4.7**).



**Scheme 4.7:** Scheme demonstrating TFA deprotection of BOC where R = an amino acid.

Subsequent to cleavage, the final Pt-peptide conjugate crude mixture was lyophilised.

The Pt-peptide conjugates, **Pt-TPP** and **Pt-ScP**, were subsequently isolated by reverse phase HPLC and the retention times are listed in **Table 4.3**. Purification afforded both Pt-peptide conjugates in typical low yield where **Pt-TPP** was obtained as 4 mg for 3.8% and **Pt-ScP** was obtained as 3.2 mg for 1.9% with respect to the resin loading.<sup>4, 13, 29</sup> It is apparent that using an unsymmetrical Pt(IV) precursor such as [Pt(IV)(Ox)(DACH)(OEt)(Ox)(succ)] did not offer an advantage in terms of increased yield as compared to the use of the symmetrical precursor, [Pt(IV)(Ox)(DACH)(Ox)(succ)<sub>2</sub>] used by McKeon *et al*, which afforded the corresponding Pt monoTPP conjugate in 3.7% yield and the Pt diTPP conjugate in 2% yield.<sup>13</sup>

<sup>195</sup>Pt NMR spectroscopy of **Pt-TPP** was used to demonstrate successful conjugation and Pt in the +IV oxidation state. A single peak was observed at 1379.14 ppm which is indicative of a Pt(IV) centre (**Figure 4.10**).

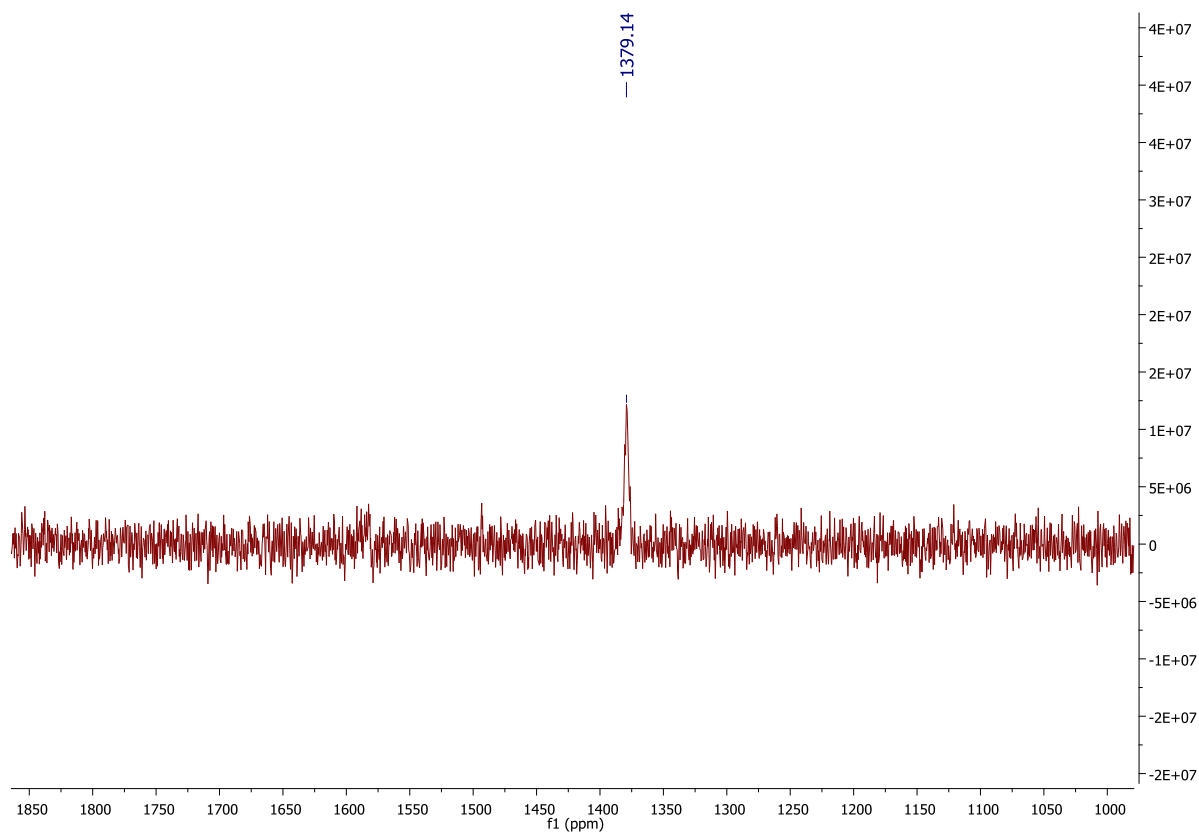


**Figure 4.10:**  $^{195}\text{Pt}$  NMR spectrum ( $\text{D}_2\text{O}$ ) of **Pt-TPP** following conjugation of [Pt(IV)(DACH)(oxalate)(ethoxide)(succinate)] and TPP.

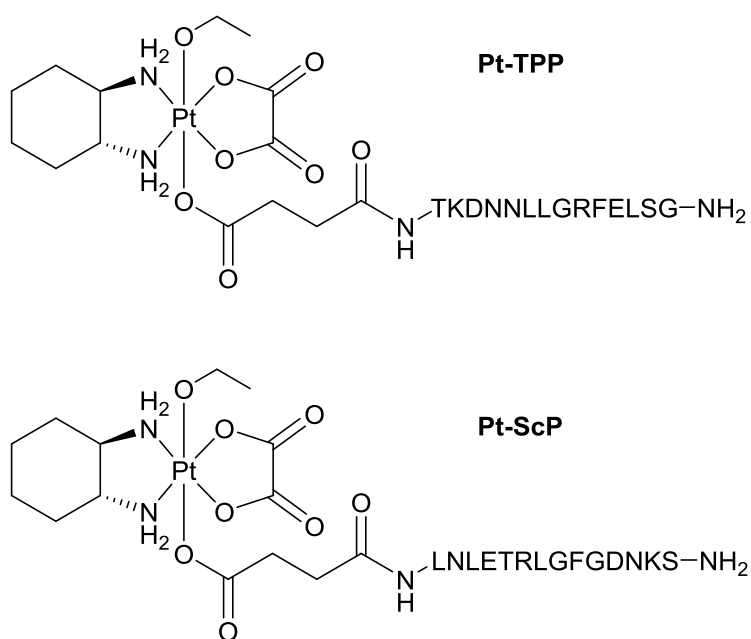


**Figure 4.11:** Chemical structures of **Pt-TPP** and **Pt-ScP**.

**Table 4.3.** HPLC data for peptide and Pt-peptide compounds.<sup>[a]</sup>

Compound	<i>t</i> R (min)	Purity %
<b>Pt-TPP</b>	38.96	100
<b>TPP</b>	38.79	95.73
<b>Pt-ScP</b>	38.56	100
<b>ScP</b>	35.90	97.08

[a] Mobile phase A: 0.1% TFA/ H<sub>2</sub>O and mobile phase B: 0.1% TFA/ MeOH were used with a gradient of 5 – 85 – 5% B over 65 min with a flow rate of 1 mL/min;  $\lambda$ : 214/254 nm.

The analytical HPLC traces of **TPP**, **ScP** and their respective **Pt-TPP** and **Pt-ScP** conjugates all showed purities > 95%, with the Pt-peptide conjugates found to be 100% pure (**Table 4.3** and **Figure 4.12**). McKeon *et al.* reported >97% and >90% purity for their Pt mono- and Pt di-conjugates respectively. With regards to the >90 % value associated with the Pt di-conjugate, an additional 8.01 % of this was attributed to the corresponding Pt mono-conjugate. The Pt peptide conjugates therefore were easier to isolate and purify relative to the strategy employed by McKeon *et al.*, given only one Pt-peptide conjugate could be generated in their individual reactions.

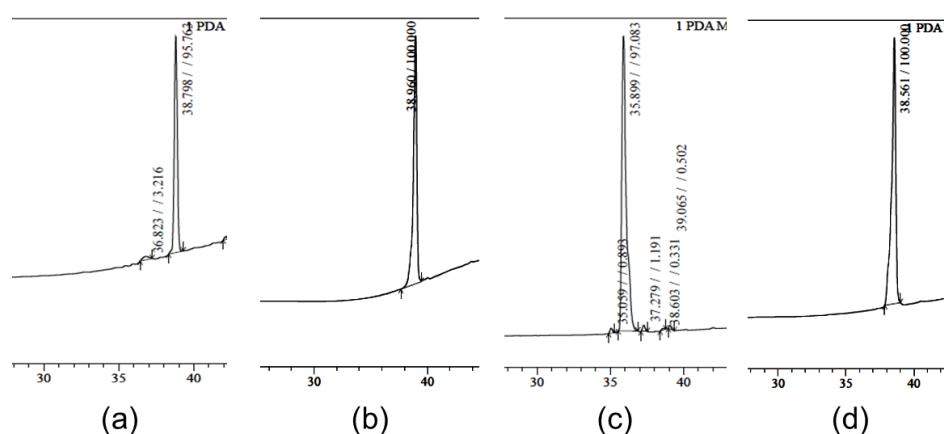


**Figure 4.12:** Expanded region between 30 and 40 min of analytical HPLC traces for (a) TPP, (b) Pt-TPP, (c) ScP, (d) Pt-ScP. HPLC conditions; (mobile phase A: 0.1% TFA/ H<sub>2</sub>O and mobile phase B: 0.1% TFA/ MeOH were used with a gradient of 5 – 85 – 5% B over 65 min with a flow rate of 1 mL/min;  $\lambda$ : 214/254 nm).

Subsequent to semi-preparative HPLC, the purity of the conjugates was determined and the chemical identities were confirmed by HRMS (**Table 4.4**).

**Table 4.4.** ESI-HRMS data for peptide and Pt-peptide compounds.

Compound	Exact Mass <sub>calcd</sub>	[M+H] <sup>+</sup>	[M+2H] <sup>2+</sup>	[M+3H] <sup>3+</sup>
<b>Pt-TPP</b>	2104.1700	[d]	1054.4160 <sup>[a]</sup>	[d]
<b>TPP</b>	1561.82	1561.71 <sup>[a][b]</sup>	782.1 <sup>[c]</sup>	521.9 <sup>[c]</sup>
<b>Pt-ScP</b>	2104.1700	[d]	1054.3705 <sup>[a]</sup>	[d]
<b>ScP</b>	1561.82	1561.55 <sup>[a][b]</sup>	782.2 <sup>[c]</sup>	522 <sup>[c]</sup>

[a] highest intensity peak observed, HRMS [b], LRMS [c], no such peak observed [d]

Regarding the MS data, the experimental mass spectral data observed are in good agreement with the predicted values. The [M+H]<sup>+</sup> peaks for the Pt-peptide conjugates were not evident but the chemical identities were unambiguously characterised by examining the 2<sup>+</sup> and/or 3<sup>+</sup> mass distribution patterns (**Table 4.4**). The peptides TPP and ScP were also identified in a similar manner.

These findings correlate with previously reported Pt-peptide conjugates of McKeon *et al.* and Abramkin *et al.*<sup>4, 13</sup> In these instances, the [M+H]<sup>+</sup> peaks were not observed in the spectra of both ESI and MALDI-TOF techniques and the conjugates were identified through the 2<sup>+</sup> and/or 3<sup>+</sup> molecular ions, as is the approach for characterising high molecular mass peptides.<sup>4, 13</sup>

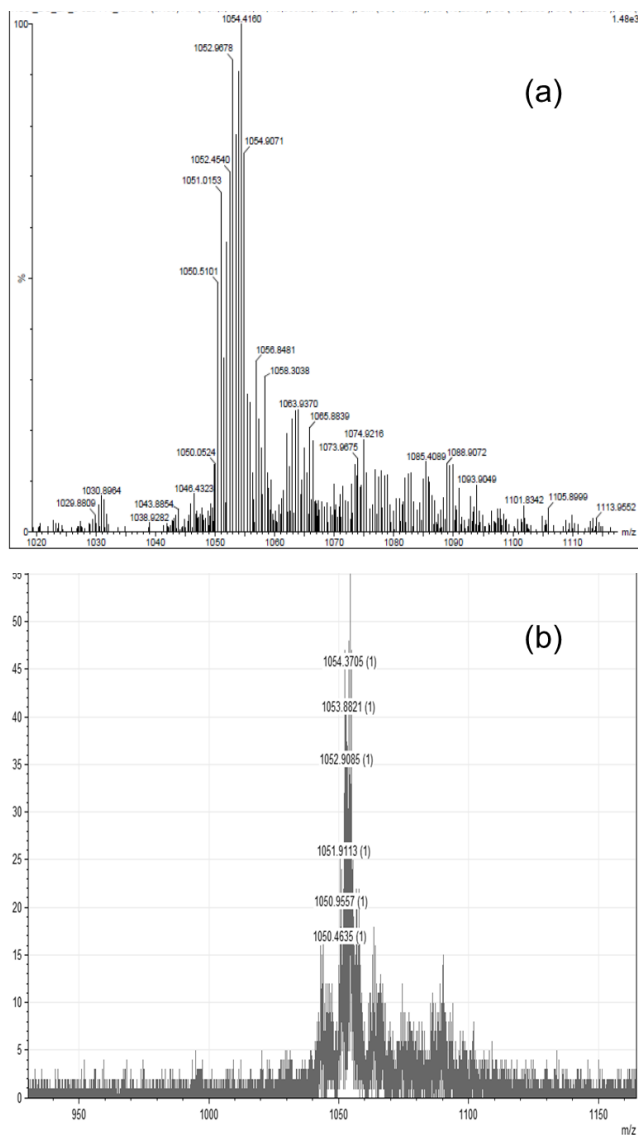


**Figure 4.13:** HRMS ESI MS of Pt-TPP (a) and Pt-ScP (b) with  $m/z$  values of 1054.4160 and 1054.3705 a.m.u. respectively.



## *In vitro* analysis of Pt-peptide conjugates

### *In vitro* cytotoxicity

HT29 and HCT116 wt colorectal cancer cells were selected for *in vitro* cytotoxicity experiments as (i) HT29 represents a relatively resistant cell line and HCT116 a relatively sensitive cell line to oxaliplatin treatment as per the *in vitro* MTS cytotoxicity data, (ii) HT29 exhibited the highest expression of memHSP70 and HCT116 the lowest and (iii) McKeon *et al.* selected the same cell lines to investigate the ability of their Pt TPP conjugates to induce cell death using the Annexin V/ Propidium Iodide (PI) assay. It is noteworthy that McKeon and co-workers did not determine IC<sub>50</sub> values for their Pt TPP conjugates.<sup>10-13</sup>

Therefore, *in vitro* cytotoxicity experiments were undertaken ( $n = 3$ ) to investigate the response of HCT116 wt and HT29 cells to treatment with oxaliplatin, Pt(IV) complex **26** (herein referred to as **Pt(IV)**), peptides **TPP** and **ScP**, and the Pt-peptide mono-conjugates **Pt-TPP** and **Pt-ScP**. Stock solutions of these test compounds were prepared fresh in culture medium and diluted to various working concentrations as per **Table 4.5**.

**Table 4.5:** The range of drug concentration used per cell line.

Compound	HCT116 wt	HT29
<b>Oxaliplatin</b>	0.078 - 10 $\mu$ M	0.39 - 100 $\mu$ M
<b>Oxaliplatin and TPP</b>	0.078 - 10 $\mu$ M	0.39 - 100 $\mu$ M
<b>Pt(IV)</b>	0.625 - 100 $\mu$ M	0.39 - 250 $\mu$ M
<b>Pt-TPP</b>	0.078 - 10 $\mu$ M	0.78 - 100 $\mu$ M
<b>Pt-ScP</b>	0.078 - 10 $\mu$ M	0.78 - 100 $\mu$ M
<b>TPP</b>	0.078 - 200 $\mu$ M	0.39 - 200 $\mu$ M
<b>ScP</b>	0.078 - 200 $\mu$ M	0.39 - 200 $\mu$ M

All test compounds were synthesised as outlined in Chapter 2. *In vitro* cytotoxicity was determined by an MTS inner salt assay, as outlined in Chapter 3. Dose-response plots based on 72 h treatment ( $n = 3$ ) were generated using GraphPad Prism and IC<sub>50</sub> values, defined as the drug concentration required to inhibit cell growth by 50 %, were generated (**Table 4.6**).

**Table 4.6:** IC<sub>50</sub> values calculated for colorectal cancer cell lines.<sup>[a]</sup>

Compound	HCT116 wt (μM)	HT29 (μM)	Resistance factor
<b>Oxaliplatin</b>	0.893 ± 0.04	26.66 ± 2.96	29.85
<b>Oxaliplatin + TPP</b>	0.714 ± 0.03	16.45 ± 2.76	23.04
<b>Pt(IV)</b>	39.22 ± 1.66	162.3 ± 10.08	4.14
<b>Pt-TPP</b>	2.539 ± 0.22	78.15 ± 15.88	30.78
<b>Pt-ScP</b>	8.175 ± 0.69	>100	>10
<b>TPP</b>	>200	>200	-
<b>ScP</b>	>200	>200	-

[a] after 72 treatment. Error shown as ± SEM.

Both peptides TPP and ScP were found to be non-toxic against both cell lines, with little or no activity at the highest concentration investigated, 200 μM. Oxaliplatin, the drug of choice for late stage colorectal cancer treatments, exhibited the best cytotoxicity, with IC<sub>50</sub> values of 0.893 and 26.66 μM in the HCT116wt and HT29 cell lines respectively, correlating with previous literature reports.<sup>18, 30-32</sup>

**Pt(IV)** was found to be significantly less cytotoxic compared to the other Pt containing complexes, with IC<sub>50</sub>s of 39.22 and 162.3 μM against the HCT116 wt and HT29 cell lines. Although **Pt(IV)** exhibited lower activity when compared to its Pt(II) core analogue oxaliplatin, this lower activity is frequently observed for Pt(IV) complexes when compared against their Pt(II) analogues.<sup>20-21, 31, 33</sup> For example, the Pt(IV) oxaliplatin analogues [Pt(DACH)(Ox)(OH)<sub>2</sub>] and [Pt(DACH)(ox)(succ)<sub>2</sub>] were found to have IC<sub>50</sub>s of 54 and 69 μM respectively as compared to oxaliplatin's IC<sub>50</sub> of 0.55 μM against HCT116 wt cells.<sup>31</sup>

Pt(IV) complexes are widely considered to internalise in cells solely through passive diffusion in most instances,<sup>34-36</sup> whereas Pt(II) may utilise both passive diffusion and cationic transport proteins<sup>36</sup> amongst other influx/efflux transporter systems.<sup>37-38</sup> Other recent studies have found that Pt(IV) complexes with a cisplatin-like core may also be subject to active transport mechanisms in addition to passive diffusion.<sup>39</sup>

The reduction of Pt(IV) to Pt(II) is universally considered an essential step in the activity of so called Pt(IV) prodrugs. It is important therefore to note that the (i) identity of axial ligands, (ii) reduction potential of the Pt(IV) complex and (iii), rate

of reduction of the Pt(IV) complex are important contributory factors to cytotoxicity amongst many others.

For example, recent investigations of the *in vitro* cytotoxicities of Pt(IV) complexes possessing mono- and di- carboxy axial ligands such as acetates and succinates, have shed some light on the importance of these factors.<sup>33 20-21, 40-41</sup>

For example, hydroxy (OH) ligands have shown lower reduction potential when compared to groups such as acetates (OAc) and succinate (succ).<sup>42-43</sup> OH is considered to have the slowest rate of reduction of axial ligands of Pt(IV), with one study reporting the trend as OH<OAc<Cl<OCOCF<sub>3</sub>. Interestingly, this trend also correlated with the cytotoxicity value of the Pt(IV) complexes tested.<sup>43</sup> The rate of reduction of **Pt(IV)** is likely a major factor in its low cytotoxicity, given the low reduction potential of Pt(IV) complexes bearing OEt ligands.

Interestingly, Pt(IV) complexes have been demonstrated to undergo reduction at a slower rate in the HT29 cell line as compared to the A2780cis and A2780P cell lines, highlighting that cell lines also influence the reducing behaviour of these complexes.<sup>44</sup>

Another interesting discovery has been that there is no trend between the rate of reduction and reduction potential of an axial ligand.<sup>7</sup>

As active Pt(II) drugs often fail to reach cells as a result of deactivation during distribution there is still a desire clinically for slower reacting Pt(II) drugs and Pt(IV) prodrugs to allow them sufficient time to reach their target site by remaining biologically inert. Therefore, *in vitro* cytotoxicity of Pt(IV) drugs is not necessarily representative of their potential *in vivo* activity and/or application. In addition, longer experimental *in vitro* cytotoxicity study times (96-120 h) are required to reveal a more accurate picture of the potential activity of these complexes as has previously been reported.<sup>44-45</sup>

**Pt-TPP** showed good activity against the HCT116 wt cell line with an IC<sub>50</sub> value of 2.55 µM. Although the cytotoxicity is lower (c. 3 fold) when compared against oxaliplatin (0.893 µM) it is a significant improvement on **Pt(IV)** (39.22 µM) which **Pt-TPP** was derived from.

**Pt-TPP** exhibits an  $IC_{50}$  of 78.15  $\mu M$  against the HT29 which was unexpected and significantly larger compared to oxaliplatin (26.66  $\mu M$ ) given the previously reported over expression of memHSP70+ in this cell line and favourable reports on the ability of Pt-TPP conjugates to induce cell death in HT29 cells.<sup>13</sup> These previous reports would suggest that **TPP** containing Pt(IV) conjugates would demonstrate greater cytotoxicity,<sup>10</sup> but as with the HCT116 wt cell line the  $IC_{50}$  value is three times that of oxaliplatin. Once more, **Pt-TPP** displays significantly greater cytotoxicity compared to **Pt(IV)** (162.3  $\mu M$ ), although it is by a smaller margin compared to the HCT116 wt cell line.

**Pt-ScP** functioned as a negative control, as the **ScP** scrambled peptide sequence does not exhibit the targeting function of **TPP**. However, the level of activity of **Pt-ScP** against the HCT116 wt cells (8.175  $\mu M$ ) was larger than expected given the nature of **ScP** and as such was predicted to give a comparable  $IC_{50}$  value to **Pt(IV)**'s 39.22  $\mu M$ . A number of factors can be put forward to explain this, for example the biocompatible nature of a peptide could improve its natural cellular uptake<sup>46</sup> or the peptide could improve the Pt(IV) reduction rate of **Pt-ScP** compared to **Pt(IV)**. However given **Pt-TPP** gave a significant response three times greater than **Pt-ScP** in the HCT116 wt cell line the superior targeting potential of **TPP** has been clearly demonstrated.

In the HT29 cell line, the upper limit of this study for **Pt-ScP** was 100  $\mu M$ , which did not reach the 50% cell viability threshold.

In an additional control experiment, oxaliplatin and **TPP** were co-administered in 1:1 concentrations against both cell lines. Similar  $IC_{50}$ s compared to oxaliplatin alone were recorded of 0.714 and 16.45  $\mu M$  in the HCT116 wt and HT29 cell lines respectively, which were found to be non-significant using an unpaired Student's t-test, compared to oxaliplatin alone.

The **Pt-ScP** activity was greater than predicted, given the previous investigation by McKeon and co-workers<sup>13</sup> found substitution of TPP in the Pt(IV) peptide conjugates with ScP essentially abolished the induction of cell death. As it is well known that Pt(IV) complexes generally act as prodrugs and must first be reduced in the cell to the Pt(II) form, it is possible that the cytotoxic effect of these complexes is delayed by the time taken for reduction to occur. Similar observations are predicted for the

**Pt-TPP** complex or indeed other future Pt(IV) mono/di TPP conjugates. Recent publications in this field show similar findings in most instances.<sup>4, 33</sup> In future work a longer time period e.g. 96 h testing may address these issues.

One possibility is the seeding cell population has multiplied by the time activity occurs thus reducing the drug to cell ratio. Another possibility is the effects of these drugs are less apparent in *in vitro* cytotoxicity experiments as compared to flow cytometry experiments measuring cell death. Finally, 72 h may not be enough time for this delayed activity to be efficiently observed. Keppler *et al.* typically determine IC<sub>50</sub>s for Pt(IV) complexes at 96 h and not 72 h as was the case in this study.<sup>31</sup>

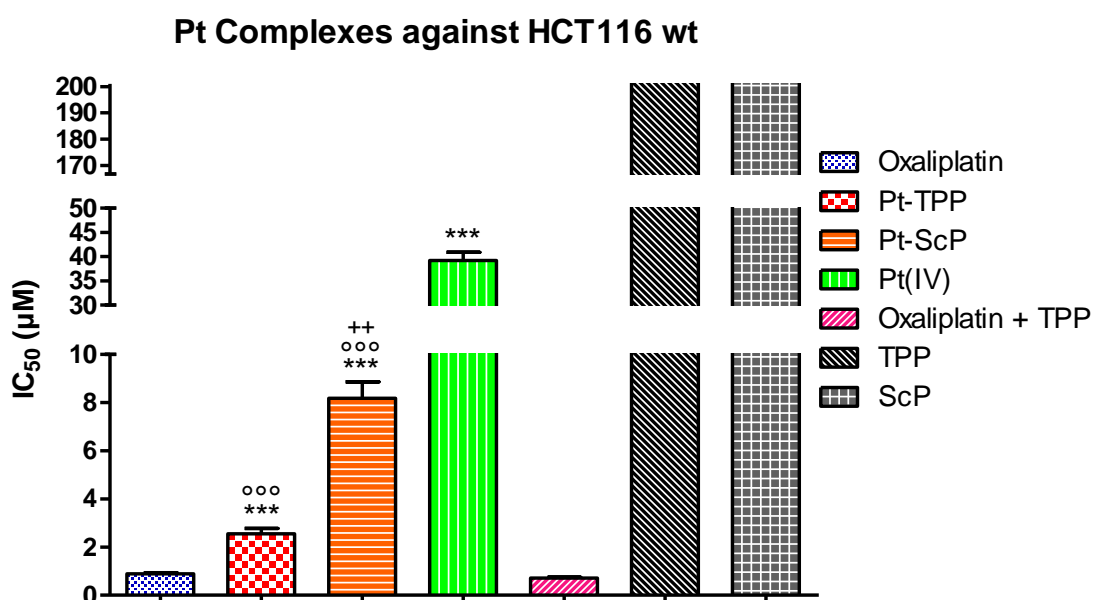


**Figure 4.13:** Statistical significance was determined using an unpaired Student's t-test, where \*\* p value  $\leq 0.01$ , \*\*\* p value  $\leq 0.001$  indicates the difference in activity where \* is significance compared to oxaliplatin, ° is significance compared to **Pt(IV)** and + is significance compared to **Pt-TPP**.

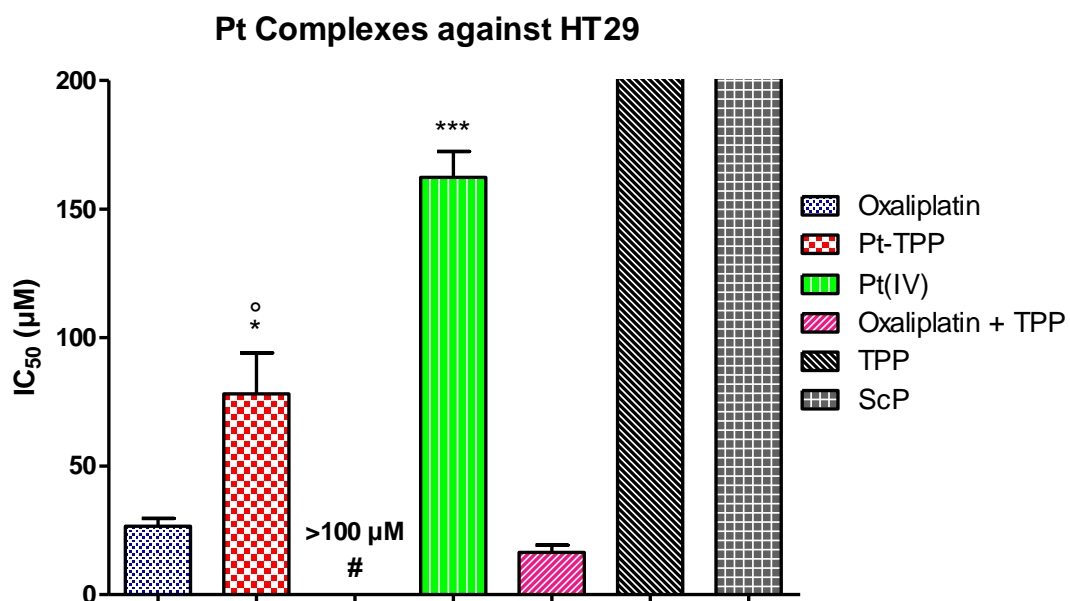


**Figure 4.14:** Statistical significance was determined using an unpaired Student's t-test, where \* p value  $\leq 0.05$ , \*\*\* p value  $\leq 0.001$  indicates the difference in activity where \* is significance compared to oxaliplatin and ° is significance compared to **Pt(IV)**. # IC<sub>50</sub> of Pt-ScP was >100  $\mu\text{M}$ , thus was excluded from graph for clarity.

## Conclusion

A novel unsymmetrical Pt(IV) complex, derived from oxaliplatin, with two unique axial ligands was synthesised and characterised to assess its suitability for conjugation with a cell penetrating peptide by amide bond formation. The complex, **26**, was brought forward for conjugation with the peptides TPP and ScP to form the corresponding Pt-mono peptide conjugates.

*In vitro* cytotoxicity data was determined for oxaliplatin, Pt(IV) complex **26**, **Pt-TPP**, **Pt-ScP**, TPP and ScP against colorectal cancer cell lines HT29 and HCT116 wt. In addition, the co administration of oxaliplatin and TPP in equal concentrations was investigated.

Although cytotoxicity values were not as low as expected following the results of McKeon *et al.*, the cells may still be apoptotic making the **Pt-TPP** conjugate valuable.

“Free” peptide TPP does not improve the cytotoxicity of Pt when co-administered. This is a clear indication that TPP behaves only as a cell penetrating peptide, as expected.

Despite implementing a strategy designed to increase the yield by semi-prep HPLC purification, the yield remained low for the Pt-peptide conjugates **Pt-TPP** and **Pt-ScP**. However, the purification process was greatly sped up as only the mono-peptide conjugate was present and the purification of the complex was higher than previous reported examples.

### Future Work

Flow cytometry *in vitro* experiments could be used to determine an alternative cytotoxic activity, apoptosis, of these drugs compared to the performed MTS assay, which determines cell proliferation. In conjunction with MTS assays run over longer time periods (i.e. 96 h) to account for Pt(IV) reduction, it may be possible to identify the feasibility of these complexes as potential next generation functional chemotherapeutic agents. Thus far, the apoptosis and cell proliferation patterns observed do not correlate meaning the mode and mechanism of action must be further investigated.

As such, cellular accumulation by ICP-MS to determine % Pt uptake is proposed to identify the extent of cellular uptake of Pt-TPP compared to the other Pt(II) and Pt(IV) derivatives, and if the level of cytotoxicity may be correlated. The rate of reduction can also be monitored and determined through time dependent HPLC studies. These two methods are proposed for the next stage of investigation.

Gel electrophoresis may also be used to show the level of DNA damage of Pt(IV) complexes when exposed to DNA with ascorbic acid. This has already been employed in Pt(IV) DNA binding studies to determine reduction rates and times.

Alternate novel or unexploited unsymmetrical Pt(IV) complex “carrier” mono ligands (e.g. OAc, COO(C<sub>x</sub>H<sub>x+2</sub>)) should be synthesised in other to improve upon the model produced here. For example, Pt(IV) drugs with lipophilic axial ligands have been found to induce greater levels of toxicity, which has largely been attributed to greater cellular accumulation through passive diffusion.<sup>33</sup> Additionally, this unsymmetrical Pt(IV) model has potential to be used to conjugate an tertiary functional group i.e. an inhibitor molecule i.e. a tri-active complex.



## References

1. Wheate, N. J.; Walker, S.; Craig, G. E.; Oun, R., The status of platinum anticancer drugs in the clinic and in clinical trials *Dalton Trans.* **2010**, 39, 8113-8127.
2. Kelland, L., The resurgence of platinum-based cancer chemotherapy. *Nat. Rev.* **2007**, 7 (8), 573-584.
3. Galluzzi, L.; Vitale, I.; Michels, J.; Brenner, C.; Szabadkai, G.; Harel-Bellan, A.; Castedo, M.; Kroemer, G., Systems biology of cisplatin resistance: past, present and future. *Cell Death & Disease* **2014**, 5, e1257.
4. Abramkin, S.; Valiahdi, S. M.; Jakupec, M. A.; Galanski, M.; Metzler-Nolte, N.; Keppler, B. K., Solid-phase synthesis of oxaliplatin-TAT peptide bioconjugates. *Dalton Transactions* **2012**, 41 (10), 3001-3005.
5. Bruno, P. M.; Liu, Y.; Park, G. Y.; Murai, J.; Koch, C. E.; Eisen, T. J.; Pritchard, J. R.; Pommier, Y.; Lippard, S. J.; Hemann, M. T., A subset of platinum-containing chemotherapeutic agents kills cells by inducing ribosome biogenesis stress. *Nat. Med.* **2017**, 23 (4), 461-471.
6. Dasari, S.; Tchounwou, P. B., Cisplatin in cancer therapy: molecular mechanisms of action. *European journal of pharmacology* **2014**, 0, 364-378.
7. Wexselblatt, E.; Gibson, D., What do we know about the reduction of Pt(IV) pro-drugs? *Journal of Inorganic Biochemistry* **2012**, 117, 220-229.
8. Bhargava, A.; Vaishampayan, U. N., Satraplatin: leading the new generation of oral platinum agents. *Expert Opinion on Investigational Drugs* **2009**, 18 (11), 1787-1797.
9. Kelland, L. R.; Abel, G.; McKeage, M. J.; Jones, M.; Goddard, P. M.; Valenti, M.; Murrer, B. A.; Harrap, K. R., Preclinical Antitumor Evaluation of Bis-acetato-ammine-dichloro-cyclohexylamine Platinum(IV): an Orally Active Platinum Drug. *Cancer Research* **1993**, 53 (11), 2581.
10. Novohradsky, V.; Zerkankova, L.; Stepankova, J.; Vrana, O.; Raveendran, R.; Gibson, D.; Kasparkova, J.; Brabec, V., Antitumor platinum(IV) derivatives of oxaliplatin with axial valproato ligands. *Journal of Inorganic Biochemistry* **2014**, 140, 72-79.
11. Ang, W. H.; Khalaila, I.; Allardyce, C. S.; Juillerat-Jeanneret, L.; Dyson, P. J., Rational Design of Platinum(IV) Compounds to Overcome Glutathione-S-Transferase Mediated Drug Resistance. *Journal of the American Chemical Society* **2005**, 127 (5), 1382-1383.
12. Ang, W. H.; Pilet, S.; Scopelliti, R.; Bussy, F.; Juillerat-Jeanneret, L.; Dyson, P. J., Synthesis and Characterization of Platinum(IV) Anticancer Drugs with Functionalized Aromatic Carboxylate Ligands: Influence of the Ligands on Drug Efficacies and Uptake. *Journal of Medicinal Chemistry* **2005**, 48 (25), 8060-8069.
13. McKeon, A. M.; Noonan, J.; Devocelle, M.; Murphy, B. M.; Griffith, D. M., Platinum(IV) oxaliplatin-peptide conjugates targeting memHsp70+ phenotype in colorectal cancer cells. *Chemical Communications* **2017**, 53 (82), 11318-11321.
14. Gehrman, M.; Stangl, S.; Foulds, G. A.; Oellinger, R.; Breuninger, S.; Rad, R.; Pockley, A. G.; Multhoff, G., Tumor Imaging and Targeting Potential of an Hsp70-Derived 14-Mer Peptide. *PLOS ONE* **2014**, 9 (8), e105344.
15. Khalil, A. A.; Kabapy, N. F.; Deraz, S. F.; Smith, C., Heat shock proteins in oncology: Diagnostic biomarkers or therapeutic targets? *Biochimica et Biophysica Acta (BBA) - Reviews on Cancer* **2011**, 1816 (2), 89-104.
16. Murphy, M. E., The HSP70 family and cancer. *Carcinogenesis* **2013**, 34 (6), 1181-1188.
17. Laufen, T.; Mayer, M. P.; Beisel, C.; Klostermeier, D.; Mogk, A.; Reinstein, J.; Bukau, B., Mechanism of regulation of Hsp70 chaperones by DnaJ cochaperones. *Proceedings of the National Academy of Sciences* **1999**, 96 (10), 5452.
18. McKeon, M. A.; Egan, A.; Chandanshive, J.; McMahon, H.; Griffith, M. D., Novel Improved Synthesis of HSP70 Inhibitor, Pifithrin- $\mu$ . In Vitro Synergy Quantification of

Pifithrin- $\mu$  Combined with Pt Drugs in Prostate and Colorectal Cancer Cells. *Molecules* **2016**, *21* (7).

19. Abramkin, S.; Valiahdi, S. M.; Jakupec, M. A.; Galanski, M.; Metzler-Nolte, N.; Keppler, B. K., Solid-phase synthesis of oxaliplatin-TAT peptide bioconjugates. *Dalton Trans.* **2012**, *41* (10), 3001-5.
20. Feazell, R. P.; Nakayama-Ratchford, N.; Dai, H.; Lippard, S. J., Soluble Single-Walled Carbon Nanotubes as Longboat Delivery Systems for Platinum(IV) Anticancer Drug Design. *Journal of the American Chemical Society* **2007**, *129* (27), 8438-8439.
21. Sommerfeld, N. S.; Hejl, M.; Klose, M. H. M.; Schreiber Brynzak, E.; Bileck, A.; Meier, S. M.; Gerner, C.; Jakupec, M. A.; Galanski, M.; Keppler, B. K., Low Generation Polyamidoamine Dendrimers as Drug Carriers for Platinum(IV) Complexes. *European Journal of Inorganic Chemistry* **2016**, *2017* (12), 1713-1720.
22. Merrifield, R. B., Solid Phase Peptide Synthesis. I. The Synthesis of a Tetrapeptide. *Journal of the American Chemical Society* **1963**, *85* (14), 2149-2154.
23. Carpino, L. A.; Han, G. Y., 9-Fluorenylmethoxycarbonyl amino-protecting group. *The Journal of Organic Chemistry* **1972**, *37* (22), 3404-3409.
24. Jones, J., *Amino Acid and Peptide Synthesis*. 2nd ed.; Oxford University Press: 2002.
25. Carpino, L. A., 1-Hydroxy-7-azabenzotriazole. An efficient peptide coupling additive. *Journal of the American Chemical Society* **1993**, *115* (10), 4397-4398.
26. Iwasawa, T.; Wash, P.; Gibson, C.; Rebek, J., Reaction of an Introverted Carboxylic Acid with Carbodiimide. *Tetrahedron* **2007**, *63* (28), 6506-6511.
27. Wehrstedt, K. D.; Wandrey, P. A.; Heitkamp, D., Explosive properties of 1-hydroxybenzotriazoles. *J Hazard Mater* **2005**, *126* (1-3), 1-7.
28. Still, B. M.; Kumar, P. G. A.; Aldrich-Wright, J. R.; Price, W. S., 195Pt NMR-theory and application. *Chemical Society Reviews* **2007**, *36* (4), 665-686.
29. Parker, J. P.; Devocelle, M.; Morgan, M. P.; Marmion, C. J., Derivatisation of buforin IIb, a cationic henicosapeptide, to afford its complexation to platinum(ii) resulting in a novel platinum(ii)-buforin IIb conjugate with anti-cancer activity. *Dalton Transactions* **2016**, *45* (33), 13038-13041.
30. Balin-Gauthier, D.; Delord, J.-P.; Rochaix, P.; Mallard, V.; Thomas, F.; Hennebelle, I.; Bugat, R.; Canal, P.; Allal, C., In vivo and in vitro antitumor activity of oxaliplatin in combination with cetuximab in human colorectal tumor cell lines expressing different level of EGFR. *Cancer Chemotherapy and Pharmacology* **2006**, *57* (6), 709-718.
31. Goschl, S.; Schreiber-Brynzak, E.; Pichler, V.; Cseh, K.; Heffeter, P.; Jungwirth, U.; Jakupec, M. A.; Berger, W.; Keppler, B. K., Comparative studies of oxaliplatin-based platinum(iv) complexes in different in vitro and in vivo tumor models. *Metallomics* **2017**, *9* (3), 309-322.
32. Florindo, P. R.; Pereira, D. M.; Borralho, P. M.; Rodrigues, C. M. P.; Piedade, M. F. M.; Fernandes, A. C., Cyclopentadienyl-Ruthenium(II) and Iron(II) Organometallic Compounds with Carbohydrate Derivative Ligands as Good Colorectal Anticancer Agents. *Journal of Medicinal Chemistry* **2015**, *58* (10), 4339-4347.
33. Varbanov, H. P.; Valiahdi, S. M.; Kowol, C. R.; Jakupec, M. A.; Galanski, M.; Keppler, B. K., Novel tetracarboxylatoplatinum(iv) complexes as carboplatin prodrugs. *Dalton Transactions* **2012**, *41* (47), 14404-14415.
34. Gabano, E.; Ravera, M.; Zanellato, I.; Tinello, S.; Gallina, A.; Rangone, B.; Gandin, V.; Marzano, C.; Bottone, M. G.; Osella, D., An unsymmetric cisplatin-based Pt(iv) derivative containing 2-(2-propynyl)octanoate: a very efficient multi-action antitumor prodrug candidate. *Dalton Transactions* **2017**, *46* (41), 14174-14185.
35. Raveendran, R.; Braude, J. P.; Wexselblatt, E.; Novohradsky, V.; Stuchlikova, O.; Brabec, V.; Gandin, V.; Gibson, D., Pt(iv) derivatives of cisplatin and oxaliplatin with phenylbutyrate axial ligands are potent cytotoxic agents that act by several mechanisms of action. *Chemical Science* **2016**, *7* (3), 2381-2391.
36. Zajac, J.; Kostrehunova, H.; Novohradsky, V.; Vrana, O.; Raveendran, R.; Gibson, D.; Kasparkova, J.; Brabec, V., Potentiation of mitochondrial dysfunction in tumor cells by

- conjugates of metabolic modulator dichloroacetate with a Pt(IV) derivative of oxaliplatin. *Journal of Inorganic Biochemistry* **2016**, *156*, 89-97.
37. Ravera, M.; Gabano, E.; Zanellato, I.; Bonarrigo, I.; Alessio, M.; Arnesano, F.; Galliani, A.; Natile, G.; Osella, D., Cellular trafficking, accumulation and DNA platination of a series of cisplatin-based dicarboxylato Pt(IV) prodrugs. *Journal of Inorganic Biochemistry* **2015**, *150*, 1-8.
  38. Johnstone, T. C.; Suntharalingam, K.; Lippard, S. J., The Next Generation of Platinum Drugs: Targeted Pt(II) Agents, Nanoparticle Delivery, and Pt(IV) Prodrugs. *Chemical reviews* **2016**, *116* (5), 3436-3486.
  39. Göschl, S.; Varbanov, H. P.; Theiner, S.; Jakupec, M. A.; Galanski, M.; Keppler, B. K., The role of the equatorial ligands for the redox behavior, mode of cellular accumulation and cytotoxicity of platinum(IV) prodrugs. *Journal of Inorganic Biochemistry* **2016**, *160*, 264-274.
  40. Shi, Y.; Liu, S.-A.; Kerwood, D. J.; Goodisman, J.; Dabrowiak, J. C., Pt(IV) complexes as prodrugs for cisplatin. *Journal of Inorganic Biochemistry* **2012**, *107* (1), 6-14.
  41. Zhang Jenny, Z.; Bonnitcho, P.; Wexselblatt, E.; Klein Alice, V.; Najajreh, Y.; Gibson, D.; Hambley Trevor, W., Facile Preparation of Mono , Di and Mixed Carboxylato Platinum(IV) Complexes for Versatile Anticancer Prodrug Design. *Chemistry óA European Journal* **2012**, *19* (5), 1672-1676.
  42. Hambley, T. W.; Battle, A. R.; Deacon, G. B.; Lawrenz, E. T.; Fallon, G. D.; Gatehouse, B. M.; Webster, L. K.; Rainone, S., Modifying the properties of platinum(IV) complexes in order to increase biological effectiveness. *Journal of Inorganic Biochemistry* **1999**, *77* (1), 3-12.
  43. Choi, S.; Filotto, C.; Bisanzo, M.; Delaney, S.; Lagasee, D.; Whitworth, J. L.; Jusko, A.; Li, C.; Wood, N. A.; Willingham, J.; Schwenker, A.; Spaulding, K., Reduction and Anticancer Activity of Platinum(IV) Complexes. *Inorganic Chemistry* **1998**, *37* (10), 2500-2504.
  44. Nemirovski, A.; Kasherman, Y.; Tzaraf, Y.; Gibson, D., Reduction of cis,trans,cis-[PtCl<sub>2</sub>(OCOCH<sub>3</sub>)<sub>2</sub>(NH<sub>3</sub>)<sub>2</sub>] by Aqueous Extracts of Cancer Cells. *Journal of Medicinal Chemistry* **2007**, *50* (23), 5554-5556.
  45. Tolan, D.; Gandin, V.; Morrison, L.; El-Nahas, A.; Marzano, C.; Montagner, D.; Erxleben, A., Oxidative Stress Induced by Pt(IV) Pro-drugs Based on the Cisplatin Scaffold and Indole Carboxylic Acids in Axial Position. *Scientific Reports* **2016**, *6*, 29367.
  46. Dubikovskaya, E. A.; Thorne, S. H.; Pillow, T. H.; Contag, C. H.; Wender, P. A., Overcoming multidrug resistance of small-molecule therapeutics through conjugation with releasable octaarginine transporters. *Proceedings of the National Academy of Sciences* **2008**, *105* (34), 12128.

## **Chapter 5**

**Development of gold(III) and platinum(II) complexes using a novel and versatile 1,4-disubstituted 1,2,3-triazole based ligand possessing diverse secondary and tertiary coordinating groups**

## Abstract

A novel 1,4-disubstituted 1,2,3-triazole-based ligand, 2-(4-(pyridin-2-yl)-1*H*-1,2,3-triazol-1-yl)propane-1,3-diamine (PTPD), which possesses pyridyl and diamino secondary and tertiary coordinating groups was synthesised in excellent yield. The reactivity of 2-(1-phenyl-1*H*-1,2,3-triazol-4-yl)pyridine (PTP), di-*tert*-butyl (2-azidopropane-1,3-diyl)dicarbamate (BOC<sub>2</sub>-PTPD) and PTPD.3HCl were investigated with Au(III) and Pt(II) precursors. Analysis, including X-ray crystal structures of [Au(III)Cl<sub>3</sub>(PTP)], [Au(III)Cl<sub>2</sub>(PTPD)][Au(I)Cl<sub>2</sub>][OH]{[NaAuCl<sub>4</sub>.2H<sub>2</sub>O]}<sub>n</sub> and [Pt(II)Cl<sub>2</sub>(PTPDH<sub>2</sub>)][PtCl<sub>4</sub>] revealed that PTPD (i) may serve as a monodentate ligand for Au(III), coordinating to the metal centre *via* the pyridine nitrogen only, (ii) preferentially coordinates Au(III) *via* the bidentate diamino group over the monodentate pyridine group, (iii) can coordinate Pt(II) in a bidentate fashion *via* the pyridyl nitrogen and the triazole N3 and (iv) can bridge two Pt(II) centres through bidentate chelation at the diamino group and bidentate chelation *via* the pyridyl nitrogen and the triazole N3. PTPD represents a versatile ligand template for the development of mixed metal complexes. The synthesis and analysis of six complexes is described herein, demonstrating the versatility of substituted triazoles as an interesting class of polydentate ligands.

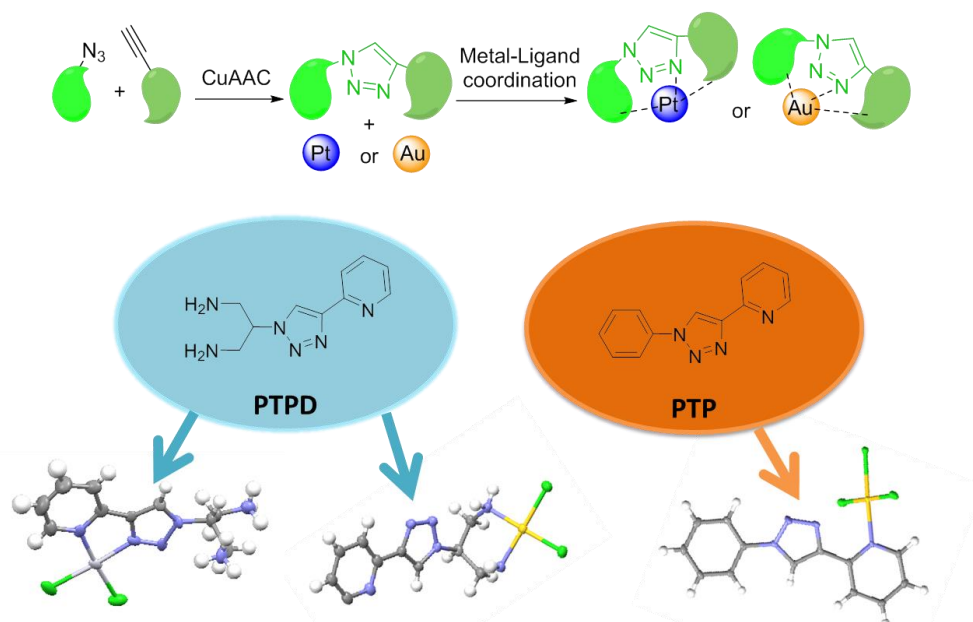


**Figure 5.1:** Graphical abstract. Crystal structures solved utilising click 1,2,3-triazole ligands PTP and PTPD coordinated to Pt(II) and Au(III).

## Introduction

Recently there has been much interest in the development of novel triazole based ligands, to construct for example a diverse range of fascinating coordination complexes,<sup>1-5</sup> including supramolecular cage structures<sup>6-7</sup>, cylinders<sup>8-10</sup> and polymers.<sup>11</sup> Triazoles represent unique building blocks and in turn, triazole coordination chemistry is strongly associated with a variety of applications including drug development, catalysis, metal ion sensing and imaging.<sup>1-2, 5</sup>

1,4-disubstituted 1,2,3-triazole based ligands are largely synthesized by the well-known copper catalysed 1,3-dipolar cycloaddition, the Cu alkyne-azide cycloaddition (CuAAC) reaction between an azide and terminal alkyne, **Figure 5.2A**.<sup>2</sup>

The 1,2,3-triazole heterocyclic ring readily coordinates metal centres through a variety of modes; N2, N3 and C5 coordination for instance, **Figure 5.2Ba-d**. Furthermore, selective alkylation (e.g. methylation) of 1,2,3-triazoles generates the corresponding 1,2,3-triazolylidenes, which can be metalated to give the corresponding 1,2,3-triazolylidene coordination complexes, **Figure 5.2Be**.<sup>1</sup>

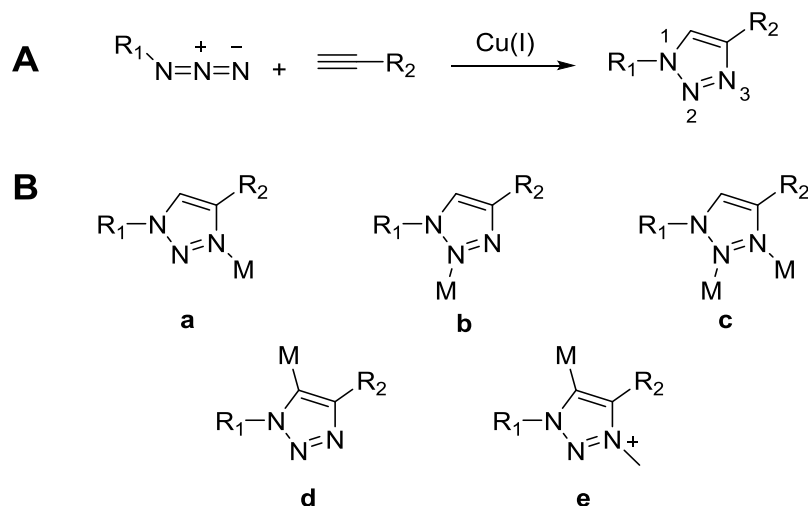


**Figure 5.2:** Copper catalysed alkyne-azide cycloaddition (A) and coordination modes associated with 1,4-disubstituted 1,2,3-triazole ligands (B).

Triazoles are ideally suited to build countless multidentate ligand systems, given the high synthetic flexibility associated with click chemistry.<sup>1-2</sup> Secondary coordination groups can be introduced at the 1 and/or 4-positions to supplement the inherent coordinating ability of the triazole group. For example, 1,2,3-triazoles have been

tethered to nitrogen containing heterocycles such as pyridine, pyrimidine and pyrazine rings, and coordination complexes of numerous metal centres have been reported, as demonstrated for pyridyl substituted triazoles in **Figure 5.3**.<sup>5, 12-16</sup>

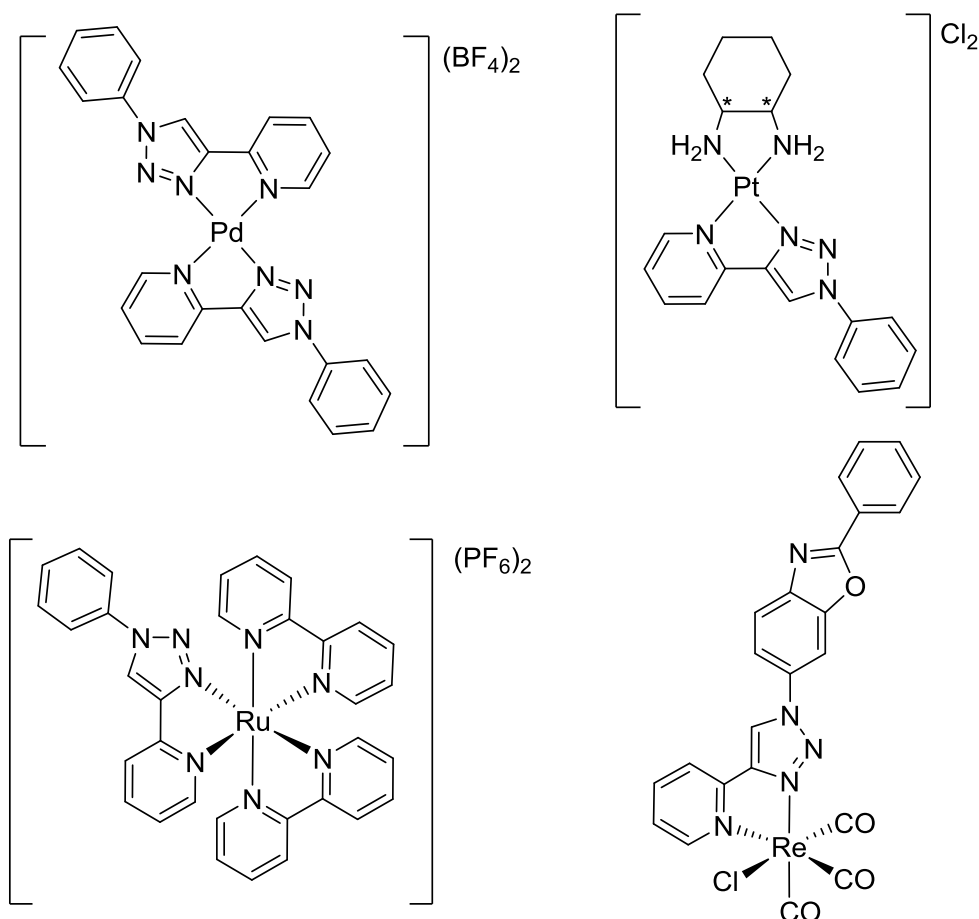


**Figure 5.3:** Representative examples of 2-pyridyl 1,2,3-triazoles Pd(II), Pt(II) Ru(II) and Re(I) coordination complexes.<sup>9, 13-14 15</sup>

In addition to the “regular” coordination *via* the N3 of 1,4-disubstituted 1,2,3-triazoles, N2 coordination is observed in the case of “inverse” triazoles, which are essentially generated by switching the R groups associated with the original alkyne and azide (**Figure 5.4**).

Inverse 1,2,3-triazole ligands such as 2-(4-phenyl-1*H*-1,2,3-triazole-1-yl)pyridine have also been developed and their palladium(II), platinum(II), rhenium(I) and ruthenium(II) complexes synthesized, **Figure 5.4**.<sup>17</sup>

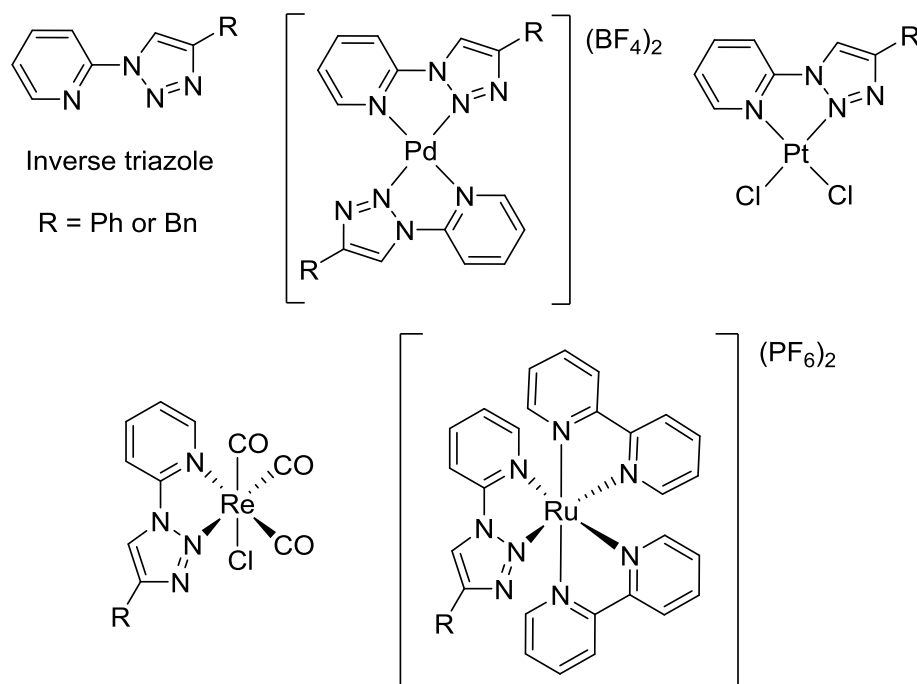


**Figure 5.4:** Structure of inverse 1,4-disubstituted 2-pyridyl 1,2,3 triazole ligands and their palladium(II), platinum(II), rhenium(I) and ruthenium(II) complexes.<sup>17</sup>

### Rationale

Novel ligand design and synthesis is fundamental to coordination chemistry and the development of coordination complexes with applications in drug development,<sup>16, 18</sup> catalysis,<sup>5</sup> and photophysics for example.<sup>19-21</sup> A novel 1,4-disubstituted 1,2,3-triazole based ligand, 2-(4-(pyridin-2-yl)-1*H*-1,2,3-triazol-1-yl)propane-1,3-diamine (PTPD) was developed, and its corresponding Au(III) and Pt(II) complexes synthesised to demonstrate that this original ligand is both flexible and versatile and could serve as a polydentate ligand for the synthesis of mixed metal complexes.



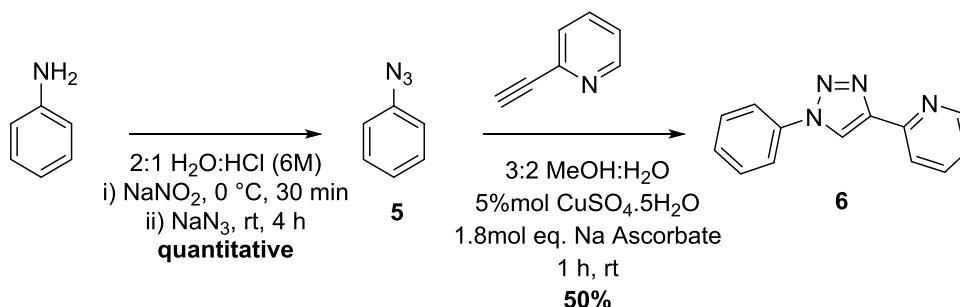
## Chapter Aims

- ◁ To synthesise and characterise a novel polydentate 1,4-disubstituted 1,2,3-triazole ligand *via* CuAAC.
- ◁ To synthesise and characterise Pt(II) and Au(III) complexes of the novel ligand.
- ◁ To establish the coordination modes associated with the novel ligand.

## Synthesis of click ligand complexes

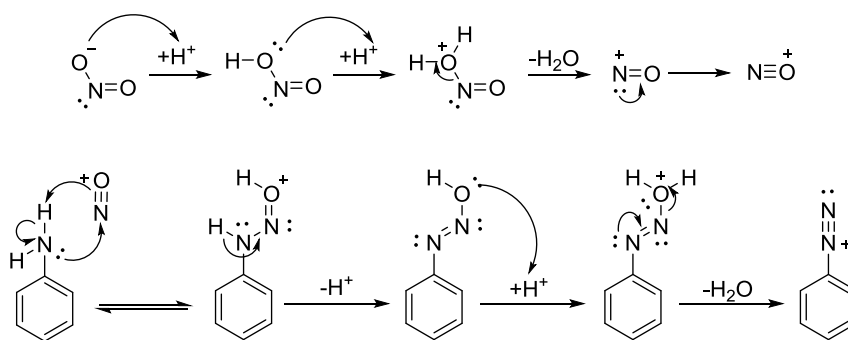
### PTP synthesis

The synthesis of 2-(1-phenyl-1*H*-1,2,3-triazol-4-yl)pyridine (PTP) **6** was carried out in 2 steps, (**Scheme 5.1**). Firstly azidobenzene (**5**) was synthesised from aniline *via* a diazonium salt intermediate and secondly, PTP was generated from azidobenzene *via* CuAAC with 2-ethynylpyridine as previously reported.<sup>12</sup>

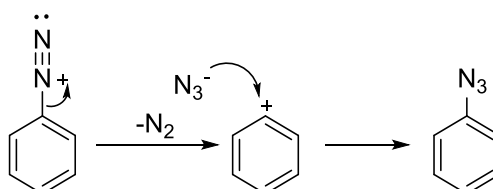


**Scheme 5.1:** Synthetic route to PTP **6**.

The mechanism for the synthesis of **5** is outlined below in **Scheme 5.2** and **5.3**, which describe formation of the diazonium salt and the nucleophilic aromatic substitution of the diazonium salt by N<sub>3</sub><sup>−</sup> to give azidobenzene.



**Scheme 5.2:** Reaction scheme demonstrating diazonium salt formation.



**Scheme 5.3:** Reaction scheme demonstrating the formation of azidobenzene by S<sub>N</sub>1 nucleophilic aromatic substitution.

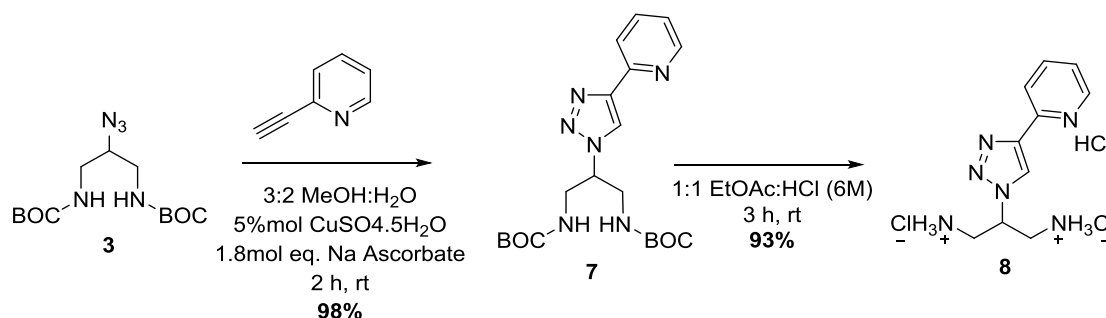
**5** was characterised by  $^1\text{H}$  NMR and  $^{13}\text{C}$  ( $\text{CDCl}_3$ ) spectroscopy, fully agreeing with previously reported values. In the  $^1\text{H}$  NMR spectrum for example, the notable loss of the single diagnostic peak of the amino protons found in aniline was observed.

Compound **5** undergoes CuAAC with 2-ethynylpyridine to form PTP (**6**). The mechanism of CuAAC is outlined in **Scheme 1.4**. (Chapter 1), showing how Cu assists in the regioselective formation of triazole rings with 1,4-disubstituted R groups.

**6** was characterised by  $^1\text{H}$  and  $^{13}\text{C}$  NMR ( $\text{CDCl}_3$ ) spectroscopy and the data is in full agreement with the previously reported synthesis.<sup>12</sup>

### PTPD synthesis

The synthesis of 2-(4-(pyridin-2-yl)-1*H*-1,2,3-triazol-1-yl)propane-1,3-diamine (PTPD) **8** was carried out in 2 steps starting with reaction of **3** (**Scheme 5.4**) with 2-ethynylpyridine using standard CuAAC methods followed by BOC deprotection using HCl in a similar manner to a method outlined in **Chapter 3**.



**Scheme 5.4:** Synthetic route to PTPD.3HCl **8**.

**7** was characterised by  $^1\text{H}$  NMR ( $\text{CDCl}_3$ ) spectroscopy, where a single peak at 8.60 ppm correlates for the one proton of the newly formed triazole ring, serving as the diagnostic signal. ESI-MS in positive mode aided the identification of the  $\text{M}+\text{H}$  with a mass peak of 419.3 a.m.u.

**8** was characterised by  $^1\text{H}$  and  $^{13}\text{C}$  NMR ( $\text{D}_2\text{O}$ ) spectroscopy, where the absence of the broad single peak at 1.43 ppm in the  $^1\text{H}$  NMR spectrum and the large signal at 28.5 ppm in the  $^{13}\text{C}$  NMR spectrum of **7** demonstrated successful BOC deprotection. The triazole proton serves as an important diagnostic signal and is found as a singlet downfield at 9.12 ppm. Three signals associated with the pyridyl protons are observed between 8.01 and 8.78 ppm and integrated for four in total as required. The

1,3-diaminopropane (DAP) methine proton and methylene protons are found at 5.55 and 3.81 ppm respectively. The  $^{13}\text{C}$  NMR spectrum exhibited the required nine signals including the triazole C5 carbon found at 127.3 ppm, as determined by C-H COSY (**Figure 5.5**). ESI-MS in positive mode aided the identification of PTPD+H and PTPD+Na with mass peaks of 219.1 and 241.1 a.m.u. Elemental analysis (EA) for **8** is consistent with the theoretical value. Furthermore, **8** features as a ligand in the X-ray crystal structure described below.

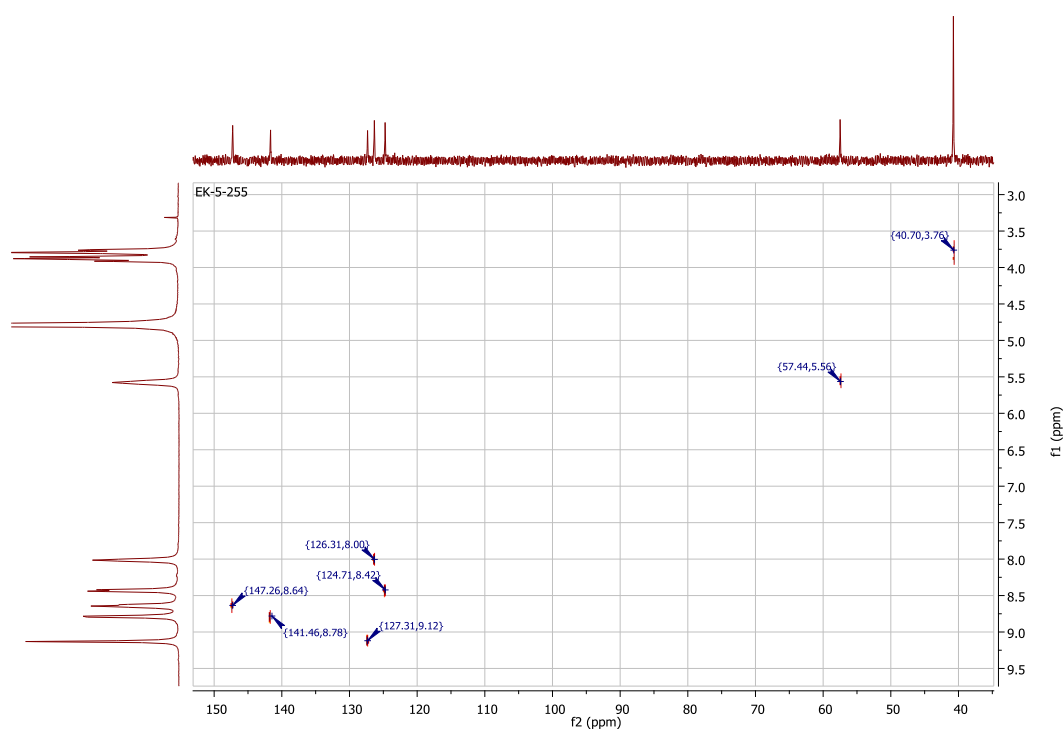
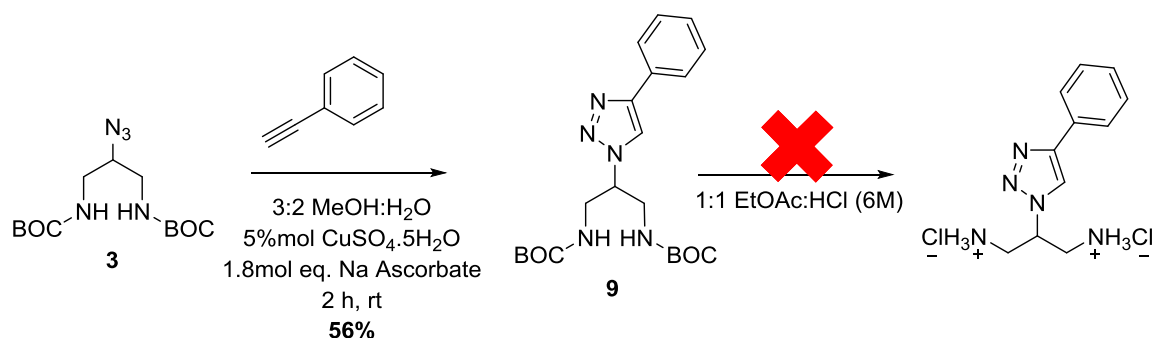


**Figure 5.5:** CH correlation NMR of **8** identifying the C4 carbon of the triazole ring at 127.3 ppm, correlating to the proton at 9.12 ppm.

### BOC<sub>2</sub>-PhTPD synthesis

The synthesis of di-*tert*-butyl (2-(4-(phenyl)-1*H*-1,2,3-triazol-1-yl)propane-1,3-diyl)dicarbamate (BOC<sub>2</sub>-PhTPD) **9** was carried out in a single step, starting with **3** (**Scheme 5.5**) using standard CuAAC methods.



**Scheme 5.5:** Synthetic route to BOC<sub>2</sub>-PhTPD **9**, displaying the unsuccessful BOC deprotection reaction.

**9** was characterised by <sup>1</sup>H NMR (CDCl<sub>3</sub>) spectroscopy, where a single peak at 7.83 ppm correlates for the one proton of the newly formed triazole ring, serving as the diagnostic signal. The five protons of the phenyl group were identified by the three resonances found at 7.81, 7.43 and 7.34, integrating in the ratio 2:2:1. In addition, the BOC peak which integrates for 18 protons was found at 1.43 ppm. The <sup>13</sup>C NMR spectrum also displays the desired number of carbon peaks.

The BOC deprotection method previously used to generate the hydrochloride salts of compounds **4** and **8** was unsuccessful in this instance and the synthesis was abandoned. Alternate BOC deprotection reactions using varied reaction times, higher and lower HCl concentrations and using TFA deprotection methods were also unsuccessful.

## Synthesis of Metal PTP and PTPD complexes

Using click ligands PTP and PTPD (**6** and **8**), a number of Pt(II) and Au(III) complexes were generated in single step reactions with a metal precursor complex.

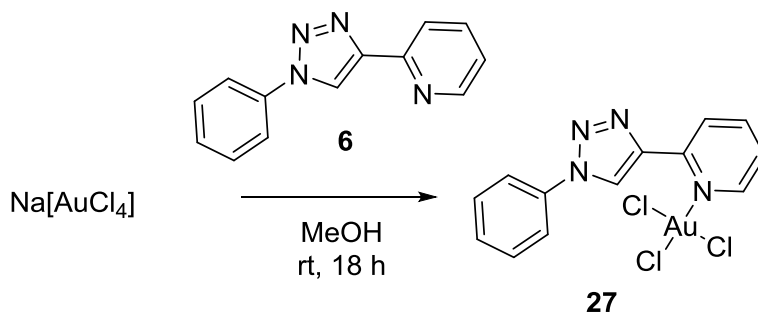
### Synthesis of Au complexes

#### [AuCl<sub>3</sub>(PTP)] synthesis

[AuCl<sub>3</sub>(PTP)] was synthesised by Mr. Zehao Zhou, a visiting exchange student from Soochow University, China, during a research placement with the Griffith group and a student I was tasked with supervising.

**6** was synthesized to serve as a model ligand to investigate the reactivity of Na[Au(III)Cl<sub>4</sub>] with the 2-pyridyl-1,2,3-triazole moiety (**8**), which also possesses the additional DAP group.

[AuCl<sub>3</sub>(PTP)], **27** was synthesised in a single step (**Scheme 5.6**) by reacting Na[AuCl<sub>4</sub>] with PTP in MeOH at rt for 18 h. The complex readily forms as a precipitate which was collected by vacuum filtration in good yield (80 %).



**Scheme 5.6:** Synthetic route to [AuCl<sub>3</sub>(PTP)].

The characterisation was informed by <sup>1</sup>H NMR (Acetone-*d*<sub>6</sub>) spectroscopy, ESI-MS, EA, X-ray crystallography and FT-IR. In the <sup>1</sup>H NMR spectrum, the triazole proton is the most downfield signal as a singlet at 9.63 ppm. Six signals associated with the pyridyl and phenyl protons are observed between 9.31 and 7.62 ppm and integrated for nine in total as required. ESI-MS in positive mode demonstrated ion fragments associated with PTP+H and AuCl<sub>3</sub>+H with mass peaks of 223.1 and 303.2 a.m.u. respectively. EA for **27** is consistent with values required for [AuCl<sub>3</sub>(PTP)].0.5MeOH. In addition, the X-ray crystal structure of the complex was solved as seen in **Figure 5.6**.

**X-ray crystal analysis of [Au(III)(PTP)Cl<sub>3</sub>] (27)**

The ORTEP structure of **27** is shown in **Figures 5.6** and **5.7**, while the data relating to the crystal and refinement patterns is reported in **Table 5.4**. The square planar Au(III) is coordinated to the pyridine nitrogen with Au-N = 2.072(3) Å, **Figure 5.6**. A long-range interaction with the triazole nitrogen (N8) is observed, N...Au = 2.853(4) Å (**Figure 5.7**), similar to that seen in [Au(III)Cl<sub>3</sub>Rbipy] (R = (1-phenyl)ethyl, N...Au = 2.758 Å).<sup>22</sup> There is also a twist between the pyridine and triazole rings of 23.427(12) Å to accommodate this interaction, slightly shallower than that of ca. 28.4 Å in [Au(III)Cl<sub>3</sub>Rbipy]. The coordination sphere of the Au(III) centre is completed as a symmetry generated dimer with long Au-Cl intermolecular contacts of 3.6911(17) Å and the dimer is stabilized by a weak bifurcated C-H...Cl interaction ( $d_{C...Cl} = 2.73\text{Å}, 2.77\text{Å}$ ), **Figure 5.7**. This type of dimerization has been seen previously in the literature<sup>23-32</sup> with a median Au...Cl distance of 3.65 Å. The coordination geometry around the Au(III) centre is a distorted octahedron.

The molecular structure of [Au(III)(PTP)Cl<sub>3</sub>] shown in **Figure 5.6** shows Au(III) in a square planar configuration. The bond angles of the Au substituents N(1)-Au(1)-Cl(1), N(1)-Au(1)-Cl(3), Cl(2)-Au(1)-Cl(1) and Cl(2)-Au(1)-Cl(3) are approximately 90 ° respectively, as expected (**Table 5.1**).

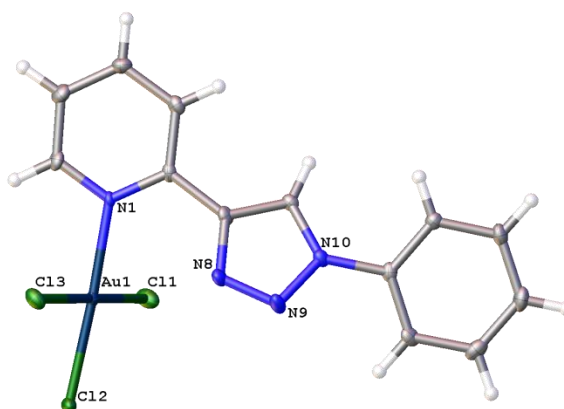


**Figure 5.6:** Molecular structure of [Au(III)Cl<sub>3</sub>(PTP)], (**27**) with selected atom labelling. Atomic displacement shown at 50% probability.

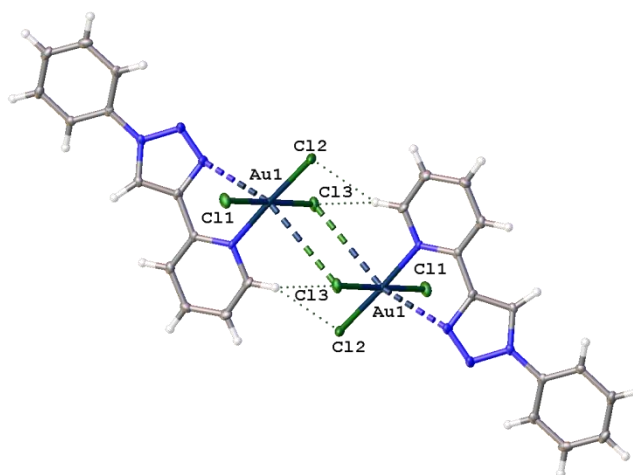


**Figure 5.7:** Symmetry generated dimer of  $[\text{Au(III)Cl}_3(\text{PTP})]$  (**27**) (symmetry generation = 1-x, 1-y, 2-z). Au-Cl intermolecular contacts are 3.6911(17) Å and the dimer is stabilized by a weak bifurcated C-H...Cl interaction ( $d_{\text{C}\cdots\text{Cl}} = 2.73\text{Å}$ ,  $2.77\text{Å}$ ). Octahedral coordination geometry for Au(III). Selected atoms labelled and displacement shown at 50% probability.

**Table 5.1.** Selected bond lengths [Å] and angles [°] determined for **27**.

Bond	Length Å	Bond	Angles °
Au(1)-N(1)	2.072(3)	N(1)-Au(1)-Cl(1)	90.29(10)
Au(1)-Cl(1)	2.2923(13)	N(1)-Au(1)-Cl(3)	90.22(10)
Au(1)-Cl(2)	2.2673(13)	Cl(2)-Au(1)-Cl(1)	89.32(5)
Au(1)-Cl(3)	2.2897(13)	Cl(2)-Au(1)-Cl(3)	90.10(5)
Au(1)-N(8)	2.853(4)	N(1)-Au(1)-Cl(2)	176.62(10)
Cl(3)-Au(1)#1	3.6911(17)	Cl(3)-Au(1)-Cl(1)	178.72(4)
		Au(1)-Cl(3)- Au(1)#1	100.34(5)



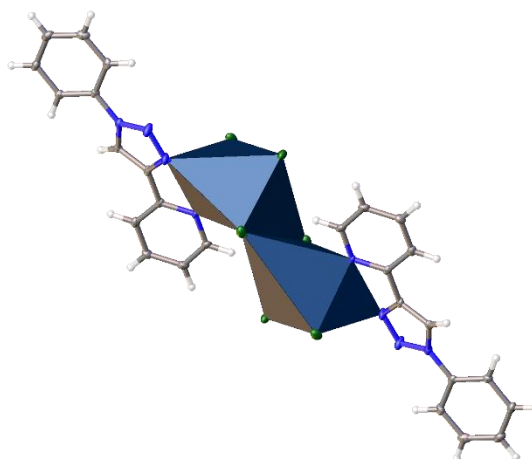
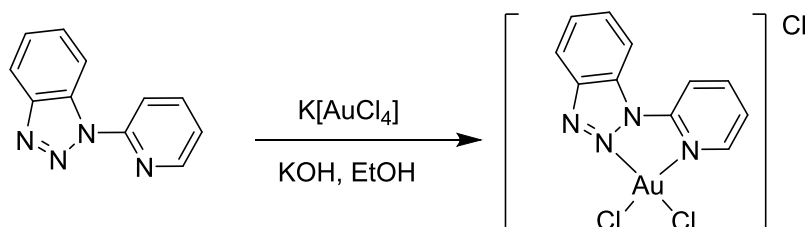


**Figure 5.8:** Polyhedral representation of coordination geometry around the Au(III) centre in **27** showing edge sharing. Atomic displacement shown at 50% probability.

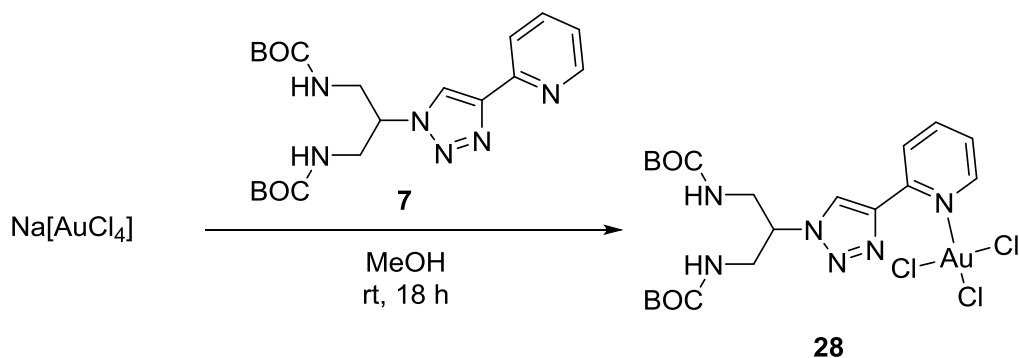
While there are multiple reports in the literature of Au(I) 1,2,3-triazoylidene complexes,<sup>33-35</sup> to the best of our knowledge there is only one report in the literature describing Au(III) coordination to a triazole N2 or N3. Yang *et al.* reported the synthesis of an Au(III) complex of 1-(pyridin-2-yl)-1*H*-benzo[d][1,2,3]triazole (PBT), **Scheme 5.7**, as a catalyst for the synthesis of E-U-haloenones.<sup>36</sup> The complex, which features an inverse triazole with respect to the pyridine, was formulated as [AuCl<sub>2</sub>(PBT)]Cl as per elemental analysis and in turn the PBT ligand is proposed to act as a bidentate chelating ligand *via* the pyridine nitrogen and triazole N2 as per **Figure 5.6**. It is possible, given the crystal structure described here within, that the Au(III) centre in the proposed [AuCl<sub>2</sub>(PBT)]Cl is coordinated to three chlorido ligands and not two, and if so, should be reformulated as [AuCl<sub>3</sub>(PBT)].



**Scheme 5.7:** Synthesis of [AuCl<sub>2</sub>(PBT)]Cl featuring the reported bidentate pyridyl triazole coordination.<sup>36</sup>

**[AuCl<sub>3</sub>(BOC<sub>2</sub>-PTPD)] synthesis**

Having established that Au(III) readily coordinates to **6** *via* the 2-pyridyl group only, we investigated the reactivity of Au(III) with **7**, where the DAP group is not free to coordinate to Au(III). [AuCl<sub>3</sub>(BOC<sub>2</sub>-PTPD)], **28** was synthesised in a single step (**Scheme 5.8**) by mixing Na[AuCl<sub>4</sub>] with **7** in MeOH at rt for 18 h. The complex readily forms as a precipitate which was collected by vacuum filtration as **28** in excellent yield (91%).



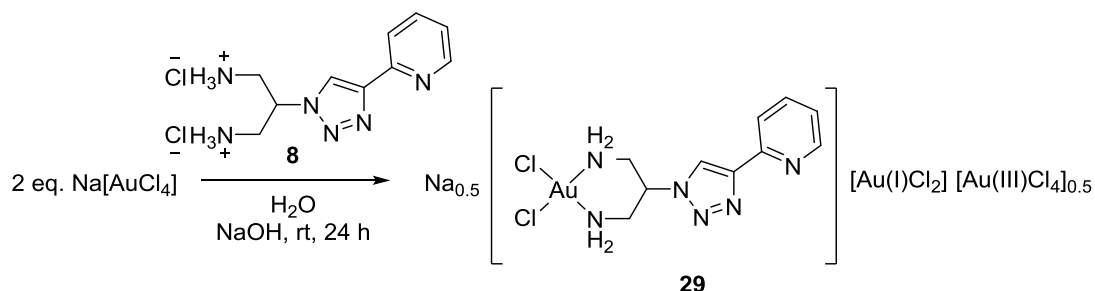
**Scheme 5.8:** Synthetic route to [AuCl<sub>3</sub>(BOC<sub>2</sub>-PTPD)].

The characterisation was informed by <sup>1</sup>H and <sup>13</sup>C NMR (acetone-*d*<sub>6</sub>) spectroscopy, ESI-MS, EA, and FT-IR. The resonances observed in the <sup>1</sup>H and <sup>13</sup>C NMR spectrum correlate with predicted values. ESI-MS in positive mode aided the identification of product ion fragments relating to AuCl<sub>2</sub>(BOC<sub>2</sub>-PTPD) (685.1 a.m.u.), AuCl<sub>2</sub>(BOC<sub>2</sub>-PTPD)-*t*Bu (629.1 amu.) and AuCl<sub>2</sub>(BOC<sub>2</sub>-PTPD)-2*t*Bu (573.1 a.m.u.). In the IR spectrum, the carbamate b(C=O) is evident at 1667 cm<sup>-1</sup>. EA for **28** is consistent with values for one ligand (**7**) and three chlorido ligands per Au(III) centre and the formula, [AuCl<sub>3</sub>(BOC<sub>2</sub>-PTPD)].1.25CH<sub>3</sub>OH. The X-ray crystal structure previously described for **27**, fully supports the proposition that **7** serves as a monodentate ligand in **28**, binding Au(III) by the pyridine nitrogen only and in turn Au(III) bound by three mono dentate chlorido ligands.

**Na<sub>0.5</sub>[Au(III)Cl<sub>2</sub>(PTPD)][Au(I)Cl<sub>2</sub>][Au(III)Cl<sub>4</sub>]<sub>0.5</sub> synthesis**

Having established that Au(III) readily reacts with both **6** and **7**, the reactivity of Au(III) with **8** was investigated as a fully deprotected multidentate ligand, PTPD, which possesses a pyridyl and a DAP group in addition to the 1,2,3-triazole. Na[AuCl<sub>4</sub>] was reacted in water with PTPD, post neutralisation of PTPD.3HCl (**8**)

with base, to rapidly give a yellow solid (**29**, **Scheme 5.9**), which is essentially insoluble in laboratory solvents, deuterated or not.



**Scheme 5.9:** Synthetic route to **29**.

The characterisation was informed by ESI-MS, X-ray crystallography and FT-IR. ESI-MS in positive mode aided the identification of the  $\text{AuCl}_2(\text{PTPD})^+$  with a mass peak of 485.1 a.m.u. Following determination of the X-ray crystal structure for **29**, examination of the EA revealed for the bulk solid that the analysis was consistent with the formula,  $\text{Na}_{0.5}[\text{Au}(\text{III})\text{Cl}_2(\text{PTPD})][\text{Au}(\text{I})\text{Cl}_2][\text{Au}(\text{III})\text{Cl}_4]_{0.5}$ . In addition, the crystal structure of the complex was solved as seen in **Figure 5.9**.

Given the poor solubility, it was fortunate that single crystals suitable for X-ray diffraction analysis were obtained by slow evaporation from the filtrate at rt. As expected, **8** preferentially coordinates Au(III) *via* the bidentate DAP group over the monodentate pyridine group (**Figure 5.9**).

#### X-ray crystal analysis of $[\text{Au}(\text{III})\text{Cl}_2(\text{PTPD})][\text{Au}(\text{I})\text{Cl}_2][\text{OH}][\{\text{NaAuCl}_4 \cdot 2\text{H}_2\text{O}\}]_n$

The ORTEP structure is reported in **Figure 5.9**, while the data relating to the crystal and refinement patterns is reported in **Table 5.4**.

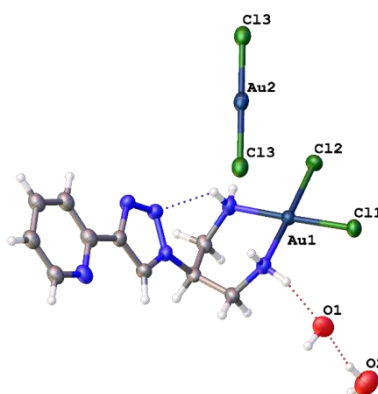


**Figure 5.9:** Hydrogen bonded hydroxide/ $\text{AuCl}_2$  (50% occupied each) charge balanced complex in **29**. The  $[\text{Au}(\text{III})\text{Cl}_2(\text{PTPD})][\text{Au}(\text{I})\text{Cl}_2][\text{OH}]$  complex also has

{[NaAuCl<sub>4</sub>.2H<sub>2</sub>O]}<sub>n</sub> site sharing with the hydroxide at a lower occupancy (**Figure 5.15b**). Selected labelling and atomic displacement shown at 50% probability.

**Table 5.2.** Selected bond lengths [Å] and angles [°] determined for **29**.

Bond	Length Å	Bond	Angles °
Au(1)-Cl(1)	2.2786(14)	Cl(2)-Au(1)-Cl(1)	90.63(5)
Au(1)-Cl(2)	2.2750(15)	N(14)-Au(1)-Cl(2)	88.69(14)
Au(1)-N(14)	2.037(5)	N(14)-Au(1)-N(16)	90.7(2)
Au(1)-N(16)	2.056(5)	N(16)-Au(1)-Cl(1)	89.89(14)
		N(14)-Au(1)-Cl(1)	178.11(15)
		N(16)-Au(1)-Cl(2)	178.18(15)

There are relatively few examples of [Au(III)Cl<sub>2</sub>]<sup>+</sup> coordinated by diamine groups in the literature. Three ethane diamine coordinated examples have been reported with chloride and nitrate counter ions.<sup>37-39</sup> Several cyclohexane diamine chloride complexes are also known.<sup>40-41</sup> In these complexes, Au-N distances are ca. 2.02 – 2.038 Å. The structure of **29**, **Figure 5.9**, features the ligand **8** with an Au(III)Cl<sub>2</sub><sup>+</sup> group coordinated by the bidentate DAP group. The Au-N distances, (2.037(5) and 2.053(5) Å) are slightly longer than in previous examples, but shorter than that seen in **27**. The Au(III)Cl<sub>2</sub>N<sub>2</sub> moiety is planar. The counter ions are the linear [Au(I)Cl<sub>2</sub>]<sup>-</sup> anion and hydroxide (O1), which are half occupied. The coordination sphere of the Au(III) centre is completed by a chloride from the linear [Au(I)Cl<sub>2</sub>]<sup>-</sup> anion (Cl3...Au1 = 3.238 Å) and a chloride from the neighbouring [Au(III)Cl<sub>2</sub>(PTPD)]<sup>+</sup> cation (Cl1, symmetry generation = x, 3/4-y, -1/2+z; Cl1...Au1 = 3.524 Å) forming a distorted elongated octahedron, as seen in **27** for the Au(III) centre, **Figure 5.6**. These cations pack tail to tail (pyridyl to pyridyl) and form a π stacked assembly (**Figure 5.10-5.12**). In the extended structure, the hydroxide anion is hydrogen bound to a water molecule and this forms a hydrogen bonded scaffold tying the [Au(III)Cl<sub>2</sub>(PTPD)][Au(I)Cl<sub>2</sub>] chains together along the bc plane (**Figure 5.10**). The partially occupied [NaAuCl<sub>4</sub>.2H<sub>2</sub>O]<sub>n</sub> (with disordered chlorides in three locations)

also form chains which run parallel to the b-axis and separate pairs of anion bridged cations of **29** (Figure 5.11).

The molecular structure of **29** ( $[\text{Au}(\text{III})\text{Cl}_2(\text{PTPD})][\text{Au}(\text{I})\text{Cl}_2][\text{OH}]\{\text{[NaAuCl}_4\cdot 2\text{H}_2\text{O}]\}_n$ ) (Figure 5.10) shows all Au(III) molecules coordinated to the PTPD ligand in a square planar configuration. In contrast to complex **27**, there was no coordination of Au(III) with the nitrogen of the 2-pyridinyl group. This is clear evidence for the stronger affinity of gold for the DAP amines over the pyridine nitrogen. The bond angles of the Au substituents Cl(2)-Au(1)-Cl(1), N(14)-Au(1)-Cl(2), N(14)-Au(1)-N(16), and N(16)-Au(1)-Cl(1) are approx.  $90^\circ$  respectively, demonstrating this geometry (Table 5.2.).

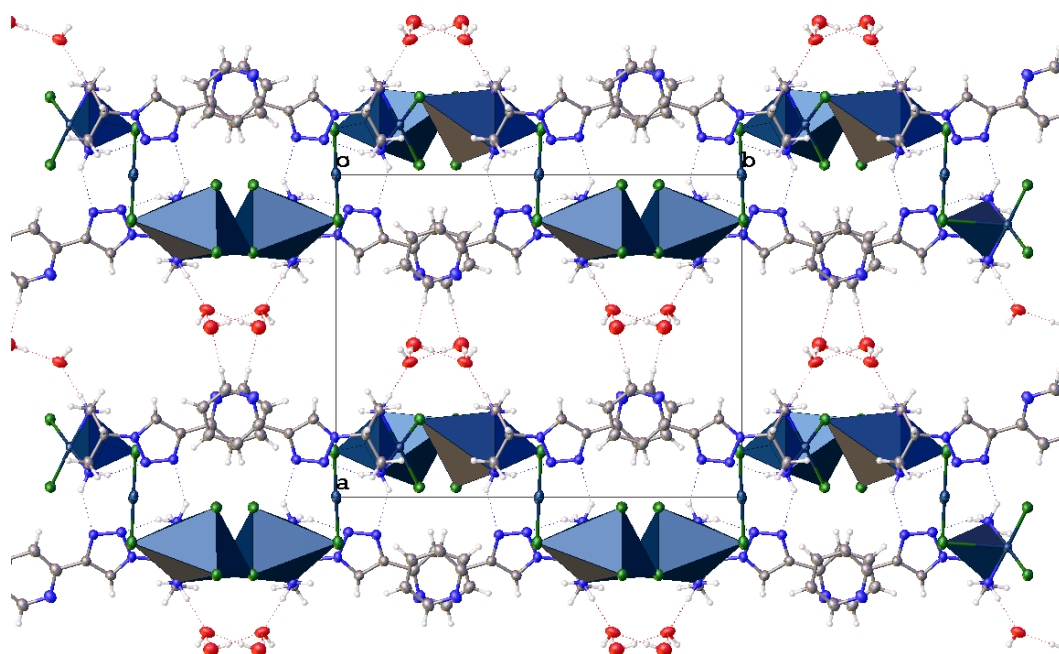


**Figure 5.10:** Extended structure of **29** showing the channel occupied in this instance with the water hydrogen bonded hydroxide ion. Polyhedra represent the coordination geometry around the Au(III) centres in  $[\text{AuCl}_2(\text{PTPD})]^+$  completed by bridging  $[\text{Au}(\text{I})\text{Cl}_2]^-$  cations. These Au(III) anions pack tail to tail (pyridyl to pyridyl) and form a  $\pi$  stacked assembly (N1-C6-C4-C4-C3-C2) to symmetry generated pyridyl ( $x, \frac{1}{2}-y, -1/2+z$ ) with a centroid to centroid distance = 3.588 Å (shift distance = 1.196 Å) and also to another symmetry generated pyridyl ( $x, \frac{1}{2}-y, \frac{1}{2}+z$ ) with a centroid to centroid distance = 3.588 Å (shift distance = 1.163 Å). Distorted octahedra and  $\pi$  stacking as well as hydrogen bonding combine to form 2 sheets linked by the  $[\text{Au}(\text{I})\text{Cl}_2]^-$  anion which extend parallel to the bc plane.

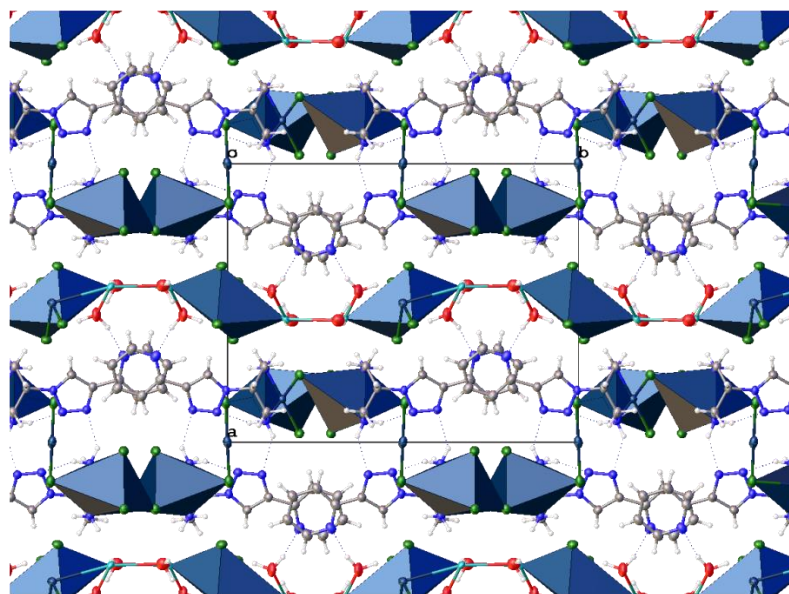


**Figure 5.11:** Extended structure of **29** showing the channel occupied in this instance with the partially occupied  $[\text{Na}(\text{AuCl}_4) \cdot 2\text{H}_2\text{O}]_n$  charge neutral species. Polyhedra represent the coordination geometry around the Au(III) centres in  $[\text{AuCl}_2(\text{PTPD})]^+$  completed by bridging  $[\text{Au}(\text{I})\text{Cl}_2]^-$  ions as well as the  $[\text{AuCl}_4]^-$  centres.

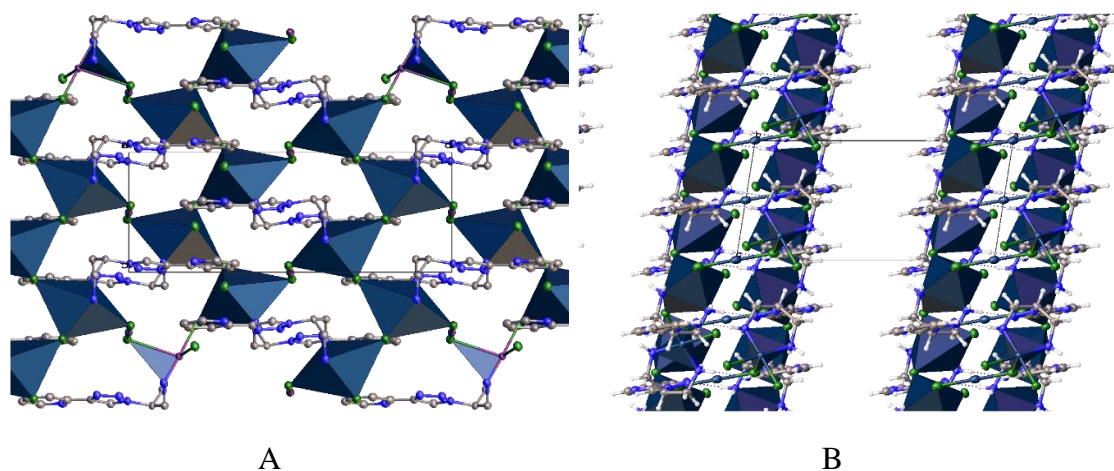


**Figure 5.12:** Polyhedral representation of **29** of the anion bridged Au(III)Cl<sub>2</sub> units in forming vertex shared distorted octahedral viewed normal to the (A) a-axis and (B) b-axis. Hydrogen bonded hydroxide and  $[\text{NaAuCl}_4 \cdot 2\text{H}_2\text{O}]_n$  chains omitted for clarity.

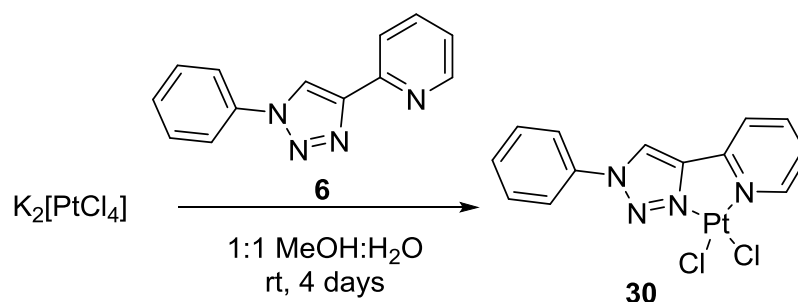
There are many reports in the literature in relation to the reduction of Au(III) centres on reaction with nucleophiles in aqueous solution,<sup>42-44</sup> including pyridine.<sup>45</sup> Specifically Đurović *et al.* reported that reaction of  $[\text{AuCl}_4]^-$  with equimolar amounts of pyridine gave the substitution product whereas in the presence of excess pyridine a second step involved reduction of Au(III) to Au(I).<sup>45</sup>

## Synthesis of Pt complexes

### [PtCl<sub>2</sub>(PTP)] synthesis

As highlighted above, **6** was synthesized to serve as a model ligand to investigate the reactivity of the 2-pyridyl 1,2,3-triazole moiety of **8**, which additionally possesses the DAP group. A [PtCl<sub>2</sub>(PTP)] complex and its X-ray crystal structure was previously reported by Schweinfurth *et al* (compound **30**).<sup>13</sup> The structure clearly highlights the propensity of the 2-pyridyl 1,2,3-triazole moiety to act as a bidentate ligand for Pt(II) centres (**30**, **Scheme 5.10**). Below are details of a novel synthetic route to the two previously reported methods.<sup>46-47</sup>

[PtCl<sub>2</sub>(PTP)], **30** was synthesised in a single step (**Scheme 5.10**) by mixing an aqueous solution of K<sub>2</sub>[PtCl<sub>4</sub>] with a methanolic solution of **6** for 4 days at rt. The complex readily forms as a precipitate which was collected by vacuum filtration as **30**. The previously reported synthesis described a 1 h stir of the ligand with [PtCl<sub>2</sub>(COD)] in DCM<sup>46</sup> and a 24 h reflux of [PtCl<sub>2</sub>(DMSO)<sub>2</sub>] with the ligand in MeOH.<sup>47</sup>



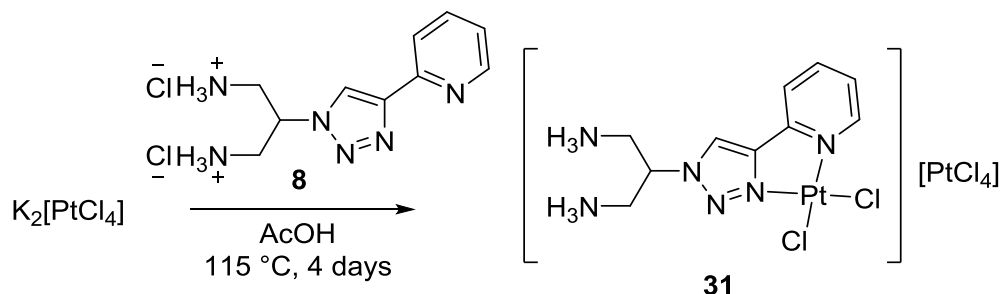
**Scheme 5.10:** Synthetic route to [PtCl<sub>2</sub>(PTP)], **30**.

The characterisation was informed by <sup>1</sup>H and <sup>13</sup>C (DMF-*d*<sub>7</sub>) NMR spectroscopy, ESI-MS, EA and FT-IR. EA for **30** is consistent with values for [PtCl<sub>2</sub>(PTP)].0.5CH<sub>3</sub>OH. All other analysis correlated with those previously reported.<sup>46-47</sup>

### [PtCl<sub>2</sub>(PTPDH<sub>2</sub>)] [PtCl<sub>4</sub>] synthesis

To demonstrate that the 2-pyridyl 1,2,3-triazole moiety in our novel multidentate ligand PTPD could also effectively bind to Pt(II) centres, K<sub>2</sub>[PtCl<sub>4</sub>] was reacted with **8** in AcOH under reflux for 4 days to give a precipitate upon cooling, as [Pt(II)Cl<sub>2</sub>(PTPDH<sub>2</sub>)] [PtCl<sub>4</sub>] (**31**, **Scheme 5.11**) in excellent yield (91%). In selecting

acetic acid as a solvent the DAP group was “protected” and less likely to coordinate Pt(II) as the amines are protonated in an acidic solvent.



**Scheme 5.11:** Synthetic route to  $[\text{PtCl}_2(\text{PTPDH}_2)][\text{PtCl}_4]$ , **31**.

The characterisation was informed by  $^1\text{H}$  NMR ( $\text{D}_2\text{O}$ ) spectroscopy, ESI-MS, X-ray crystallography and FT-IR. Of the resonances observed in the  $^1\text{H}$  NMR spectrum the triazole is the furthest downfield signal as a singlet at 8.98 ppm. Four poorly resolved signals associated with the pyridyl protons are observed between 8.66, 8.11, 7.99 and 7.43 ppm and integrate for four in total as required. The six ammonium protons are observed as a multiplet at 8.40 ppm. The methine and methylene protons are found at 5.40 and 3.42 ppm respectively. ESI-MS in positive mode aided the identification of the product ion fragments  $\text{PtCl}_2\text{PTPD}+\text{H}$  and  $\text{PtCl}_2\text{PTPD}+2\text{Na}$  with mass peaks of 484.6 and 532.4 a.m.u. respectively. EA for **31** is consistent with values for  $[\text{PtCl}_2(\text{PTPDH}_2)][\text{PtCl}_4].0.5\text{CH}_3\text{COOH}$ . In addition, crystals were obtained by slow filtration at rt and the structure was solved as seen in **Figure 5.13**.

#### X-ray crystal analysis of $[\text{Pt}(\text{II})\text{Cl}_2(\text{PTPD})][\text{PtCl}_4]$

The ORTEP structure of the major conformation of **31** is shown in **Figure 5.13**, while the data relating to the crystal and refinement patterns is reported in **Table 5.4**. In **31**, the metal chloride is coordinated to the pyridyl and triazole nitrogen atoms with Pt-N distances of 2.001(10), 2.16(3) and 1.994(10), 1.84(2) Å respectively. Pt-Cl distances are 2.284(3) and 2.290(3) Å for both complexes. The metal ligand moiety is essentially planar in both unique molecules in the structure. There are few congeners with substituents on the triazole (pyridyl,<sup>48</sup> phenyl,<sup>13</sup> hexyl<sup>49</sup>) reported in the literature. In these few examples, pyridyl N-Pt distances range from 2.028 - 2.047 Å, triazole N-Pt 1.986-1.994 Å and Pt-Cl 2.283-2.292 Å. Also in these complexes, the metal ligand moiety is essentially planar. In **31** however, the  $[\text{Pt}(\text{II})\text{Cl}_2(\text{PTPDH}_2)]^{2+}$  groups stack parallel to the b-axis in an ABCDA motif with a



separation of ca. 3.4 Å. The Pt atoms do not line directly over each other but are offset with a  $d_{\text{Pt}\dots\text{Pt}}$  of 3.308 and 3.588 Å. The anions  $[\text{PtCl}_4]^{2-}$  surround the stacks along the (001) plane.

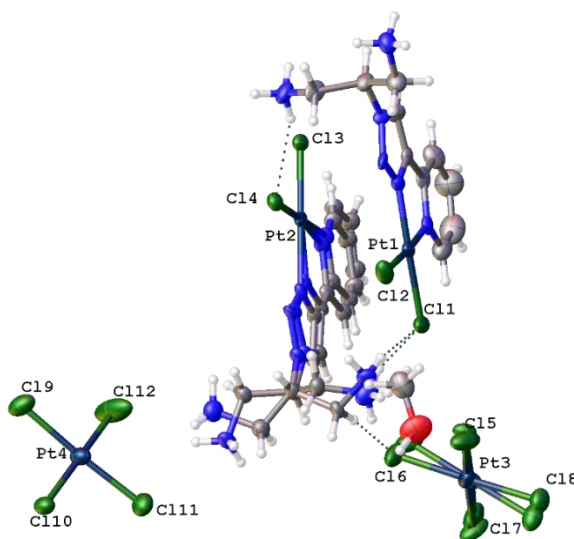


**Figure 5.13:** Disordered asymmetric unit of **31** showing the fully disordered ligand coordinated to Pt2, and the fully disordered anion  $[\text{PtCl}_4]^{2-}$ . MeOH is only partially occupied. Unresolved disordered solvent was also removed using SQUEEZE (approx. 5MeOH, 6H<sub>2</sub>O per unit cell).

**Table 5.3.** Selected bond lengths [Å] and angles [°] determined for **31**.

Bond	Length Å	Bond	Angles °
Pt(1)-N(1)	2.001(10)	N(1)-Pt(1)-Cl(1)	94.7(3)
Pt(1)-N(11)	1.994(10)	Cl(2)-Pt(1)-Cl(1)	90.14(14)
Pt(1)-Cl(1)	2.290(3)	N(11)-Pt(1)-N(1)	80.0(4)
Pt(1)-Cl(2)	2.284(4)	N(11)-Pt(1)-Cl(2)	95.2(3)
		N(1)-Pt(1)-Cl(2)	175.1(3)
		N(11)-Pt(1)-Cl(1)	174.6(3)

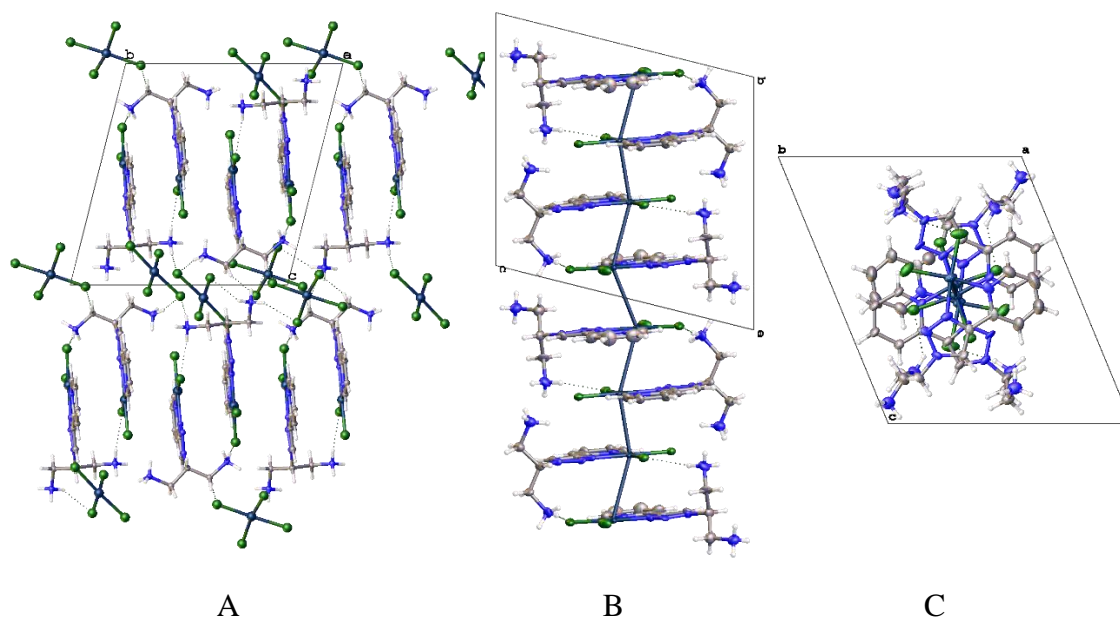
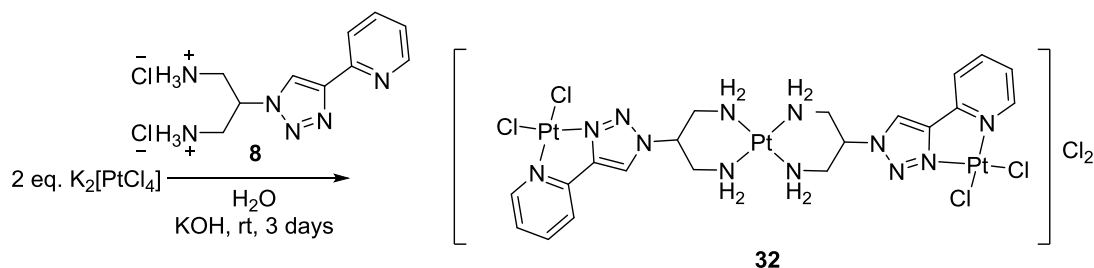


**Figure 5.14:** Packing diagrams of **31** viewed (A) normal to the *a*-axis showing the Pt(II)Cl<sub>2</sub>(PTPDH<sub>2</sub>) stacks with the PtCl<sub>4</sub> anion filler along the (001) plane (B) normal to the *a*-axis showing the links between Pt centres and (C) normal to the *b*-axis, down the Pt axis.

#### [Pt<sub>3</sub>Cl<sub>4</sub>(PTPD)<sub>2</sub>]Cl<sub>2</sub> synthesis

Given that Pt(II) readily reacts with both **6** and PTPDH<sub>3</sub> **8**, the reactivity of Pt(II) with the deprotonated ligand **8**, PTPD, was also investigated. The novel and fully deprotected multidentate ligand, PTPD, possesses a pyridyl and a DAP group in addition to the 1,2,3-triazole. **32** was synthesised in a single step by mixing K<sub>2</sub>[PtCl<sub>4</sub>] with PTPD in a 2:1 ratio in H<sub>2</sub>O for 3 days at rt to give the proposed [Pt(II)<sub>3</sub>Cl<sub>4</sub>(PTPD)<sub>2</sub>]Cl<sub>2</sub> (**32**, Scheme 5.12).



**Scheme 5.12:** Synthetic route to [Pt<sub>3</sub>Cl<sub>4</sub>(PTPD)<sub>2</sub>]Cl<sub>2</sub>.

The characterisation was informed by HR ESI-MS, EA and FT-IR. EA for **32** is consistent with two PTPD ligands and six chlorine atoms per three Pt(II) centres, C<sub>20</sub>H<sub>28</sub>Cl<sub>6</sub>N<sub>12</sub>Pt<sub>3</sub>.

Given **32** is essentially insoluble in common laboratory solvents, NMR spectroscopic characterisation was not successfully undertaken. HRMS helped identify the product ion fragment associated with  $\text{PtCl(PTPD)}$  (449.027) and  $\text{PtCl}_2(\text{PTPD})+\text{H}$  (485.034) and significantly  $\text{Pt}_2(\text{PTPD})_2\text{Cl}_3$  (933.100)  $\text{Pt}_2(\text{PTPD})_2\text{Cl}_4+\text{H}$  (969.065) and  $\text{Pt}_3(\text{PTPD})_2\text{Cl}_5$  (1198.993), **Figure 5.15**.

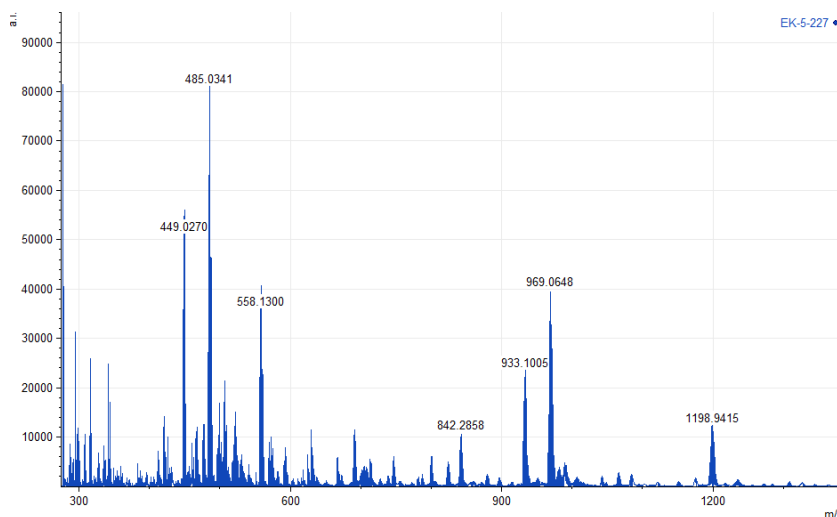


**Figure 5.15:** HR ESI-MS of **32**.

Though bis(diammino) complexes are more closely associated with  $\text{Pd(II)}$  centres,  $\text{Pt(II)}$  bis(diammino) complexes are well represented in the literature,<sup>50-51</sup> including  $\text{Pt}$  complexes of 1,3-diaminopropane.<sup>52</sup> In addition, bis(ethylenediamino)platinum(II) chloride is commercially available. In turn we suggest that our novel ligand PTPD in **32** bridges two  $\text{Pt(II)}$  centres and that the two PTPD ligands coordinate three  $\text{Pt(II)}$  centres as per the proposed coordination compound for **32** (**Scheme 5.11**).

## Crystallographic data

The x-ray crystal structures in this chapter were determined by Dr. Brendan Twamley at the School of Chemistry, Trinity College Dublin.

**Table 5.4.** Crystallographic details for all structures **27**, **29** and **31**.

Compound	<b>27</b>	<b>29</b>	<b>31</b>
Empirical formula	$\text{C}_{13}\text{H}_{10}\text{AuCl}_3\text{N}_4$	$\text{C}_{20}\text{H}_{36.60}\text{Au}_{3.80}\text{C}_{19.21}\text{N}_{12}$ $\text{Na}_{0.80}\text{O}_{4.40}$	$\text{C}_{10.25}\text{H}_{17}\text{Cl}_6\text{N}_6\text{O}_{0.25}$ $\text{Pt}_2$
Formula weight	525.57	1608.97	831.18
Temperature (K)	100(2)	100(2)	100(2)
Wavelength (Å)	0.71073	0.71073	0.71073
Instrument	ECO	ECO	ECO
Crystal system	Triclinic	Monoclinic	Triclinic
Space group	$\text{P}^-$	$\text{P2}_1/\text{c}$	$\text{P}^-$
$a$ (Å)	6.960(3)	15.2675(6)	12.4400(6)
$b$ (Å)	9.060(4)	18.9896(7)	13.3881(6)
$c$ (Å)	12.468(6)	7.1416(3)	15.1617(7)
$\alpha$ (°)	88.87(3)	90	76.6984(17)
$\beta$ (°)	76.044(16)	99.1035(11)	68.0193(18)
$\gamma$ (°)	86.372(11)	90	89.2239(19)
Volume (Å <sup>3</sup> )	761.5(6)	2044.44(14)	2271.40(19)
Z	2	2	4
(calc. Mg/m <sup>3</sup> )	1.472	2.614	2.431
(mm <sup>-1</sup> )	2.292	14.250	13.018
F(000)	492	1483	1522
Crystal size (mm <sup>3</sup> )	0.28 x 0.24 x 0.16	0.18 x 0.08 x 0.08	0.13 x 0.03 x 0.03
Theta range for data collection (°)	2.806 to 28.414	2.908 to 26.468	2.269 to 26.560
Reflections collected	11304	40737	36729
Independent reflections	3795 [R(int) = 0.0462]	4212 [R(int) = 0.0293]	9231 [R(int) = 0.0891]
Max. and min. transmission	0.7457 and 0.3481	0.0276 and 0.0080	0.7454 and 0.4504
Data / restraints /	3795 / 0 / 190	4212 / 965 / 232	9231 / 604 / 648

parameters			
Goodness-of-fit on $F^2$	1.067	1.106	1.030
Final R indices [ $I > 2\sigma(I)$ ]	R1 = 0.0260, wR2 = 0.0550	R1 = 0.0258, wR2 = 0.0657	R1 = 0.0495, wR2 = 0.0980
R indices (all data)	R1 = 0.0337, wR2 = 0.0579	0.0297, wR2 = 0.0673	R1 = 0.0928, wR2 = 0.1131
Largest diff. peak and hole ( $e.\text{\AA}^{-3}$ )	1.195 and -2.065	1.233 and -0.853	1.977 and -2.523

## Conclusion

The synthesis and characterisation of a novel polydentate 1,4-disubstituted 1,2,3-triazole based ligand, 2-(4-(pyridin-2-yl)-1*H*-1,2,3-triazol-1-yl)propane-1,3-diamine (PTPD) is described. X-ray structural characterisation of  $[\text{Au(III)Cl}_3(\text{PTP})]$  (**27**),  $[\text{Au(III)Cl}_2(\text{PTPD})][\text{Au(I)Cl}_2][\text{OH}]\{\text{[NaAuCl}_4\cdot 2\text{H}_2\text{O}]\}_n$  (**29**) and  $[\text{Pt(II)Cl}_2(\text{PTPDH}_2)][\text{PtCl}_4]$  (**31**) and characterisation of  $[\text{Au(III)Cl}_3(\text{BOC}_2\text{-PTPD})]$  (**28**) and  $[\text{Pt(II)}_3\text{Cl}_4(\text{PTPD})_2]\text{Cl}_2$  (**32**) support the proposition that PTPD is an interesting multidentate ligand that can bind metal centres through a variety of coordination modes including bidentate coordination through the DAP group, bidentate through the triazole N3 and pyridyl nitrogen and monodentate through the pyridyl nitrogen. Ultimately PTPD is a versatile and ideal ligand template for the development of mixed metal complexes of Pt and Au and Pt/Au and other transition metals.

## Future Work

Although the complexes were well characterised, the poor solubility of many of the polydentate metal complexes described potentially limit their application. For example, if  $[\text{Pt(II)}_3\text{Cl}_4(\text{PTPD})_2]\text{Cl}_2$  possessed superior water solubility, it could be investigated as a triplatinum type anticancer agent, which were designed to clamp DNA *via* formation of DNA adducts.

Future investigations could be undertaken to improve the solubility of these complexes. Ultimately, PTPD should be employed as a multidentate ligand to generate mixed metal complexes of Pt, Au and other transition metals. Reactions could be undertaken stepwise, where metals are reacted sequentially or in one pot.

In addition, it would be worthwhile to synthesise the “inverse” PTPD ligand and its Au(III) and Pt(II) complexes for comparison with the complexes described here within.

## References

- Schulze, B.; Schubert, U. S., Beyond click chemistry - supramolecular interactions of 1,2,3-triazoles. *Chem. Soc. Rev.* **2014**, 43 (8), 2522-2571.
- Crowley, J. D.; McMorran, D. A., Click-Triazole" Coordination Chemistry: Exploiting 1,4-Disubstituted-1,2,3-Triazoles as Ligands. In *Click Triazoles*, Košmrlj, J., Ed. Springer-Verlag Berlin Heidelberg: 2012; Vol. 28, pp 31-84.
- Suntrup, L.; Kleoff, M.; Sarkar, B., Serendipitous discoveries of new coordination modes of the 1,5-regioisomer of 1,2,3-triazoles enroute to the attempted synthesis of a carbon-anchored tri-mesoionic carbene. *Dalton Trans.* **2018**.
- Struthers, H.; Mindt, T. L.; Schibli, R., Metal chelating systems synthesized using the copper(i) catalyzed azide-alkyne cycloaddition. *Dalton Trans.* **2010**, 39 (3), 675-696.
- van Hilst, Q. V. C.; Lagesse, N. R.; Preston, D.; Crowley, J. D., Functional metal complexes from CuAAC "click" bidentate and tridentate pyridyl-1,2,3-triazole ligands. *Dalton Trans.* **2018**, 47 (4), 997-1002.
- Kocher, L.; Durot, S.; Heitz, V., Control of the cavity size of flexible covalent cages by silver coordination to the peripheral binding sites. *Chem. Comm.* **2015**, 51 (67), 13181-13184.
- Ballester, P.; Claudel, M.; Durot, S.; Kocher, L.; Schoepff, L.; Heitz, V., A Porphyrin Coordination Cage Assembled from Four Silver(I) Triazolyl-Pyridine Complexes. *Chemistry (Weinheim an der Bergstrasse, Germany)* **2015**, 21 (43), 15339-48.
- Vellas, S.; Lewis, J.; Shankar, M.; Sagatova, A.; Tyndall, J.; Monk, B.; Fitchett, C.; Hanton, L.; Crowley, J., [Fe2L3]4+ Cylinders Derived from Bis(bidentate) 2-Pyridyl-1,2,3-triazole "Click" Ligands: Synthesis, Structures and Exploration of Biological Activity. *Molecules* **2013**, 18 (6), 6383.
- Kumar, S. V.; Lo, W. K. C.; Brooks, H. J. L.; Crowley, J. D., Synthesis, structure, stability and antimicrobial activity of a ruthenium(II) helicate derived from a bis-bidentate "click" pyridyl-1,2,3-triazole ligand. *Inorg. Chim. Acta* **2015**, 425, 1-6.
- Vasdev, R.; Preston, D.; Scottwell, S.; Brooks, H.; Crowley, J.; Schramm, M., Oxidatively Locked [Co2L3]6+ Cylinders Derived from Bis(bidentate) 2-Pyridyl-1,2,3-triazole "Click" Ligands: Synthesis, Stability, and Antimicrobial Studies. *Molecules* **2016**, 21 (11), 1548.
- Schulze, B.; Friebe, C.; Hoeppener, S.; Pavlov, G. M.; Winter, A.; Hager, M. D.; Schubert, U. S., Ruthenium(II) metallo-supramolecular polymers of click-derived tridentate ditopic ligands. *Macromolecular rapid communications* **2012**, 33 (6-7), 597-602.
- Bolje, A.; Urankar, D.; Košmrlj, J., Synthesis and NMR Analysis of 1,4-Disubstituted 1,2,3-Triazoles Tethered to Pyridine, Pyrimidine, and Pyrazine Rings. *European Journal of Organic Chemistry* **2014**, 2014 (36), 8167-8181.
- Schweinfurth, D.; Pattacini, R.; Strobel, S.; Sarkar, B., New 1,2,3-triazole ligands through click reactions and their palladium and platinum complexes. *Dalton Trans.* **2009**, (42), 9291-9297.
- Kilpin, K. J.; Gavey, E. L.; McAdam, C. J.; Anderson, C. B.; Lind, S. J.; Keep, C. C.; Gordon, K. C.; Crowley, J. D., Palladium(II) Complexes of Readily Functionalized Bidentate 2-Pyridyl-1,2,3-triazole "Click" Ligands: A Synthetic, Structural, Spectroscopic, and Computational Study. *Inorg. Chem.* **2011**, 50 (13), 6334-6346.
- Wang, J.; Delavaux-Nicot, B.; Wolff, M.; Mallet-Ladeira, S.; Metivier, R.; Benoist, E.; Fery-Forgues, S., The unsuspected influence of the pyridyl-triazole ligand isomerism upon the electronic properties of tricarbonyl rhenium complexes: an experimental and theoretical insight. *Dalton transactions (Cambridge, England : 2003)* **2018**.
- Pages, B. J.; Sakoff, J.; Gilbert, J.; Zhang, Y.; Li, F.; Preston, D.; Crowley, J. D.; Aldrich-Wright, J. R., Investigating the cytotoxicity of platinum(II) complexes incorporating bidentate pyridyl-1,2,3-triazole "click" ligands. *J. Inorg. Biochem.* **2016**, 165, 92-99.
- Lo, W. K. C.; Huff, G. S.; Cubanski, J. R.; Kennedy, A. D. W.; McAdam, C. J.; McMorran, D. A.; Gordon, K. C.; Crowley, J. D., Comparison of Inverse and Regular 2-

- Pyridyl-1,2,3-triazole “Click” Complexes: Structures, Stability, Electrochemical, and Photophysical Properties. *Inorg. Chem.* **2015**, *54* (4), 1572-1587.
18. Riedl, C. A.; Hejl, M.; Klose, M. H. M.; Roller, A.; Jakupec, M. A.; Kandioller, W.; Keppler, B. K., N- and S-donor leaving groups in triazole-based ruthena(ii)cycles: potent anticancer activity, selective activation, and mode of action studies. *Dalton Trans.* **2018**, 47 (13), 4625-4638.
  19. Urankar, D.; Košmrlj, J., Preparation of diazenecarboxamide–carboplatin conjugates by click chemistry. *Inorg. Chim. Acta* **2010**, *363* (14), 3817-3822.
  20. Kitteringham, E.; Wu, D.; Cheung, S.; Twamley, B.; O'Shea, D. F.; Griffith, D. M., Development of a novel carboplatin like cytoplasmic trackable near infrared fluorophore conjugate via strain-promoted azide alkyne cycloaddition. *J. Inorg. Biochem.* **2018**, *182*, 150-157.
  21. Scattergood, P. A.; Elliott, P. I. P., An unexpected journey from highly tunable phosphorescence to novel photochemistry of 1,2,3-triazole-based complexes. *Dalton Trans.* **2017**, 46 (47), 16343-16356.
  22. Cinellu, M. A.; Zucca, A.; Stoccoro, S.; Minghetti, G.; Manassero, M.; Sansoni, M., Synthesis and characterization of gold(III) adducts and cyclometallated derivatives with 6-benzyl- and 6-alkyl-2,2'-bipyridines. *J. Chem. Soc., Dalton Trans.* **1996**, (22), 4217-4225.
  23. von Wachenfeldt, H.; Polukeev, A. V.; Loganathan, N.; Paulsen, F.; Röse, P.; Garreau, M.; Wendt, O. F.; Strand, D., Cyclometallated gold(iii) aryl-pyridine complexes as efficient catalysts for three-component synthesis of substituted oxazoles. *Dalton Trans.* **2015**, 44 (12), 5347-5353.
  24. Shaikjee, A.; Levendis, D. C.; Marques, H. M.; Mampa, R., A gold(III) complex and a tetrachloroaurate salt of the neuroepileptic drug gabapentin. *Inorg. Chem. Commun.* **2011**, *14* (4), 534-538.
  25. Hashmi, A. S.; Lothschütz, C.; Ackermann, M.; Doepp, R.; Anantharaman, S.; Marchetti, B.; Bertagnolli, H.; Rominger, F., Gold catalysis: in situ EXAFS study of homogeneous oxidative esterification. *Chemistry (Weinheim an der Bergstrasse, Germany)* **2010**, *16* (27), 8012-9.
  26. Ortego, L.; Meireles, M.; Kasper, C.; Laguna, A.; Villacampa, M. D.; Gimeno, M. C., Group 11 complexes with amino acid derivatives: Synthesis and antitumoral studies. *J. Inorg. Biochem.* **2016**, *156*, 133-144.
  27. Glišić, B. Đ.; Savić, N. D.; Warzajtis, B.; Djokic, L.; Ilic-Tomic, T.; Antić, M.; Radenković, S.; Nikodinovic-Runic, J.; Rychlewska, U.; Djuran, M. I., Synthesis, structural characterization and biological evaluation of dinuclear gold(iii) complexes with aromatic nitrogen-containing ligands: antimicrobial activity in relation to the complex nuclearity. *Med. Chem. Comm.* **2016**, *7* (7), 1356-1366.
  28. Schimanski, A.; Freisinger, E.; Erxleben, A.; Lippert, B., Interactions between [AuX<sub>4</sub>]<sup>-</sup> (X = Cl, CN) and cytosine and guanine model nucleobases: salt formation with (hemi-) protonated bases, coordination, and oxidative degradation of guanine. *Inorg. Chim. Acta* **1998**, *283* (1), 223-232.
  29. Bruni, B.; Ferraroni, M.; Orioli, P.; Speroni, G., A Biologically Active Gold Complex: Trichloro[(2-pyridyl)methanol-N]gold(III). *Acta Cryst.* **1996**, *C52*, 1423-1424.
  30. Segapelo, T. V.; Guzei, I. A.; Spencer, L. C.; Zyl, W. E. V.; Darkwa, J., (Pyrazolylmethyl)pyridine platinum(II) and gold(III) complexes: Synthesis, structures and evaluation as anticancer agents. *Inorg. Chim. Acta* **2009**, *362* (9), 3314-3324.
  31. Sánchez-Delgado, R. A.; Navarro, M.; Lazard, K.; Atencio, R.; Capparelli, M.; Vargas, F.; Urbina, J. A.; Bouillez, A.; Noels, A. F.; Masi, D., Toward a novel metal based chemotherapy against tropical diseases 4. Synthesis and characterization of new metal-clotrimazole complexes and evaluation of their activity against *Trypanosoma cruzi*. *Inorg. Chim. Acta* **1998**, *275-276*, 528-540.
  32. Warzajtis, B.; Glišić, B. Đ.; Radulović, N. S.; Rychlewska, U.; Djuran, M. I., Gold(III) complexes with monodentate coordinated diazines: An evidence for strong electron-withdrawing effect of Au(III) ion. *Polyhedron* **2014**, *79*, 221-228.



33. Kilpin, K. J.; Paul, U. S. D.; Lee, A.-L.; Crowley, J. D., Gold(i) "click" 1,2,3-triazolyldienes: synthesis, self-assembly and catalysis. *Chem. Commun.* **2011**, 47 (1), 328-330.
34. Xi, Y.; Wang, Q.; Su, Y.; Li, M.; Shi, X., Quantitative kinetic investigation of triazole-gold(i) complex catalyzed [3,3]-rearrangement of propargyl ester. *Chem. Commun.* **2014**, 50 (17), 2158-2160.
35. Canseco-Gonzalez, D.; Petronilho, A.; Mueller-Bunz, H.; Ohmatsu, K.; Ooi, T.; Albrecht, M., Carbene Transfer from Triazolyldiene Gold Complexes as a Potent Strategy for Inducing High Catalytic Activity. *J. Am. Chem. Soc.* **2013**, 135 (35), 13193-13203.
36. Yang, Y.; Hu, W.; Ye, X.; Wang, D.; Shi, X., Preparation of Triazole Gold(III) Complex as an Effective Catalyst for the Synthesis of  $\alpha$  Haloenones. *Adv. Synth. Catal.* **2016**, 358 (16), 2583-2588.
37. Motley, D. M.; Walmsley, J. A.; Zukerman-Schpector, J.; Tiekink, E. R. T., Crystal and Molecular Structure of Dichloro(ethylenediamine)gold(III) Nitrate: [Au(NH<sub>2</sub>CH<sub>2</sub>CH<sub>2</sub>NH<sub>2</sub>)Cl<sub>2</sub>]NO<sub>3</sub>. *J. Chem. Cryst.* **2009**, 39 (5), 364-367.
38. Altaf, M.; Ahmad, S.; Kawde, A.-N.; Baig, N.; Alawad, A.; Altuwaijri, S.; Stoeckli-Evans, H.; Isab, A. A., Synthesis, structural characterization, electrochemical behavior and anticancer activity of gold(III) complexes of meso-1,2-di(1-naphthyl)-1,2-diaminoethane and tetraphenylporphyrin. *New J. Chem.* **2016**, 40 (10), 8288-8295.
39. Zhu, S.; Gorski, W.; Powell, D. R.; Walmsley, J. A., Synthesis, Structures, and Electrochemistry of Gold(III) Ethylenediamine Complexes and Interactions with Guanosine 5'-Monophosphate. *Inorg. Chem.* **2006**, 45 (6), 2688-2694.
40. Al-Jaroudi, S. S.; Fettouhi, M.; Wazeer, M. I. M.; Isab, A. A.; Altuwaijri, S., Synthesis, characterization and cytotoxicity of new gold(III) complexes with 1,2-diaminocyclohexane: Influence of stereochemistry on antitumor activity. *Polyhedron* **2013**, 50 (1), 434-442.
41. Omer, K. H.; Seliman, A. A.; Altaf, M.; Casagrande, N.; Aldinucci, D.; Altuwaijri, S.; Isab, A. A., Synthesis, characterization and anticancer activity of gold(III) complexes with (1R,2R)-(-)-1,2-diaminocyclohexane. *Polyhedron* **2015**, 102, 773-781.
42. Ericson, A.; I. Elding, L.; K. C. Elmroth, S., Kinetics and mechanism of reduction of gold(III) complexes by dimethyl sulfide. *J. Chem. Soc. Dalton Trans.* **1997**, (7), 1159-1164.
43. Skibsted, L. H., Ligand Substitution and Redox Reactions of Gold(III) Complexes. In *Advances in Inorganic and Bioinorganic Mechanisms*, Sykes, A. G., Ed. Harcourt Brace Jovanovich: London, 1986; Vol. 4, pp 137-184.
44. Chipman, A.; Gouranourimi, A.; Farshadfar, K.; Olding, A.; Yates, B. F.; Ariafard, A., A Computational Mechanistic Investigation into Reduction of Gold(III) Complexes by Amino Acid Glycine: A New Variant for Amine Oxidation. *Chemistry (Weinheim an der Bergstrasse, Germany)* **2018**, 24 (33), 8361-8368.
45. Durovic, M. D.; Puchta, R.; Bugarcic, Z. D.; van Eldik, R., Studies on the reactions of [AuCl<sub>4</sub>]- with different nucleophiles in aqueous solution. *Dalton Trans.* **2014**, 43 (23), 8620-8632.
46. Schweinfurth, D.; Pattacini, R.; Strobel, S.; Sarkar, B., New 1,2,3-triazole ligands through click reactions and their palladium and platinum complexes. *Dalton Transactions* **2009**, (42), 9291-9297.
47. Lo, W. K. C.; Huff, G. S.; Cubanski, J. R.; Kennedy, A. D. W.; McAdam, C. J.; McMorran, D. A.; Gordon, K. C.; Crowley, J. D., Comparison of Inverse and Regular 2-Pyridyl-1,2,3-triazole "Click" Complexes: Structures, Stability, Electrochemical, and Photophysical Properties. *Inorganic Chemistry* **2015**, 54 (4), 1572-1587.
48. McCarney, E. P.; Hawes, C. S.; Blasco, S.; Gunnlaugsson, T., Synthesis and structural studies of 1,4-di(2-pyridyl)-1,2,3-triazole dpt and its transition metal complexes; a versatile and subtly unsymmetric ligand. *Dalton Trans.* **2016**, 45 (25), 10209-10221.
49. Huff, G. S.; Lo, W. K. C.; Horvath, R.; Turner, J. O.; Sun, X.-Z.; Weal, G. R.; Davidson, H. J.; Kennedy, A. D. W.; McAdam, C. J.; Crowley, J. D.; George, M. W.; Gordon, K. C., Excited States of Triphenylamine-Substituted 2-Pyridyl-1,2,3-triazole Complexes. *Inorg. Chem.* **2016**, 55 (23), 12238-12253.

50. W., W. G.; S., K. D., The unit cell dimensions of bis(ethylenediamine)platinum(II) chloride. *Acta Cryst.* **1963**, *16* (9), 932-932.
51. Sato, S., Structure of bis(ethylenediamine)platinum(II) dichloride. *Acta Crystallogr. Sect. C* **1990** *46* (6), 1107-1108.
52. Alvarez-Valdés, A.; Pérez, J. M.; López-Solera, I.; Lannegrand, R.; Continente, J. M.; Amo-Ochoa, P.; Camazón, M. J.; Solans, X.; Font-Bardía, M.; Navarro-Ranninger, C., Preparation and Characterization of Platinum(II) and (IV) Complexes of 1,3-Diaminepropane and 1,4-Diaminebutane: Circumvention of Cisplatin Resistance and DNA Interstrand Cross-Link Formation in CH1cisR Ovarian Tumor Cells. *J. Med. Chem.* **2002**, *45* (9), 1835-1844.
53. Spek, A. L., Structure validation in chemical crystallography. *Acta Cryst.* **2009**, *D65*, 148-155.

## **Chapter 6**

### **Platinum(II) complexes with click functionalised ligands**

## Abstract

Click Chemistry has a very important role to play in the functionalisation of Pt-based drugs. This chapter builds on the research carried out in Chapters 3 and 5 and comprises three mini chapter sections. Specifically, novel strategies (i) to conjugate a previously reported cage ligand to a fluorophore conjugate *via* click chemistry, (ii) to synthesise novel Pt steroid conjugates *via* click chemistry and (iii) to develop novel Pt(II) tetrazine iEDDA click capable complexes/templates are described.

## Introduction

Metal chelating ligands are frequently used in the design of self-assembled structures in supramolecular coordination chemistry. Metal cage structures for example have biological applications for the encapsulation of (counter)ions and metallodrug complexes (e.g. cisplatin) as drug delivery systems (**Figure 6.1**).<sup>1-2</sup> The Kühn and Casini research groups for instance developed metal (Pt and Pd) cage structures using rigid bis(monodentate) pyridyl ligands as scaffolds and Casini demonstrated that their Pd cage could be used as a system to deliver the anticancer drug cisplatin.

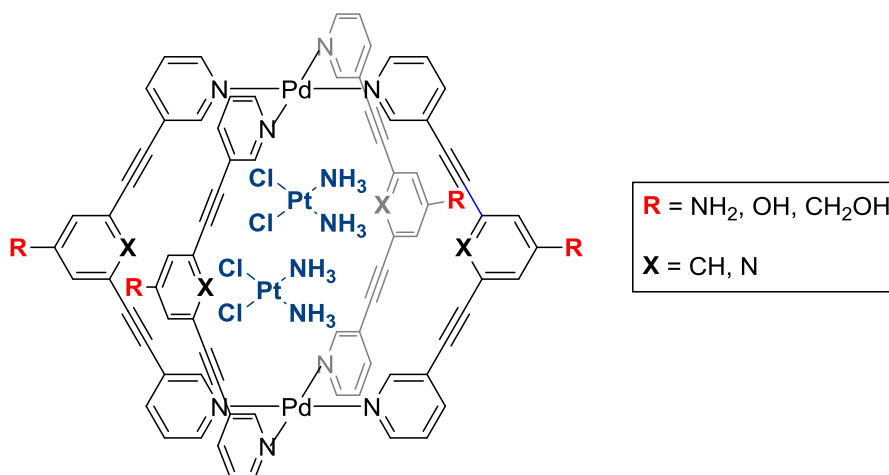


**Figure 6.1:** Pd metallocage complexes previously synthesised which encapsulated two cisplatin molecules.<sup>1</sup>

Casini and coworkers wish to improve upon the functionality of their metallocages and to track the metallocages in cells. Dr. Griffith and Prof. Casini (Cardiff University) initiated a collaboration, where it was agreed that the Griffith group

would functionalise the cage ligands with an azide group, establish a protocol for the click reaction and click the cage ligand with a NIR-AZA fluorophore provided by Prof. Donal O'Shea.<sup>1-2</sup> This work was a natural fit with the theme of this thesis and therefore the synthesis of a novel click chemistry cage ligand with an azide handle and its potential for functionalisation was investigated.

Anticancer hormone therapy utilising steroids and their derivatives is one of the oldest clinical techniques for treatment of cancer.<sup>3</sup> It has been demonstrated that hormone sensitive cancer cell lines e.g. breast,<sup>4-6</sup> prostate<sup>7</sup> and ovarian,<sup>8</sup> are sensitised to Pt drugs when administered with steroid compounds. For example, estrogen and progesterone have been shown to improve the anticancer effect of cisplatin and improve its activity against Pt resistant cancer cell lines.<sup>9</sup> This is due to the increased demand by cancer cells for steroids in their growth and as such the upregulated number of steroid hormone receptors (SHRs) they exhibit.<sup>10</sup>

To date, a number of Pt-steroid derivatives have been successfully synthesised and exhibit cytotoxicity but they are not more cytotoxic than the parent Pt drug alone in most instances.<sup>6, 11</sup> However, it is feasible that conjugation of steroids to Pt drugs may help with the goal of overcoming Pt resistance either by inhibition of an essential pathway or through an alternate Pt cellular uptake mechanism. In this chapter, a series of novel bidentate steroid derived ligands and their corresponding Pt(II) complexes were developed.

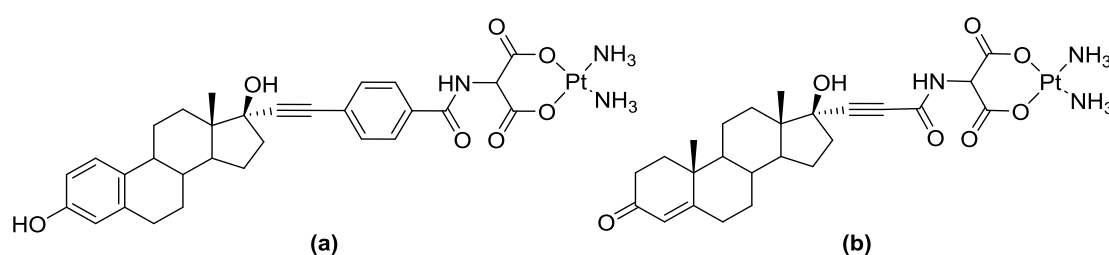


**Figure 6.2:** Examples of Pt-steroid complexes (a) Pt(II) benzamide-malonate estradiol<sup>12</sup> and (b) Pt(II) malonate testosterone.<sup>13</sup>

iEDDA is rapidly becoming one of the most promising bioorthogonal click approaches employed due to the rapid rate at which it occurs and the diversity of templates commercially available for use. Functionalisation of a Pt complex with a tetrazine moiety would allow for rapid conjugation *in vitro* and *in vivo* with a corresponding cyclooctyne or *trans*-cyclooctene group. These cyclooct-yne and -ene

groups may be attached to a myriad of compounds such as fluorescent probes, targeting moieties and secondary drug molecules.<sup>14-15</sup> To the best of our knowledge, this strategy has not yet been employed with a Pt complex.

### **Rationale**

This chapter comprises novel strategies in the fields of Pt and click chemistry, which do not tie directly with topics covered in chapters 3, 4 or 5 and/or merit a stand-alone chapter. It will serve to increase our understanding of and further demonstrate the importance of click chemistry to Pt conjugation strategies.

### **Chapter Aims**

- ◁ To develop a strategy to conjugate a previously reported cage ligand to a fluorophore conjugate *via* click chemistry.
- ◁ To synthesise novel Pt steroid conjugates *via* click chemistry.
- ◁ To develop novel Pt(II) tetrazine iEDDA click capable complexes/templates.

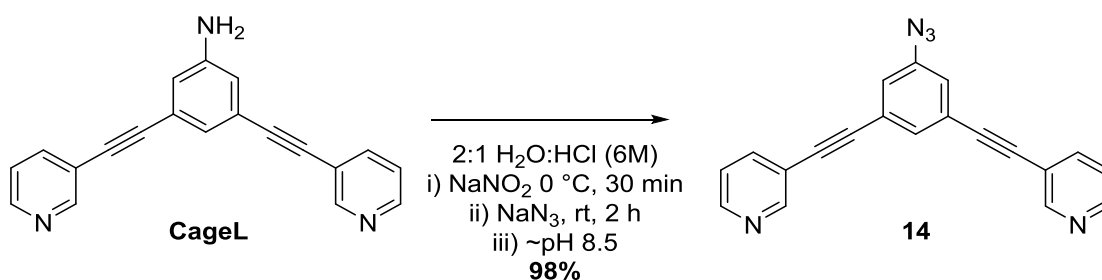
## Synthesis of azide cage ligands

### 3,3'-((5-azido-1,3-phenylene)bis(ethyne-2,1-diyl))dipyridine (CageL-N<sub>3</sub>)

#### synthesis

As discussed, rigid bis(monodentate) pyridyl ligands (**CageL**, **Scheme 6.1**) were employed by Casini and coworkers to develop Pd and Pt cage complexes of formula M<sub>2</sub>L<sub>4</sub> (**Figure 6.6**). The introduction of an azide handle on to the benzene ring of these ligands would facilitate click reactions and easy functionalisation of the cage ligands.

CageL-N<sub>3</sub>, **14**, was synthesised from its corresponding amino precursor in a single step in high yield (98%), following the previously described method for the synthesis of **5** and as shown below in **Scheme 6.1**.



**Scheme 6.1:** Synthetic route to compound **14**.

**14** was characterised by <sup>1</sup>H and <sup>13</sup>C NMR (CDCl<sub>3</sub>) spectroscopy, where the absence of the broad single peak at 3.91 ppm in the proton spectrum indicated the loss of the NH<sub>2</sub> group (**Figure 6.3**). The aromatic protons were observed as six signals at 8.77, 8.59, 7.82, 7.51, 7.32 and 7.19 ppm and integrating in total for eleven as required. ESI-MS in positive mode aided the identification of the M+H with a mass peak of 322.4 a.m.u. In addition, the M-N<sub>2</sub> and M-N<sub>3</sub> fragmentation peaks were observed at 294.3 and 279.2 a.m.u. respectively. A sharp peak was observed in the FT-IR spectrum at 2107 cm<sup>-1</sup>, which is indicative of the newly formed azide functional group.

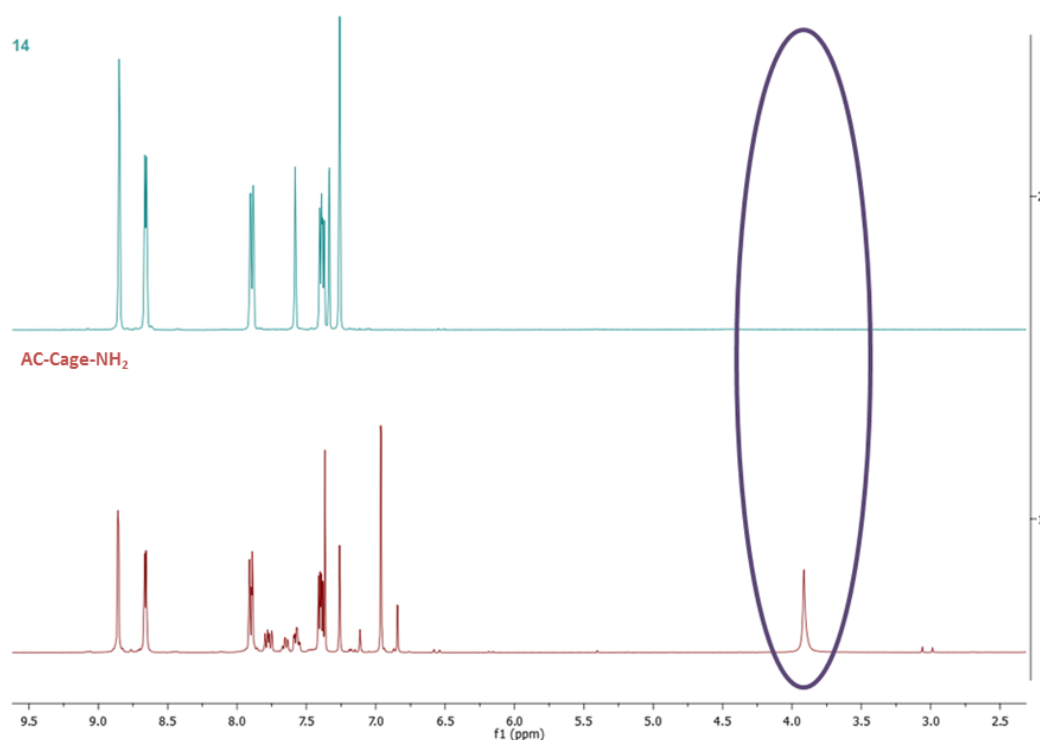


**Figure 6.3:**  $^1\text{H}$  NMR overlap of CageL- $\text{N}_3$ , **14** (top) and the starting compound CageL- $\text{NH}_2$  (bottom). The circle highlights the loss of the amino group.

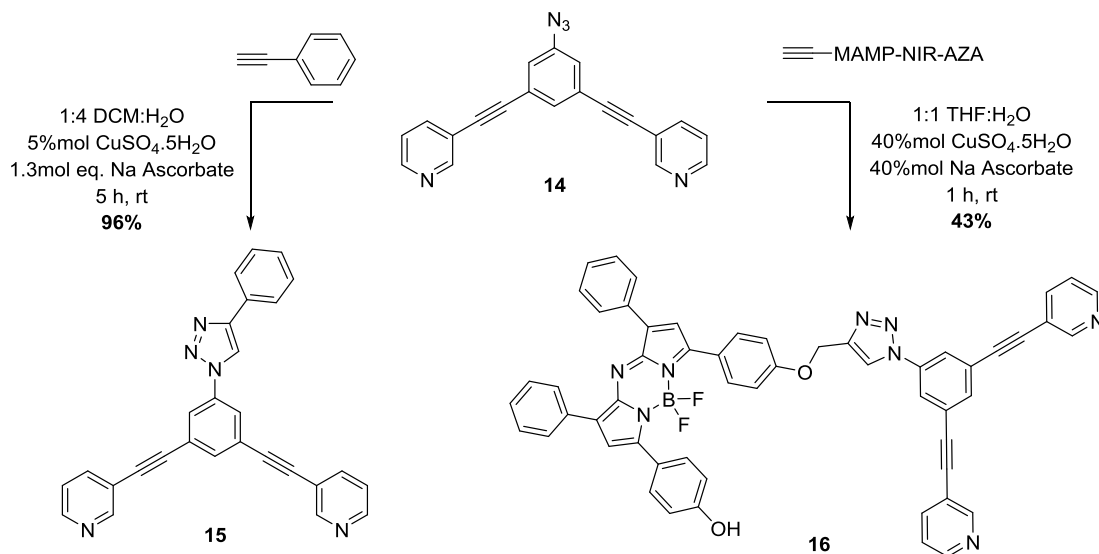
### Click reactions of CageL- $\text{N}_3$

Two click reactions were performed on **14** via CuAAC (**Scheme 6.2**). In the first instance, 3,3'-((5-(4-phenyl-1*H*-1,2,3-triazol-4-yl)-1,3-phenylene)bis(ethyne-2,1-diyl))dipyridine (**15**) was synthesised on reaction of CageL- $\text{N}_3$  with phenacetylene as a proof of concept for the click reaction and to ensure that potential interactions between the Cu(I) catalyst and the pyridyl group N atoms did not adversely affect reaction progression. **15** was characterised by  $^1\text{H}$  and  $^{13}\text{C}$  NMR ( $\text{CDCl}_3$ ) spectroscopy. In the  $^1\text{H}$  NMR spectrum, the three aromatic signals at 7.91, 7.84 and 7.78 ppm which integrate in the ratio of 2:2:1 are attributed to the phenyl group protons. Additionally, the single proton resonance at 8.27 ppm represents the newly formed triazole proton. ESI-MS in positive mode aided the identification of the  $\text{M}+\text{H}$  with a mass peak of 424.2 a.m.u. The previously observed azide peak was absent from the FT-IR spectrum indicating a complete click reaction and formation of **15**.

Subsequent to the successful synthesis of **15**, CageL- $\text{N}_3$  was reacted with the MAMP NIR-AZA fluorophore to give 3,3'-((5-(4-(MAMP-NIR-AZA)-1*H*-1,2,3-triazol-4-



yl)-1,3-phenylene)bis(ethyne-2,1-diyl)dipyridine (Cage-T-MAMP), **16**, the desired cage ligand fluorophore conjugate.



**Scheme 6.2:** Synthetic route to compound **15** and **16** via CuAAC.

**16** was characterised by <sup>1</sup>H and <sup>19</sup>F NMR (DMSO-*d*<sub>6</sub>) spectroscopy and ESI-MS. In the <sup>1</sup>H NMR spectrum of **16**, the signal at 3.92 ppm corresponds to the methylene of the ether bridge between the triazole and aromatic ring of the **MAMP** fluorophore. Four aromatic signals at 8.17-7.95, 7.52, 7.31 and 6.95 ppm, which integrate in the ratio of 8:8:2:2 and are associated with the **MAMP** fluorophore aromatic rings are observed. The remaining aromatic signals correspond to the three aryl and pyridyl groups of the cage ligand moiety. The <sup>19</sup>F spectrum of **16** exhibits a standard quartet signal at -130.40 ppm, which is standard for BODIPY compounds.<sup>16-17</sup> ESI-MS in negative mode aided the identification of the M-H with a mass peak of 887.4 a.m.u.

### Fluorescent properties and analysis of Cage-T-MAMP

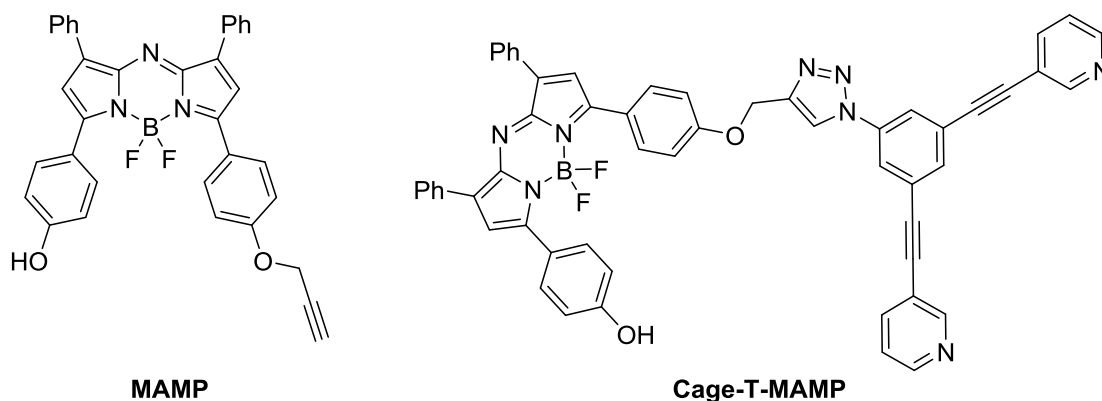


**Figure 6.4:** Structures of **MAMP** and **Cage-T-MAMP** (**16**).

As discussed in chapter 3, NIR-AZA compounds are known for having good photostability and NIR properties. In this instance the click conjugate **16** in  $\text{CHCl}_3$  ( $\lambda_{\text{max abs}} = 680 \text{ nm}$ ,  $\lambda_{\text{max em}} = 716 \text{ nm}$ ) was found to maintain the excellent NIR spectral properties of the free fluorophore (**MAMP**) with only minor differences in the  $\lambda_{\text{max em}}$  observed while the  $\lambda_{\text{max abs}}$  was unchanged (**Figure 6.5**).

These spectral properties correlate with other clicked derivatives of **MAMP** reported by Murtagh *et al.* for example, which also demonstrated minor changes in the  $\lambda_{\text{max abs}}$  and  $\lambda_{\text{max em}}$  on conjugation using click chemistry.

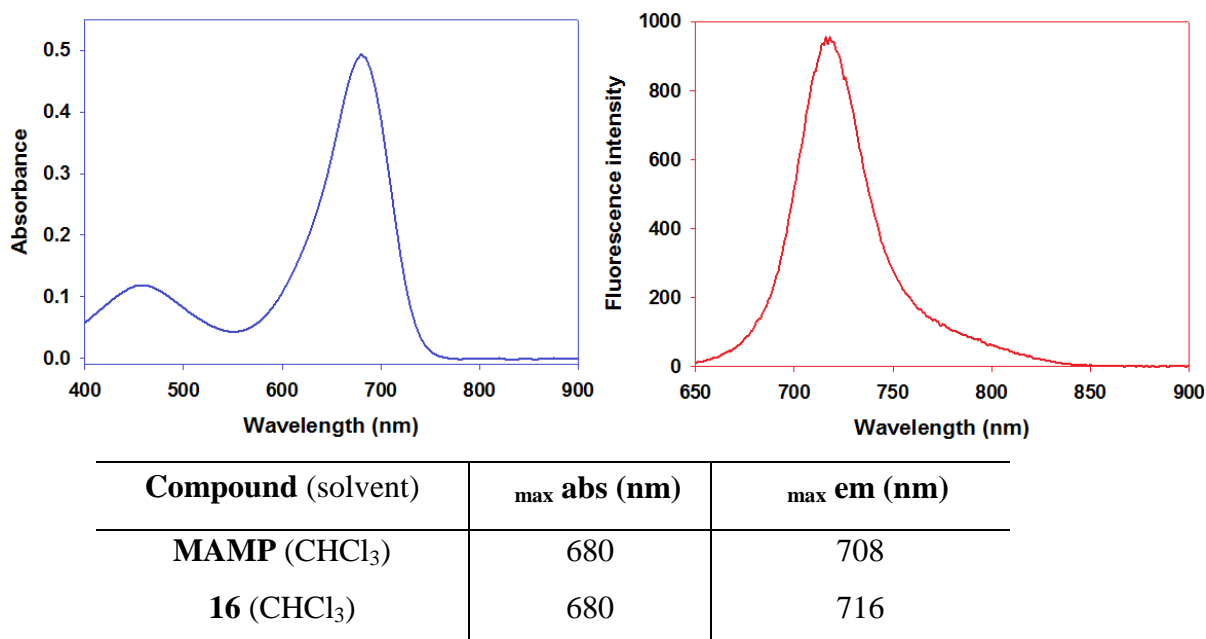


**Figure 6.5:** UV-vis and fluorescence properties of **MAMP** and **16**. Graph displaying absorbance (blue) and fluorescent emission (red) of **16**.

**14** and **16** were synthesised successfully in good yields. Notably the 2 step reactions were very rapid and produced clean products. **14** and **16** will be supplied to Casini and coworkers, where reaction with Pt and Pd precursors will generate the corresponding  $M_2L_4$  cage complexes by self-assembly (**Figure 6.6**). The cage complexes of **14** could potentially be modified *in cellulo* using SPAAC or iEDDA click chemistry, for example, and the uptake, transport and localisation of the cage complex of **16** which features a fluorophore will be tracked.

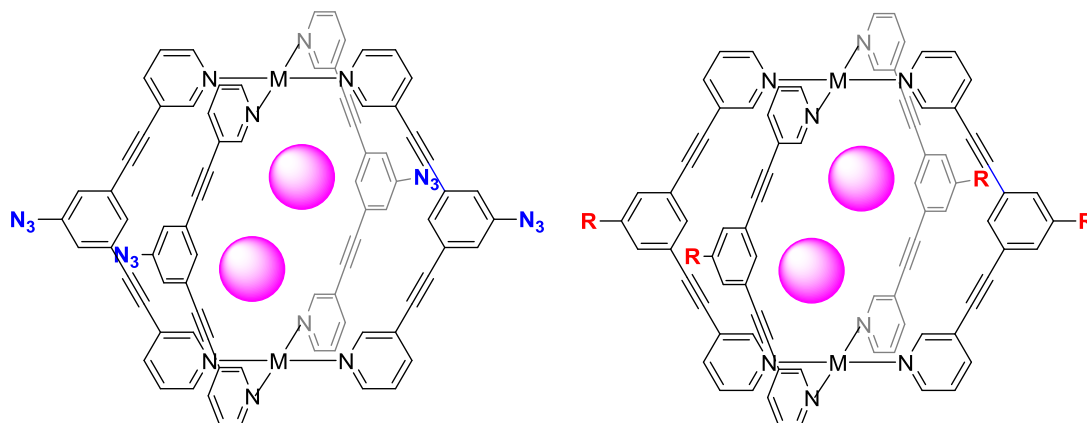


**Figure 6.6:** Potential  $M_2L_4$  metal cage structures of **14** and **16**, where  $M = Pt$  or  $Pd$  and  $R = MAMP$  fluorophore or another potential clicked structure derived from **14**. Encapsulated ion or drug indicated by purple sphere.

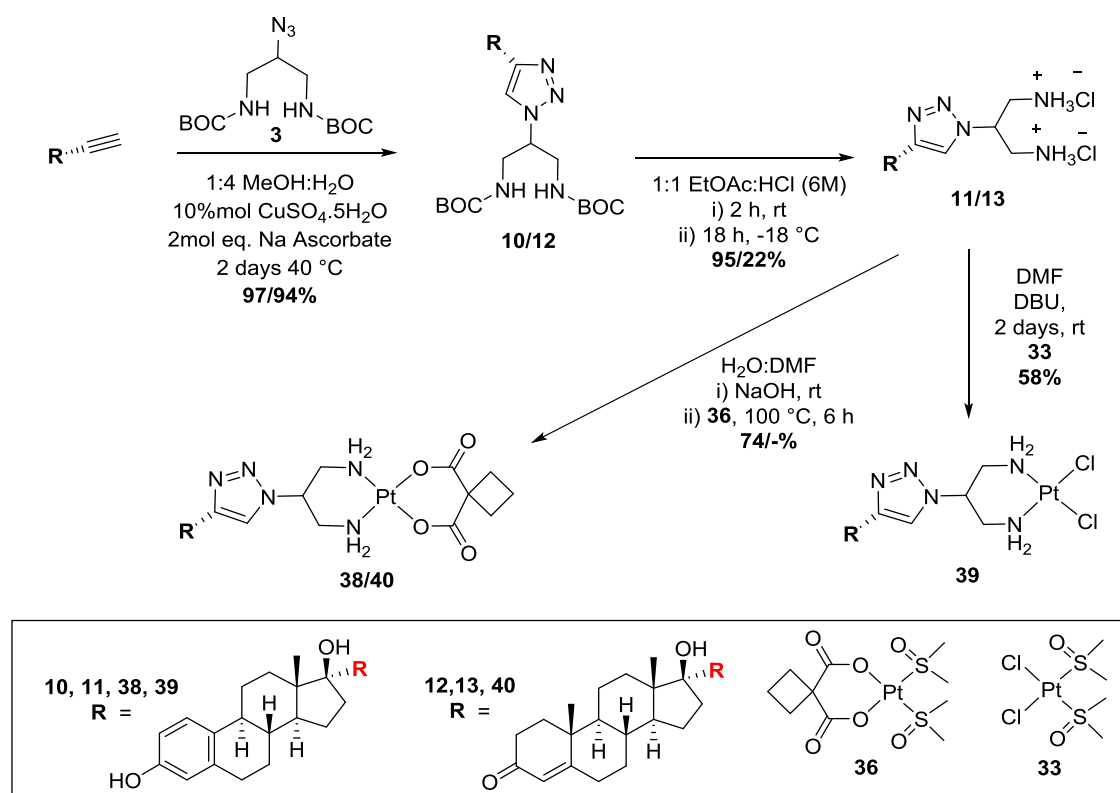
## Synthesis of Pt steroid complexes

The same synthetic strategy was developed to synthesise a Pt-estradiol complex and a Pt-testosterone complex as described below.

In the first step, I employed CuAAC to click **3** with the terminal alkyne steroid derivative as per **Scheme 5.4** (chapter 5) to generate **10** and **12**. In the second step, BOC deprotection of the amines using acid was used to form the hydrochloride salts of **11** and **13**, as per Chapter 5, **Scheme 5.4**. In the third step, reaction of **11** or **13** with two equivalents of base (NaOH or DBU) in a water:DMF mixture and subsequent reaction with the Pt precursors **33** or **36** gave corresponding Pt-steroid complexes **38-40** (**Scheme 6.3**, **Figure 6.7**).

From here on in, the neutralised steroid ligands of the estradiol derivative **11** and the testosterone derivative **13** will be referred to as DAP-estradiol and as DAP-testosterone respectively.

### Pt-Steroid complexes



**Scheme 6.3:** Planned synthetic route to [Pt(II)(CBDCA)(DAP-estradiol)] **38**, [Pt(II)Cl<sub>2</sub>(DAP-estradiol)] **39** and [Pt(II)(CBDCA)(DAP-testosterone)] **40**.

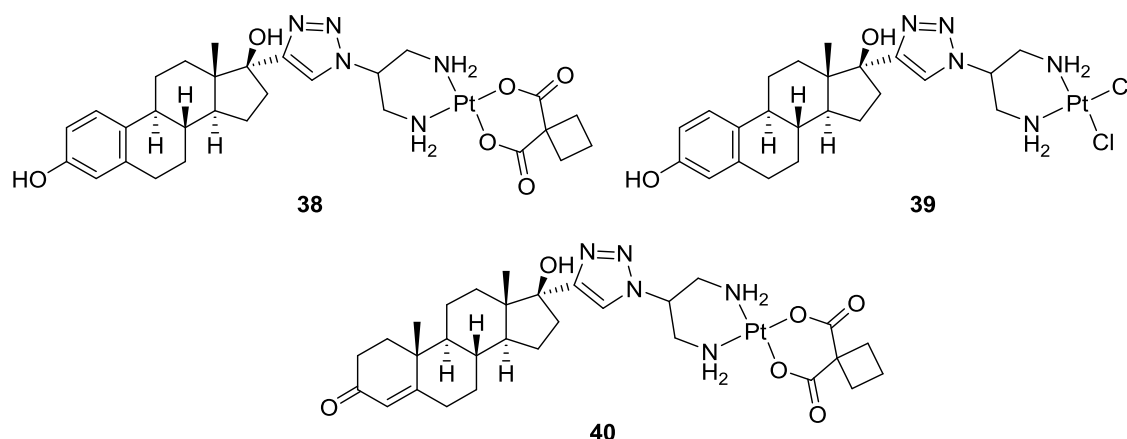


**Figure 6.7:** Structures of proposed Pt-steroid complexes **38** [Pt(II)(CBDCA)(DAP-Estradiol)], **39** [Pt(II)Cl<sub>2</sub>(DAP-Estradiol)] and **40** [Pt(II)(CBDCA)(DAP-Testosterone)].

The characterisation for each compound was informed using a variety of <sup>1</sup>H, <sup>13</sup>C and <sup>195</sup>Pt NMR spectroscopy, ESI-MS, EA and FT-IR, which correlated with the theoretical values demonstrating the formation of the desired complex, with the exception of complex **40**, which was not successfully synthesised.

#### DAP-Estradiol synthesis

The BOC protected product **10** was characterised by <sup>1</sup>H NMR (CDCl<sub>3</sub>) spectroscopy, where a single, large peak at 1.42 ppm correlates to the two symmetrical BOC groups attached. The triazole peak was found as a singlet at 7.65 ppm (**Figure 6.8**). The remaining 30 protons are accounted for by the remaining 14 signals, with 5 protons overlapping with the large BOC peak integrating for 49 protons in total. The <sup>13</sup>C NMR spectrum displayed 26 signals accounting for the 26 unique carbons of the 33 carbon structure of **10**. ESI-MS in positive mode aided the identification of the M+H and M+Na mass peaks of 612.5 and 634.5 a.m.u. respectively.

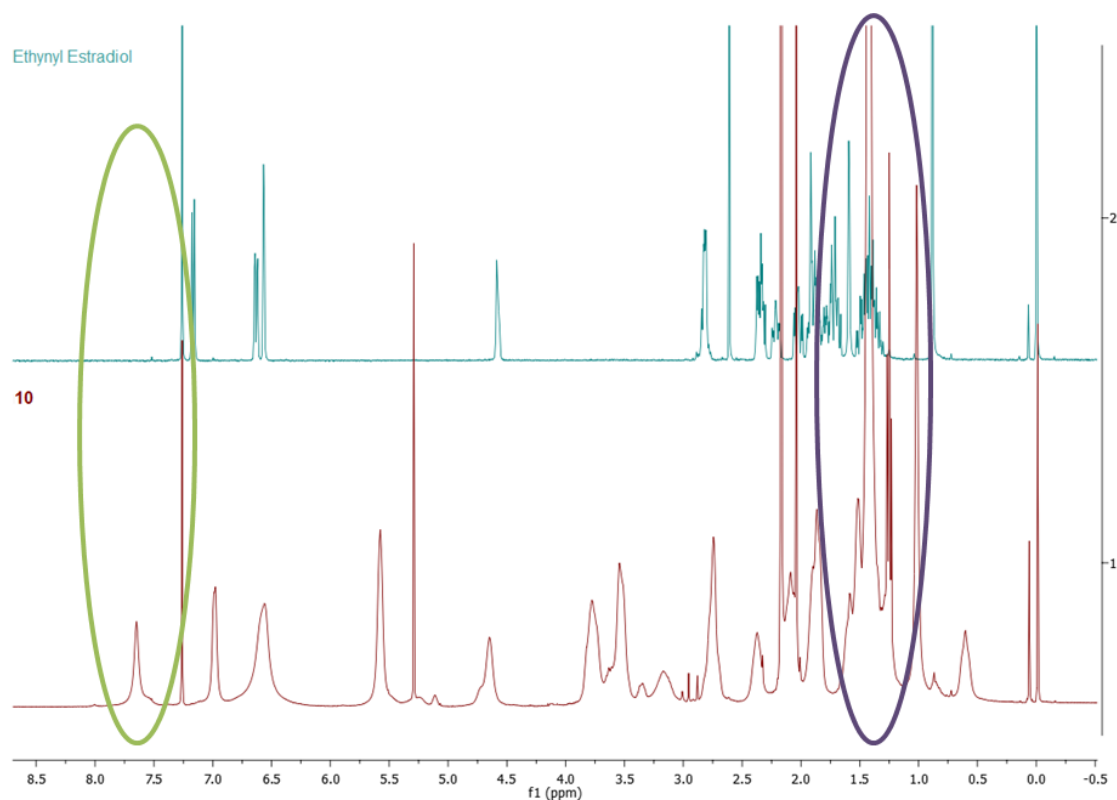


**Figure 6.8:** Overlap  $^1\text{H}$  NMR of estradiol starting material, ethynyl estradiol and **10**. The emergence of the new signal for the triazole proton at 7.65 ppm is circled in green, and the appearance of the large signal of 18 protons of the two BOC groups is shown in purple at 1.42 ppm.

The dihydrochloride salt product **11** was characterised by  $^1\text{H}$  NMR ( $\text{D}_2\text{O}$ ) spectroscopy where the absence of a single, large upfield signal that correlates to the two BOC groups demonstrated the successful deprotection of the compound. In addition, the  $^1\text{H}$  NMR spectra exhibited 28 protons across 15 signals, compared to the predicted 35 protons of **11**, which correlated with the predicted structure given that  $\text{NH}_3$  and OH protons typically aren't observed due to the broadening of the signal associated with  $\text{NH}_3$  due to H-bonding and exchange of and OH in  $\text{D}_2\text{O}$ . The  $^{13}\text{C}$  NMR spectrum displayed the predicted 23 carbon signals and the absence of the relatively large BOC carbon signals. ESI-MS in positive mode aided the identification of the M-2Cl and M-Cl mass peaks of 412.4 and 446.5 a.m.u. respectively.

### Platinum DAP-estradiol synthesis

Two unique Pt-estradiol complexes, **38** and **39** were successfully synthesised by two variant Pt complexation methods, where **38**, the dicarboxylato complex serves as a carboplatin analogue and **39**, the dichlorido complex serves as a cisplatin analogue.

The characterisation of **38** was informed by  $^1\text{H}$  NMR ( $\text{DMF-}d_7$  and  $\text{DMSO-}d_6$ ),  $^{195}\text{Pt}$  NMR ( $\text{DMSO-}d_6$ ) spectroscopy, EA and FT-IR. The resonances observed in the  $\text{DMF-}d_7$   $^1\text{H}$  NMR spectrum correlate with predicted values. 32 protons were accounted for of the expected **39**. Outstanding proton signals are found within the DMF and water residual solvent peaks, in line with the number observed for the free ligand **11**. Likewise, 32 protons were accounted for in a similar manner in the  $\text{DMSO-}d_6$   $^1\text{H}$  NMR. The  $^{195}\text{Pt}$  NMR spectrum of **39** displayed a single peak at -3245.61 ppm, which falls into the predicted range of  $\text{Pt(II)(O,O')N}_2$  type complexes.<sup>20-21</sup> Elemental analysis for **38** is consistent with the theoretical values of  $[\text{Pt(II)(CBDCA)(DAP-Estradiol)}].1.5\text{H}_2\text{O}$ . FT-IR shows the carbonyl  $\text{C=O}$  peak of the bidentate CBDCA at  $1648\text{ cm}^{-1}$ .

The characterisation of **39** was informed by  $^1\text{H}$  NMR ( $\text{DMF-}d_7$ ),  $^{195}\text{Pt}$  NMR ( $\text{DMSO-}d_6$ ) spectroscopy, EA and FT-IR. The resonances observed in the  $\text{DMF-}d_7$   $^1\text{H}$  NMR spectrum integrate for 34 protons, which correlate with predicted values for **39** and with the free ligand **11**. The  $^{195}\text{Pt}$  NMR spectrum of **39** displayed a single peak at -2277.74 ppm, which falls into the predicted range of  $\text{Pt(II)N}_2\text{Cl}_2$  type complexes.<sup>20-21</sup> Elemental analysis for **39** is consistent with the theoretical values of  $[\text{Pt(II)Cl}_2(\text{DAP-Estradiol})].0.25\text{H}_2\text{O}$ .

Unlike previously reported Pt-steroid complexes connected *via* N,N-bidentate ligands (**Figure 6.9**), the novel complexes **38** and **39** are coordinated to the Pt(II) metal centre from the steroid over a shorter distance, and utilise a click triazole spacer moiety (**Figure 6.7**). In addition, the previously reported examples of Pt-estrogen complexes have used a variety of modifications to the steroid frame to form a ligand, through C17 on the D ring (**Figure 6.9a**),<sup>12</sup> as reported with complexes **38** and **39**, through C15 of the D ring (**Figure 6.9b**), which utilises a PEG spacer group<sup>22</sup> and by C7 of the B ring (**Figure 6.9c**).<sup>21</sup>

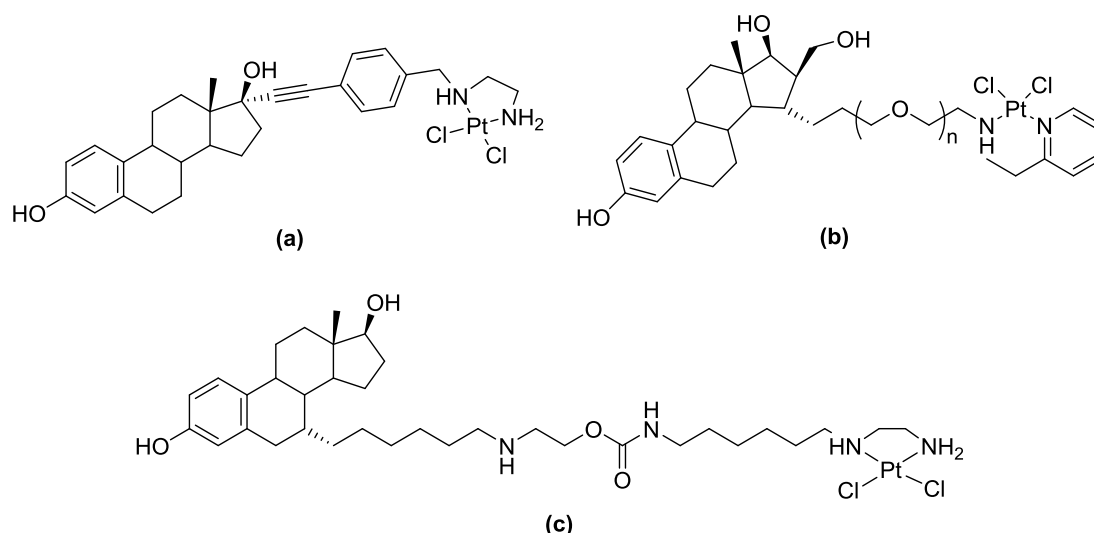


**Figure 6.9:** Examples of Pt(II) estrogen complexes which use *N,N*-bidentate linkers.<sup>12, 21-22</sup>

#### DAP-Testosterone synthesis

The BOC protected product **12** was characterised by  $^1\text{H}$  NMR ( $\text{CDCl}_3$ ) spectroscopy where a single, large peak at 1.42 ppm correlates to the two symmetrical BOC groups attached. The triazole peak serving as the diagnostic signal was found as a singlet at 7.58 ppm, integrating for one proton (**Figure 6.10**). The predicted 53 protons were identified in the  $^1\text{H}$  NMR spectrum across 16 signals. Furthermore, the  $^{13}\text{C}$  NMR spectrum displayed the expected 26 unique peaks for the 34 carbon structure of **12**. ESI-MS in positive mode aided the identification of the  $\text{M}+\text{H}$  and  $\text{M}+\text{Na}$  mass peaks of 628.5 and 650.5 a.m.u. respectively.



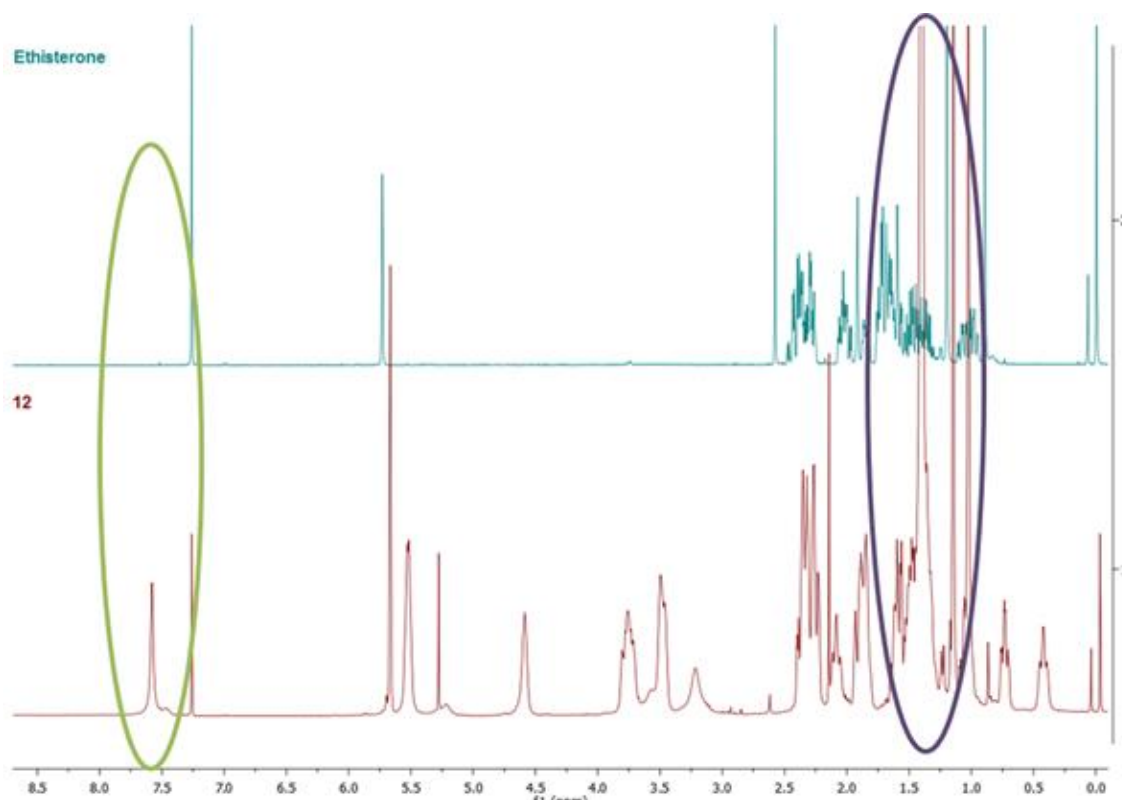


**Figure 6.10:** Overlap  $^1\text{H}$  NMR of testosterone starting material, ethisterone and **12**. The emergence of the new triazole proton at 7.58 ppm is circled in green, and the appearance of the 18 protons of the two BOC groups is shown in purple at 1.42 ppm are evidence of **12**'s formation.

The dihydrochloride salt product **13** was characterised by  $^1\text{H}$  NMR ( $\text{MeOD-}d_4$ ) spectroscopy where the absence of the single, large upfield signal that correlates to the two BOC groups demonstrated the successful deprotection of the compound. In addition, the  $^1\text{H}$  NMR spectra exhibited 31 protons across 14 signals, compared to the predicted 39 protons of **13**, which correlated with the predicted structure given that the outstanding protons are accounted for due to (i) the broadening of the signal associated with  $\text{NH}_3$  H-bonding in  $\text{MeOD-}d_4$ , (ii) exchange of OH protons with  $\text{MeOD-}d_4$  and (iii) the final proton predicted to be masked by the residual water solvent peak. The  $^{13}\text{C}$  NMR spectrum was as expected, also showing the absence of the large BOC carbon peaks. ESI-MS in positive mode aided the identification of the M-2Cl mass peak of 428.5 a.m.u.

**Platinum DAP-testosterone attempted synthesis**

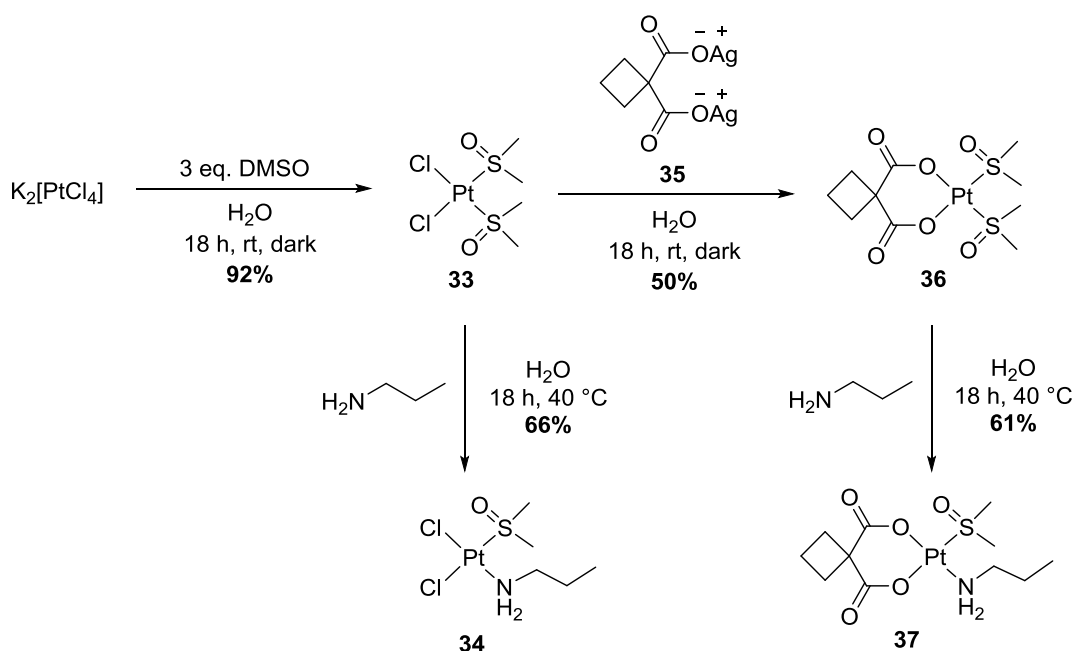
The carboplatin-like testosterone derivate was not successfully synthesised. There is evidence in the  $^1\text{H}$  NMR ( $\text{DMF-}d_7$ ) and ESI-MS spectra that the ligand scaffold (**13**) decomposes under the reaction conditions. In the  $^1\text{H}$  NMR, 31 protons are observed across 14 signals compared to the predicted 43 protons. ESI-MS in positive mode gave an unidentified signal at 570.3 a.m.u. which displays a Pt(II) mass pattern. Furthermore the EA of attempted reaction **40** also did not agree with the required values.

Within the literature and reviews on this topic there are relatively few examples of Pt-testosterone complexes reported when compared with the number of Pt estrogen type complexes, as evident in the reviews of Gust *et al.*, La Bideau *et al.* and Johnstone *et al.*<sup>6, 11, 23</sup> This may be due in part to the relatively poorer aqueous solubility and solubility in aqueous miscible solvents of testosterone in comparison to estradiol,<sup>24-25</sup> making it more challenging to successfully complex with Pt(II).

Although a Pt-testosterone derivative could not be synthesised, the two novel Pt-estradiol complexes, **38** and **39**, as carboplatin and cisplatin analogues were successfully generated in good with yield and analysis. These Pt-steroid conjugates, which may be endowed with improved targeting and cancer selectivity relative to cisplatin and carboplatin, represent interesting novel candidates for *in vitro* cytotoxicity testing.

## Synthesis of Pt DMSO *n*-propylamine complexes

Pt DMSO *n*-propylamine (*n*-pa) complexes, [PtCl<sub>2</sub>(DMSO)(*n*-pa)] and [Pt(CBDCA)(DMSO)(*n*-pa)] were selected as ideal precursors for the synthesis of Pt mixed amine dichlorido complexes and CBDCA complexes featuring a tetrazine handle and as cisplatin and carboplatin analogues respectively.



**Scheme 6.4:** Synthetic route for the synthesis of Pt dichlorido and Pt CBDCA complexes containing DMSO and *n*-pa ligands **34** and **37**.

**Table 6.1.** Overview of the peaks observed by IR spectroscopy.

Complex	(-H) stretch	(-H) bend	( C = O ) s	( S = O ) s
<b>33</b>	---	---	---	1016 cm <sup>-1</sup>
<b>34</b>	3248, 3202 cm <sup>-1</sup>	1572 cm <sup>-1</sup>	---	1039 cm <sup>-1</sup>
<b>35</b>	---	---	1495 cm <sup>-1</sup>	---
<b>CBDCAH<sub>2</sub></b>	---	---	1687 cm <sup>-1</sup>	---
<b>36</b>	---	1602 cm <sup>-1</sup>	1660 cm <sup>-1</sup>	1025 cm <sup>-1</sup>
<b>37</b>	3252, 3203 cm <sup>-1</sup>	1615 cm <sup>-1</sup>	1655 cm <sup>-1</sup>	1030 cm <sup>-1</sup>

***cis*-[Pt(II)Cl<sub>2</sub>(DMSO)<sub>2</sub>] synthesis**

*cis*-[Pt(II)Cl<sub>2</sub>(DMSO)<sub>2</sub>], **33** was synthesised in a single step following the previous published method of Shahabadi *et al.*<sup>18</sup> K<sub>2</sub>[PtCl<sub>4</sub>] was dissolved in H<sub>2</sub>O with 3 eq. of DMSO and stirred at rt for 18 h in the dark to yield **33** (Scheme 6.4). The characterisation was informed by FT-IR and EA, which correlated with the previously reported analysis.<sup>18</sup>

***cis*-[Pt(II)Cl<sub>2</sub>(DMSO)(*n*-pa)] synthesis**

*cis*-[Pt(II)Cl<sub>2</sub>(DMSO)(*n*-pa)], **34** was synthesised in a single step by stirring a suspension of **33** in H<sub>2</sub>O with *n*-pa at 40 °C for 2 h to yield **34** (Scheme 6.4).

The characterisation was informed by <sup>1</sup>H and <sup>13</sup>C NMR (D<sub>2</sub>O) spectroscopy, ESI-MS and FT-IR. The resonances observed in the <sup>1</sup>H NMR spectrum correlate with predicted values and splitting pattern of *n*-pa, giving three diagnostic peaks; at 2.83-2.70 ppm the most down field CH<sub>2</sub> due to the amine groups deshielding effect, at 1.67 ppm the central CH<sub>2</sub> group and at 0.91 ppm, the terminal CH<sub>3</sub> of *n*-pa. Combined with the presence of the 6 protons of the DMSO ligand from 3.54-3.40 ppm, this confirms a successful synthesis. ESI-MS in positive mode aided the identification of the M+Na with a mass peak of 426.3 a.m.u. Elemental analysis for **34** is consistent with theoretical values. In addition, the crystal structure of the complex was solved as seen in the ORTEP structure, in Figure 6.11. The novel unpublished structure was identified, with a polymeric ladder formation running parallel to the b-axis formed by long Pt-Cl interactions (Figure 6.12). The data relating to the crystal and refinement patterns is reported in Table 6.2.

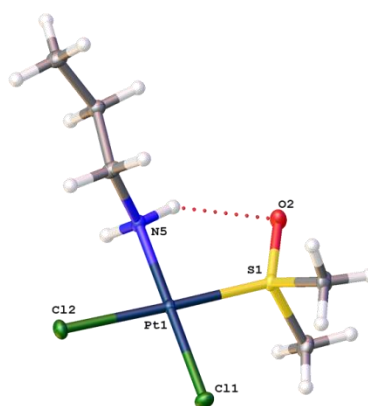


**Figure 6.10:** ORTEP diagram of **34** with atomic displacement parameters shown at 50% probability. Non-carbon atoms labelled and hydrogen atoms omitted for clarity.

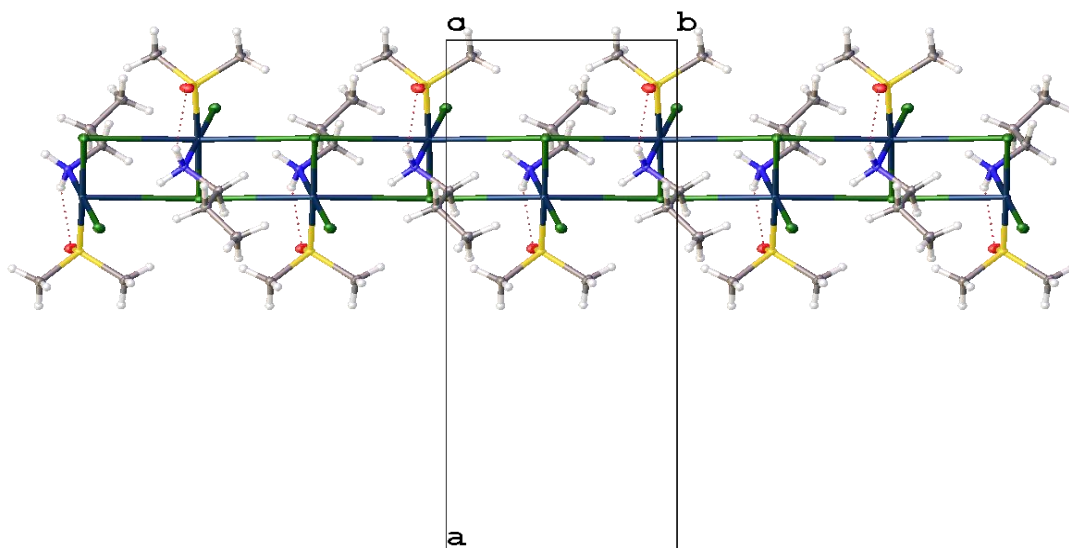


**Figure 6.11:** Polymeric ladder formation of **34** running parallel to the b-axis formed by long Pt...Cl interactions ( $\text{Cl2}\dots\text{Pt}\$1 = 3.8031(5)\text{\AA}$ ,  $\text{Pt1}\dots\text{Cl2\_}\$1 = 3.7283(5)\text{\AA}$ ; symmetry transformation  $\$1 = 1.5-X, -0.5+Y, 0.5-Z,$ ).

**Table 6.2.** Selected bond lengths [ $\text{\AA}$ ] and angles [ $^\circ$ ] determined for **34**.

Bond	Length $\text{\AA}$	Bond	Angles $^\circ$
Pt(1)-Cl(1)	2.3211(5)	Cl(1)-Pt(1)-Cl(2)	91.170(19)
Pt(1)-Cl(2)	2.3192(5)	S(1)-Pt(1)-Cl(1)	91.170(19)
Pt(1)-S(1)	2.1850(5)	N(5)-Pt(1)-S(1)	89.08(5)
Pt(1)-N(5)	2.0474(17)	N(5)-Pt(1)-Cl(2)	88.59(5)
Pt(1)-Cl(2)#1	3.7283(5)	S(1)-Pt(1)-Cl(2)	177.343(18)
		N(5)-Pt(1)-Cl(1)	179.59(5)

The molecular structure of *cis*-[Pt(II)Cl<sub>2</sub>(DMSO)(*n*-pa)] (**34**) in **Figure 6.10** clearly shows the typical Pt(II) square planar geometry. The bond angles of the central Pt substituents Cl(1)-Pt(1)-Cl(2), S(1)-Pt(1)-Cl(1), N(5)-Pt(1)-S(1) and N(5)-Pt(1)-Cl(1) are at approximately 90° and the S(1)-Pt(1)-Cl(2) and N(5)-Pt(1)-Cl(1) are approximately 180°, (**Table 6.2**). The Pt-Cl bond lengths are 2.32  $\text{\AA}$ , the Pt-S 2.19  $\text{\AA}$  and Pt-N 2.05  $\text{\AA}$ .

**[Pt(II)(CBDCA)(DMSO)<sub>2</sub>] synthesis**

[Pt(II)(CBDCA)(DMSO)<sub>2</sub>], **36** was synthesised in a single step following the previous published method of Bitha *et al.*<sup>19</sup> Ag<sub>2</sub>CBDCA (**35**) and **33** were suspended in H<sub>2</sub>O and stirred at rt for 18 h in the dark to yield **36** (Scheme 6.4).

The characterisation was informed by <sup>1</sup>H and <sup>13</sup>C NMR (D<sub>2</sub>O) spectroscopy, ESI-MS and FT-IR. Elemental analysis for **36** is consistent with theoretical values and all other analysis correlated with those previously reported.<sup>19</sup>

**[Pt(II)(CBDCA)(DMSO)(*n*-pa)] synthesis**

[Pt(II)(CBDCA)(DMSO)(*n*-pa)], **37** was synthesised in a single step by stirring a suspension of **36** in H<sub>2</sub>O with *n*-pa at 40 °C for 2 h to yield **37** (Scheme 6.4), as previously reported.<sup>19</sup>

The characterisation was informed by <sup>1</sup>H and <sup>13</sup>C NMR (D<sub>2</sub>O) spectroscopy, ESI-MS and FT-IR. The resonances observed in the <sup>1</sup>H NMR spectrum correlate with predicted values, with the *n*-pa protons giving three diagnostic peaks at 2.66-2.58 ppm as the most down field CH<sub>2</sub> due to the amine groups deshielding effect, 1.72-1.60 ppm; the central CH<sub>2</sub> group (CH<sub>2</sub>) and 0.89 ppm as the terminal CH<sub>3</sub> of *n*-pa. The remaining signals integrate for the CBDCA and DMSO ligands confirming the successful synthesis. ESI-MS in positive mode aided the identification of the M+H, M+Na, 2M+H and 2M+Na with mass peaks of 475.2, 497.1, 949.3 and 971.4 a.m.u. respectively. Elemental analysis for **37** is consistent with theoretical values. In addition, the previously unreported crystal structure of the complex was solved as seen in the ORTEP structure in Figure 6.12. The data relating to the crystal and refinement patterns is reported in Table 6.3.

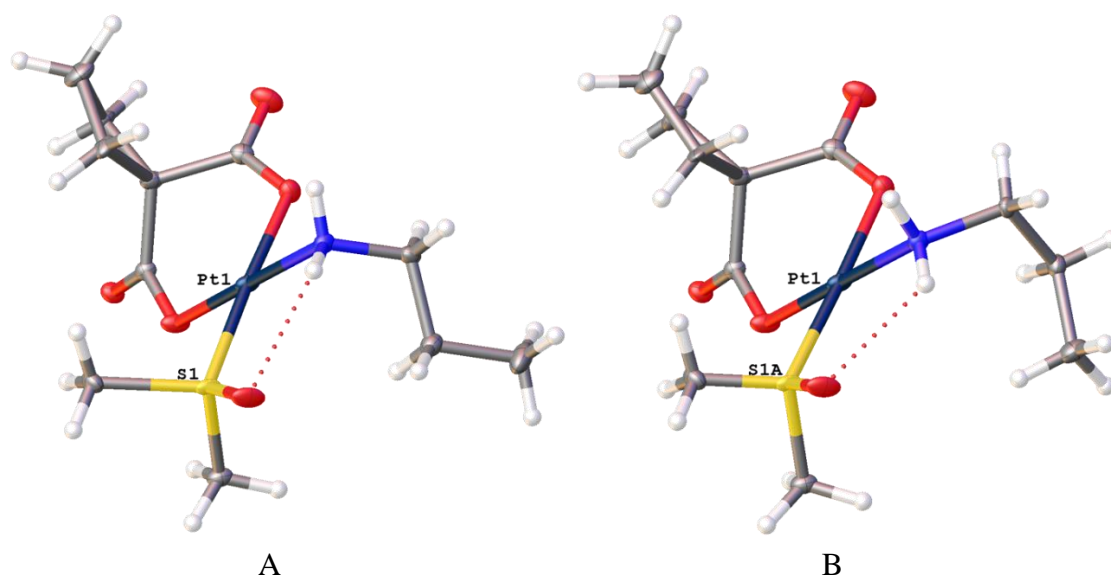


**Figure 6.12:** ORTEP diagram of **37** with atomic displacement parameters shown at 50% probability. Non-carbon atoms labelled and hydrogen atoms omitted for clarity. Individual images of each disordered moiety (A) DMSO, propylamine and cyclobutane groups disordered with occupancies of 67, 57 and 57 % and (B) 33, 43 and 43% respectively.

**Table 6.3.** Selected bond lengths [Å] and angles [°] determined for **37-A**.

Bond	Length Å	Bond	Angles °
Pt(1)-S(1)	2.180(8)	O(0AA)-Pt(1)-S(1)	90.04(18)
Pt(1)-O(0AA)	2.0232(15)	O(0AA)-Pt(1)-O(12)	90.77(6)
Pt(1)-O(12)	2.0276(16)	O(12)-Pt(1)-N(13)	87.12(7)
Pt(1)-N(13)	2.0375(17)	N(13)-Pt(1)-S(1)	91.97(18)
		O(0AA)-Pt(1)-N(13)	177.20(7)
		O(12)-Pt(1)-S(1)	177.0(2)

The molecular structure of [Pt(II)(CBDCA)(DMSO)(*n*-pa)] (**37**) in **Figure 6.12** clearly shows the typical Pt(II) square planar geometry. The bond angles of the central Pt substituents O(0AA)-Pt(1)-S(1), O(0AA)-Pt(1)-O(12), O(12)-Pt(1)-N(13) and N(13)-Pt(1)-S(1) are approximately 90° and the O(0AA)-Pt(1)-N(13) and O(12)-Pt(1)-S(1) are approximately 180 ° (**Table 6.3**). The Pt-O bond lengths are 2.03 Å,

the Pt-S 2.18 Å and Pt-N 2.04 Å, where the Pt-S and Pt-N are very similar to those in **34**.

Two crystal conformations of complex **37** were observed due to the free bond rotation of the *n*-pa ligand in contrast to **34** where only a single structural conformation observed in the solid state.

**33**, **34**, **36** and **37** were synthesised in good yield and high purity as important platinum precursors in investigations described below.

**Table 6.4.** Crystal data and structure refinement for **34** and **37**.

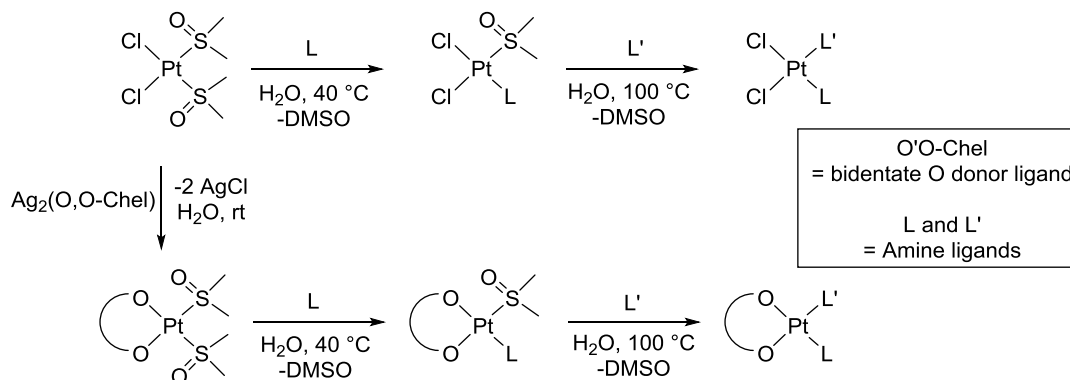
Compound	<b>34</b>	<b>37</b>
Empirical formula	C <sub>5</sub> H <sub>15</sub> Cl <sub>2</sub> NOPtS	C <sub>11</sub> H <sub>21</sub> NO <sub>5</sub> PtS
Formula weight	403.23	474.44
Temperature	100 K	100 K
Wavelength	0.71073 Å	0.71073 Å
Crystal system	Monoclinic	Monoclinic
Space group	C2/c	P2 <sub>1</sub> /n
Unit cell dimensions	a = 20.9490(8) Å, U = 90°. b = 20.9490(8) Å, V = 121.1433(12)°. c = 16.9429(7) Å, [ = 90°.	a = 8.2289(3) Å, U = 90°. b = 9.9801(3) Å, V = 94.9380(10)°. c = 17.8668(6) Å, [ = 90°.
Volume	2224.63(16) Å <sup>3</sup>	1461.87(8) Å <sup>3</sup>
Z	8	4
Density (calculated)	2.408 Mg/m <sup>3</sup>	2.156 Mg/m <sup>3</sup>
Absorption coefficient	13.236 mm <sup>-1</sup>	9.756 mm <sup>-1</sup>
F(000)	1504	912
Crystal size	0.26 x 0.22 x 0.08 mm <sup>3</sup>	0.29 x 0.14 x 0.04 mm <sup>3</sup>
Theta range for data collection	3.005 to 30.645°.	2.823 to 33.342°.
Index ranges	-30 ≤ h ≤ 28, -9 ≤ k ≤ 10, -18 ≤ l ≤ 24	-12 ≤ h ≤ 12, -15 ≤ k ≤ 15, -27 ≤ l ≤ 27
Reflections collected	19325	44917
Independent reflections	3431 [R(int) = 0.0276]	5646 [R(int) = 0.0369]
Completeness to theta = 26.000°	99.9 %	99.9 %



Absorption correction	Semi-empirical from equivalents	Semi-empirical from equivalents
Max. and min. transmission	0.7461 and 0.4115	0.7465 and 0.3931
Refinement method	Full-matrix least-squares on $F^2$	Full-matrix least-squares on $F^2$
Data / restraints / parameters	3431 / 2 / 111	5646 / 154 / 247
Goodness-of-fit on $F^2$	1.105	1.117
Final R indices [ $I > 2\sigma(I)$ ]	$R1 = 0.0157$ , $wR2 = 0.0341$	$R1 = 0.0195$ , $wR2 = 0.0423$
R indices (all data)	$R1 = 0.0182$ , $wR2 = 0.0349$	$R1 = 0.0223$ , $wR2 = 0.0431$
Largest diff. peak and hole	0.763 and -1.594 e. $\text{\AA}^{-3}$	1.738 and -1.961 e. $\text{\AA}^{-3}$

### Attempted synthesis of Pt-tetrazine

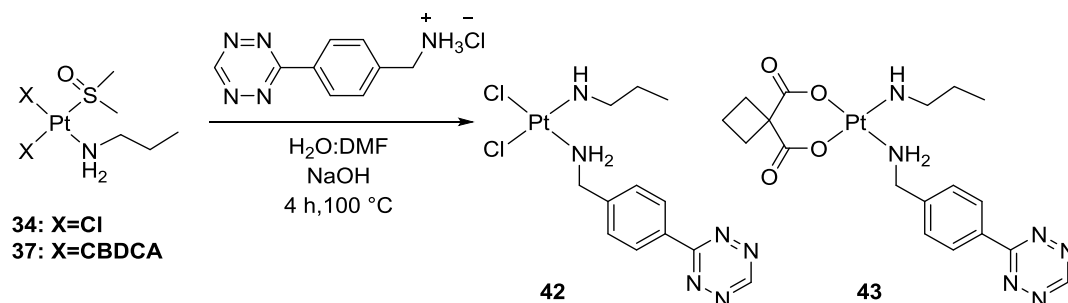
*cis*-[Pt(II)Cl<sub>2</sub>(DMSO)(*n*-pa)], **34** and [Pt(II)(CBDCA)(DMSO)(*n*-pa)], **37** were selected for reaction with tetrazine amine. Bitha *et al.* previously reported **37** as an ideal precursor for the synthesis of mixed am(m)ine complexes as per **Scheme 6.5**.<sup>19</sup> However, this approach was not explored for dichlorido Pt complexes.



**Scheme 6.5:** Synthesis of mixed am(m)ine complexes by 2 step ligand exchange.<sup>19</sup>

In turn it was hypothesised that reaction of both **34** and **37** with tetrazine amine as per **Scheme 6.6** would generate complexes **42** and **43**, which would serve as cisplatin and carboplatin type complexes featuring an iEDDA tetrazine click handle.

Reaction of tetrazine amine with complexes **34** and **37** did not generate the desired products, and analysis of the products isolated failed to reveal their identity. There are no literature reports of Pt binding to tetrazine moieties, so it is likely that the tetrazine ligand was not stable under the experimental conditions employed. This supposition is supported by the publication of Karver *et al.*, which describes the decomposition of tetrazine amine in aqueous solution over time and where decomposition was accelerated with heating.<sup>26</sup>



**Scheme 6.6:** Synthetic route for the synthesis of Pt-tetrazine complexes **42** and **43**.

Ultimately, a novel strategy is likely required to incorporate a tetrazine handle into a Pt complex.

## Conclusion and Future Work

Casini and coworkers bis(monodentate) pyridyl ligands, designed for the self-assembly of Pt and Pd metallocage structures, were successfully derivatised with an azide functional group to give **14**. A protocol was established for the successful click reaction of the azide derived ligands with phenacetylene and a BODIPY derived fluorophore MAMP (**16**) and standard photophysical properties of **16** determined.

**14** and **16** will be supplied to Casini and coworkers (Cardiff University) and their Pt(II) and Pd(II) metallocages synthesised and their activity studied.

A series of steroid derivatives of estradiol and testosterone were synthesised and their coordination to Pt investigated. Using CuAAC click chemistry techniques, bidentate *N,N*-carrier ligands coupled to estradiol and testosterone (**11** and **13**) were successfully synthesised. Estradiol compound **11** was successfully conjugated to two Pt complexes (**33** and **36**) to generate Pt-estradiol complexes **38** and **39**. However, due to poorer stability of the testosterone ligand, it was not possible to generate the Pt-testosterone complex **40**.

Future work would look towards reacting **13** with Pt-DMSO type precursors<sup>27</sup> in organic solvents (such as DCM), in order to obtain a Pt-testosterone complex. In addition to this, *in vitro* studies are currently being carried out on complexes **38** and **39** in collaboration with Dr. Diego Montagner (Maynooth University).

A Pt ammine dichlorido DMSO complex *cis*-[PtCl<sub>2</sub>(DMSO)(*n*-pa)] (**34**) was successfully synthesised and characterised by NMR, MS, EA and IR, in addition to its crystal structure being determined. The crystal structure for the previously reported [Pt(CBDCA)(DMSO)(*n*-pa)] (**37**) was also determined.

Future work on this topic aims to further test the report of Bitha *et al.* that [Pt(ammine)Cl<sub>2</sub>(DMSO)] and [Pt(ammine)(dicarboxylato)(DMSO)] complexes are reliable precursors for the synthesis of the corresponding mixed ammine complexes on reaction with a secondary amine.<sup>19</sup> In addition, another suitable tetrazine based ligand should be sourced or synthesised, which is stable at elevated temperatures (100 °C) in aqueous solution to generate the desired Pt-complex featuring an IEDDA capable handle.

## References

- Schmidt, A.; Molano, V.; Hollering, M.; Pöthig, A.; Casini, A.; Kühn Fritz, E., Evaluation of New Palladium Cages as Potential Delivery Systems for the Anticancer Drug Cisplatin. *Chemistry óA European Journal* **2016**, 22 (7), 2253-2256.
- Kaiser, F.; Schmidt, A.; Heydenreuter, W.; Altmann Philipp, J.; Casini, A.; Sieber Stephan, A.; Kühn Fritz, E., Self-Assembled Palladium and Platinum Coordination Cages: Photophysical Studies and Anticancer Activity. *European Journal of Inorganic Chemistry* **2016**, 2016 (33), 5189-5196.
- Evolution of Cancer Treatments: Hormone Therapy. *American Cancer Society* **2014**.
- Early Breast Cancer Trialists' Collaborative Group, Relevance of breast cancer hormone receptors and other factors to the efficacy of adjuvant tamoxifen: patient-level meta-analysis of randomised trials. *The Lancet* **2011**, 378 (9793), 771-784.
- Carlsson, J.; Nordgren, H.; Sjöström, J.; Wester, K.; Villman, K.; Bengtsson, N. O.; Ostenstad, B.; Lundqvist, H.; Blomqvist, C., HER2 expression in breast cancer primary tumours and corresponding metastases. Original data and literature review. *British Journal Of Cancer* **2004**, 90, 2344.
- Johnstone, T. C.; Suntharalingam, K.; Lippard, S. J., The Next Generation of Platinum Drugs: Targeted Pt(II) Agents, Nanoparticle Delivery, and Pt(IV) Prodrugs. *Chemical reviews* **2016**, 116 (5), 3436-3486.
- Hu, R.; Dunn, T. A.; Wei, S.; Isharwal, S.; Veltri, R. W.; Humphreys, E.; Han, M.; Partin, A. W.; Vessella, R. L.; Isaacs, W. B.; Bova, G. S.; Luo, J., Ligand-Independent Androgen Receptor Variants Derived from Splicing of Cryptic Exons Signify Hormone-Refractory Prostate Cancer. *Cancer Research* **2009**, 69 (1), 16.
- Albanito, L.; Madeo, A.; Lappano, R.; Vivacqua, A.; Rago, V.; Carpino, A.; Oprea, T. I.; Prossnitz, E. R.; Musti, A. M.; Andò, S.; Maggiolini, M., G Protein-Coupled Receptor 30 (GPR30) Mediates Gene Expression Changes and Growth Response to 17 $\beta$ -Estradiol and Selective GPR30 Ligand G-1 in Ovarian Cancer Cells. *Cancer Research* **2007**, 67 (4), 1859.
- He, Q.; Liang, C. H.; Lippard, S. J., Steroid hormones induce HMG1 overexpression and sensitize breast cancer cells to cisplatin and carboplatin. *Proceedings of the National Academy of Sciences* **2000**, 97 (11), 5768.
- Ahmad, N.; Kumar, R., Steroid hormone receptors in cancer development: A target for cancer therapeutics. *Cancer Letters* **2011**, 300 (1), 1-9.
- Gust, R.; Beck, W.; Jaouen, G.; Schönenberger, H., *Optimization of cisplatin for the treatment of hormone dependent tumoral diseases Part 1: Use of steroidal ligands*. 2009; Vol. 253, p 2742-2759.
- Gabano, E.; Cassino, C.; Bonetti, S.; Prandi, C.; Colangelo, D.; Ghiglia, A.; Osella, D., Synthesis and characterisation of estrogenic carriers for cytotoxic Pt(ii) fragments: biological activity of the resulting complexes. *Organic & Biomolecular Chemistry* **2005**, 3 (19), 3531-3539.
- Gandolfi, O.; C. Apfelbaum, H.; Migron, Y.; Blum, J., *Syntheses of cis-dichlorodiammineplatinum analogs having steroidal hormones bound to the metal atom via malonato bridges*. 1989; Vol. 161, p 113-123.
- Oliveira, B. L.; Guo, Z.; Bernardes, G. J. L., Inverse electron demand Diels-Alder reactions in chemical biology. *Chemical Society Reviews* **2017**, 46 (16), 4895-4950.
- Knall, A.-C.; Slugovc, C., Inverse electron demand Diels-Alder (iEDDA)-initiated conjugation: a (high) potential click chemistry scheme. *Chemical Society Reviews* **2013**, 42 (12), 5131-5142.
- Wu, D.; Cheung, S.; O'Sullivan, C. J.; Gao, Y.; Chen, Z.-l.; O'Shea, D. F., Strained alkyne substituted near infrared BF<sub>2</sub> azadipyromethene fluorochrome. *RSC Adv.* **2016**, 6 (90), 87373-87379.
- Kitteringham, E.; Wu, D.; Cheung, S.; Twamley, B.; O'Shea, D. F.; Griffith, D. M., Development of a novel carboplatin like cytoplasmic trackable near infrared fluorophore

conjugate via strain-promoted azide alkyne cycloaddition. *Journal of Inorganic Biochemistry* **2018**, *182*, 150-157.

18. Shahabadi, N.; Heidari, L., Synthesis, characterization and multi-spectroscopic DNA interaction studies of a new platinum complex containing the drug metformin. *Spectrochimica Acta Part A: Molecular and Biomolecular Spectroscopy* **2014**, *128*, 377-385.

19. Bitha, P.; Morton, G. O.; Dunne, T. S.; Delos Santos, E. F.; Lin, Y. I.; Boone, S. R.; Haltiwanger, R. C.; Pierpont, C. G., (Malonato)bis[sulfinylbis[methane]-S]platinum(II) compounds: versatile synthons for a new general synthesis of antitumor symmetrical and dissymmetrical (malonato)platinum(II) complexes. *Inorganic Chemistry* **1990**, *29* (4), 645-652.

20. Still, B. M.; Kumar, P. G. A.; Aldrich-Wright, J. R.; Price, W. S., 195Pt NMR-theory and application. *Chemical Society Reviews* **2007**, *36* (4), 665-686.

21. Kim, E.; Rye, P. T.; Essigmann, J. M.; Croy, R. G., A bifunctional platinum(II) antitumor agent that forms DNA adducts with affinity for the estrogen receptor. *Journal of inorganic biochemistry* **2009**, *103* (2), 256.

22. Provencher-Mandeville, J.; Descôteaux, C.; Mandal, S. K.; Leblanc, V.; Asselin, É.; Bérubé, G., Synthesis of 17 $\beta$ -estradiol-platinum(II) hybrid molecules showing cytotoxic activity on breast cancer cell lines. *Bioorganic & Medicinal Chemistry Letters* **2008**, *18* (7), 2282-2287.

23. Le Bideau, F.; Dagorne, S., Synthesis of Transition-Metal Steroid Derivatives. *Chemical Reviews* **2013**, *113* (10), 7793-7850.

24. 17 $\beta$ -Estradiol Product Information. *Cayman Chemical Item No. 100006315*, CAS No. 50-28-2.

25. Testosterone Product Information. *Merck: Sigma-Aldrich Item No. T1500 Sigma*, CAS No. 58-22-0.

26. Karver, M. R.; Weissleder, R.; Hilderbrand, S. A., Synthesis and Evaluation of a Series of 1,2,4,5-Tetrazines for Bioorthogonal Conjugation. *Bioconjugate Chemistry* **2011**, *22* (11), 2263-2270.

27. Schweinfurth, D.; Pattacini, R.; Strobel, S.; Sarkar, B., New 1,2,3-triazole ligands through click reactions and their palladium and platinum complexes. *Dalton Transactions* **2009**, (42), 9291-9297.

## Thesis Conclusion

This thesis was focused on the functionalisation of platinum based drugs through click chemistry strategies. A number of successful click syntheses and conjugation approaches were investigated, generating novel ligands and Pt complexes. Furthermore, the chemical, photophysical and biological properties of a number of these functionalised Pt conjugates were determined.

Chapter 3 investigated the synthesis and *in vitro* analysis of a novel Pt NIR-AZA fluorophore conjugate. This complex was generated using SPAAC click chemistry, the first example where the azide handle resides on the stable ammine carrier ligand. It was designed to structurally mimic the anticancer Pt drug carboplatin so as to track its movement throughout the cytoplasm of the cell. *In vitro* analysis in ovarian cancer cells A2780P and A2780cis showed that the Pt-fluorophore conjugate was non-toxic in a cellular environment and was effectively internalised as shown by widefield NIR cellular imaging. The Pt-fluorophore complex developed shows good fluorescent imaging properties in the NIR range, demonstrating its viability as a carboplatin-like click probe. The core Pt complex [Pt(CBDCA)(DAP-N<sub>3</sub>)], which has click capabilities, displayed a similar cytotoxic profile to carboplatin, highlighting it as a good carboplatin mimic and as a bioorthogonal Pt drug complex. The novel X-ray crystal structure of [Pt(CBDCA)(DAP-N<sub>3</sub>)] was determined.

In chapter 4, the synthesis of 14-mer TPP and corresponding scrambled peptide sequence, ScP, with identical amino acid composition has been reported. In addition, novel Pt-peptide mono-conjugates were successfully synthesised for each peptide as [Pt(DACH)(OEt)(Ox)(succTPP)] and [Pt(DACH)(OEt)(Ox)(succScP)]. The resulting Pt-peptide conjugates were subsequently characterised and their *in vitro* cytotoxicity against colorectal cancer cells, HCT116 wt and HT29, determined. The data suggests that while the Pt-TPP conjugate was less cytotoxic than oxaliplatin, conjugation of the TPP targeting peptide to the Pt(IV) core ([Pt(DACH)(OEt)(Ox)(succ)]) endowed [Pt(DACH)(OEt)(Ox)(succTPP)] with the potential for targeting cancerous cells due to its enhanced cytotoxicity. In addition, the co-administration of oxaliplatin and TPP did not enhance the cytotoxic profile indicating TPP functions as a targeting moiety only. This study will be expanded to

determine the cellular accumulation of the Pt complexes described to further demonstrate the enhanced targeting ability of the TPP conjugated Pt complexes.

In chapter 5, the synthesis and characterisation of a novel polydentate 1,4-disubstituted 1,2,3-triazole based ligand, 4-(pyridin-2-yl)-1*H*-1,2,3-triazol-1-yl)propane-1,3-diamine (PTPD) is described. The reactivity of PTPD and the previously reported PTP ligand with Au(III) and Pt(II) centres was investigated. X-ray structural characterisation of [Au(III)Cl<sub>3</sub>(PTP)], [Au(III)Cl<sub>2</sub>(PTPD)][Au(I)Cl<sub>2</sub>][OH]{[NaAuCl<sub>4</sub>.2H<sub>2</sub>O]}<sub>n</sub> and [Pt(II)Cl<sub>2</sub>(PTPDH<sub>2</sub>)][PtCl<sub>4</sub>] and characterisation of [Au(III)Cl<sub>3</sub>(BOC<sub>2</sub>-PTPD)] and [Pt(II)<sub>3</sub>Cl<sub>4</sub>(PTPD)<sub>2</sub>]Cl<sub>2</sub> support the proposition that PTPD is an interesting multidentate ligand that can bind metal centres through a variety of coordination modes including bidentate coordination through the DAP group, bidentate through the triazole N3 and pyridyl nitrogen and monodentate through the pyridyl nitrogen. Ultimately, PTPD is a versatile and ideal ligand template for the development of mixed metal complexes of Pt and Au, and Pt/Au and other transition metals.

In the final chapter, three connected topics were explored which investigated the application and functionalisation of Pt complexes and ligands using a click chemistry approach. In the first instance, a metallocage ligand was functionalised with an azide moiety to give CageL-N<sub>3</sub>. A synthetic protocol was established for the CuAAC click reaction of CageL-N<sub>3</sub> with phenacetylene and an alkyne derivative of a BODIPY fluorophore. Significantly, the cage fluorophore clicked product, Cage-T-MAMP, retained its fluorescent properties. Subsequent metallocage assembly will be performed by Prof. Casini and coworkers and an investigation undertaken to track the metallocage fluorophore conjugate as a drug delivery vector *in vitro*.

Novel estradiol and testosterone bidentate ligands were successfully generated using click chemistry. The estradiol ligand was successfully coordinated in two instances to Pt, to give [Pt(II)Cl<sub>2</sub>(DAP-estradiol)] and [Pt(II)(CBDCA)(DAP-estradiol)] as cisplatin and carboplatin derivatives respectively. These complexes are currently undergoing *in vitro* testing. The Pt-testosterone derivatives were not successfully synthesised.

The final investigation sought to develop iEDDA click capable Pt-tetrazine containing complexes. Two Pt complexes, *cis*-[PtCl<sub>2</sub>(DMSO)(*n*-pa)] and

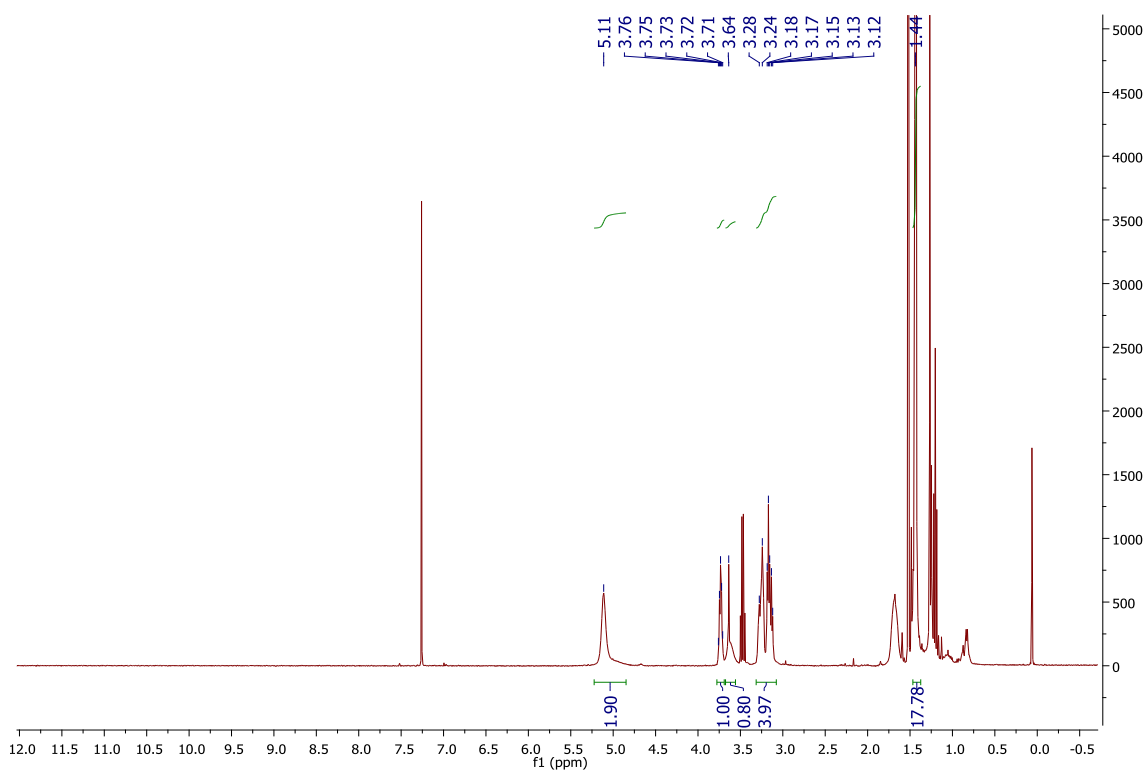
[Pt(CBDCA)(DMSO)(*n*-pa)], were synthesised as ideal precursors for the synthesis of mixed am(m)ine complexes. The novel crystal structures of both these complexes were solved. Reaction of *cis*-[PtCl<sub>2</sub>(DMSO)(*n*-pa)] and [Pt(CBDCA)(DMSO)(*n*-pa)] with the amine tetrazine ligand failed to generate the desired Pt tetrazine complex. This was hypothesised to be due to the instability of the tetrazine under the reaction conditions used. Future work will focus on optimising the reaction conditions and/or sourcing an alternative tetrazine ligand.

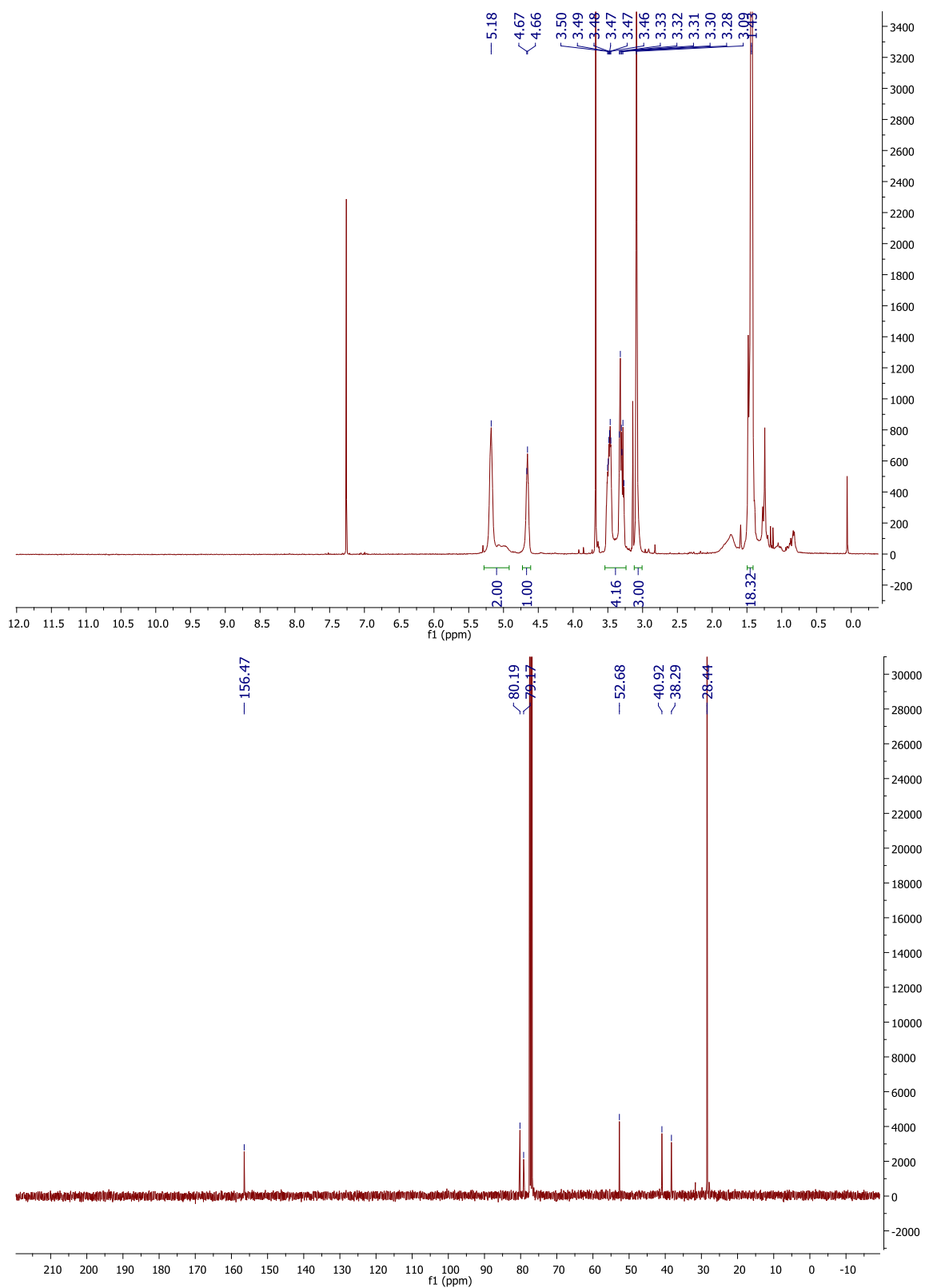
Click chemistry can be used to synthesise functional ligands with extremely useful moieties for the coordination to metal complexes, such as Pt. In addition, click chemistry can be used to generate Pt drug conjugations with desirable functional groups to improve *in vitro* applications. In conclusion, this thesis demonstrates why click chemistry is an invaluable tool to the modern medicinal inorganic chemist.

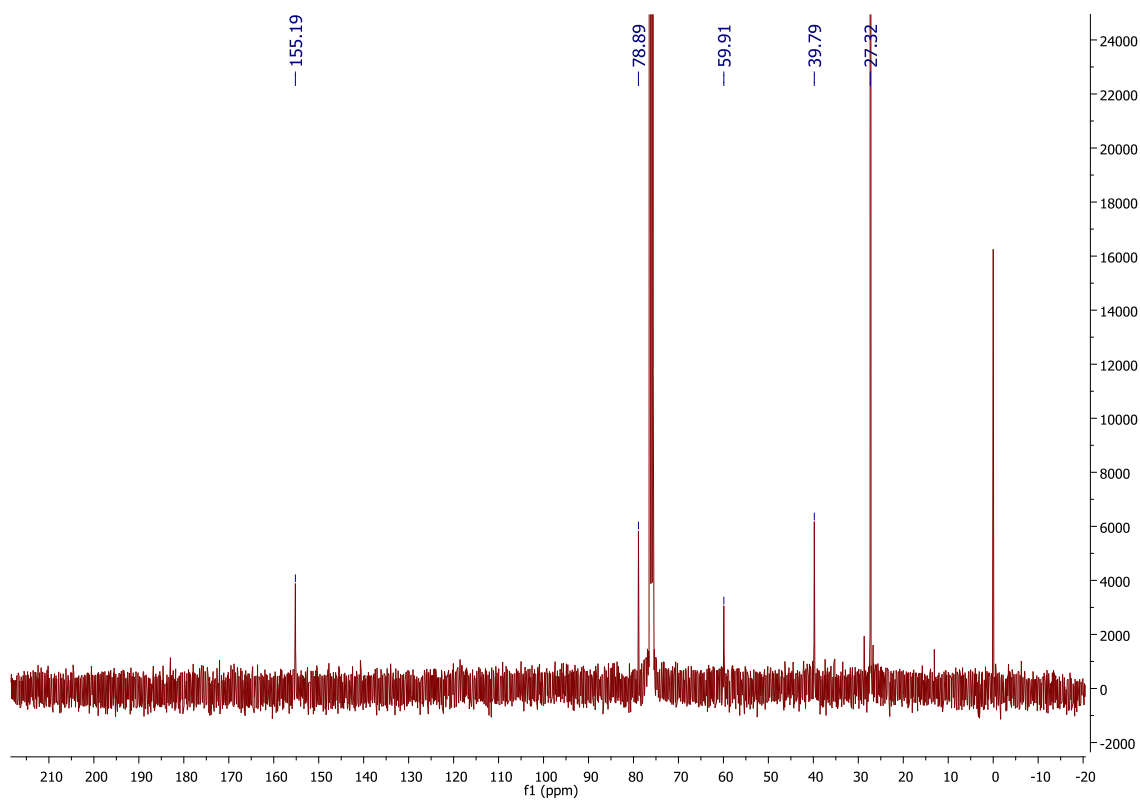
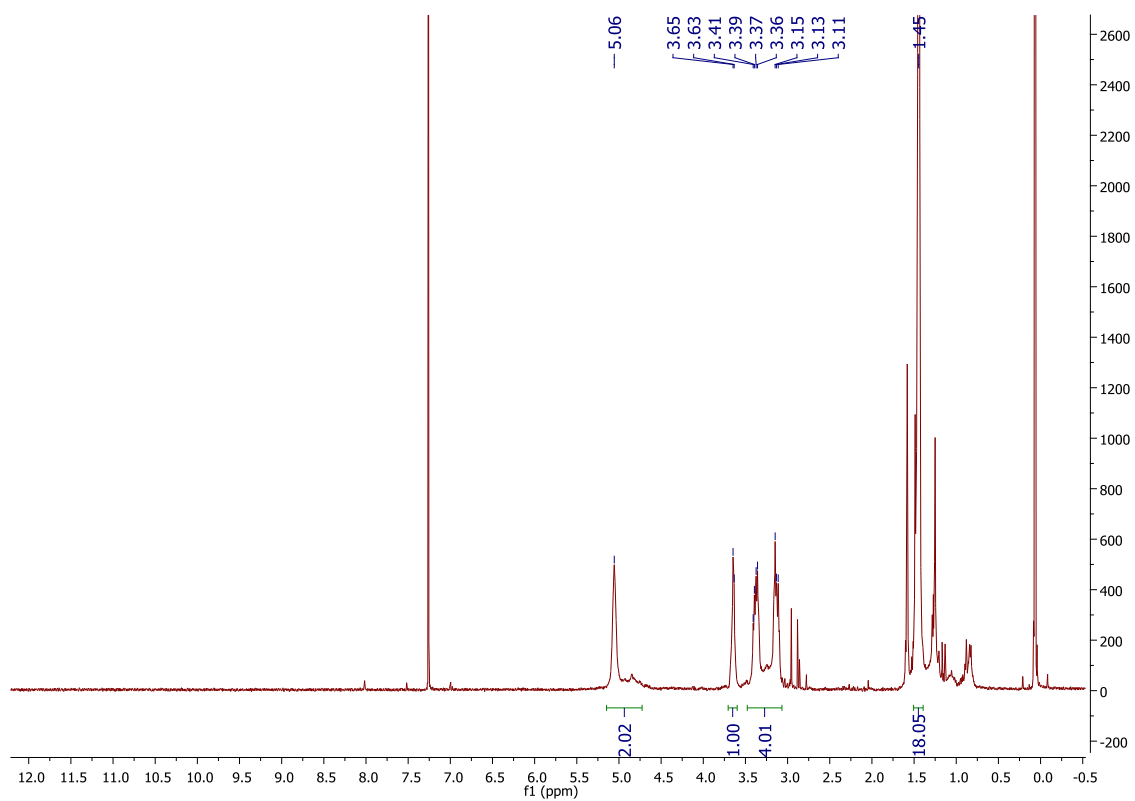


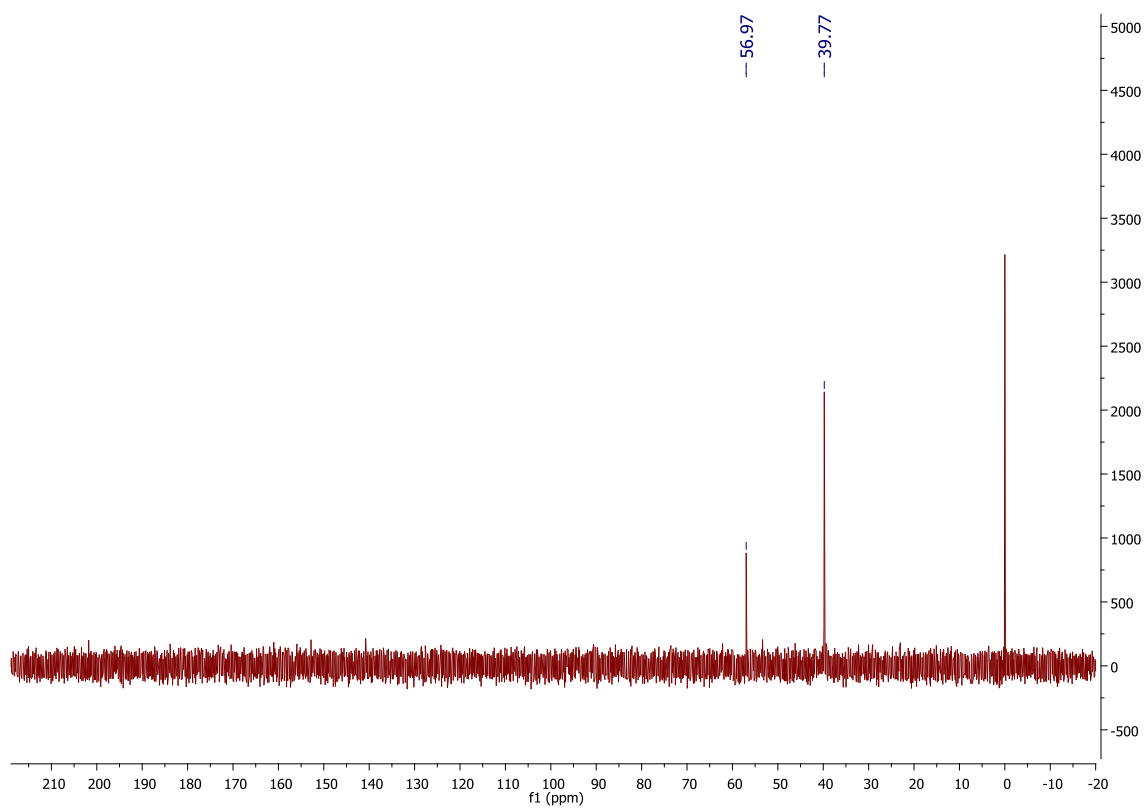
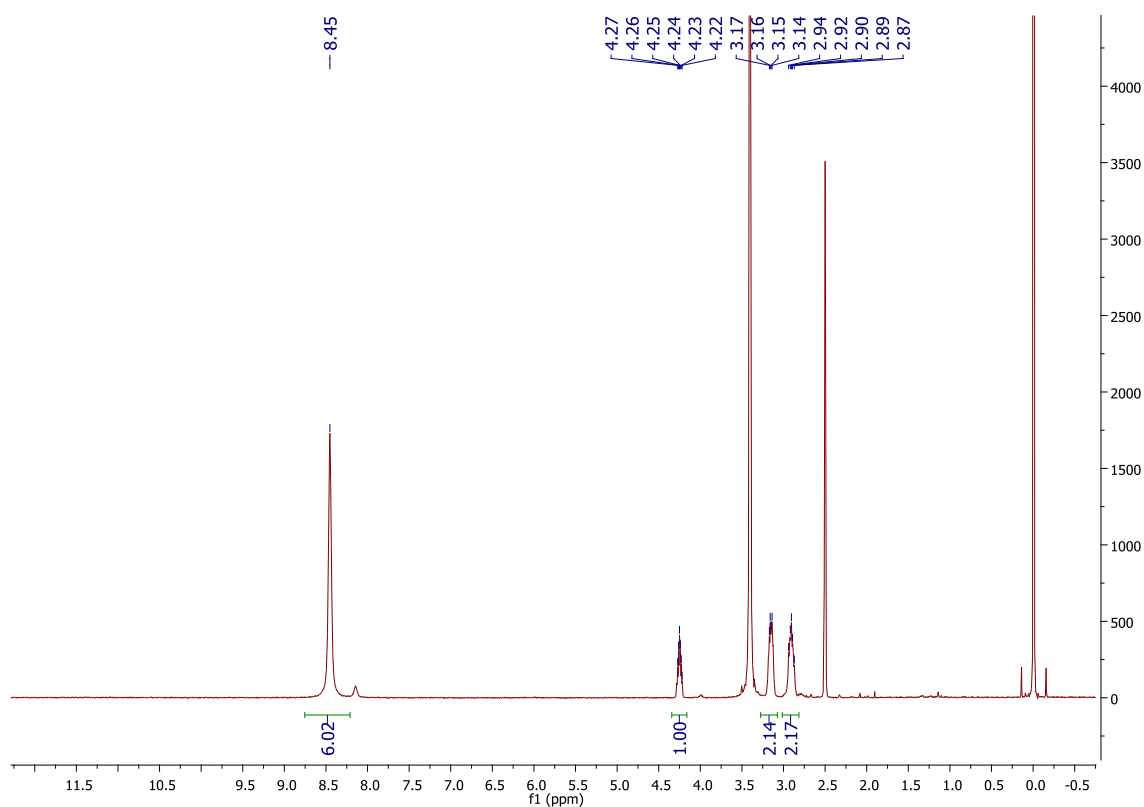
## **Appendix**

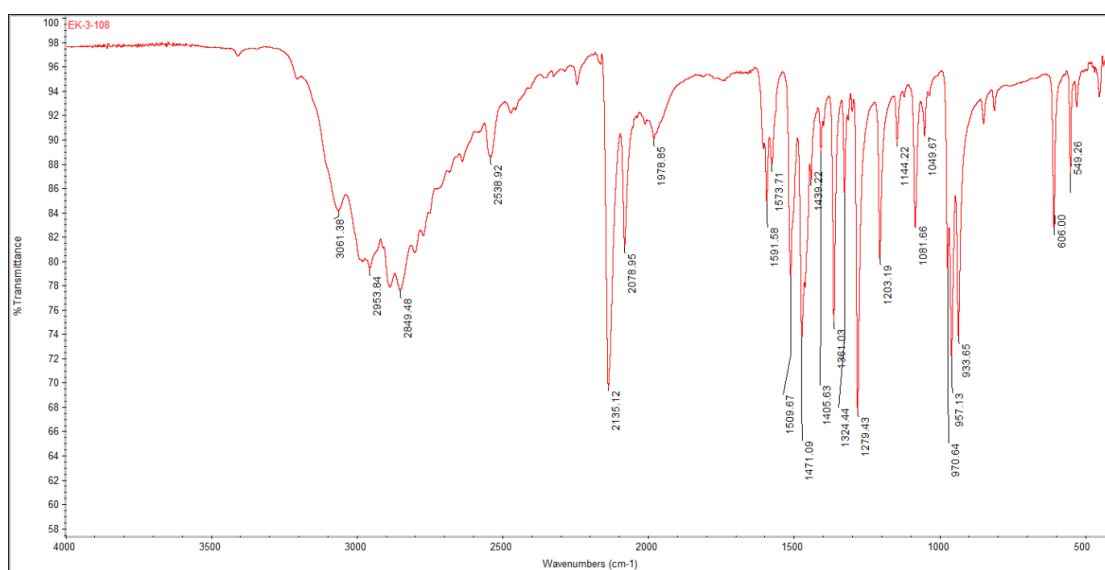
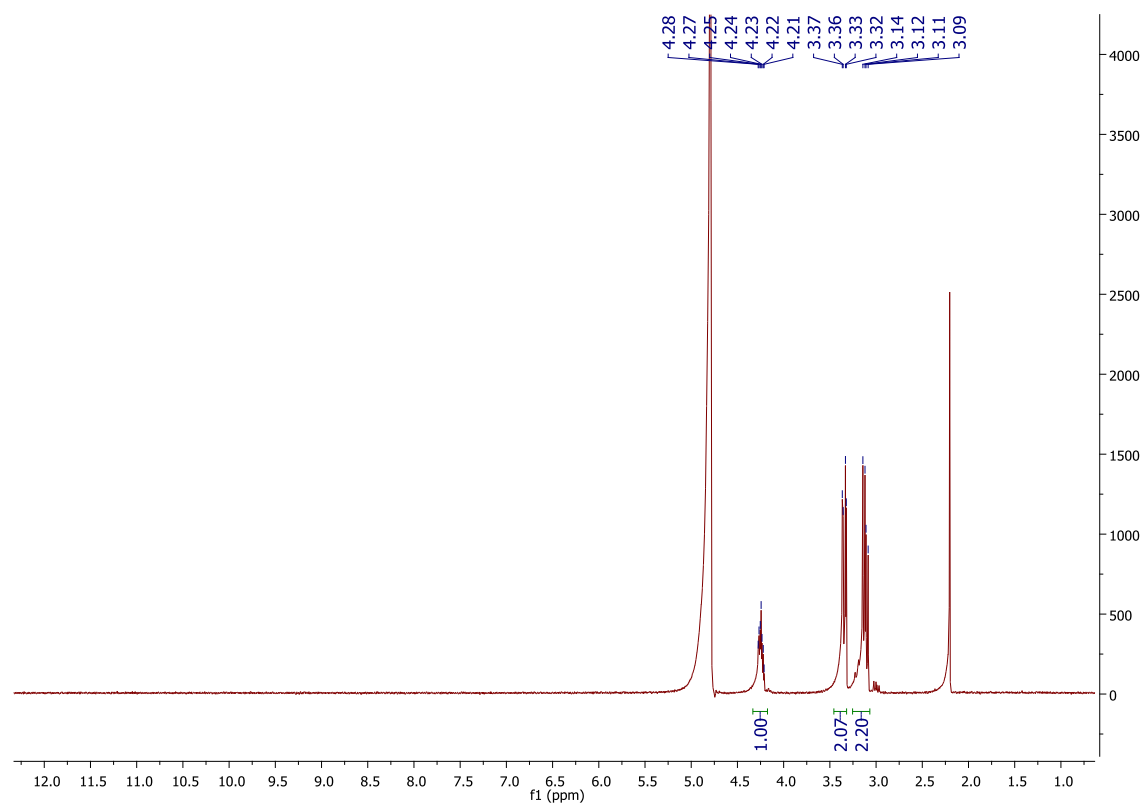
## Organic syntheses

Di-*tert*-butyl (2-hydroxypropane-1,3-diyl)dicarbamate (1)

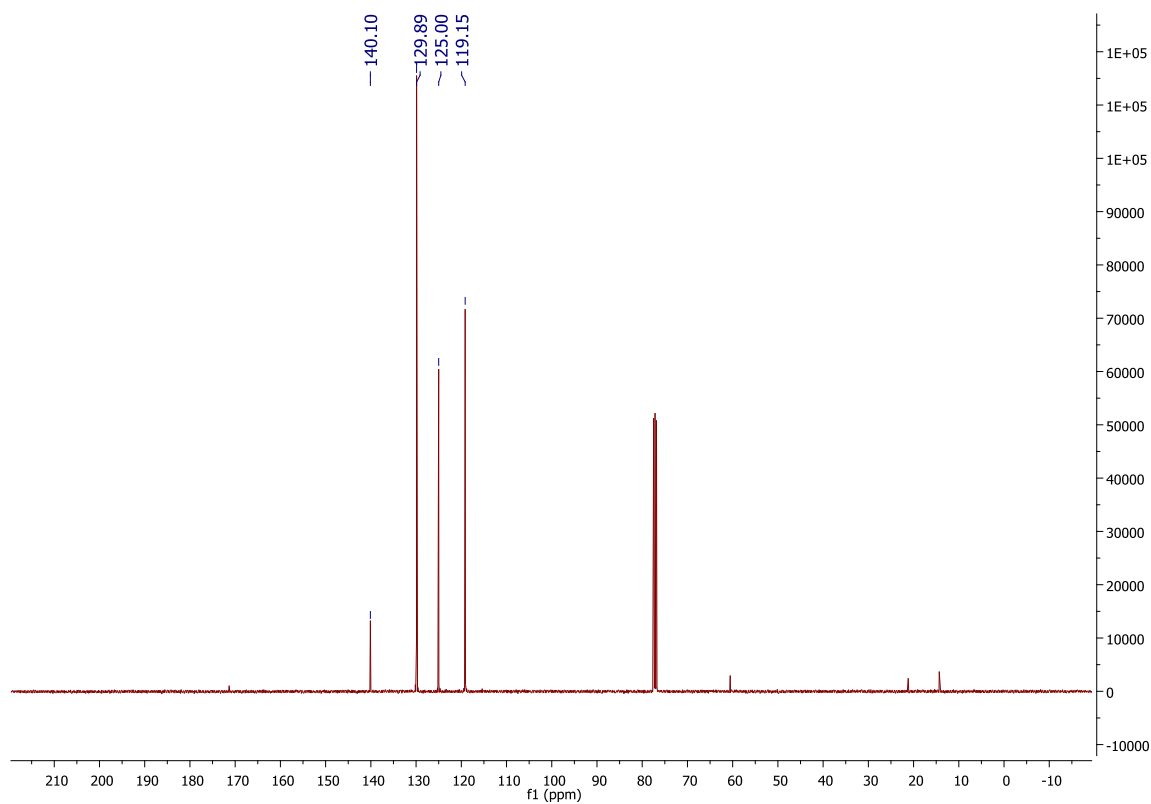
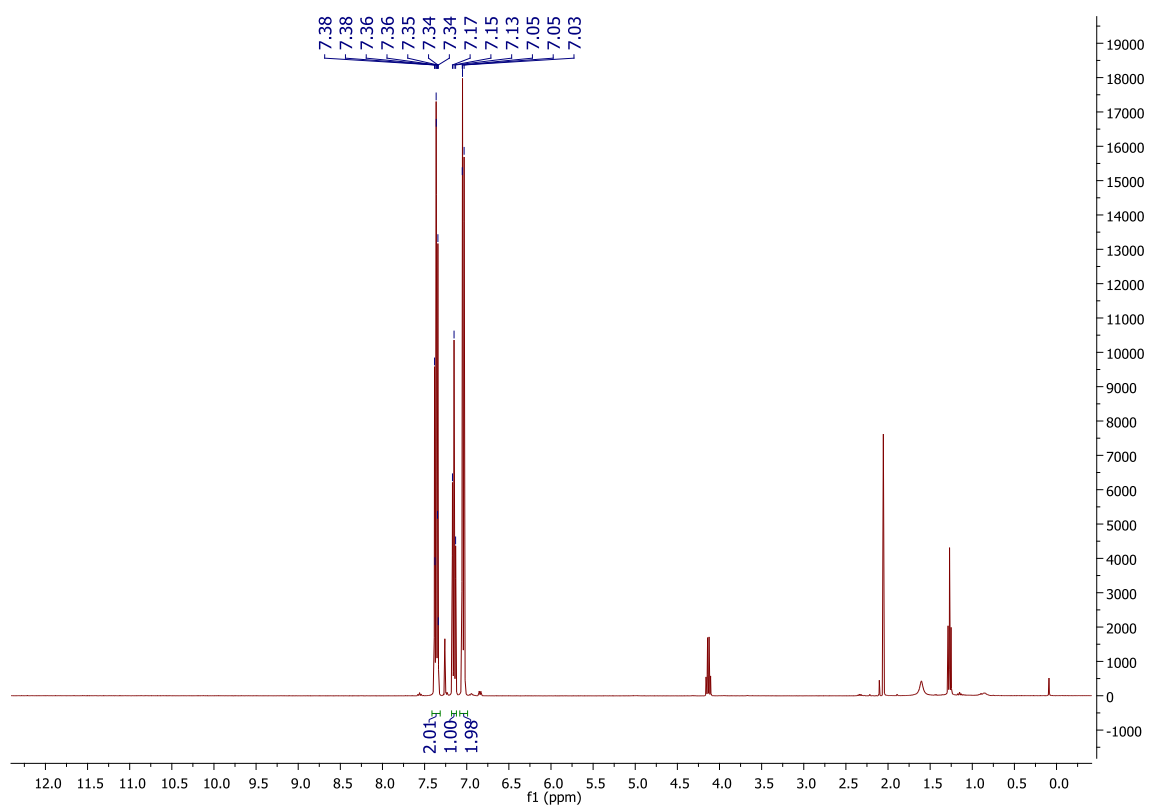
**Di-*tert*-butyl ((propan-2-yl methanesulfonate)-1,3-diyl)dicarbamate (2)**

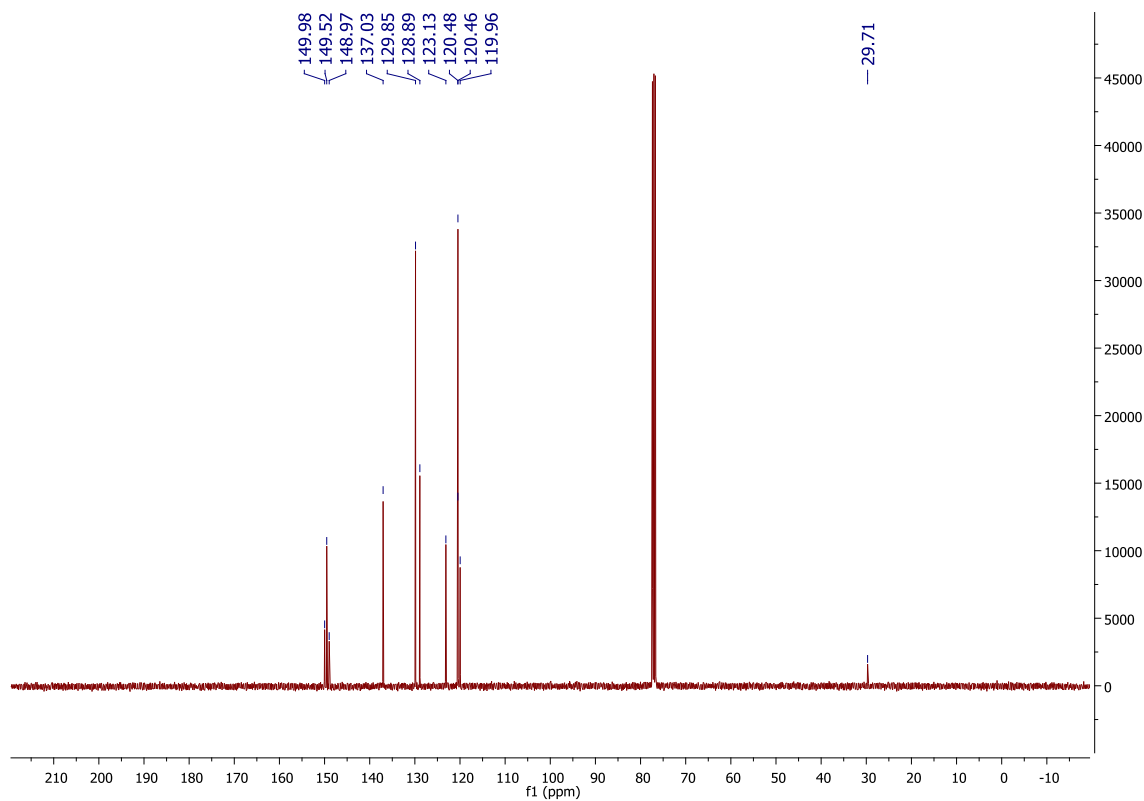
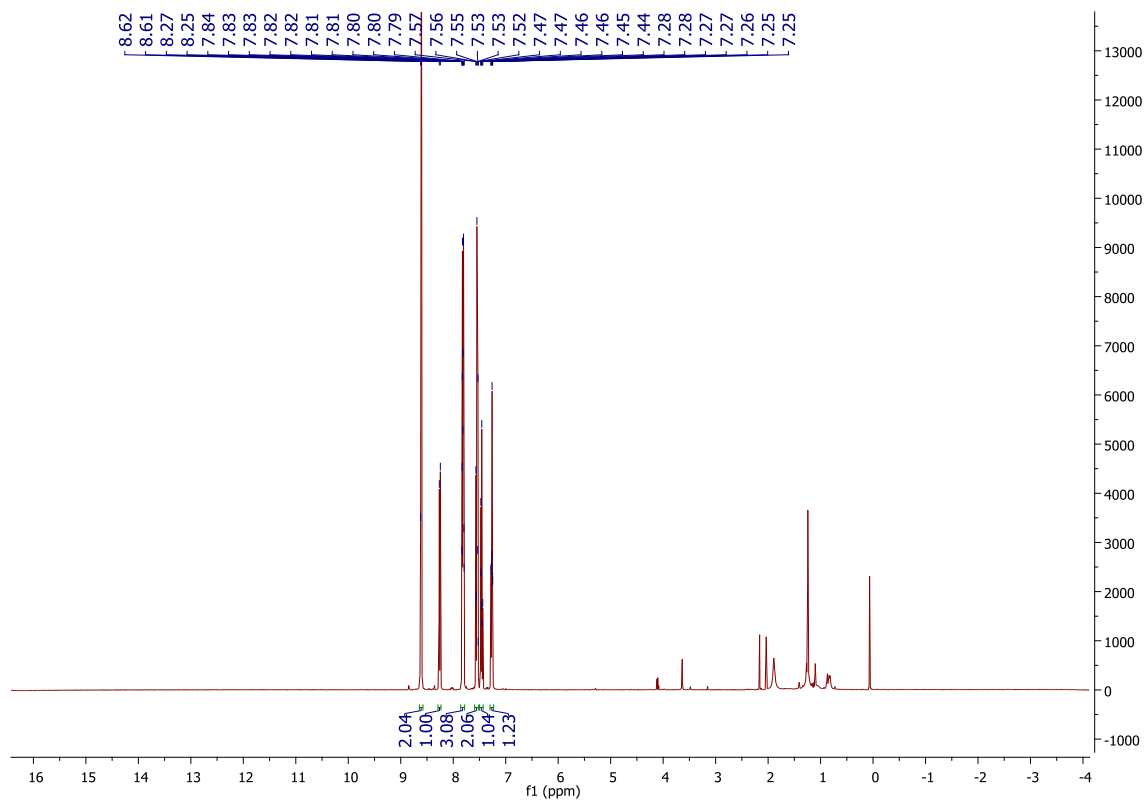
**Di-*tert*-butyl (2-azidopropane-1,3-diyl)dicarbamate (3)**

**2-azidopropane-1,3-diamine dihydrochloride - DAP-N<sub>3</sub>.2HCl (4)**

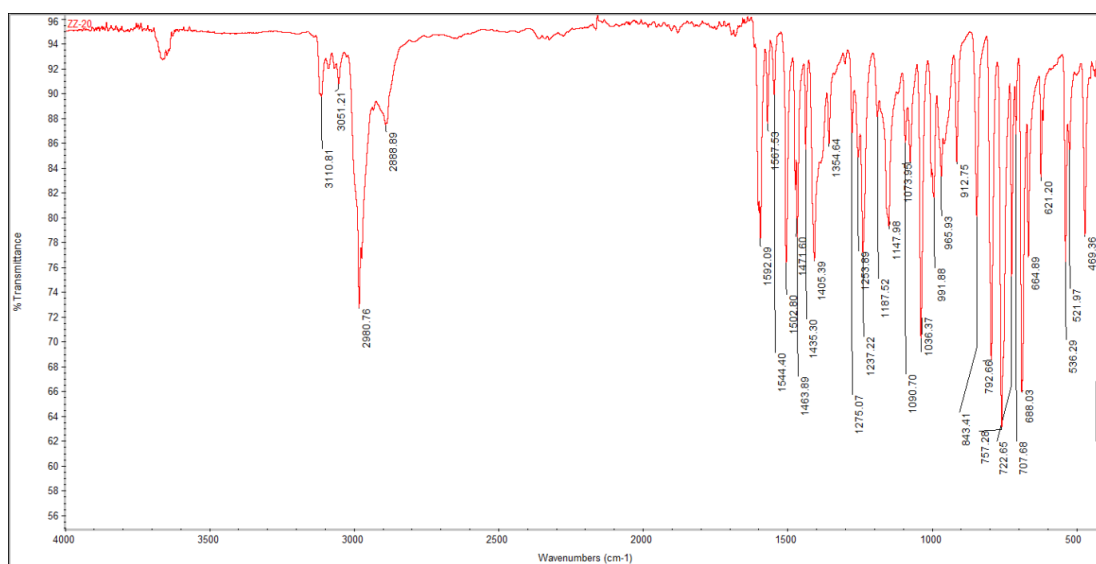


## Azidobenzene (5)

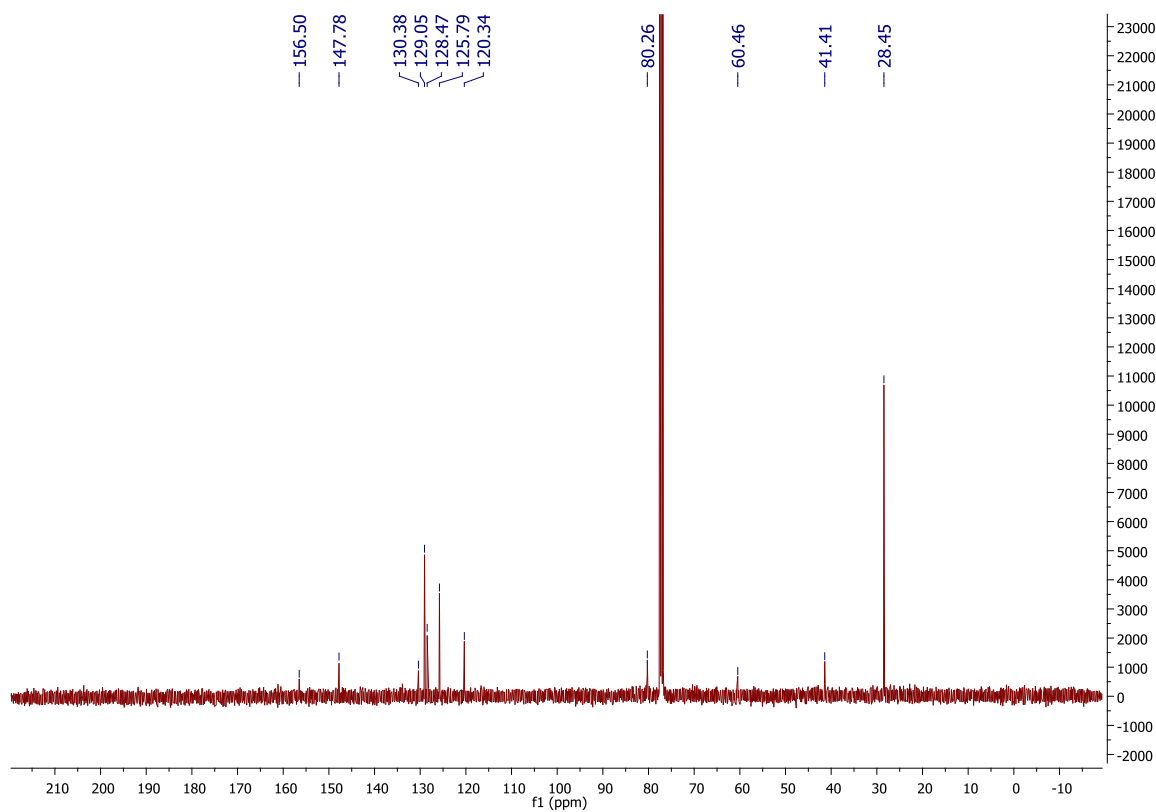
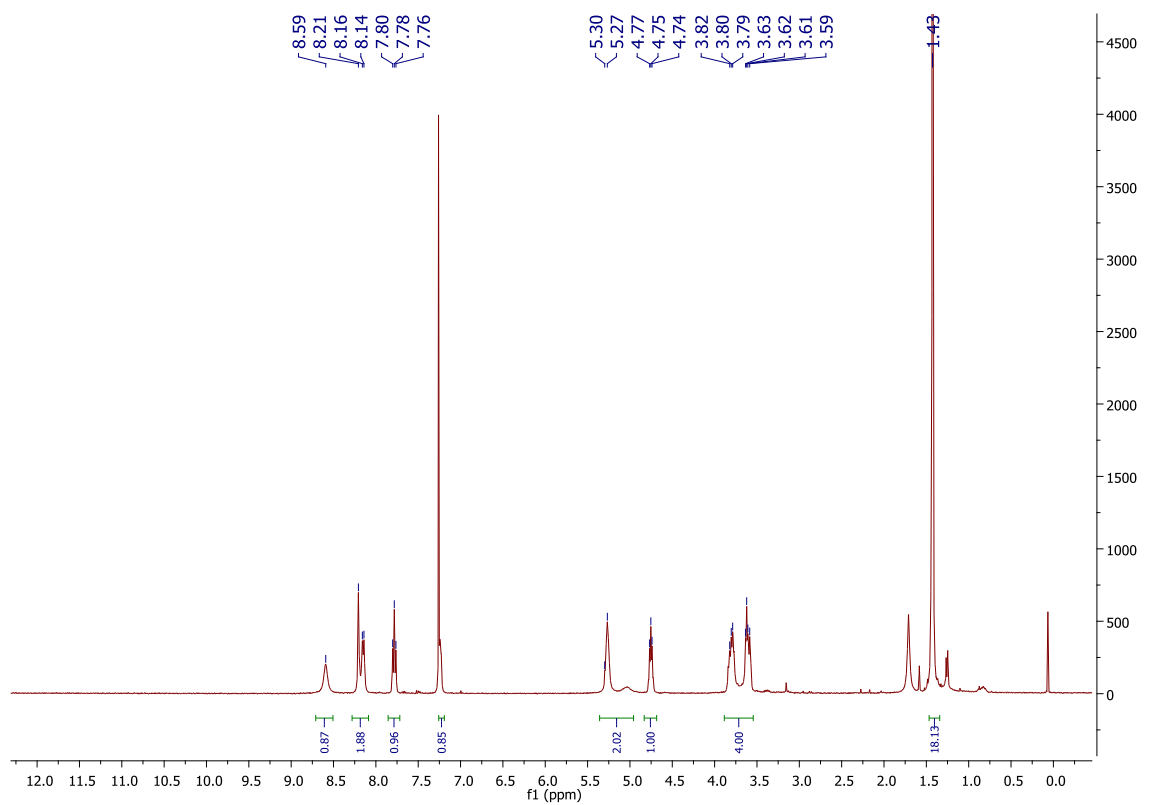


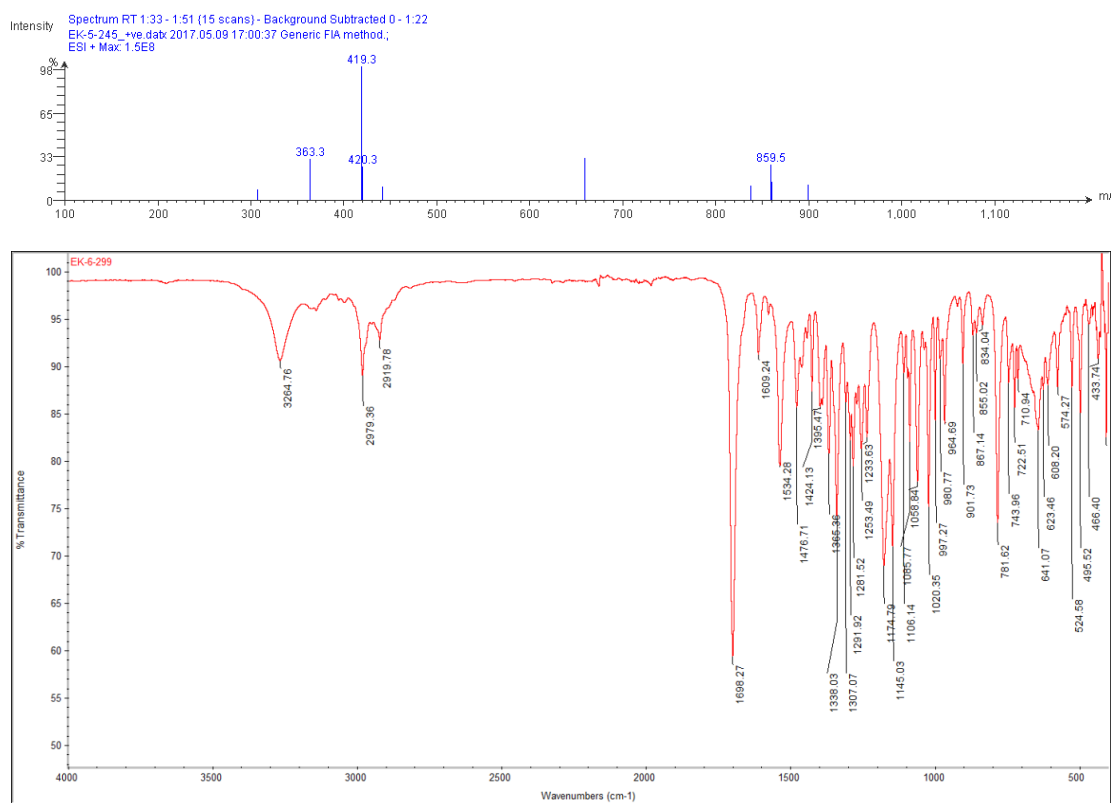
**2-(1-phenyl-1*H*-1,2,3-triazol-4-yl)pyridine (PTP) (6)**

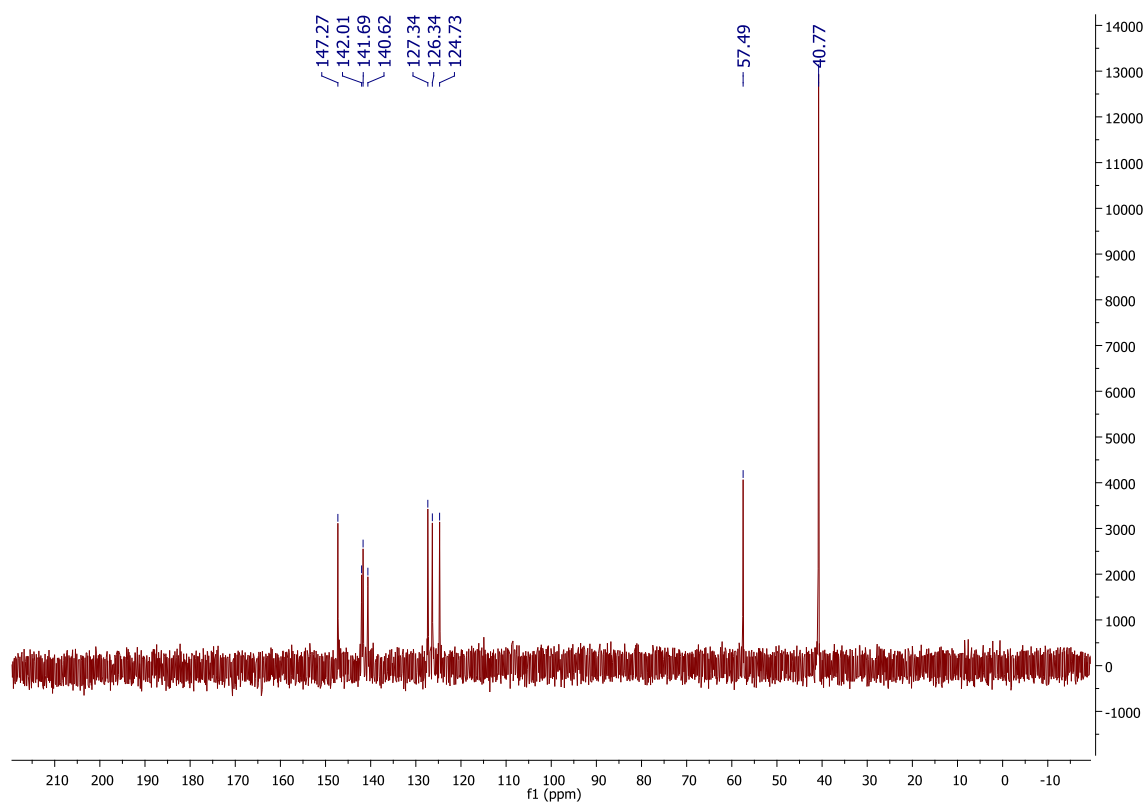
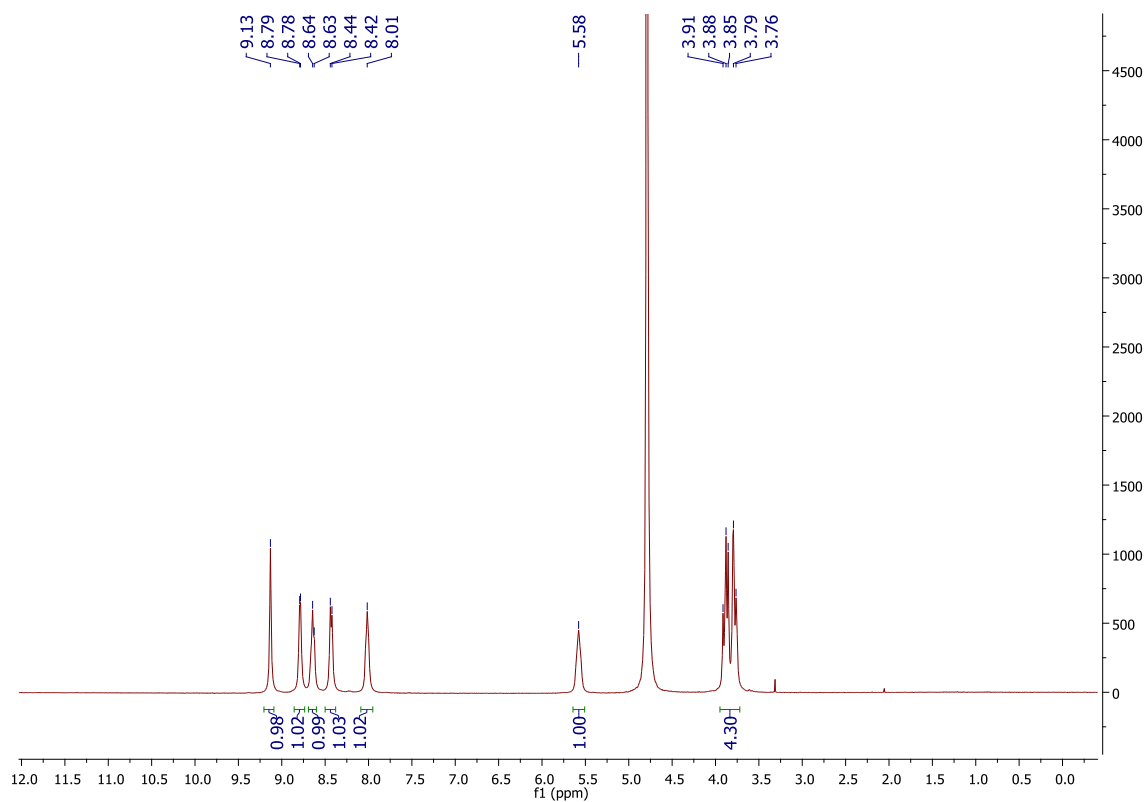




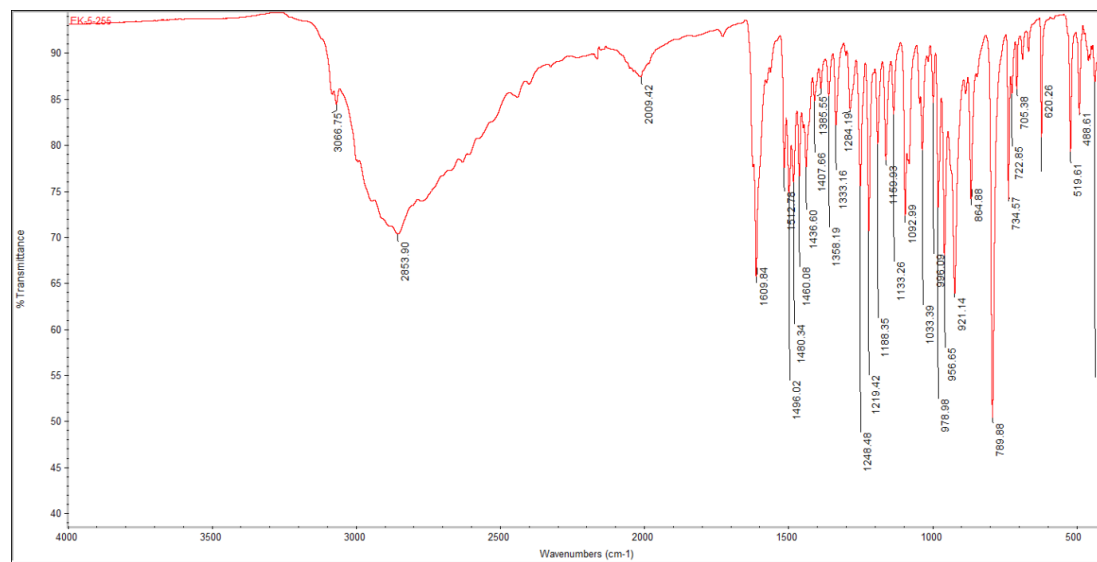
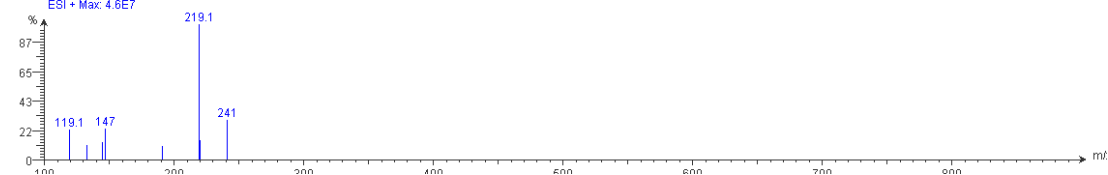
**Di-*tert*-butyl (2-(4-(pyridin-2-yl)-1*H*-1,2,3-triazol-1-yl)propane-1,3-diyl)dicarbamate (BOC<sub>2</sub>-PTPD) (7)**



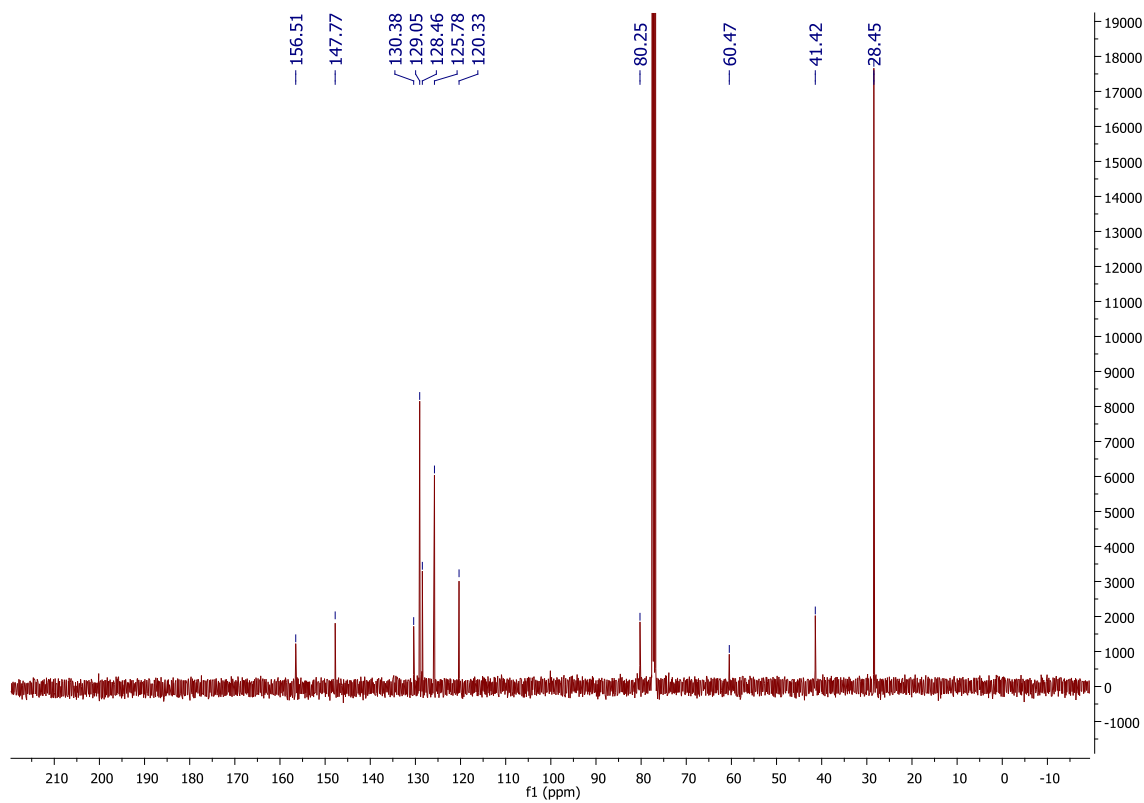
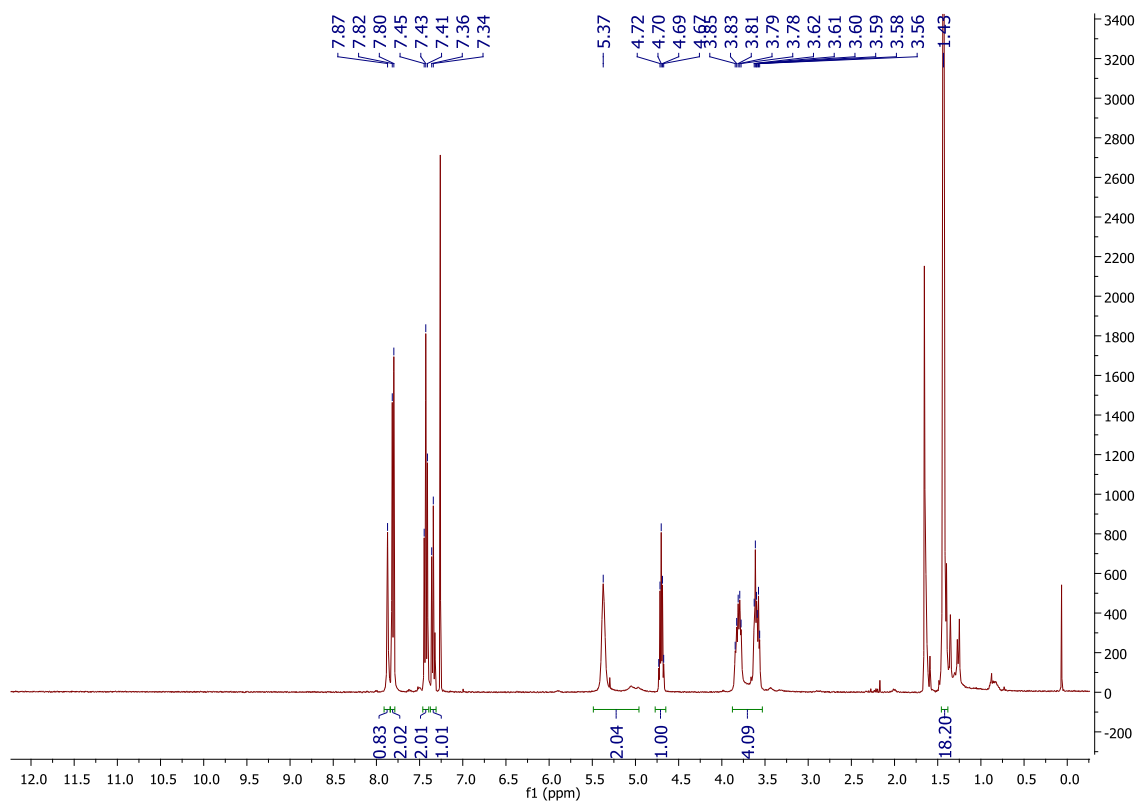


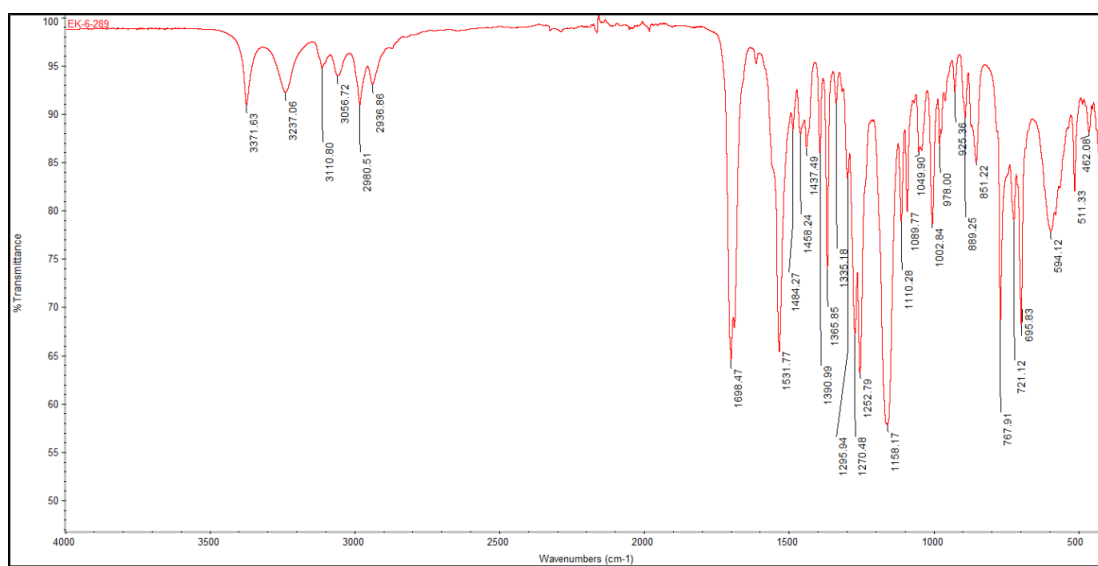
**2-(4-(pyridin-2-yl)-1*H*-1,2,3-triazol-1-yl)propane-1,3-diamine trihydrochloride - PTPD.3HCl (8)**

Spectrum R1 U:3/- U:48 (12 scans) - Background Subtracted U:02 - U:32  
EK-5-232\_+ve.datx 2016.11.14 16:48:38 Generic FIA method;  
ESI + Max: 4.6E7

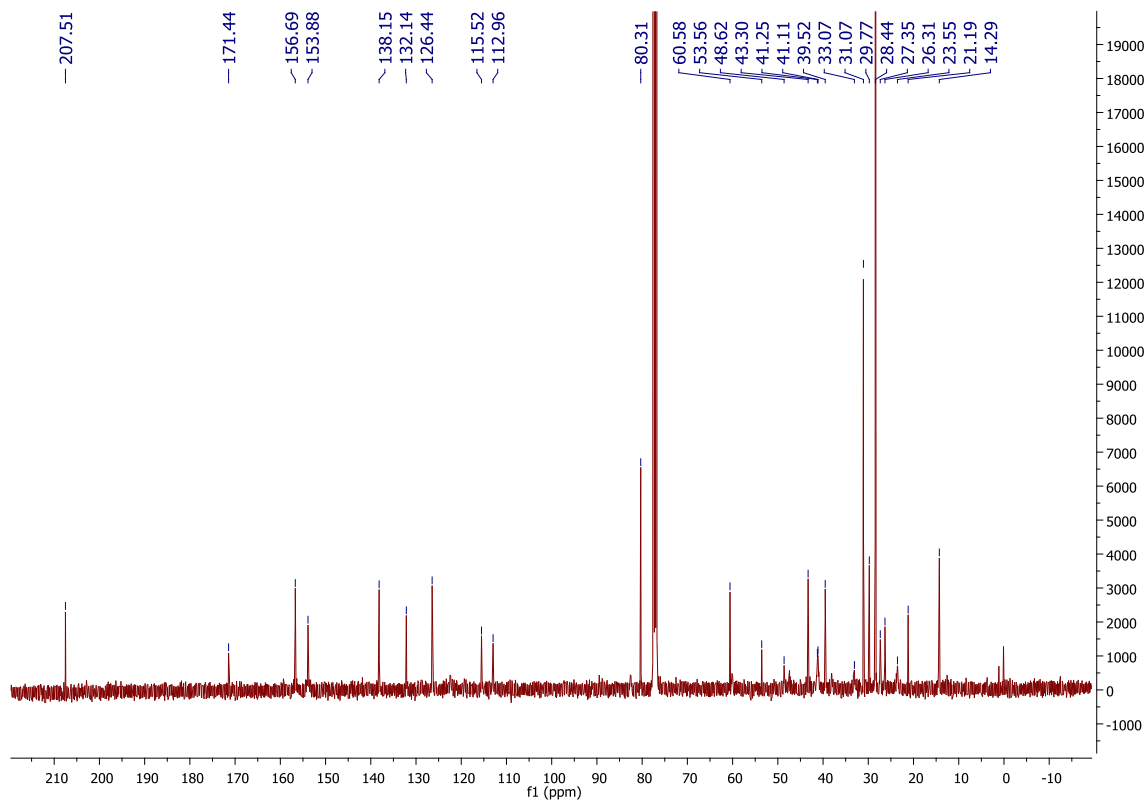
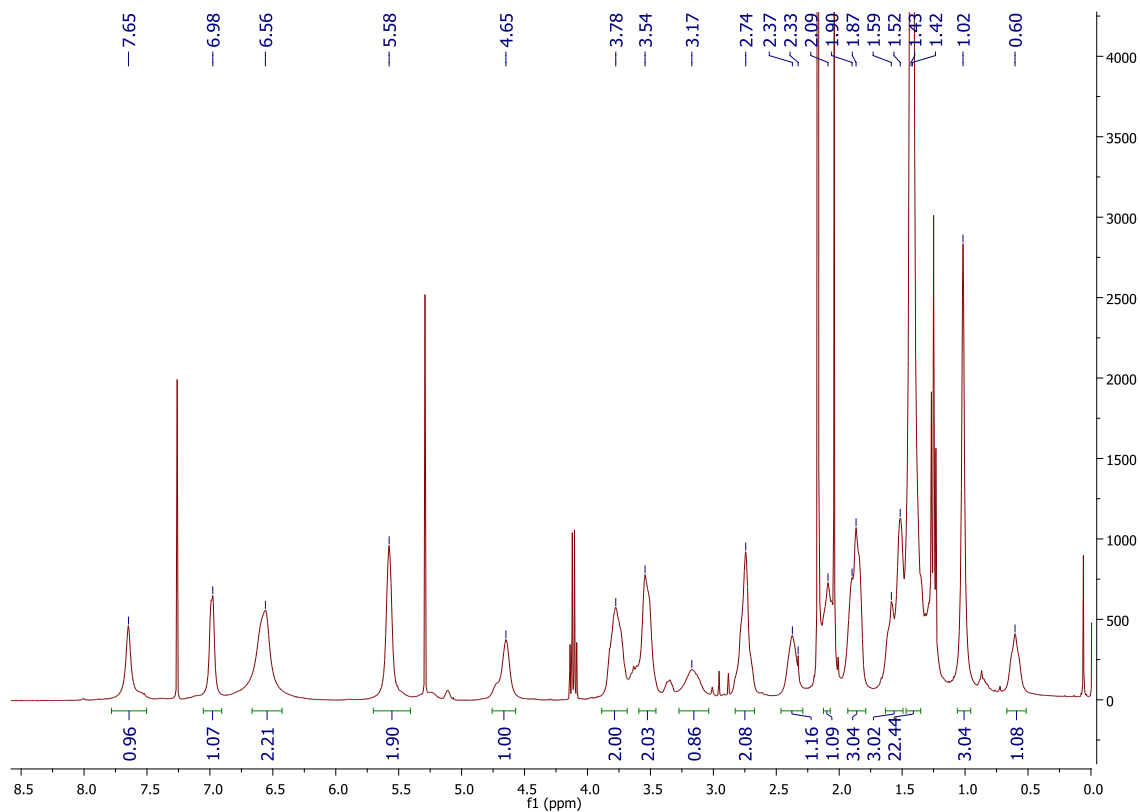


**Di-*tert*-butyl (2-(4-(phenyl)-1*H*-1,2,3-triazol-1-yl)propane-1,3-diyl)dicarbamate**  
**(9)**

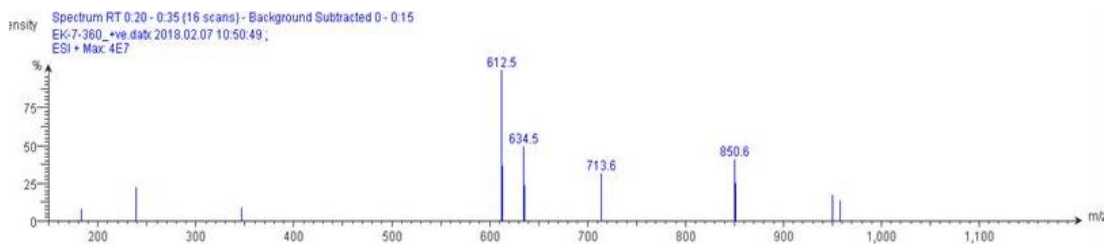




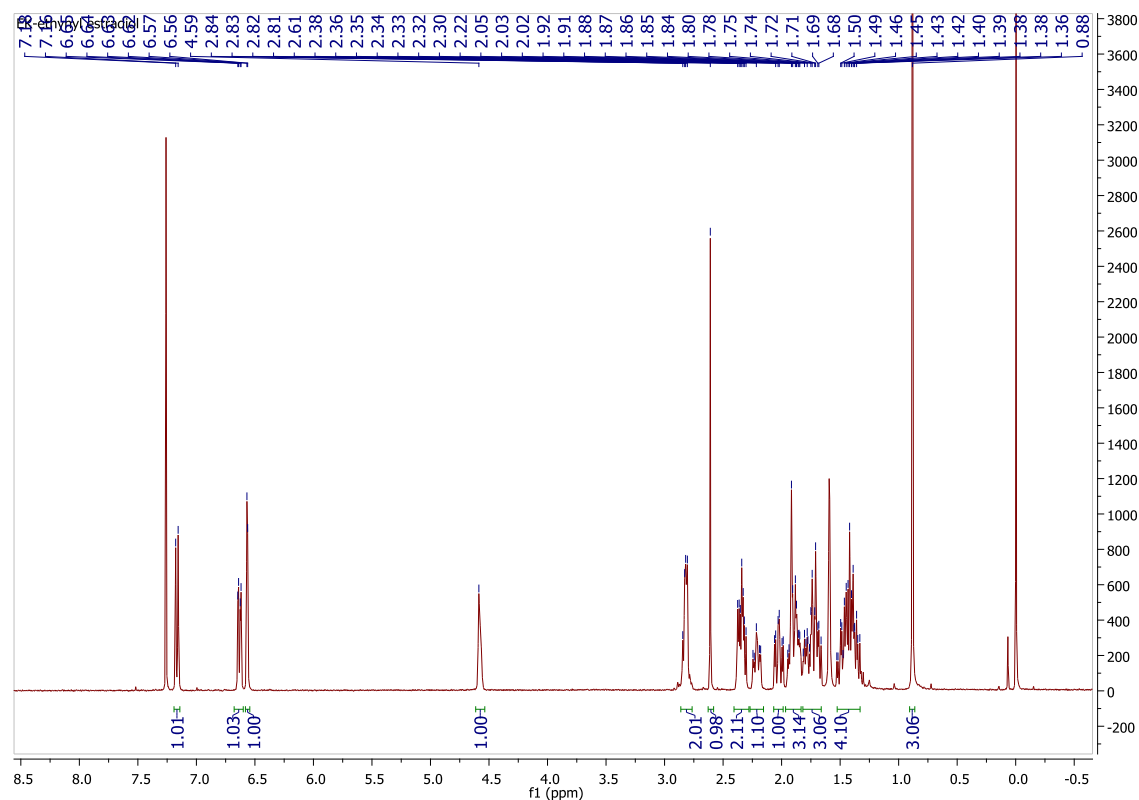
**Di-*tert*-butyl (2-(4-(estradiol)-1*H*-1,2,3-triazol-1-yl)propane-1,3-diyl)dicarbamate (10)**



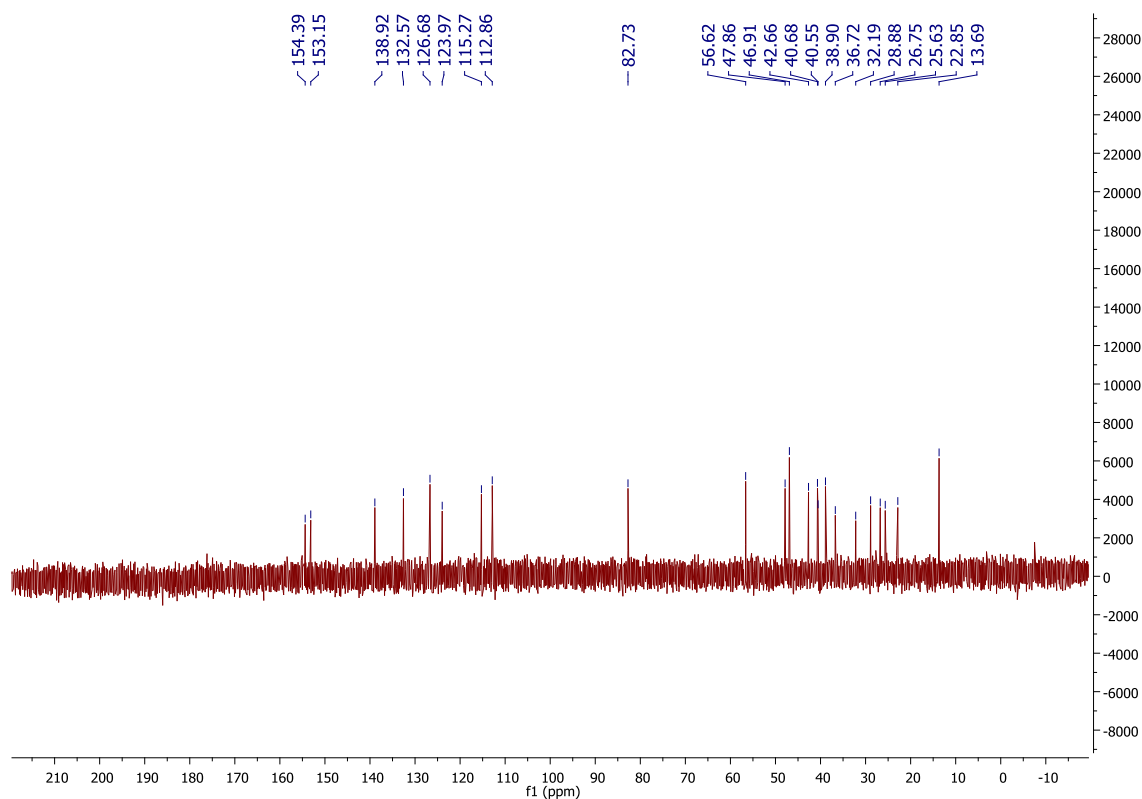
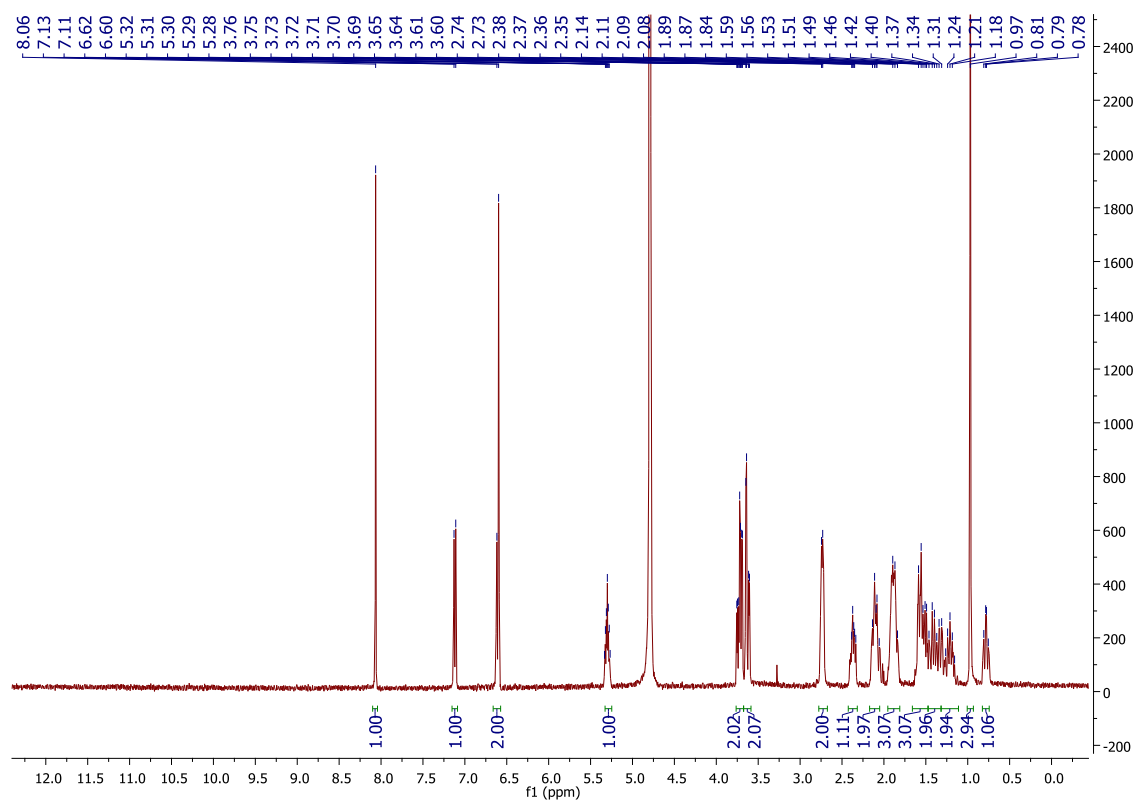


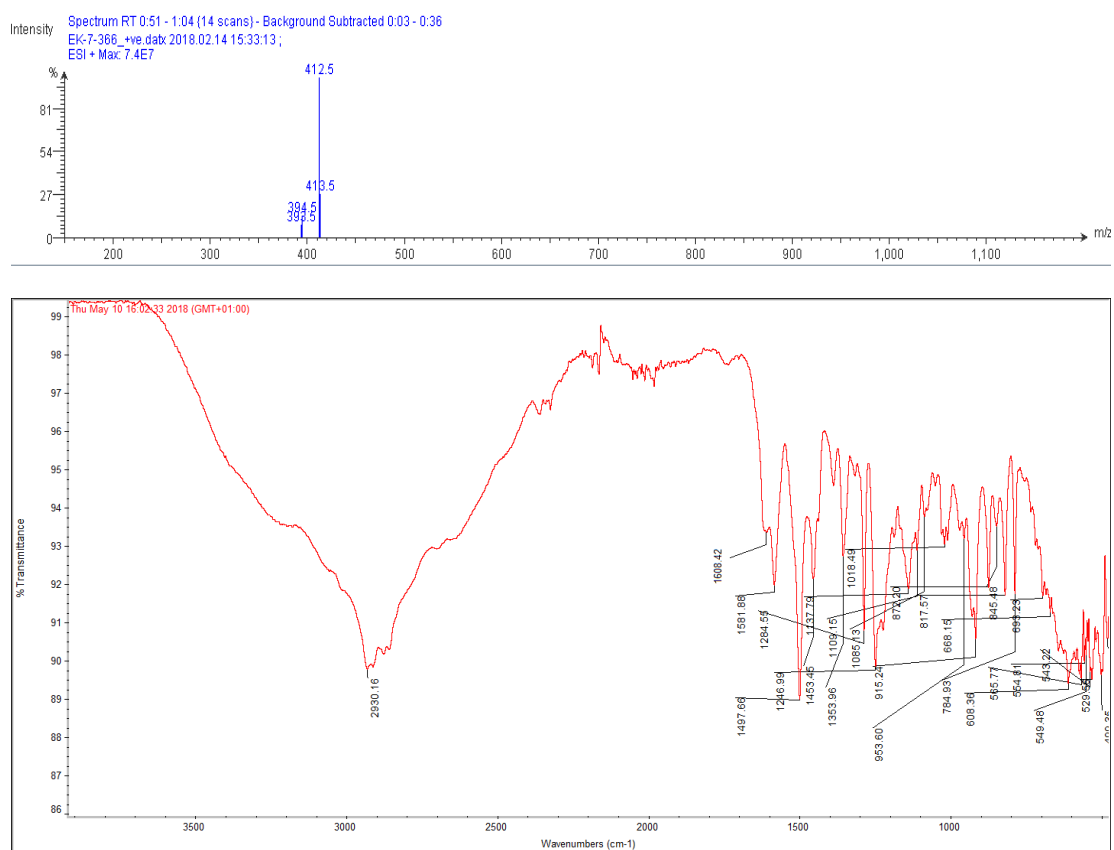


### Ethynyl estradiol reference NMR

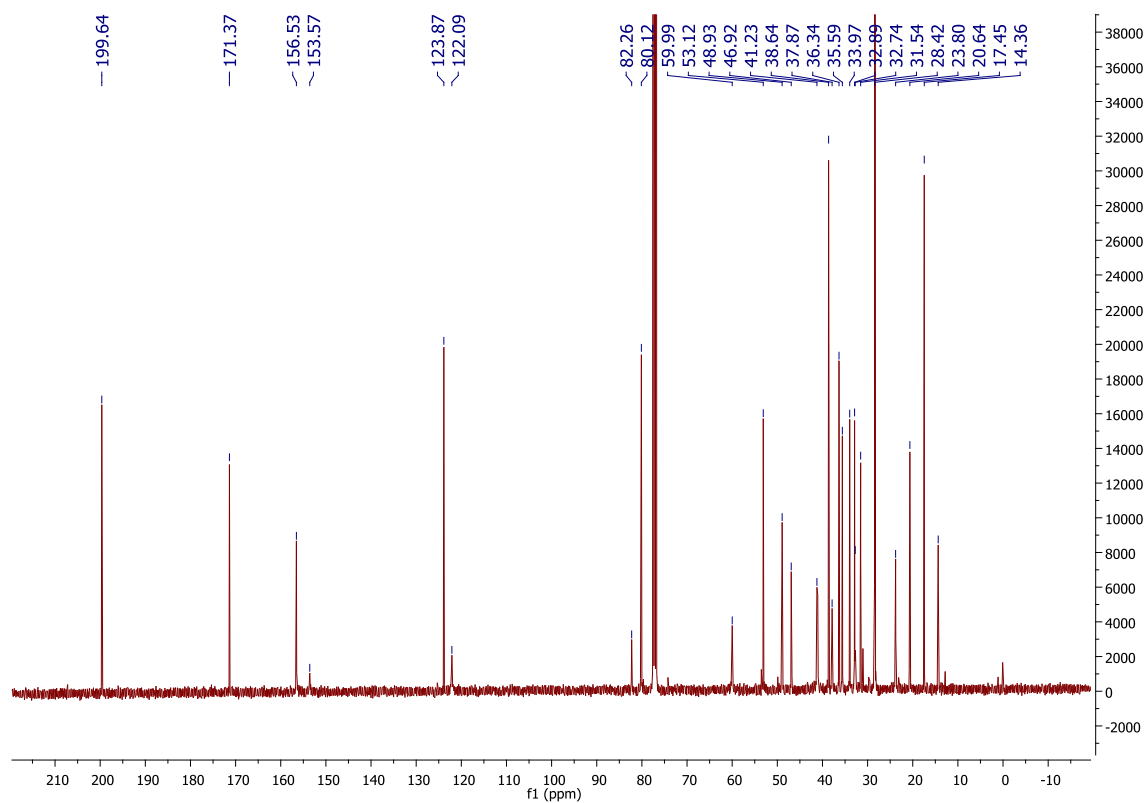
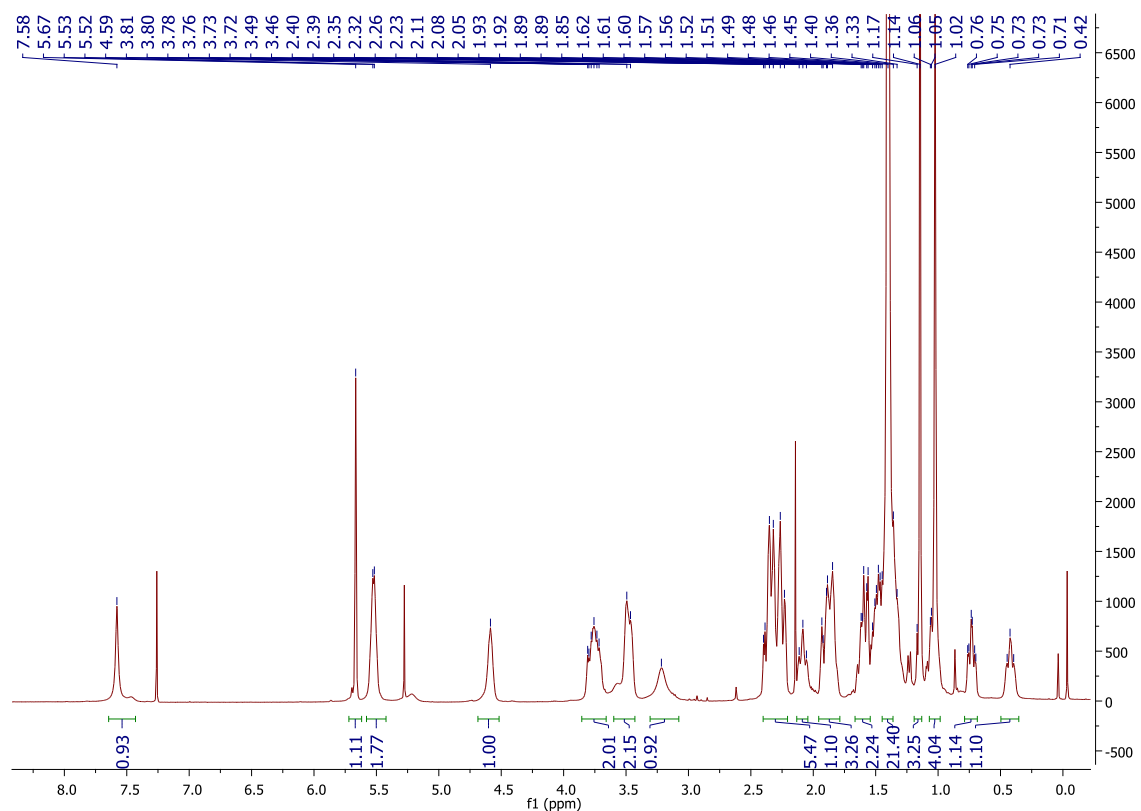


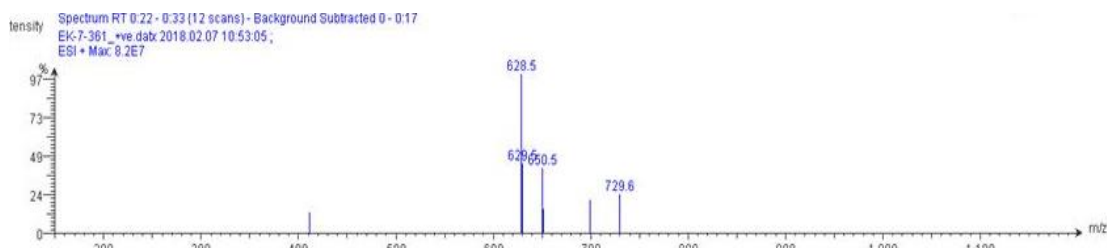
$^1\text{H}$  NMR (400 MHz,  $\text{CDCl}_3$ )  $\delta$ : 7.17 (d,  $J$  = 8.4 Hz, 1H), 6.63 (dd,  $J$  = 8.4, 2.6 Hz, 1H), 6.57 (d,  $J$  = 2.5 Hz, 1H), 4.59 (s, 1H), 2.82 (dd,  $J$  = 9.5, 6.2 Hz, 2H), 2.61 (s, 1H), 2.34 (m, 2H), 2.27 – 2.15 (m, 1H), 2.07 – 1.99 (m, 1H), 1.97 – 1.83 (m, 3H), 1.82 – 1.66 (m, 3H), 1.53 – 1.33 (m, 4H), 0.88 (s, 3H) ppm.

**(2-(4-(estradiol)-1*H*-1,2,3-triazol-1-yl)propane-1,3-diyl) dihydrochloride (11)**

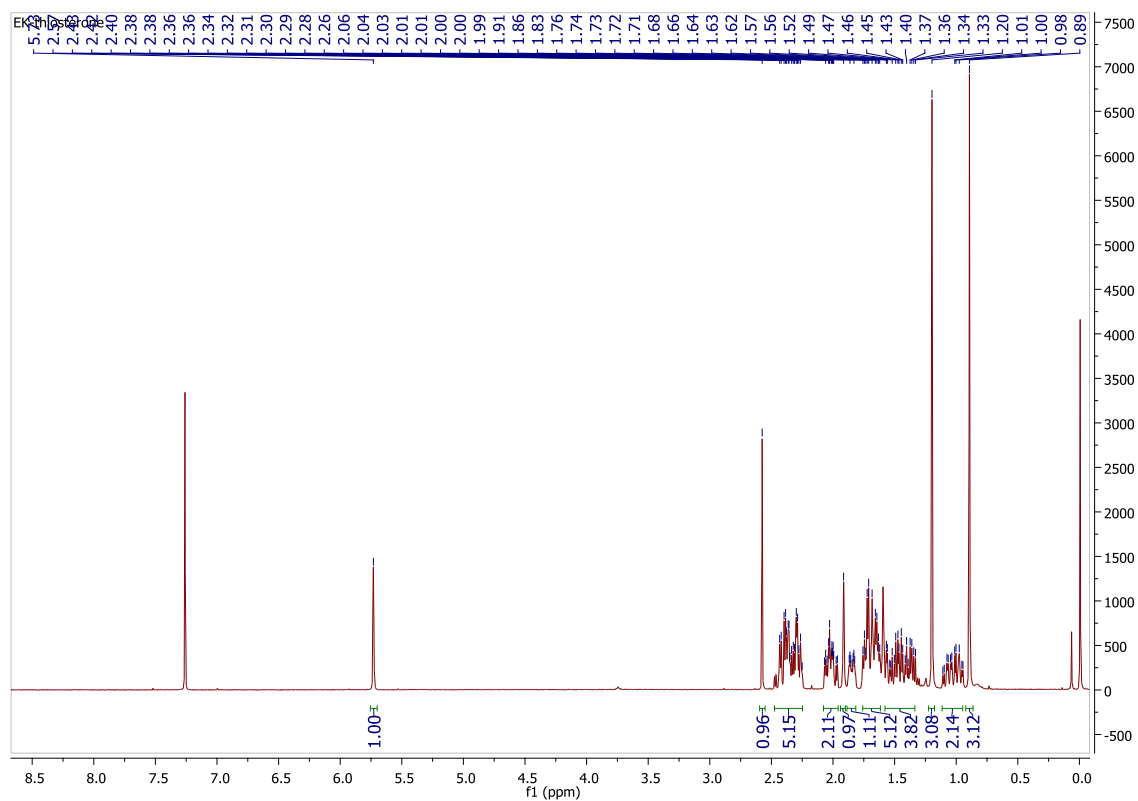


**Di-*tert*-butyl (2-(4-(testosterone)-1H-1,2,3-triazol-1-yl)propane-1,3-diyl)dicarbamate (12)**





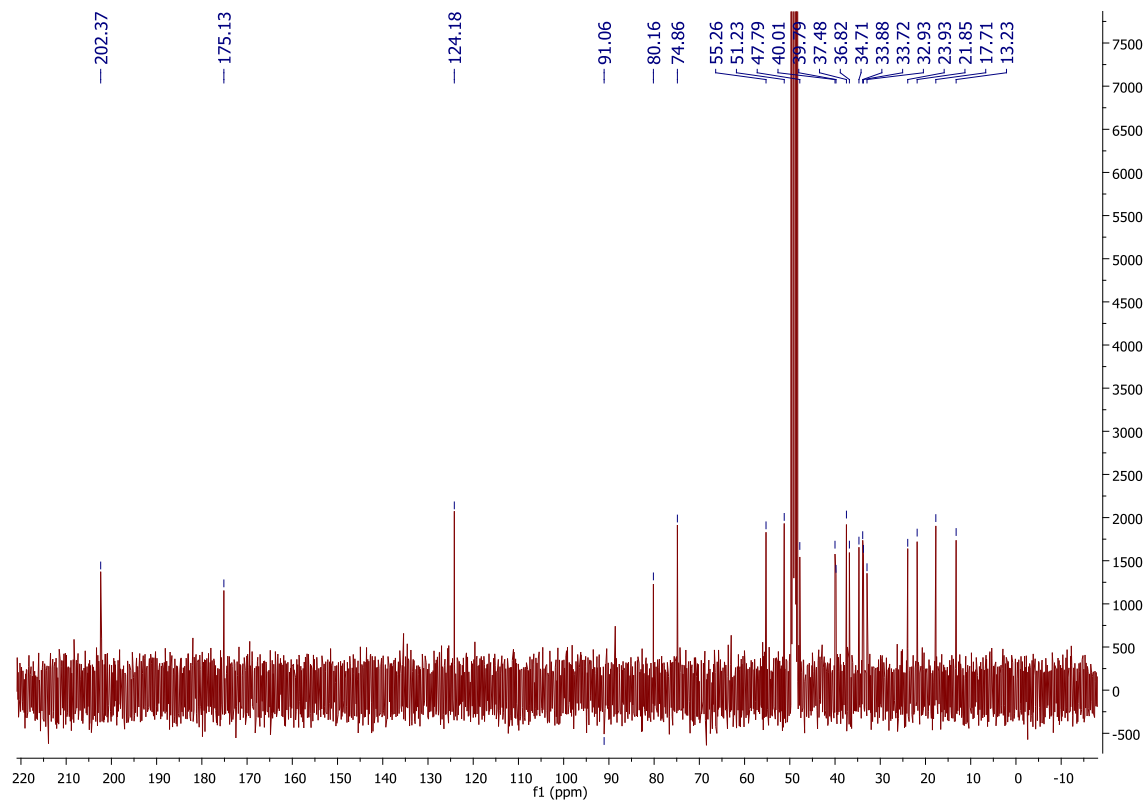
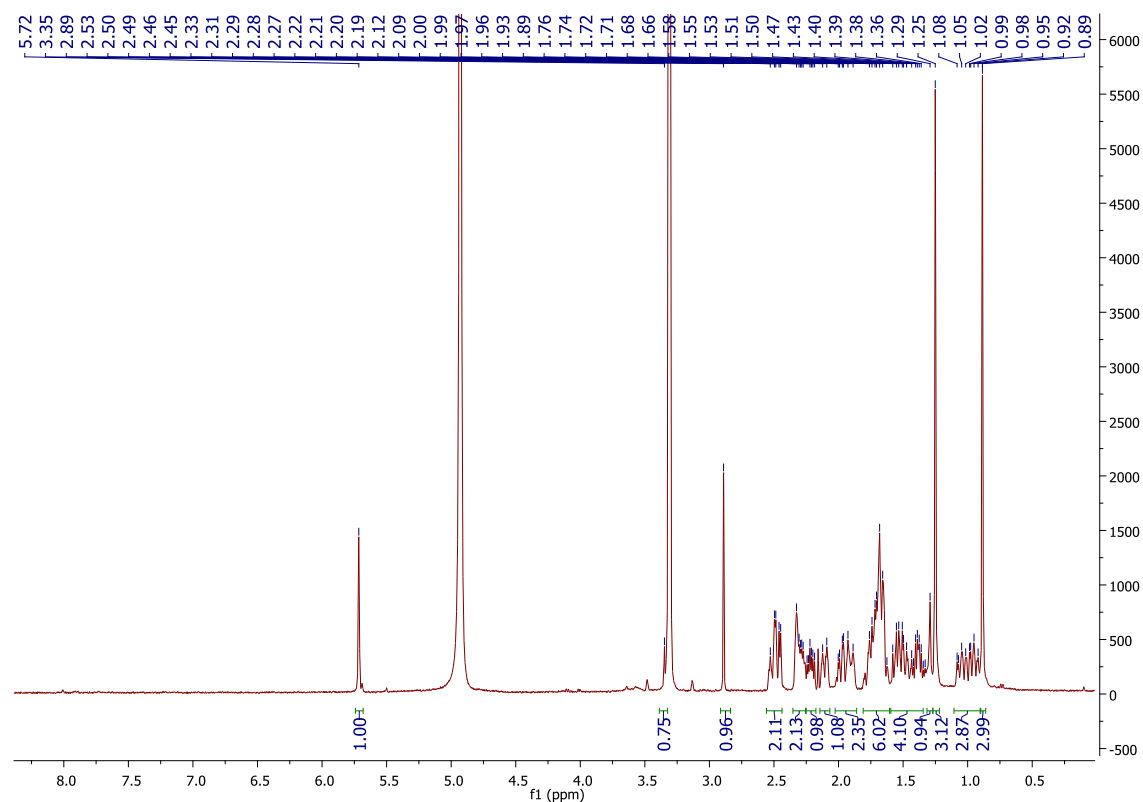
### Ethisterone reference NMR

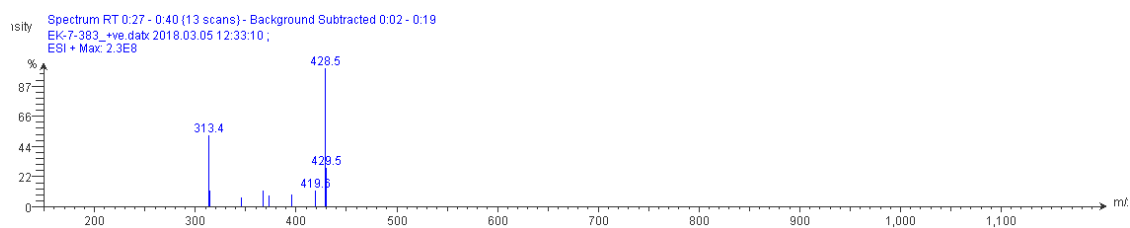


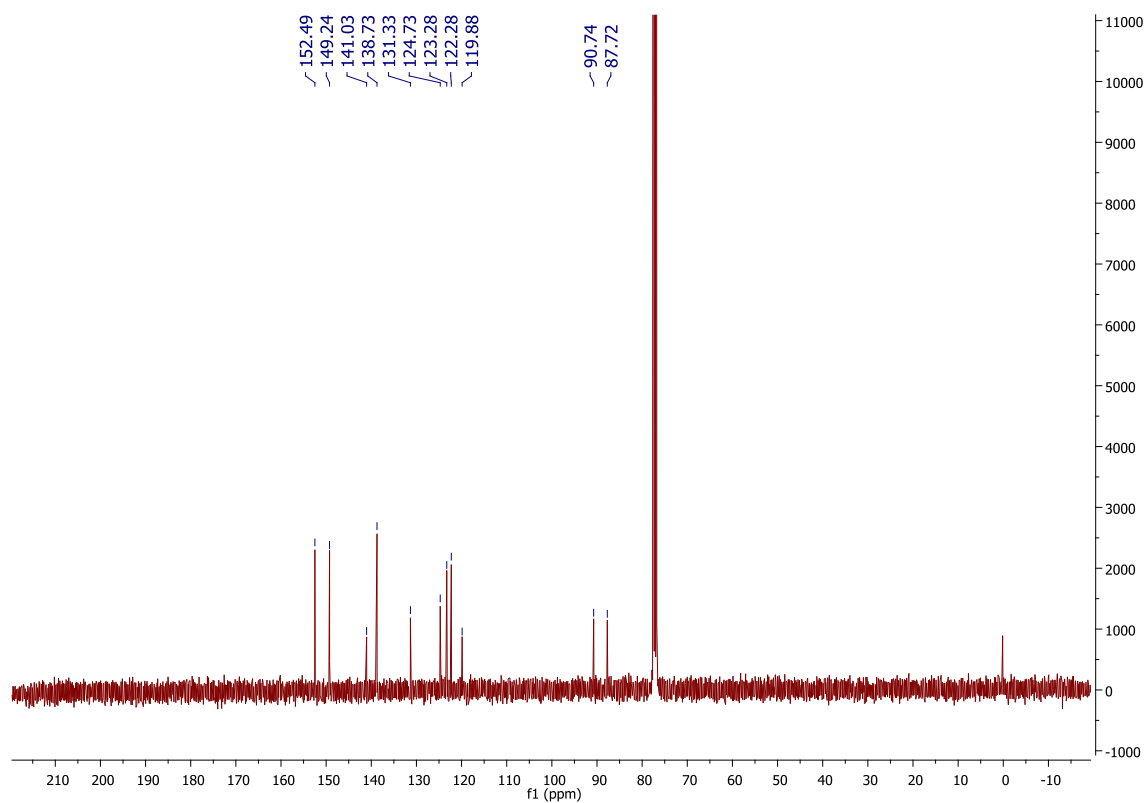
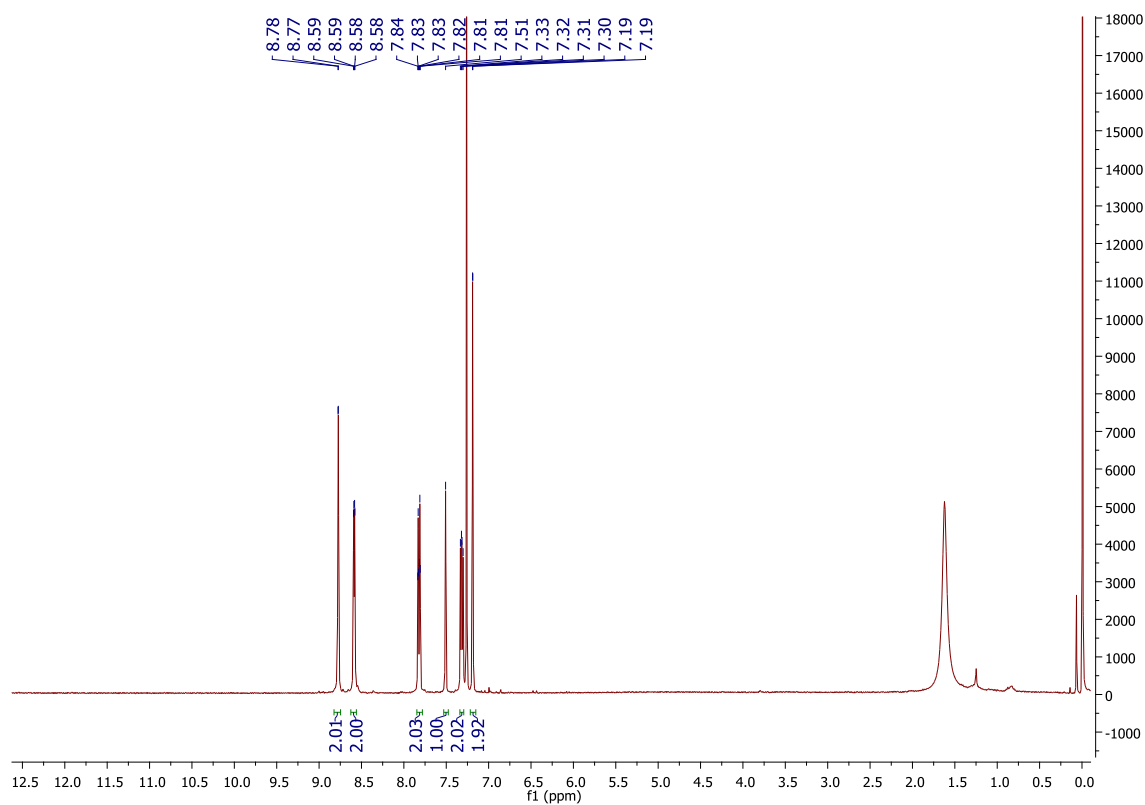
<sup>1</sup>H NMR (400 MHz, CDCl<sub>3</sub>) δ: 5.73 (s, 1H), 2.57 (s, 1H), 2.34 (m, 5H), 2.08 – 1.96 (m, 2H), 1.91 (s, 1H), 1.89 – 1.81 (m, 1H), 1.76 – 1.62 (m, 5H), 1.58 – 1.34 (m, 4H), 1.20 (s, 3H), 1.11 – 0.95 (m, 2H), 0.89 (s, 3H) ppm.

**(2-(4-(testosterone)-1*H*-1,2,3-triazol-1-yl)propane-1,3-diyl) dihydrochloride (13)**

MeOD

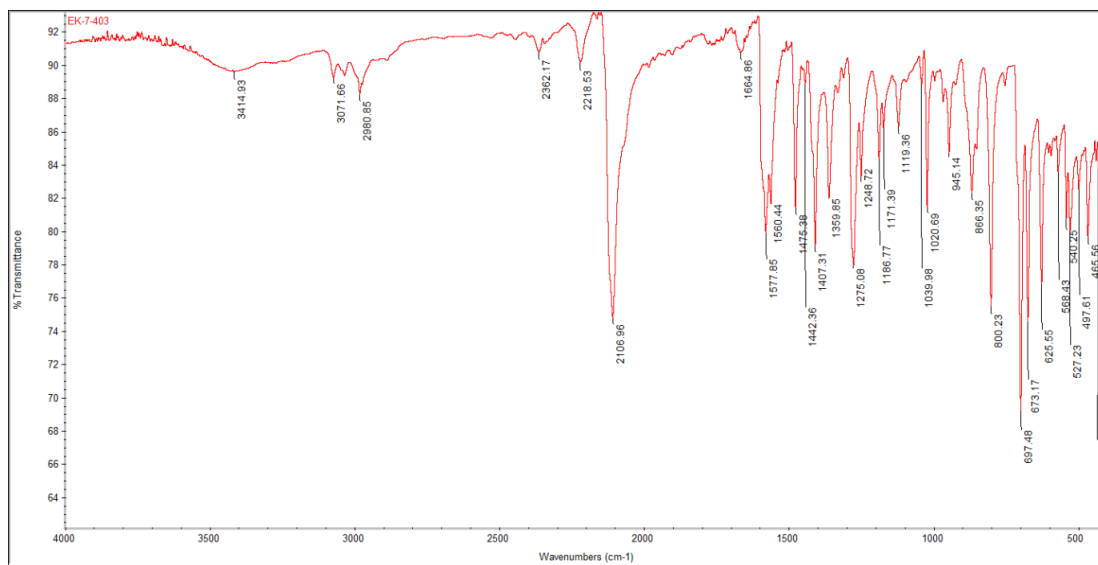
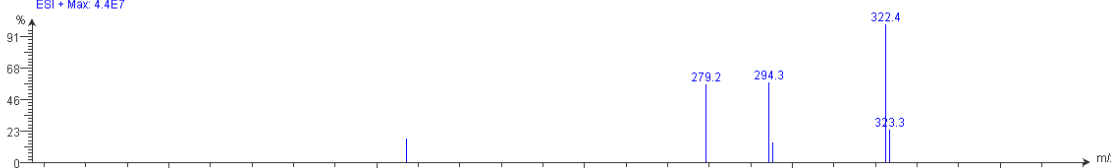




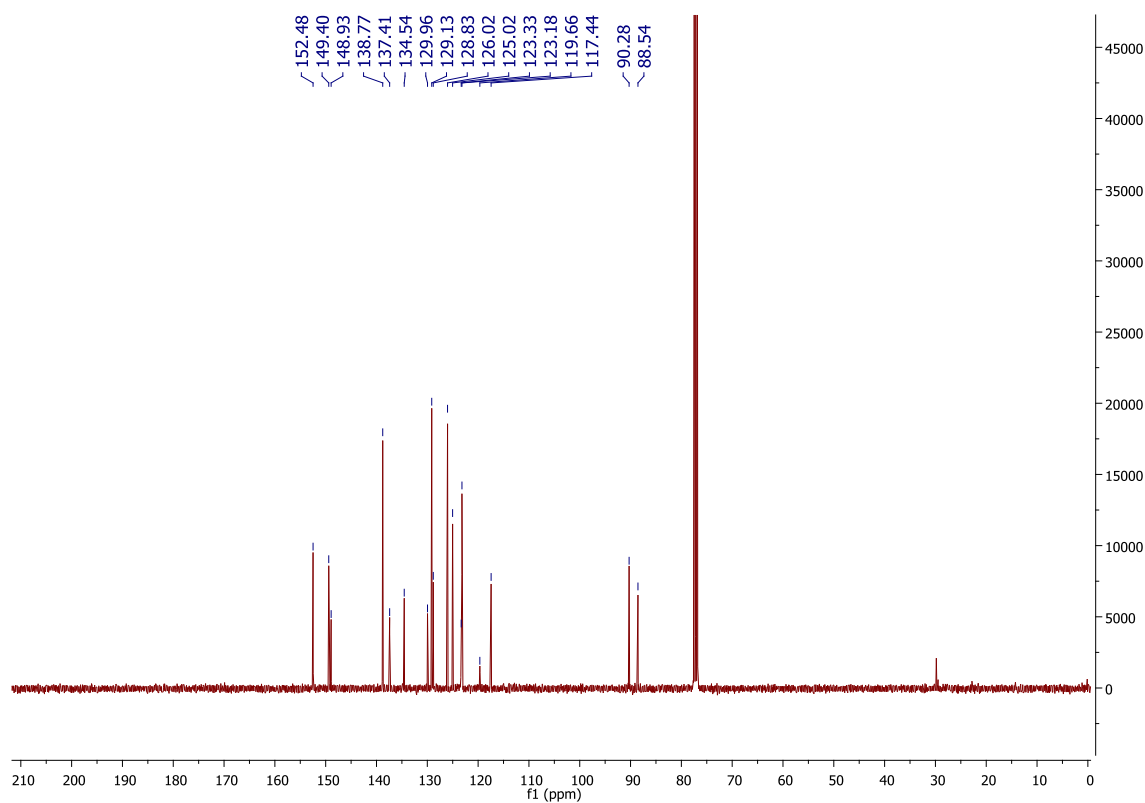
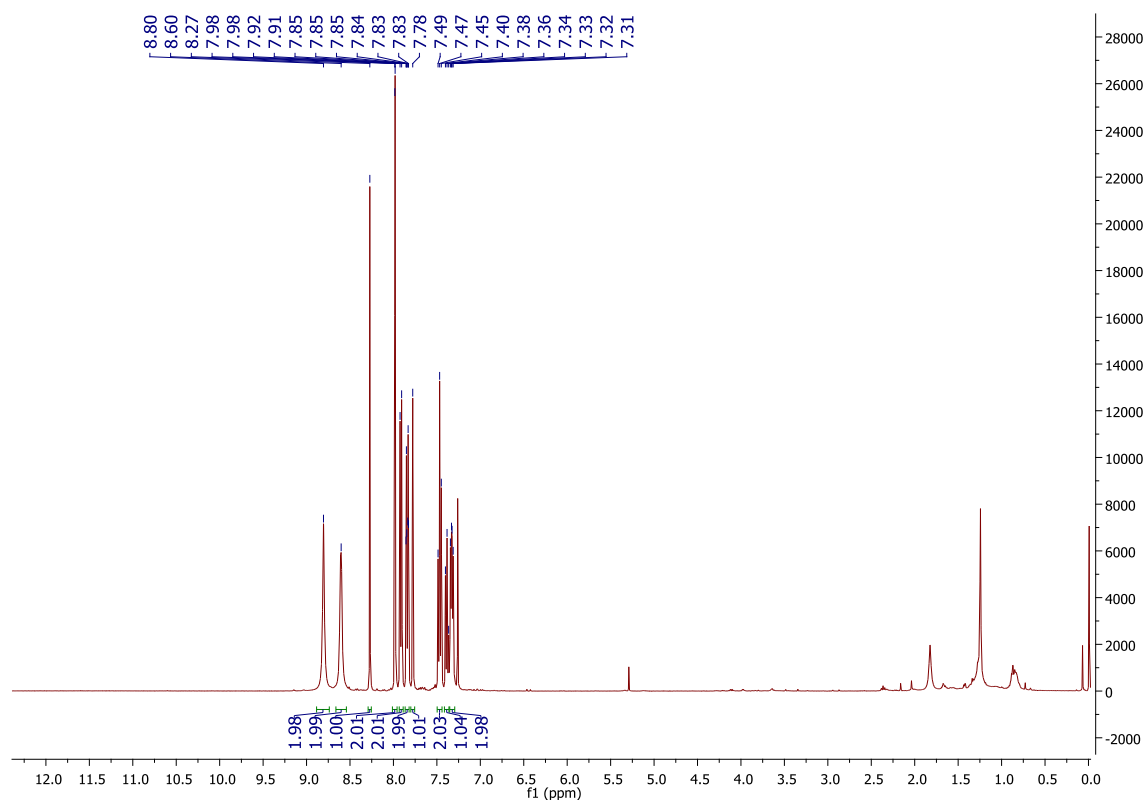
**3,3'-((5-azido-1,3-phenylene)bis(ethyne-2,1-diyl))dipyridine (CageL-N<sub>3</sub>) (14)**

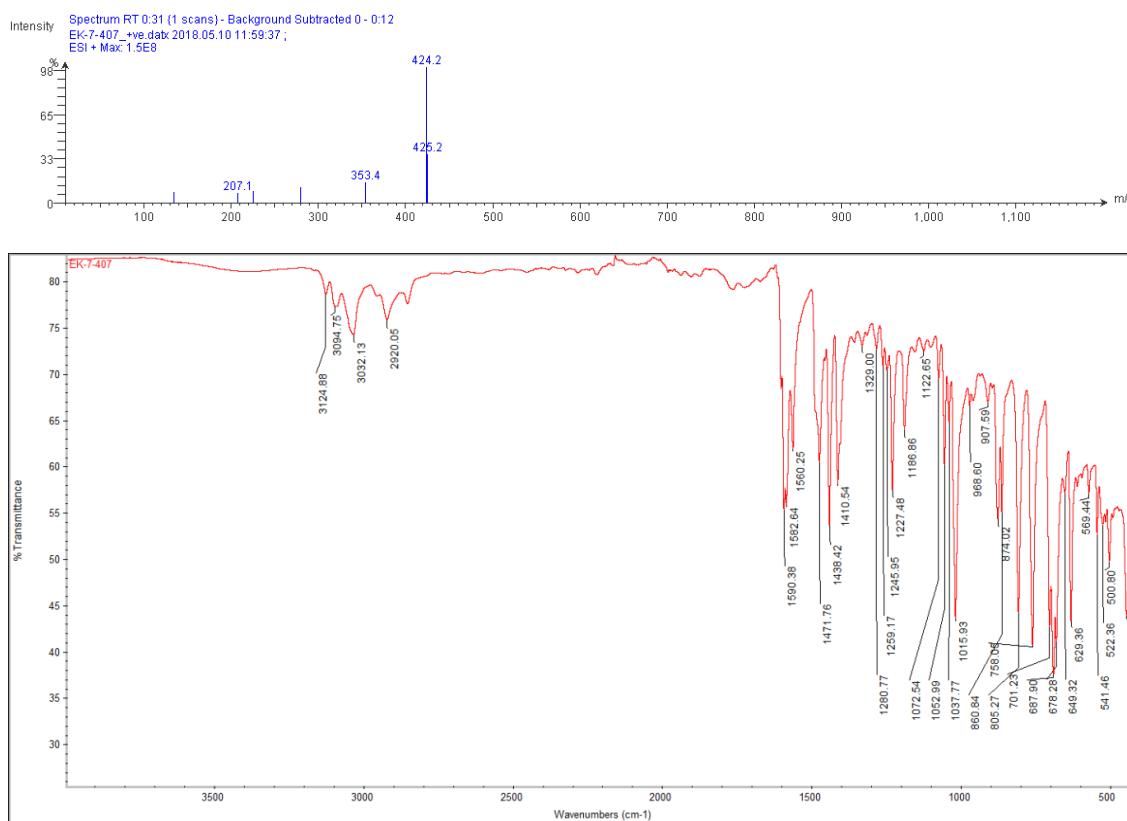


Intensity Spectrum: R1 0.38 - 0.33 (21 scans) - Background subtracted 0 - 0.20  
EK-7-391\_B\_+ve.dat 2018.04.13 12:06:33;  
ESI + Max: 4.4E7

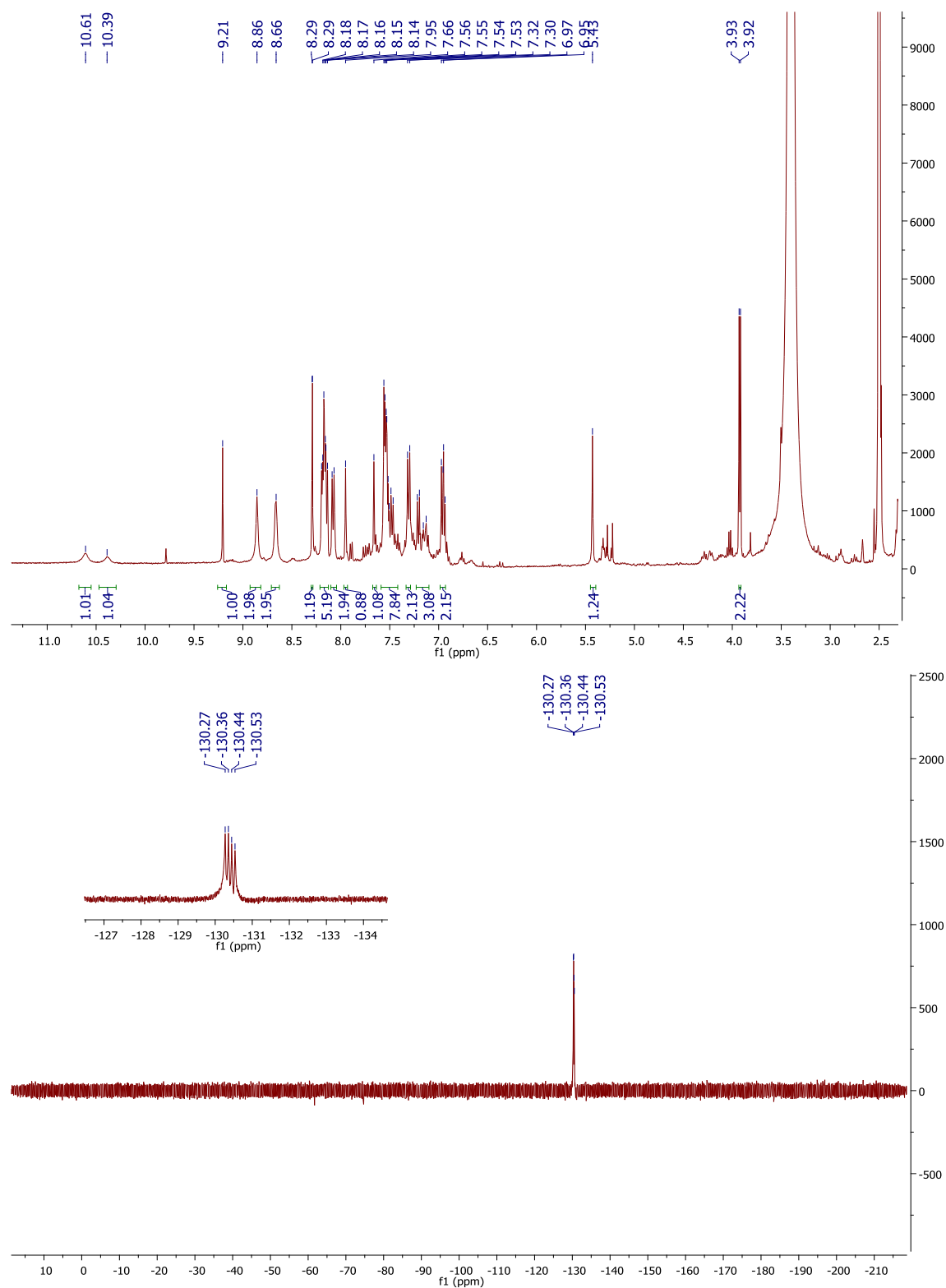


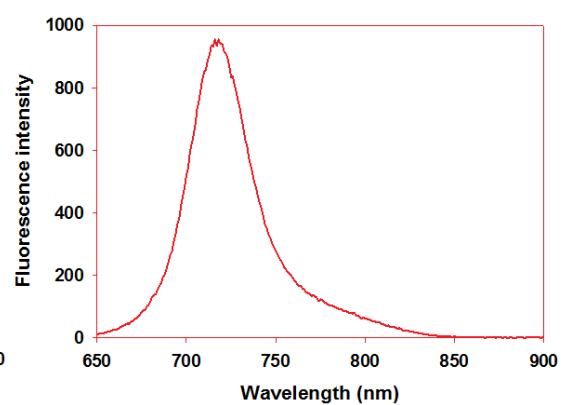
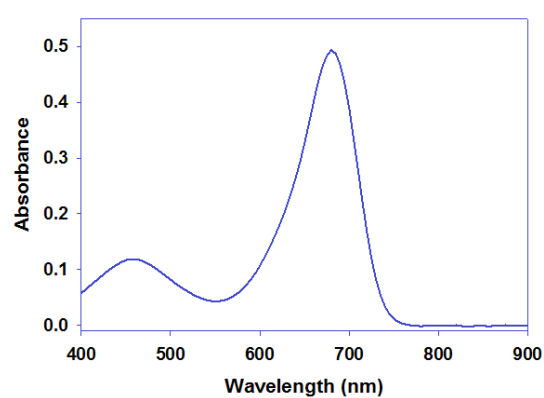
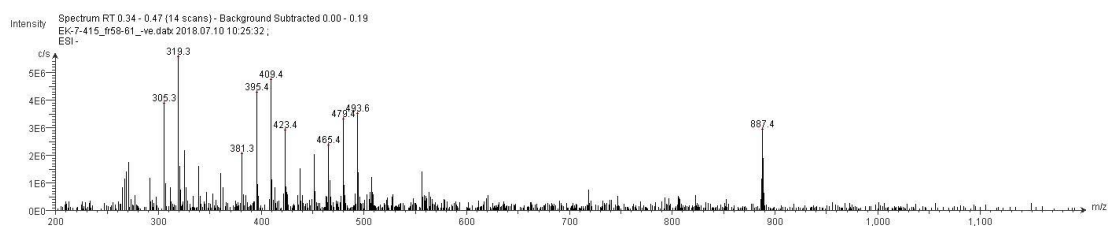
**3,3'-((5-(4-phenyl-1*H*-1,2,3-triazol-4-yl)-1,3-phenylene)bis(ethyne-2,1-diyl))dipyridine (Cage-T-Ph) (15)**



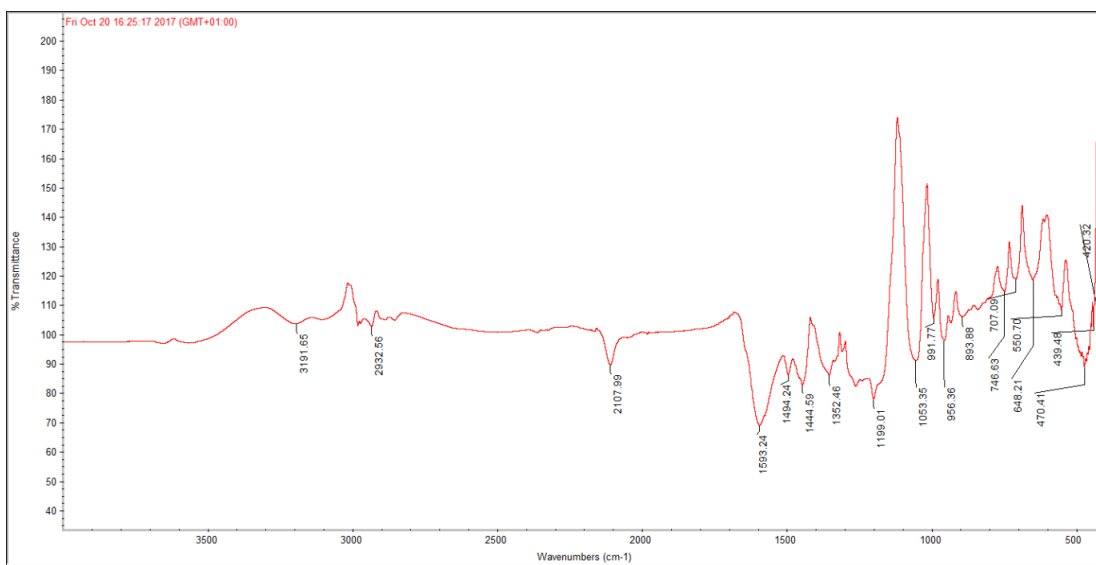
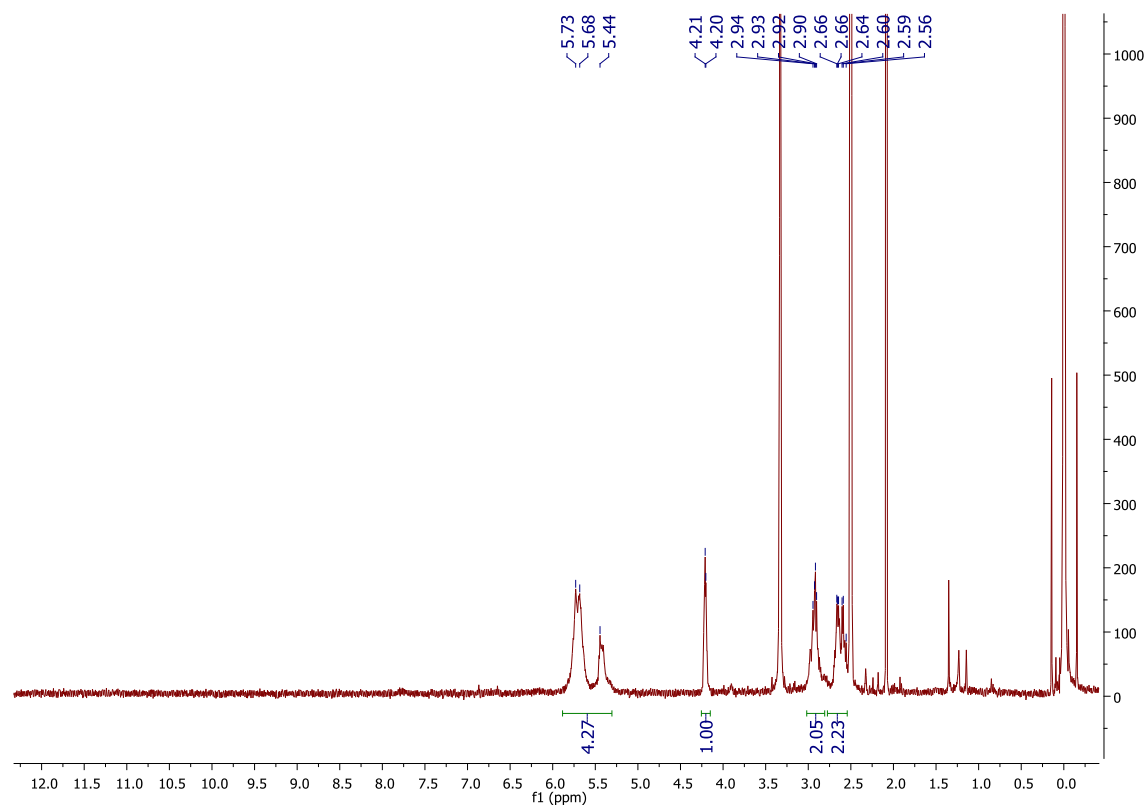


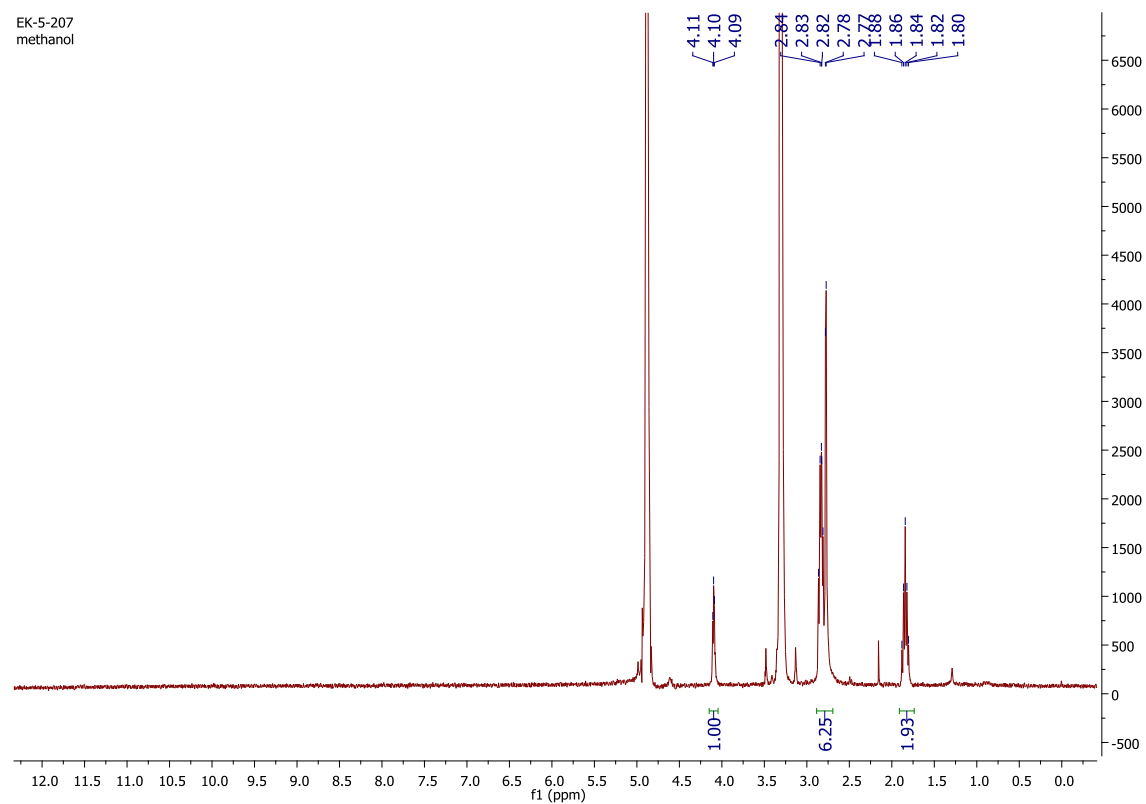
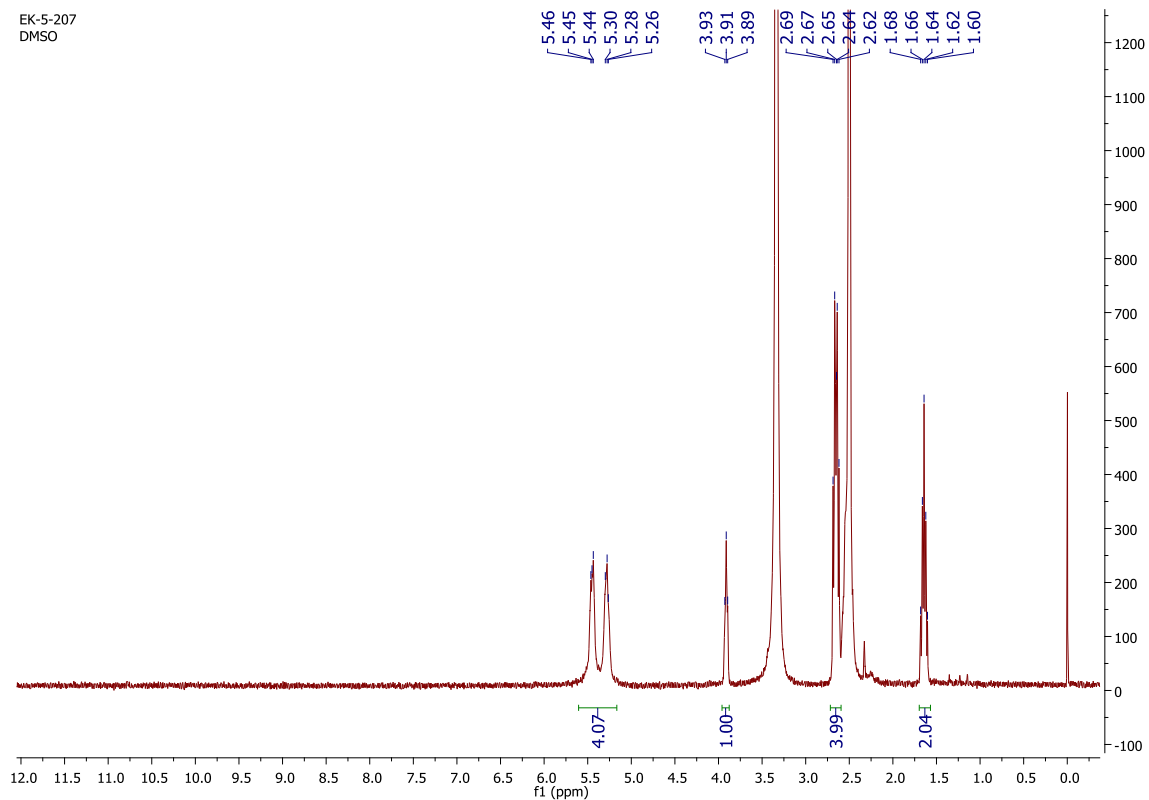
**3,3'-((5-(4-( MAMP-NIR-AZA)-1*H*-1,2,3-triazol-4-yl)-1,3-phenylene)bis(ethyne-2,1-diyl))dipyridine (Cage-T-MAMP) (16)**

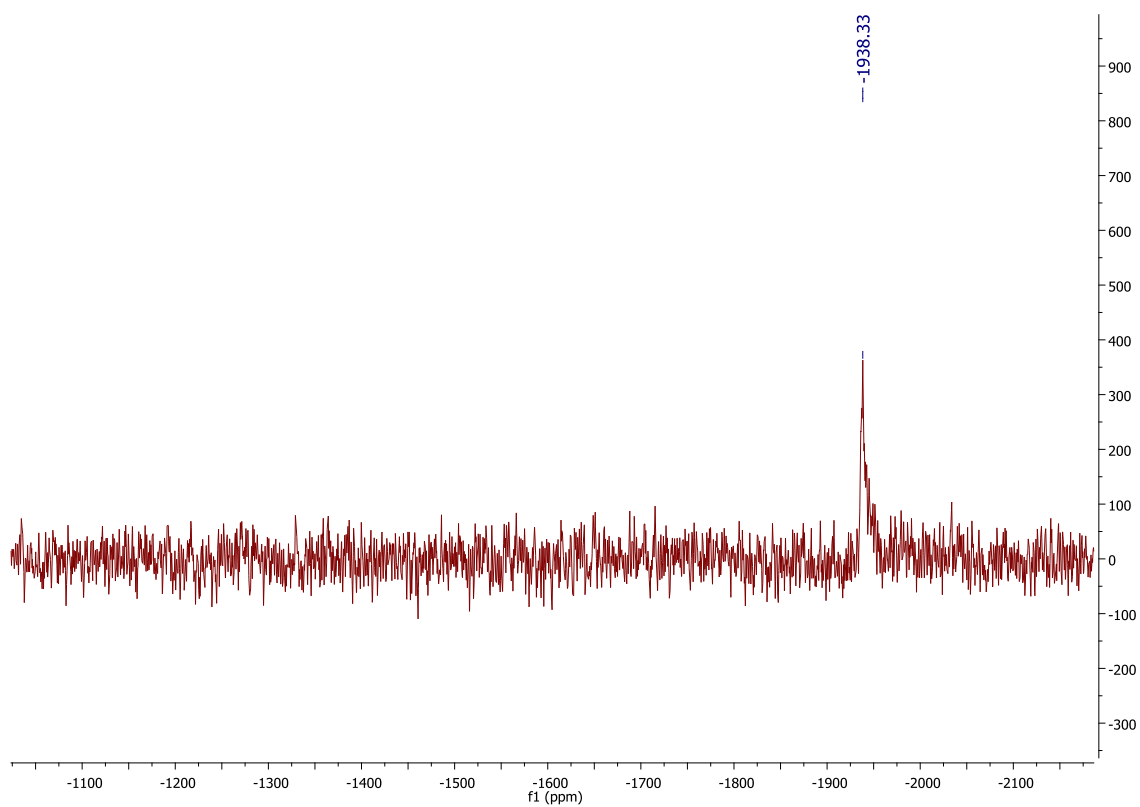
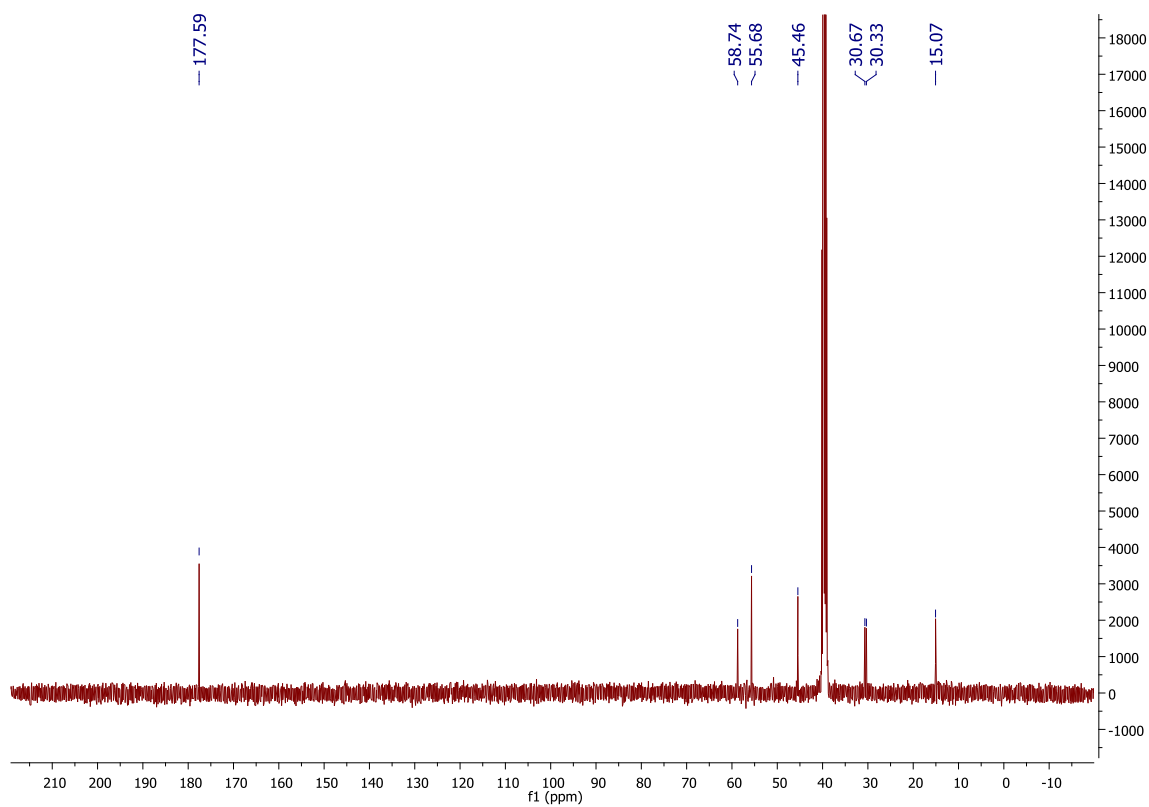




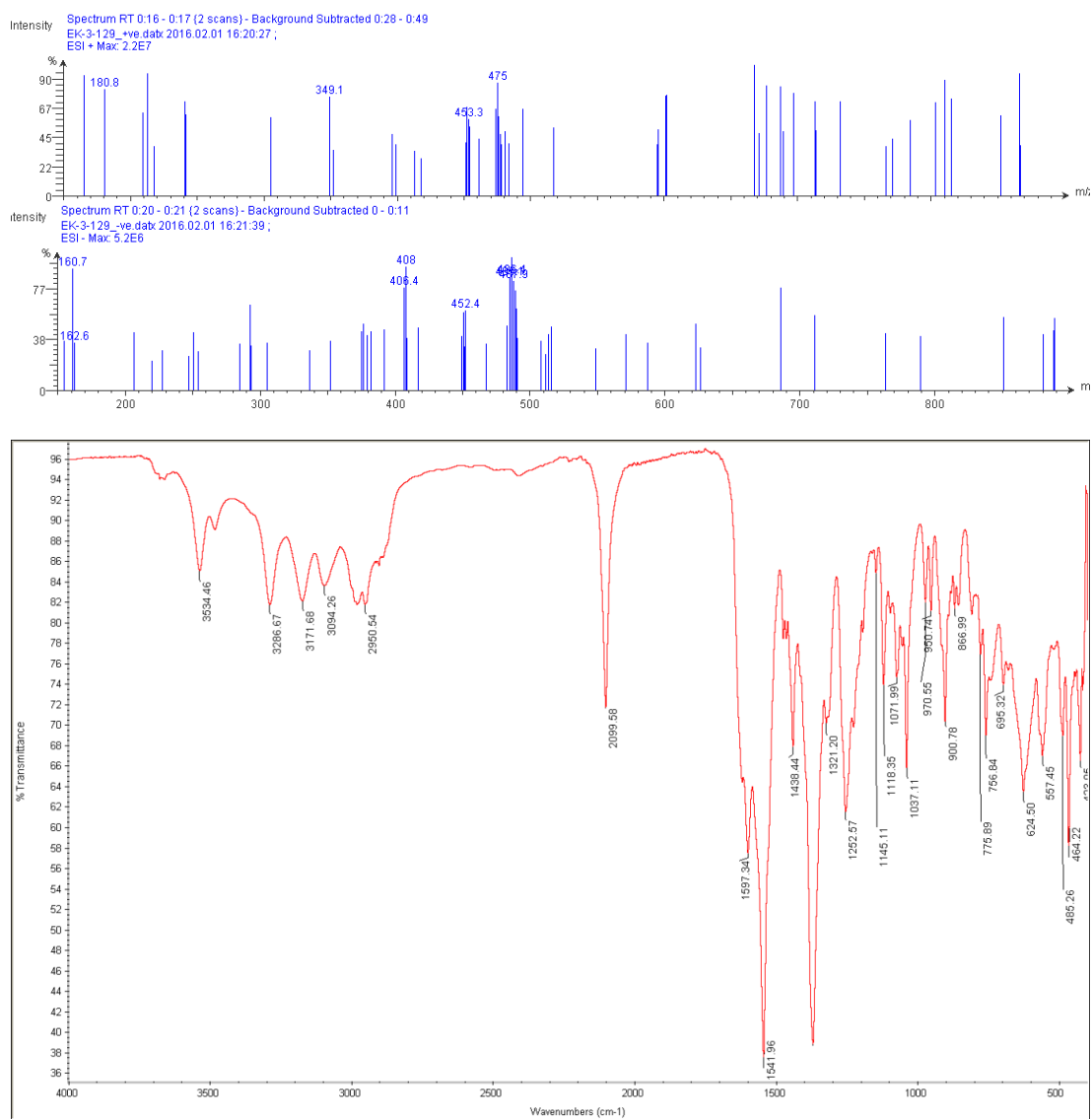
## Inorganic syntheses

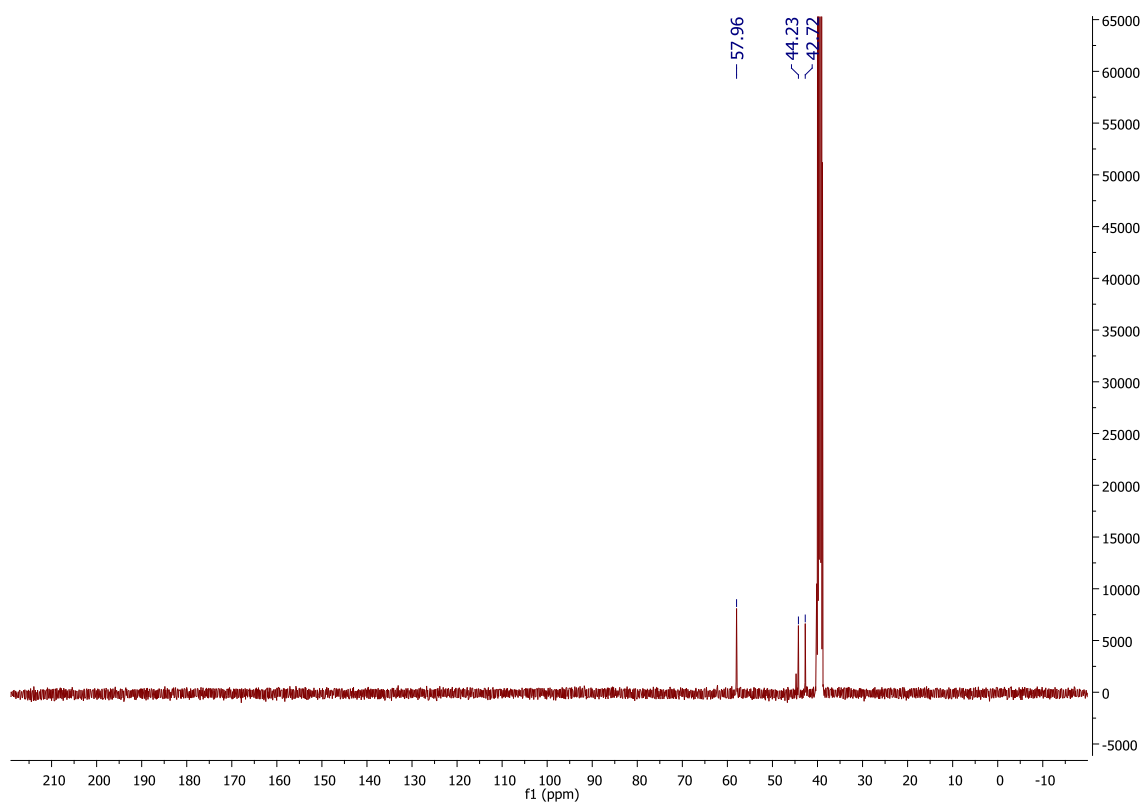
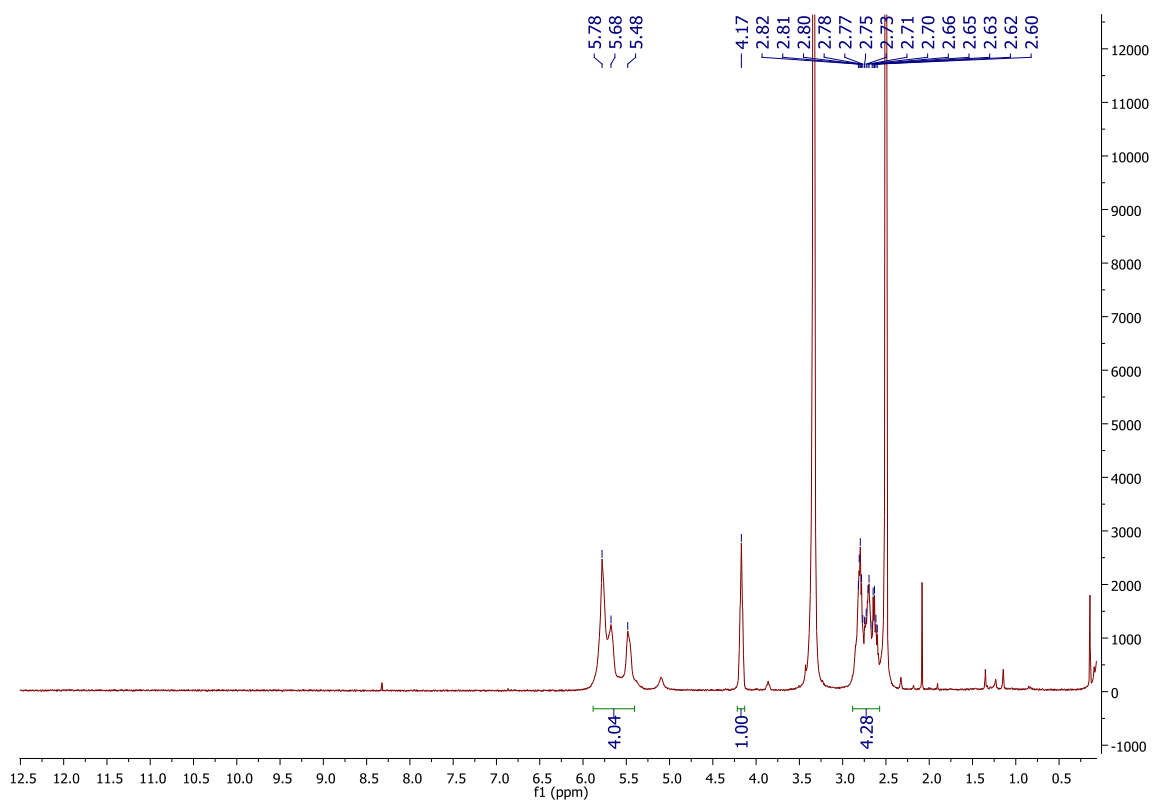
*cis*-[Pt(II)(I)<sub>2</sub>(DAP-N<sub>3</sub>)] (17)

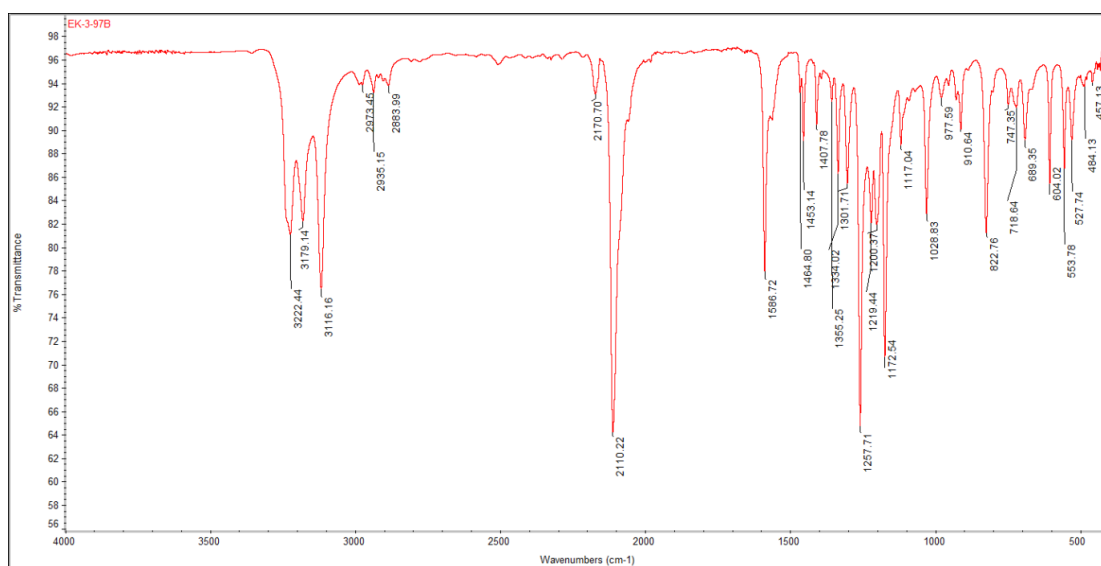
**[Pt(II)(CBDCA)(DAP-N<sub>3</sub>)] (18)**



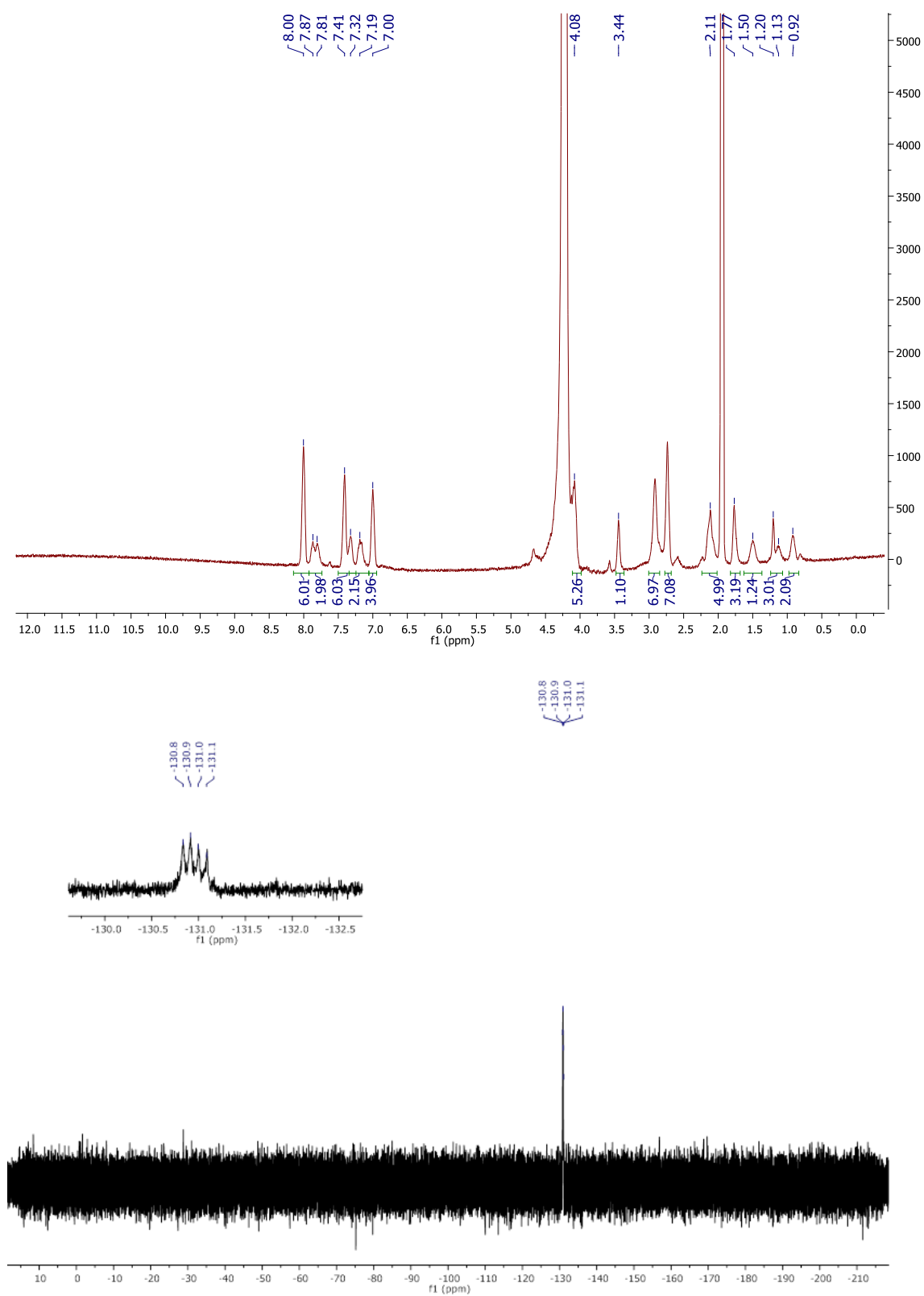


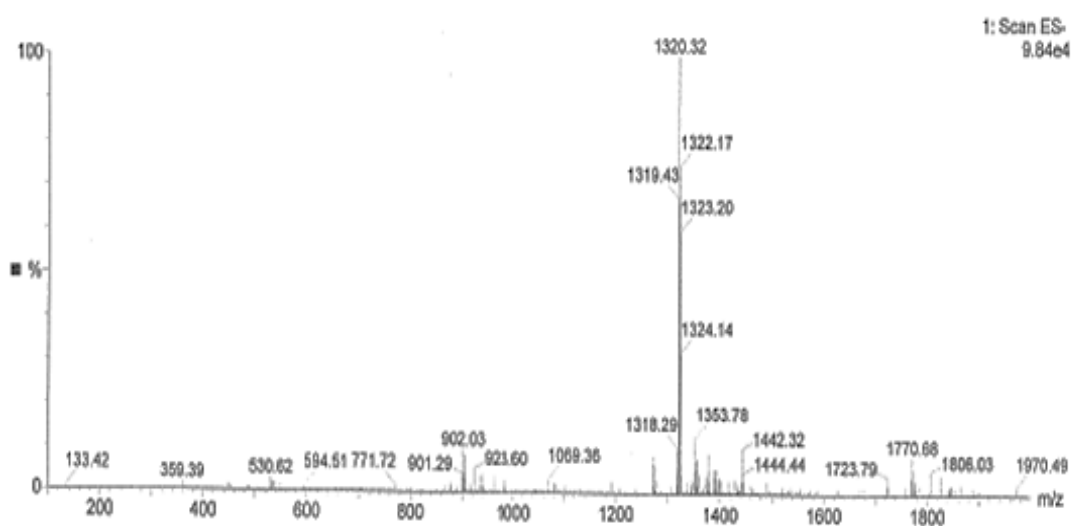
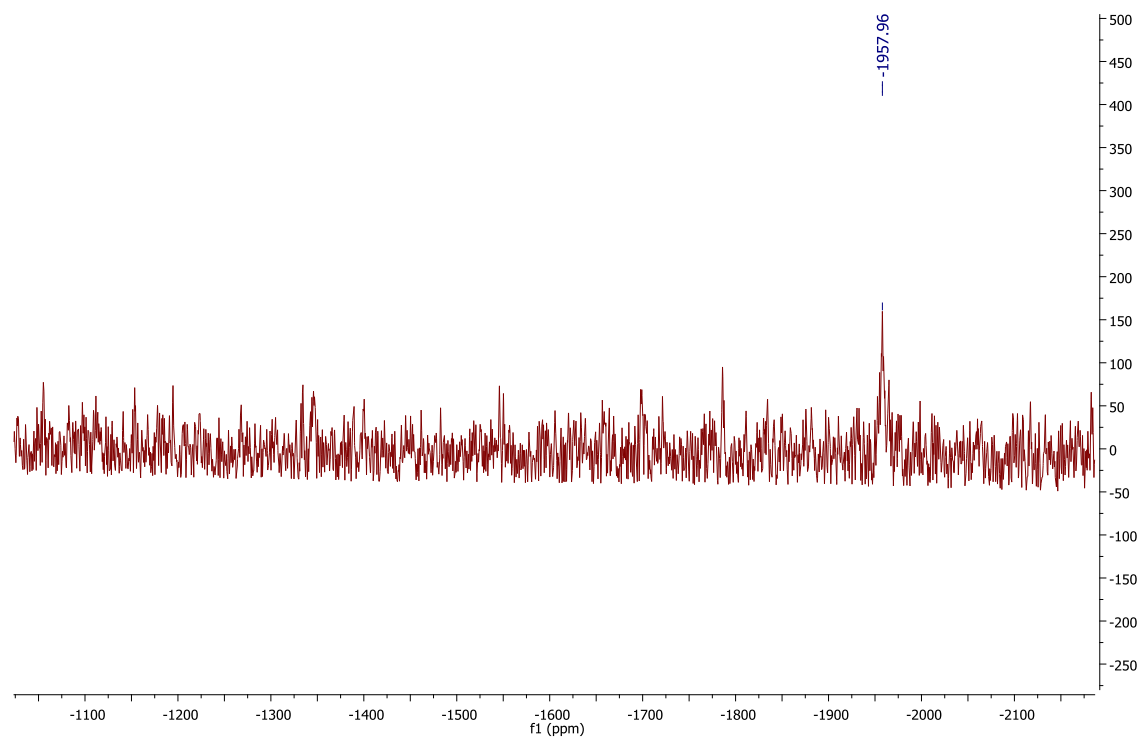


**[Pt(II)Cl<sub>2</sub>(DAP-N<sub>3</sub>)] (19)**



**[Pt(II)(CBDCA)(DAP-BCN-NIR-AZA)] fluorophore conjugate - Pt-Flu (20)**





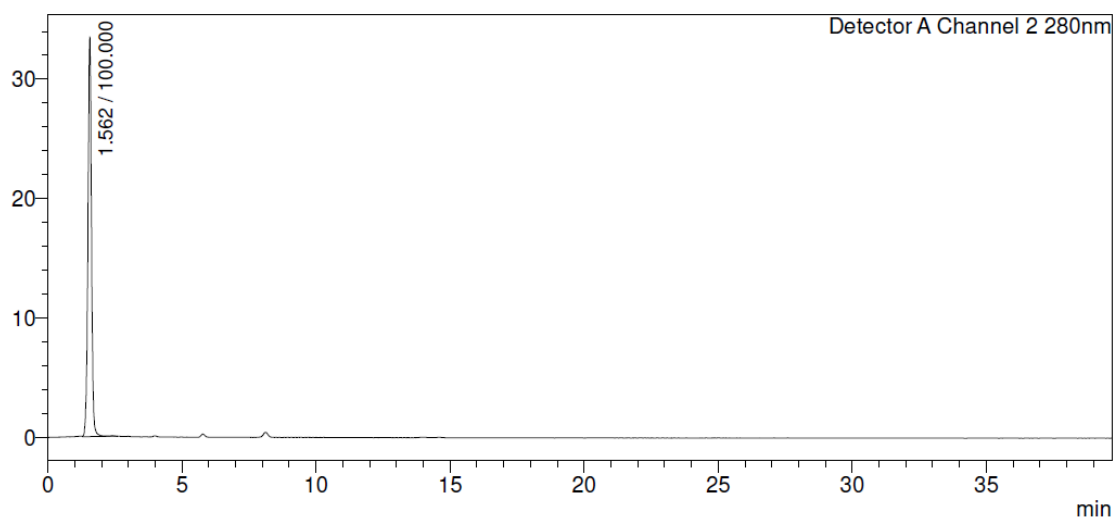
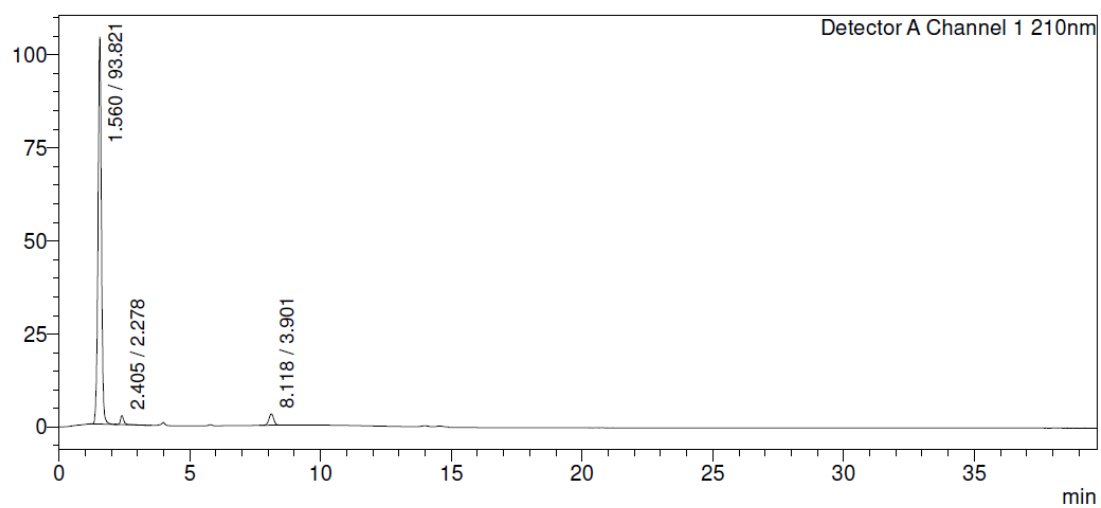
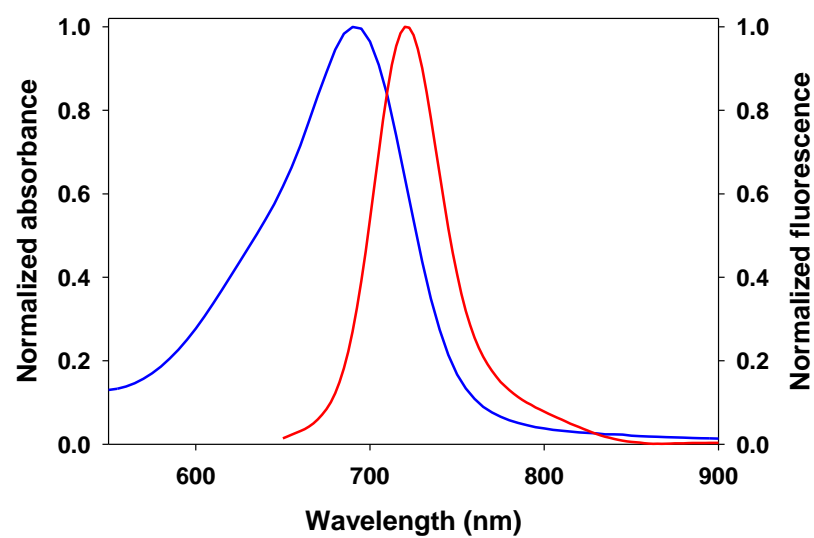
DG\_EK\_5-249\_ESINEG\_CONE40 39 (1.253) AM (Cen.4, 80.00, Ar,1.0,554.26,0.70,LS 1); Sm (Mn, 4x7.00); Sb (16,20.00 ); Cm (39:41)

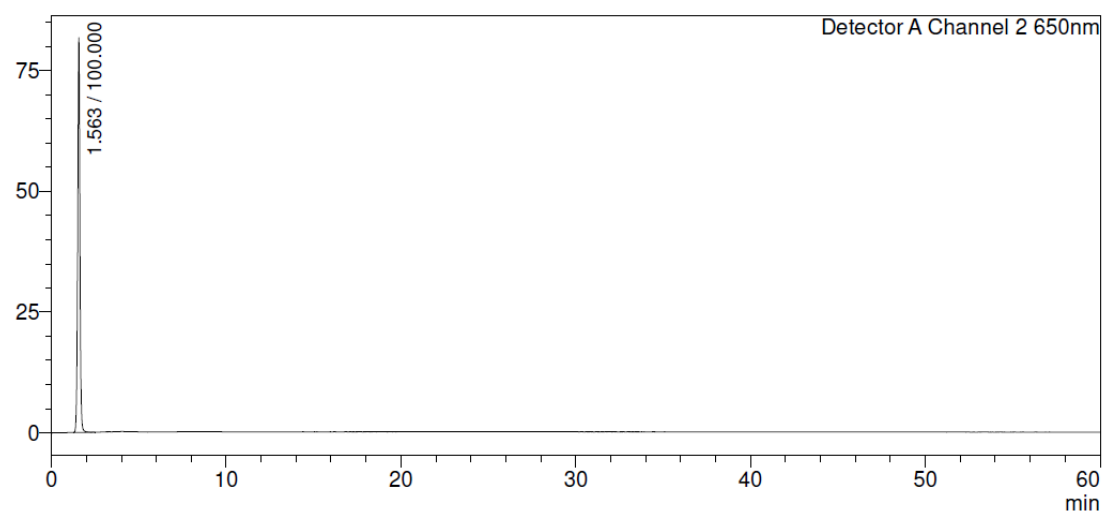
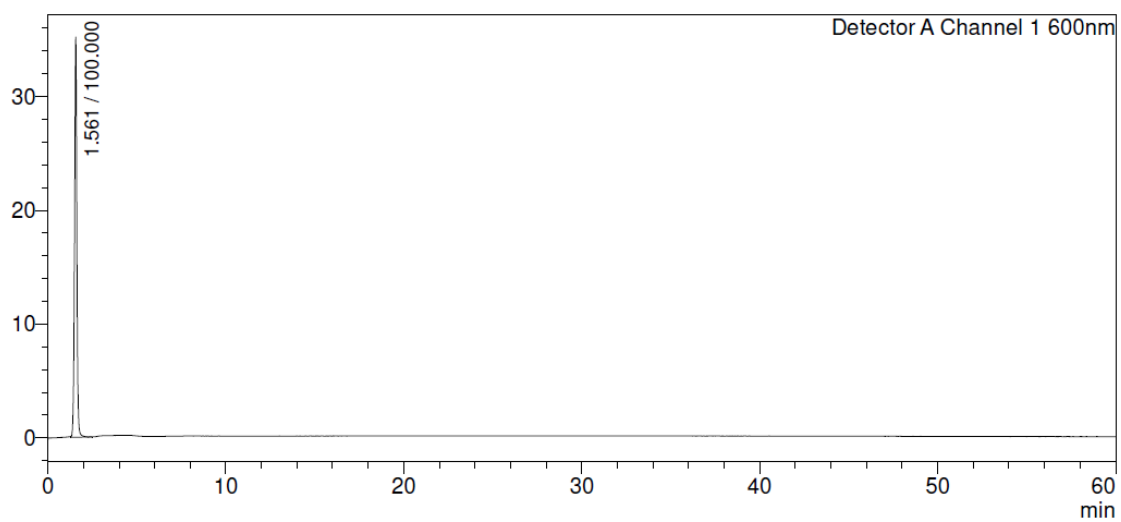
1: TOF MS ES-

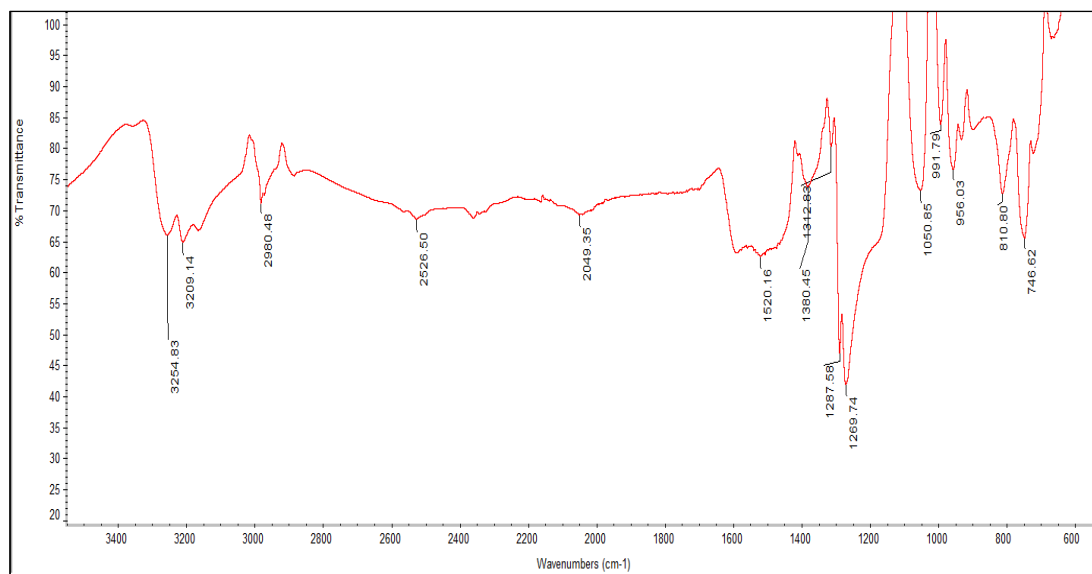
124

Mass	Calc. Mass	mDa	PPM	DBE	Score	Formula
1320.3612	1320.3685	-7.3	-5.6	34.0	1	C57 H58 B N9 O11 F2 S Pt

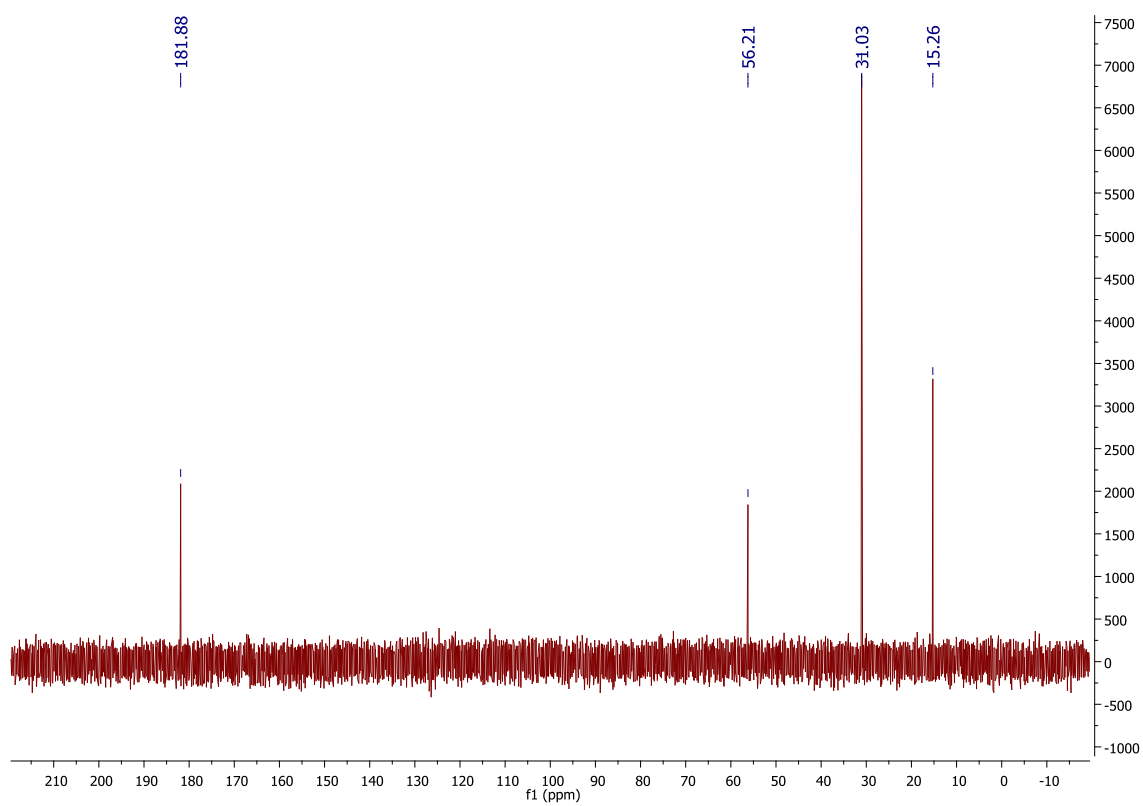
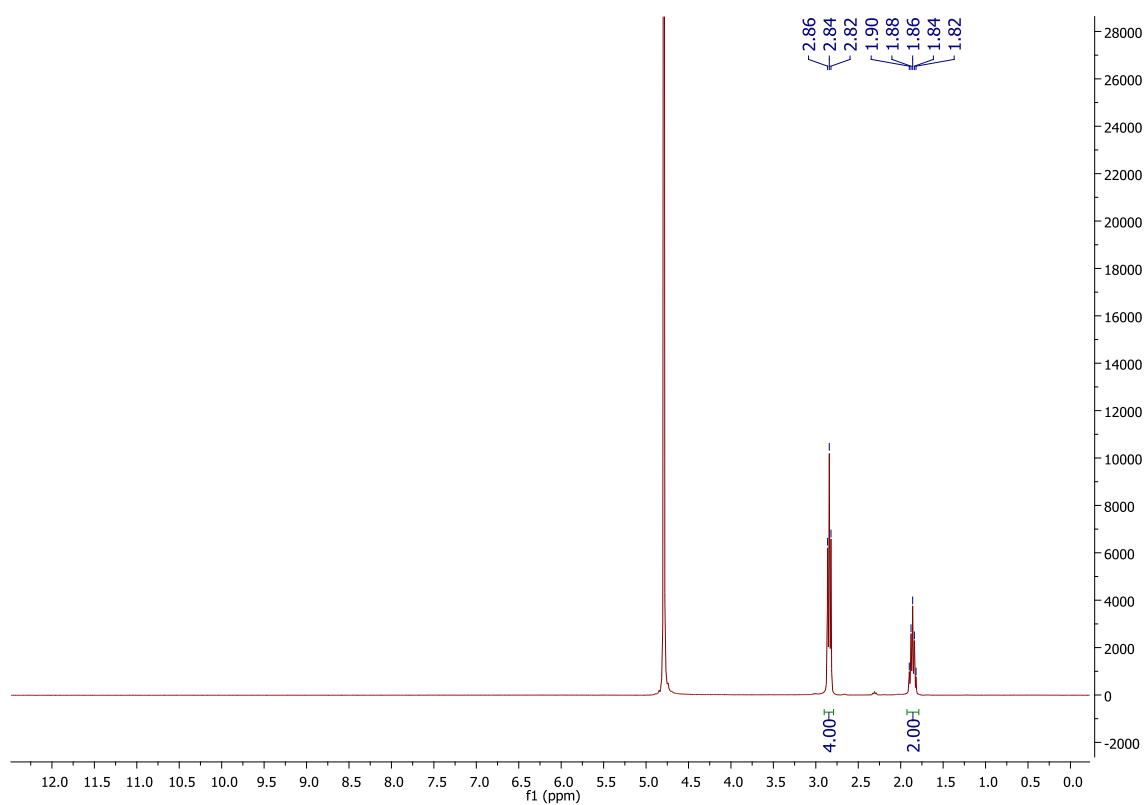
Minimum: -1.5  
Maximum: 50.0

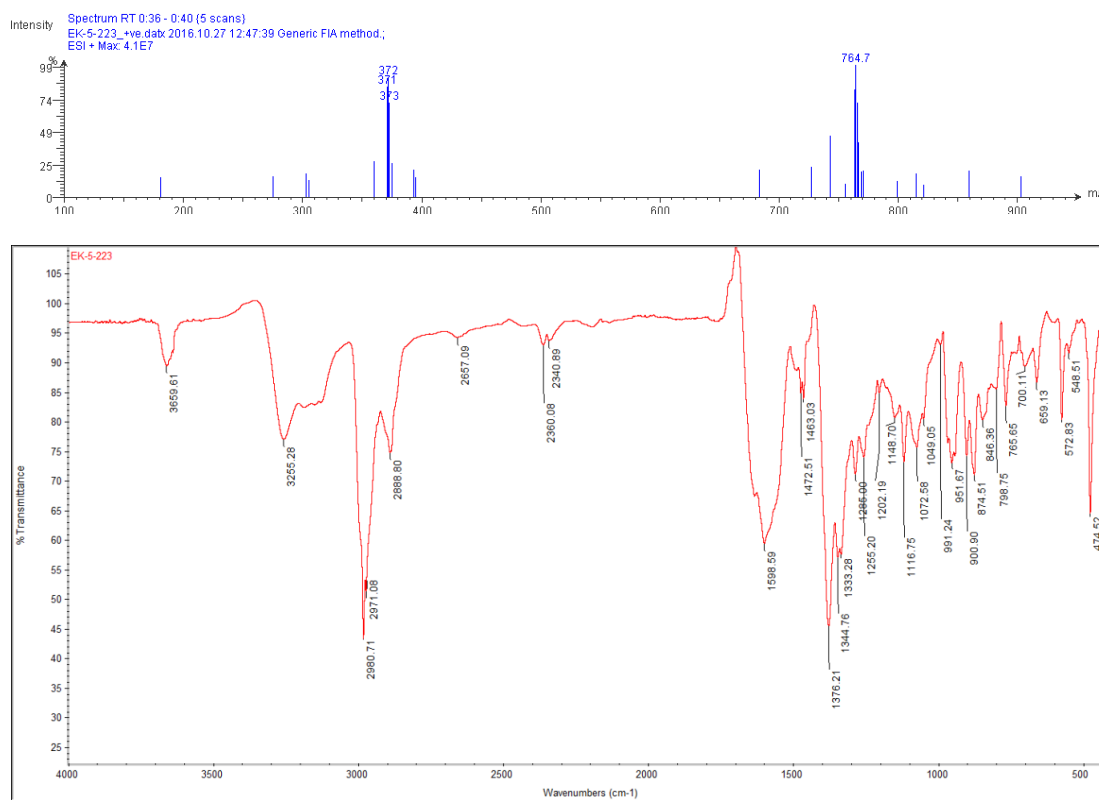


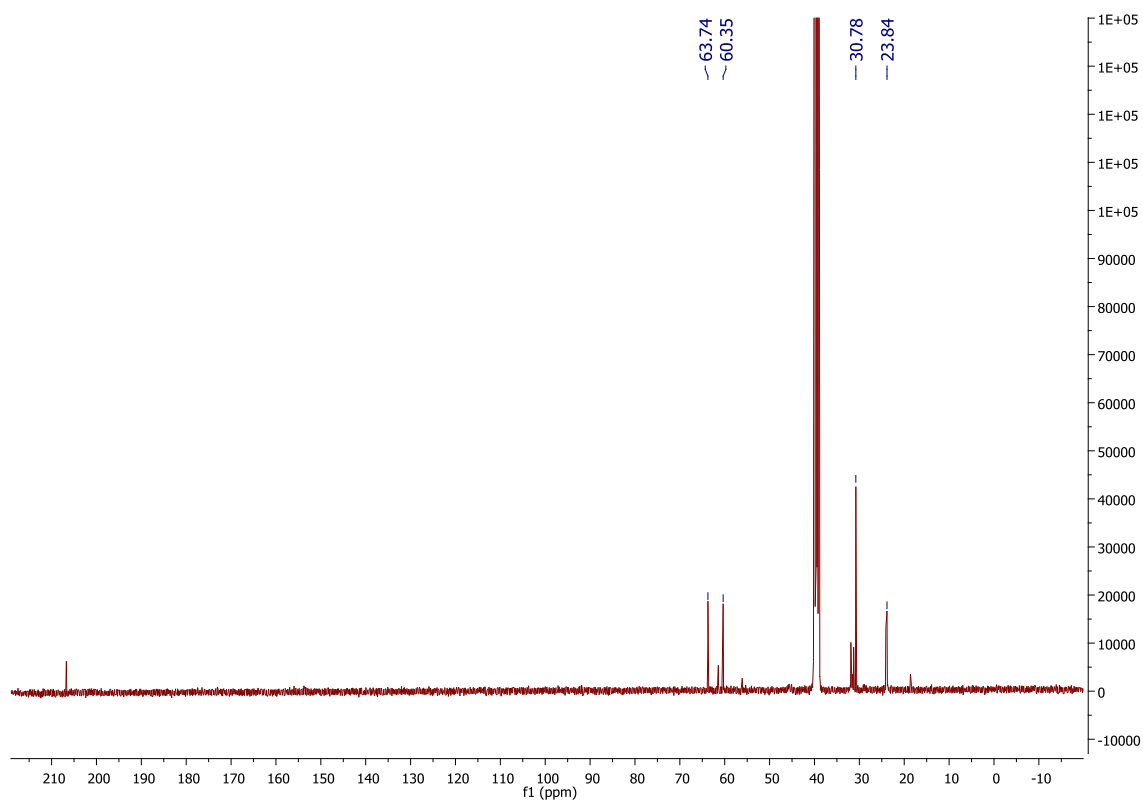
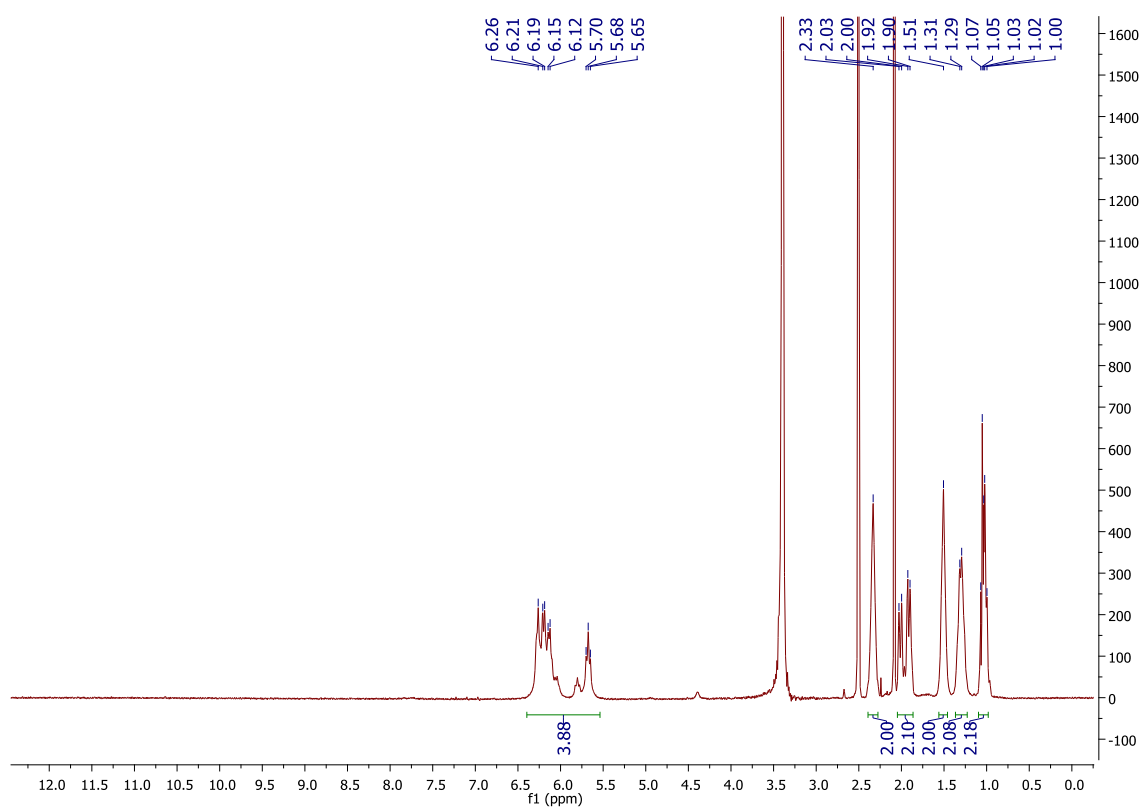


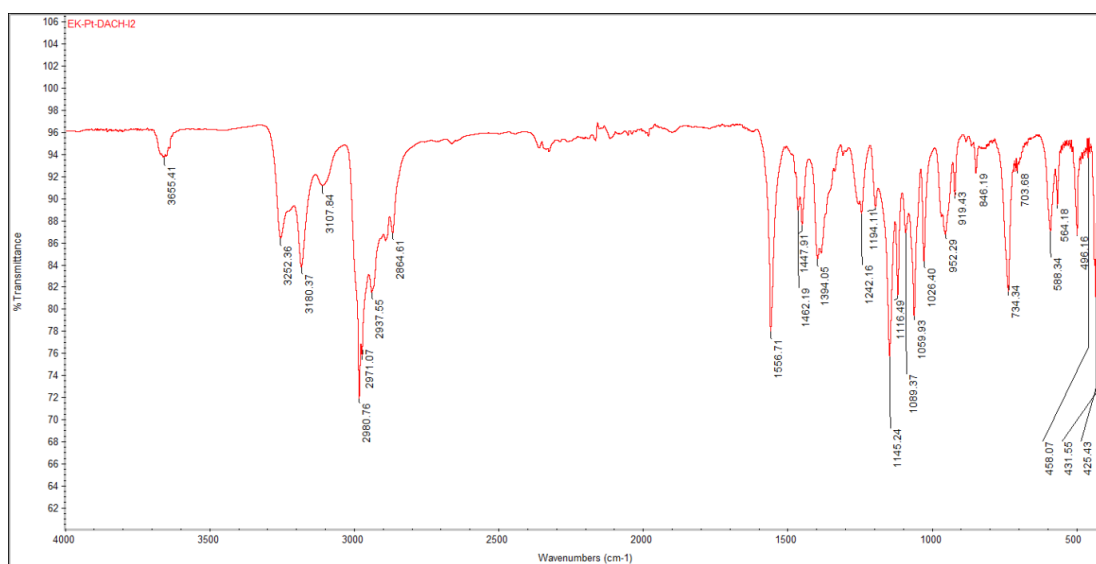
***cis*-[Pt(II)(I)<sub>2</sub>(NH<sub>3</sub>)<sub>2</sub>] –iodoplatin (21)**

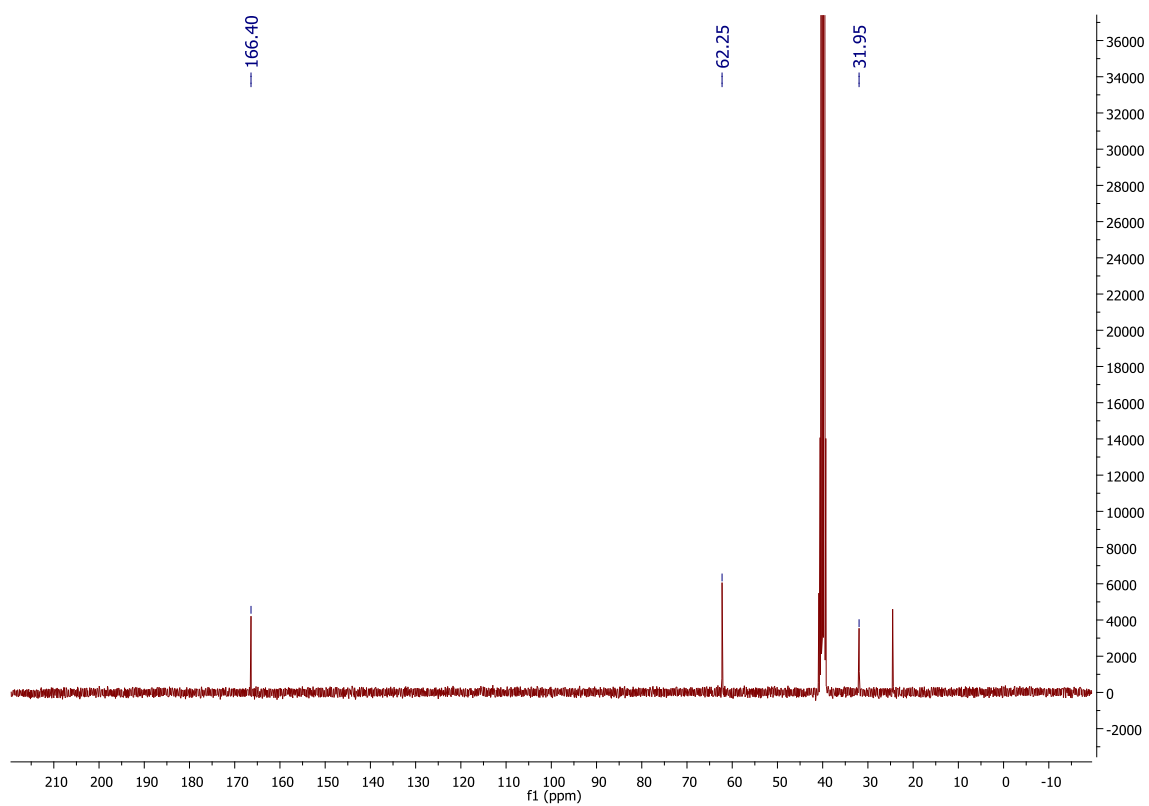
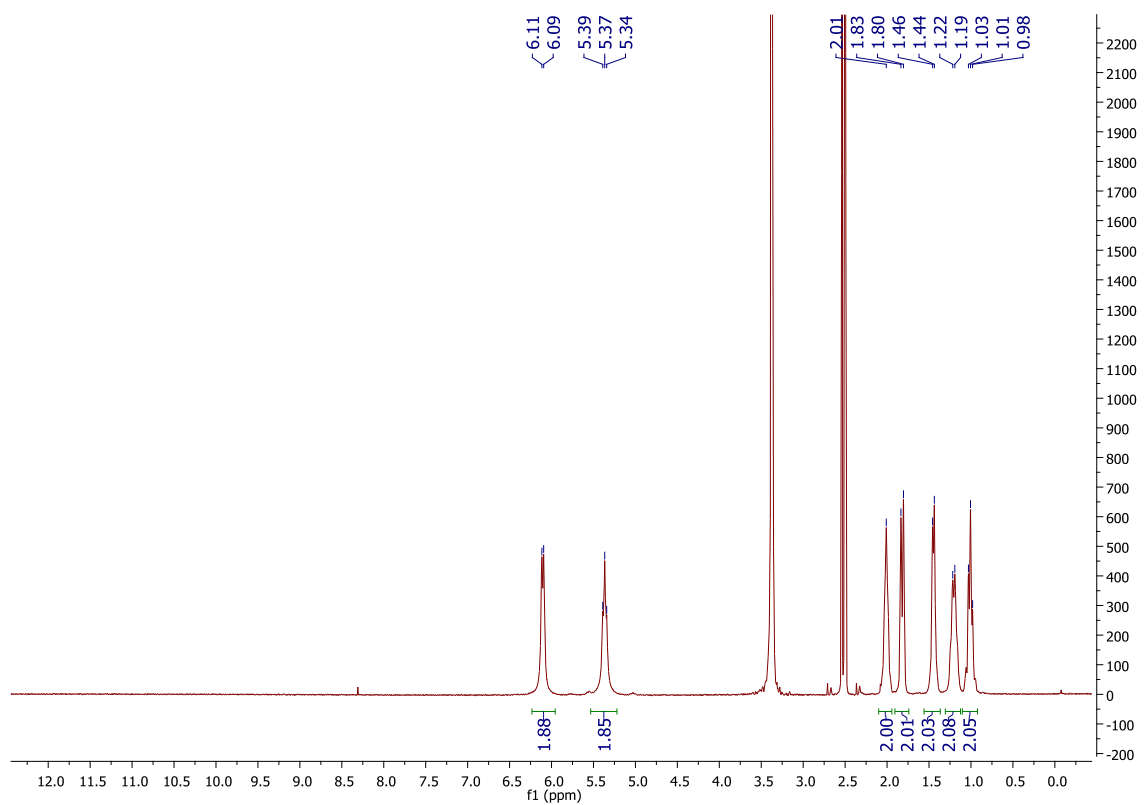


**[Pt(II)(CBDCA)(NH<sub>3</sub>)<sub>2</sub>] –Carboplatin (22)**

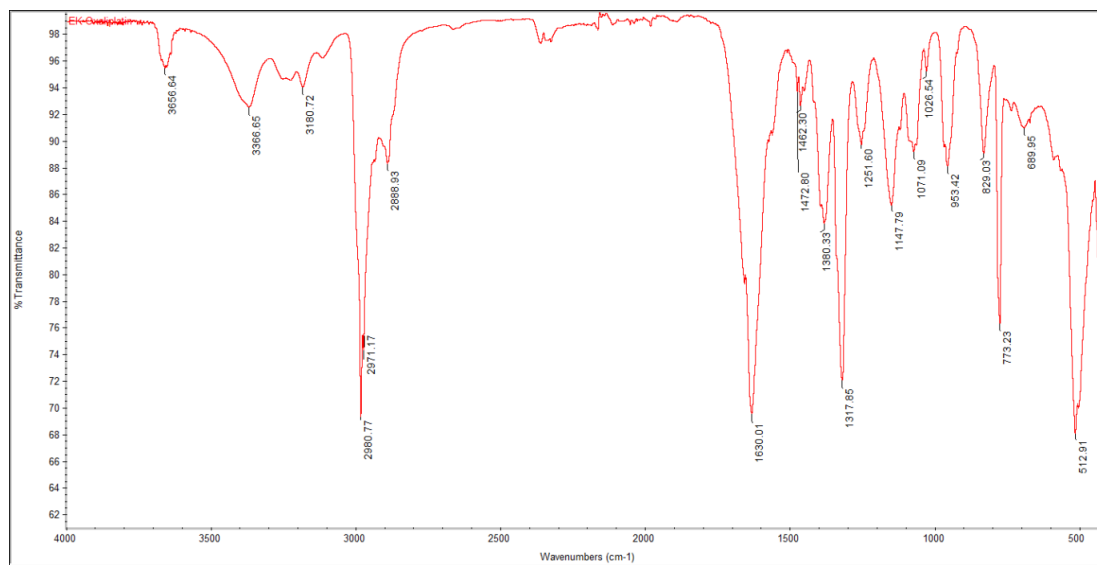
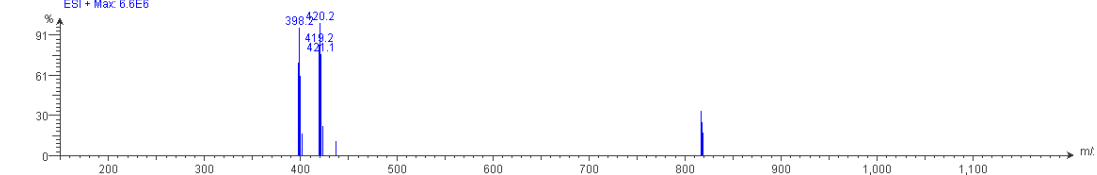


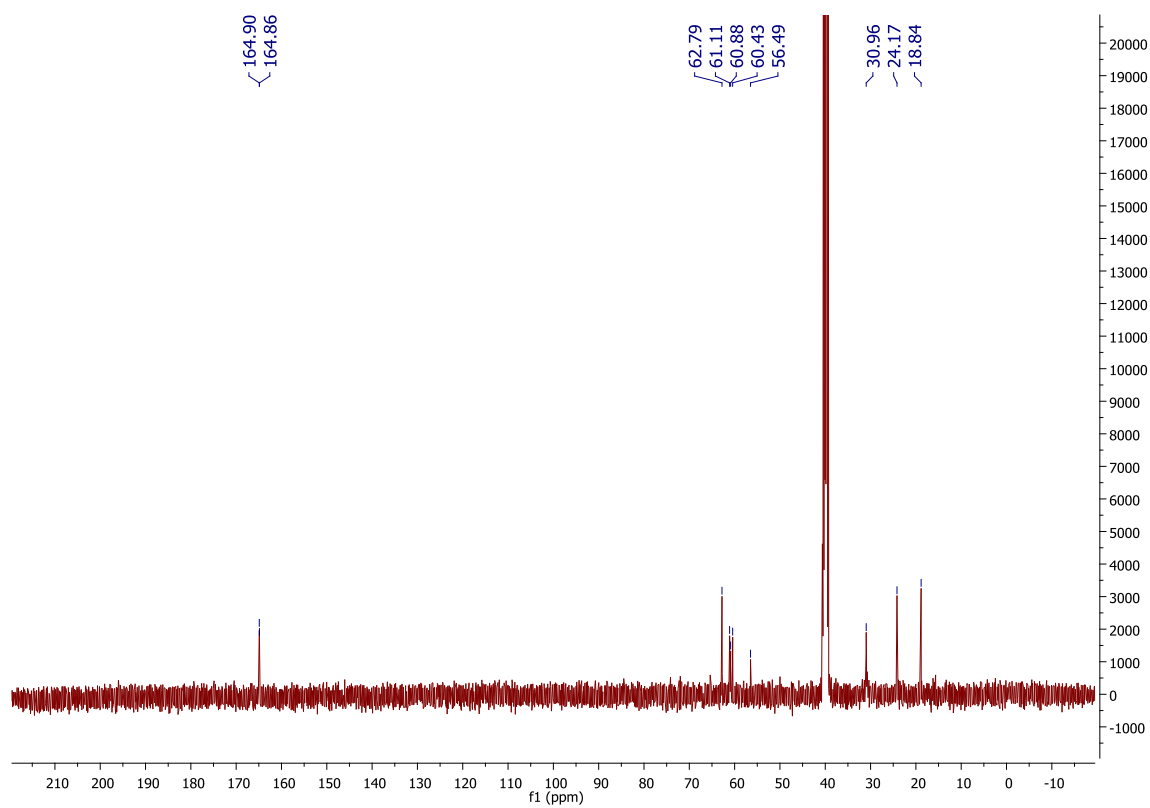
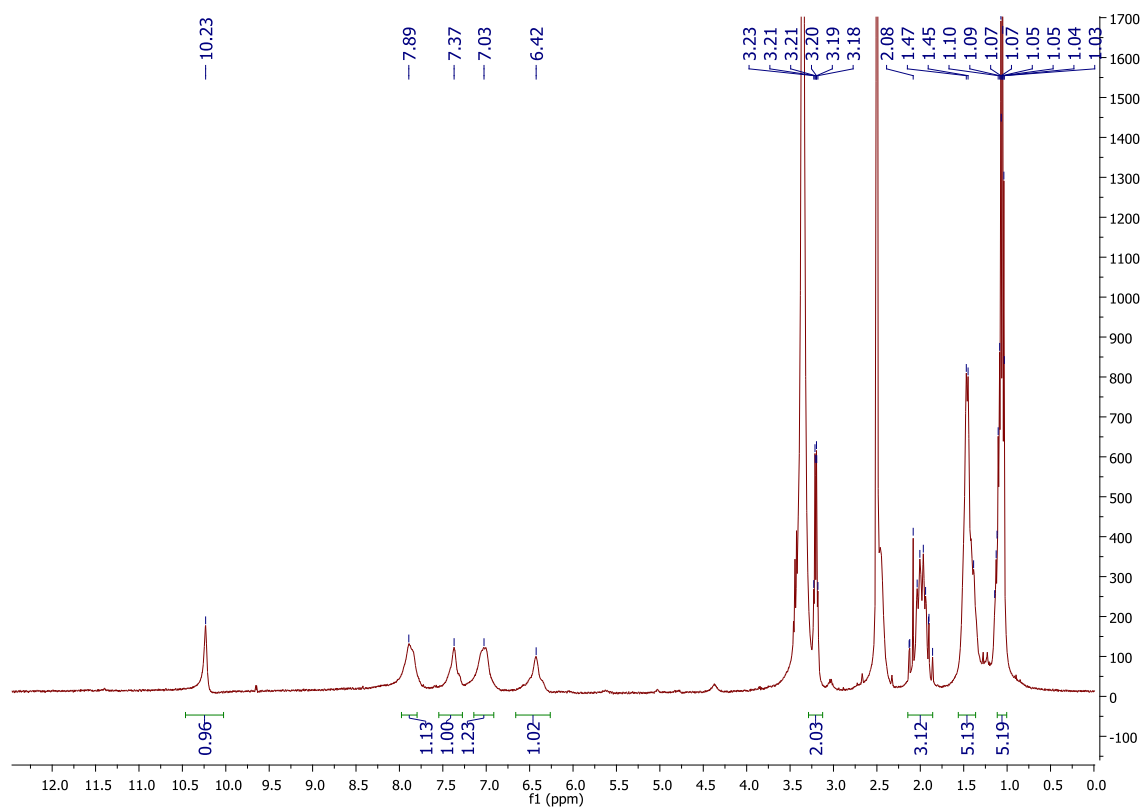
**[Pt(II)I<sub>2</sub>(DACH)] (23)**

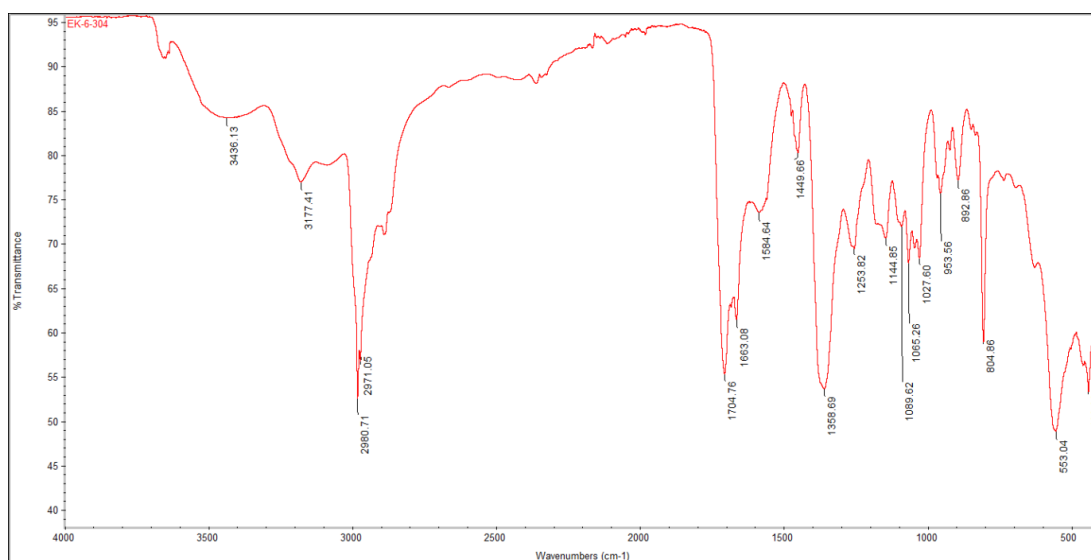
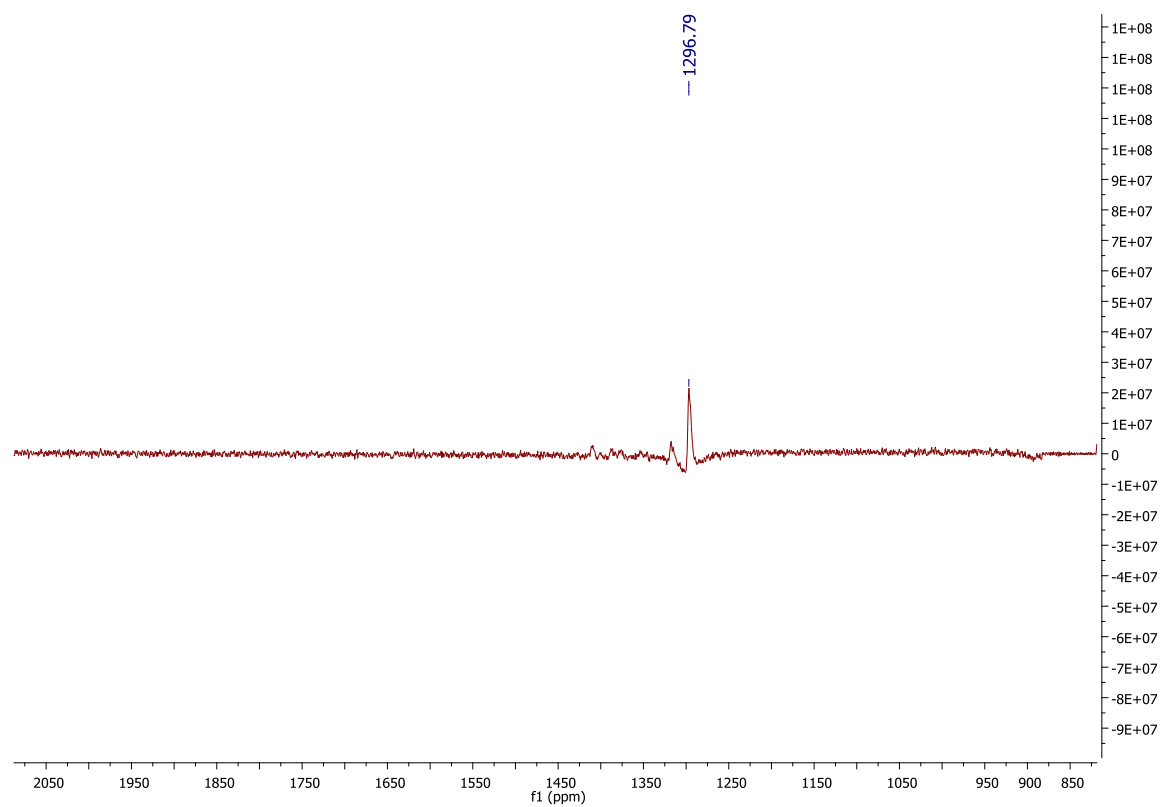


**[Pt(II)(DACH)(oxalato)] –oxaliplatin (24)**

Intensity Spectrum RT 1.20 - 1.38 (19 scans) - Background Subtracted 0.04 - 1.03  
EK-6-325\_+ve.dab 2017.12.09 16:51:34;  
ESI + Max: 6.6E6



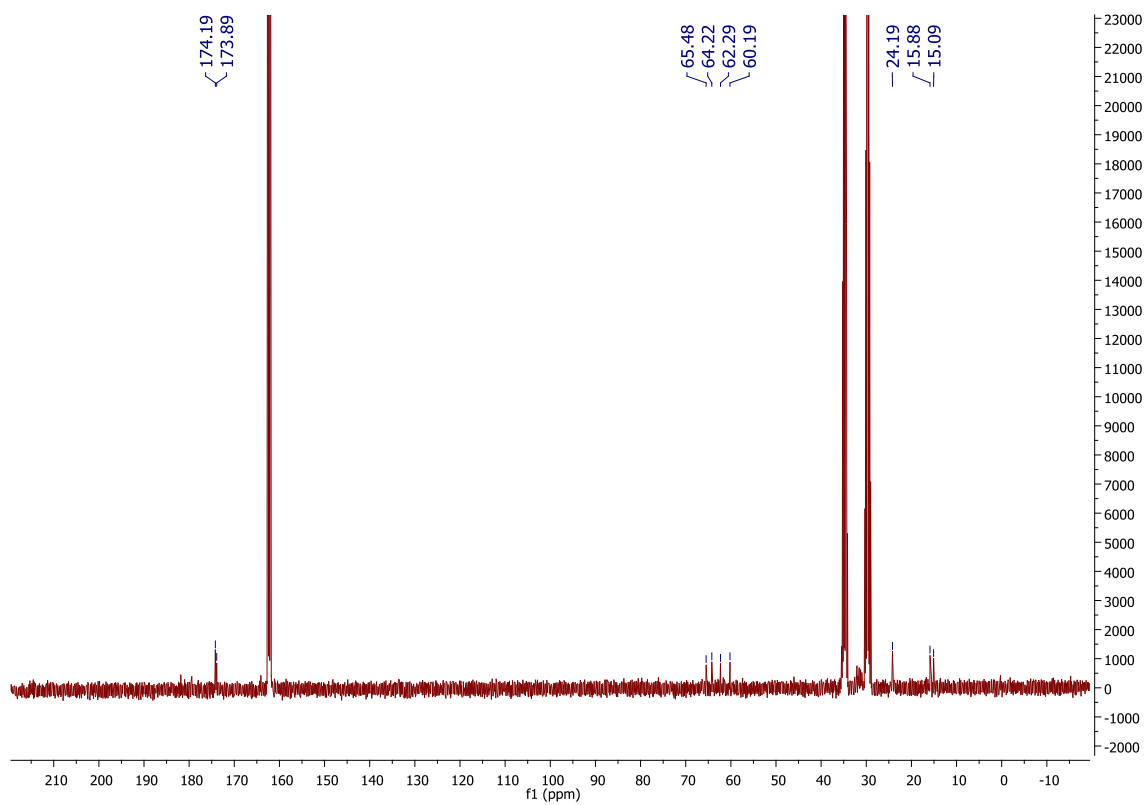
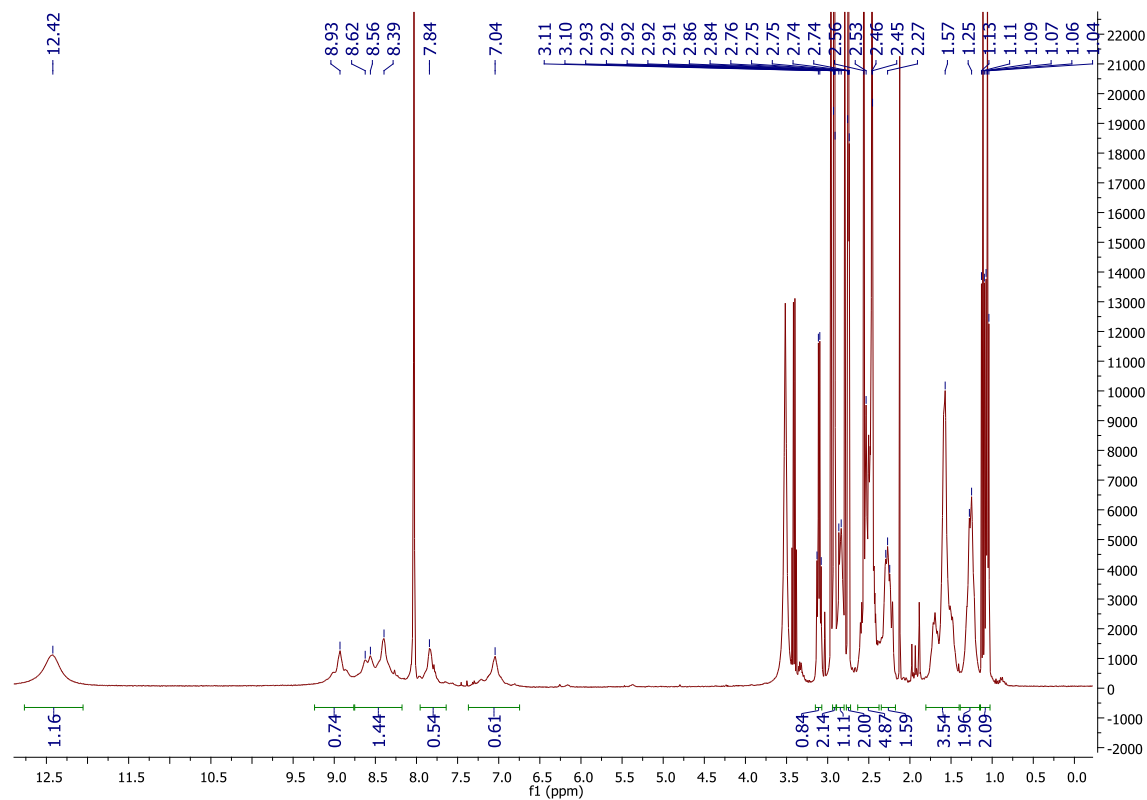
**[Pt(IV)(DACH)(OEt)(OH)(oxalato)] (25)**



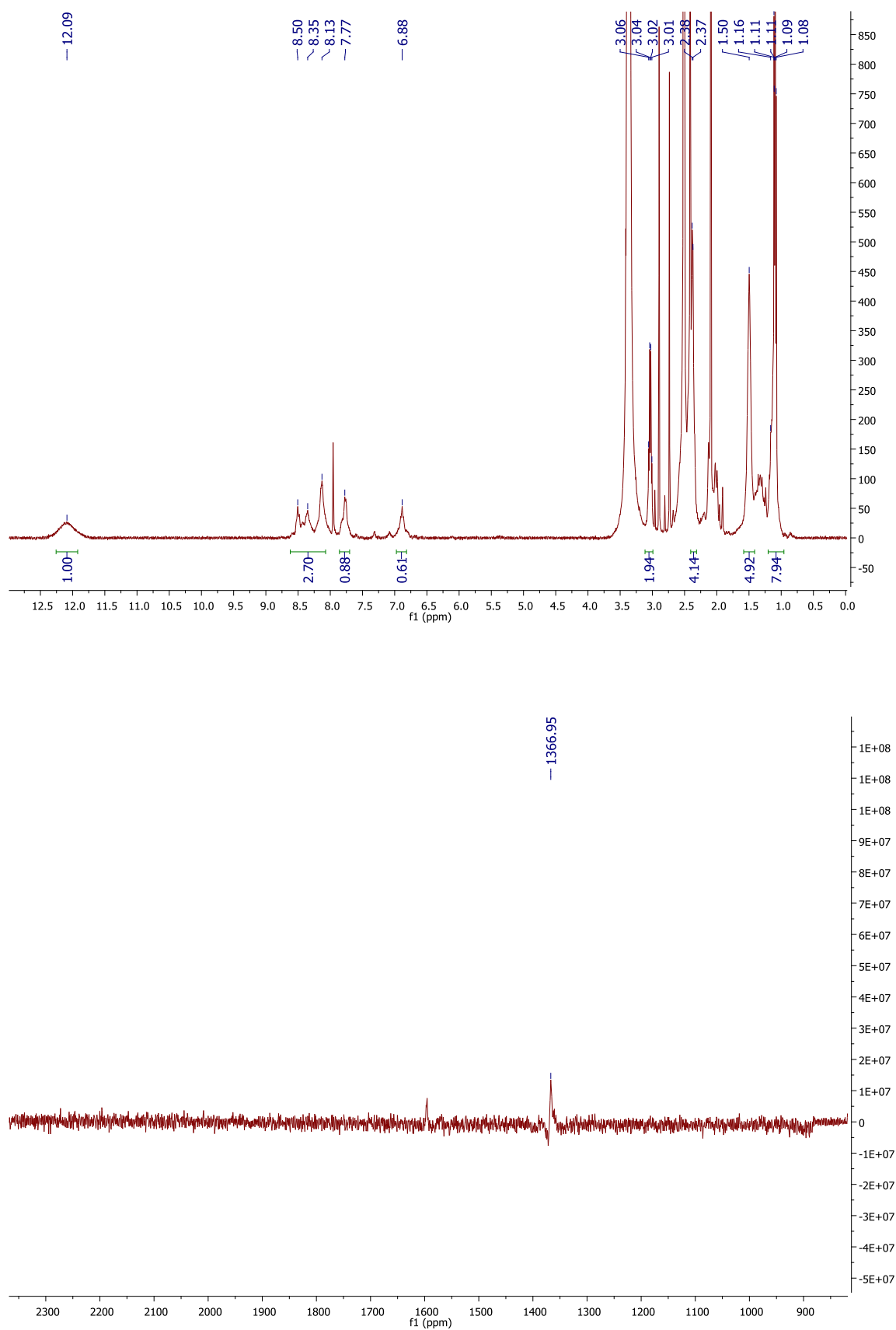


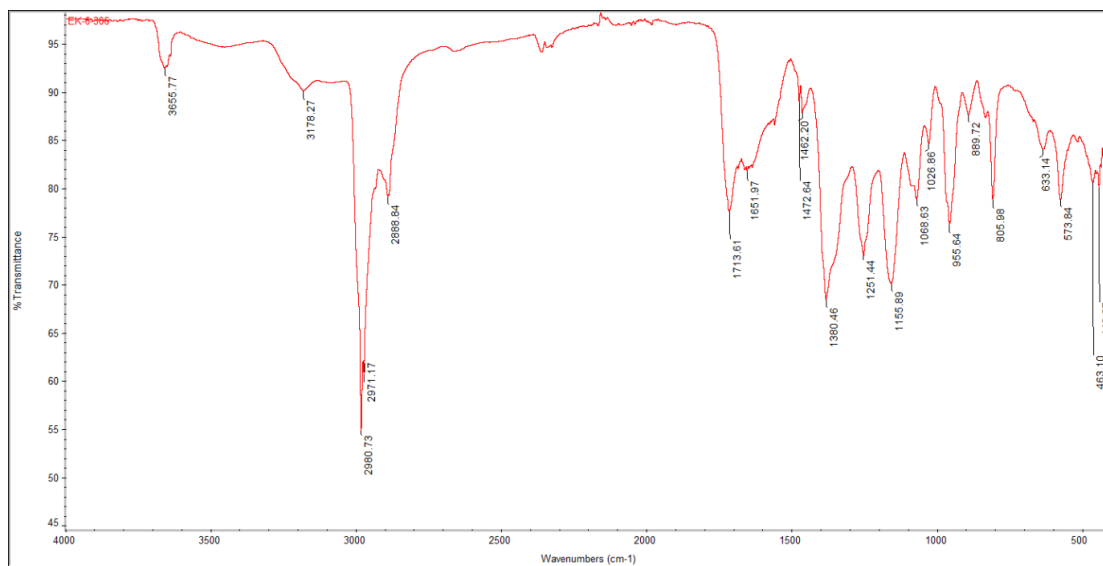
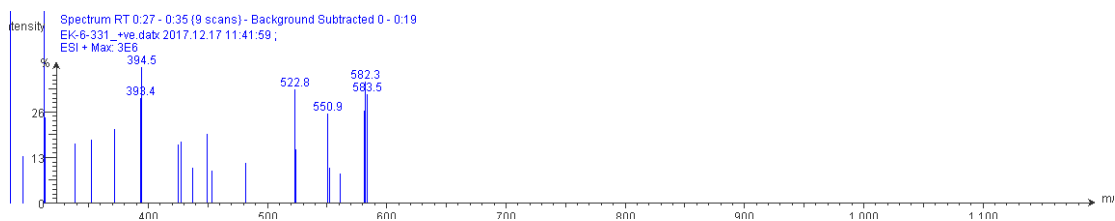
**[Pt(IV)(DACH)(OEt)(oxalato)(succinato)] (26)**

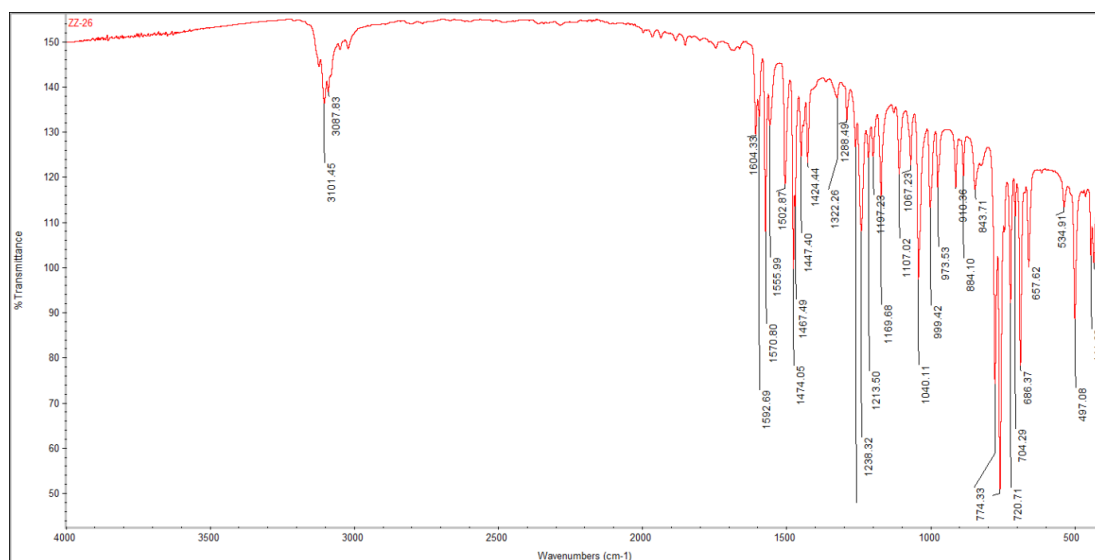
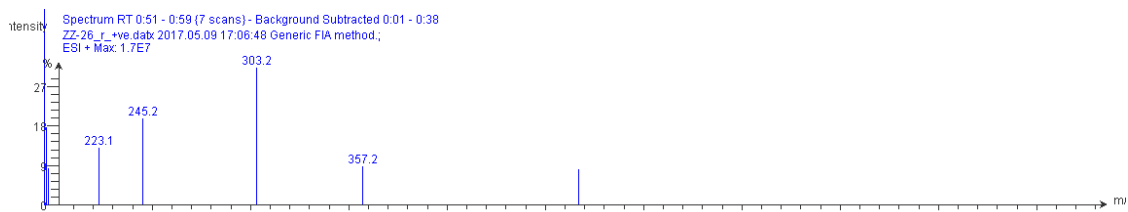
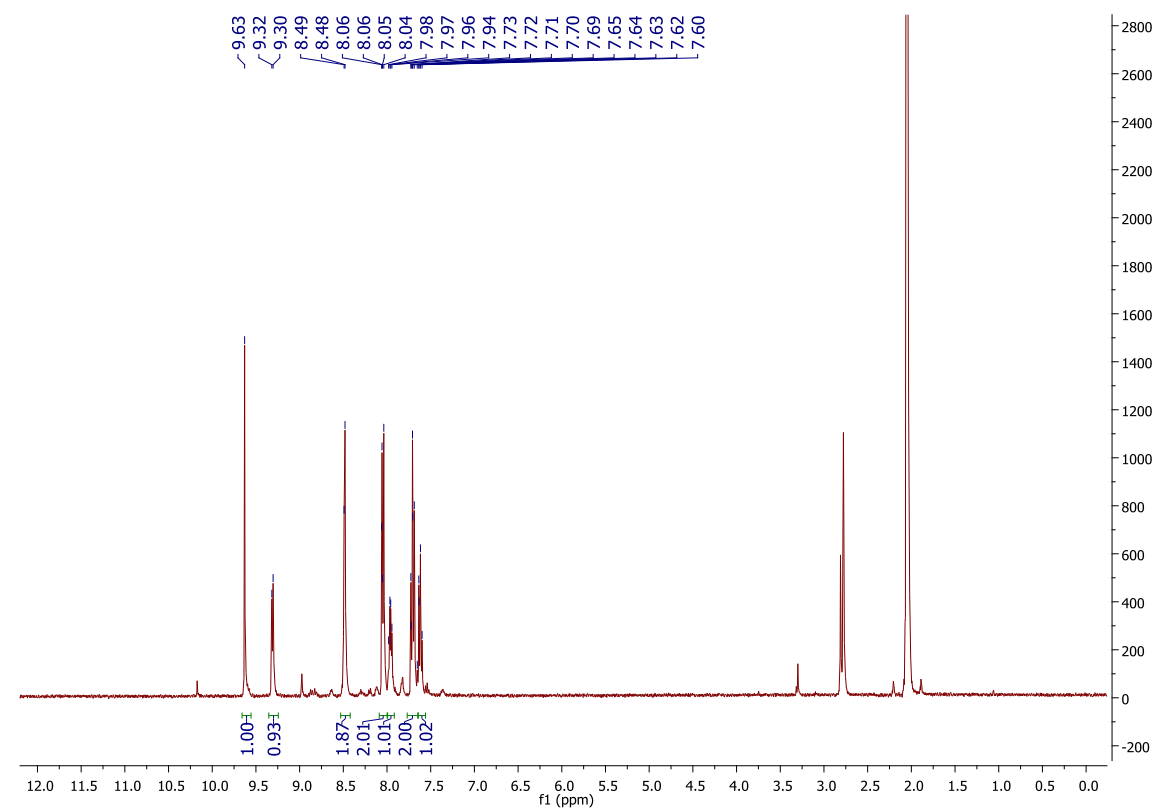
DMF



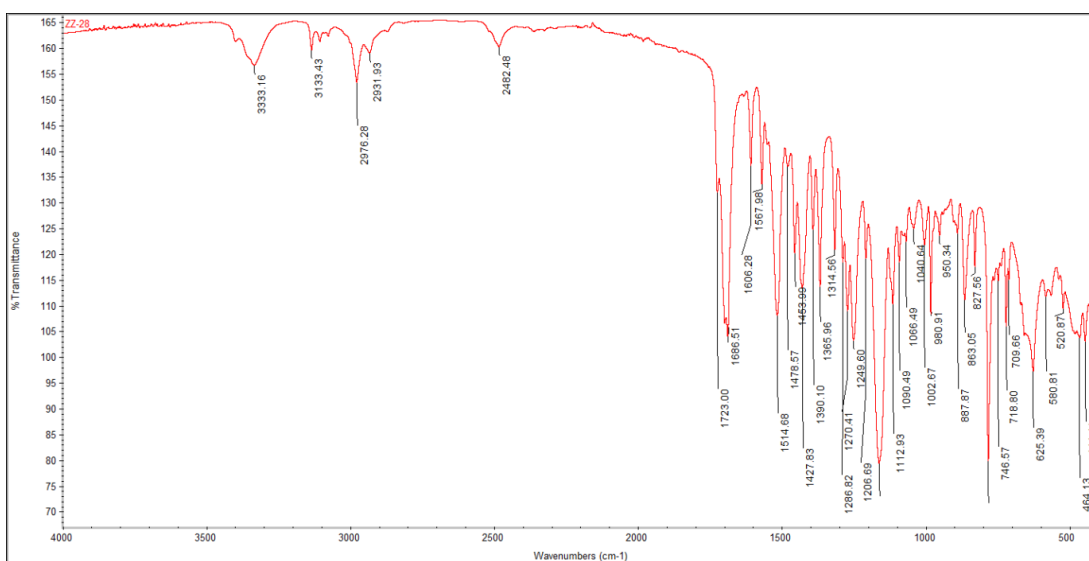
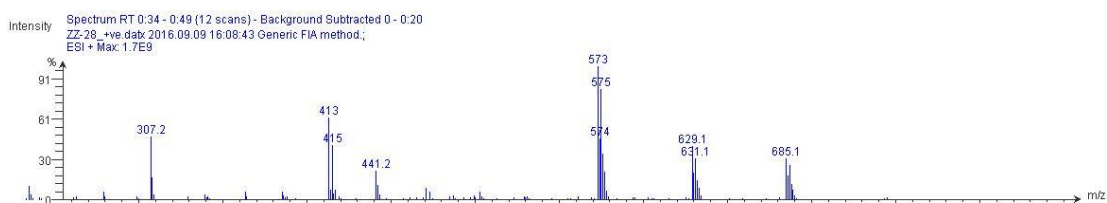
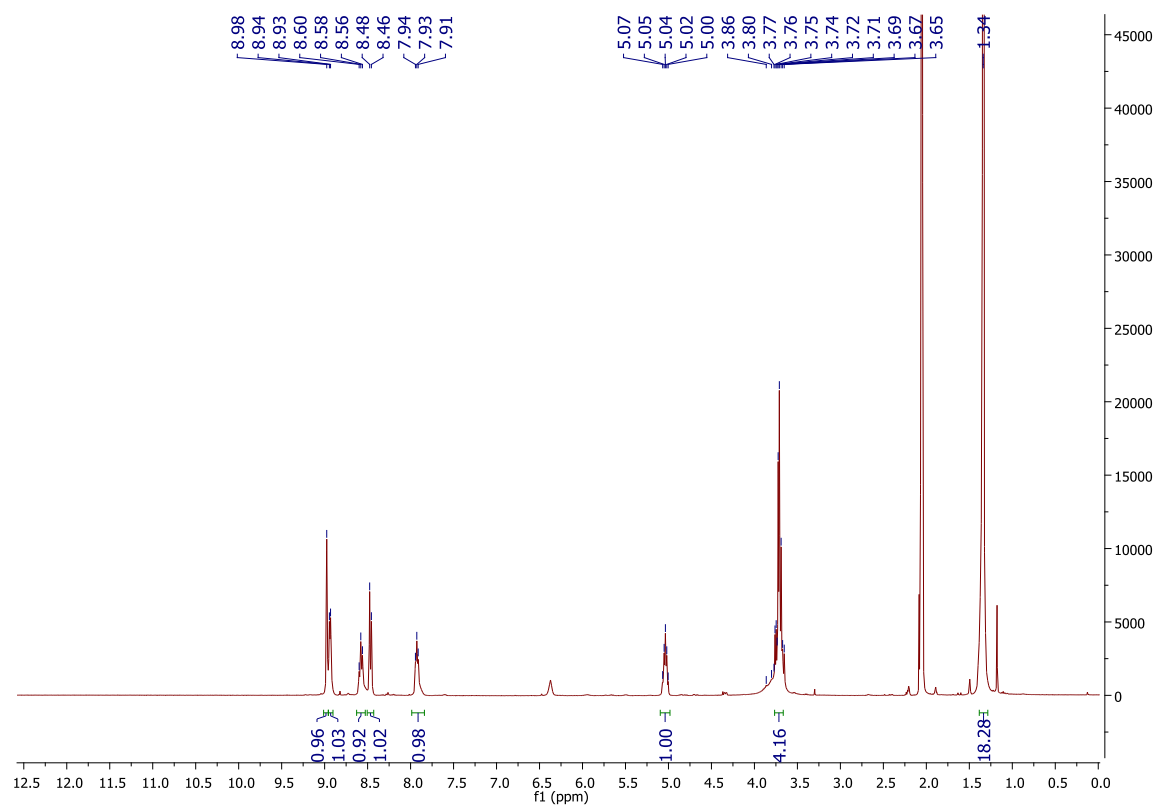
DMSO

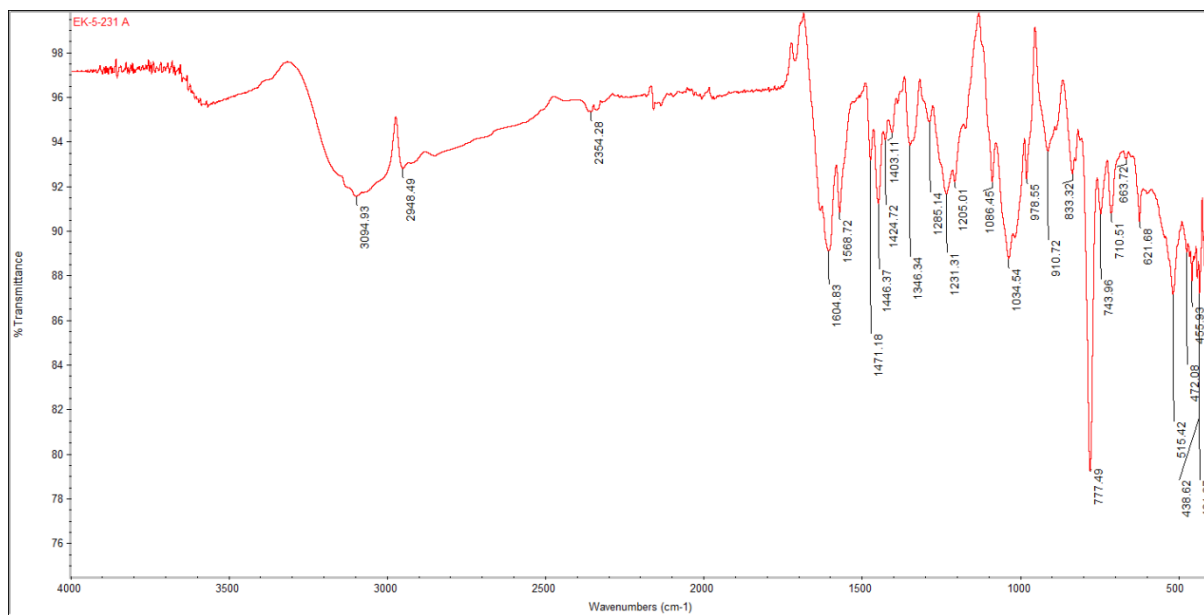
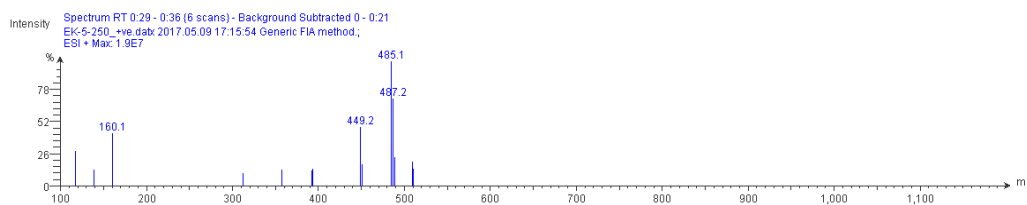


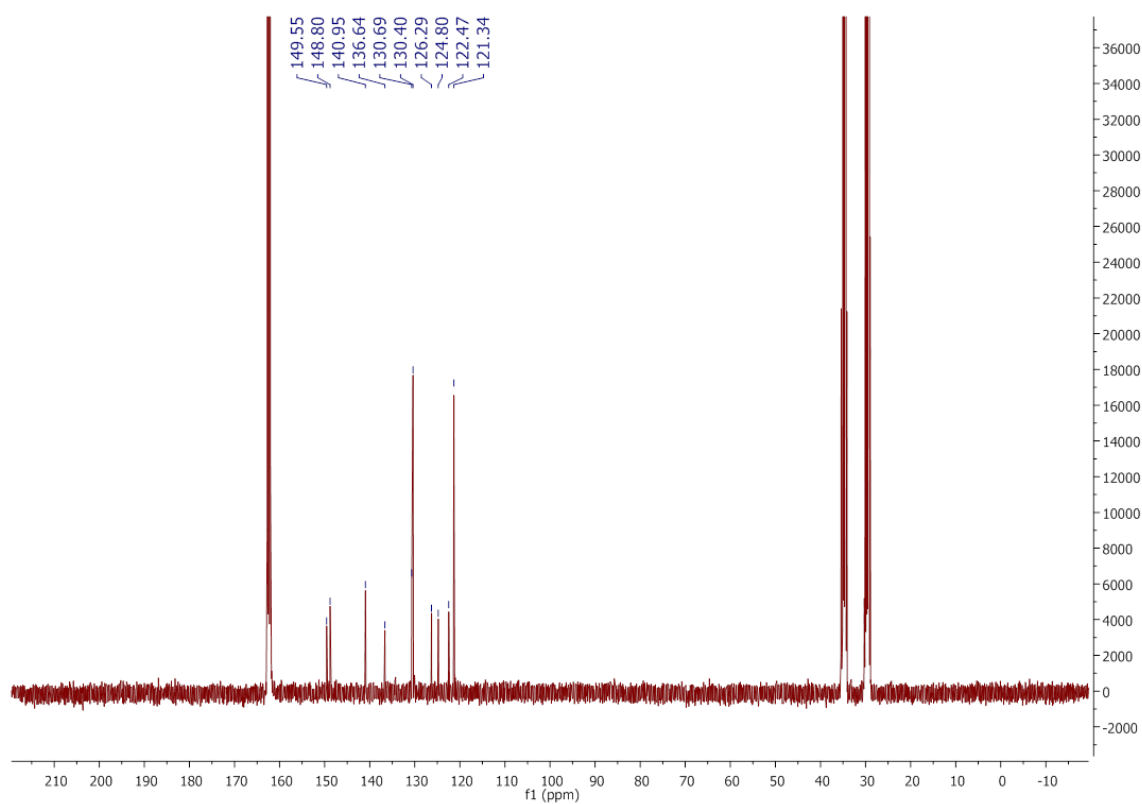
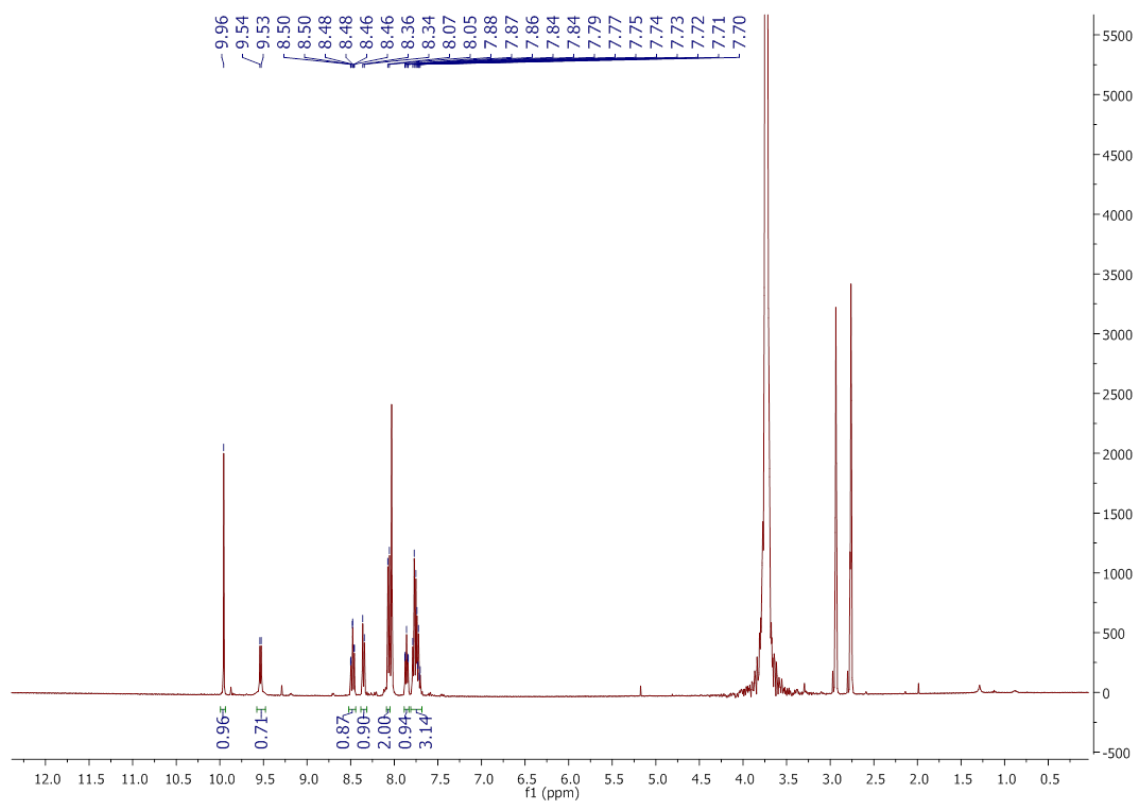


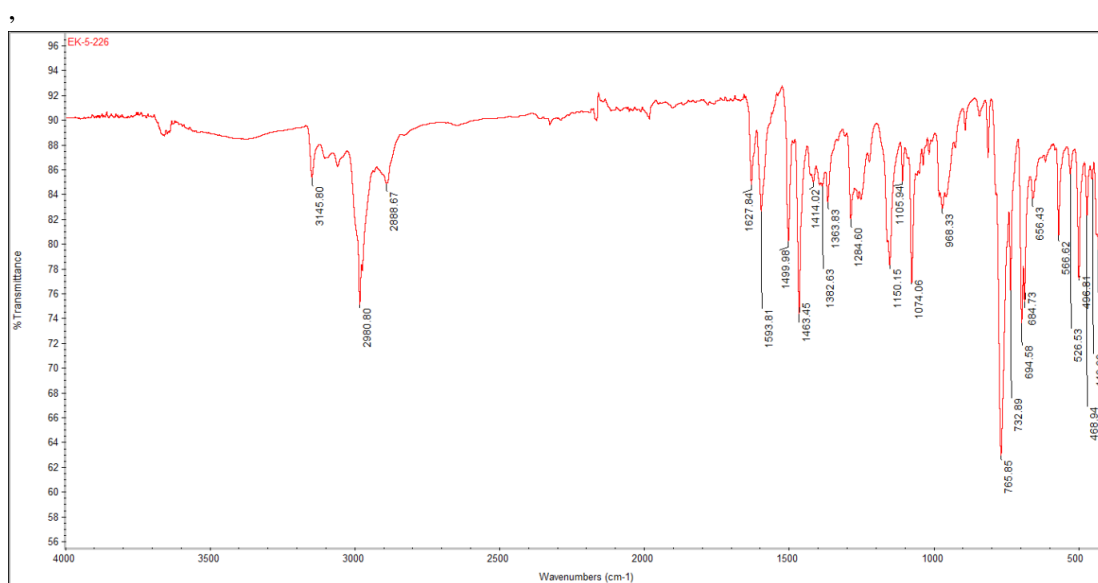
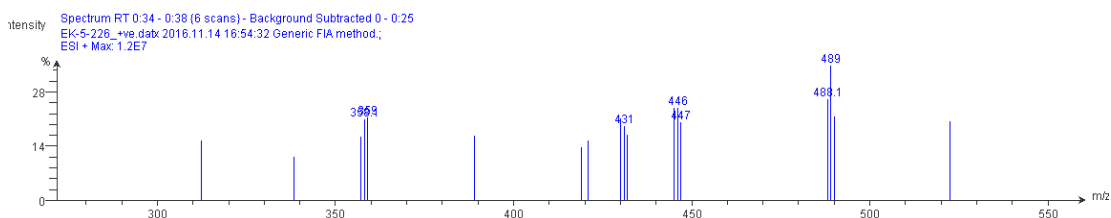
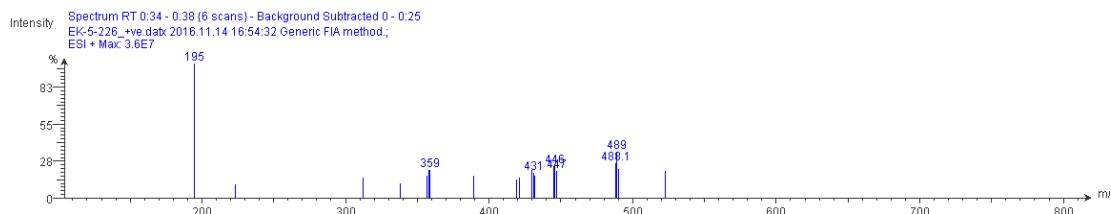
**[Au(III)Cl<sub>3</sub>(PTP)] (27)**

**[Au(III)Cl<sub>3</sub>(BOC<sub>2</sub>-PTPD)] (28)**



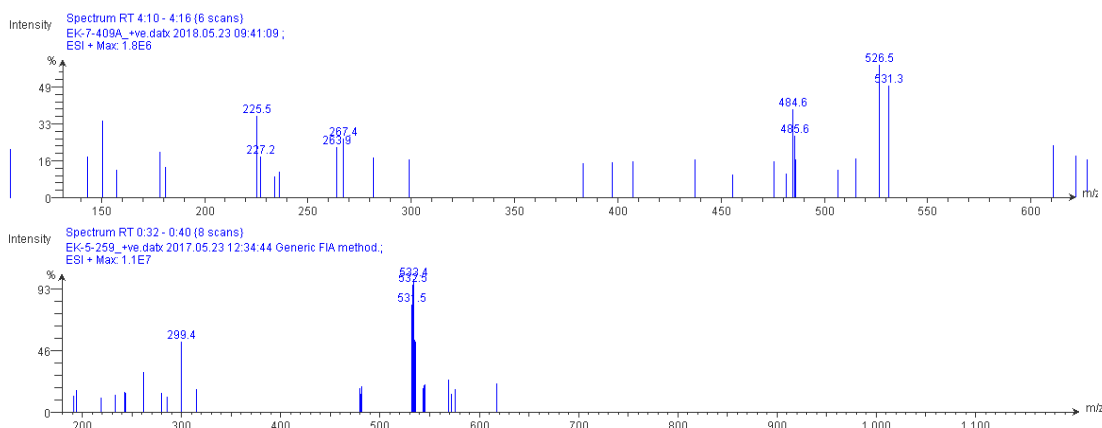
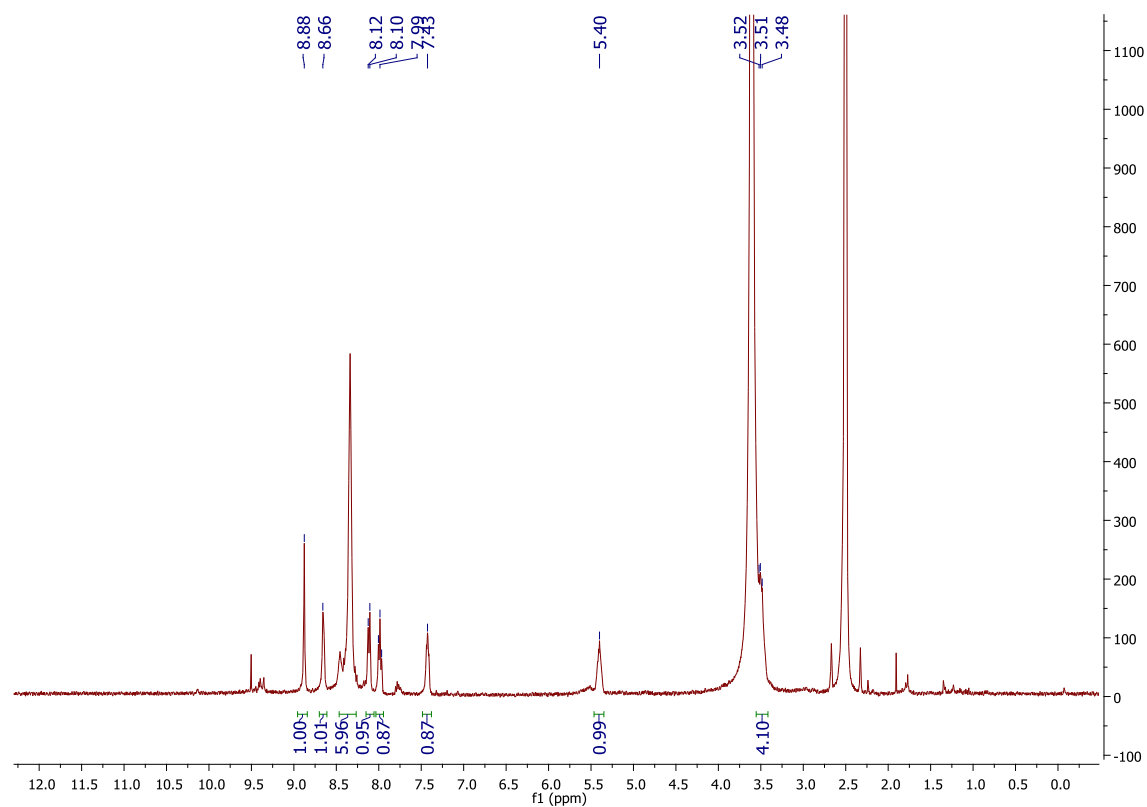
**Na<sub>0.5</sub>[Au(III)Cl<sub>2</sub>(PTPD)][Au(I)Cl<sub>2</sub>][Au(III)Cl<sub>4</sub>]<sub>0.5</sub> (29)**

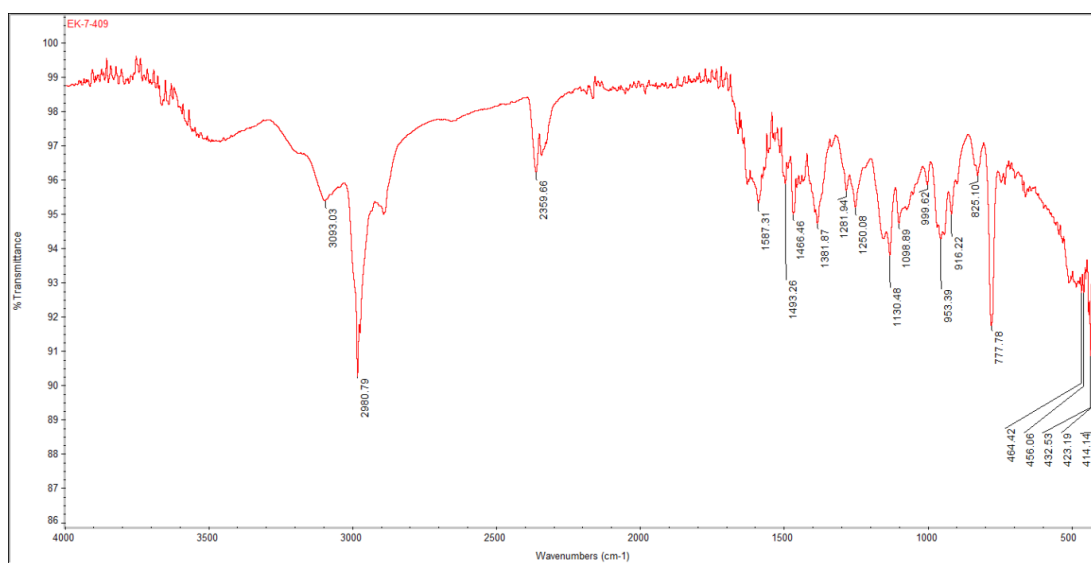
**[Pt(II)Cl<sub>2</sub>(PTP)] (30)**



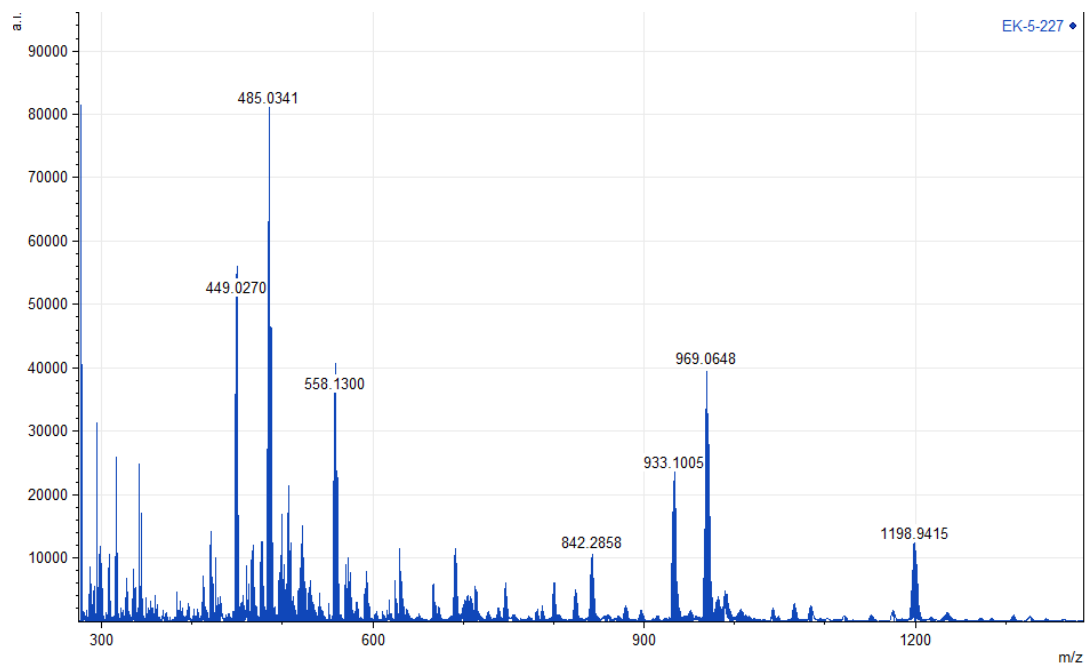


**[Pt(II)Cl<sub>2</sub>(PTPDH<sub>2</sub>)] [PtCl<sub>4</sub>] (31)**

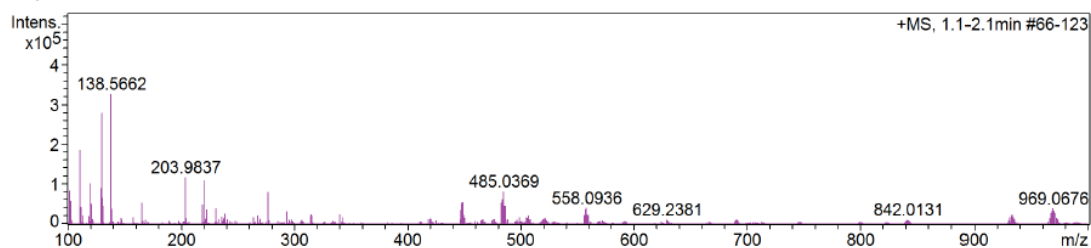




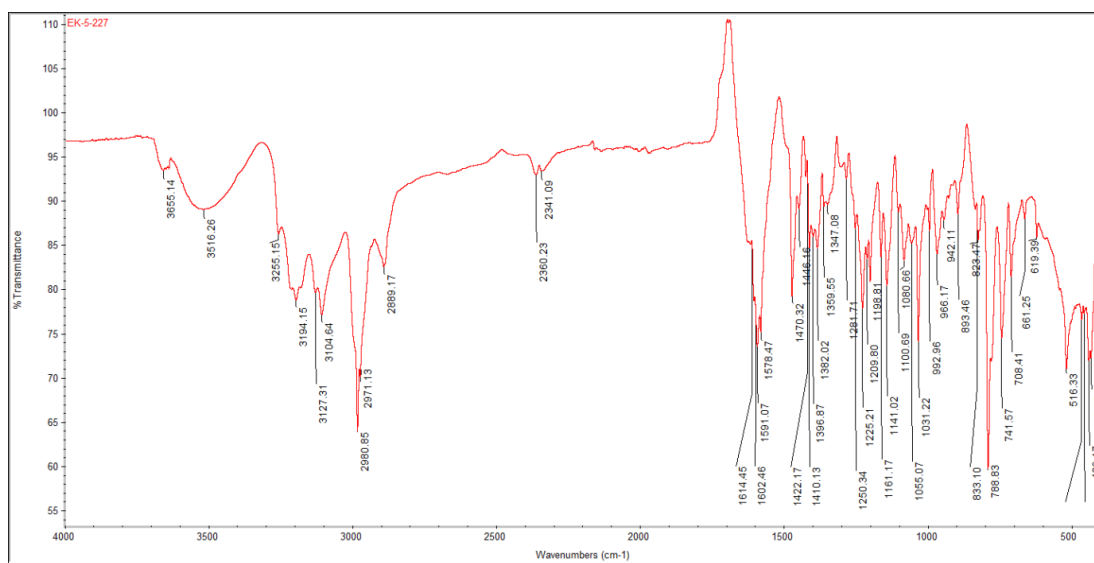
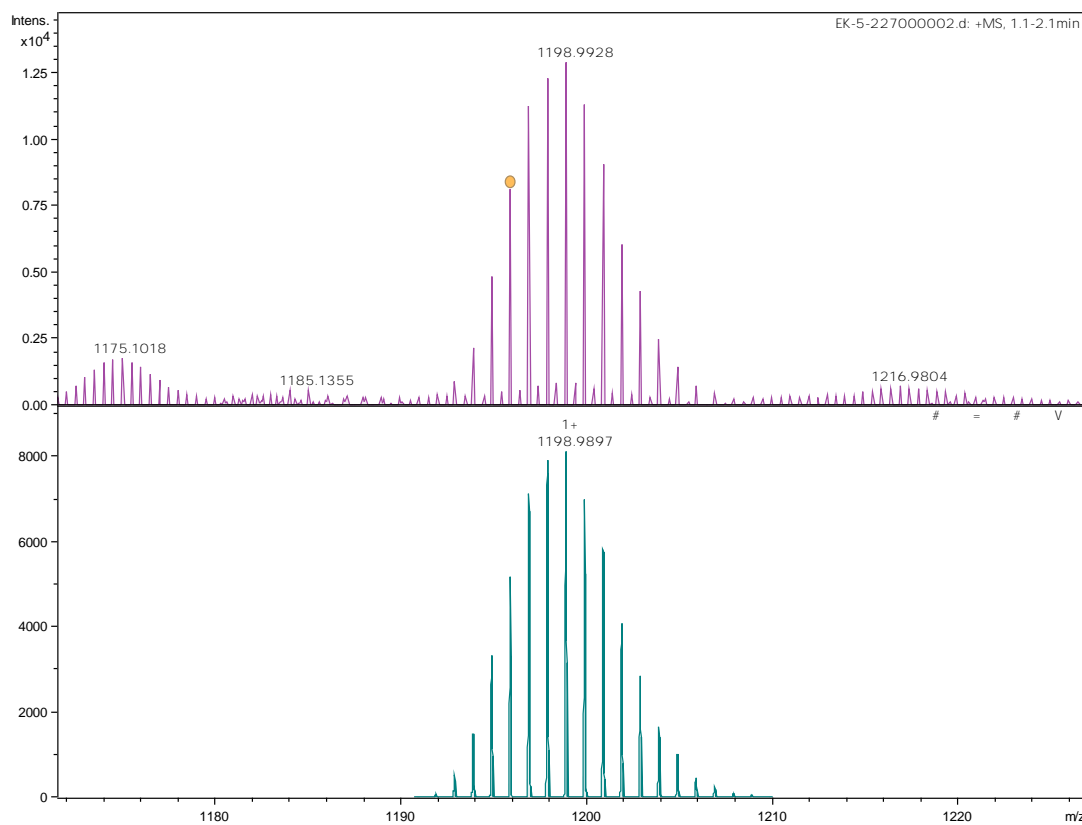
**[Pt(II)<sub>3</sub>Cl<sub>4</sub>(PTPD)<sub>2</sub>]Cl<sub>2</sub> (32)**

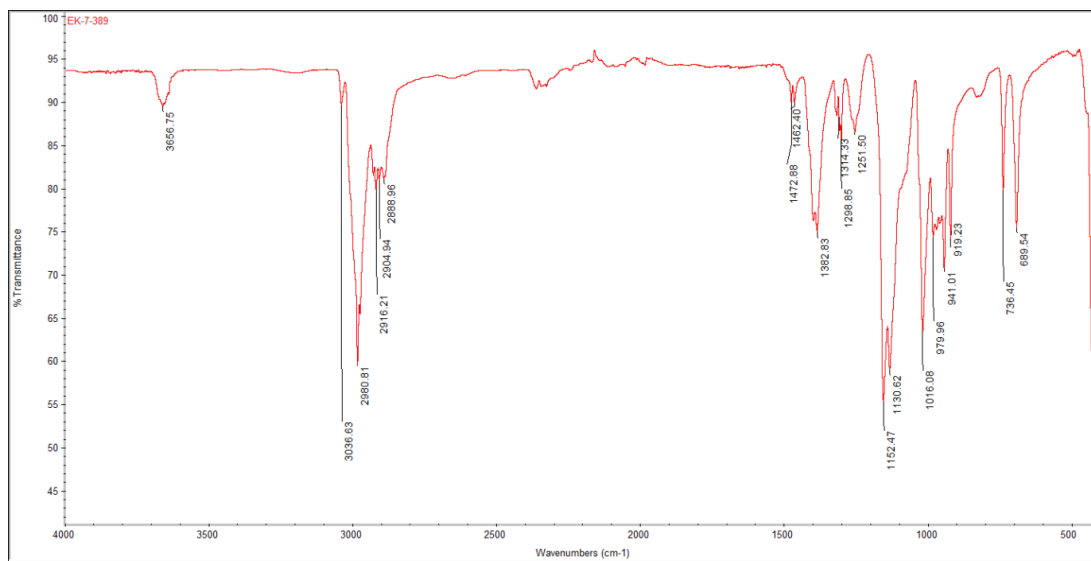


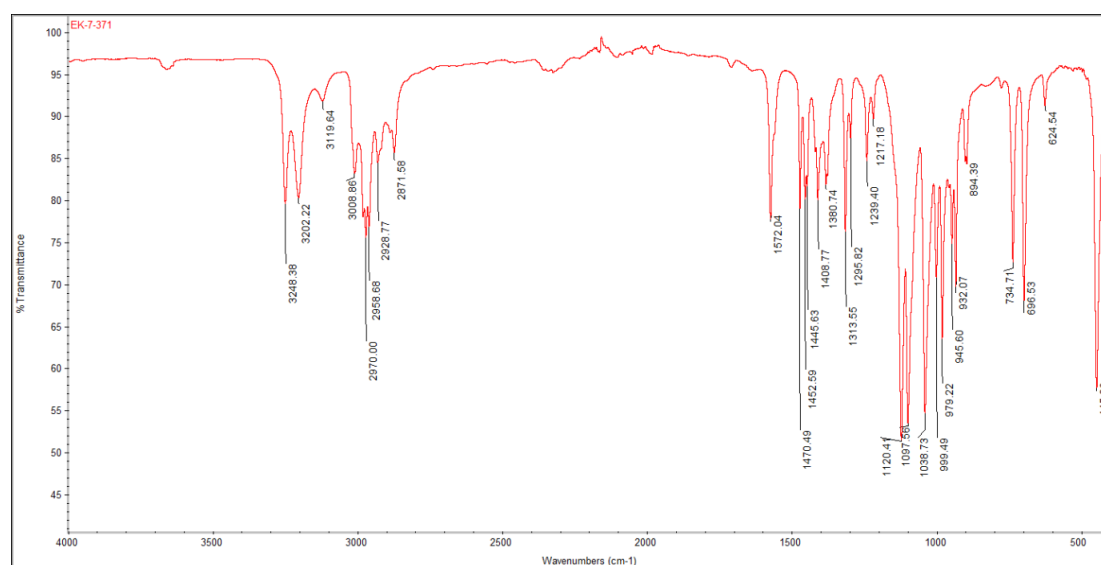
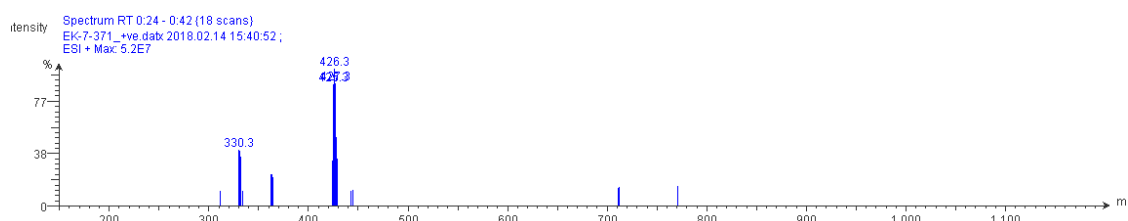
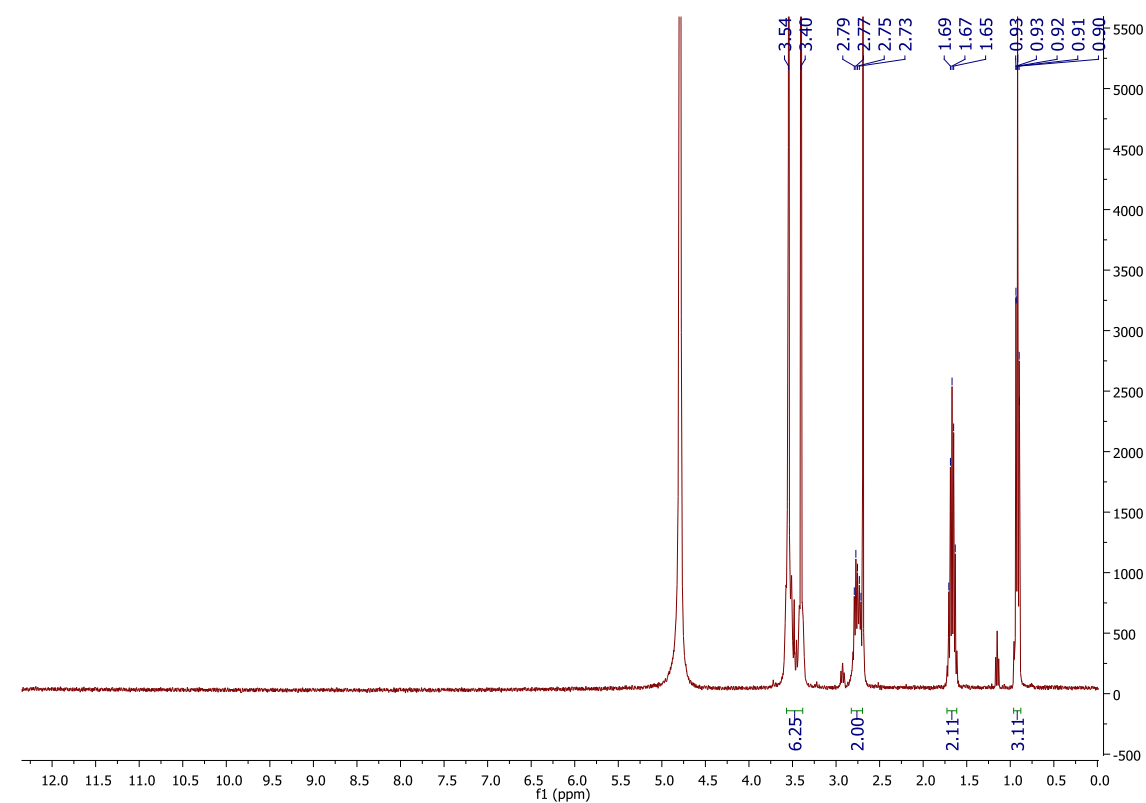
**+MS, 1.1-2.1min #66-123**

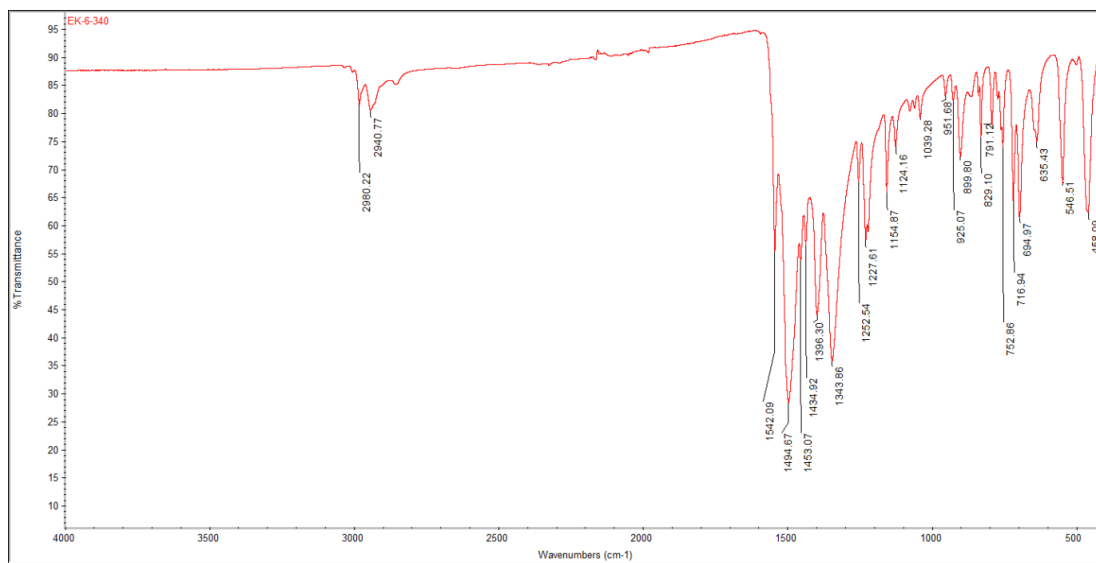
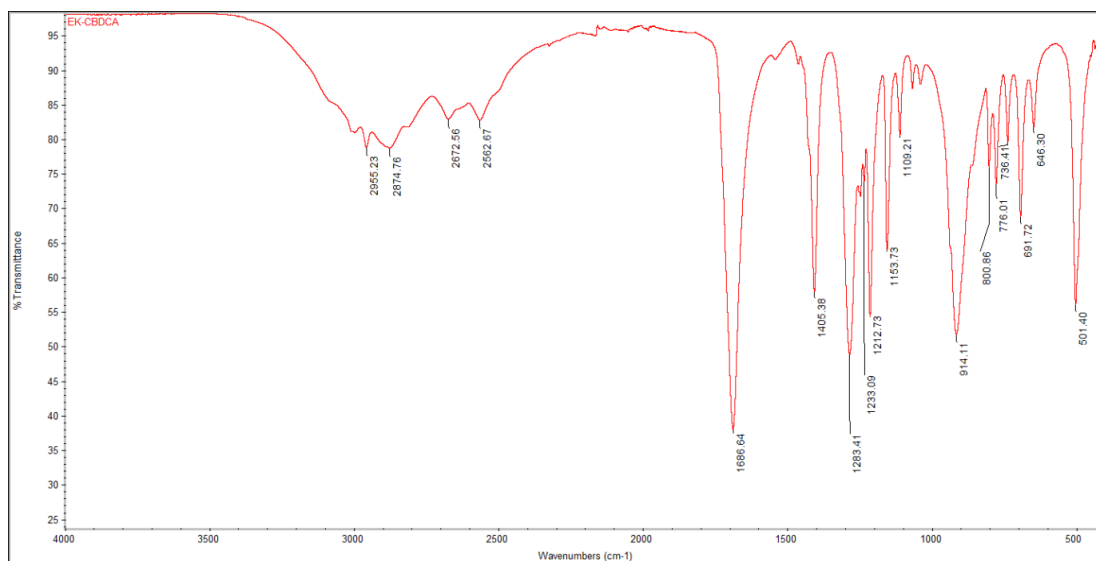


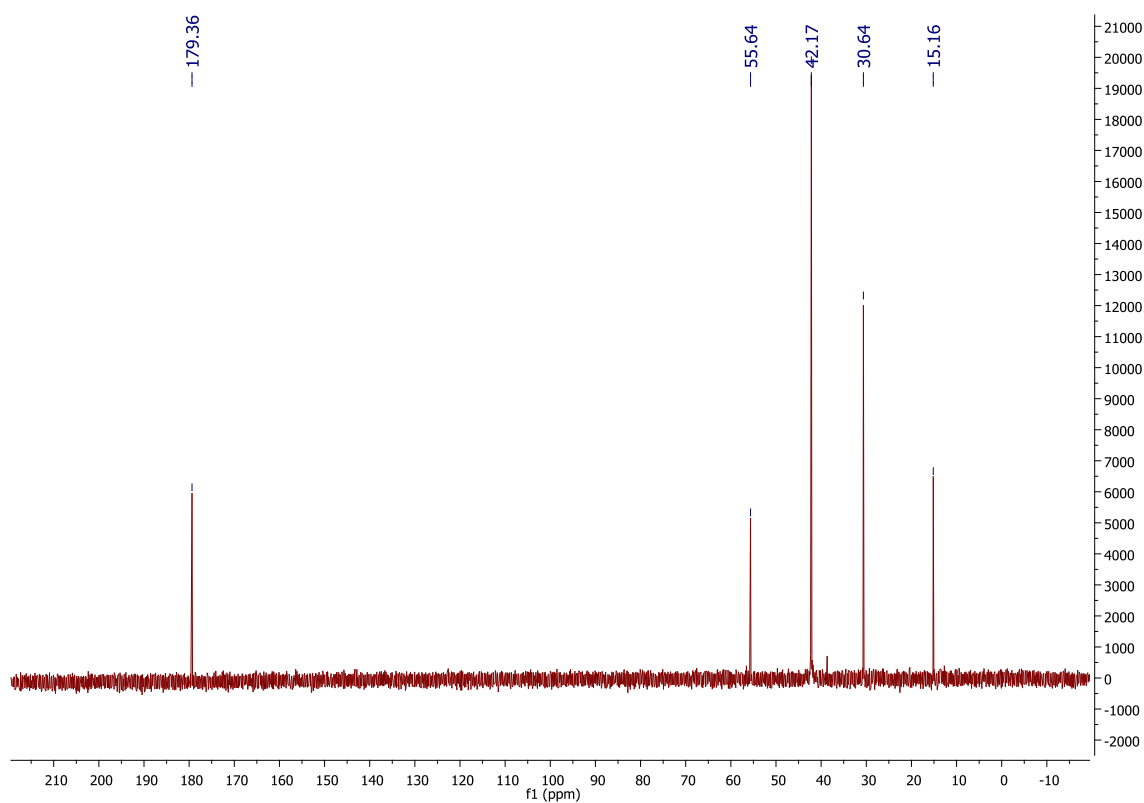
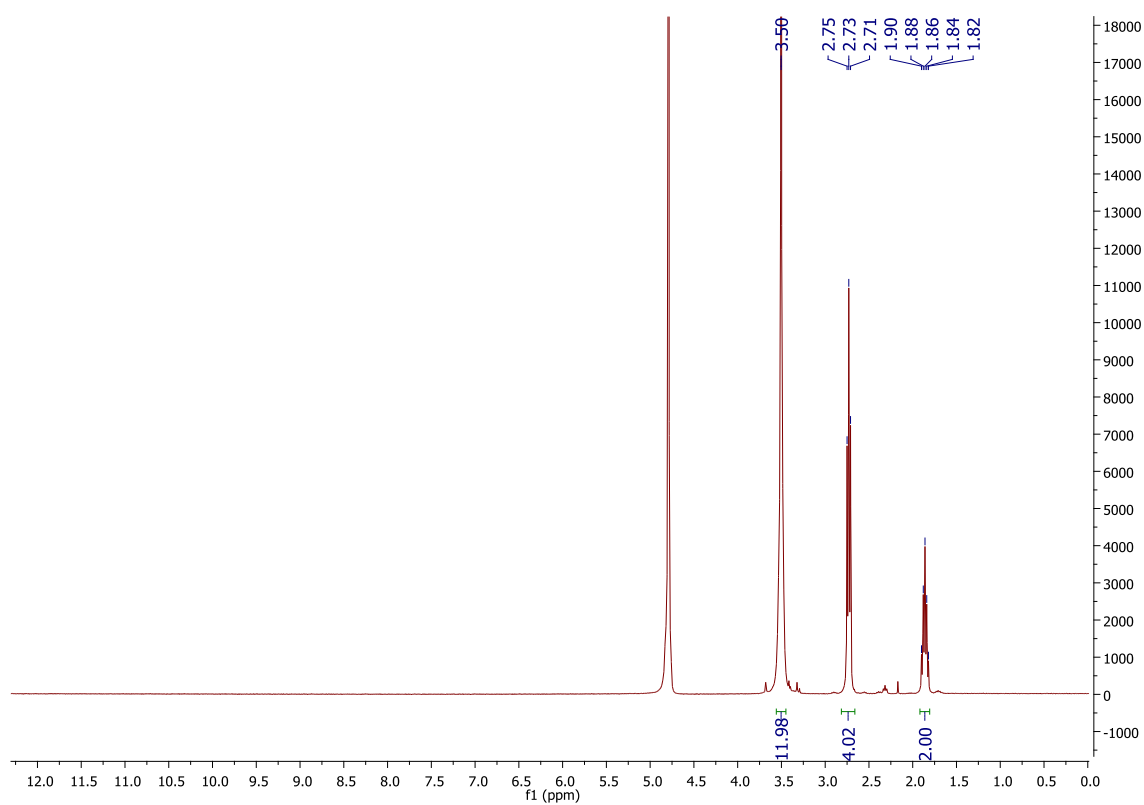
Meas. m/z	#	Ion Formula	m/z	err [ppm]	mSigma	# mSigma	Score	rdb	e <sup>-</sup> Conf	N-Rule
1195.9938	1	C <sub>20</sub> H <sub>28</sub> Cl <sub>5</sub> N <sub>12</sub> Pt <sub>3</sub>	1195.9941	-3.1	16.9	1	100.00	11.0	even	-



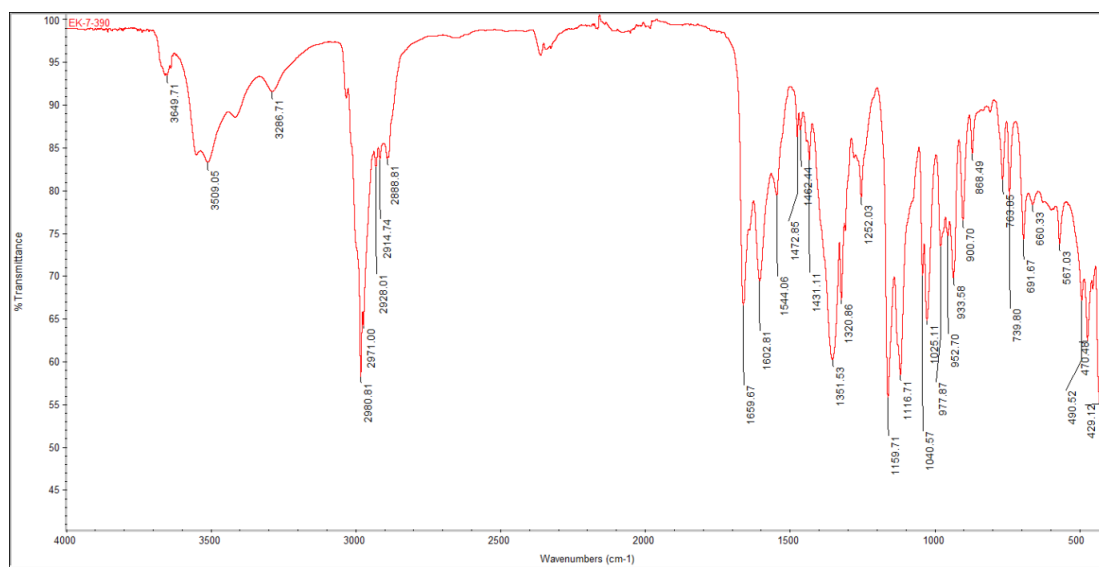
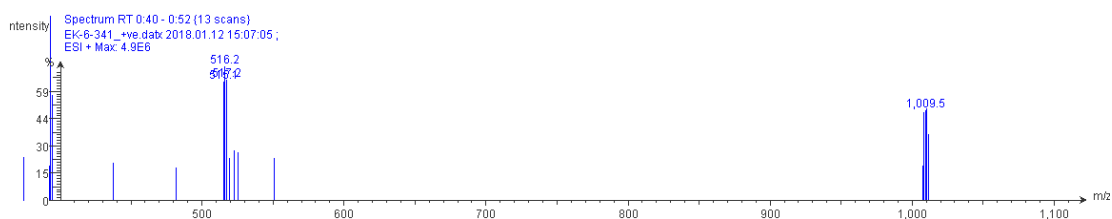
*cis*-[Pt(II)Cl<sub>2</sub>(DMSO)<sub>2</sub>] (33)

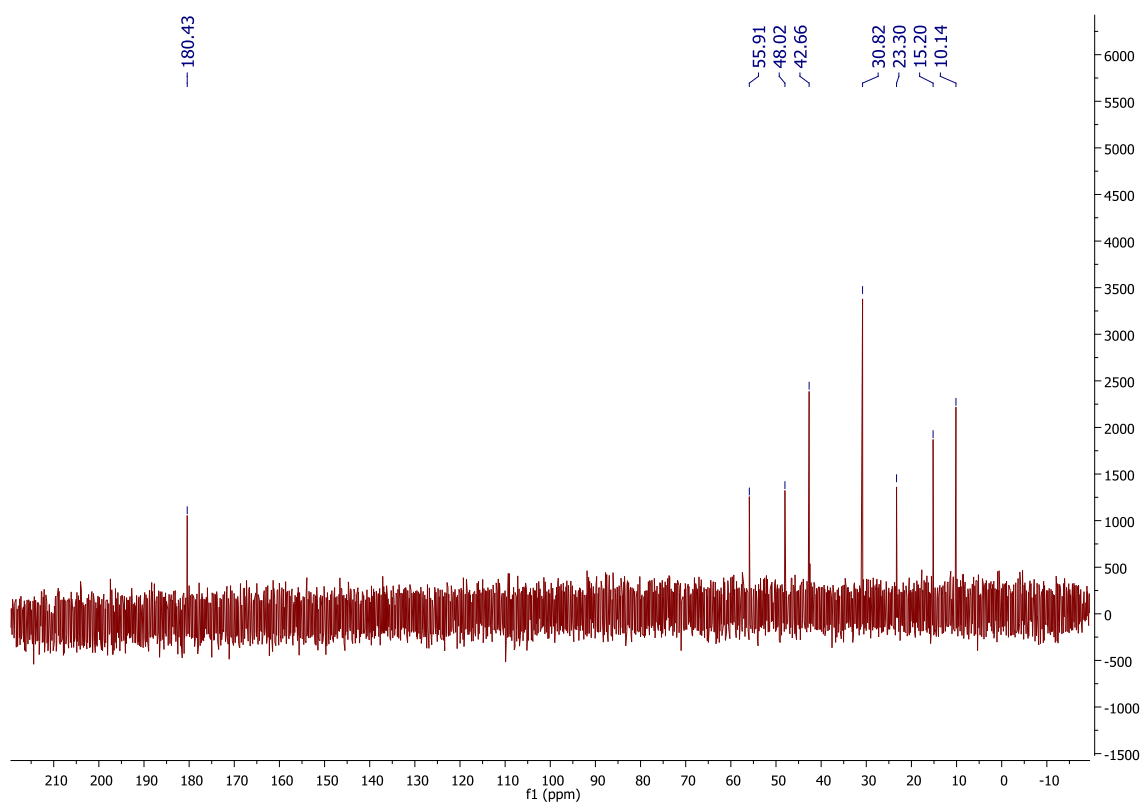
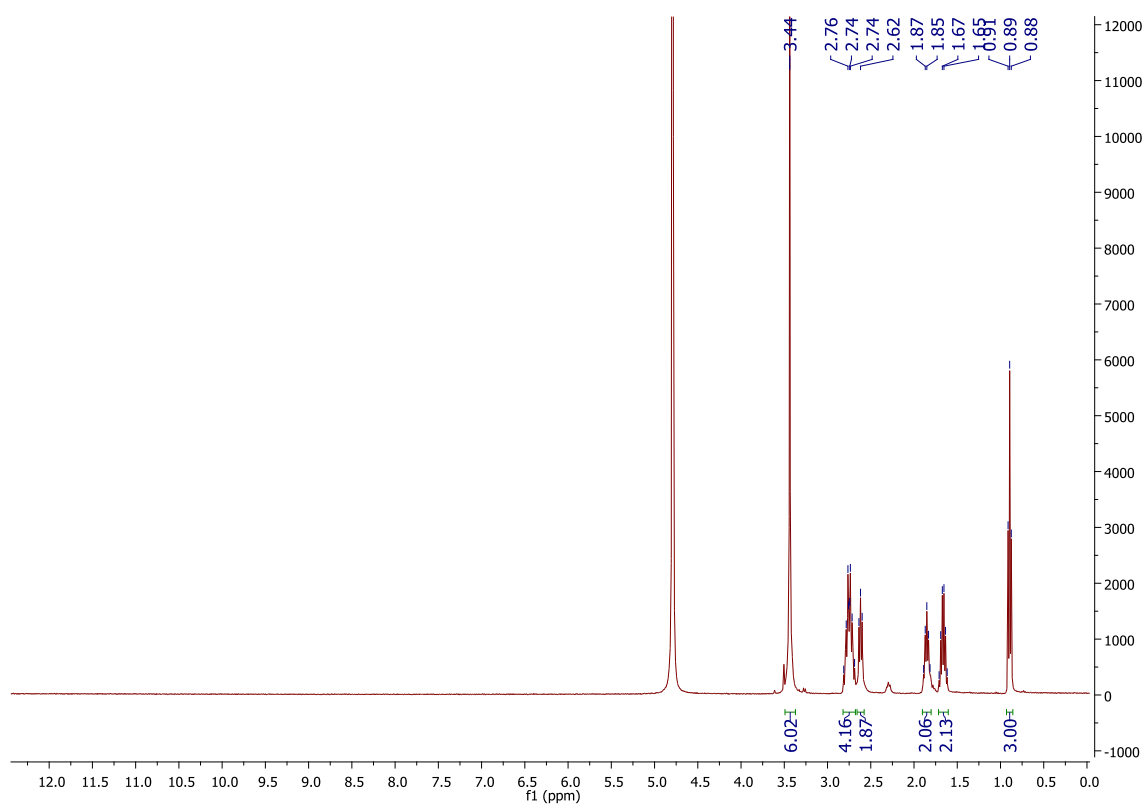
***cis*-[Pt(II)Cl<sub>2</sub>(DMSO)(*n*-propylamine)] (34)**

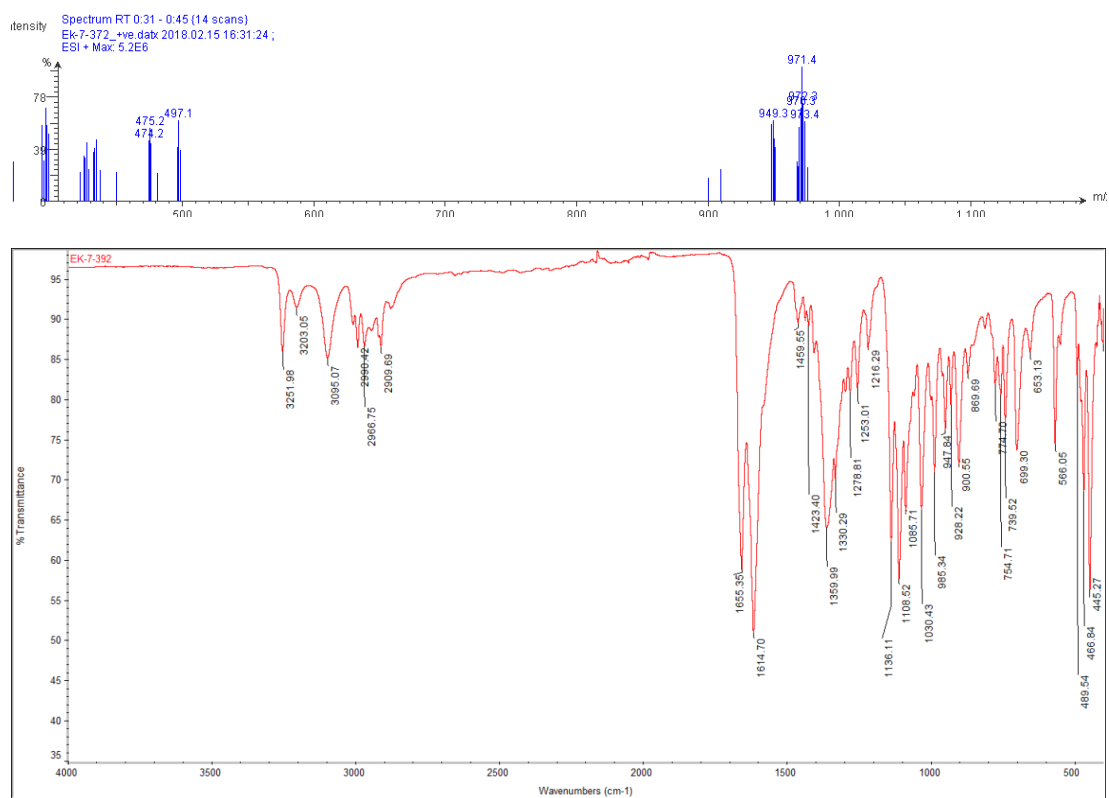
**[Ag<sub>2</sub>(CBDCA)] (35)****Free ligand: CBDCAH<sub>2</sub>**

*cis*-[Pt(II)(CBDCA)(DMSO)<sub>2</sub>] (36)



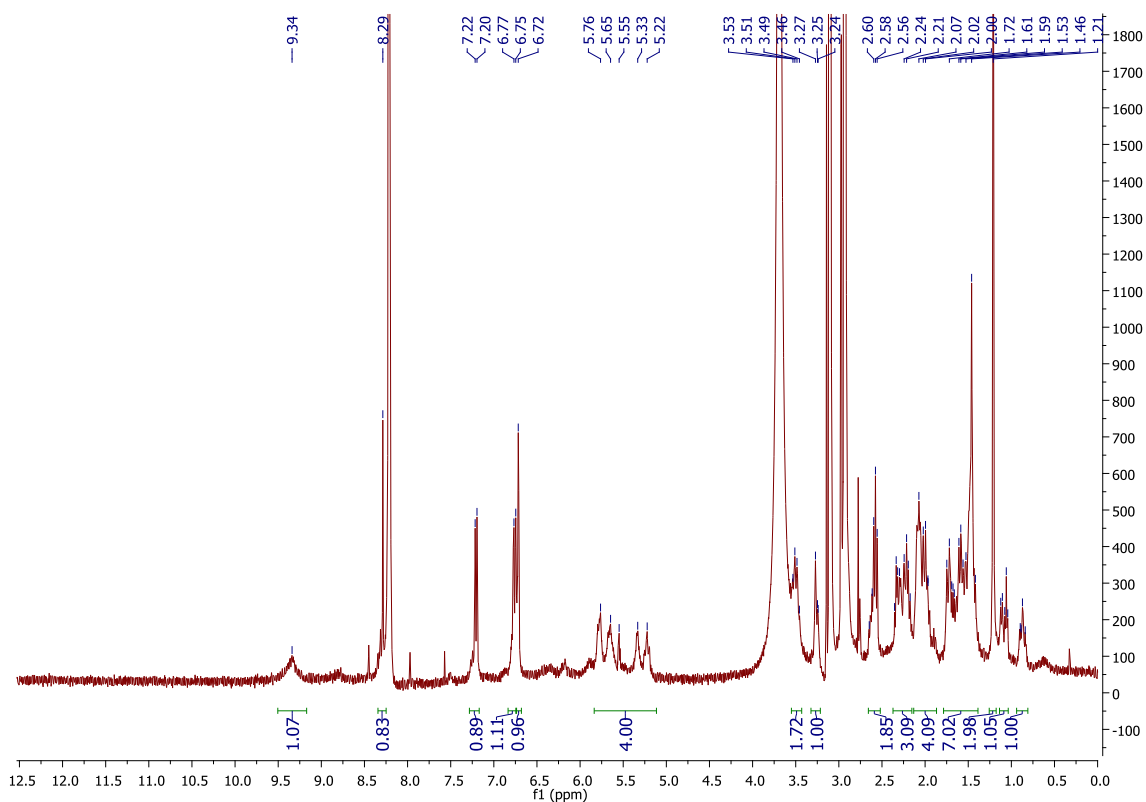


***cis*-[Pt(II)(CBDCA)(DMSO)(*n*-propylamine)] (37)**

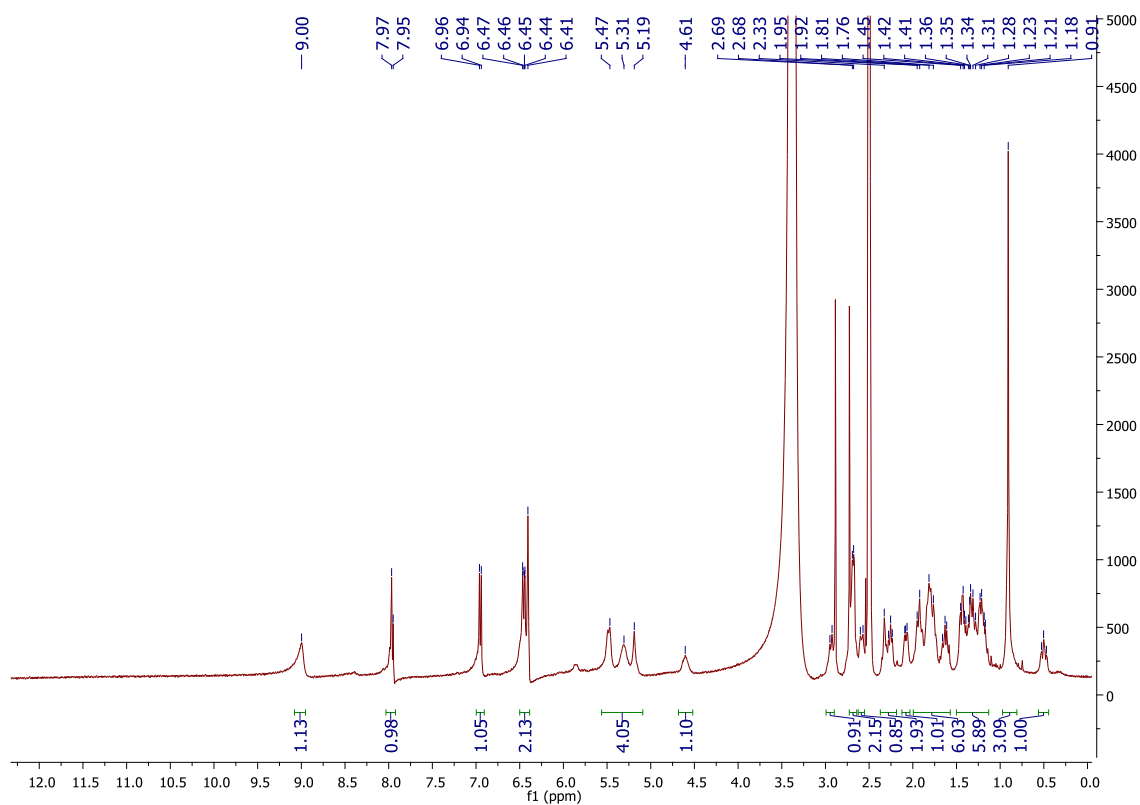


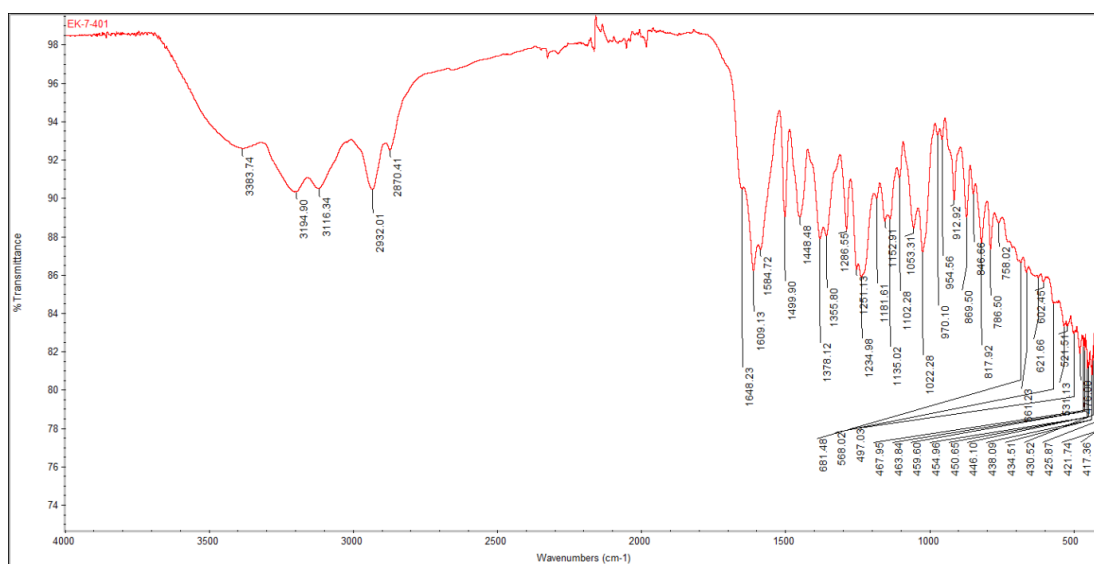
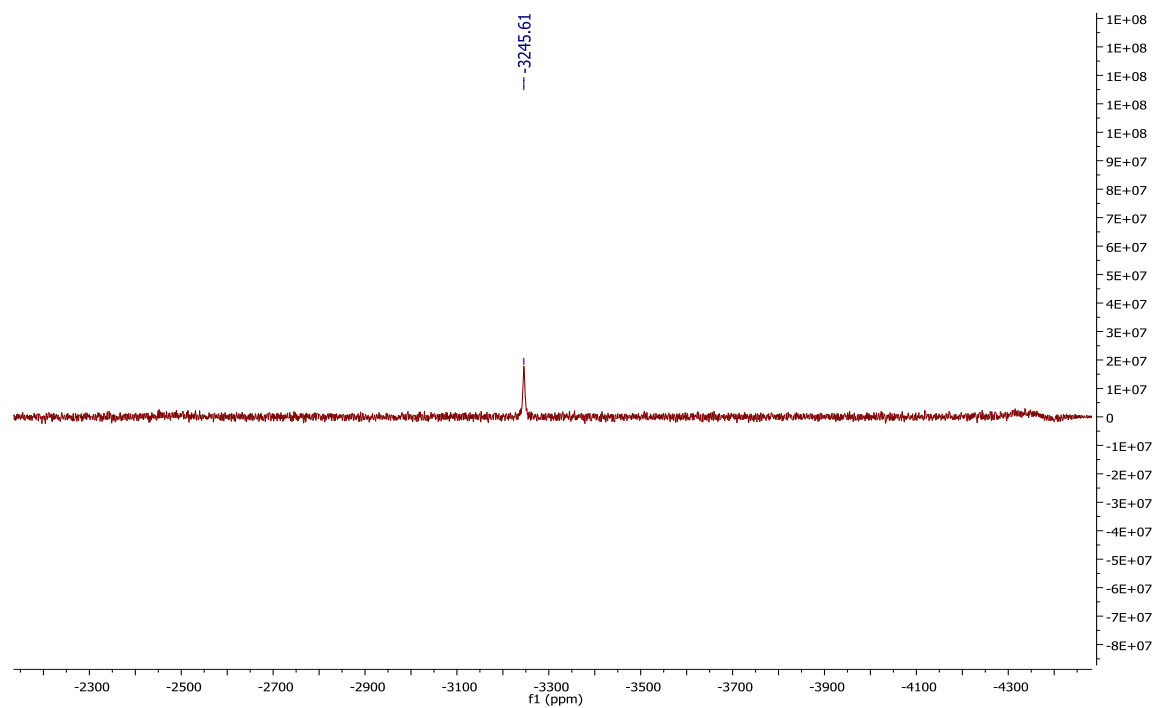
**[Pt(II)(CBDCA)(2-(4-(estradiol)-1*H*-1,2,3-triazol-1-yl)propane-1,3-diyl)] (38)**

DMF

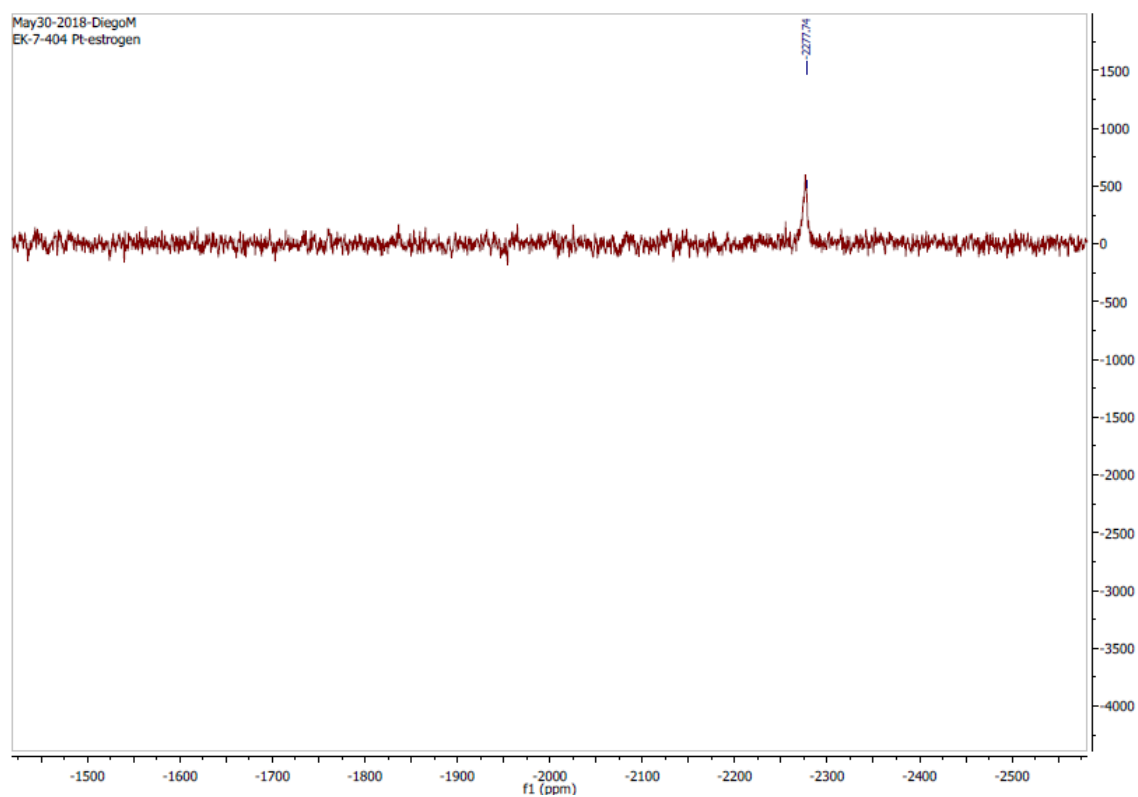
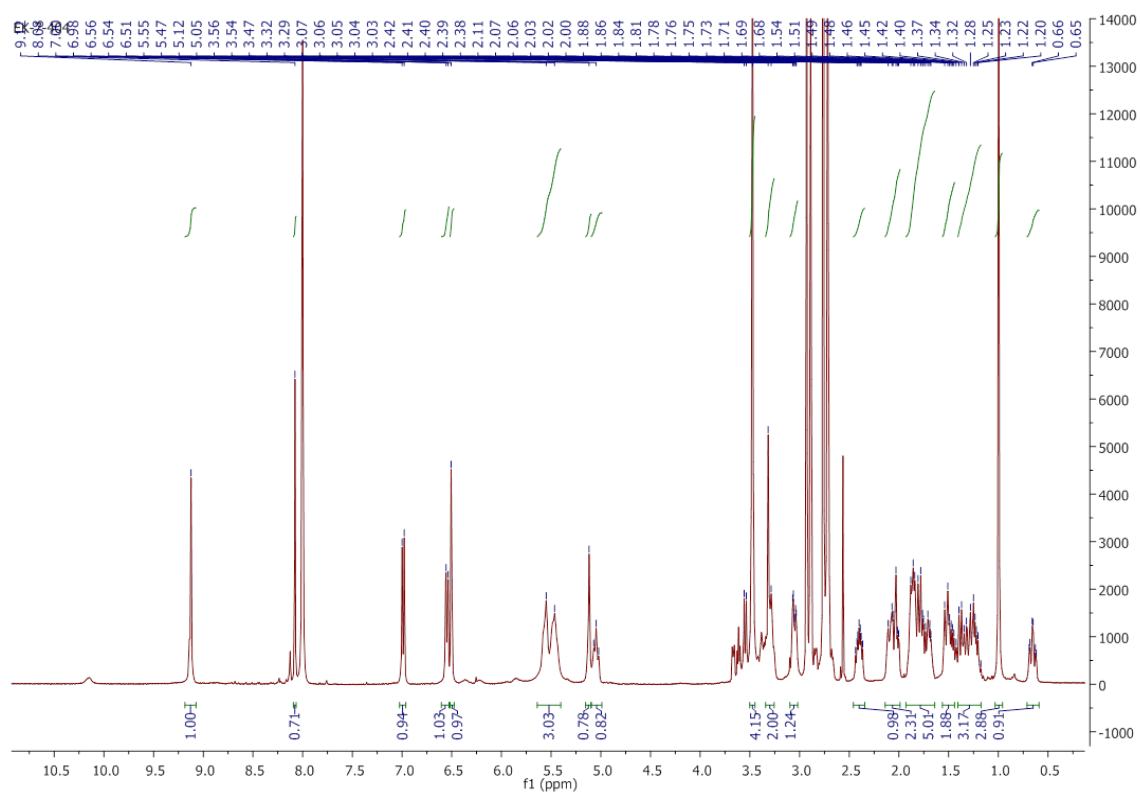


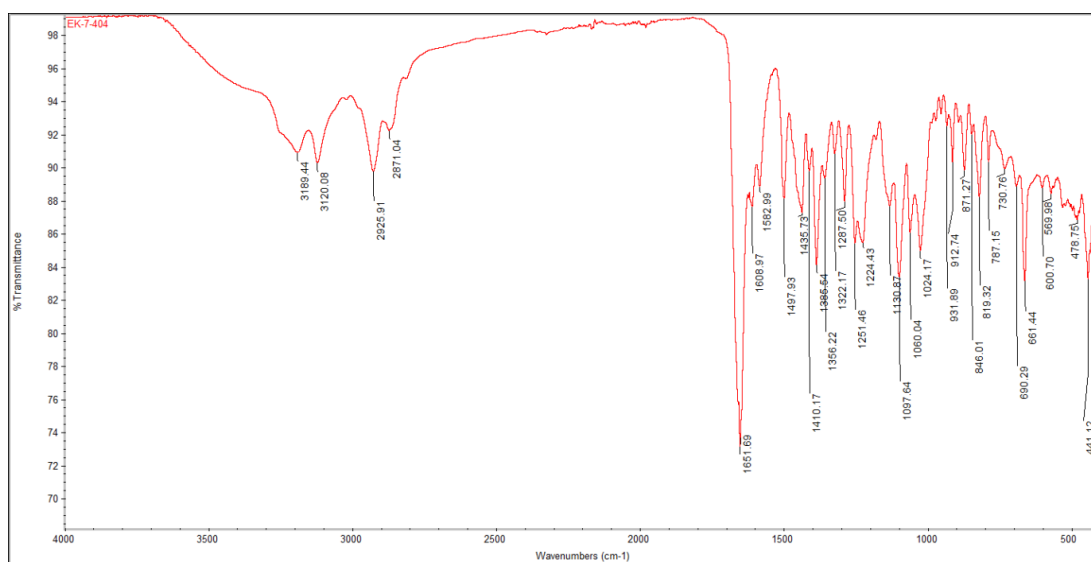
DMSO



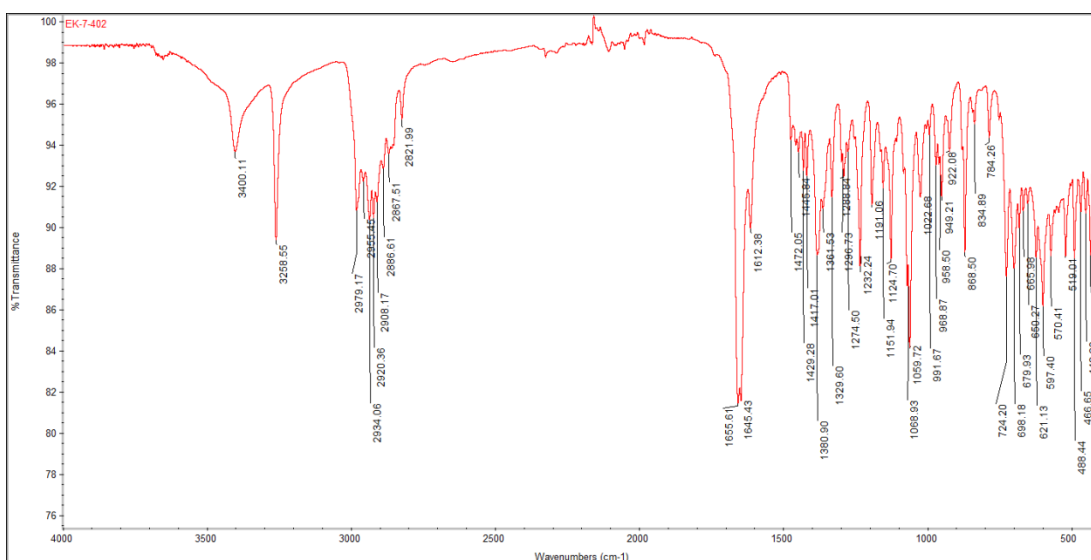
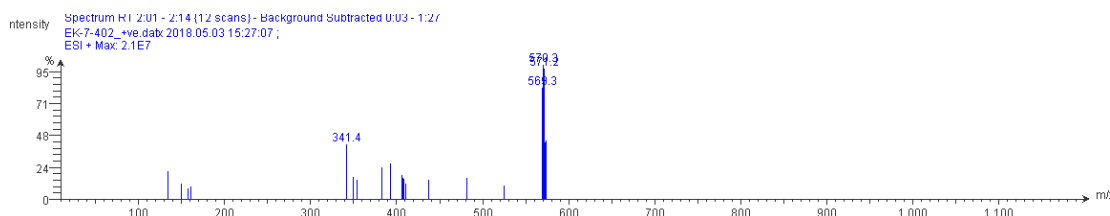
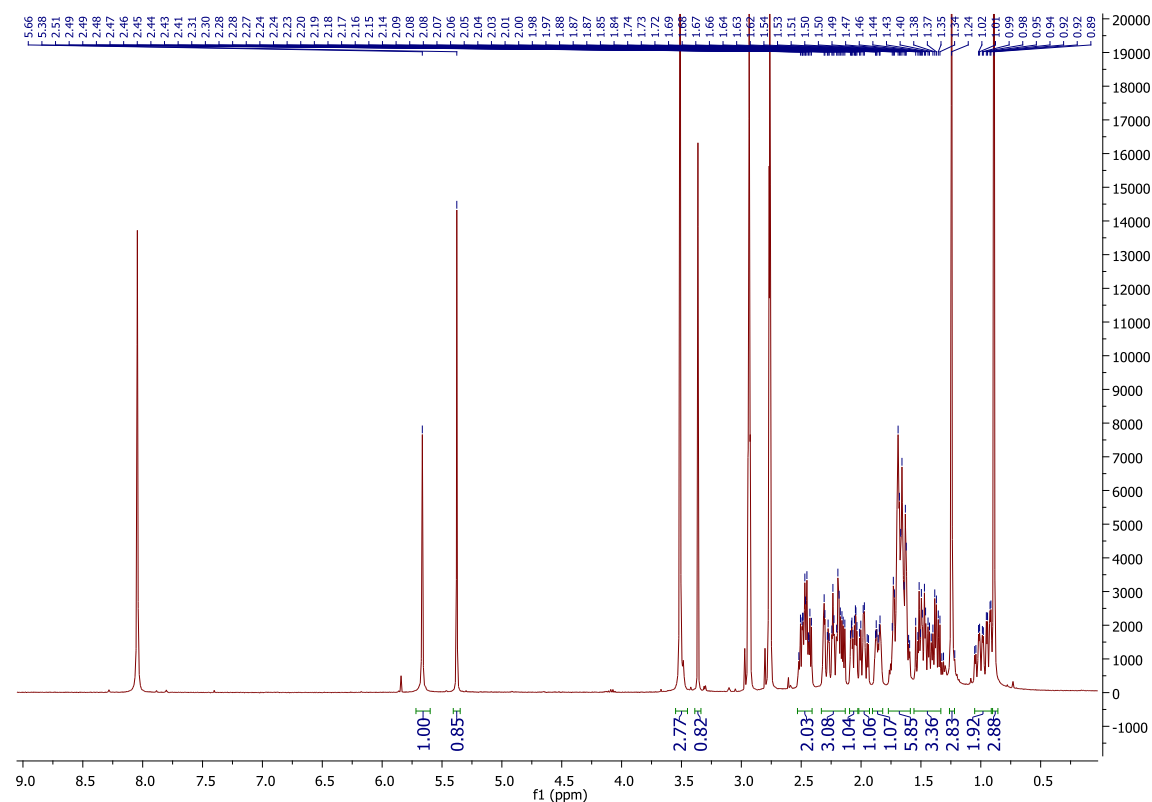


**[Pt(II)Cl<sub>2</sub>(2-(4-(estradiol)-1H-1,2,3-triazol-1-yl)propane-1,3-diyl)] (39)**





# Attempted synthesis of [Pt(II)(2-(4-(testosterone)-1*H*-1,2,3-triazol-1-yl)propane-1,3-diyl)] (40)



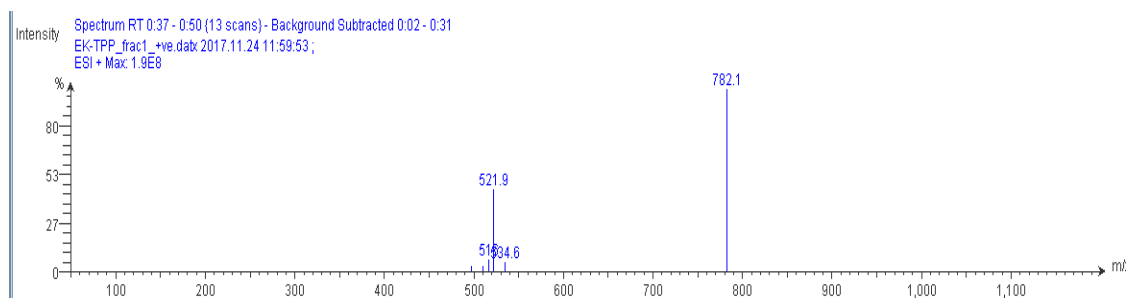
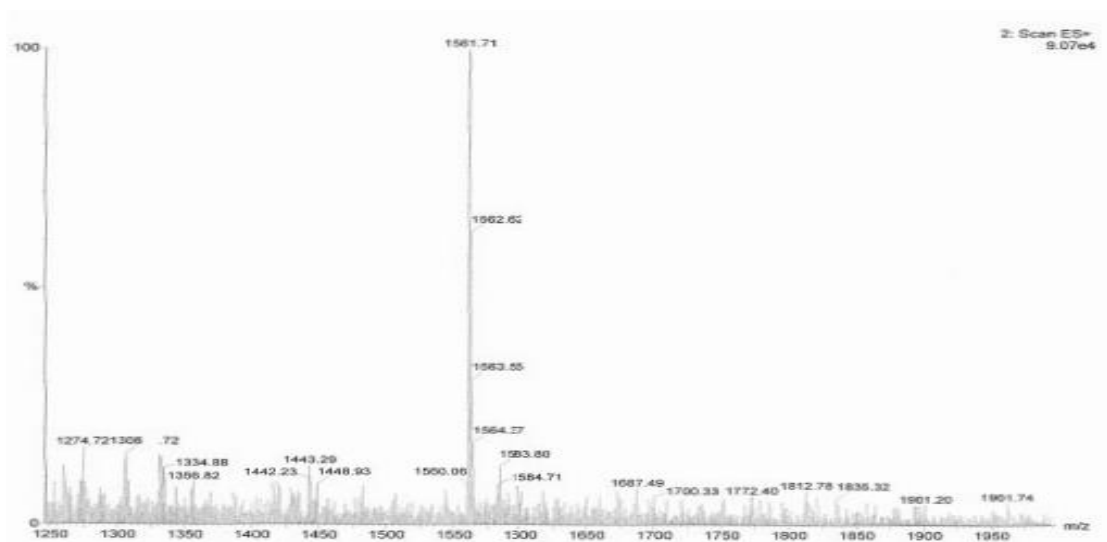
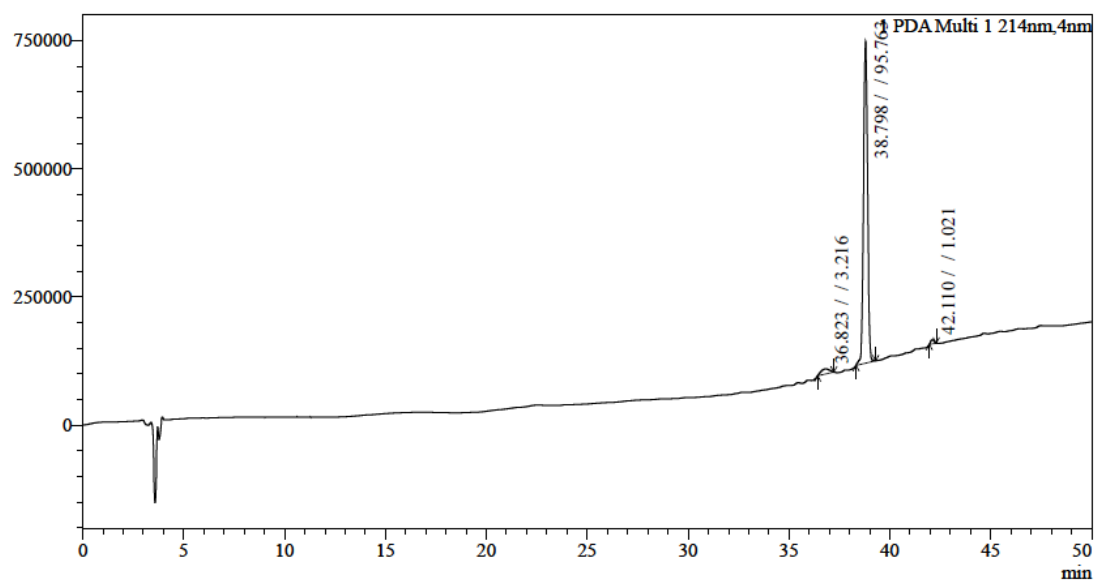


## Peptides

## TPP

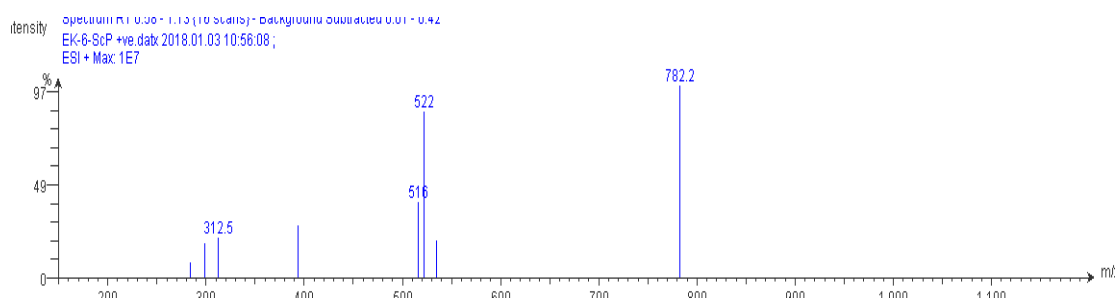
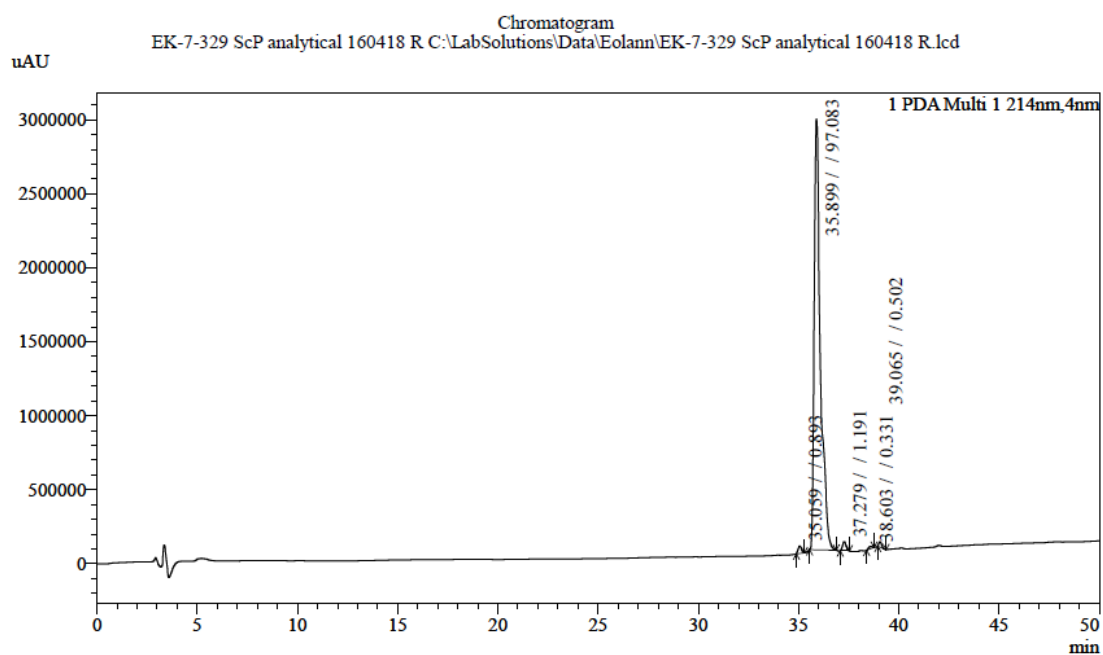
## Chromatogram

Chromatogram  
Eolann TPP fr1 prod fr1 analytical 130418 C:\LabSolutions\Data\Eolann\TPP Analytical\Eolann TPP fr1 prod fr1 analytical 130418.lcd  
uAU



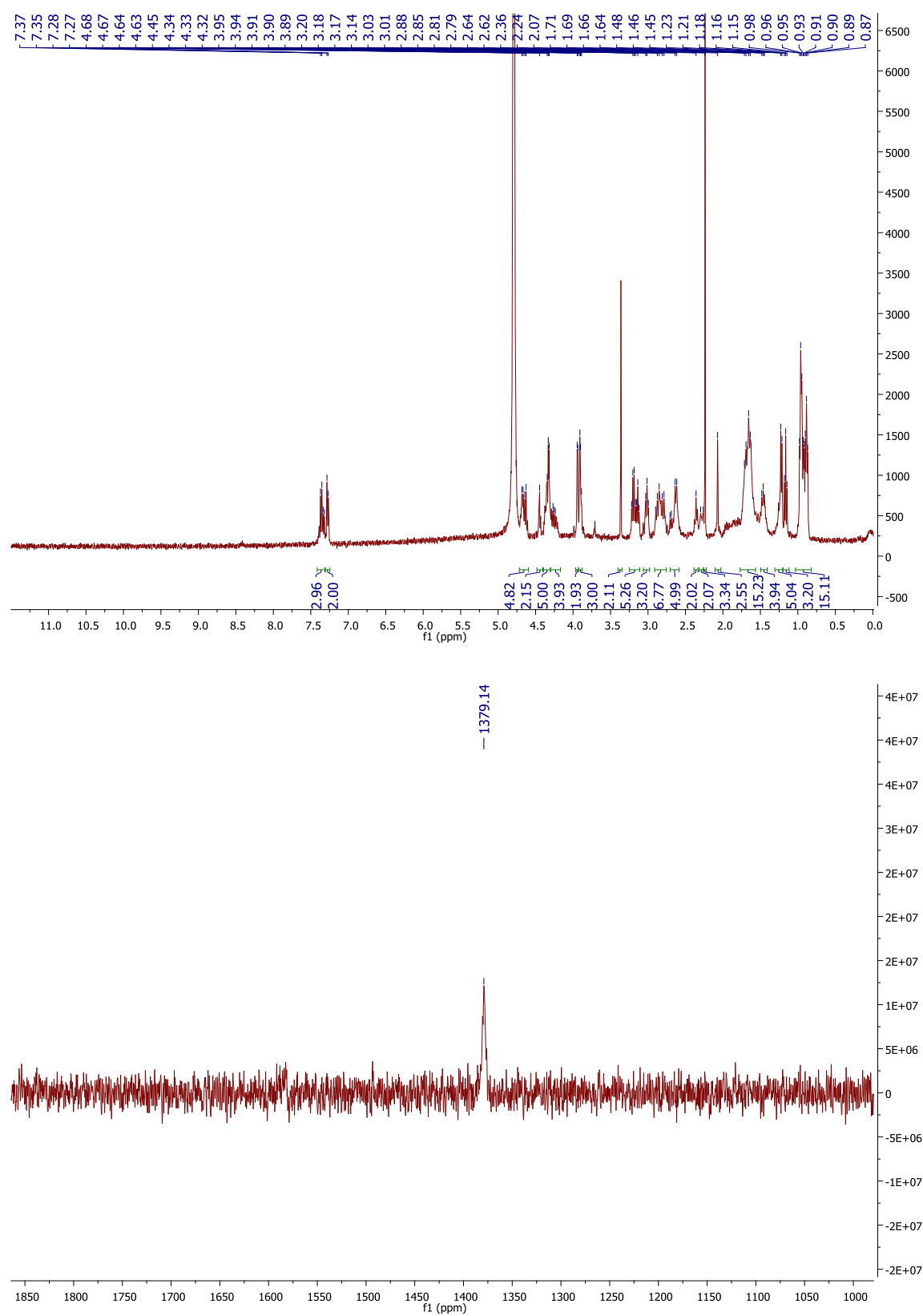
## ScP

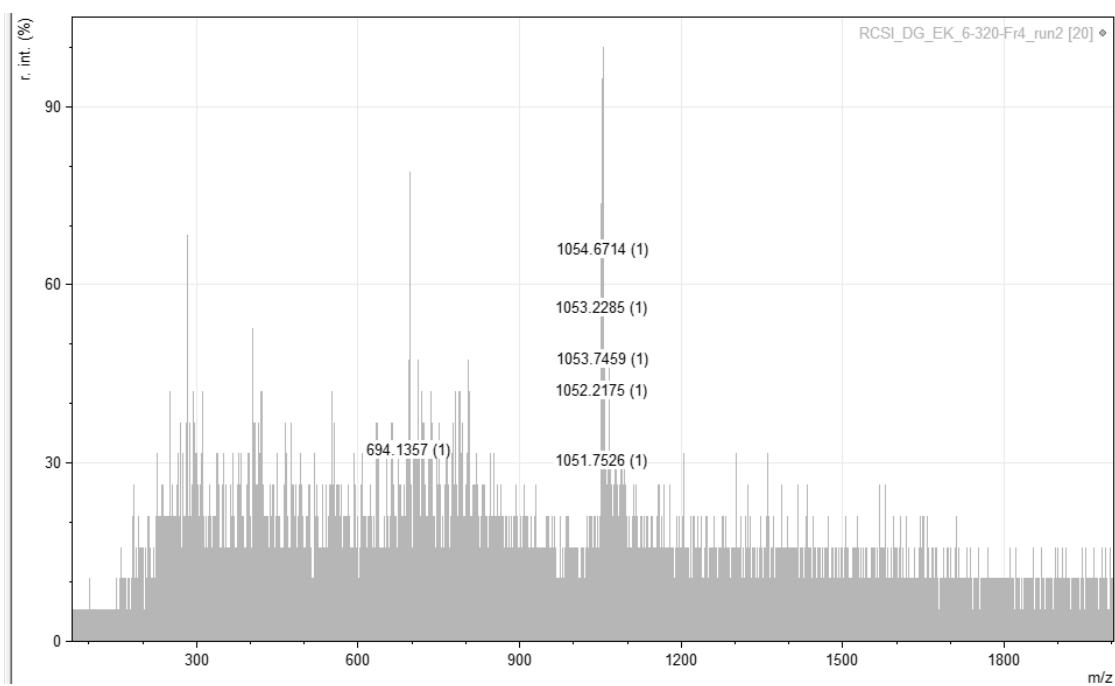
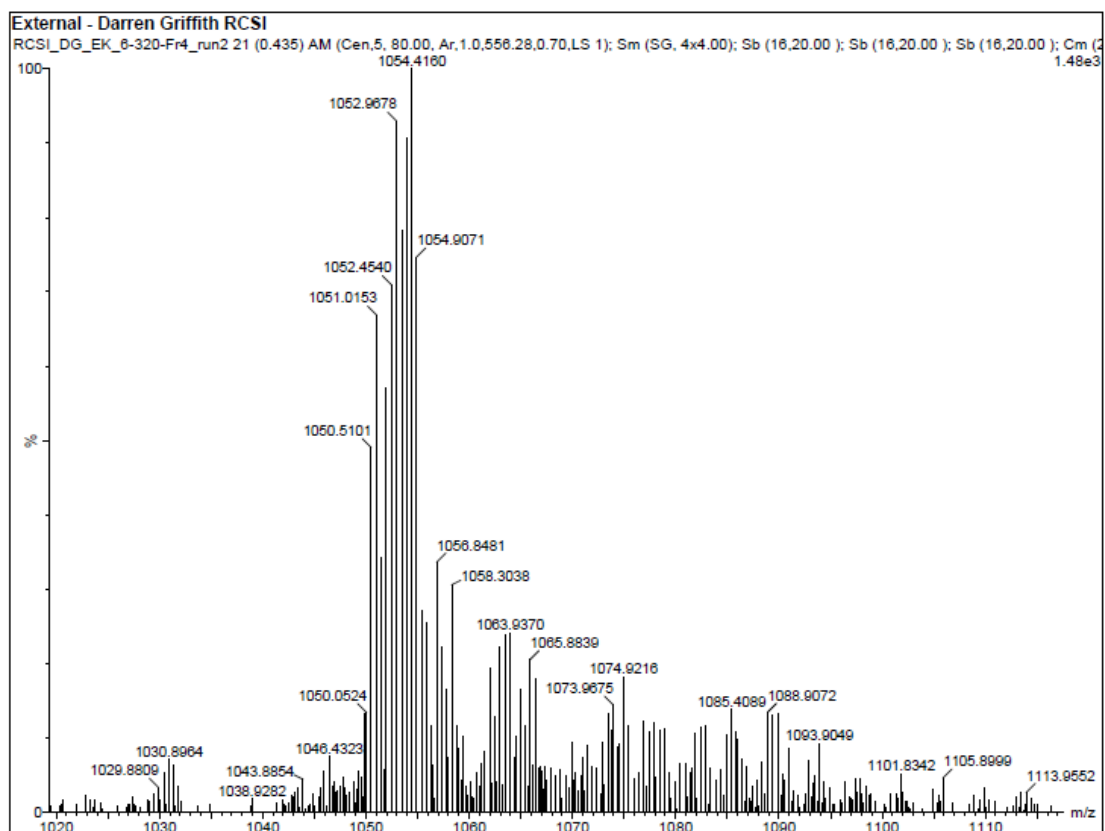
## Chromatogram

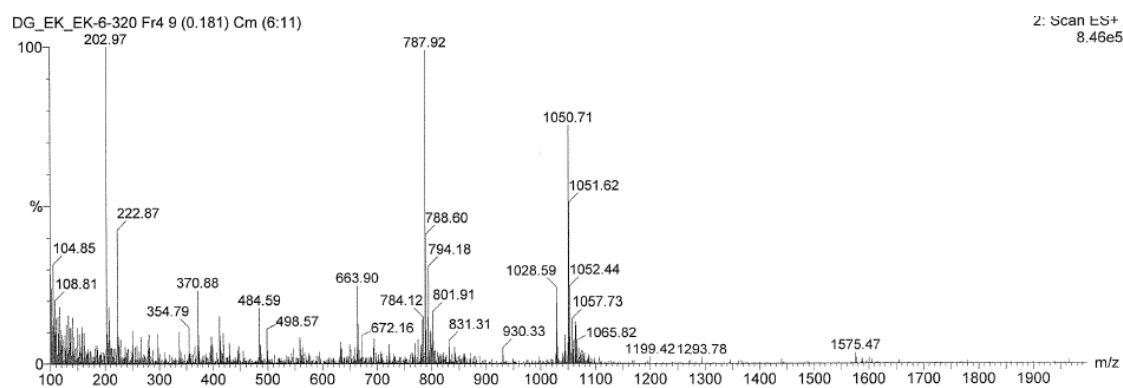


## Pt-Peptides

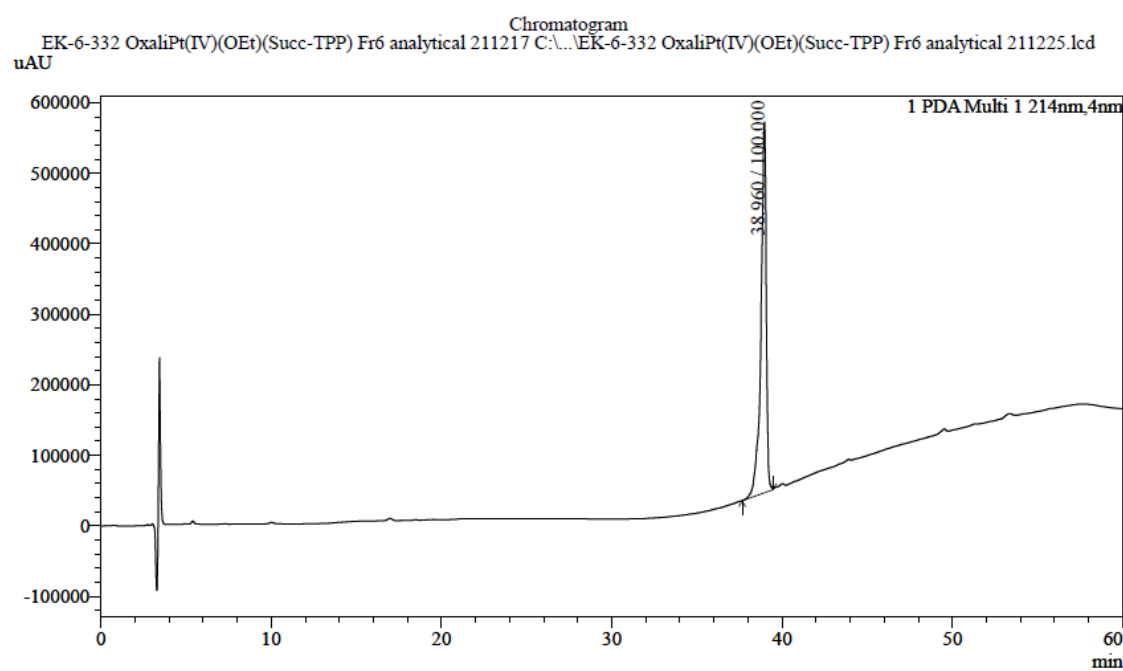
## Pt-TPP

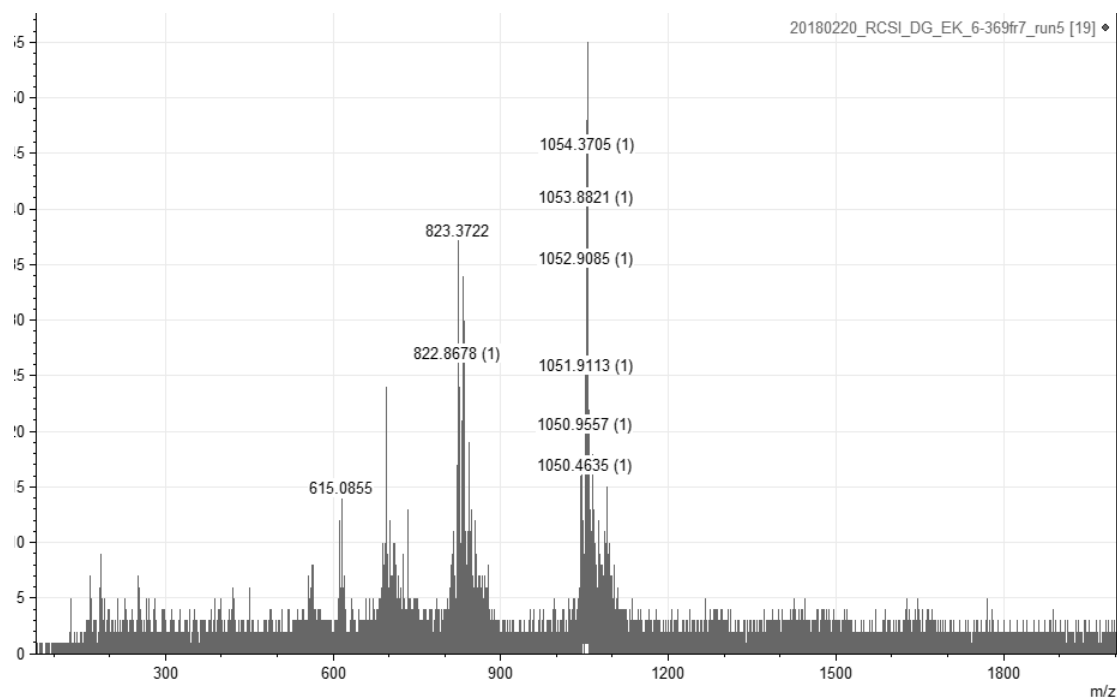
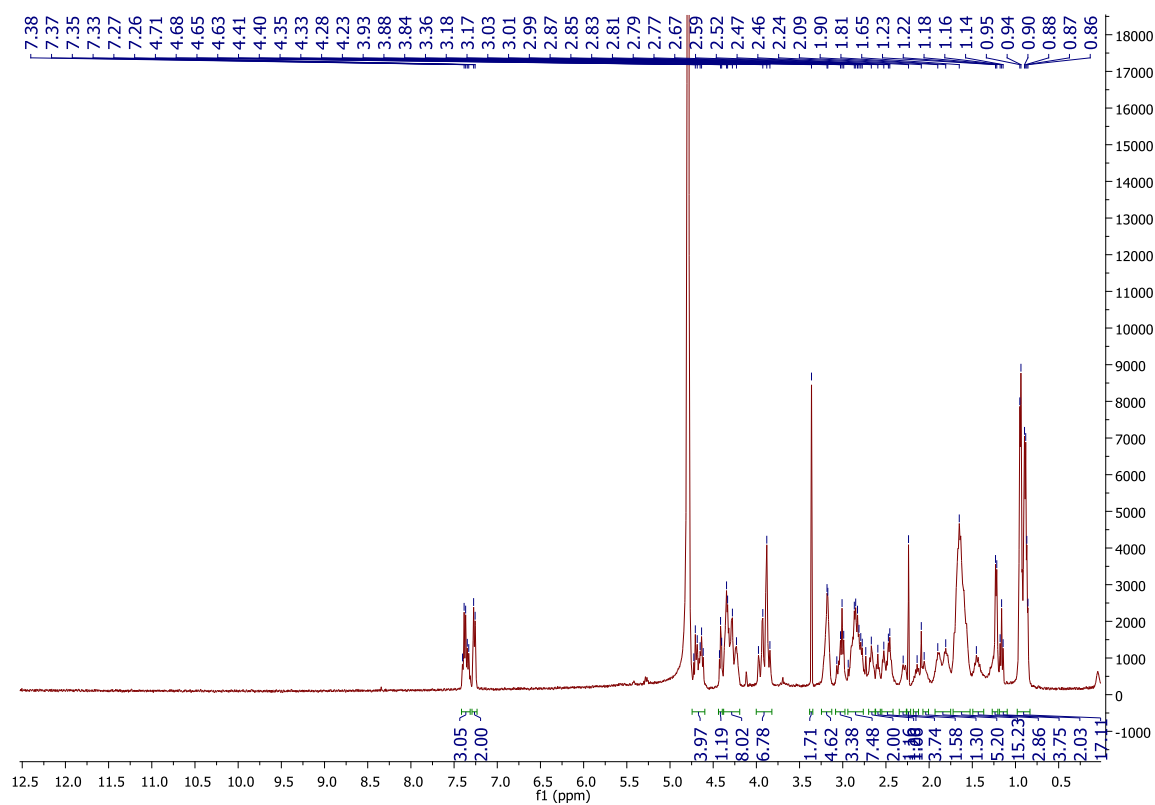


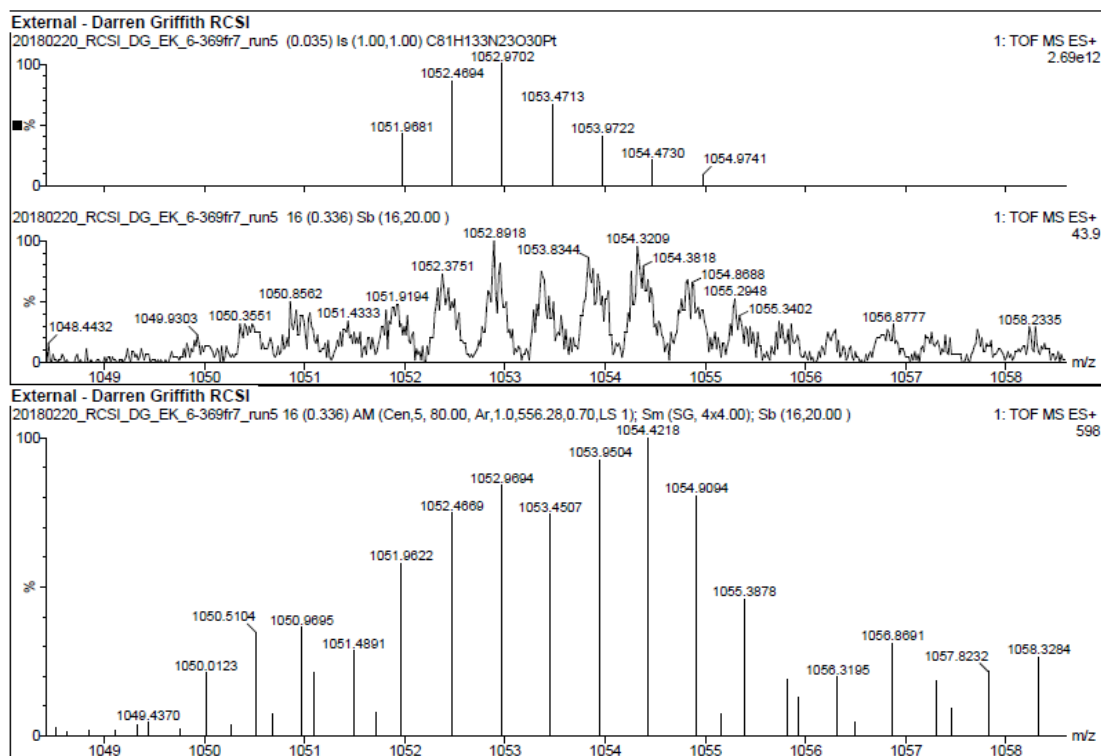




### Chromatogram

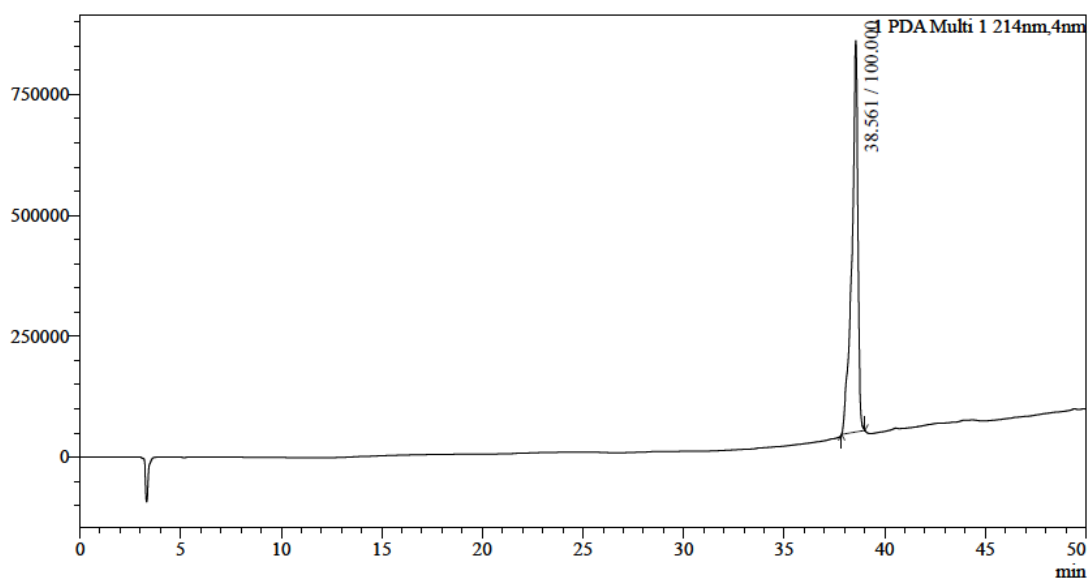


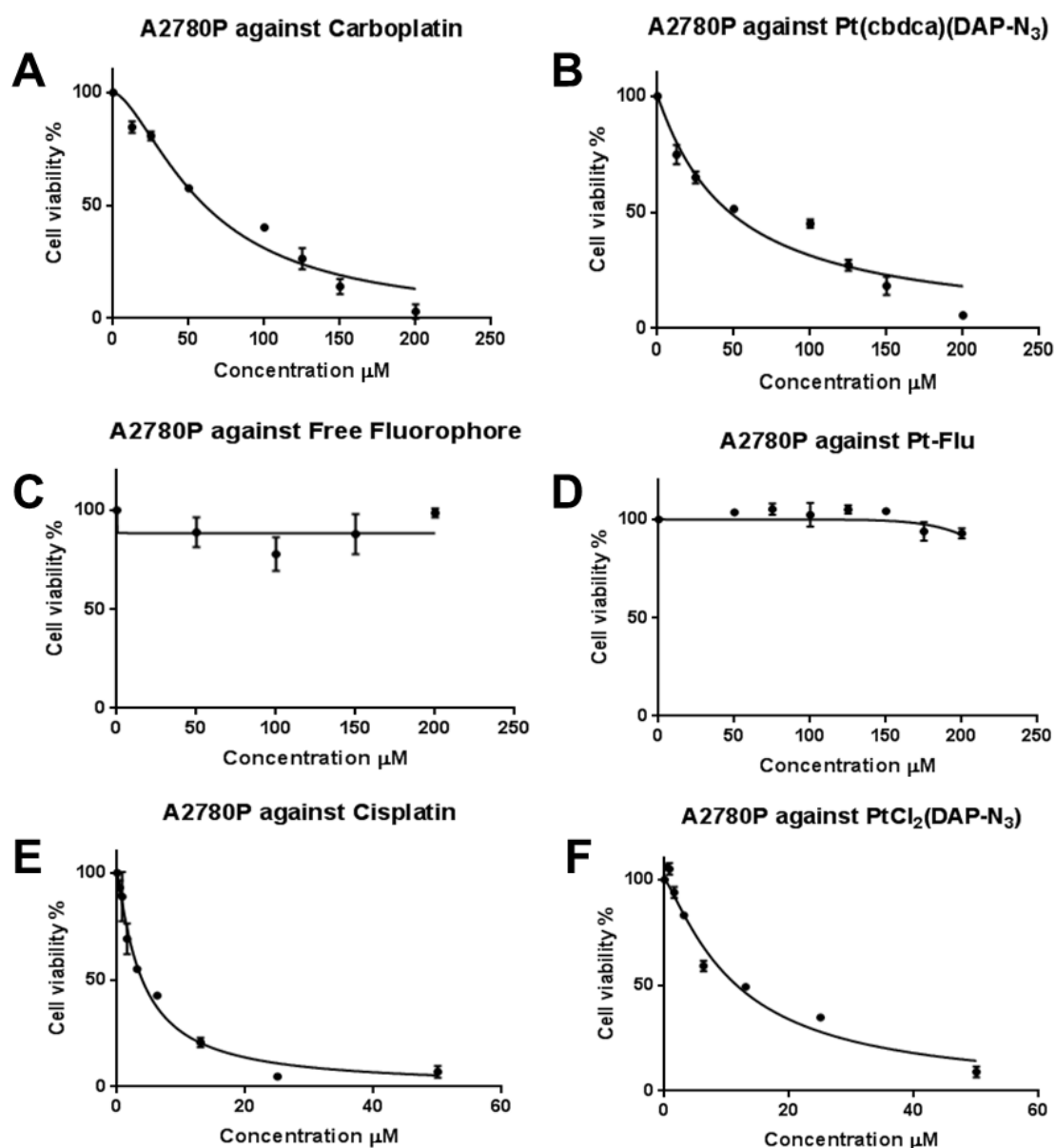
**Pt-ScP**



## Chromatogram

Chromatogram  
EK-7-369 Pt-Scp Fr7 pure analytical 160218 C:\LabSolutions\Data\Eolann\EK-7-369 Pt-Scp Fr7 pure analytical 160219.lcd  
uAU



*In vitro* cytotoxicity data - Cell proliferation curves

**Figure S1:** Cell proliferation curves ( $n = 3$ ) after 72 h treatment compounds against A2780P cells with IC<sub>50</sub> values (A) carboplatin 71.9 μM, (B) [Pt(CBDCA)(DAP-N<sub>3</sub>)] 4 μM, (C) Flu and (D) Pt-Flu >200 μM, (E) cisplatin 4.5 μM and (F) [PtCl<sub>2</sub>(DAP-N<sub>3</sub>)] 12.0 μM.



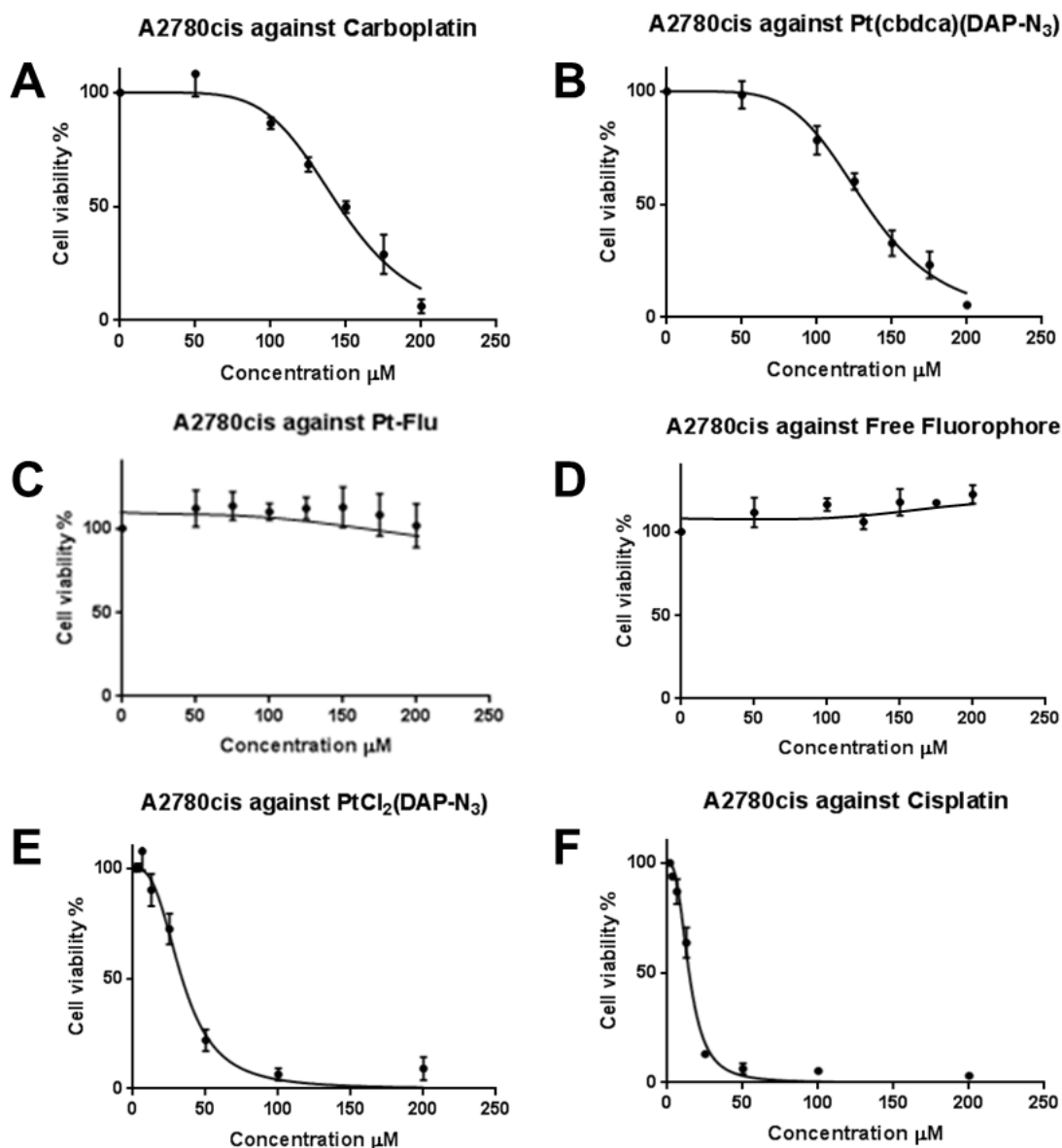


**Figure S2:** Cell proliferation curves ( $n = 3$ ) after 72 h treatment compounds against A2780cis cells with IC<sub>50</sub> values (A) carboplatin 149.8  $\mu\text{M}$ , (B) [Pt(CBDCA)(DAP-N<sub>3</sub>)] 134.3  $\mu\text{M}$ , (C) Flu and (D) Pt-Flu >200  $\mu\text{M}$ , (E) cisplatin 15.8  $\mu\text{M}$  and (F) [PtCl<sub>2</sub>(DAP-N<sub>3</sub>)] 36.2  $\mu\text{M}$ .

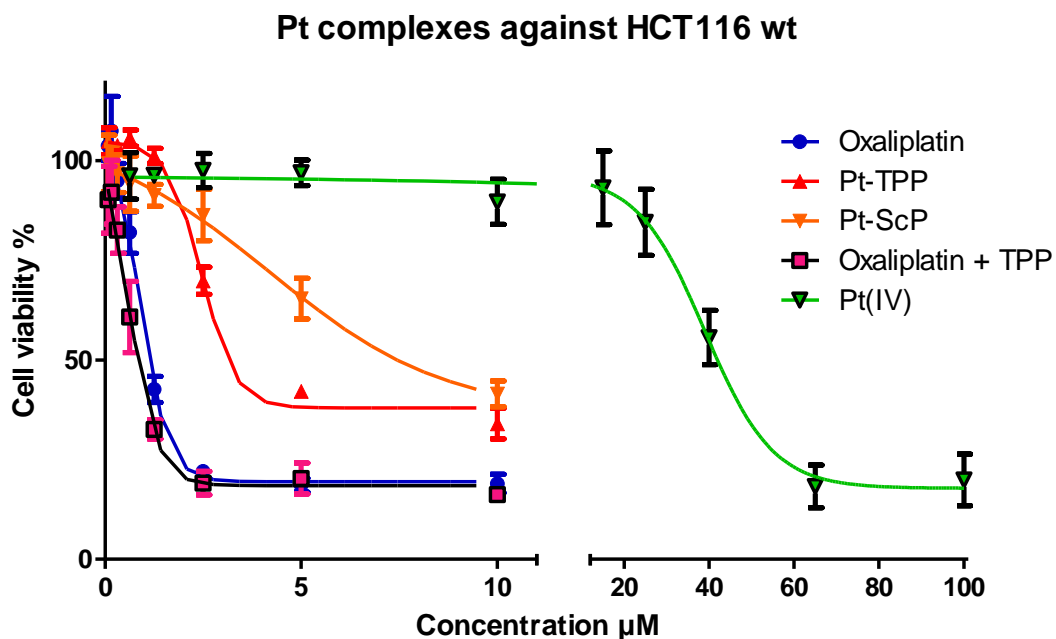


**Figure S3:** HCT116 wt cell proliferation curves ( $n = 3$ ) after 72 h treatment with compounds  $\text{IC}_{50}$  values: oxaliplatin  $0.89 \mu\text{M}$ , Pt-TPP  $2.4 \mu\text{M}$ , Pt-ScP  $8.18 \mu\text{M}$ , oxaliplatin + TPP  $0.71 \mu\text{M}$  and Pt(IV)  $39.22 \mu\text{M}$ .

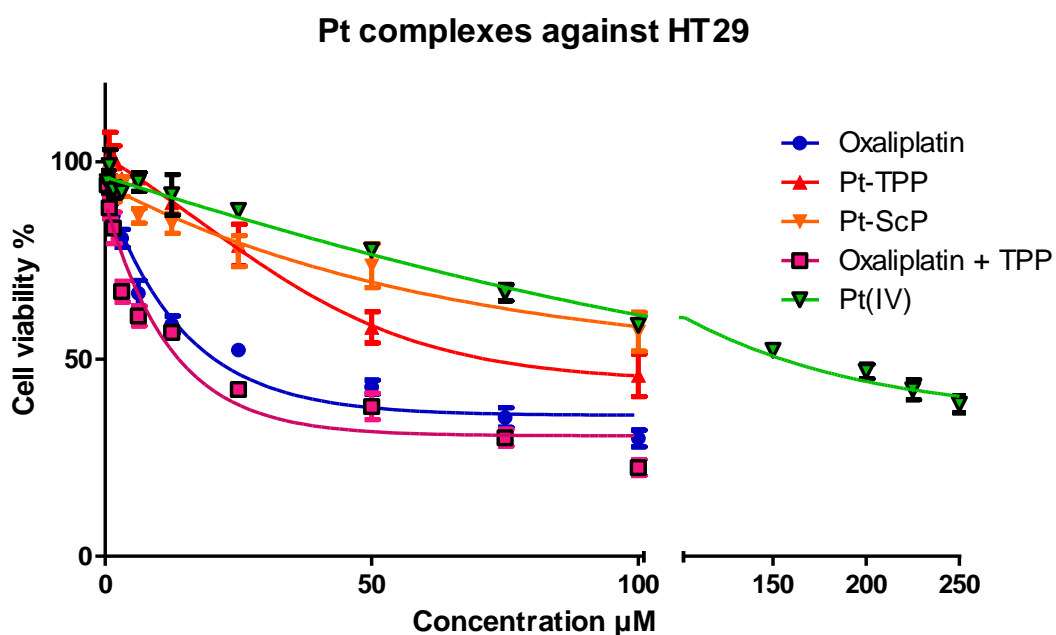


**Figure S4:** HT29 cell proliferation curves ( $n = 3$ ) after 72 h treatment with compounds  $\text{IC}_{50}$  values: oxaliplatin  $26.66 \mu\text{M}$ , Pt-TPP  $78.15 \mu\text{M}$ , Pt-ScP  $>100 \mu\text{M}$ , oxaliplatin + TPP  $16.45 \mu\text{M}$  and Pt(IV)  $162.3 \mu\text{M}$ .